Physical and Geochemical Conditions of Organic Metamorphism Next to Selected Dikes, Victoria, Australia

Charles E. Barker

Department of Geology and Geophysics

The University of Adelaide

December, 1994

TABLE OF CONTENTS

TABLE OF CONTENTS (continued)

Page

Page

TABLE OF CONTENTS (continued)

Page

ABSTRACT

Studies of ten basalt dikes from 0.06 m to 40 m thick in the Devonian Buchan Rift and Mesozoic Gippsland Basin, Victoria were used to examine the physical and chemical parameters or processes that are important during contact metamorphism of coaly sedimentary organic matter (SOM). These natural experiments can persist decades longer than reasonable for laboratory experiments and consequently should be improved analogues of burial heating that occurs over geological time scales. Previous studies using this analogue concept of organic geochemical experiments have been limited in that direct paleotemperature and heating duration measurements were not available. This study applies fluid inclusion geothermometry to directly measure peak paleotemperature (T_{peak}) and apatite fission track (AFT) annealing studies to attempt measurement of heating duration during contact metamorphism by dikes. These measurements are compared to heat flow models and a vitrinite reflectance geothermometer (VRG).

In the Buchan Rift, a study of one dike in a limestone host shows that burial history of the host rock prior to intrusion is important in determining the extent of the contact aureole. Development of a geothermometer based on solid bitumen reflectance shows that T_{peak} in the Buchan Rift approached 200°C. After exhumation and cooling of the host rocks, a 2.2 m thick dike was intruded during the Tertiary. The host rock burial history and its apparently unsaturated condition during intrusion resulted in a nominal response to contact temperatures of near 600°C.

In the Gippsland Basin, dikes intruded the Upper Jurassic to Lower Cretaceous Strzelecki Group strata which was then at a temperature of about 100°C. Contact metamorphism in the host rocks next to thin dikes (in this study, < 3.4 m thick) caused the T_{peak} interpreted from fluid inclusions to systematically increase towards the dike margin to near 550°C. These T_{peak} data are in fair agreement with those predicted by a heat flow model

that considers the effects of latent heat in the magma and pore water in the host rocks. These studies suggest that heat absorbed by the pore water and consequent advection are important controls on the T_{peak} reached next to the dikes that did not show an extended zone of elevated Rv-r.

The estimated T_{peak} next to some larger dikes (20-40 m thick) in the Gippsland Basin did not fit the conductive heat flow models used in this study and these dikes showed an extended zone of elevated Rv-r. Geochemical studies are interpreted to indicate that convective heat and fluid transfer are causing the extended zone of increased temperature. Thus, thick dikes tend to show cooling by convection effects and thin dikes tend to show advection or incipient convection effects. Away from the immediate dike contact, a VRG for hydrothermal metamorphism shows good agreement with the T_{peak} interpreted from fluid inclusion data from a thin and a thick dike. Close to the dike margin, Rv-r becomes inaccurate and the VRG cannot be used.

Heating duration studies using AFT annealing found that the host rock was at too high a temperature during intrusion and heating duration information was not recorded.

Rock-Eval, Rv-r, stable isotopes, gas chromatography (GC), and ^{13}C CP MAS nuclear magnetic resonance studies are used to characterize hydrocarbon generation from the host rocks during contact metamorphism by dikes in the western onshore portion of the Gippsland Basin. The evidence from the natural samples, supplemented by hydrous pyrolysis experiments, show that coaly SOM in the Strzelecki Group is capable of generating oil and gas. GC shows that the oils generated by hydrous pyrolysis are good matches to some natural oils trapped in the Upper Cretaceous to Tertiary Upper Latrobe Group that have a highly mature geochemical signature. These highly mature oils have been attributed to Lower Latrobe Group coal sources even though the observed Rv-r of these coals makes them poor candidates for this source rock to oil match.

STATEMENT

This thesis contains no material which has been accepted for the award of any other degree or diploma in any University and, to the best of the candidate's belief, the thesis contains no material previously published or written by another person, except where reference is made in the text of the thesis.

The author consents to the thesis being made available for photocopying and loan if applicable if accepted for the award of the degree.

Signed,

Charles E. Barker — Date: Dec. 19 1994

Acknowledgments

This work was made possible by the continuing support and encouragement of Dr. Yvonne Bone. Yvonne arranged for the scholarships that funded the Australian portion of the study. I owe a great debt to her for believing that this project could be done and making it so.

Yvonne is also Chair of the thesis committee. The thesis committee members were David McKirdy and John Foden, who also provided much scientific guidance for this study. Susan Marshallsea, Ian Duddy, and Paul Green of Geotrack International provided much information and guidance on the Gippsland portion of the study. Ian Duddy suggested the Gippsland area, and along with Paul Green contributed much on the geologic background of the onshore Gippsland Basin and on AFT annealing studies in general. Sue Marshallsea did the fission track annealing study of the onshore Gippsland Basin samples and on the Walsen Dike in Colorado. These scientists enthusiastically got involved in this study because of their acute interest in understanding all aspects of geothermometry and the AFT annealing method. I greatly appreciate their interest and support.

Mike Middleton was instrumental in setting up sampling of potential dike sites in the Perth and Canning Basins. Mike also provided guidance on how to approach this study and worked with me on measuring thermal conductivity using his transient method. Mike and his wife, Lynn graciously provided lodging and transportation while in Perth.

I thank Malcolm Wallace (University of Melbourne) for arranging trip to sample of the Ellendale 38 intrusion. Malcolm and Margaret Wallace are thanked for taking care of us in Melbourne with a place to stay, fun and discussions on the Buchan and Gippsland geology.

Bob Dalgarno, Victoria Geological Survey, who first introduced me to the geology of the Buchan Rift, was a key person in helping me sample cores at the Core Library. He also arranged for sampling permits for the Gippsland study. Bob Dalgarno was truly interested in this study and was a important element in the success of this thesis.

I also thank A.H.M. VandenBerg of the Victoria Survey for his informative discussion on the geology of Buchan Rift and for reviewing an early version the Buchan chapter.

Dennis Arne, Dalhousie University, provided us with samples from the Buchan Rift from what proved to be a key locality. He also was a reviewer of the Buchan Chapter and made a strong contribution to improving the text.

The Department of Geology and Geophysics, University of Adelaide, especially Victor Gostin and Patrick James, are gratefully acknowledged for field and administrative support. The department also provided: thin sections made by Wayne Mussared, Christine Badcock, and Geoff Trevelyan; drafting by Sherry Proferes; and photography by Rick Barrett.

Graham Jones, Waite Solid State NMR Facility, The University of Adelaide, performed the ^{13}C NMR analyses. Dr. Jones also helped me understand the NMR method and interpretation.

The USGS Laboratories, Denver, Colorado provided the following analyses: Rock-Eval by T.A. Daws; C, O Isotopes by Augusta Warden and C.N. Threlkeld; the source rock extractions were completed by the author under supervision of P.G. Lillis and Mark Monk; some of the solid bitumen reflectance for the Buchan study were run by M. J. Pawlewicz; X-ray diffraction traces were run by T.M. Finn; M.D. Lewan supervised the hydrous pyrolysis experiments; drafting was performed by Tom Kostick. Computer support was provided by Ray Obuch and Jim Brewton.

Drs. J. H. Sass and C. F. Williams, USGS, Menlo Park, California performed the P-T bomb thermal conductivity measurements.

John Draper, Ray Smith, J.W. Beeston, Luke Sorby, Russell Darcy and Brad John of the Geological Survey of Queensland discussed with me the possibility of studying the dikes exposed in the Moreton Basin, Queensland. Unfortunately, the area had been too hot in the past.

T. James Reynolds, Fluid Inc., Denver, Colorado provided much discussion and advice on the fluid inclusions studied and how to approach reequilibrated inherited fluid inclusions. He also provided the use of a heating stage when ours decrepitated.

This research was supported by an Australian Overseas Postgraduate Research Scholarship and a University of Adelaide Graduate Scholarship.

The U.S. Geological Survey (USGS) granted study leave for a portion of this project. This study leave was made possible through the support of Don Gautier, Gary Hill, Ted Dyman, Tom Ahlbrandt, Bonnie Claus and Kathy Varnes.

I owe a great debt to all of these people, the laboratories, and especially the citizens of Australia and the United States who support their Universities and scholarship programs.

A special acknowledgment is due to those who reviewed chapters or appendices : Yvonne Bone, Bonnie L. Crysdale, Mike Lewan, Sue Marshallsea, Mike Middleton, Mark J. Pawlewicz and Fleur Tiver.

This study would not have been completed even on a geological time scale if Mark Pawlewicz, Mike Lewan, Tom Kostick and Jim Reynolds had not gone beyond the call of duty in the last moments.

Special recognition is due to Pamela Young, my wife, who was a constant companion during the field work. Pam also spent long hours at sample preparation, drafting and data entry, error-checking rewritten chapters and in general expedited the completion of the thesis.

DEDICATION

To all my friends who have demonstrated so many times late at night:

No poem was ever written by a drinker of water.

--Horace, Roman Poet

65 - 8 B.C.

ABBREVIATIONS AND ACRONYMS USED

General Physical Terms

Direction: N = north; S = south; E = east; W = west

K = permeability in air

K = thermal conductivity, measured water saturated at elevated P-T.

κ = thermal diffusivity

P = pressure

P_c = confining pressure

P_i = internal pressure

P_{eff} = effective pressure = P_c-P_i

T = temperature (always given in degrees Celsius also annotated as °C)

T_{peak} = peak temperature reached during the geologic history of the sample

T_{magma} = temperature of the igneous magma during intrusion

T_{host} = initial temperature of the host rock,

$T_{contact}$ = initial temperature of the host rock at its contact with the dike

t = time

Heating duration = elapsed time of a heating event. The heating duration is dependent on what limits are set to define what constitutes a heating event. For example, during burial diagenesis, it is often taken as the elapsed time within 15% of T_{peak}. A chemically significant heating duration for kinetic studies is difficult to define in geological systems.

X = distance from dike contact in meters. X maybe annotated with the direction from dike margin, if appropriate. X may also be given as the sample interval relative to the dike margin on the side of the dike suggested by the direction (i.e. 0.1 to 0.2 m west) . If a single number is given, X indicates the sample interval midpoint from the dike contact

(i.e. 0.15 m west).

Analytical Techniques, Units, and Terms

AFT = apatite fission track

CL = Cathodoluminescence microscopy

Carbon and oxygen isotopic analyses of carbonate minerals, CO_2 gas, and C in CH_4 gas.

$\delta\ ^{13}C$ or $\delta\ ^{18}O$ (in $^{o}/_{oo}$) = $[R_{sample}/(R_{standard}-1)] \times 1000$

Where R_{sample} is the ratio of heavy to light isotope and $R_{standard}$ is the respective ratio in an internationally accepted standard (in this case PDB).

$^{o}/_{oo}$ = parts per thousand (also referred to as 'per mil')

^{13}C CP MAS NMR = carbon 13 cross polarization magic angle spinning nuclear magnetic resonance technique

f_a = aromatic fraction

f_{all} = aliphatic fraction

FI = fluid inclusion(s).

A type A, B or C fluid inclusion refers to one trapped along a Type A, B or C fracture, respectively. See definition of fracture types below.

T_e = eutectic temperature, i.e. temperature that first liquid appears in a completely crystallized (frozen) fluid inclusion (Roedder, 1984). In this study, T_e refers to the first appearance of liquid as the frozen fluid inclusion is warmed up on the heating stage. Goldstein and Reynolds (1994) discuss optical changes in a fluid inclusions contents that suggest the onset of melting.

T_h = temperature of total fluid inclusion homogenization to a single phase. The phase into which homogenization occurs is usually also noted.

T_f = temperature of melting. In this study it refers to the melting of ice in aqueous fluids.

T_t = temperature of fluid inclusion trapping

Chip no. = a sequence number representing the order of measurement in the heating stage. The chip number indicates the order in which each small piece of rock cut or broken from the polished thin section was examined in the heating stage. The chip number is used to keep track of the heating history of each chip. When a new chip is inserted into the heating stage it is known that spurious T_h data cannot be caused by overheating susceptible fluid inclusions.

C.P. fading = loss of the distinction of liquid and vapor phases at the critical point. This loss is observed as a fading of the meniscus between the two phases.

wt.-% NaCl equivalent = the salinity, i.e. the concentration of dissolved solids in an aqueous fluid inclusion, expressed as if it were solely composed of a NaCl-H_2O solution. See Goldstein and Reynolds (1994) for discussion

SF = shape of the fluid inclusion vacuole. An empirical determination made by the microscopist based on shapes suggested by Bodnar et al. (1989).

FIA = fluid inclusion assemblage

ICP-AES = inductively coupled plasma atomic emission spectroscopy

LOI = Loss on ignition (sample fusion) for ICP-AES analysis

ppm = parts per million

Rock-Eval pyrolysis

Unit definitions for Rock Eval data in Appendix 5 are as follows:

HC = hydrocarbon

gC = grams carbon

mg = milligrams

rk = rock;

wt.-% = weight percent.

S_1 = yield of distillable hydrocarbons

S_2 = yield of pyrolysiable hydrocarbons

S_3 = yield of CO_2 during pyrolysis

TOC = total organic carbon

HI = hydrogen Index = $(S_2/TOC)x100$

OI = oxygen Index = $(S_3/TOC)x100$

PI = transformation ratio = $S_1/(S_1+S_2)$

T_{max} = pyrolysis program temperature for the inflection point of the S_2 peak

Rb = Solid bitumen reflectance

Rb-r = mean random reflectance of solid bitumen

Rb-m = mean maximum reflectance of solid bitumen

max = microscope stage rotation to maximum reflectance and this value measured

ran = no rotation, random reflectance measured

Rv = vitrinite reflectance

Rv-r = mean random reflectance of vitrinite

Rv-m = mean maximum reflectance of vitrinite

SOM = sedimentary organic matter-- includes dispersed organic matter and coal

VRG = vitrinite reflectance geothermometer

XRD = powder X-ray diffraction

Statistical Analysis

mean or ave = arithmetic average

s or σ = sample or population standard deviation, respectively

n = sample size

range = the difference between the lower and upper data edge

mode = most frequent measurement or class in distribution

UM or U Mode = uppermost mode in distribution

Best mode = the mode assessed to be representative of a skewed or polymodal distribution in weathered vitrinite samples. For example, in weathered vitrinite populations Rv can be reduced and an upper mode may be assessed to be representative of the unweathered reflectance. In bitumen reflectance studies, the best mode is taken as the upper data edge.

LDE = lower data edge

UDE = upper data edge

N/A = data not available or not applicable

N/R = data not reported

est = estimated

Coefficient of variation (V) = standard deviation/mean. In Rv-r analyses, a $V < 0.1$ indicates a reliable mean and a $V > 0.2$ suggests an unreliable mean in such small samples ($n<10$).

? = A query mark next to a data point suggests some uncertainty in the data usually because the sample is weathered, or contained too little or poor material for a well constrained measurement, or uncertainty in the position of the sample.

Quality

Quality in the data tables refers to sample quality. For Rv-r this is assessed by the method described in Appendix 1. For fluid inclusion data it is a subjective assessment (see Appendix 4).

B = assessed to be barren of measurable material or objects.

P = assessed to be poor for sample suite

F = assessed to be average for sample suite

G= assessed to be good for sample suite

Sample Lithology

ss = sandstone

mdst = mudstone

sltst = siltstone

carb = carbonaceous

coaly = indicates presence of coaly fragments

picked coal = grains of coal picked out of a mixed lithology or weathered coal sample

cc = calcite

Q-d = Quartz -detrital; a framework grain of quartz within a sandstone

Fracture Types

Type A. Fracture cross cuts several sedimentary features such as framework grains, cement, matrix and so forth. Type A fractures are clearly diagenetic.

Type B. Fractures which clearly involve grain edge and matrix breakage but do not noticeably crosscut other framework grains, and are likely post-depositional in

origin. The best examples are fractures lined with diagenetic minerals like those found in the matrix and are likely formed in this rock.

Type C. A fracture wholly contained within a detrital grain and is likely an inherited fracture.

Chapter 1.

Geothermometry and Geochronology of Contact Metamorphism Caused by Dikes

1.1 INTRODUCTION

Contact metamorphism by igneous dikes has long been used as a natural laboratory for studying thermal effects on rocks. More recently, contact metamorphism caused by dikes has been emphasized as a natural analogue of pyrolysis, a laboratory heating technique that simulates natural thermal maturation of sedimentary organic matter (SOM) (Cooles et al., 1986; Clayton and Bostick, 1986; Bishop and Abbott, 1993, 1995). This study further develops laboratory pyrolysis as the analogue of contact metamorphism caused by dikes by refining the knowledge of the physical conditions during metamorphism using geothermometry, geochemistry, geochronology, and geophysics.

A major limitation of previous studies of contact metamorphism caused by dikes is that the peak temperature (T_{peak}) reached in the host rock next to the dike could not be measured directly. This problem lead to the indirect calibration of geothermometers based on models of heat flow theory (Lovering, 1935; Jaeger, 1959), electron spin resonance (Peters et al., 1978), laboratory bomb experiments (Bostick, 1979), and clay minerals (Pytte and Reynolds, 1989), among many techniques. One aspect of this study is to measure the homogenization temperature (T_h) of fluid inclusions reequilibrated during contact metamorphism caused by dikes and assess this temperature as a direct recording geothermometer.

For contact metamorphism of sedimentary rocks, a widely used method of assessing temperature is vitrinite reflectance. Vitrinite reflectance is primarily set by heating to T_{peak} (Suggate, 1982; Barker, 1983; Price, 1983; Bone and Russell, 1988; Barker and Goldstein,

1990; among others). Credible vitrinite reflectance geothermometers (VRG) have been calibrated for burial heating and hydrothermal metamorphism (Barker and Pawlewicz, 1994; Appendix 11) using the T_h of reequilibrated fluid inclusions to estimate T_{peak}. Vitrinite reflectance has been calibrated to apparent T_{peak} and heating duration of contact metamorphism caused by dikes using bomb experiments and predictions from heat flow theory (Bostick, 1979; Peters et al., 1978; among others). While the application of heat flow theory is a theoretically robust technique, its application to rocks uses many simplifying assumptions that limit its accuracy. Bomb experiments are usually much shorter in duration compared to the length of time elapsed in contact metamorphism and if the bomb sample is run dry (that is, with rock only and no immersion in water) the experiment is a poor analogue of natural systems which usually consist of water saturated rock (Lewan, 1993a; Smith et al., 1994).

In the past there has been no way to get at an external confirmation of the predictions from a heat flow model or the results of bomb experiments by either direct temperature or heating duration data. Thus, it is poorly known whether these simplified models or bomb experiments realistically represent nature.

This study focuses on direct assessment of temperature and heating duration using fluid inclusions and apatite fission track (AFT) annealing studies to check the viability of a heat flow model. To make it more realistic, the heat flow model uses direct measurements of thermal conductivity at elevated temperatures and pressure rather than a standard or established value.

Study Objectives

1. Characterize regional burial and thermal history to assess the influence of contact metamorphism on thermal maturation of SOM, and the effect of the pre-existing T_{peak} on

the impact of contact metamorphism;

2. Measure Rock-Eval pyrolysis, gas chromatography, and ^{13}C NMR responses of vitrinite-rich SOM to contact metamorphism caused by dikes, to characterize this system as a natural version of laboratory pyrolysis and define the natural conditions of this pyrolysis;
3. Develop the use of post-depositional or reequilibrated inherited fluid inclusions as a peak temperature indicator in contact metamorphosed sedimentary rocks;
4. Use AFT annealing to estimate heating duration in contact metamorphosed sedimentary rocks;
5. Measure rock thermal and physical parameters on samples from the specific sites to develop a model of T_{peak} based on heat flow theory for contact metamorphism caused by dikes;
6. Test the typical assumptions in some previous dike studies--A) that dike contact aureoles are symmetrical on either side of the dike; B) that dikes have a limited effect on source rock thermal maturation and are ineffective in heating large portions of rock; and C) that heat flow models based on conductive cooling in a closed geologic system adequately describe contact metamorphism.
7. If the hydrothermal VRG proves inaccurate, develop a VRG for dike contact metamorphism based on direct estimates of T_{peak} from fluid inclusions and Rv-r.

The direct paleotemperature measurements made in this study emphasize those made on fluid inclusions in fractured and healed quartz taken from contact metamorphosed sandstones next to dikes. Dikes offer several advantages in such a study: 1) they are typically well exposed because they crosscut generally subhorizontal strata; and 2) they are thought to typically show symmetry in their contact metamorphism aureole such that only one side of the dike need be studied. Sills are excluded from this study because they seem to

retard contact metamorphic reactions by trapping reaction products below them (Peters et al., 1978).

1.2 TEMPERATURE ESTIMATED FROM FLUID INCLUSIONS

Fluid inclusions are formed by crystal defects that trap liquids and(or) gases during crystal growth (growth bound or primary inclusions) or in fractures (fracture bound or secondary inclusions) (see review by Hollister, 1981). Fluid inclusions trap liquids, solids and gases as separate phases or as dissolved gases and solids in a single homogeneous phase. To be used for geothermometry, a fluid inclusion must have trapped a homogeneous phase rather than a combination of fluid, solid, and(or) gas as separate phases. To maintain a record of the initial trapping conditions, the mass and volume of the inclusion contents (fluid density) must remain constant. In fluid inclusions that have trapped a homogeneous phase, dissolved solids, gases and(or) vapor can precipitate as separate phases upon sufficient cooling.

Point A In Fig. 1-1 represents a fluid inclusion trapped at 200 bars hydrostatic pressure and at 150°C. Fig. 1-1 also shows lines of equal density (isochores) for the pure water system in P-T space. Given the initial constant volume assumption in fluid inclusion geothermometry, pressure within the inclusion is dependent on temperature. In nature, temperature is the externally controlled variable which determines the internal pressure (P_i) within the fluid inclusion, because the crystal containing the fluid inclusion is strong enough to resist considerable pressure differences without significant volume change. The confining pressure (P_c) acting on the crystal containing the fluid inclusion is generally controlled by depth and hydrostatic to lithostatic load conditions. Within the fluid inclusion, however, if constant mass and volume constraints are followed, the pressure inside the fluid inclusion generally follows a constant density (isochoric) path (Sterner, 1992a). As the crystal cools,

the density of the embedded fluid inclusion initially follows a path along the isochore represented by the dashed line (at about 0.93 g/cm^3) from point A to point B, the boundary where two phases, vapor and liquid, are stable. With further cooling to point C, P_i within the fluid inclusion follows a curving path constrained by the two-phase boundary. During continued cooling to near surface conditions, the phase proportions change because of decreasing density in the vapor phase and increasing density of the liquid phase (Goldstein and Reynolds, 1994). These changes in density are most obvious to the observer as an increasing volume of the vapor phase during cooling.

In the laboratory, heating in a microscope stage reverses the changes in phase proportions that occurred during cooling. The homogenization temperature (T_h) is the temperature measured at atmospheric pressure where the fluid, vapor, and solid phases that have precipitated in an inclusion homogenize to a single phase. T_h is used along with composition data derived by freezing point or other chemical analyses of the inclusion contents to define the constant fluid density path (isochore) along which this fluid inclusion was trapped. T_h represents the minimum trapping P-T conditions for an inclusion of that density. Thus, if the inclusion was originally trapped a single phase, this trapping could only occur along the isochore, and T_h represents the lowest trapping T and P along that isochore. To explain this concept, the pure water system is considered (Fig. 1-1). A pure water fluid inclusion in the laboratory would contain two phases, vapor and liquid. With heating, the two phase fluid inclusion is constrained to follow the two phase boundary. At the intersection of the isochore along which the fluid inclusion was trapped and the two phase boundary, the fluid inclusion homogenizes (the vapor phase is lost).

Fig. 1-1. Pure water system isochores. Figure based on Fisher (1976), and modified from Crawford (1981). View of fluid inclusion refers to the image projected to the microscopist during heating or cooling on a heating stage. CP is the critical point. See text for discussion of point A.

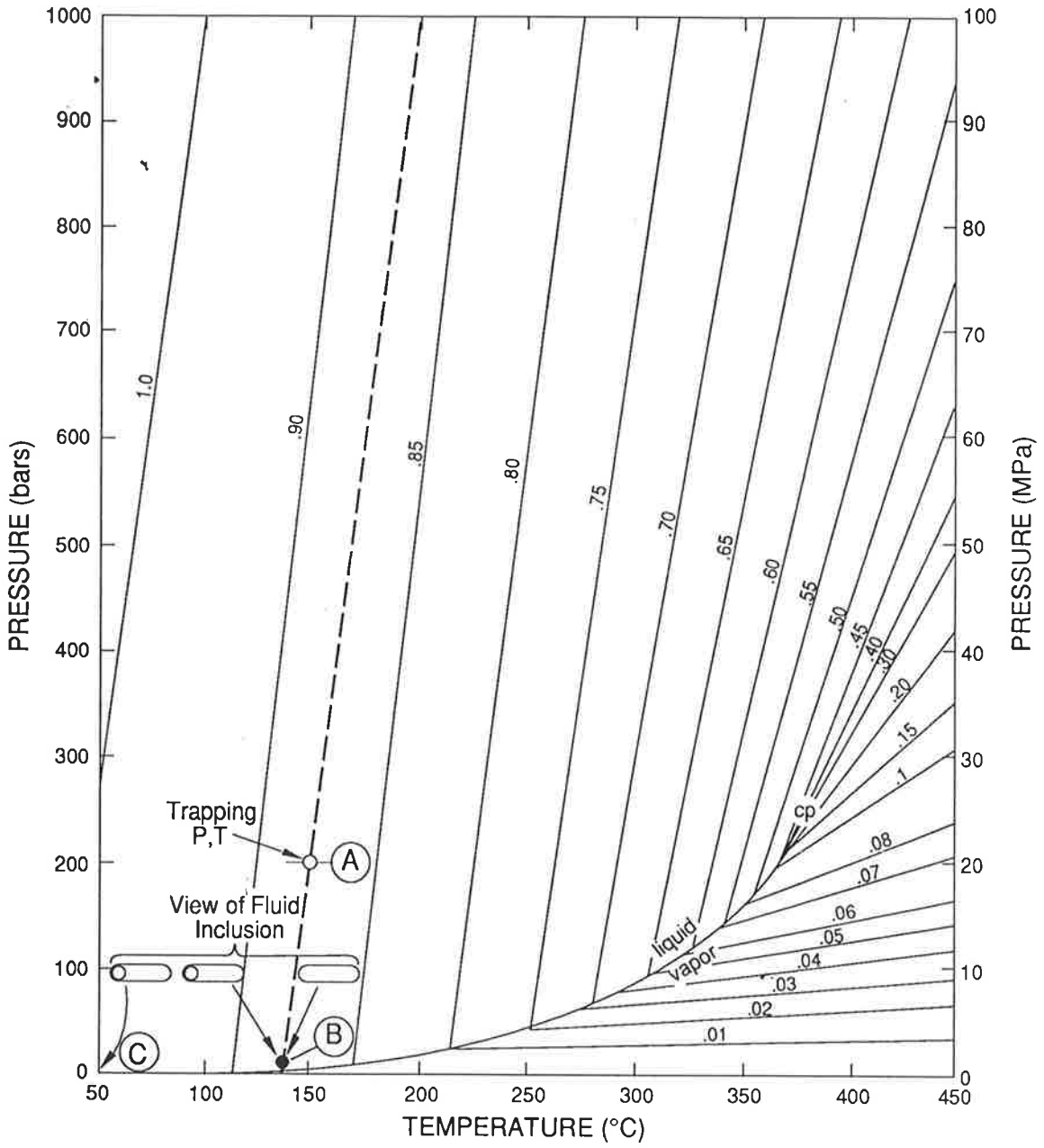
PRESSURE (bars)
PRESSURE (MPa)
TEMPERATURE (°C)
1000
900
800
700
600
500
400
300
200
100
0
100
90
80
70
60
50
40
30
20
10
0
50
100
150
200
250
300
350
400
450
1.0
.90
.85
.80
.75
.70
.65
.60
.55
.50
.45
.40
.30
.20
.15
.1
.08
.07
.06
.05
.04
.03
.02
.01
cp
liquid
vapor
Trapping
P,T
A
View of Fluid
Inclusion
B
C

This type of homogenization occurs along the vapor-liquid phase boundary up to the critical point (CP). At the critical point, the fluid inclusion would homogenize by the meniscus fading to a supercritical fluid. Fluid inclusions trapped at fluid densities less than the critical density homogenize to a vapor phase.

In nature, most inclusions would not form exactly at the pressure of trapping indicated by T_h. To determine the trapping conditions an external estimate of the trapping pressure is required. The temperature of the intersection of the isochore and the trapping pressure is the trapping temperature. The difference between trapping temperature and T_h is termed the pressure correction.

The simplest interpretation of T_h data is to just use it as a minimum estimate of the trapping temperature and not apply a pressure correction. Determining the trapping pressure is a not a trivial determination (Roedder and Bodnar, 1980; Burruss, 1989) and the presence of dissolved gases associated with the petroleum source rocks used in this study may make a pressure correction inaccurate (Hanor, 1980). A common method to correct T_h to T_t requires knowledge of the composition of the phases present in an inclusion, the isochores of relevant chemical system, and the depth of inclusion formation. Further, it must be known whether the fluid inclusion was trapped under a hydrostatic gradient (9.8 MPa/km for fresh water to 12.5 MPa/km for strong brines; North, 1985) or a lithostatic gradient which averages 24.4 MPa/km; Hunt, 1979).

Determination of the pressure gradient is a complex problem itself. For example, the determination of hydrostatic conditions existing during trapping asserts that the fluid forming the inclusion is connected by a permeable pathway to the earth surface. This fact may be difficult to establish. After a depth of about 1.2 km fluid overpressures exceeding hydrostatic pressure can occur (Hunt, 1979). However, present day conditions in the Gippsland Basin are hydrostatic in the Upper Cretaceous and Tertiary strata to at least 3.5 km depth

(Miyazaki, 1989). Overpressuring and underpressuring are considered transient effects and thus, the pressure regime at present may not reflect conditions during fluid inclusion trapping in the past. The upper limit of P-T conditions for diagenesis, at the onset of metamorphism, generally occurs at depths over 3 km and typically occurs under lithostatic pressure conditions (Winkler, 1976). Considering only the problem of fluid paleopressure determination suggests the difficulty of pressure correction of fluid inclusion data.

The fluid inclusions used in this study are from oil and gas source rocks and typically contain some natural gases. Using a crushing stage (Roedder, 1984), the presence of hydrocarbon gases in vein calcite were detected by opening fluid inclusions in kerosene. The presence of natural gases can produce a large error in the pressure correction of T_h data to trapping temperature (Hanor, 1980). The T_h of natural-gas-bearing aqueous inclusions approaches the minimum temperature of entrapment and in such cases, T_h may be the most reliable estimate attainable given the uncertainties outlined above (Goldstein and Reynolds, 1994). Consequently, no pressure correction was applied to data in this study and T_h is used as a minimum trapping temperature estimate.

1.3 REEQUILIBRATION OF FLUID INCLUSIONS IN QUARTZ

Reequilibration is any process that causes the mass or volume of a fluid inclusion to change. The driving force of reequilibration is the elastic strain energy caused when P_i is not equal to P_c. The magnitude of the energy driving reequilibration is described by the effective pressure which is the difference between the confining and internal pressure: $P_{eff} = P_c - P_i$ (Vityk et al., 1994). Theoretical, laboratory and geological studies have established that aqueous fluid inclusions in quartz can reequilibrate if P_{eff} is not zero (Leroy, 1979; Pecher, 1981; Gratier and Jenatton, 1984; Bodnar et al., 1989; Boullier et al., 1989; Sterner and Bodnar, 1989; Lacazette, 1990). The following discussion is only concerned with the case

when $P_i > P_c$, and P_{eff} is negative, as this is the relevant case for the overpressuring of fluid inclusions caused by heating related to simple contact metamorphism. When $P_i > P_c$ reequilibration can occur by decrepitation, stretching (elastic deformation) of the vacuole and(or) possibly diffusion of the inclusion contents into the crystal. Decrepitation is caused by a fluid inclusion rupturing by a fracture cutting into the host crystal. In extreme cases, the crystal fractures through to the outside and inclusion contents are mixed with the enclosing pore fluid. In milder cases, the fracture partially extends into the host crystal effectively increasing the vacuole volume and reducing P_i to the point where the fracture does not propagate to the crystal exterior. In this case, the composition of fluid inclusion contents are preserved but T_h would change.

Stretching is caused by a permanent plastic deformation of the vacuole in the host crystal. Stretching increases the volume of the fluid inclusion and consequently the fluid density decreases because mass remains constant. Reequilibration causes T_h to increase and approach the T_{peak} extant in the rock (Gratier and Jenatton, 1984; Barker and Goldstein, 1990). The increase in T_h is a result of reequilibration processes that decrease fluid density and P_i within the vacuole.

Reequilibrated fluid inclusions do not record the conditions initially set during crystal growth and follow different isochores than originally set during trapping. If the fluid inclusion decrepitates, then both T_h and salinity of the fluid contents are reset to the ambient pore fluid conditions (Gratier and Jenatton, 1984). If stretching, solution and precipitation, or diffusion are the agents of reequilibration then, because these are kinetic processes, time may also be a factor in the degree of reequilibration.

The assessment of P_{eff} acting on a fluid inclusion can be made using thermobaric gradients constructed for pressures from hydrostatic to lithostatic and the isochores representative of the fluid inclusion contents (Figs 1-2 and 1-3). If the thermobaric path

followed by the fluid inclusion host crystal during burial has a higher slope (dP/dT) than the slope of the isochore for the fluid inclusion contents, prograde reequilibration (to a lower fluid density) is not possible by P_i driven effects alone. Sedimentary basins that have geothermal gradients of less than about 8°C/km for hydrostatic conditions and 10°C/km for lithostatic conditions will not induce prograde reequilibration. If thermobaric gradients are above 10°C/km, fluid inclusions can theoretically reequilibrate in either hydrostatic or lithostatic conditions. The vast majority of sedimentary basins have geothermal gradients above 20°C/km and it is possible for P_i to exceed P_c but resulting P_{eff} may be too low to cause reequilibration. Each of these cases can be evaluated using Figs 1-2 and 1-3 for the pure water system. Of course, the pure water system is just one end member of possible natural aqueous fluids. Increasing salt concentration of the fluid inclusion contents causes an increasingly lower slope of the isochore from that shown for pure water except near the critical temperature (Bodnar and Vityk, 1994). Saline fluid inclusions generally have a reduced tendency to reequilibrate compared to pure water because P_i is lower for a given P_c. For example, a pure water inclusion trapped at 150°C and then overheated to 200°C will have a P_i about 20 MPa higher than a 15 wt-% NaCl equivalent fluid inclusion (Crawford, 1981). Thus, saline fluid inclusions generally require more overheating to initiate reequilibration because at the same conditions of overheating the P_i is lower. The pure water system generally indicates the optimal conditions for reequilibrating fluid inclusions that contain no dissolved gas. Dissolved gas in a fluid inclusion enhances the tendency to reequilibrate by increasing P_i at a given temperature (Goldstein and Reynolds, 1994).

Fig. 1-2. Pure water system isochores with thermobaric gradients for fresh-water hydrostatic (9.8 MPa/km) pressure and a surface temperature of 10°C. Isochores based on Fisher (1976) and Crawford (1981). Crosses show P_i for overheating of the fluid inclusion at the indicated temperature (in °C). CP is the critical point. See text for discussion of the fluid inclusion represented by point A.

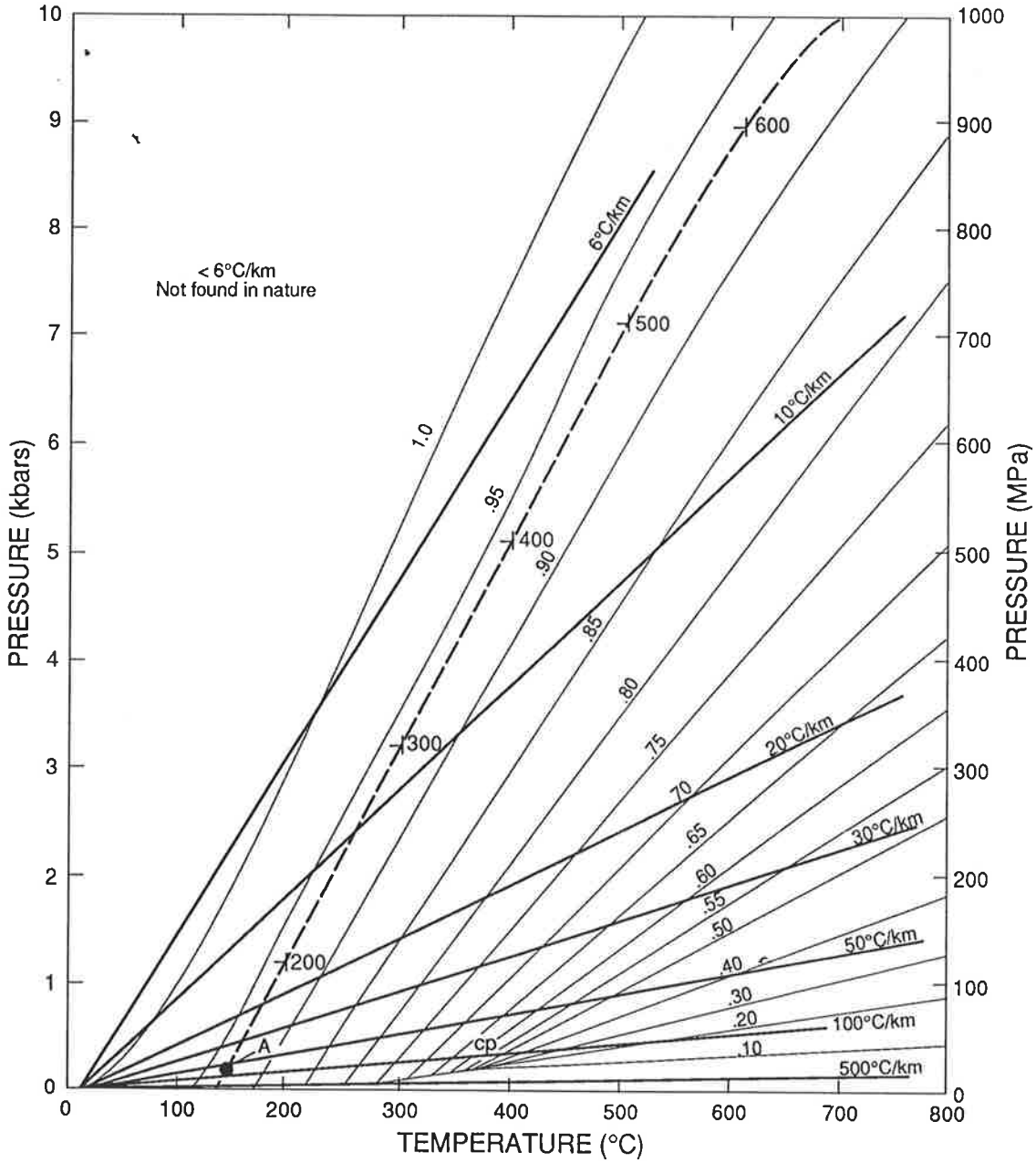
PRESSURE (kbars)
PRESSURE (MPa)
TEMPERATURE (°C)
< 6°C/km
Not found in nature
6°C/km
10°C/km
20°C/km
30°C/km
50°C/km
100°C/km
500°C/km
1.0
.95
.90
.85
.80
.75
.70
.65
.60
.55
.50
.40
.30
.20
.10
200
300
400
500
600
A
cp

Fig. 1-3. Pure water system isochores with thermobaric gradients for lithostatic (24.4 MPa/km) pressure based on an average rock density and a surface temperature of 10°C. Isochores based on Fisher (1976) and Crawford (1981). Crosses show P_l for overheating of the fluid inclusion at the indicated temperature (in °C). CP is the critical point. See text for discussion of the fluid inclusion represented by point A.

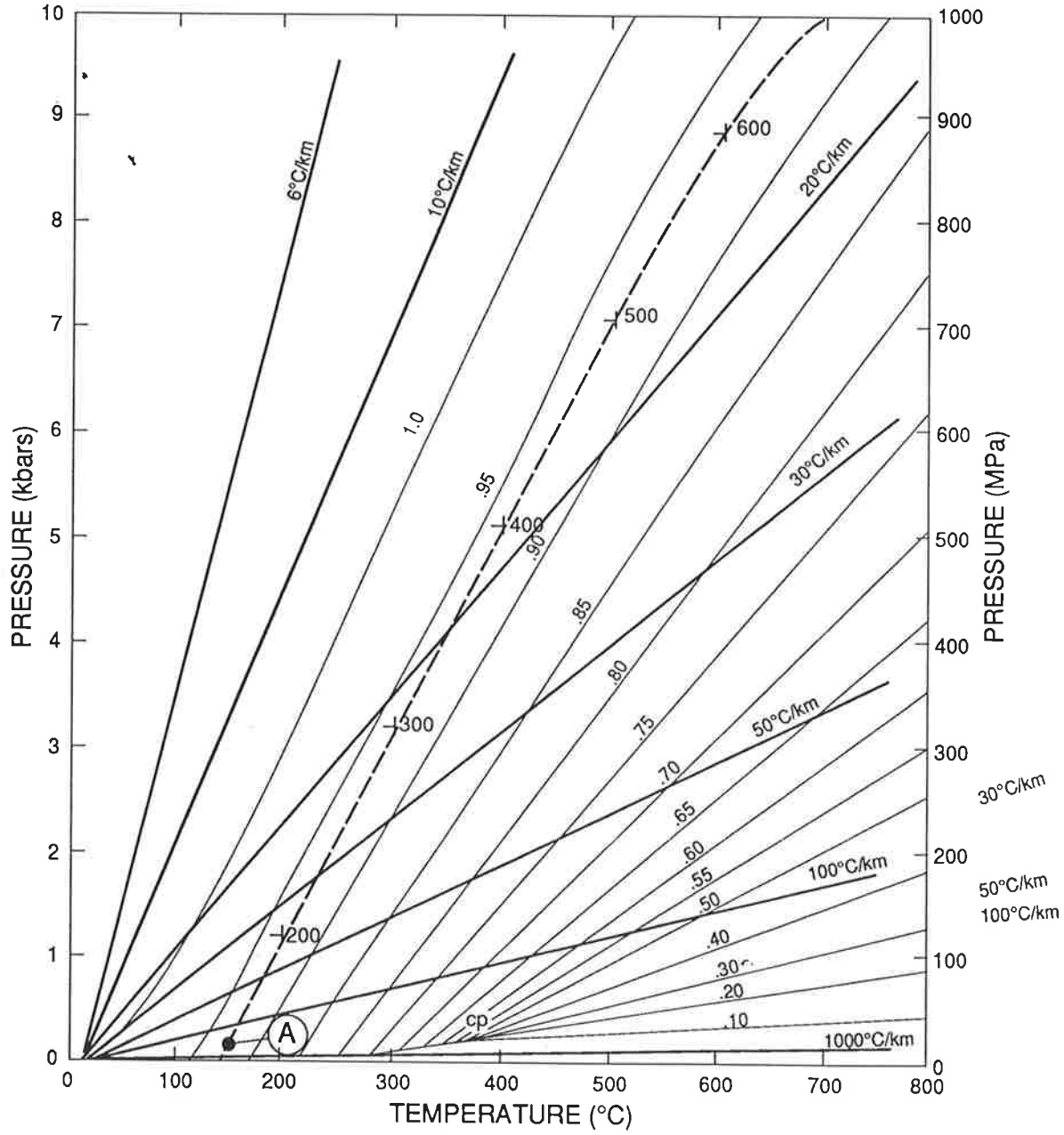
PRESSURE (kbars)
PRESSURE (MPa)
TEMPERATURE (°C)
0
100
200
300
400
500
600
700
800
1
2
3
4
5
6
7
8
9
10
900
1000
6°C/km
10°C/km
20°C/km
30°C/km
50°C/km
100°C/km
1000°C/km
1.0
.95
.90
.85
.80
.75
.70
.65
.60
.55
.50
.40
.30
.20
.10
200
300
400
500
600
cp
A

The P_{eff} changes possible during heating are illustrated by a pure water fluid inclusion that was trapped at 20 MPa hydrostatic pressure and at 150°C (represented by point A in Figs 1-2 and 1-3). P_i is described by the 0.93 g/cm^3 isochore at temperatures above T_h. In this example, the variation of P_c during heating is described by the thermobaric gradient line labeled 50°C/km within the natural pressure envelope between hydrostatic (Fig. 1-2) and lithostatic (Fig. 1-3) conditions. Heating fluid inclusion A to 200°C by burial in a 50°C/km gradient would produce a P_i of about 120 MPa and a P_c of 30 MPa for hydrostatic and a P_c of 90 MPa for lithostatic conditions. The magnitude of P_{eff} in this case ranges from -90 MPa for hydrostatic conditions to -30 MPa for lithostatic conditions. If the host crystal containing fluid inclusion A were heated to 600°C by an intruding dike, in contrast to the burial heating case, P_c remains essentially constant because dike intrusion is essentially an instantaneous event that occurs at constant burial depth and pressure. To examine the results of heating on fluid inclusions trapped in quartz near the dike margin, consider again fluid inclusion A at its initial trapping pressure of 20 MPa hydrostatic pressure. Fluid inclusion A upon being heated to 600°C would experience a P_{eff} of about -900 MPa under hydrostatic conditions and - 800 MPa under lithostatic conditions.

In quartz, reequilibration has been shown to be largely controlled by P_{eff} (Vityk et al., 1994), inclusion volume and shape (Bodnar et al., 1989; Lacazette, 1990), and strength of the host crystal (Lacazette, 1990). Reequilibration in quartz requires a higher P_{eff} compared to calcite because the resistance of quartz to tensile fracturing is greater (Lacazette, 1990). Fig. 1-4 estimates the decrepitation pressure (essentially P_{eff} in the example) required to fracture and open a fluid inclusion versus the diameter of a fluid inclusion for selected shapes, and a calcite or quartz host mineral containing the fluid inclusion. Because decrepitation, as used by Lacazette (1990), is the opening of an inclusion vacuole to the external fluid by fracturing, the pressures estimated using this figure represent the upper limit

of possible effective pressure for reequilibration. Stretching can occur at P_{eff} less than the decrepitation pressure. Lacazette's (1990) analysis (Fig. 1-4) suggests that a fluid inclusion A trapped in quartz would not decrepitate after reaching a P_{eff} of -30 to -90 MPa during heating to 200°C during diagenesis or contact metamorphism. This would be the case regardless of shape if the fluid inclusion size of 2-10 μm for fluid inclusions formed during diagenesis and about 2 to 20 μm for inherited fluid inclusions. Conversely, at 600°C and a P_{eff} of -800 to -900 MPa reached in shallowly buried rocks near the dike contact, all fluid inclusions over 2 μm diameter in quartz would reequilibrate by decrepitation. Because 2 μm is about the limit of visibility for observing fluid inclusions, essentially all usable fluid inclusions in the sample will have reequilibrated near the dike margin (excluding fluid inclusions formed after the intrusive event). At the levels of P_{eff} reached near the dike most fluid inclusions probably reequilibrate by decrepitation. The healing of these narrow fractures in quartz is rapid (Gratier and Jenatton, 1984; Sterner and Bodnar, 1984; Brenan, 1991) and these decrepitated fluid inclusions should heal and trap fluids under conditions near T_{peak} and P_c.

Experiments at P_c = atmospheric (0.1 MPa) generally suggest that less than 10 percent of fluid inclusions in quartz will be modified by reequilibration (mostly by decrepitation) if P_{eff} remains lower than -200 MPa (Robinson et al., 1992 and references cited herein). In nature, similar results to the experiments and models have been observed. Swanenburg (1980) found 1 μm fluid inclusions that had attained a P_{eff} of -600 MPa during metamorphism without reequilibration. Burruss and Hollister (1979) found in a study of a hydrothermal system in the Valles Caldera, New Mexico that P_{eff} of -100 MPa is necessary to decrepitate nearly pure water fluid inclusions in quartz.

Fig. 1-4. Pressure required to decrepitate a fluid inclusion of given diameter and shape in a quartz or calcite host. This figure was provided by Lacazette as a supplement to Lacazette (1990). Note that decrepitation pressure refers to the P_{eff} required to rupture the inclusion at a P_c of 0.1 MPa (1 atm) in the laboratory. Because $P_{eff} = P_c - P_i$, in this case P_{eff} is essentially equal to $-P_i$ at decrepitation.

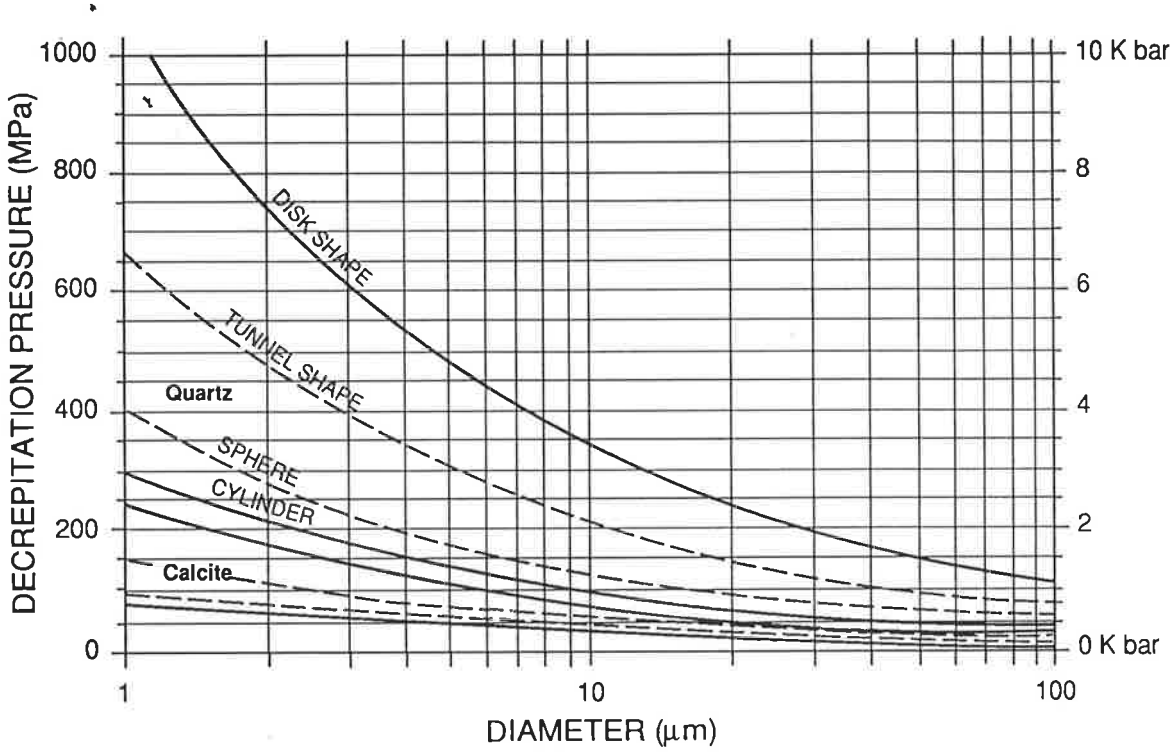
DECREPITATION PRESSURE (MPa)
1000
800
600
400
200
0
10 K bar
8
6
4
2
0 K bar
DISK SHAPE
TUNNEL SHAPE
Quartz
SPHERE
CYLINDER
Calcite
1
10
100
DIAMETER (μm)

Robinson et al. (1992), in their review of evidence of reequilibration in diagenetic quartz conclude that typical size (<10 μm) fluid inclusions trapped under diagenetic T and P_c conditions, require a P_{eff} of about -200 MPa generated by heating to about 200°C to initiate decrepitation during burial. Of course, fluid inclusion reequilibration by stretching may occur at lower P_{eff} and at a lower degree of overheating than the 200°C that they calculate for decrepitation during diagenesis. As pointed out by Robinson et al. (1992) 200°C overheating of a diagenetic fluid inclusion is difficult to attain as this temperature level is generally considered metamorphism. This analysis suggests it is difficult to reequilibrate fluid inclusions by simple burial diagenesis.

As discussed below, while it is easy to demonstrate reequilibration during experiments because the T_h increases at some point during overheating, such an observation is not possible in natural systems as we can only observe the fluid inclusion after reequilibration. Direct evidence of reequilibration from imprints left in the rock are rare. Thus, studies of fluid inclusion reequilibration are usually restricted to inferring that reequilibration has occurred.

The discussion so far has assumed that fractures opening a fluid inclusion only occur by decrepitation (pure tensile fracturing). Kerrich (1976) shows that fluid inclusions in deformed quartz crystals show higher T_h compared to those in adjacent undeformed quartz (Fig. 1-5a). The increased T_h (suggesting reduced fluid density) is thought to be due to fluid leakage, perhaps into the crystal structure, occurring during compressive folding and tectonic recrystallization of the quartz. This type of reequilibration related to shear or tear fracturing is not classical decrepitation by tensile fracturing. Increased T_h caused by tensile fracturing reequilibration is shown in Fig. 1-5b. Reequilibration due to shear or tear fracturing of the quartz crystal is indistinguishable from tensile decrepitation in its effect on the scattering of the T_h measurements and the resetting of some fluid inclusions to T_{peak}. Perhaps these

processes may be distinguished by petrographic evidence of recrystallization or strain reduction such as reduced undulosity in quartz. Kerrich (1976) concludes that "this study has demonstrated that even a small degree of intracrystalline strain may cause leakage of fluid inclusions resulting in anomalously high homogenization temperatures." The T_h distribution found to be a result of fracturing of either type (Fig. 1-5a and b) is typical of a reequilibrated population found by this study. The processes that Kerrich (1976) describes appear to have occurred at about 210°C and suggest that lower temperature reequilibration of fluid inclusions in quartz may be enhanced by other mechanisms than pure tensile fracturing. To accommodate the insertion of the dike, the host rock must experience mechancial stress in proportion to the thickness of the dike. The studies of Kerrich (1976) suggest this mechanical stress may be an effective mechanism to promote reequilibration at lower P_{eff} than required for decrepitation.

Contact metamorphism caused by dikes also causes a thermal shock by introducing a horizontal temperature gradient on the order of 100 to 1000°C/m. This thermal shock can cause reequilibration of fluid inclusions by fracturing because of differential thermal expansion of the framework grains due to the high temperatures reached next to dikes (Somerton, 1992) and(or) rapid changes in thermal gradients (Simmons and Richter, 1976). Somerton (1992) describes a series of dry heating experiments using various sandstone types to show a six-fold increase in framework grain fracturing during heating to 600°C.

Fig. 1-5. A) T_h measured in undeformed versus deformed quartz within a single crystal. The increased T_h is attributed to leakage of fluid from inclusions because of intracrystalline strain. Fig 1-5A from Kerrich (1976). B) The T_h histogram resulting from laboratory overheating of fluid inclusions with an original T_h of 135°C. Heating was at 180°C for 80 days at P_c = 0.1 MPa (atmospheric pressure). The increase in T_h is attributed to reequilibration by decrepitation of fluid inclusions in natural quartz. Note added in proof: In Fig. 1-5b, the number of measured fluid inclusions increases from 9 to 12 before and after heating respectively. This means that the figure is confusing in that additional fluid inclusions have been measured after heating and they may have had a higher T_h to begin with. Fig. 1-5B from Gratier and Jenatton (1984).

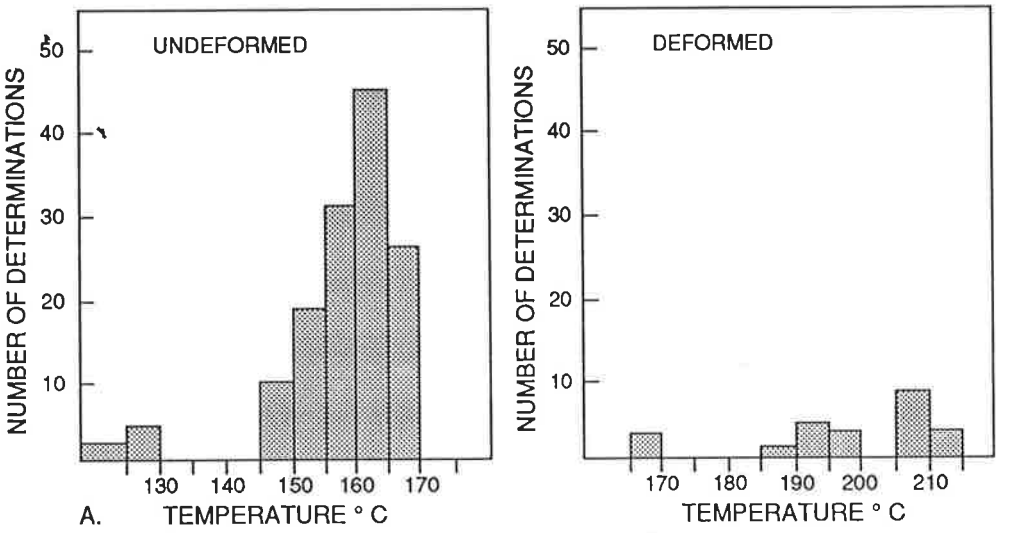
UNDEFORMED
DEFORMED
NUMBER OF DETERMINATIONS
50
40
30
20
10
130
140
150
160
170
180
190
200
210
A.
TEMPERATURE ° C

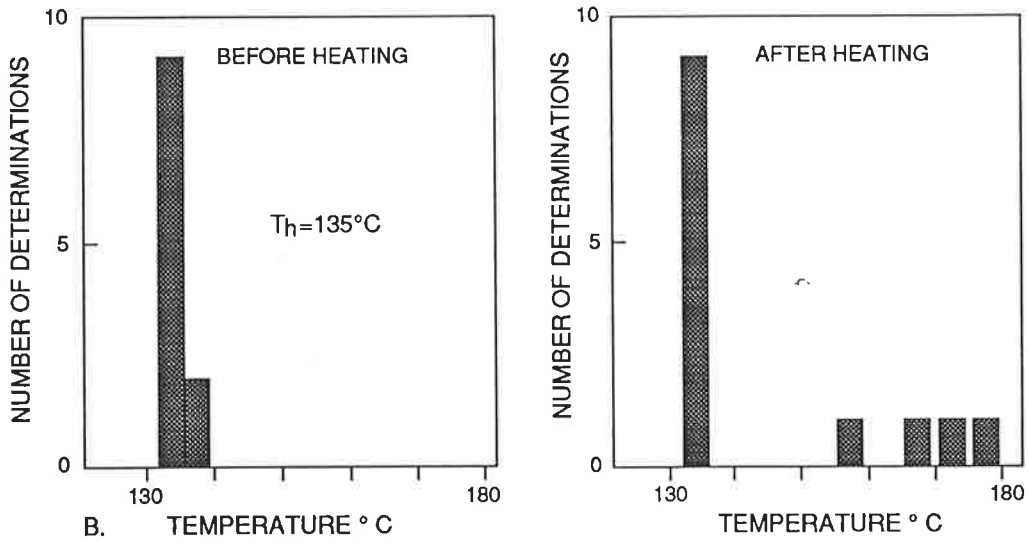
BEFORE HEATING
AFTER HEATING
T_h=135°C
NUMBER OF DETERMINATIONS
10
5
0
130
180
B.
TEMPERATURE ° C

These purely thermal expansion fractures, when they intersect a fluid inclusion, would cause the fluid inclusion contents to reequilibrate. Healing of fractured quartz grains appears to occur rapidly and it would be expected that these fluid inclusions would record the heating event and approach T_{peak}. Healing of the thermally induced fractures cutting the grains would also occur, forming post-depositional fracture-bound fluid inclusion planes that would also record the heating event.

Time Effects in Reequilibration

The question arises that if quartz can reequilibrate during contact metamorphism caused by dikes, why isn't quartz widely observed to reequilibrate during heating stage experiments? The answer seems to lie in the fact that reequilibration can require some time for significant changes in T_h to occur. Gratier and Jenatton (1984) suggest the rate of reequilibration process is a function of: A) temperature and P_i; B) nature and structure of mineral, and C) inclusion geometry. As shown by Lacazette (1990) inclusion geometry includes shape and size of the inclusion. Quartz annealing experiments by Boullier et al. (1989) confirm that changes of fluid inclusion shape are solution-deposition phenomena and that in the absence of decrepitation, plastic deformation is largely responsible for density changes, but diffusion processes cannot be ruled out. Solution/precipitation reactions and diffusion are time dependent and may explain why reequilibration in quartz is a geological process. Note that long-term heating experiments on reequilibration in quartz (Bodnar et al.,1989) indicate that P_{eff} required for the onset of reequilibration showed no change during heating experiments that lasted two years. This study infers that there is a P_{eff} threshold for reequilibration to occur and time effects are only important after reequilibration is initiated. However, as described above, P_{eff} is not a controlling factor in fractures caused by mechanisms other than decrepitation.

Conclusions on Reequilibration during Contact Metamorphism

An important conclusion from Lacazette's work and other studies is that almost all sizes and shapes of fluid inclusions in quartz host crystals could be reequilibrated during heating to the P_{eff} conditions near the contact of a dike intruding shallowly buried rocks. At the edge of the contact metamorphic aureole reequilibration is unlikely as P_{eff} is much lower.

Fig. 1-4 predicts that small diameter fluid inclusions are more difficult to reequilibrate, regardless of shape. So, in general, small inclusions require more overheating and larger inclusions less overheating to develop P_i sufficient for reequilibration. Because natural populations of fluid inclusions occur over a considerable size range but, within a healed fracture or growth zone, originally formed over a narrow temperature range, reequilibrated fluid inclusion populations will show a wide range of T_h and show polymodal T_h histograms.

1.4 IDENTIFICATION OF FLUID INCLUSION ORIGIN

The existence of reequilibrated fluid inclusions requires modification of the concept of fluid inclusion origin. Primary fluid inclusions are those determined by their textural relationships to be trapped during crystal growth and secondary fluid inclusions are those trapped after crystal growth. The distinction of primary versus secondary fluid inclusions (Roedder, 1984) in reequilibrated populations may have significance only in petrographic terms. During reequilibration, a fluid inclusion that is texturally "primary" may have altered its fluid density by reequilibration and not recorded the conditions extant during crystal growth implied by the term "primary". Subtle decrepitation, or stretching or diffusion are not easily detectable using optical microscopy, so reequilibrated fluid inclusions cannot be identified by this method. Similarly reequilibrated secondaries would not record the conditions extant when the fracture healed. In this study, the descriptive terms "growth bound" and "fracture bound" are used instead of the respective interpretative terms "primary" and "secondary".

Classification of Fracture Bound Fluid Inclusions

In sedimentary rocks, the fluid inclusions observed are present because of either trapping in the source terrain or trapping after deposition. Post-depositional features that trap growth bound fluid inclusions are cements and authigenic minerals such as dolomite. This type of fluid inclusion is rare in the host rocks studied and is not discussed further. Fluid inclusions trapped after deposition of the host rock are observed in healed fractures crossing framework grains, matrix and(or) cement. These post-depositional fractures are type A and B fractures (Appendix 1). Some fluid inclusions formed after sediment deposition are shown in Fig. 1-6. In this discussion, a fluid inclusion trapped along a type A or B fracture are termed a type A or type B fluid inclusions, respectively. Type C fluid inclusions are those inherited from the source terrain (Fig. 1-6). Sometimes it is necessary to distinguish fluid inclusion subgroups in type C, such as fracture bound, growth bound, isolated, or three dimensional cluster.

Type C fluid inclusions are trapped in the source terrains and are transported within the framework grains to the depositional site. Type C fluid inclusions differ from post-depositional fluid inclusions as they were definitely present during contact metamorphism and have experienced the thermal event. Identifiable growth-bound fluid inclusions are rarely observed in detrital grains, often because the grains are so small and the textural information used to distinguish a relationship to crystal growth is much larger. In small grains it is difficult to observe enough of the texture to interpret a growth bound fluid inclusion. When using inherited fluid inclusions, this study preferentially uses those trapped along type C fractures for reconstructing T_{peak} near the dike. Reequilibrated type C fractures at room temperature will have fluid inclusions with a wide range of V/L ratios. Of course, this reequilibration could have occurred in the source terrains. Thus, it is necessary to demonstrate in several framework grains that the estimated T_{peak} has a relationship to the dike contact. It is not

necessary to assume that the type C fracture is actually an inherited fracture because if it is wrongly identified, then it must be post-depositional and could validly record T_{peak} during a heating event regardless of its origin. Type C fractures are used as one line of fluid inclusion evidence to determine T_{peak}.

Determination of T_{peak} in Fluid Inclusions of Diverse Origin

As discussed above, reequilibrated fluid inclusions characteristically show a population of fluid inclusions that originally had a narrow T_h range, and during heating have changed density by stretching or by decrepitating and trapping a later, higher temperature fluid. This reequilibration process gives different T_h distributions for type A and type B fluid inclusions formed during post-depositional heating and for type C inherited fluid inclusions.

Post-depositional fluid inclusions were likely trapped at relatively low temperature and most of the fluid inclusions could potentially overheat and reequilibrate during contact metamorphism caused by dikes (Fig. 1-8). New fluid inclusions can also form during contact metamorphism by the fracturing and healing processes described above. In this case, the reequilibrated preexisting diagenetic fluid inclusions and newly formed fracture-bound fluid inclusions can be recognized as they will be in the higher range of T_h observed in the post-depositional fluid inclusion populations. Type A and B fractures that heal after T_{peak} and trap fluid inclusions will not interfere with the determination of T_{peak} because their T_h will be lower. The temperature that the sample approached is estimated by the uppermost mode of the homogenization temperature histogram for growth bound fluid inclusions (Barker and Goldstein, 1990) or the upper data edge (UDE) when considering type A and B fluid inclusions. The use of UDE for type A and B fluid inclusions assumes that any fluid inclusions along these healed fractures that have necked down and have disproportionately distributed their liquid and vapor contents are excluded as they can have spurious T_h .

Fig. 1-6. Fracture types A, B and C shown in transmitted white light. These photographs are all taken of samples of the Upper Jurassic to Lower Cretaceous Strzelecki Group sandstones within the Mesozoic Gippsland Basin that host Cretaceous dikes. The geology of these dikes and their location is discussed in chapters 3 and 4.

A) Thin section of sandstone, San Remo 1 dike, at a distance (X) from the dike margin = 0.07 m east. A type A fracture cross cutting several framework grains (white arrows). Black arrow points to the position of the fluid inclusion shown in photographs B and C in this 200 μm (widest dimension) quartz grain. The horizontal field of view is 1.2 mm.

B) Close up view of same fluid inclusion bearing grain seen in frame A . The horizontal field of view is 0.26 mm.

C) As in frame B but with the lens focused further into the quartz grain. Arrow points to 8 by 4 μm fluid inclusion which had a T_h of 250°C. The horizontal field of view is 0.26 mm.

D) Type C fractures crosscutting 140 μm quartz grain. Note the lack of any breakage at grain boundary which is characteristic of type C fractures.

E) Thin section of sandstone from Bena 3 dike, X = 3 m east. Type B fracture containing vapor-rich fluid inclusions. The inclusions are about 2 μm wide and up to 15 μm long. Note the breakage at the grain edge with mineral matter intruding into or precipitated along the fracture. This mineral matter is typical of type B fractures. The horizontal field of view is 0.26 mm.

F) San Remo 1 dike, X = 0.07 m east. A special case of type B fracture in which the inclusion itself is connected to the grain edge (white arrows). The lower fluid inclusion decrepitated during heating. The horizontal field of view is 0.26 mm.

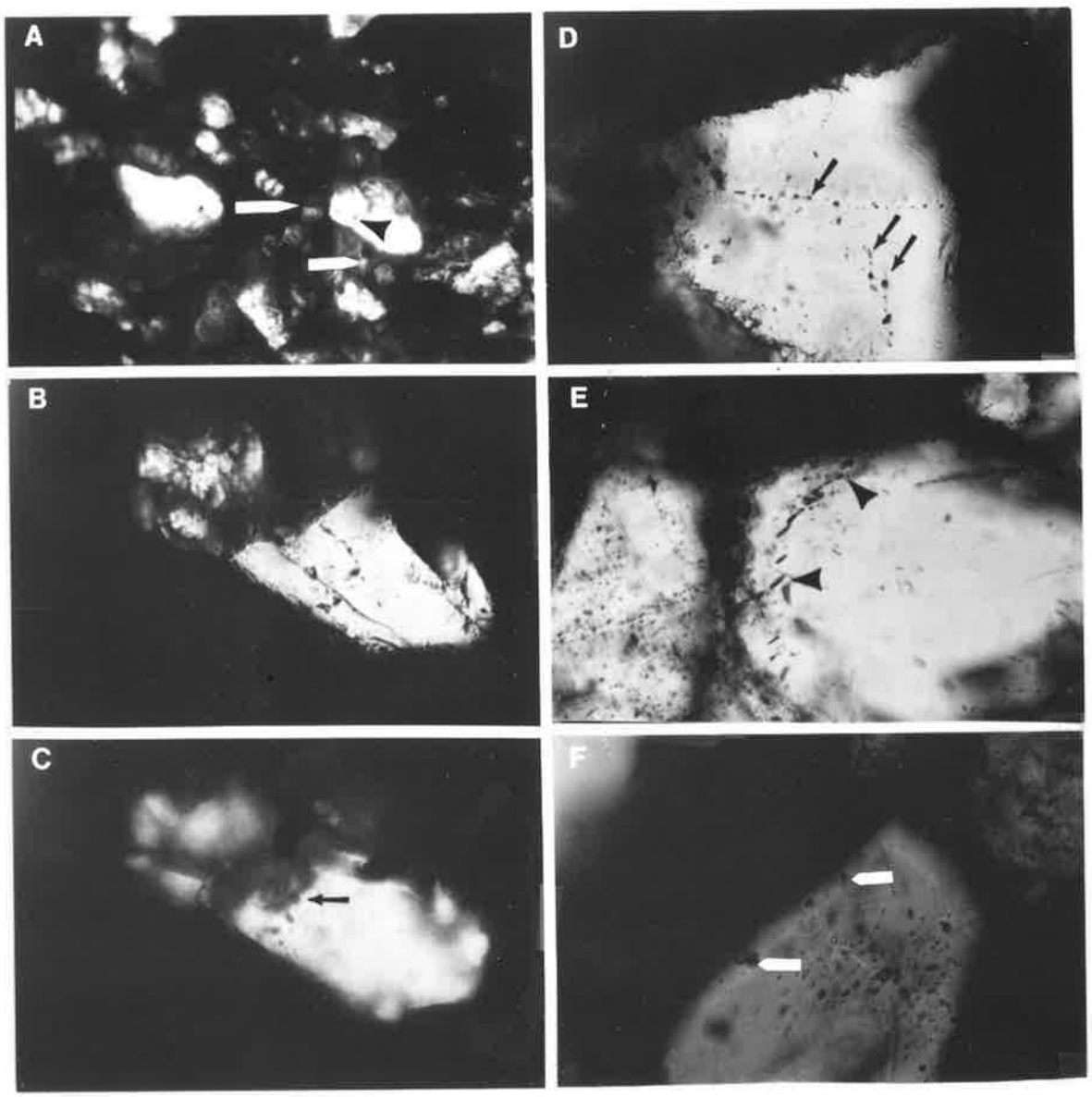
A
D
B
E
C
F

Fig. 1-7. Fracture types A and B shown in transmitted white light. These photographs are all taken of samples of the Strzelecki Group sandstones within the Gippsland Basin that host Cretaceous dikes. The geology of these dikes and their location is discussed in chapters 3 and 4.

A) Thin section of sandstone, Bena 3 dike, X = 13 m east. Arrow points to faintly visible type A fracture cross cutting two framework grains. The horizontal field of view is 1.2 mm.

B) Close up view of photograph A. The arrow points to faint type A fracture cross cutting two framework grains. The break seems caused by compaction. The horizontal field of view is 0.26 mm.

C) Thin section of sandstone, San Remo 1 dike, X = 0.11 m west. The horizontal field of view is 1.2 mm. The arrow points to a type A fracture filled with mineral matter.

D) Close up view of photograph C. The horizontal field of view is 0.26 mm.

E) Thin section of sandstone, Bena 3 dike, x = 3 m east. Mineral matter filled Type B fractures (one indicated by the arrow) crosscutting framework grains. The horizontal field of view is 1.2 mm.

F) Thin section of sandstone, Bena 3 dike, X = 13 m east. The arrow points to a faint type A fracture cross cutting broken and offset framework grains. The break seems caused by compaction. The horizontal field of view is 1.2 mm.

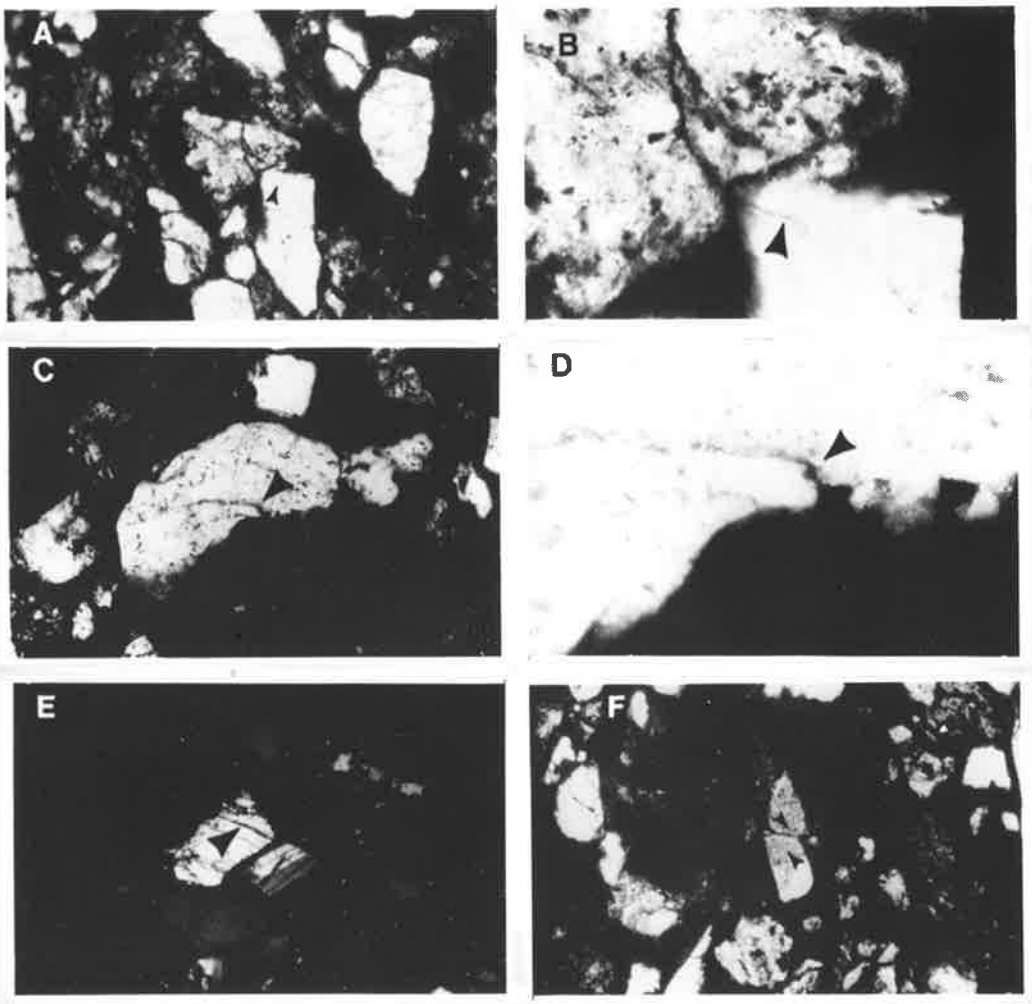
A
B
C
D
E
F

Fig. 1-8. Schematic of reequilibration of post-depositional (diagenetic) Type A and B fluid inclusions near an intrusion as seen by changes in the T_h distribution. For contact metamorphism caused by dikes in host rocks that otherwise have only undergone burial diagenesis, trapping of fracture bound fluid inclusions can only occur at or below T_{peak} and thus, there is no possibility of masking the upper data edge (UDE).

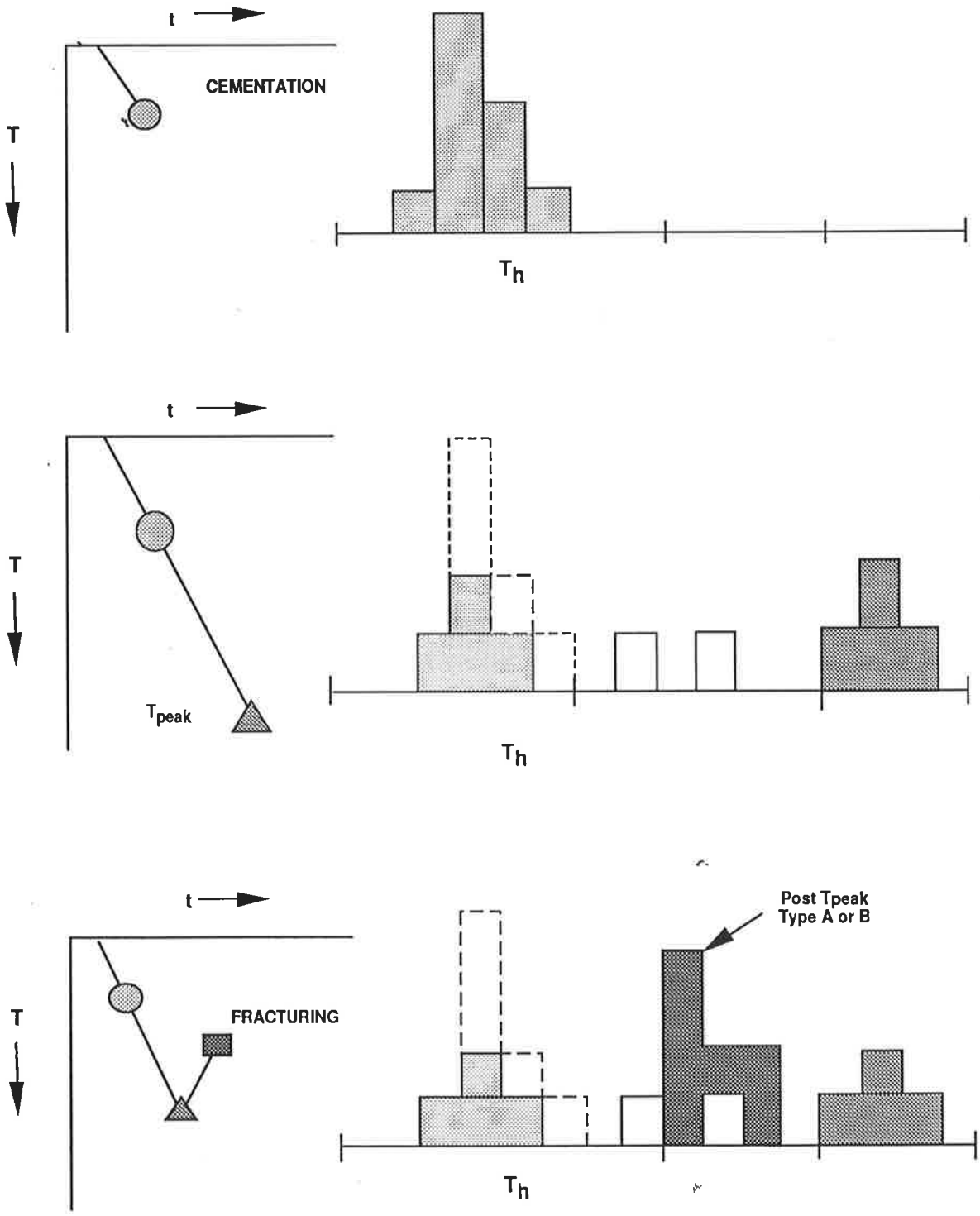
t
CEMENTATION
T
Th
t
T
Tpeak
Th
t
Post Tpeak
Type A or B
T
FRACTURING
Th

Fig. 1-9. Schematic of reequilibration of type C inherited fluid inclusions as seen by the changes in the T_h distribution. Note that preservation of T_h below T_{peak} in inherited fluid inclusions can mask the lower mode. When using type C fluid inclusions it is crucial to infer that the inherited fluid inclusions considered for paleotemperature determination have been reequilibrated during contact metamorphism.

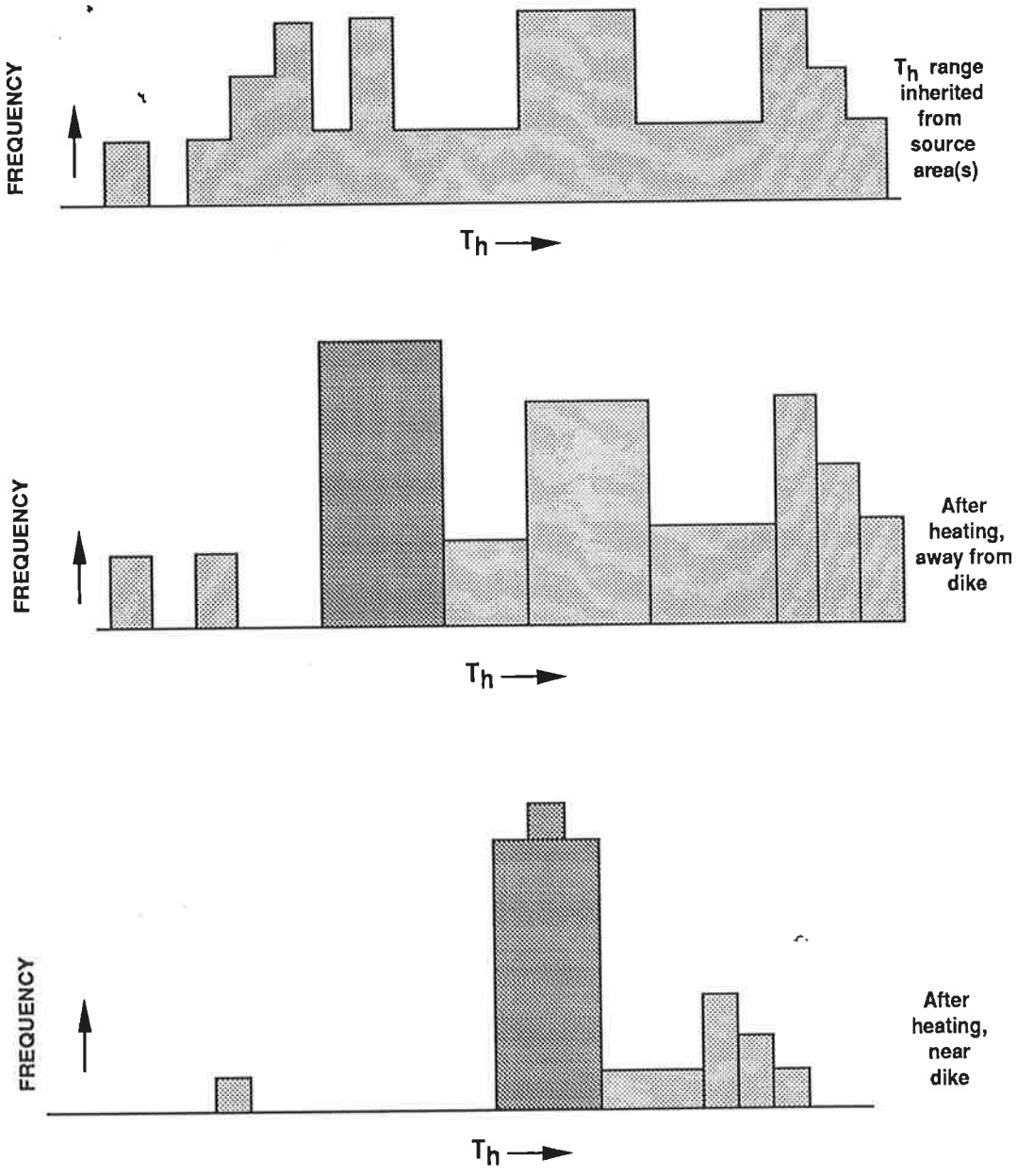
FREQUENCY
T_h
T_h range inherited from source area(s)
FREQUENCY
T_h
After heating, away from dike
FREQUENCY
T_h
After heating, near dike

The problem with type A and B fluid inclusions is that they are rare in the matrix rich, framework-grain poor sandstones as found in Upper Jurassic to Lower Cretaceous Strzelecki Group of the Mesozoic Gippsland Basin. Identifiable post-depositional fractures are rare simply because grain to grain contacts can be uncommon but these contacts are by definition necessary to identify a type A fracture. In general, few framework grains have broken, which is required to trap post-depositional fluid inclusions. Thus, studying type C fluid inclusions is important because some assurance is needed that the minimum temperature suggested by the UDE of the T_h distribution from type A and B fluid inclusions is in fact approaching T_{peak}. Other types of peak-recording geothermometers such as vitrinite reflectance can also be used in confirming T_{peak}.

Type C fluid inclusions have usually been trapped over a wide range of temperature (Fig. 1-9) as well as fluid salinity. During contact metamorphism, the only type C fluid inclusions that reequilibrate are those in which P_{eff} becomes large enough as T_{peak} is approached. Some fluid inclusions will potentially have a sufficiently low density (i.e. high T_h) that P_{eff} remains small enough that they do not reequilibrate. These Type C fluid inclusions will have their original T_h that is higher than those fluid inclusions that have reequilibrated and will tend to fall above the low mode (Fig. 1-9c). Figure 1-9c optimistically assumes that almost all type C fluid inclusions near the dike will reequilibrate. In fact, the discussion of reequilibration presented above shows it is possible that a significant number of type C fluid inclusions can retain their original T_h through contact metamorphism. The crucial problem in using inherited fluid inclusions for paleotemperature estimates is the inference that they have been reequilibrated during contact metamorphism caused by the dike.

Using fracture bound type C fluid inclusions is more precise than just considering all inherited fluid inclusions because they can show clear evidence of reequilibration. The evidence of reequilibration comes from the observation that fluid inclusions trapped along

fractures commonly have formed above the two phase boundary and have trapped a homogeneous fluid that is expressed as consistent V/L ratios when viewed at surface temperature. After reequilibration, these fluid inclusions will have different fluid densities and at surface temperature are observed to have a variable V/L ratio, a factor used to identify reequilibrated fluid inclusions. However, this reequilibration could have occurred in the detrital source areas for Type C fluid inclusions. The evidence for reequilibration during contact metamorphism is: 1) a variable V/L ratio in fluid inclusions trapped along the same fracture; 2) that the low mode temperature shows an increase as the dike is approached; and 3), if enough post-depositional fluid inclusions are found, the T_{peak} indicated by UDE found in Type A and B fluid inclusions should overlap the low mode temperature from type C fluid inclusions.

In a pilot study of estimating T_{peak} next to dikes using fluid inclusions, Barker et al. (1992b) estimated T_{peak} using the lower inflection point of the lowest mode of a population that includes all type C fluid inclusion types: isolated, clusters and fracture bound (Fig. 1-9), as well as type A and B. It is now recognized that when using isolated type C fluid inclusions there is usually no way to infer that reequilibration has occurred by observing them in an optical microscope. Nevertheless, this pilot study showed good agreement between T_{peak} estimated from fluid inclusions and a VRG.

This study now uses fracture-bound type C fluid inclusions with a variable V/L to estimate a minimum T_{peak} from the temperature of the lower mode of the T_h distribution. The temperature of the lower mode of T_h data from fracture bound type C fluid inclusions, which gives a minimum T_{peak} estimate, are compared to T_h from type A and type B fluid inclusions which approach T_{peak} near the UDE. Because of undetected fluid inclusion necking and the fact that T_h only approaches T_{peak}, what is expected is an overlap in the T_h data from type C fluid inclusions with the T_h data from type A and B fluid inclusions.

Other Evidence of Reequilibration

If fluid inclusions reequilibrate by decrepitation and resealing, the salinity of the fluid should reflect that of the pore fluid present. Consequently, it may be possible to distinguish reequilibration by a sudden change to a uniform salinity --as found during laboratory experiments where the fluid composition is kept constant. However, it is expected that during hydrothermal metamorphism caused by dikes, the salinity of the fluid will increase as mineral reactions proceed (Ellis and Mahon, 1977), and that a range of salinities would be found trapped in the fluid inclusions. Further, size and shape should also be factors in the measured T_h of reequilibrated fluid inclusions. The shape of equilibrated fluid inclusions in quartz tends to approach that of a negative crystal (Bodnar et al., 1989; Vityk et al., 1994). All of these aspects are used in this study to infer which fluid inclusion measurements can be related to dike contact metamorphism.

Limitations of Studies Using Reequilibrated Inherited Fluid Inclusions

Reequilibrated type C fluid inclusions are in many respects the most problematic to work with because: 1) the timing of formation (the primary versus secondary concept) is irrelevant due to the possibility of subsequent density changes; 2) salinity measurements have a reduced value because they may either reflect the inherited fluid or the fluid composition attained during crack-seal reequilibration. Further, the composition of reequilibrated external fluids is difficult to establish; 3) crushing stage studies to establish the presence of non-condensible gases is also ambiguous because of inherited gases. For these reasons, using salinity and the types of gases present to characterize reequilibration were not widely used in this study. This is unfortunate because in experimental studies where the external fluid composition is known, crack-seal reequilibration is demonstrated by the sudden

approach of the inclusion contents to that of the enclosing fluid. Fluid inclusions that simply stretch during reequilibration show no change in salinity and so salinity is at best an ambiguous line of evidence in demonstrating reequilibration. This thesis is limited in scope to the assumption that reequilibration is occurring because of the marked overheating caused by intrusion and cooling next to the dike. Salinity is not used as a major line of evidence in this determination. T_h is a far more sensitive measure of reequilibration.

1.5 HEATING DURATION FROM APATITE FISSION TRACK ANNEALING

General discussions of the AFT annealing method are found in Green et al. (1989) and Naeser et al. (1989). Practical aspects of the method are discussed by Hurford and Green (1982). Bray et al. (1992) and Arne and Zentilli (1994) discuss the usefulness of combining the AFT annealing and vitrinite reflectance methods to extend the temperature range of AFT annealing with Rv-r data and use AFT annealing to constrain the possible thermal histories suggested by vitrinite reflectance. Arne et al. (1990a, b), Arne (1991, 1992) and Barker (1991) discuss using fission track analysis to study the temperature and duration of heat pulses related to ore deposition or geothermal systems and these studies are based on similar methods applied to dikes in this study. The discussion of AFT annealing methods and interpretation of data summarized here are compiled from these studies and other specific studies cited below.

Fission tracks are linear damage features produced in a crystal lattice by the spontaneous fission of trace amounts of ^{238}U. Fission tracks in apatite form throughout the history of a crystal but remain invisible until they are enlarged by etching with acid. Uranium-bearing minerals may be age dated by etching the crystal and measuring the number of spontaneous fission tracks and determining the number of induced fission tracks, usually using external detectors, artificially produced by neutron bombardment (Naeser, 1979).

After formation, tracks begin to anneal (shorten) by an atomic diffusion process. Diffusion is a temperature controlled process that can be described by kinetic equations (Naeser, 1981; Gleadow et al., 1981; Laslett et al., 1987; Duddy et al, 1988; Green et al., 1986; 1989). Temperature is thought to be the external factor controlling annealing (Fleischer et al., 1975). Crystal composition, especially chlorine content in apatite, is an important internal factor (Green et al., 1985; Corrigan, 1993). Apatite becomes more resistant to annealing with increasing Cl content and retains tracks to higher temperatures. In summary, the measured fission track density for apatite is the result of: 1) ^{238}U content of the crystal; 2) time elapsed since the initial cooling of the crystal and, 3) the thermal history of the crystal if tracks are being annealed (Arne et al., 1990b).

In sedimentary basins, the apatite fission track age is largely controlled by annealing in the temperature range of 20°C to 150°C over geological time scales (1 to 200 m.y.). During burial in sedimentary basins, fission track annealing occurs in apatite over the temperature range of 60°C to 150°C. Newly formed fission tracks are about 15 μm long but combined effects of temperature and time are recorded by track length reduction. The processes of track formation and annealing over the life of the crystal form a record of the cumulative thermal history in track length distribution. Interpretation of track length distributions then provides information about the manner of cooling in the temperature range of 60°C to 150°C (Gleadow et al., 1986).

Estimating cooling history next to dikes using AFT annealing is possible because although temperatures are much higher, the heating duration is much less (10^{-2} to 10^{5} yr; Mundry, 1968) than temperature and heating time scales in burial diagenesis (10^{6}-10^{8} yr). Experiments on fission track annealing show that at 370°C complete annealing of fission tracks in apatite occurs in one hour (Green et al., 1989). These experiments also suggest that each 10°C decrease from 370°C increases the time required for complete annealing by

an order of magnitude. Next to the basaltic dikes used in this study, temperatures near the dike contact approached 600°C. All apatite fission tracks will be annealed at the dike contact (Fig. 1-10). Next to dikes that cool by conduction, temperatures decrease outward in the sandstone host rock until the regional burial temperature is reached. At some point temperature and heating duration will decrease to the point that all of the fission tracks are preserved. At this point, contact metamorphism has not affected the host rocks and these rocks will have an apparent age reflecting the mixture of ages from the detrital apatite crystals contributed by the source areas to the sedimentary host rock.

For the heating duration to be estimated from kinetic models, the T_{peak} at which some measurable portion of fission tracks have been annealed must be determined. For application to AFT annealing models, it is convenient to use the T_{peak} at the point at which 50 percent of the spontaneous tracks are annealed (or the apparent fission track age has been reduced by 50 percent). At the point of 50% AFT annealing, the T_{peak} is estimated from fluid inclusion data, and(or) VRG. The elapsed time (heating duration) needed to produce 50% AFT annealing at the estimated T_{peak} is evaluated using kinetic models (such as Laslett et al., 1987). This process is illustrated in chapter 4. In this study, because of the time intensive nature of AFT annealing and fluid inclusion work in sandstones, the T_{peak} at 50 % fission track loss is interpolated from a series of T_{peak} and age determinations made at spaced intervals from the dike margin.

Fig. 1-10. Schematic of the response of apparent fission track ages to increasing contact metamorphism temperature as a dike is approached. The apparent age decreases as apatite fission tracks are annealed. After the rapid cooling typical of dikes intruding much cooler sedimentary rocks, the cooling age of the intrusion is recorded by the completely annealed apatite crystals at the dike contact that begin to accumulate tracks once again.

Annealing of Apatite Fission Tracks as a Dike is Approached

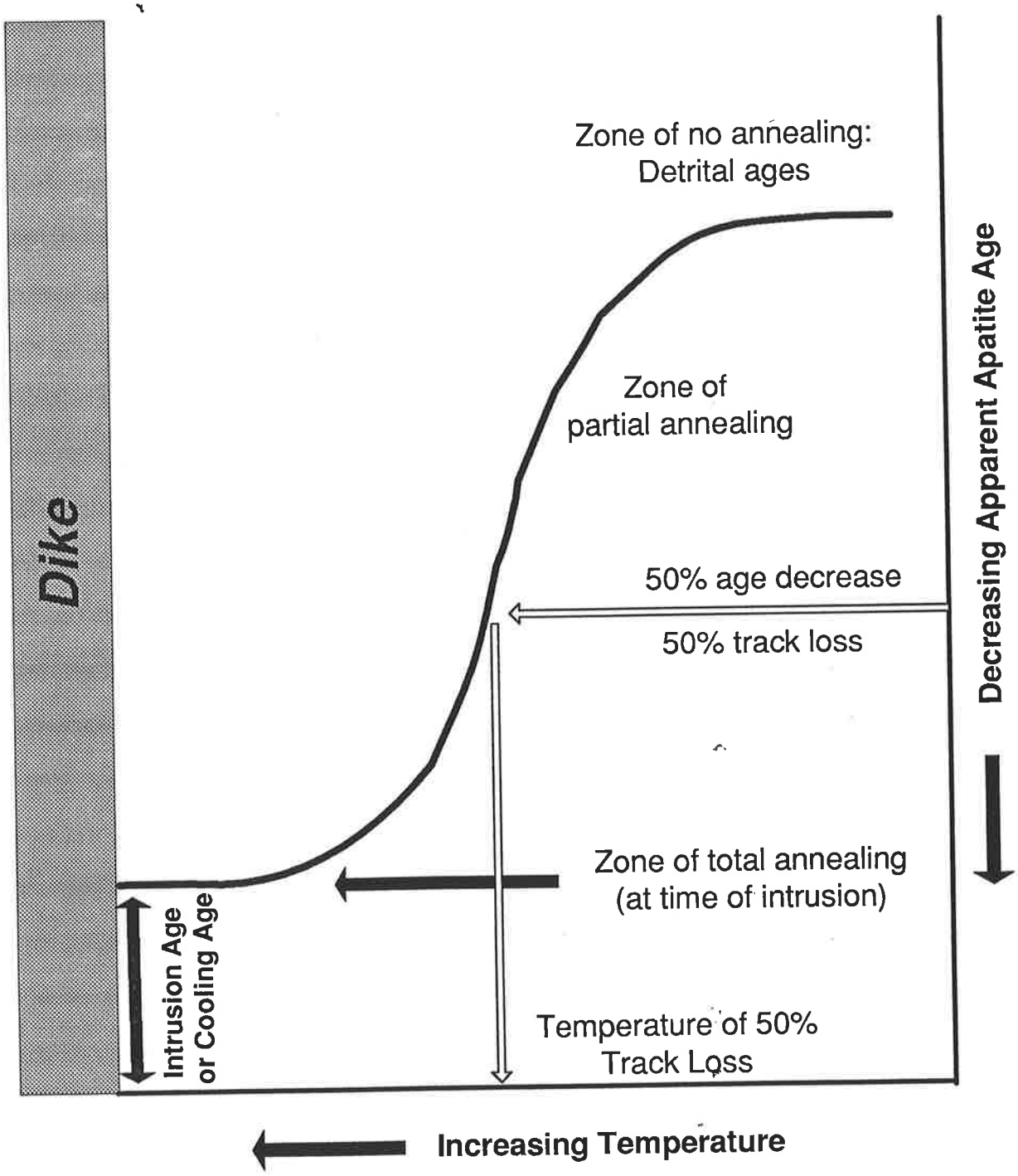

1.6 VITRINITE REFLECTANCE GEOTHERMOMETRY DURING CONTACT METAMORPHISM

In this study, vitrinite reflectance is used as a check on the geothermometry indicated by fluid inclusions because this parameter is more easily measured and it has been calibrated to many of the organic geochemistry techniques used in this study. Further, the purpose of thermal maturation parameters, such as vitrinite reflectance, is to measure the degree of heating (Barker and Pawlewicz, 1994). This use of vitrinite reflectance makes its calibration to T_{peak} important because T_{peak} constitutes an absolute thermal maturation parameter. Studies using temperature-based comparisons rather than thermal maturation parameters have an obvious advantage in that standards and instrumentation are readily available worldwide and their connection to other physical sciences is quantitative.

T_{peak} can be determined by using fluid inclusions, AFT annealing, or measurements on equilibrium mineral assemblages and by direct measurement in strata that can be demonstrated to be at the highest temperature attained in their geologic history. AFT annealing studies are limited in that tracks are not generally retained above about 150°C. Studies of equilibrium mineral assemblages are also limited in that during burial heating, equilibration can be difficult to attain or may not be recorded by mineral precipitation. These problems make it advantageous to measure other more commonly available and easily measured thermal maturation parameters. Thus, T_{peak} is presently not considered a replacement for, but supplementary to, vitrinite reflectance, AFT annealing, or other thermal maturation studies.

A purpose of this study is to develop a VRG for contact metamorphism caused by dikes. First, the VRG for hydrothermal metamorphism (Barker and Pawlewicz, 1994) will be tested for accuracy in the special case of contact metamorphism caused by dikes. The heating of water-wet host rocks by dikes causes hydrothermal alteration. However, the VRG

for hydrothermal metamorphism is largely developed for open-system hydrothermal alteration like that seen in geothermal systems or ore deposits. Contact metamorphism next to dikes may be more closed. Thus, the published hydrothermal VRG may not be applicable in this case. This study will attempt to determine system openness next to selected dikes so that a determination of the applicability of the VRG for hydrothermal metamorphism can be made. In a pilot study (Barker et al., 1992b), using mostly data form type C fluid inclusions the VRG for hydrothermal metamorphism showed fair agreement with the fluid inclusion data from Gippsland Basin. Perhaps the accuracy of the calibration can be improved using constraints on T_{peak} discussed above. In any case, calibration of a VRG based on T_{peak} estimated from fluid inclusion data should be more accurate than previous published geothermometers for contact metamorphism next to dikes as they were calibrated using bomb experiments or heat flow models to indirectly estimate T_{peak} .

1.7 LONG TERM PYROLYSIS OF ORGANIC MATTER

The natural pyrolysis of sedimentary rocks by igneous intrusions is in some respects analogous to the standard geochemical techniques, Rock-Eval (anhydrous open pyrolysis) and hydrous pyrolysis (closed, sample immersed in excess water), developed to evaluate petroleum source rock potential under controlled heating conditions. Such pyrolysis experiments are thought to be adequate experiments to simulate SOM thermal maturation except that, in the laboratory, the geological heating-duration factor can not be directly assessed. Consequently, natural pyrolysis occurring in sedimentary rocks metamorphosed next to dikes of increasing size and heating duration are useful as a series of longer term geological experiments (10^{-2} to 10^{5} yr; Mundry, 1968) overlapping with experiments on laboratory time scales (10^{-4} to 10^{1} yr) for oil generation studies. The overlap between the laboratory and natural heating durations enables the relevant organic maturation and oil

generation reactions to be tracked from the controlled laboratory conditions to nature. The key to this study is that T and t dependence of oil generation can be clearly resolved by making accurate measurements by fluid inclusion-AFT annealing techniques of reaction conditions and heating duration between the laboratory experiments and natural hydrous pyrolysis occurring next to igneous intrusions of increasing size. The previous lack of accurate T_{peak} and heating duration data in natural systems, has been a block in determining the conditions extant during the metamorphic event.

Contact metamorphism is a natural (usually hydrous) pyrolysis experiment occurring over a much longer time frame than laboratory conditions and as heating duration is extended, it becomes comparable to burial metamorphism. Thus by studying hydrocarbon generation in exposed rocks it is possible to investigate this process as it may occur in the deeper portions of the basin. This observation is not new but previous studies have been less quantitative in that they do not directly measure T and heating duration conditions during natural pyrolysis, only model them.

Study Areas

The multidisciplinary approach used in this study required several sample attributes that in some ways are mutually exclusive: 1) rocks that have been intruded ideally have not been previously heated above 60°C such that the source rocks are preserved and apatite still retains fission tracks; 2) samples that contain usable fluid inclusions in easily reequilibrated minerals such as calcite, or common fluid inclusions that were formed during the intrusion; and 3) samples must contain sufficient unweathered thermally immature organic matter and apatite for alteration by contact metamorphism. These ideal samples proved difficult to find, as dikes are symptomatic of high heat flow and high regional burial temperatures. Also, because the study considered exposed dikes, weathering may be a significant problem.

Extended efforts to find appropriate intrusives in limestone or calcite cemented sandstone have resulted in no useful cases. The Bowen, Calide, Canning, Moreton, Perth, and Sydney Basins of Australia were all profiled from the literature and pilot studies were done on three of these basins to determine if the samples were appropriate. All of these basins proved inadequate in some aspect.

The Buchan Rift was also sampled but was shown to be overmature, generally deficient in humic SOM, and showed little change during contact metamorphism. This portion of the study was limited to characterization of one dike, development of a geothermometer based on solid bitumen reflectance, a regional reflectance study and development of the burial and thermal history of the area to explain the response of the host rock to contact metamorphism by the dike.

The Gippsland Basin was finally selected for an extended study because it is characterized by especially good exposures of dikes intruding marginally mature to mature potential source rocks on the basin flank. The dikes in this basin are often so well exposed in sea cliffs, wave cut terraces, and(or) road cuts that in some cases it was possible to accurately measure sample distances from the dikes to centimeter, and in one case (San Remo 3, a 0.06 m thick dike), a few millimeters accuracy.

Chapter 2.

Contact Metamorphism in an Overmature Basin:

The Buchan Rift, Victoria, Australia

2.1 INTRODUCTION

Generally contact metamorphism next to a 2.2 m thick basalt dike intruding the Buchan Caves Limestone in the Buchan Rift (Fig. 2-1 and 2-2a,b) would produce increased thermal maturation out to a distance equal to about one dike thickness (Dow, 1977). A pilot study, however, showed that the rocks generally had not responded to contact metamorphism (Barker et al., 1992a). Initially it was considered that the local host rocks may have been altered by other nearby intrusions. Teichert and Talent (1958) mapped a thin dike 100 m south southeast of the dike sampled for study. Other intrusives are exposed in the road cut 300 m to the north of the dike we studied (Teichert and Talent, 1958; McAndrew and Marsden, 1968; Orth et al., in press) and 1 km north northeast, a 0.3 m thick dike is reported in the Murrindal cave (Mill et al., 1980). Additional caves and outcrops in the Buchan Rift where dikes are exposed are also described by Joyce and King (1980), Arne et al. (1994) and Orth et al. (in press).These other dikes are too distant from the sampled roadcut to have much influence on the host rocks we studied.

Further work has shown that this lack of response was apparently caused by the rocks having been heated to relatively high burial temperatures before intrusion (Barker and Bone, 1995; Appendix 11). The initial studies also found that vitrinite was sparse in these rocks but that solid bitumen was common in the Buchan Group limestones. Solid bitumen responds to increased heating in a fashion similar to vitrinite, and bitumen reflectance can be used to assess thermal history like vitrinite reflectance (Robert, 1988). However, a relationship of solid bitumen reflectance (Rb) to peak temperature (T_{peak}) had not been established, and initially we could not compare Rb results to other geothermometry.

The purpose of this chapter is to: 1) document the burial and thermal history of the Buchan Group limestones as an explanation for their minimal response to contact metamorphism; 2) establish the relationship of solid bitumen reflectance to T_{peak}; and 3) use Rb and fluid inclusion geothermometry to establish the degree of regional burial heating in the Buchan Rift.

2.2 BURIAL AND THERMAL HISTORY

The general geology of Buchan Rift has been updated by Orth et al. (in press) and their work forms the geologic foundation for our study. The burial history presented here synthesizes stratigraphic and age data from Cas (1983; 1988), Ramsay and VandenBerg (1990), Webb (1991), and Orth et al. (in press). The geologic history is placed in the context of global tectonics and climatic change by the use of Veevers (1984).

An integration of these studies shows that the Buchan Rift formed in the Early Devonian (410-385 Ma) during an extensional tectonic phase that affected eastern Victoria after the Latest Silurian (Webb, 1991) to earliest Devonian Bowning Deformation (Cas, 1983; 1988) . Initially, the Rift (Fig. 2-1) was filled with Snowy River Volcanics (410-395 Ma) which are mostly subaerial rhyolitic volcanic deposits. Later, with further subsidence, marine deposits of the Buchan Group (395-385 Ma) covered the Snowy River Volcanics.

Fig. 2-1. Locality map showing the extent of the Buchan Group, Snowy River Volcanics, and the Buchan Rift, Eastern Victoria. Modified from O'Shea (1980).

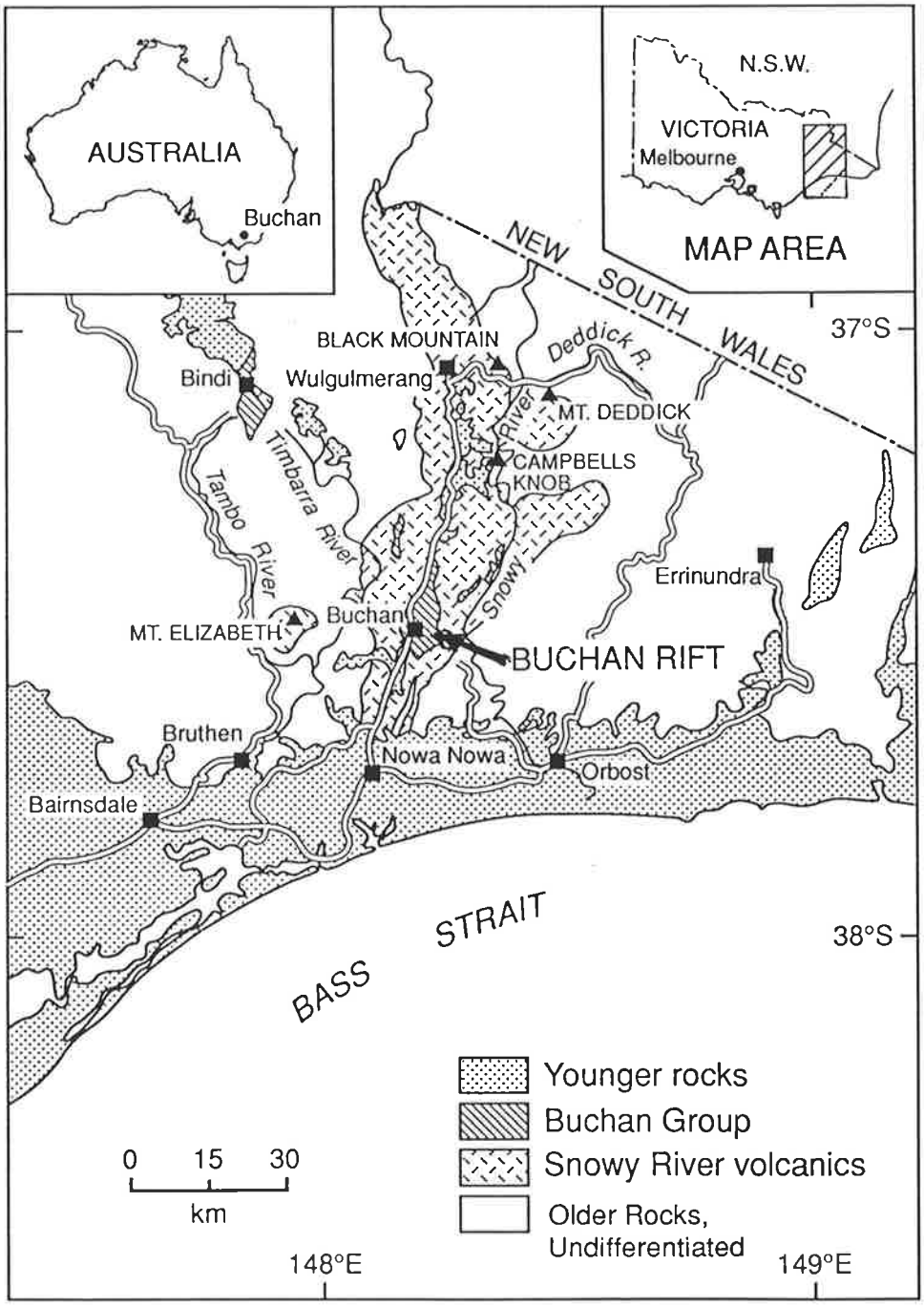
AUSTRALIA
Buchan
N.S.W.
VICTORIA
Melbourne
MAP AREA
NEW SOUTH WALES
37°S
BLACK MOUNTAIN
Deddick R.
Bindi
Wulgulmerang
River
MT. DEDDICK
CAMPBELLS KNOB
Timbarra River
Tambo River
Snowy
Errinundra
MT. ELIZABETH
Buchan
BUCHAN RIFT
Bruthen
Nowa Nowa
Orbost
Bairnsdale
BASS STRAIT
38°S
Younger rocks
Buchan Group
Snowy River volcanics
Older Rocks, Undifferentiated
0 15 30
km
148°E
149°E

Fig. 2-2. A. Roadcut at Murrindal where the 2.2 m thick dike was sampled (arrow). B. The basaltic dike exposed in the roadcut. The dike is 2.2 m thick where sampled near the white card. The sampled bed is marked by the white card on right hand side of the dike. Note the sheared and altered dike contacts which show as dark bands adjacent to the host rock contact near the white card.

A

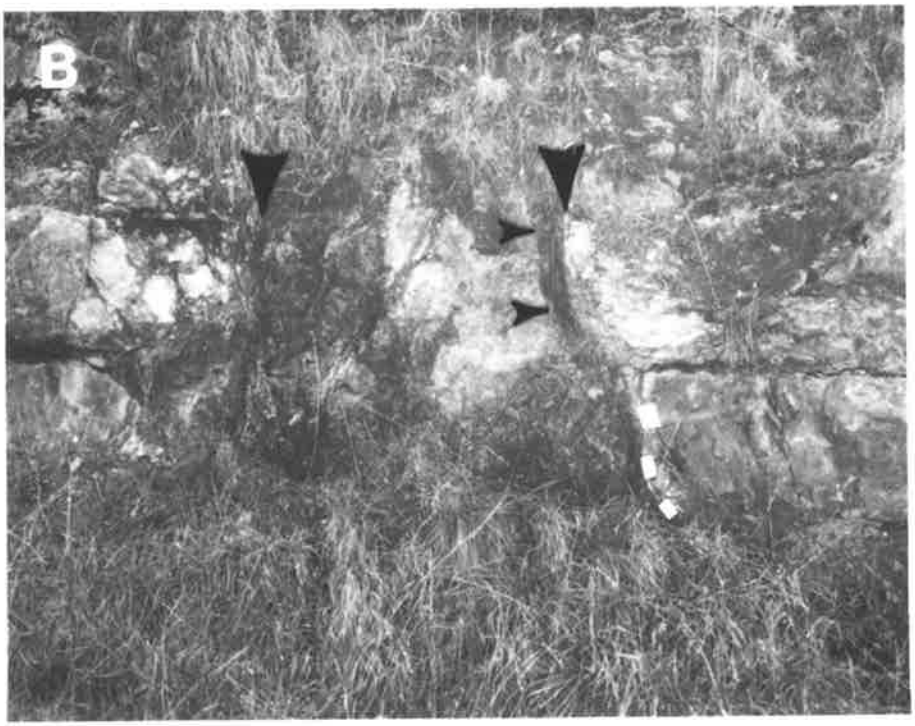

The basal Buchan Group consists of shallow-water algal limestones of the Buchan Caves Limestone which underlie the Taravale Marlstone. The Buchan Caves Limestone is 260-280m thick in the Murrindal area (Fig. 2-3a,b). The basal portion of the Buchan Caves Limestone was dolomitized but grades upward into limestone. Overlying the Buchan Caves Limestone is the Pyramids Marl which is 60m thick in the Murrindal area. The Taravale Marlstone is a somewhat younger mudstone unit deposited in deeper water. Although eroded, it is still up to 600 m thick. The last phase of shallow water limestone deposition during the Early Devonian produced the Murrindal Limestone. The Murrindal Limestone consists of carbonate shelf deposit up to 290 m thick. Our burial history reconstruction estimates that 200 m of the Murrindal Limestone and about 1.2 km of the Taravale Marlstone have been eroded from the Buchan Rift. The average surface temperature during the Early Devonian was about 25°C (Fig. 2-4).

The Middle Devonian Tabberabberan Deformation (385-380 Ma) folded and faulted the rocks of the Buchan Rift. The Tabberabberan Deformation marks the end of Paleozoic deposition in the Buchan Rift (Orth et al., in press), and the onset of erosion, and thus also marks the time of peak burial. The Devonian was also a time of extensive granitic plutonism that produced some 200 separate intrusions in Victoria (Fig. 2-5). Evidence of continuing magmatic activity after deposition of the Buchan Group is a pre-Tabberabberan dike exposed at the Back Creek mine (Arne et al., 1994). A heat flow of about 110 mW/m^2 is required to heat the Buchan Caves Limestone to the observed T_{peak} of 200°C at the modeled peak burial of 2.7 km at about 380 Ma (Fig.2-3a) and a surface temperature of 25°C (Fig. 2-4).

Fig. 2-3. Burial depth reconstruction, Buchan Rift, Victoria. (A) modeled burial depth history and inferred paleotemperature from a variable heat flow history, deepest formation in the figure is the Snowy River Volcanics followed by the Buchan Caves Limestone and (B) time versus maturity (Rv) and paleotemperature near the top of the Buchan Caves Limestone.

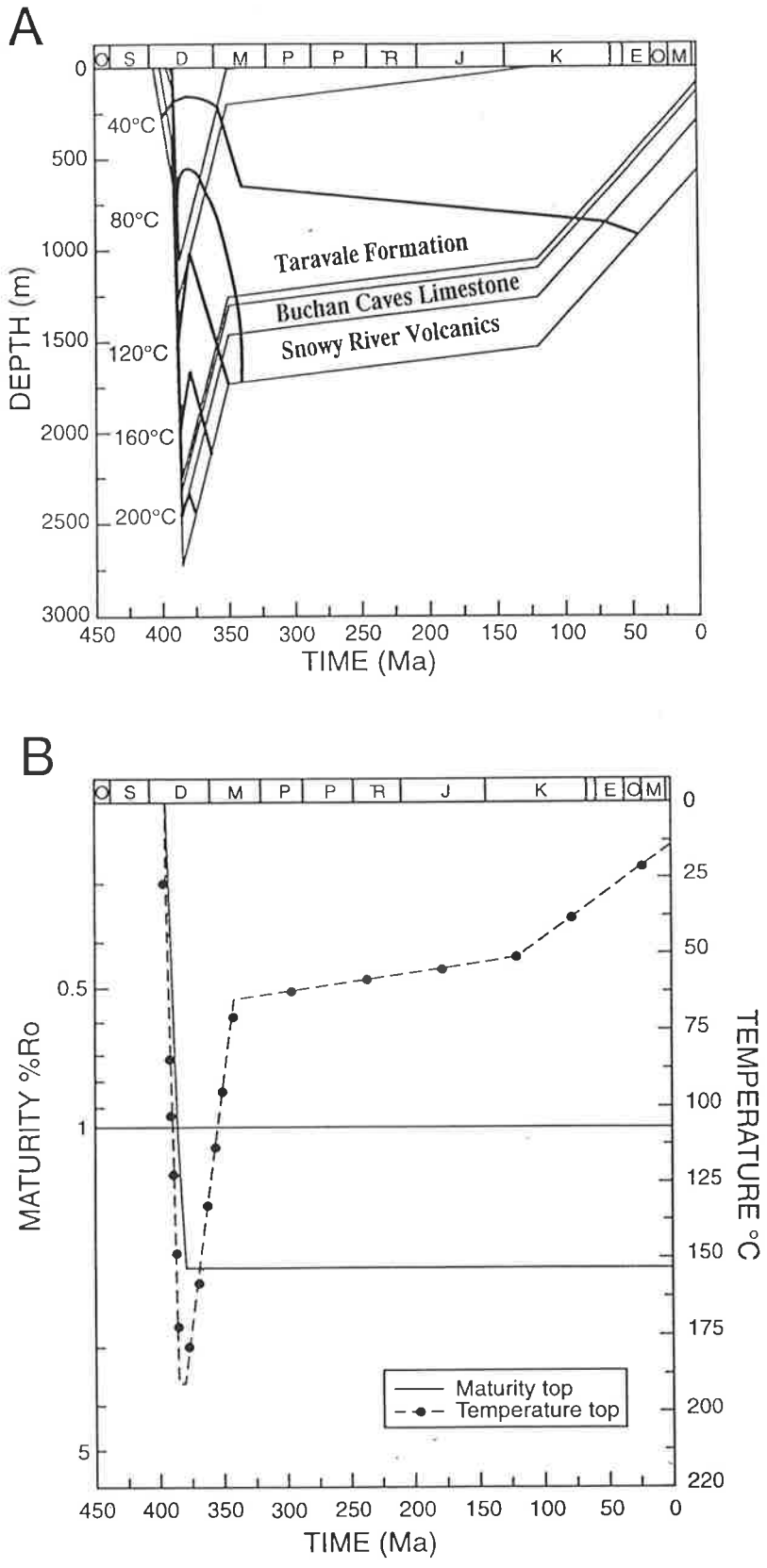
A
O S D M P P R J K E O M
0
500
1000
1500
2000
2500
3000
DEPTH (m)
40°C
80°C
120°C
160°C
200°C
Taravale Formation
Buchan Caves Limestone
Snowy River Volcanics
450 400 350 300 250 200 150 100 50 0
TIME (Ma)
B
O S D M P P R J K E O M
0.5
1
5
MATURITY %Ro
0
25
50
75
100
125
150
175
200
220
TEMPERATURE °C
Maturity top
Temperature top
450 400 350 300 250 200 150 100 50 0
TIME (Ma)

Fig. 2-4. Summary of paleoclimate and paleosurface temperature estimates based on paleolatitude reconstruction. Modified for the Buchan area from Veevers (1984). Average annual surface temperatures of climatic zones from Savin (1977). Paleolatitude for southern Victoria scaled from the continent drift maps of Veevers (1984, his figure 10). Global trend of surface temperature (dotted line) from Frakes and Rich (1982). E and SE on the figure indicate these parts of Australia. Dashed line indicates inferred value. Question mark indicates uncertainty in the data.

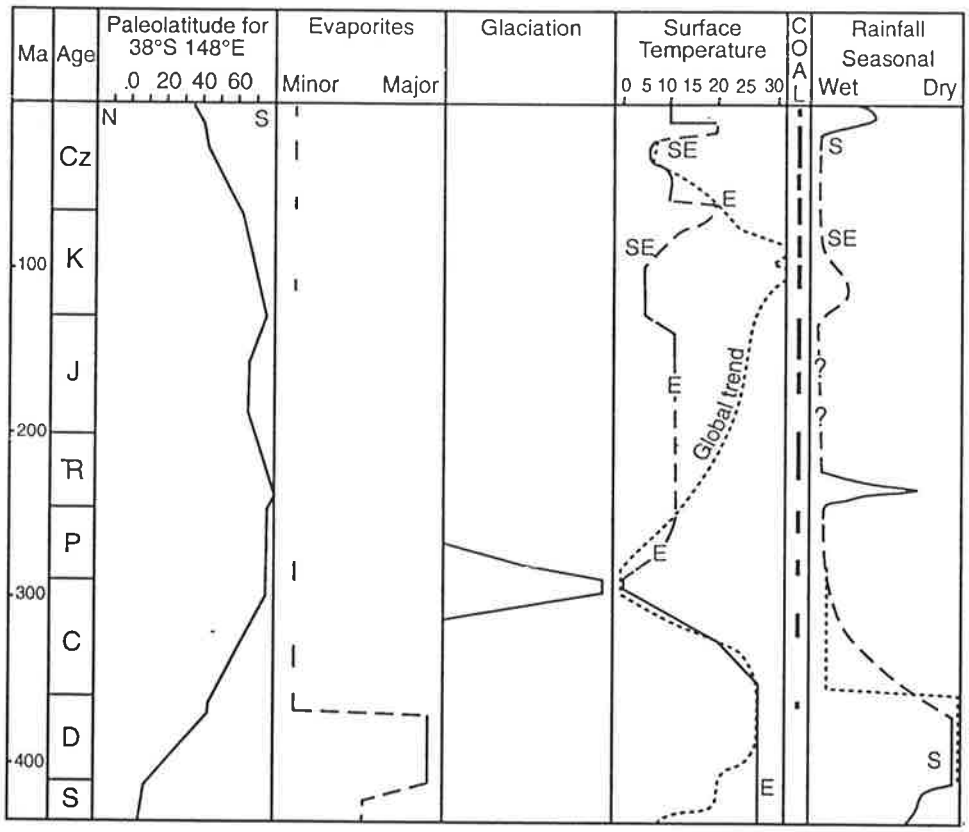
Ma
Age
Paleolatitude for 38°S 148°E
.0 20 40 60
N
S
Evaporites
Minor
Major
Glaciation
Surface Temperature
0 5 10 15 20 25 30
COAL
Rainfall Seasonal
Wet
Dry
Cz
K
J
R
P
C
D
S
100
200
300
400
SE
E
SE
E
Global trend
E
E
S
SE
?
?
S

The high heat flow at the time of peak burial in the mid-Devonian is attributed to: 1) continuance of the high heat flow associated with extrusion of the Snowy River Volcanics in the Early Devonian; and(or), 2) contemporary intrusions and evidence for reset age dates in the region suggesting an ongoing high heat flow regime in eastern Victoria (Fig. 2-5).

Allen and Allen (1990) show a range of heat flows for active rifts or volcanic areas that extends to 200 mW/m^2. In our burial history reconstruction, we have used a more conservative heat flow but have increased the burial depth of the Buchan Caves Limestone by adding 1.4 km of strata (now eroded) deposited above the existing 600m of Taravale Marlstone. This thickness of eroded strata in the Buchan area is suggested by the apatite fission track analysis of Dumitru et al. (1991; Fig. 2-6) who estimate at least 1.5-3.0 km of strata were eroded from the craton edge after the rebound of southeast Australia caused by the rifting and separation from Antarctica during the Cretaceous.

The Tabberabberan Deformation was followed in the Early Carboniferous (about 350 Ma) by the Kanimblan Deformation. This deformation was not very intense in eastern and central Victoria and cooling of the rocks in the Buchan area generally continued. Dumitru et al. (1991) suggest that burial temperatures in the Devonian rocks of eastern Victoria decreased to less than 60°C after about 300 Ma (Fig. 2-4). Our burial history reconstruction suggests the marked temperature decrease is the result of: 1) continuing exhumation of the Buchan Caves Group after the Tabberabberan Deformation; 2) an apparent decrease in heat flow to 65 mW/m^2 (the average global heat flow; Allen and Allen, 1990) in response to the cessation of igneous and orogenic activity; and 3) decreasing surface temperatures that preceded a glacial period in the Early Permian (Fig. 2-4).

Fig. 2-5. K-Ar age frequency distributions segregated into western, central and eastern Victoria. Modified from Richards and Singleton (1981). The smallest tick mark is equal to one age determination. Note that thermal events occurring during the Devonian have reset the age of many older intrusions to an apparent Devonian age (Orth et al., in press). However, the resetting of K-Ar ages suggests that the Devonian is a time of high heat flow consistent with the burial history reconstruction (Fig. 2-3) that suggests peak burial and T_{peak} in the Buchan Rift was reached at about 380 Ma in the Buchan Caves Limestone. Timing of burial temperature reduction to less than 60°C based on Dumitru et al. (1991). Tectonic events from Cooper and Grindley (1982) and Cas (1983; 1988).

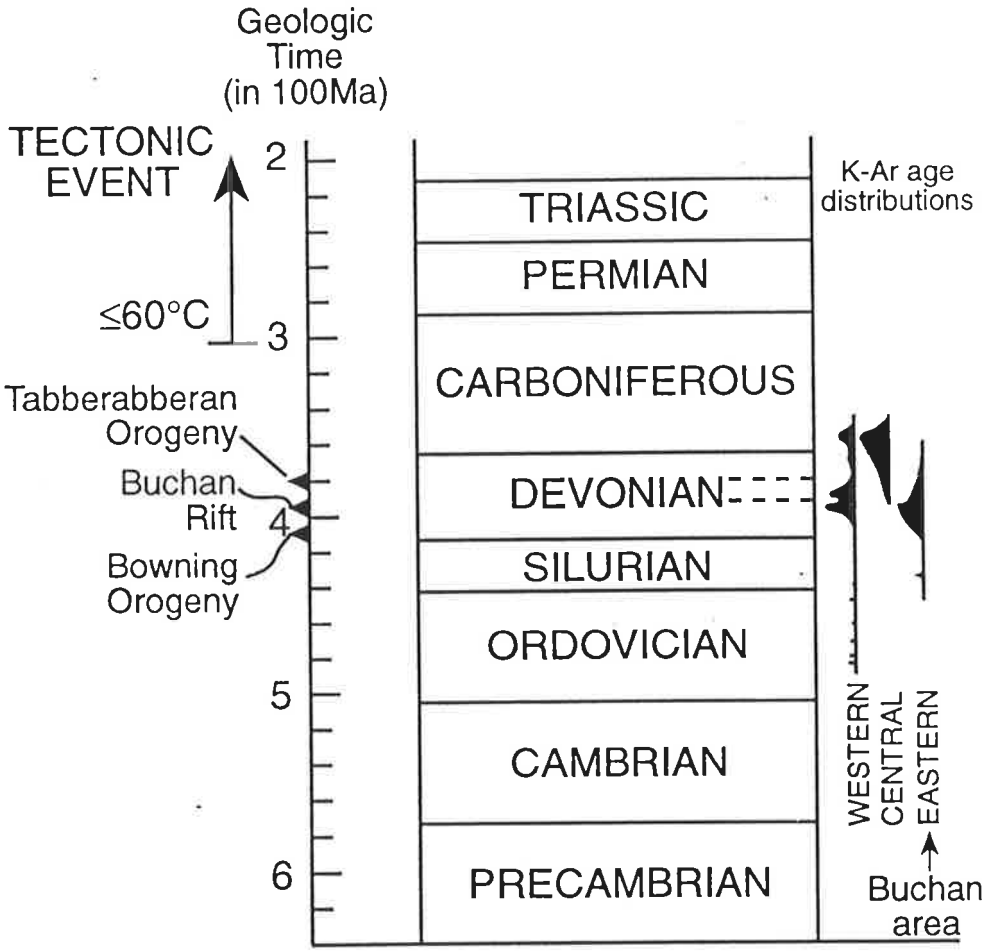
Geologic
Time
(in 100Ma)
TECTONIC
EVENT
≤60°C
Tabberabberan
Orogeny
Buchan
Rift
Bowning
Orogeny
2
3
4
5
6
TRIASSIC
PERMIAN
CARBONIFEROUS
DEVONIAN
SILURIAN
ORDOVICIAN
CAMBRIAN
PRECAMBRIAN
K-Ar age
distributions
WESTERN
CENTRAL
EASTERN
Buchan
area

Fig. 2-6. Late Paleozoic to Mesozoic cooling model for eastern Victoria based on the apatite fission track study of Dumitru et al. (1991). Note the thickness of eroded section (about 1-1.5 km) indicated by the difference in ground level at the projected position of the Buchan Rift and the dashed line showing the projected position of the now eroded strata.

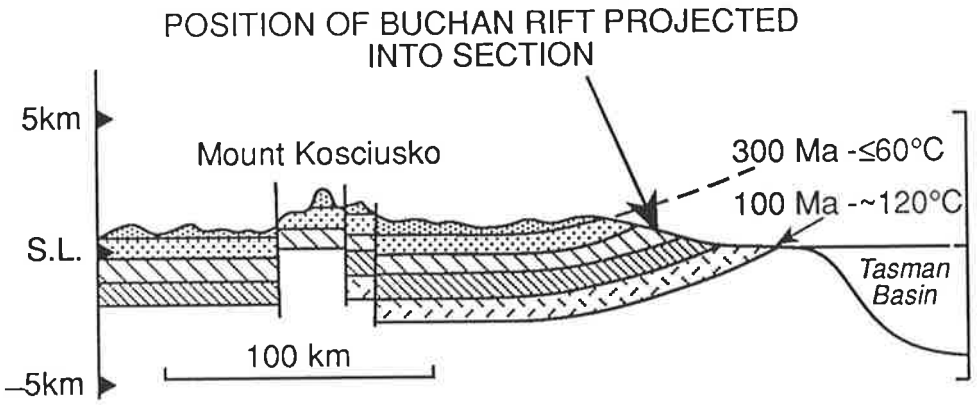
POSITION OF BUCHAN RIFT PROJECTED INTO SECTION
5km
S.L.
–5km
Mount Kosciusko
300 Ma -≤60°C
100 Ma -~120°C
Tasman Basin
100 km

Carboniferous and Permian sedimentation was mostly thin across the region. There was apparently little or no deposition from the Triassic to Jurassic, and only thin Late Cretaceous sedimentation (Abele, 1988). The Tabberabberan Deformation thus marks the onset of a long period of erosion and cooling that by mid-Cretaceous time, produced a surface of low relief and probably low elevation over most of southeast Australia (Orth et al., in press).

The history of the Buchan Rift since the Early Cretaceous has been controlled by the separation of Australia from Antarctica. At the end of the Early Cretaceous, Australia separated from Antarctica with the onset of Southern Ocean spreading. The breakup induced regional uplift in the Late Cretaceous to form the Eastern Highlands of southeast Australia which includes the Buchan area. During the Paleogene, the Buchan area was a highlands perhaps as high as 1500 m, that underwent deep incision by streams (Orth et al., in press) which transported sediments south into the Gippsland Basin and northwest to the Murray Basin. During the Eocene, karst developed in the Buchan Rift area (Finlayson et al., 1992). In the Late Eocene(?) (Orth et al., in press), the dikes near Murrindal intruded the Buchan Caves Limestone that, in part, formed the Buchan area highlands. Karst formation both preceded and post-dated the intrusions. Mill et al. (1980) reports a dike in the Murrindal cave that has been exposed on one side because continuing karst formation after intrusion has removed the host rock. Also, Orth et al. (in press) report that basalt filled a cave exposed just north of the Murrindal dike. The post Late Eocene basaltic volcanism was a brief intermission in the erosion of the highlands that generally continued from the Late Cretaceous to the present.

2.3 SOLID BITUMEN REFLECTANCE AND PEAK TEMPERATURE

Solid bitumen is commonly the only organic matter in limestones and in lower Paleozoic rocks which can lack vitrinite. In these rocks, it is often the only organic material large enough for reflectance study. Although not initially present in rocks, bitumen can be generated in a carbonate rock at less than 70°C (Tannenbaum and Aizenshtat, 1985; Aizenshtat et al., 1986) and thus is potentially present for recording most of the burial and thermal history. Bitumen is also found in igneous rocks and in veins where other types of solid organic matter are rare (Parnell et al., 1993). Unfortunately, it is possible that solid bitumen migration and formation occurred after T_{peak}, or not at all, during the burial history of a rock. This case is considered unusual because, if source rocks are present, oil generation and migration are typically widespread as T_{peak} is approached and so solid bitumen is often available during this crucial period in burial history.

Solid bitumen studies potentially have a wide application because bitumen is more common in all types of sedimentary rocks than is generally recognized. Our experience shows that solid bitumen can closely resemble, and is often erroneously reported, as vitrinite. This misreporting is especially prevalent when microscopy is done on kerogen concentrates rather than whole rock mounts. Petrographic differentiation of solid bitumen from vitrinite group macerals, in particular the maceral group gelovitrinite, is achieved by: 1) the recognition of plant-derived textures or maceral associations in vitrinite; 2) the use of fluorescence properties (Robert, 1988); 3) solid bitumen may show solubility in immersion oil or carbon disulfide; 4) a difference in reflectance (commonly) and a higher bireflectance compared to vitrinite (Jacob, 1989); 5) solid bitumen can have a cenospheric, granular mosaic or a flow texture; 6) the external morphology of solid bitumen is globular, mammillar, or botryoidal when unconfined, or conforms to the adjacent host surfaces when confined; and 7) in clastic rocks, vitrinite is a sedimentary particle transported to the site whereas bitumen commonly forms after deposition.

Besides being confused with vitrinite, other significant errors in Rb studies are

reflectance changes due to radioactivity and weathering (oxidation) as well as the difficulty in fixing the timing of oil migration and solidification. Radioactivity increases Rb (Eakin, 1989; Eakin and Gize, 1992). Eakin (1989) demonstrates a regular decrease in reflectance away from the boundaries of radioactive mineral grains, reaching a relatively stable value about 30 μm away. Thus, it is important to measure Rb away from radioactive mineral inclusions or radioactive mineral rich zones and their relatively thin halo of increased reflectance. Weathering may also effect Rb as it does vitrinite reflectance (Cornelius, 1987). By analogy to vitrinite reflectance studies, weathering effects are probably detectable as grains rimmed by a rind of lower reflectance. The reflectance of the core of the grain is probably still an accurate measure of the original reflectance except in cases of an extreme degree of weathering, as in soil zones, where the reflectance of the entire grain is lowered. Note that the common, but not exclusive, origin of bitumen after deposition greatly reduces the problem of measuring recycled sedimentary organic matter. It is expected that the problem of interlaboratory variation in analyses and operator bias shifting reflectance results like that seen in vitrinite reflectance studies (Dembicki, 1984) must also be considered in Rb studies.

The observation of solid bitumen particles with widely different reflectance within a sample may be attributable to several episodes of migration into the rock (Gentzis and Goodarzi, 1990; among others). Consequently, a rock can contain multiple solid bitumen generations which each record a different portion of thermal history and consequently have a different reflectance. The tactic used in this paper to deal with many generations of solid bitumen in one sample is to use the upper data edge of the reflectance distribution. The idea here is that the upper data edge is most likely the earliest generation of solid bitumen that has the best chance of having passed through T_{peak} and thus, show the best correlation with other peak recording geothermometers. However, this method does not insure that a solid bitumen does indeed record T_{peak}, only that it is the most likely candidate to record it.

Bitumen reflectance appears to react somewhat like vitrinite reflectance during burial

heating and contact metamorphism (Jacob, 1989) especially at higher thermal maturation levels (Teichmüller, 1987). This paper uses fluid inclusion and other geothermometry, from this study and the literature, to calibrate bitumen reflectance to T_{peak}. A positive correlation is expected because bitumen responds to increasing temperature by increasing aromaticity which is observed as a regular reflectance increase (Lobzova and Ziborova, 1988) like that observed in vitrinite (Wilson, 1987). Like vitrinite reflectance, time is probably only an effective control on bitumen reflectance for the geologically short period necessary for the chemical reactions to go to completion (Barker and Pawlewicz, 1994). Thereafter, bitumen reflectance would be mostly dependent on the T_{peak}, although pressure and heating rate may also be important.

Calibration of a Geothermometer Based on Solid Bitumen Reflectance

The calibration of Rb and T_{peak} formulated in this paper is based on a heterogeneous data set (Appendix 3) that uses different geothermometers having a variable degree of precision. The T_{peak} was mostly estimated from burial history modeling, organic petrology, laboratory experiments and fluid inclusion T_h measurements. Some of the literature cases employed in the calibration only give a relatively crude estimate of T_{peak}. These limitations in the data set make it necessary to qualify this calibration as preliminary.

Major axis regression of the T_{peak} and Rb (upper data edge value) gives a correlation coefficient(r^2) of 0.79 for 55 cases (Fig. 2-7) and preliminary equation of:

$$T_{peak} = (Rb + 0.895)/0.0199.$$

Fig. 2-7. Solid bitumen reflectance (upper data edge value used) versus apparent peak paleotemperature (T_{peak}) estimates compiled from the literature and unpublished data (listed in Barker, in preparation). The equation relating these variables is preliminary because of the variability in the quality of the T_{peak} estimate and a wide array of methods used in examples taken from the literature. The major axis regression line shown has a correlation coefficient (r^2) = 0.79 and an equation of T_{peak} = (Rb +0.8949)/0.01988. Note that this equation has changed slightly from Barker and Bone (1995) by the addition of more data (Appendix 3) since that manuscript was completed. This equation computes a T_{peak} of 196°C at 3.0% Rb-r instead of 197°C originally computed by Barker and Bone (1995) for the sample from the Pyramids area.

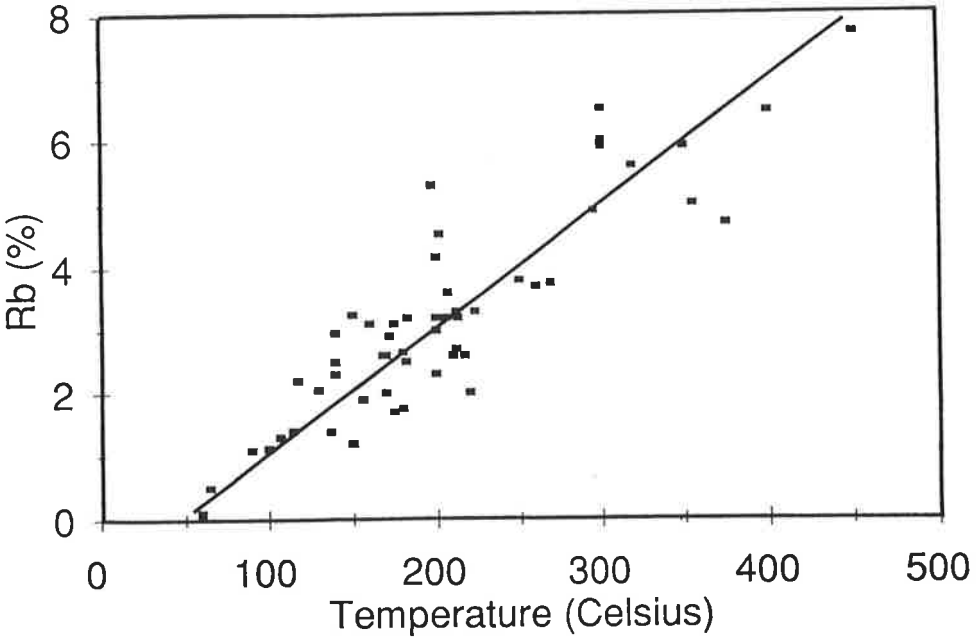
8
6
4
2
0
Rb (%)
0
100
200
300
400
500
Temperature (Celsius)

The relationship between Rb and T_{peak} seems to be a linear relationship whereas Rv-r versus T_{peak} is an exponential relationship (Barker and Goldstein, 1990). The thermal evolution of both vitrinite and bitumen are thought to be the result of reactions which increase the aromaticity of the remaining solid. Nuclear magnetic resonance studies of coal show that the aromaticity initially appears to be controlled by significant differences in the chemistry of the macerals which compose the coal. With increasing temperature these maceral differences are diminished or disappear. Aromaticity increases relative to vitrinite reflectance then settles into an apparent linear relationship between aromaticity and reflectance (Carr and Williamson, 1990). By comparison, solid bitumen has a more homogeneous chemical composition and burial heating produces a linear increase in aromaticity with increasing temperature.

2.4 REGIONAL BURIAL TEMPERATURES

Solid bitumen was commonly found in samples (Fig. 2-8) throughout the Buchan Rift. Solid bitumen occurs as mostly homogeneous grains precipitated on, or adhering to, secondary pores, fractures, burial cements, veins and stylolites (Plate2-1a). Some samples contain up to three generations of solid bitumen that produce polymodal reflectance distributions when measured. For geothermometry, only solid bitumen near the upper data edge are measured. The Rb geothermometer estimates that a T_{peak} of up to 200°C was reached in the rocks of the Buchan Rift during burial (Fig. 2-8). T_h data from fluid inclusions trapped in fluorite and calcite associated with lead-zinc deposits (Arne et al., 1994) indicate similar paleotemperatures were widespread in the Buchan Rift. For example, a sample from the Pyramids area (Fig. 2-8) has a Rb of 3.0% and an estimated T_{peak} of 196°C. This T_{peak} is in good agreement with mean fluid inclusion homogenization temperature of 188°C in fluorite and an upper mode of about 200°C (Arne et al., 1994). Our interpretation is that because the general reflectance level of solid bitumen is similar throughout the Buchan Rift, the thermal maturation level is related to regional

burial heating rather than contact metamorphism.

Temperatures of about 100°C are required to initiate oil generation, and oil generation is complete at less than 200°C. Our thermal history (Fig. 2-3b) suggests that a T_{peak} of 200°C was reached in the Middle Devonian and were reduced to less than 60°C by about 250 Ma. These data suggest oil generation and probably solid bitumen formation was confined to the Devonian in the Buchan Rift. Rock-Eval analyses of rocks in the Murrindal area confirm that no remaining hydrocarbon generation potential exists in the Buchan Group limestones.

2.5 CONTACT METAMORPHISM

Tertiary intrusions of the Murrindal area are related spatially and, in some cases, by age (Orth et al., in press) to the Older Volcanics of eastern Victoria. The intrusions are apparently the exposed feeder dikes to the flows capping karst surfaces in the area. Day (1983) described flows of Older Volcanics in the Buchan Rift area as basalts with either: 1) phenocrysts of locally embayed olivine with clinopyroxene in a groundmass of plagioclase; or 2) with glomeroporphyritic aggregates of olivine with augite and laboradorite. The petrography of the Murrindal dike is somewhat like the second type observed by Day (1983) but differs in that the dike rock contains solitary, non-glomeroporphyritic, euhedral olivine phenocrysts (about 1mm longest dimension). The difference may be that Day described flows which show textures due to crystal settling effects and we studied dikes which show quench textures. Overall, the Murrindal dike has a vesicular interstitial texture with subhedral to euhedral plagioclase and augite (titanaugite) forming a finer-grained equigranular groundmass to the olivine phenocrysts. The elongate or platy phenocrysts generally have no preferred orientation with little or no flow structure. The ferromagnesian minerals in places show a spotty surface alteration to biotite. Most of these olivine phenocrysts are now altered to antigorite(?) and an opaque mineral.

Fig. 2-8. General geology of the Buchan Rift (from Cromie, 1990: prepared by BHP Minerals) with fluid inclusion data from Cromie (1990) and solid bitumen reflectance (Rb) data (this paper). The World Hill Granite intrudes Ordovician to Silurian sedimentary rocks and so is older than the Buchan Rift sediments and is not related to their heating. T_h = the temperature of fluid inclusion homogenization to liquid. Rb is the random bitumen reflectance in oil with the upper data edge value reported. The °C value shown in parentheses is the peak temperature estimated from Rb (Fig. 2-7, major axis regression line). Not shown is a Rb value of 3.0% for the Pyramids deposit.

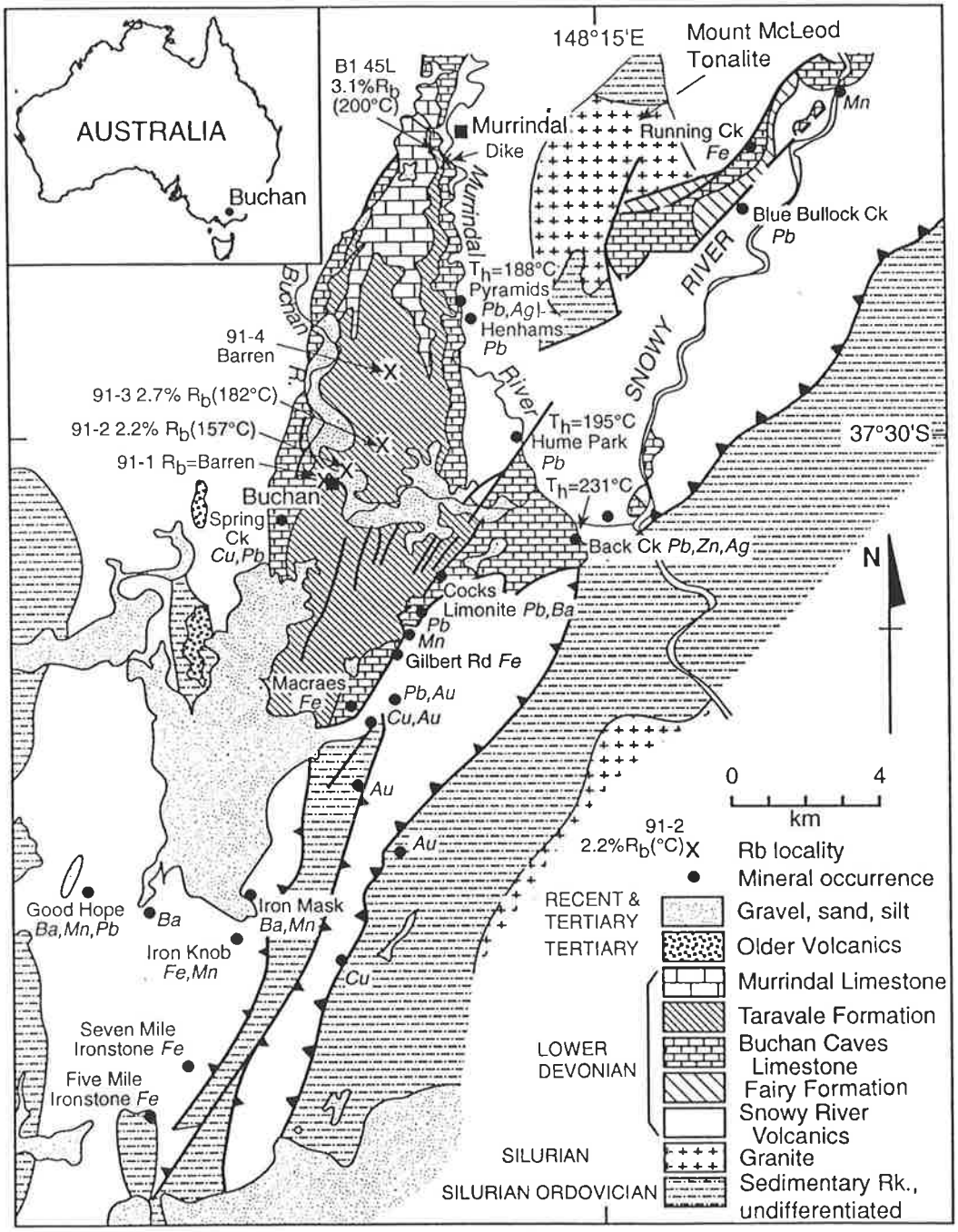
AUSTRALIA
Buchan
148°15'E
Mount McLeod
Tonalite
B1 45L
3.1%Rb
(200°C)
Murrindal
Dike
Running Ck
Fe
Mn
Blue Bullock Ck
Pb
Murrindal R.
Buchan R.
Th=188°C
Pyramids
Pb,Ag
Henhams
Pb
SNOWY RIVER
91-4
Barren
91-3 2.7% Rb(182°C)
91-2 2.2% Rb(157°C)
91-1 Rb=Barren
Th=195°C
Hume Park
Pb
Th=231°C
37°30'S
Buchan
Spring
Ck
Cu,Pb
Back Ck Pb,Zn,Ag
N
Cocks
Limonite Pb,Ba
Pb
Mn
Gilbert Rd Fe
Macraes
Fe
Pb,Au
Cu,Au
Au
0
4
km
91-2
2.2%Rb(°C)
Au
Rb locality
Mineral occurrence
Good Hope
Ba,Mn,Pb
Ba
Iron Mask
Ba,Mn
Iron Knob
Fe,Mn
Cu
RECENT &
TERTIARY
Gravel, sand, silt
TERTIARY
Older Volcanics
Murrindal Limestone
Taravale Formation
Buchan Caves
Limestone
Fairy Formation
LOWER
DEVONIAN
Snowy River
Volcanics
Seven Mile
Ironstone Fe
Five Mile
Ironstone Fe
SILURIAN
Granite
SILURIAN ORDOVICIAN
Sedimentary Rk.,
undifferentiated

Although the dike contact with the host rock is mostly obliterated (Fig. 2-2b), the solitary olivine phenocrysts are present as the altered dike margins are approached. Olivine was apparently the common phenocryst present when the magma was quenched at the dike-margin chill zones. A completely liquid melt, when quenched, forms a uniform equigranular texture without phenocrysts (Turner, 1981). Thus, the solitary olivine phenocrysts in a fine-grained equigranular groundmass indicate the dike was below the liquidus when intruded. A basaltic melt in which only olivine has precipitated suggests an intrusion temperature of about 1250 °C (Fig . 2-9) at the apparent near surface pressure. Near-surface pressure present during intrusion of the Murrindal dike is indicated by spatially related dikes that fill karst features. As expected, for a magma below the surface, this estimated intrusion temperature is just above the upper limit of measured extrusion temperatures for basalts (Carmichael et al., 1974).

Carslaw and Jaeger (1959; see also Taitt and Jaupart, 1990) suggest that T_{peak} reached in the host rock at the dike contact ($T_{contact}$) during the initial conductive heat flow stage, assuming equal thermal diffusivities for the dike and host rock and neglecting latent heat in the magma, is represented by $T_{contact} = (T_{magma} + T_{host})/2$, where T_{magma} and T_{host} are the initial temperature of the magma and host rock, respectively. T_{host} at Murrindal is estimated to have been 20°C (Fig. 2-3b) and if the dike was intruded at 1250° C, $T_{contact}$ was about 635°C.

Fig. 2-9. Liquidus mineralogy of a typical basalt. Modified from the Basaltic Volcanism Study Project (1981) and Middlemost (1985). The figure shows the first minerals to precipitate from a basaltic liquid at a given pressure and temperature. This phase diagram was used to estimate the temperature of intrusion based on the large olivine phenocrysts found in the quenched magma in the contact zone of the dike. The magma was assumed to be in equilibrium with the low hydrostatic pressure (near land surface conditions) reconstructed for the Murrindal area during intrusion.

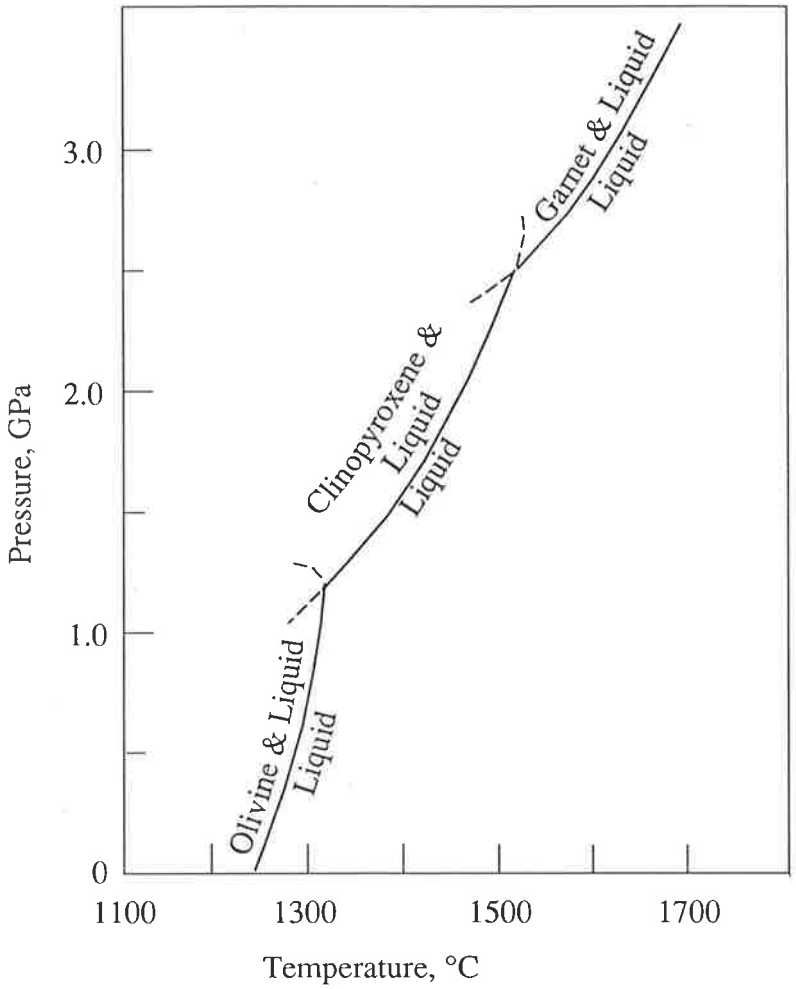
Pressure, GPa
3.0
2.0
1.0
0
1100
1300
1500
1700
Temperature, °C
Olivine & Liquid
Liquid
Clinopyroxene &
Liquid
Liquid
Garnet & Liquid
Liquid

Heat flow modeling of a 2 m dike (Fig. 2-10), using the Jaeger (1959) example of sheet intrusions into water saturated sedimentary rocks suggests an increase in host rock temperature to above the peak burial temperature of 200°C approximately 1.8 m away from the dike. The Rb in rocks closer to the dike than 1.8 m should have exceeded the peak burial temperature of 200°C and should show a reflectance above the regional level. Near the dike, however, the solid bitumen generally has a mean reflectance of about 2.4 to 2.7% and, where measured, has an upper data edge of near 3.1%. Both the mean and upper data edge values shows little or no systematic change in reflectance up to 6 m away from the dike contact (Fig. 2-11). The Rb geothermometer estimates predicts a T_{peak} of 200°C was reached during burial in the rocks next to the dike. Thus, a much thicker contact metamorphosed zone in the host rock is expected but not observed. These relationships suggest that Rb at this thermal maturation level is not very sensitive to short-term temperature increase. However, observations indicate that solid bitumen grains well away from the dike typically have a homogeneous structure (Plate 2-1a; Barker and Bone, 1995) but the proportion of grains with finely granular mosaic structure (Plate 2-1b) increases toward the dike. The increase in granular mosaic structure near the dike appears to be one of the most detectable responses of the rock to contact metamorphism at Murrindal.

Carbon and oxygen isotopes, even with an expanded axis scaling to emphasize the relatively small observed changes, also show little change except at the dike contact (Fig. 2-11). The whole rock isotope signatures vary within a range expected for analytical errors for most of the sampling sequence.

Fig. 2-10. Expected peak temperature versus distance from a dike of indicated thickness as predicted from heat flow theory using the case of water saturated sedimentary rock (Jaeger, 1959).

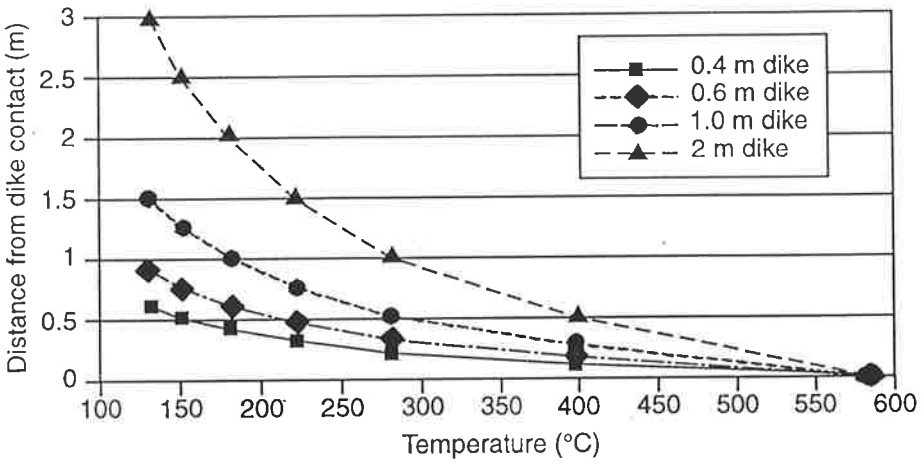
Distance from dike contact (m)
3
2.5
2
1.5
1
0.5
0
100
150
200
250
300
350
400
450
500
550
600
Temperature (°C)
0.4 m dike
0.6 m dike
1.0 m dike
2 m dike

Fig. 2-11. Oxygen and carbon isotope composition and reflectance of solid bitumen next to a 2.2 m thick dike near Murrindal, Buchan Rift, Victoria. The intrusion temperature is estimated at 1250°C and in the host rock should show a contact aureole out to about 2 meters from the dike contact. Samples immediately adjacent to the dike contact were apparently barren of solid bitumen with textures appropriate for reflectance measurement.

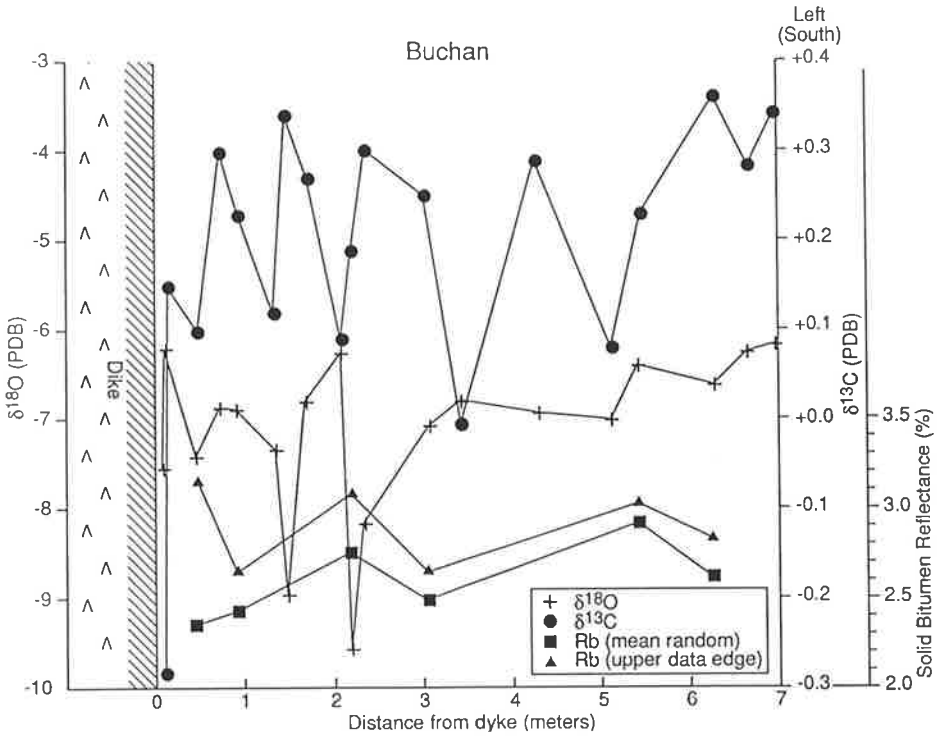
Buchan
Left
(South)
Dike
δ18O (PDB)
δ13C (PDB)
Solid Bitumen Reflectance (%)
Distance from dyke (meters)
δ18O
δ13C
Rb (mean random)
Rb (upper data edge)

PLATE 2-1

a. Solid bitumen with homogeneous structure (and reflectance) lining a stylolite. Largest piece of solid bitumen about 20 microns long. Sample from the Pyramids area (Fig. 2-8). Photograph taken under epi-illumination and oil immersion with uncrossed polars.

b. Solid bitumen showing a finely granular mosaic texture. The solid bitumen particle is about 20 microns at wide and is shown in a polished mount of an organic matter concentrate prepared by digesting the sample in dilute acid. Sample taken 93 cm south of the southerly dike contact of the Murrindal dike. Photograph taken under epi-illumination and oil immersion with uncrossed polars.

c. Host limestone at the southerly dike contact of the Murrindal dike seen in a thin section under transmitted white light illumination with uncrossed polars. The dike would have filled the clear area to the right side of the photograph. Note the strong darkening and discoloration of the host rock accompanied by the formation of a granular crystalline mass (hornfels or mylonite) at the dike contact. Field of view is about 2 cm.

d. Host limestone at the southerly dike contact of the Murrindal dike seen by cathodoluminescence (CL). The dike would have been at the right edge of the photograph. Note the bright CL in the host rock accompanied by recrystallization at the dike contact. The darkened area seen in Plate 2-1c roughly corresponds to the areas of bright CL but note that the view, although seen in the same sample, is not the same view as Plate 2-1c. Note the rapid decrease in CL brightness and the increasing preservation of fossils and the burial cements (especially the CL zones, see arrow) away from the dike contact. Field of view is about 1 cm.

e. Another view of the host limestone at the southerly dike contact of the Murrindal dike seen in a thin section under transmitted white light illumination with uncrossed polars. The dike was at the right edge of the photograph. Note the well preserved, stellate-shaped fossil some 8 mm away from the dike contact. The fossil is about 1.5 mm across.

f. A 3 by 6 mm roughly ellipsoidal-shaped pore now filled with burial cement seen by cathodoluminescence (CL). The pore is located about 2 cm away from the dike contact in the host limestone near the southerly dike contact of the Murrindal dike. The pore shows the following cementation sequence from earliest to latest (all calcite): 1) early dull or no CL; 2) bright CL in thick bands to rhombic or trigonal shape; 3) early dull and bright CL, thinly banded 4) late dull or no CL; 5) opaque minerals (arrow) on the late dull or no CL cement 6) late banded dull and bright CL with opaque minerals. Pyrite may also occur as a phase in the host rock. Field of view is about 1 cm.

g. Stylolites (arrow) crosscutting burial cements seen under cathodoluminescence excitation. Sample taken 54 cm from the northerly dike contact of the Murrindal dike. The vein here is clearly cut by the stylolite but that in outcrop near the Murrindal dike the veins crosscut and fill the stylolites and are clearly post-stylolite. Field of view is about 0.3 mm.

h. Fluid inclusions along healed fractures that crosscut burial cement 16.1 m north of the northerly dike contact of the Murrindal dike seen in a thin section under transmitted white light illumination with uncrossed polars. The rhombic-shaped fluid inclusion (arrow) is 8 microns across. The fluid inclusion above the marked inclusion has a much higher vapor to liquid ratio. The two fluid inclusions also have the appearance of inclusions that have necked down after trapping and are useless for geothermometry. Note the lack of usable fluid inclusions in the cement outside of those fluid inclusions in the secondary planes. Field of view is about 0.3 mm.

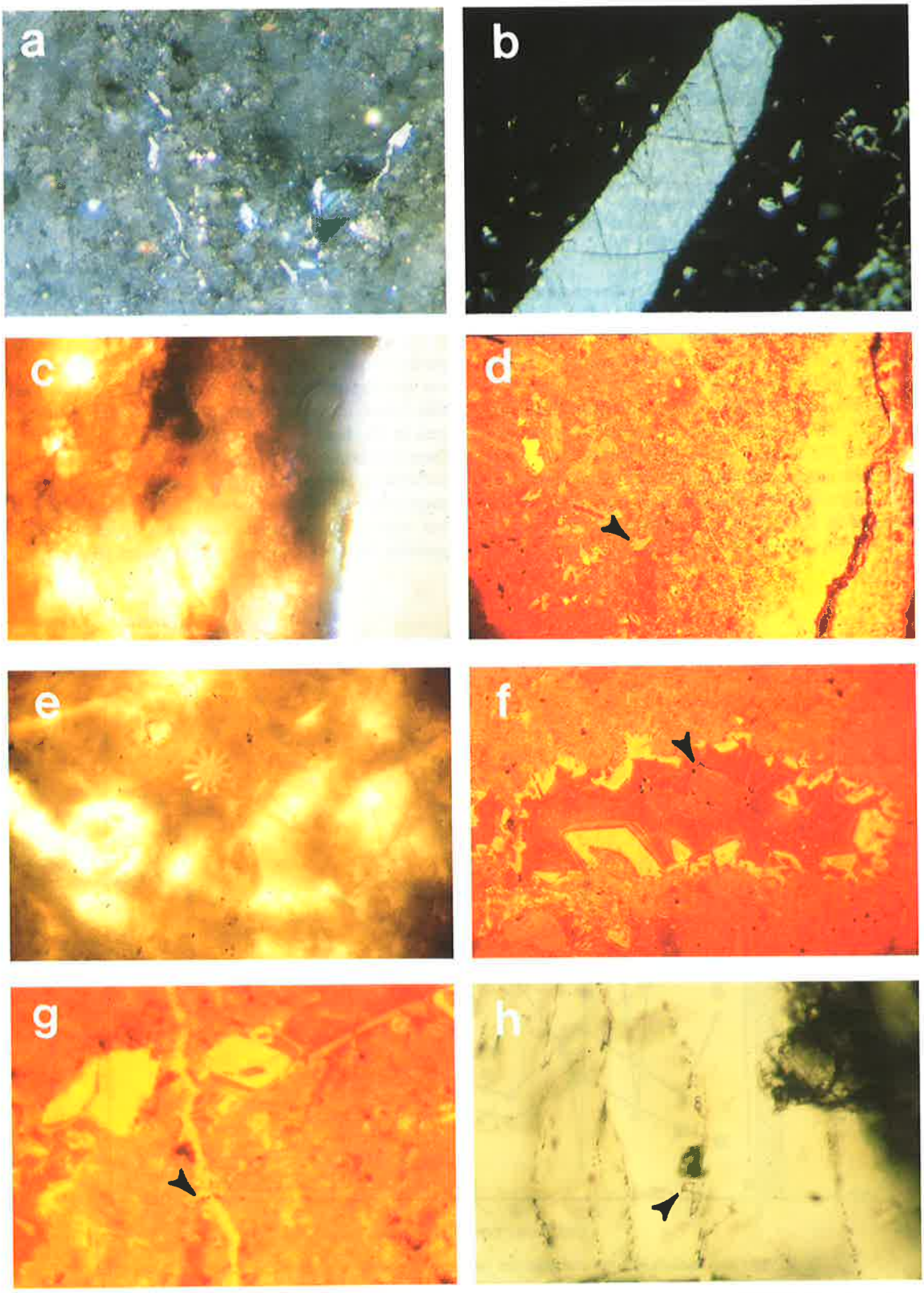
a
b
c
d
e
f
g
h

Host Rock Petrography

Host rock petrography also shows little or no systematic change except at the immediate dike contact. The host rock is darkened next to the dike for the first few centimeters away from the contact in what is commonly called the bake zone (Plate 2-1c). Except for a few centimeters next to the dike, however, these rocks do not record being heated much above regional T_{peak}. The discoloration of the host rock at the contact is one of the few metamorphic effects found and it is restricted to a narrow band next to the dike. The cathodoluminescence (CL) character of the samples near the dike (Plate 2-1d) is of a bright orange yellow within a few millimeters of the contact, which initially overprints all other features and is quite homogeneous in color. The bright CL near host rock contact with the dike decreases to a dull yellow-orange background illumination a few centimeters away. Micro-fossils are recrystallized and or obliterated near the dike contact (Plate 2-1d) but in some cases, are seemingly unaltered as close as 1 cm to the dike contact (Plate 2-1e). Similarly, trace element zonation revealed by CL is obliterated near the dike contact but a few centimeters away shows sharp banding in CL; this suggests that no CL-active trace element migration took place at the high temperatures reached there (Plate 2-1d and 2-1f) .

The detailed CL character of burial cements has been reported by Harrington (1993). Like our own observations on burial cements deposited near the Murrindal dike, Harrington observed a typical burial cementation sequence in the Buchan Group limestones. The initial cement in samples near the Murrindal dike is a thin layer of discontinuous dull or non-luminescent calcite (Plate 2-1f) typical of that which is precipitated from an oxidized fluid. On the early dull CL cement, or in some cases precipitated directly on the host rock, is subhedral to euhedral dolomite (not illustrated). The dolomite mostly shows no CL and in transmitted light consists of a transparent rim on a solid-inclusion rich, semitransparent crystal. The dolomite locally contains thin zones that show an orange-red CL. The next younger cement is calcite that has a bright yellow CL and a thick banded to a blocky form. This blocky calcite

was followed by a relatively thin band of fine zoned bright and dull CL calcite. This early fine-zoned calcite fills in most of the remaining pore space and is probably the result of precipitation in a changeable fluid chemistry, most likely the result of alternate passage of relatively oxidized meteoric and reduced basinal fluids at intermediate burial levels. The early fine-zoned cement is followed by a more uniformly dull CL calcite cement, representing a somewhat steady level of reduction during calcite precipitation, possibly induced by deep burial. The dull cement which is followed by a late cement shows thin zones of bright and dull CL that are probably the result of a changeable level of reduction in the environment during precipitation. In the context of the Buchan Rift burial history presented below and the interpretation of Harrington (1993), the burial cement sequence can be inferred to record the passage of the Buchan Group limestones through deep burial into relatively reduced fluids at about 3 km and continued cementation as exhumation allowed the introduction of less reduced fluids into the rock. Stylolites commonly cut across the entire burial cement sequence and, locally, cut across the late veins (Plate 2-1g).

Calcite veins of moderate to bright yellow-orange luminescence crosscut all of the burial cement features and most of the stylolites. These late calcite veins locally fill what were open stylolites near the Murrindal dike we studied are likely to have formed after, or during, exhumation. The veins are subparallel to healed fractures that contain common fluid inclusions (Plate 2-1h) having variable vapor to liquid ratios and containing fresh water (evidence presented below). The CL activity in these late veins may be related to some moderate yellow-orange CL bands (as well as dull bands) observed in calcareous laminated flowstone lining cavernous pores at Rocky Camp Quarry near Murrindal. A late cement with a bright yellow-orange CL apparently related to these veins locally replaces the burial cements and fills remaining pore space (which is mostly secondary porosity). These features suggest that the late veins and the bright yellow CL replacive cements are related to the Tertiary to recent karst formed in the Buchan Rift (Finlayson et al., 1992).

The CL petrography suggests a relatively complete record of the cementation history in the Buchan Group limestones but unfortunately reliable fluid inclusions for homogenization study are lacking in the samples examined. Near the Murrindal dike usable fluid inclusions were found only in the veins and healed fractures crosscutting the burial cements and stylolites. Usable fluid inclusions are those large enough to monitor during heating under the optical microscope and those present in a cement that is transparent enough so that the increasingly small vapor bubble can be observed close to T_h. Some very small (<2 μm) fluid inclusions were noted in sparry or neomorphic calcite but they proved to be unusable in our heating stage. Note that portions of the polished thin sections used for CL were not subsequently used for fluid inclusion analysis because Barker (1992) has shown that heating by the electron beam can reequilibrate fluid inclusions to over 200°C.

For reliable fluid inclusion geothermometry, among other factors, a single phase must be trapped in the inclusions, if the measured homogenization temperatures are to have meaning as a temperature of formation or peak burial temperature. This is not the case for the usable fluid inclusions trapped near the Murrindal dike. A crushing stage study using glycerine immersion and the method of Roedder (1984) shows that fluid inclusions in healed fractures crosscutting the burial cements sometimes contain a non-condensible gas. T_h measured in the two phase fluid inclusions are erratic, ranging from 73°C to 355°C, and commonly the fluid inclusions decrepitate upon heating. The wide range of T_h, together with the near fresh water in the inclusions (mean freezing point temperature of -0.1 °C for seven inclusions) and the presence of single phase inclusions along with ones of a variable vapor to liquid ratio (Plate 2-1h) all suggest that the fluid inclusions were formed by two-phase trapping in the vadose zone. T_h measured in such inclusions are considered unsuitable for geothermometry. These fluid inclusions are likely associated with fresh water recharge during the Late Cretaceous to Tertiary uplift of the area and subsequent karst formation in the Tertiary to present.

2.6 DISCUSSION

The data suggest that the Buchan Group limestones within the Buchan Rift underwent widespread moderate to high temperature burial heating. Burial history reconstruction indicates that the moderate to high temperatures were established in the Middle Devonian. The fission track data of Dumitru et al. (1991) suggests cooling to below 60°C before the Permian. These preexisting moderate burial temperatures seem to have muted the response of the rocks to contact metamorphism (heating) by the Tertiary(?) dikes.

In addition to the effect of the preexisting moderate burial heating, the lack of alteration away from the dike contact, as shown by the fluid inclusion and other data, may have been caused by the rocks being above the water table (vadose zone) during intrusion. Even if phreatic conditions existed during intrusion, these rocks only have about 5% porosity, a level that was probably reached during diagenesis in the Paleozoic and thus allowed little water to be held in the rock for enhancing metamorphism. We assert that those relatively dry, unsaturated conditions inhibited metamorphism. This hypothesis is different from the conclusions of Raymond and Murchison (1988) who conclude that in the rocks they studied, those that had less water in them during intrusion showed more pervasive metamorphic effects. Although the Murrindal rocks are much different from those studied by Raymond and Murchison (1988), we see a potential problem with their hypothesis in that the heat transmitted to the pore water in the water-rich rocks still must dissipate either by convection or conduction through the nearby rocks (Delaney, 1982). This heat, whether transmitted by conduction or convection is still available to metamorphose the organic matter in nearby rocks, if they have been exposed only to lower temperatures before intrusion. We agree with Raymond and Murchinson that rocks of increased thermal maturation show less metamorphism.

Goodarzi et al. (1989) reported that solid bitumen in algal stromatolitic limestones with interbedded dark gray shale of the Late Proterozoic Artillery Lake Formation in Canada shows little response to diabase dikes (up to 60 m thick) of the 1.2 Ga Mackenzie dike swarm. In this

case, the Artillery Lake Formation likely reached its thermal peak during pre-intrusive regional metamorphism to lower greenschist facies rather than during dike intrusion. The solid bitumen has a regional reflectance range of 3.5 to 4.5% equivalent to a T_{peak} of 220 to 270°C (Fig. 2-7 and 2-8) in fair agreement with the lower greenschist facies found in these rocks. Locally the solid bitumen has a cenospheric texture (a pyrolitic carbon) that is the result of sudden and very high temperature alteration of solid bitumen that may be related to the effect of the dikes. However, Goodarzi et al. (1989) state that field observations (we speculate they mean bake zones) show that metamorphic effects are restricted to a few centimeters of sedimentary host rock at the contact. In any case, the lower greenschist facies of the rocks attained before intrusion is consistent with our observations of a minimal response of the previously heated sedimentary host rocks to the contact metamorphism.

2.7 CONCLUSIONS

1. The Buchan Group in the Buchan Rift has undergone widespread burial heating to near 200°C.
2. Peak temperature occurred during a high heat flow period that coincided with maximum burial at about 380 Ma and with the onset of the Tabberabberan Deformation.
3. The proportion of solid bitumen grains with finely granular mosaic texture increases towards the dike and is one of the major responses of the host rock to contact metamorphism. CL shows that the host rock is recrystallized at the contact but a few centimeters away is unaffected by the intrusion. The regional moderate reflectance of the solid bitumen, which is similar to that observed next to the dike, also indicates the bitumen went through the regional peak temperature period in the Devonian and thus was present in the Buchan Group before the dike was intruded in the Tertiary.
4. A preliminary study suggests that solid bitumen reflectance shows a strong correlation with the peak temperature and is useful as a geothermometer.

2.8 SUMMARY OF CHAPTER 2

A 2.2 m thick, Late Eocene(?) dike that intruded the Devonian Buchan Caves Limestone, near Murrindal, Victoria has produced a narrow contact aureole only centimeters wide in the adjacent host rock. Mean solid bitumen reflectance ranges from about 2.4 to 2.7% and shows little change up to 6 m away from the dike contact. Carbon and oxygen isotope values also show little change except at the dike contact. The most detectable response of the rock to contact metamorphism is the proportion of solid bitumen grains with finely granular mosaic structure increase towards the dike. Also under cathodoluminescence (CL) excitation, the host rock is initially observed to be recrystallized to a uniform bright orange color. By 1 cm away from the contact, however, CL shows preservation of sharp boundaries in finely zoned burial cements.

A regional study of thermal maturation and a geothermometer based on solid bitumen reflectance indicate paleotemperatures near 200°C were widespread in the Buchan Rift during peak burial near the time of the Devonian Tabberabberan Deformation. The lack of response of the Buchan Caves Limestone to contact metamorphism is attributed to: 1) prior heating to near 200°C; and 2) the fact that the dike intruded into cool, near surface, low-porosity rocks which may have been in the vadose zone.

Implications to the Gippsland Basin Study

Prior burial history is a key factor in determining response of rocks to intrusion. This study of the Buchan Caves Limestone shows that short term contact metamorphism reached temperatures up to 400°C above the prior $T_{peak,}$ yet little reaction was detected in the host rocks. Areas of low thermal maturity are required for study if a response to intrusion is to be detectable well away from the dike.

Chapter 3.

Origin and Burial History of the Strzelecki Group, Western Onshore Gippsland Basin

3.1 MESOZOIC AND CENOZOIC EVOLUTION OF THE SOUTHEAST MARGIN OF AUSTRALIA

Southeast Australia was tectonically stable from the Permian to early Jurassic with only minor subsidence and consequently little sedimentation (as described in Chapter 2). Starting in the Latest Jurassic, however, tectonism along with major sediment accumulation has dominated the evolution of southern Australia in the Mesozoic and Cenozoic. The Otway, Bass and Gippsland Basins of southern Victoria (Fig. 3-1), were all initiated in the Latest Jurassic to Early Cretaceous with the opening of a narrow trough called the Otway rift. This initial rift was related to the separation of Australia from Antarctica that later led to sea floor spreading and the present configuration of the continents (see reviews by Lowry, 1988; Smith, 1988; Mebberson, 1989; Lowry and Longley, 1991; Duddy and Green, 1992; Willcox et al. 1992). In the Otway Rift, the Upper Jurassic-Lower Cretaceous Otway and Strzelecki Groups were deposited. The Gippsland Basin and Bass Basins are now separated from the Otway Basin by the King Island/Mornington Peninsula basement ridge. The Gippsland Basin is separated from the Bass Basin by the Bassian Rise. This discussion focuses on the Gippsland Basin.

Fig. 3-1. The initial stage of rifting that led to the separation of Australia and Antarctica (from Webb, 1991). Later in the Cretaceous sea floor spreading commenced in the area of the Tasman Rift and Southern Ocean and opened the Tasman Seaway. The Lord Howe Rise then continued on an eastward drift.

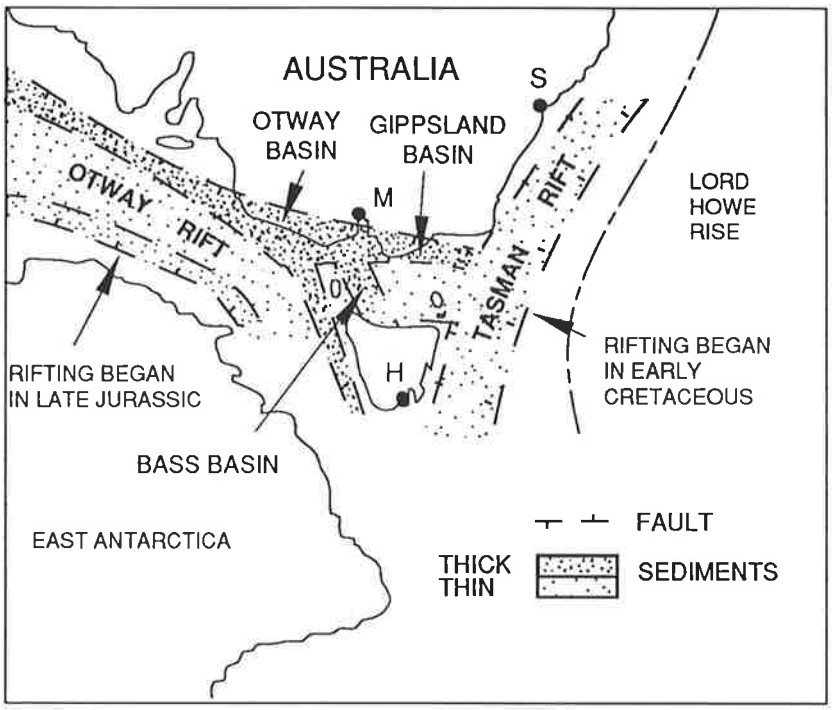
AUSTRALIA
S
OTWAY BASIN
GIPPSLAND BASIN
M
OTWAY RIFT
TASMAN RIFT
LORD HOWE RISE
RIFTING BEGAN IN LATE JURASSIC
H
RIFTING BEGAN IN EARLY CRETACEOUS
BASS BASIN
EAST ANTARCTICA
FAULT
THICK
THIN
SEDIMENTS

Fig. 3-2. Schematic of the main structural features, Gippsland Basin Region, Victoria (modified from Duddy and Green, 1992). Hatchered areas indicate the Strzelecki Ranges where the Strzelecki Group is exposed and this portion of the study was conducted. The dotted line shows the position of the King Island/Mornington Peninsula Basement Ridge.

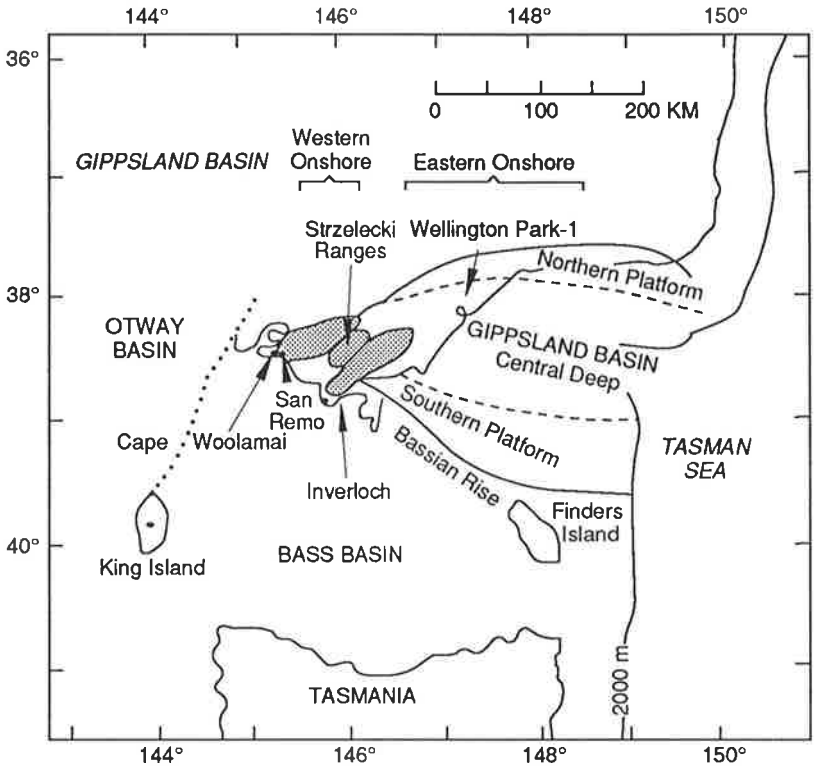
144°
146°
148°
150°
36°
38°
40°
0
100
200 KM
GIPPSLAND BASIN
Western Onshore
Eastern Onshore
Strzelecki Ranges
Wellington Park-1
Northern Platform
OTWAY BASIN
GIPPSLAND BASIN Central Deep
San Remo
Cape Woolamai
Southern Platform
Bassian Rise
TASMAN SEA
Inverloch
Finders Island
King Island
BASS BASIN
TASMANIA
2000 m

The Paleozoic metasedimentary rocks and granites that underlie the initial rift and the western onshore Gippsland Basin (Edwards et al., 1944; Willcox et al., 1992) are related to Paleozoic fold and intrusion zones that form the basement rocks of southeast Australia (Fig. 3-3). These rocks are exposed in and along the flanks of the onshore Gippsland Basin at Wonthaggi, Cape Woolamai, Wilsons Promontory and in the Eastern Highlands which includes the Buchan area. The easterly trending fault zones that formed during the initial rifting phase in the Gippsland Basin truncate the northerly trending Paleozoic basement structures (Fig. 3-3). Into this initial rift poured the wholly non-marine, volcaniclastic, quartz-poor sediments composing the Strzelecki Group. The offshore boundaries of this initial rift and related deposition are the Gippsland Rise at 149-150°E longitude in the Tasman Sea (Megallaa, 1993) and the Bassian Rise to the south. The western edge of the onshore Gippsland Basin is inferred to be the King Island/Mornington Peninsula Basement Ridge on the west. Further evidence for the edge of the basin are conglomerates in the Strzelecki Group exposed near San Remo that contain clasts derived from local basement rocks. The northern edge is in the vicinity of Latrobe Valley where the Neocomian age Tyers Conglomerate and Rintouls Creek Sandstone overlie Silurian basement at Tyers Creek (Edwards and Baker, 1943; Holdgate and McNichol; 1992). These strata form the best reservoir rocks yet found in the Strzelecki Group. Similar reservoir rocks may lie along the edges of the initial rift as it is likely that there are multiple source points of coarse sediment all along the length of what was apparently a rapidly subsiding, steep sided, narrow structural valley (Edwards and Baker, 1943 and Fig. 3-1). Because the downward migration of hydrocarbons is difficult, the source of the hydrocarbons to charge these reservoirs would likely be the associated coaly SOM in the Strzelecki Group itself.

Fig. 3-3. Structural zones of Victoria, showing the Paleozoic tectonic zones and overlying Mesozoic Basins. Modified from Ramsay and VandenBerg (1990). Pz = Paleozoic and Mz = Mesozoic.

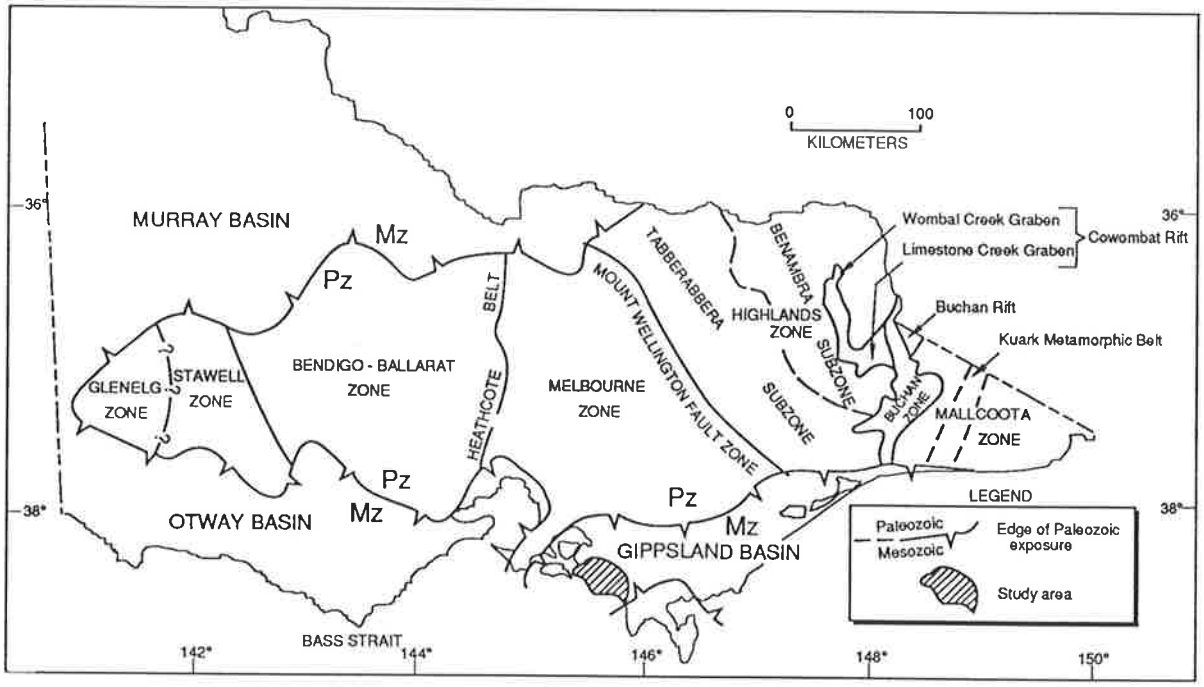
0
100
KILOMETERS
36°
38°
MURRAY BASIN
Mz
Pz
BELT
HEATHCOTE
BENDIGO - BALLARAT ZONE
GLENELG ZONE
STAWELL ZONE
MELBOURNE ZONE
TABBERABBERA
MOUNT WELLINGTON FAULT ZONE
BENAMBRA
HIGHLANDS ZONE
SUBZONE
SUBZONE
BUCHAN ZONE
Wombat Creek Graben
Limestone Creek Graben
Cowombat Rift
Buchan Rift
Kuark Metamorphic Belt
MALLACOOTA ZONE
OTWAY BASIN
Pz
Mz
GIPPSLAND BASIN
Pz
Mz
BASS STRAIT
142°
144°
146°
148°
150°
LEGEND
Paleozoic
Mesozoic
Edge of Paleozoic exposure
Study area

At the end of the Early Cretaceous, Australia separated from Antarctica but this final breakup did not extend along the Otway Rift faults into the Gippsland Basin. Instead the continents parted along western Tasmania with the commencement of Southern Ocean spreading (Fig. 3-1). The breakup at the end of the Early Cretaceous induced uplift and a major unconformity marked by deep erosion of the Strzelecki Group around the edge of the initial rift in the Gippsland Basin (Fig. 3-4) . In the mid Cretaceous, a dike swarm intruded the western Gippsland Basin (Duddy and Green, 1992). This 100 to 85 Ma dike swarm is probably related to changes in the stress regime during a shift in spreading from the Southern Ocean to the Tasman Sea (Duddy and Green, 1992) rather than the later 80 Ma opening of the Tasman Sea or subsequent intrusion and extrusion of the Older Volcanics (Day, 1983). Contact metamorphism of the Strzelecki Group by these dikes is the focus of this portion of the study.

In the mid Cretaceous, continuing rifting and the breakaway of Australia from Antarctica and the Lord Howe Rise was accompanied by 1 to 3 km of rapid uplift and erosion (Dumitru et al., 1991; Duddy and Green, 1992). The uplift was initiated in a broad area around the rifted continental margin of southeast Australia in the area of what is now the Tasman Sea and Bass Strait coastal regions. This same Late Cretaceous uplift and erosional event formed the Eastern Highlands and in the Tertiary led to the development of the Buchan karst (Webb et al., 1991).

Fig. 3-4. Generalized stratigraphy and a tectonic, thermal, and fluid development history in the Gippsland Basin, Victoria. Stratigraphy and tectonics based on Lowry and Longley (1991) and Duddy and Green (1992). The burial history reconstruction for the western onshore Gippsland Basin uses that of Duddy and Green (1992) which is based on AFT age measurements. This evidence is supplemented by the surface temperature history, T_{peak} and diagenetic history data developed in this study. The hydrocarbon generation history is largely notional based on the general course of hydrocarbon generation outlined by Tissot and Welte (1984) and Stach et al. (1982).

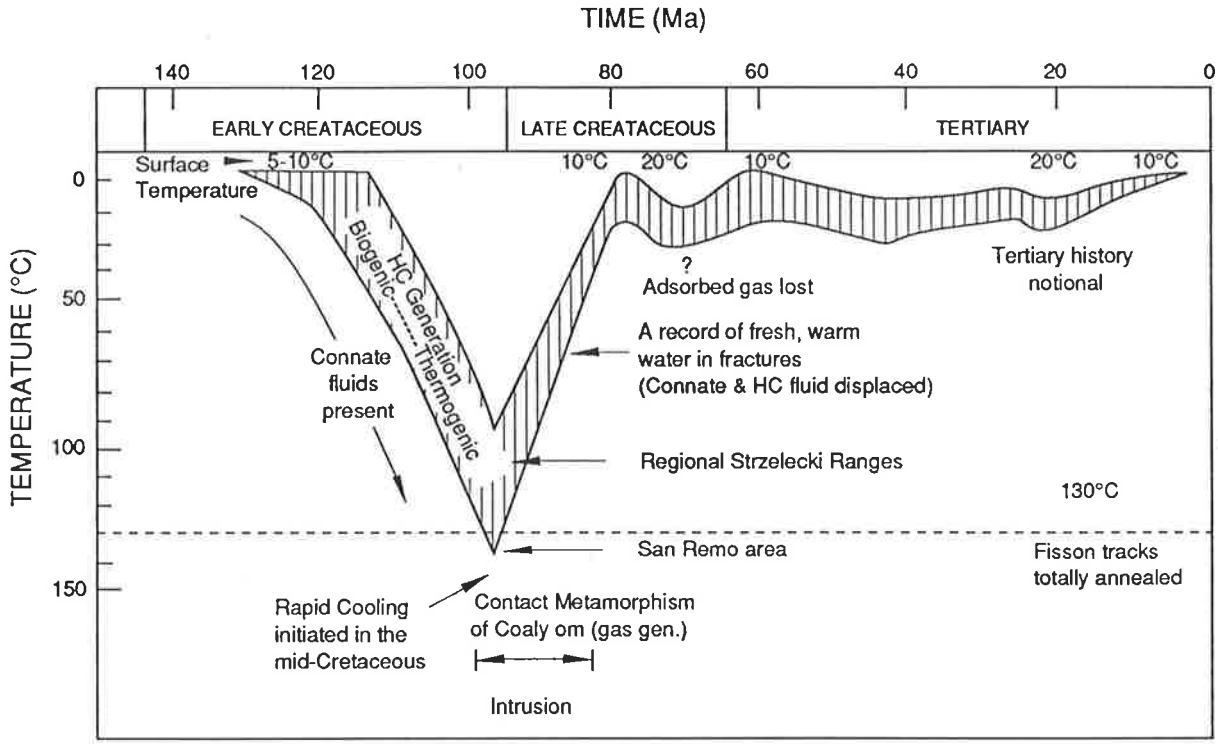
TIME (Ma)
140
120
100
80
60
40
20
0
EARLY CREATACEOUS
LATE CREATACEOUS
TERTIARY
TEMPERATURE (°C)
0
50
100
150
Surface Temperature
5-10°C
10°C
20°C
10°C
20°C
10°C
Biogenic
HC Generation
Thermogenic
Connate fluids present
?
Adsorbed gas lost
Tertiary history notional
A record of fresh, warm water in fractures (Connate & HC fluid displaced)
Regional Strzelecki Ranges
130°C
San Remo area
Fisson tracks totally annealed
Rapid Cooling initiated in the mid-Cretaceous
Contact Metamorphism of Coaly om (gas gen.)
Intrusion

This erosion event removed about 2 km of the Strzelecki Group from the western Onshore Gippsland Basin and apparently removed any flows that are related to the mid Cretaceous dike swarm. Another effect of this mid Cretaceous uplift was the formation of new basin margins and a reduced basin area for Late Cretaceous to present sedimentation in the Gippsland Basin. This later sedimentation has mostly occurred in the eastern onshore and eastern central deep areas of the Gippsland Basin.

A second phase of rifting was initiated during the mid to Late Cretaceous by the shift to northwest-southeast directed crustal extension in the Tasman Sea. This rifting phase was accompanied by deposition of the nonmarine Golden Beach Group in the Gippsland Basin over locally deformed and eroded Strzelecki Group (Lowry and Longley, 1991). This deposition apparently did not occur in the western onshore Gippsland Basin. The Golden Beach Group is composed of quartz-rich fluvial sandstones with thick lacustrine mudrock and some basalt flows. The lack of appreciable volcanic detritus in the Golden Beach Group marks the end of the voluminous Early Cretaceous volcanic activity in the vicinity of the Otway and Gippsland Basins (Gleadow and Duddy, 1981; Duddy, 1983; Duddy and Green, 1992). Post mid-Cretaceous reservoir quality is generally far better than that found in the Strzelecki Group where diagenesis of the unstable volcanic fragments, compaction and carbonate cementation has mostly obliterated porosity.

A final phase of sedimentation occurred during the Late Cretaceous and has generally continued to the present. This renewed sedimentation was caused by the onset of Tasman Sea spreading occurring between Australia and Lord Howe Rise and associated sagging of the Gippsland Basin fill. The final phase of thick sediment deposition occurred in the eastern portions of the Gippsland Basin and did not effect the western onshore Gippsland Basin. During this period, intermittent compression or wrenching formed more hydrocarbon traps. The last phase of sedimentation is initially marked by deposition of the mostly non-marine quartz-

rich sediments of the Lower Latrobe Group. Subsidence was much greater along the northern margin of the later rift, resulting in markedly thicker sediments in this region (Mebberson, 1989). A period of compression occurring in the Late Eocene to mid Miocene produced many of northeast trending anticlines which later trapped large hydrocarbon volumes in the eastern offshore Gippsland Basin. All major hydrocarbon discoveries are in the Upper Latrobe Group in fluvial to shallow marine facies (Traralgon Formation in part) sealed by transgressive marine shale or igneous rocks (Mebberson, 1989; Willcox et al., 1992). In the northern onshore Gippsland Basin, non-marine sedimentation continued from the Paleocene to Late Miocene with predominantly non-marine rocks of the Latrobe Valley Group (Bolger, 1991). Upper Latrobe Group deposition continued in the coastal portions of the Gippsland Basin. Offshore, the Eocene to Oligocene marine mudstone of the Gurnard Formation was deposited over the Upper Latrobe Group. Commencing in the Late Oligocene to Miocene and continuing to the present, a major marine transgression is marked by the deposition of marine mudstone, marl and limestone of the Seaspray Group in the central deep and initially on the northern platform portions of the Gippsland Basin. In the northern Gippsland Basin, non-marine deposition continued from the Pliocene to the Pleistocene with the clastic rocks of the Sale Group (Bolger, 1991).

These tectonic and sedimentary processes have resulted in a present day Gippsland Basin that is an easterly oriented complexly faulted and folded graben-like feature that initially deepens and becomes wider to the east (Ozimic et al., 1987). Seismic data suggest the Gippsland Basin may contain up to 12-14 km of sediment in a depocenter structurally bounded on the north and northwestern margins by a detachment ramp and on its southerly side by a listric fault system (Willcox et al., 1992). The eastern margin is open to the Tasman Sea. On the southwest, the basin is bounded by the Bassian Rise between Wilsons Promontory and Flinders Island which structurally separates the Gippsland Basin from the Bass Basin. The

Northwestern margin of the onshore portion of the Gippsland Basin is approximately formed by the Mesozoic exposures in Western Port Bay trending northeast from Phillip Island. The northern margin is formed by the Eastern Highlands. The basin fill forms a triangular wedge of a 41,000 km^2 area with 25 percent of the area onshore Thompson (1986). The restored total thickness of the Strzelecki Group is about 3.5 km. Thompson (1986) estimated some 4.5 km of post Early Cretaceous fill in the central deep. The offshore Gippsland Basin contains some 3.6 billion barrels of oil and 8.8 trillion cubic feet of gas (Carmody, 1992) dominantly sourced from humic SOM (Powell and Boreham, 1994).

3.2 THE STRZELECKI GROUP

The Strzelecki Group beds are exposed in two areas of South Gippsland: 1) A northern band, forming the study area, in the Strzelecki Ranges extending northeast from San Remo and Inverloch on the coast to Korumburra and Loch (Fig. 3-5) and onward to Moe; and 2) A southern band extending northeast from the northern portion of Wilsons Promontory. Almost all reported dikes are located in the northern band of the Strzelecki Group, as are the thicker coal beds. The northern band of exposures were sampled for this study. In the western Onshore Gippsland Basin, most major structural features trend northeast. Most dikes trend northwest but two dikes used in this study, trend northeast (Korumburra 1) and north (Cruickston 1). The exposures are bounded by faults and consist of two uplifted blocks, the westernmost one forming the San Remo Peninsula and the western part of the Strzelecki Ranges (Douglas et al., 1988). This block has a gentle northerly dip (Edwards, 1942). The Cape Paterson area dips to the south. The Strzelecki Group is covered by Tertiary sediments and basalt of the Older Voclanics in the Tarwin River Valley to Leongatha areas and to the north of Poowong and Nyora. Tertiary sediments and Older Voclanics mostly cover the Strzelecki Group in the Western Port Bay and Bass River areas.

Provenance

As discussed further in Chapter 4, the provenance of the Strzelecki Group is important to this study because it suggests the types of inherited fluid inclusions possible in the sediment.

The Strzelecki Group in the Gippsland Basin consists of alluvial fan and fluvial deposits formed by a rapid infilling of the initial Gippsland Basin rift by solely non-marine volcaniclastic and lithic sediments derived from the adjacent highlands. The volcanic rocks are thought to be derived from igneous activity penecontemporaneous with the initial rifting. Edwards and Baker (1943) discuss evidence that the rift escarpment was steep. The presence of Tyers Conglomerate in the basal portions of the Strzelecki Group (Fig. 3-6), and other conglomerates in the San Remo Area (Smith, 1988), suggests the source areas were not far removed from the margins of the initial rift.

Fig. 3-5. Strzelecki Group, western onshore Gippsland Basin, showing the location of dikes studied. This area is a portion of South Gippsland area of Victoria. Details on the dike locations are given in Table 4-1. Dike acronyms are B1 = Bena 1; B3 = Bena 3; Cru1 = Cruickston 1; I1 = Inverloch 1; I2 = Inverloch 2; I3 = Inverloch 3; K1 = Korumburra 1; SR1 = San Remo 1 and SR3 = San Remo 3.

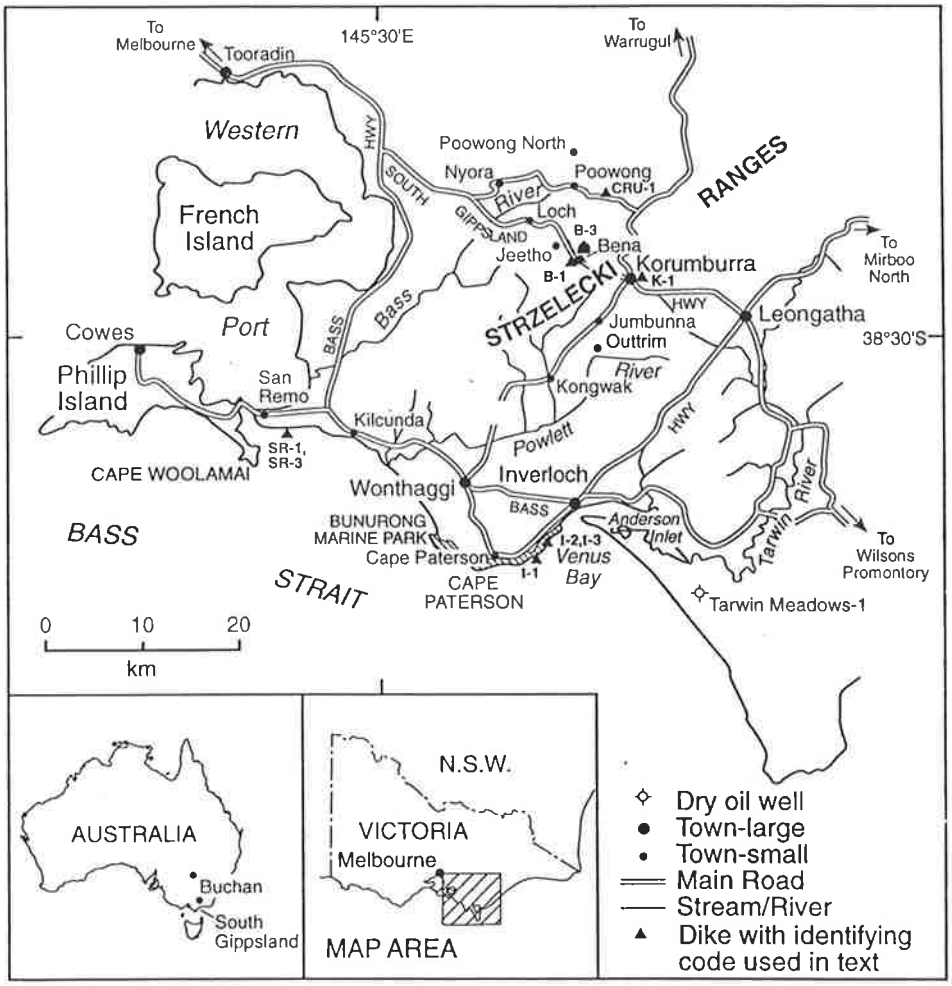
To Melbourne
Tooradin
145°30'E
To Warrugul
Western
HWY
SOUTH GIPPSLAND
Poowong North
Nyora
River
Poowong
CRU-1
RANGES
Loch
B-3
Bena
Jeetho
B-1
Korumburra
K-1
To Mirboo North
French Island
Port
Bass
BASS
STRZELECKI
HWY
Leongatha
38°30'S
Cowes
Jumbunna
Outtrim
Phillip Island
San Remo
Kongwak
River
Kilcunda
Powlett
HWY
SR-1, SR-3
CAPE WOOLAMAI
Wonthaggi
Inverloch
BASS
Anderson Inlet
Tarwin River
BUNURONG MARINE PARK
Cape Paterson
I-2,I-3
Venus Bay
I-1
CAPE PATERSON
BASS STRAIT
Tarwin Meadows-1
To Wilsons Promontory
0 10 20
km
AUSTRALIA
Buchan
South Gippsland
N.S.W.
VICTORIA
Melbourne
MAP AREA
Dry oil well
Town-large
Town-small
Main Road
Stream/River
Dike with identifying code used in text

The Tyers Conglomerate is polymictic with clasts like those found in the adjacent Eastern Highlands Paleozoic metasedimentary and igneous rocks (Holdgate and McNichol, 1992). Jenkins (1962) states that the source of a Mesozoic arkose at Ryhll on Phillip Island, apparently based on similarity of clast lithology, is the Cape Woolamai Granite just south of the exposure. At the edges of the northwestern onshore Gippsland Basin similar Paleozoic basement rocks are exposed along with the Tynong Granite (Jenkins, 1962). The metasedimentary rocks consist of cherty mudstone, mudstone, slate and sandstone. In the northern onshore Gippsland Basin, the basement consists of the Ordovician to Middle Devonian Jordan River and Wallhalla Groups with Upper Devonian Granites (Holdgate and McNichol, 1992). Direct evidence of the basement rock underlying the area are Silurian metasedimentary rocks exposed at Wonthaggi and intersected by wells in the Wonthaggi Coalfield (Edwards et al., 1944) and the Devonian granites exposed at Cape Woolamai. Along the southern edge of the onshore Gippsland at Wilsons Promontory, Devonian granites and Lower Paleozoic metasedimentary rocks are exposed. Some sedimentary rock fragments are also derived from reworked Strzelecki Group.

The Strzelecki Group is dominantly made up of volcaniclastic sediment (Edwards and Baker, 1943; Lindsay, 1982; Duddy, 1983). However, the origin of the volcaniclastic sediment is Early Cretaceous age (Gleadow and Duddy, 1981; Duddy, 1983). This origin is problematic because there are no known Early Cretaceous igneous rocks in the area. Transport from the Lord Howe Rise to the east is not considered tenable for many reasons (Gleadow and Duddy, 1981; Duddy, 1983) even though Willcox et al. (1992) reported paleocurrent markers in the Strzelecki Ranges that suggest an eastern source. The clast evidence from the conglomerates near the base of the Strzelecki Group suggest a local source, at least early in the depositional history. The presumption taken here is that the evidence for igneous activity was obliterated during the deep mid-Cretaceous erosion of southeast Australia and the problem is not

considered further here.

Petrography

The first major study of the petrography of the Strzelecki Group was made by Edwards and Baker (1943). More recently, Philip (19580, Lindsay (1982), Paten (1982), Smith (1988) and Holdgate and McNichol (1992) have studied or reviewed the petrography of the Strzelecki Group. The petrography of the related Otway Group was studied in the Otway Basin by Duddy (1983) and in the Bass Basin by Smith (1986). The results of these investigations and this study indicate that the "normal" portion of the Strzelecki Group (Fig. 3-6) is derived from a fluvial sediment with: 1) 30-40% volcanic rock fragments, mostly of intermediate composition or glassy; 2) 25-35% feldspar, mostly plagioclase and K-feldspar that are mostly cloudy; 3) 10-30% quartz, mainly monocrystalline but with locally embayed grains of volcanic origin and locally common plutonic and metamorphic polycrystalline quartz, graphic intergrowths with feldspars, or polymineralic plutonic rock fragments (as found at SR1); 4) 5-10% sedimentary rock fragments, but locally abundant with intraformational clasts composing most the rock; 5) Fossilized wood or coaly material trace to 20%, averaging an estimated 3 wt-% total organic carbon; 6) 10-20% matrix, much of which appears diagenetic and formed of chlorite, mixed-layer clay minerals, zeolite including common laumontite and carbonate and 7) 0-20% micitric or fine grained calcite or siderite, often as early displacive cement that forms concretions. There are rare quartz overgrowths and rare pore lining carbonate cements. Biotite, hornblende and pyroxene, as well as other trace mineral grains, are present (Edwards and Baker, 1943).

Original porosity is moderate to low in what was a poorly to moderately sorted grain mass. This original porosity was rapidly lost during compaction, early cementation and the formation of pseudomatrix because of the breakdown of the unstable volcanic fragments (Gleadow and Duddy, 1981; Lindsay, 1982; Duddy, 1983). Edwards and Baker (1943) report a

porosity of 2% in fresh rocks and 10% in weathered rocks similar to that determined in this study (Appendix 10). Compaction and the plastic nature of the pseudomatrix or mudstone grains has produced mostly long and concavo-convex grain contacts.

The framework grains are typically angular to subangular and may contain subrounded lithic or intraformational clasts. The modal grain size is about 150 μm but can range up to a grit or cobble conglomerate size. Polymictic conglomerates are mostly found in the basal portions of the Strzelecki Group and intraformational conglomerates sporadically occur in the section.

Overall, the Strzelecki Group is dominantly a massive bedded sandstone that is difficult to subdivide into smaller units. Its massive character is illustrated by its lack of seismic reflectors in seismic profiles and its subsurface structure is poorly known. The fluvial sandstone can also be laminated or cross-bedded. Coal and mudstone are a minor components.

3.3 BURIAL HISTORY OF THE STRZELECKI GROUP, WESTERN ONSHORE GIPPSLAND BASIN

The importance of understanding the burial history before studying thermal maturation during contact metamorphism by dikes was shown in Chapter 2. In this section the burial history of the western onshore Gippsland Basin is examined to define the burial conditions before and after mid Cretaceous intrusions before studying the contact metamorphism caused by them. More recently Duddy and Green (1992) and Holdgate and McNichol (1992) have reviewed the geology of this area. A key element of this geologic history is that after exhumation which commenced in the mid Cretaceous, the western onshore Gippsland Basin was never reburied nor generally reheated.

Reconstruction of Burial Depth and Temperature

The burial depth estimates and T_{peak} predictions from geothermal gradients are more accurate

if they consider the change of average annual surface-temperature that occurs with change in paleoclimate. Further, a 10°C change in the surface temperature during maximum burial can produce measurable changes in Rv-r. The surface temperature history for the Gippsland Basin is estimated from the paleosurface temperature reconstruction developed for the Buchan area (Fig. 2-4). This reconstruction is broadly applicable to the western onshore portion of the Gippsland Basin which has largely remained a positive erosional feature or subaerial depositional environment since the Late Mesozoic and is in close proximity to the Buchan area.

Deposition of the Strzelecki Group was commenced in the initial rift at about 140 Ma (Tithonian to Beriasian) and ceased at about 95 Ma in the Albian (Fig. 3-6) (Haskell, 1972; Holdgate and McNichol, 1992; Willcox et al., 1992). Most of the mined coals and rocks exposed in the Strzelecki Ranges are Aptian (115-110 Ma) (Gregory et al., 1989; written communication, G. Holdgate, 1994). Rapid burial to about 2 km and some 110°C occurred in the Strzelecki Ranges (Fig 3-7).

At about 95 Ma, regional erosion began. The erosion in the Gippsland Basin was associated with regional uplift of the Buchan area and southeast Australia (Dumitru et al. 1991; Duddy and Green, 1992). Depth of erosion of the Strzelecki Group is estimated at about 1 km deep on the southern platform (Mebberson, 1989), and 1.5 km at Wellington Park-1 (Fig. 3-8).

Fig. 3-6. General stratigraphy, Strzelecki Group, northern onshore Gippsland Basin. The figure is from Holdgate and McNichol (1992). The oil and gas column summarizes the oil (half moon) and gas shows (open circles) that were found in wells drilled in the onshore Gippsland area.

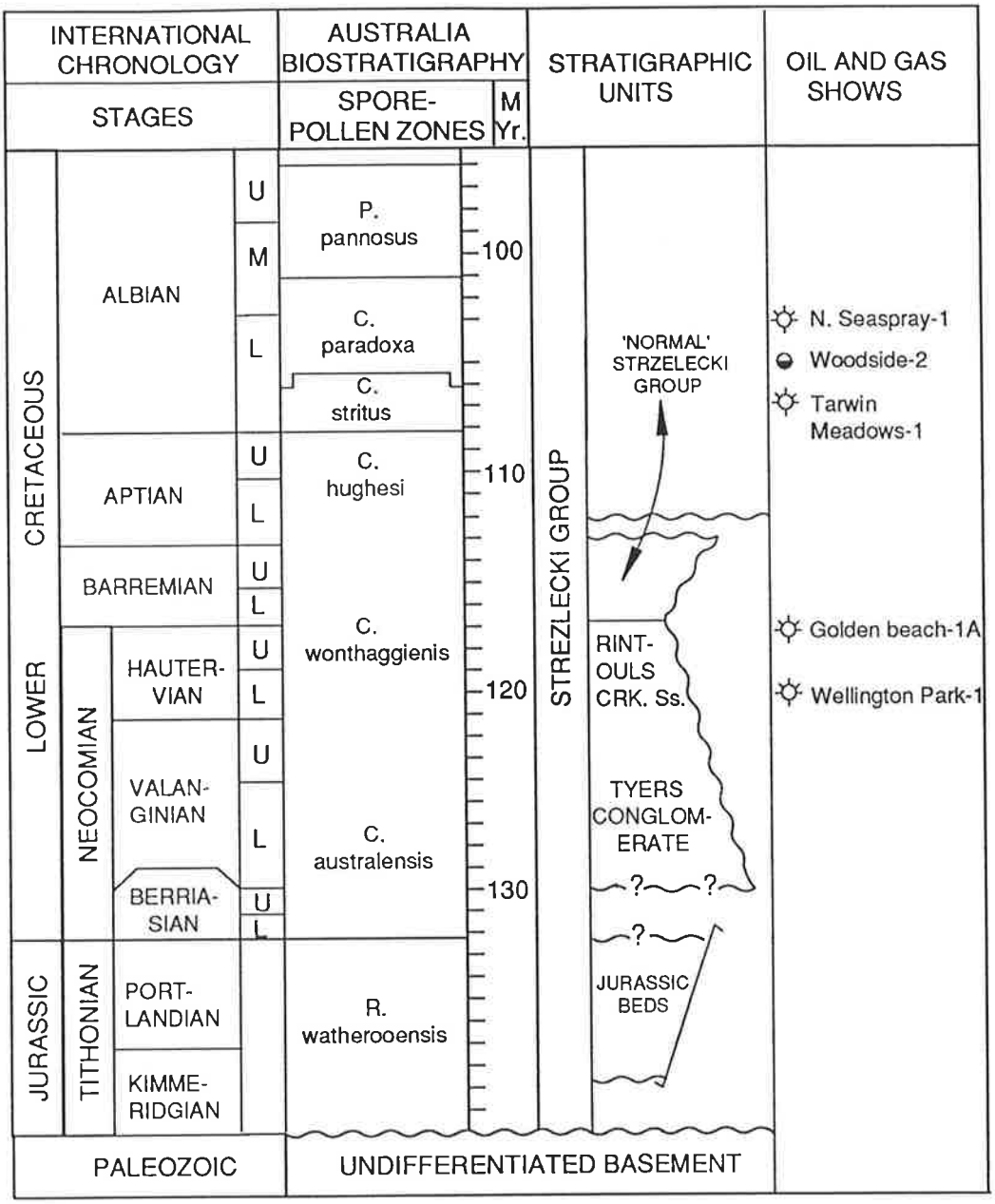
INTERNATIONAL CHRONOLOGY
STAGES
AUSTRALIA BIOSTRATIGRAPHY
SPORE-POLLEN ZONES
M Yr.
STRATIGRAPHIC UNITS
OIL AND GAS SHOWS
CRETACEOUS
LOWER
JURASSIC
ALBIAN
APTIAN
BARREMIAN
NEOCOMIAN
HAUTER-VIAN
VALAN-GINIAN
BERRIA-SIAN
TITHONIAN
PORT-LANDIAN
KIMME-RIDGIAN
U
M
L
P. pannosus
C. paradoxa
C. stritus
C. hughesi
C. wonthaggienis
C. australensis
R. watherooensis
100
110
120
130
STREZLECKI GROUP
'NORMAL' STRZELECKI GROUP
RINT-OULS CRK. Ss.
TYERS CONGLOM-ERATE
JURASSIC BEDS
N. Seaspray-1
Woodside-2
Tarwin Meadows-1
Golden beach-1A
Wellington Park-1
PALEOZOIC
UNDIFFERENTIATED BASEMENT

Fig. 3-7. Simplified thermal, fluid and hydrocarbon generation history, Gippsland Basin. The base figure is from Duddy and Green (1992). Fluid and hydrocarbon generation history from this study. Surface temperature history from Fig. 2-4. Also shown are the general times of basaltic intrusions in the Strzelecki Ranges from Duddy and Green (1992).

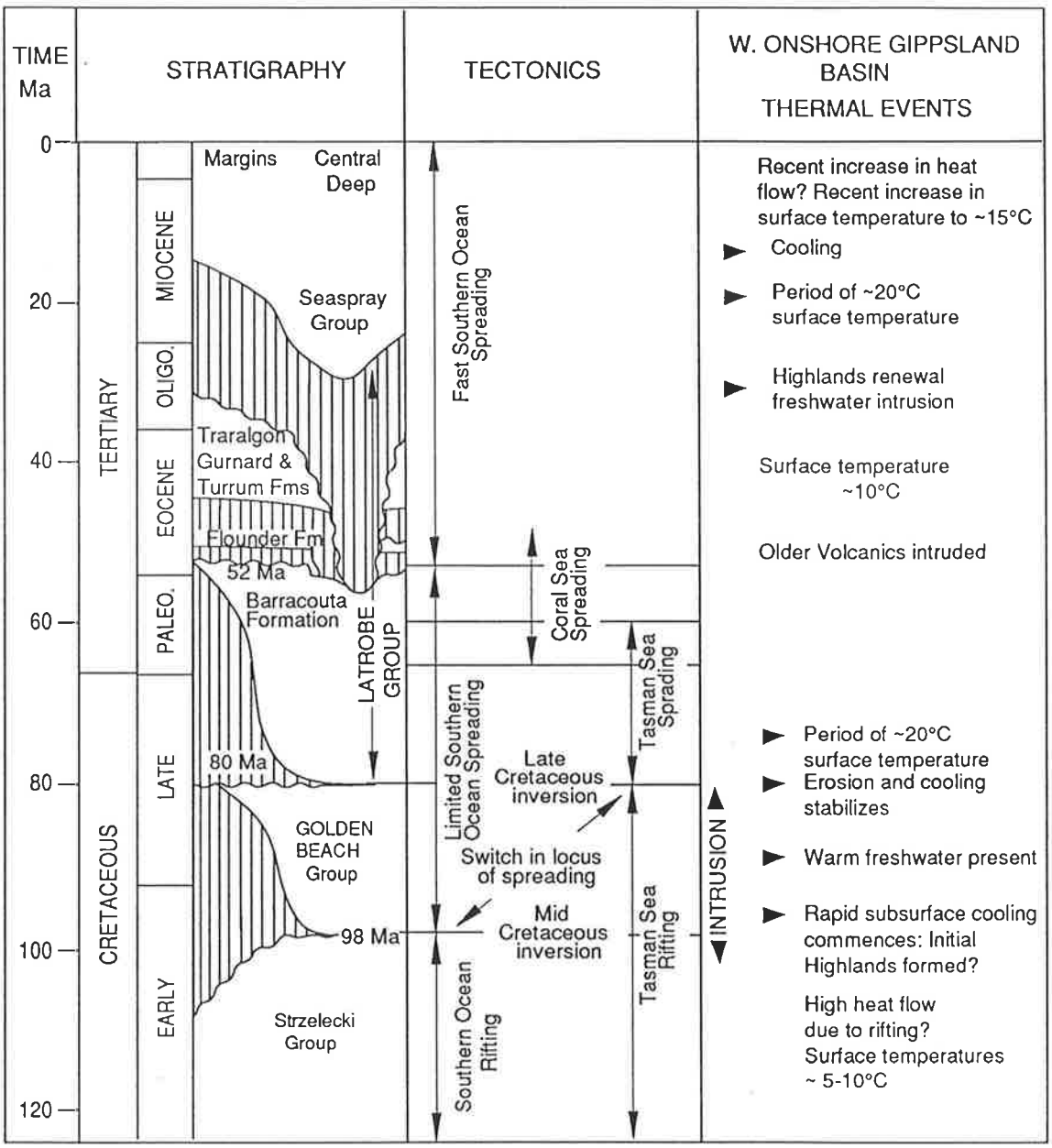
TIME
Ma
STRATIGRAPHY
TECTONICS
W. ONSHORE GIPPSLAND BASIN
THERMAL EVENTS
0
20
40
60
80
100
120
TERTIARY
CRETACEOUS
MIOCENE
OLIGO.
EOCENE
PALEO.
LATE
EARLY
Margins
Central Deep
Seaspray Group
Traralgon
Gurnard &
Turrum Fms
Flounder Fm
52 Ma
Barracouta Formation
LATROBE GROUP
80 Ma
GOLDEN BEACH Group
98 Ma
Strzelecki Group
Fast Southern Ocean Spreading
Coral Sea Spreading
Tasman Sea Spreading
Limited Southern Ocean Spreading
Late Cretaceous inversion
Switch in locus of spreading
Mid Cretaceous inversion
Tasman Sea Rifting
Southern Ocean Rifting
INTRUSION
Recent increase in heat flow? Recent increase in surface temperature to ~15°C
Cooling
Period of ~20°C surface temperature
Highlands renewal freshwater intrusion
Surface temperature ~10°C
Older Volcanics intruded
Period of ~20°C surface temperature
Erosion and cooling stabilizes
Warm freshwater present
Rapid subsurface cooling commences: Initial Highlands formed?
High heat flow due to rifting? Surface temperatures ~ 5-10°C

The depth of erosion in the vicinity of Tarwin Meadows 1 is estimated from a near surface vitrinite reflectance (Rv-r) of 0.65% measured in the well. The depth of erosion is reconstructed by using versus depth profiles. Wells penetrating uneroded rock sections have Rv-r versus depth profiles that intersect the surface at an Rv-r of about 0.2%. Projection of the Rv-r versus depth profiles (solid line) to an Rv-r of about 0.2% suggests the depth of erosion. At Tarwin Meadows 1, the estimated depth of erosion (dashed line) is about 1.5 km. This erosion estimate constitutes the minimum for the western onshore Gippsland Basin as the Strzelecki Ranges to the north and the San Remo area to the northwest are on uplifted fault blocks and are more deeply eroded.

Table 3-1. Wells studied in or near the Western Onshore Gippsland Basin

Well Name and Acronym	**Latitude (°south)**	**Longitude (°east)**	**Notes**
Tarwin Meadows-1 (TO-1)	38.7239	145.8600	Dry hole, southeast of Inverloch, Victoria in the Tarwin Meadows area. Rv-r , Rock-Eval, ^{13}C CP MAS NMR and stable isotope analyses available from this study.
Wellington Park-1 (WP-1)	38.1404	147.3750	Dry hole well in the eastern portion of the onshore Gippsland Basin. AFTA studies by Heagarty et al. (1986), and Duddy and Green (1992). Burial history study by Holdgate and McNichol (1992). Rv-r was studied by Paten (1982). Rv-r , Rock-Eval and stable isotope analyses available from this study.

Fig. 3-8. Burial history of the Wellington Park 1 well, eastern onshore Gippsland Basin. The figure is from Duddy and Green (1992) who also estimated a mid-Cretaceous paleogeothermal gradient of 45°C/km in this well. The Tertiary geothermal gradient was apparently somewhat lower. Present day geothermal gradient in the well is 44°C/Km (King et al., 1985) but this a result of a recent increase in the heat flow during the late Tertiary (Duddy and Green, 1992).

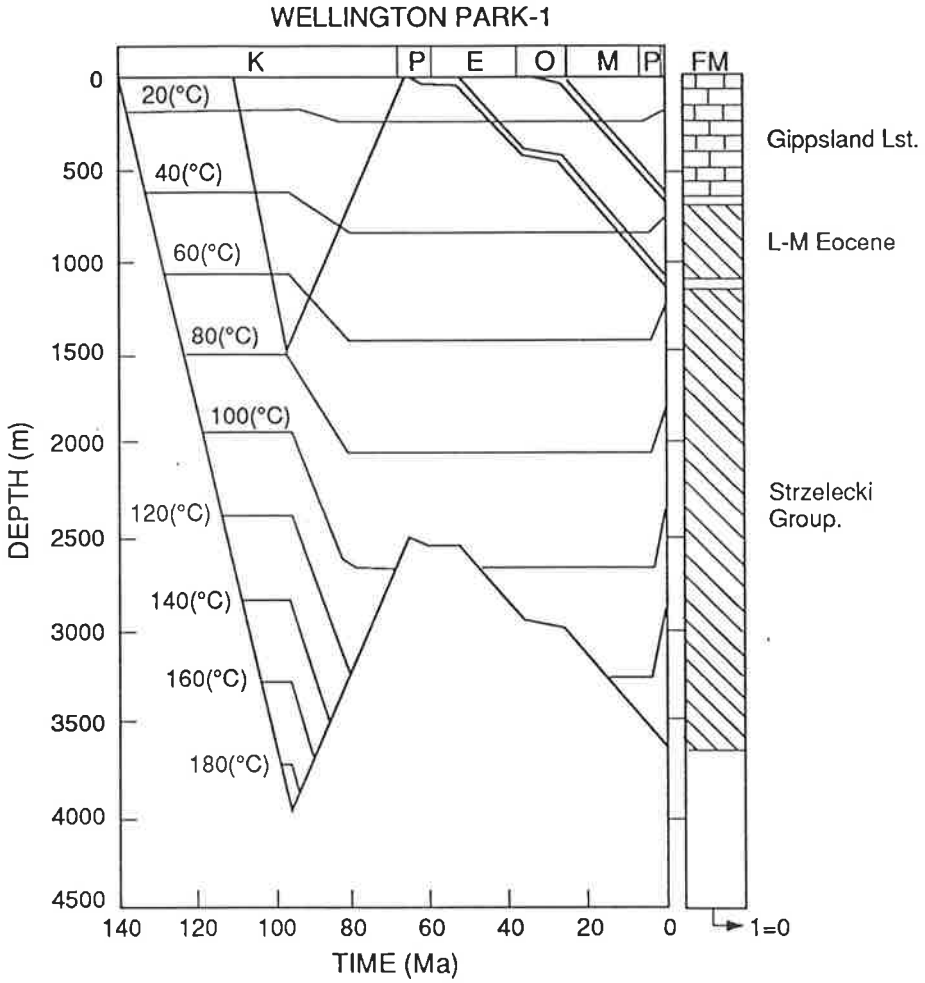
WELLINGTON PARK-1
K
P
E
O
M
P
FM
0
500
1000
1500
2000
2500
3000
3500
4000
4500
DEPTH (m)
20(°C)
40(°C)
60(°C)
80(°C)
100(°C)
120(°C)
140(°C)
160(°C)
180(°C)
140
120
100
80
60
40
20
0
TIME (Ma)
1=0
Gippsland Lst.
L-M Eocene
Strzelecki
Group.

Fig. 3-9. Erosion estimates for the Tarwin Meadows 1 well compared to that made for the Wellington Park 1 well and the San Remo area of the western onshore Gippsland Basin. As explained in the text the depth of erosion is reconstructed by projecting Rv-r versus depth profiles to a surface value of 0.2% Rv-r that is found near the surface of uneroded areas.

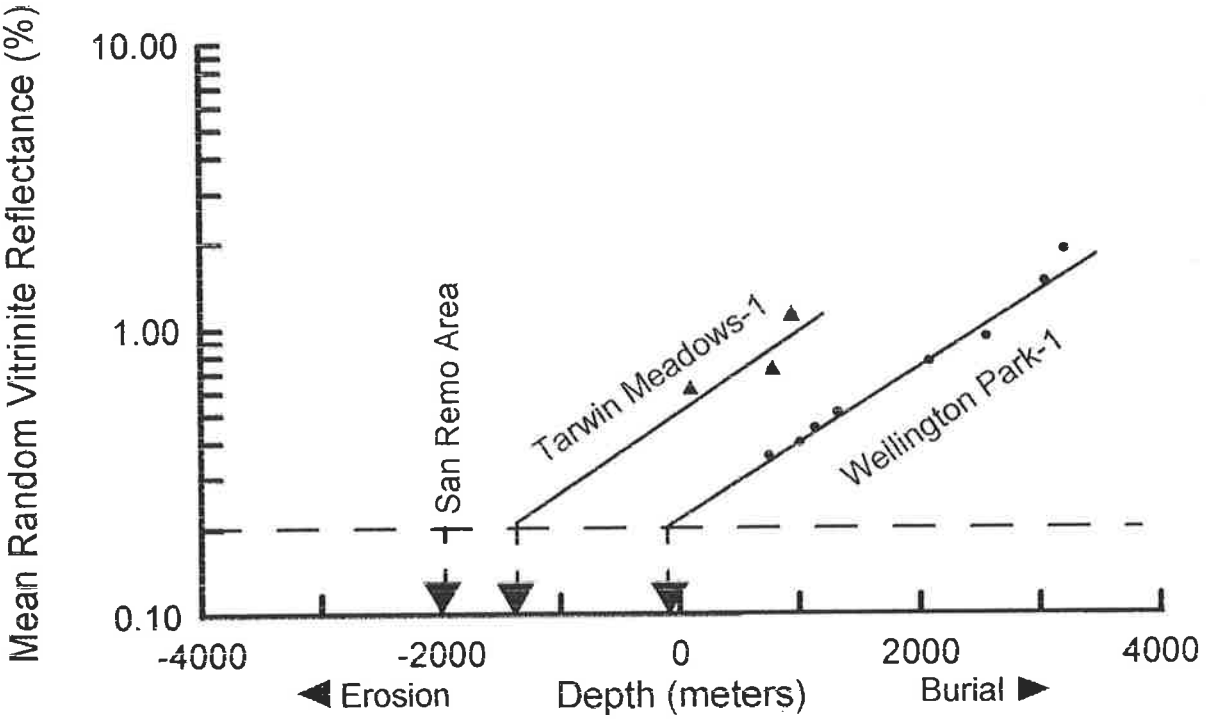
Mean Random Vitrinite Reflectance (%)
10.00
1.00
0.10
San Remo Area
Tarwin Meadows-1
Wellington Park-1
-4000
-2000
0
2000
4000
◄ Erosion
Depth (meters)
Burial ►

Note that in the Late Cretaceous and Tertiary, the Strzelecki Group in the Wellington Park-1 well was reburied and is at T_{peak} at present. Reburial has increased thermal maturation and reset the Rv-r versus depth profile. Thus, the Rv-r versus depth profile in Wellington Park 1 intersects the surface at 0.2% Rv-r. Fig. 3-8 reconstructs the erosion history of Wellington Park 1 partially based on AFTA data that is able to detect the erosional phase by preserved partial annealing of the fission tracks. Reheating in the Cenozoic has obliterated the evidence for erosion in the Rv-r data.

Maximum burial depth at San Remo is estimated using a regional surface Rv-r of about 0.7% suggesting a T_{peak} of about 110°C (Barker and Pawlewicz, 1994). Duddy and Green (1992) estimated a mid-Cretaceous geothermal gradient of about 50°C/km and Fig. 2-4 suggesting a mid Cretaceous surface temperature of 10°C. Calculations using these data show that 110°C would have been reached at 2 km during peak burial in the mid Cretaceous. This depth of burial is consistent with estimates from AFT annealing evidence (Duddy and Green, 1992). Because these rocks are exposed at the surface, an erosion of 2 km of rock from the coastal San Remo area is indicated.

The erosion and igneous activity of the Buchan Trough and Gippsland Basin area have also been related since the Cretaceous (Webb et al., 1991) (Fig. 3-10). The record preserved in the Tertiary shows that times of erosion are linked to the times of volcanic activity. This relationship is thought to reflect uplift in the Eastern Highlands related to crustal underplating occurring during times of volcanism. Fig. 3-10 has been extended to the Strzelecki Ranges area by the Strzelecki Group sedimentation being related to the apparent erosion of an Early Cretaceous age volcanic area edging the initial rift (Duddy, 1983) and the mid-Cretaceous age dike swarm in the Strzelecki Ranges (Duddy and Green, 1992; Appendix 9).

Fig. 3-10. Depositional history of the eastern and western Gippsland Basin compared to basalt ages in the southern portion of the Eastern Highlands (including the Buchan area). The figure is modified from Webb et al. (1991). Reasons for the erosion and deposition cycles in the western Gippsland Basin are discussed in the text. Times of erosion suggested by vertically ruled areas. Solid line in the eastern Gippsland column suggests shifts in depositional environment from: L = land (non-marine); M = mixed non-marine and shallow marine; S = shallow marine.

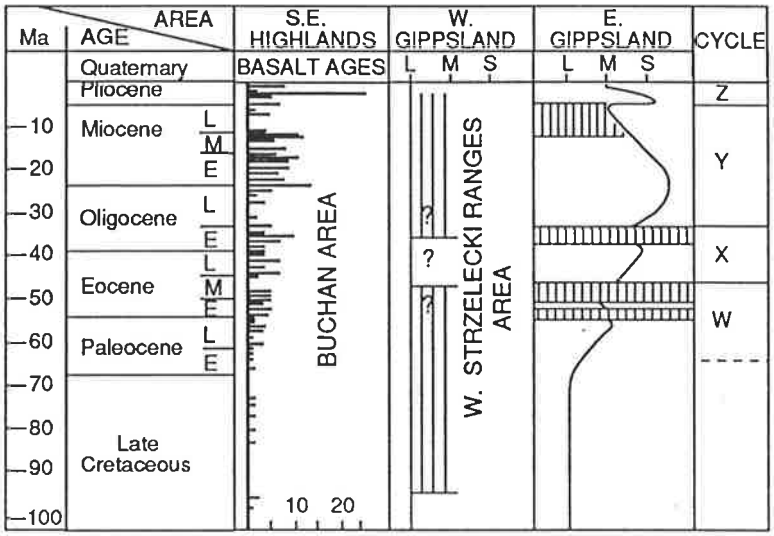
Ma
AGE
AREA
S.E. HIGHLANDS
W. GIPPSLAND
E. GIPPSLAND
CYCLE
Quaternary
Pliocene
Miocene
Oligocene
Eocene
Paleocene
Late Cretaceous
L
M
E
BASALT AGES
BUCHAN AREA
W. STRZELECKI RANGES AREA
10
20
30
40
50
60
70
80
90
100
Z
Y
X
W

3.4 ADDITIONAL CONSTRAINTS ON THE THERMAL AND FLUID HISTORY

Fluid Inclusion and Isotopic Evidence from Post-Dike Veins

Calcite veins that crosscut a dike, or sparry calcite precipitated in vugs within the dikes, are clearly post intrusion. Fluid inclusion homogenization temperatures (T_h) suggest the late calcite precipitated at about 70°C at San Remo 1 and about 80 °C at Bena 3 (Appendix 4). As discussed in Chapter 1, no pressure correction was applied to these T_h data because crushing stage studies on these veins showed the presence of hydrocarbon and possibly CO_2 gases in the fluid inclusions. Similar computations to those presented above for depth of erosion show that this paleotemperature would have existed at about 1.5 km depth according to the paleogeothermal gradient and surface temperature history estimated for the area in the Late Cretaceous to Paleogene. The mean freezing point depression for these fluid inclusions was near 0°C. The fluid inclusion and burial history data on the San Remo 1 dike late calcite suggests precipitation from warm fresh water at a depth of about 1.5 km during the uplift that occurred in Late Cretaceous to Paleocene time.

Isotopically, the vug calcite within San Remo 1 dike is similar in composition ($\delta\ ^{18}0$ = -22.76 and $\delta^{13}C$ = -5.58; Appendix 7, sample R-26) to those found regionally in concretions, late veins and calcite cemented host rock (Fig. 3-11). The carbonate in the concretions has been interpreted as formed during early diagenesis from isotopically light meteoric waters found in the southern polar area (Gregory et al., 1989). Gregory et al. reported a $\delta\ ^{18}0$ = -1 to -27 (converted to PDB standard from SMOW; Arthur et al., 1983) and $\delta^{13}C$ = -26 to +20 PDB for an extensive regional sample set from the Otway and Strzelecki Groups. This regional isotope range completely envelops the more limited range found in this study for the Strzelecki Group host rock, veins and concretions. These cements are apparently formed under similar conditions to those interpreted by Gregory et al. (1989).

The late veins fill the NNW trending joint set that the dikes intrude. Thus, AFT age dating of the dikes indicates the joints were apparently established by 100-85 Ma, at or just after peak burial. Cement zones in these veins are parallel to the vein margin. The cement zoning is formed by physical incorporation of host rock fragments that have been ripped off the vein wall and cemented in place by vein calcite. In some cases, this crack seal process that incorporates the host rock fragments has been repeated as the fracture widened and the veins took on a banded appearance. CL observations show a relatively homogenous cement interrupted by the bands of host rock fragments. The commonly uniform CL color of the calcite cement suggests that the trace metal content of CL-active elements and by inference, the pore fluid chemistry, has remained relatively constant during vein formation. The apparent timing of fracture opening, isotopic signature, and vein textures suggest that the vein calcite has formed in regional fracture set that widened during exhumation. The calcite in these dilational fractures also precipitated from what appears to be fluid similar to the regional meteoric fluid extant in the mid to Late Cretaceous or from carbonate solutions derived from the early cements (Gregory et al., 1989).

Fig. 3-11. Isotope analyses of calcite in host rock, veins and concretions, western onshore Gippsland Basin. Isotope analyses are relative to the PDB standard. Numerical results and locality information are tabulated in Appendix 7.

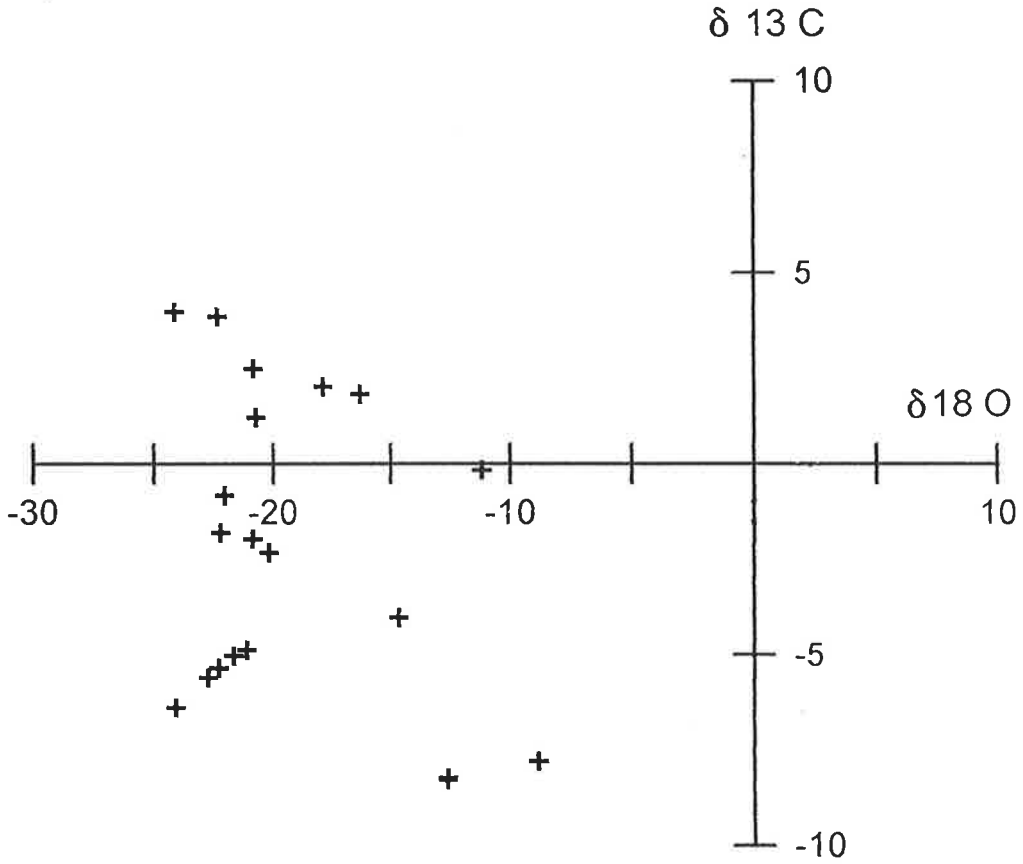
δ 13 C
10
5
δ18 O
-30
-20
-10
10
-5
-10

The fresh water in the fluid inclusions is interpreted to be trapped recharge water driven by the topographic relief that likely developed during this time of uplift. During the Paleogene, the Buchan area was a highlands perhaps as high as 1500 m (Orth et al., in press). Although the Strzelecki Group strata would have eroded faster than the dense carbonates at Buchan, some elevation is expected for the Strzelecki Ranges that underwent rapid uplift during the Late Cretaceous to Paleocene. The presence of Paleocene age Older Volcanics, which cover the portions of the northern Strzelecki Ranges, demonstrates that erosion was accomplished by the time of extrusion. This fixes the time of freshwater intrusion into the deeply buried Strzelecki Group to pre-Eocene.

This fluid inclusion and burial history evidence suggests that the fresh water now observed in the offshore Gippsland Basin may be just the latest occurrence of recharge that is being driven into the deeply buried strata (Kuttan et al., 1986; Harrison, 1989). The Late Cretaceous to Paleocene intrusion of fresh water into the Strzelecki Group at San Remo apparently precedes the later intrusion of fresh water that is Oligocene to Miocene in age, related to a later renewal of the Strzelecki Ranges (Bolger, 1991) and other structures (Harrison, 1989) required to generate the topographic head necessary to drive the recharge into deeply buried strata. The significance of an older recharge system is that any biogenic or thermogenic hydrocarbons in the Strzelecki may have been swept into the deeper portions of the offshore Gippsland Basin by the recharge. These hydrocarbons may have also been biodegraded by bacterial activity that such recharge makes possible by introducing cooler, oxygenated fluids in the present day offshore Gippsland Basin (Mebberson, 1989).

3.5 REGIONAL VITRINITE REFLECTANCE AND ROCK-EVAL ANALYSES

The burial history of the Strzelecki Group has produced an eroded surface in the western onshore Gippsland that exposes rocks that have of an Rv-r of 0.5 to 0.7 % away from dikes (Fig. 3-12) consistent with their exhumation from depths of about 2 km. Individually dikes do not seem to influence thermal maturation much beyond their immediate contacts (as shown in Chapter 4). Fig. 3-12 suggests that in the dike swarm area the regional values of Rv-r, taken away from dike contacts, are commonly higher than the regional values measured well away from the dike swarm.

3.6 IMPLICATIONS

The burial history of the Strzelecki Group has produced a regional Rv-r of about 0.5-0.7%. In the area of the dike swarm, increased Rv-r above this regional level may be due to increased heat flow from an unexposed magma at depth feeding the dikes or undetected dikes near the sample localities. As discussed in Chapter 5, advection of pore water heated by the cooling of dikes may also be a factor. In any case, in the western onshore Gippsland Basin, the dike swarms seem to be an indicator of areas of increased thermal maturation. Increased source rock maturation in the western Gippsland Basin has led to little or no hydrocarbon trapping because erosion has removed or breached most structures. However, in the eastern Gippsland Basin, reburial in the Late Cretaceous has preserved more of the Strzelecki Group, increased its T_{peak}, generated hydrocarbons and introduced reservoirs and seals above it. In addition, the reaction of the Strzelecki Group to increased burial heating offshore can be studied by examining the reactions occurring in the contact aureoles of the dikes. This aspect is discussed in Chapters 4 and 5.

Fig. 3-12. Rv-r measured on near-surface samples from the western onshore Gippsland Basin compared to dike occurrences. The dikes mapped include both dikes found during this study and localities compiled from the literature. Dike locations compiled from Edwards (1934; 1942), Edwards et al. (1944), Ferguson (1909), Kitson (1903; 1917), Rosengren (1984), Stirling (1890; 1892; 1893), Tickell (1971), Whitelaw (1922) and this study. Post Cretaceous geology from Spencer-Jones et al. (1975); and Douglas (1976).

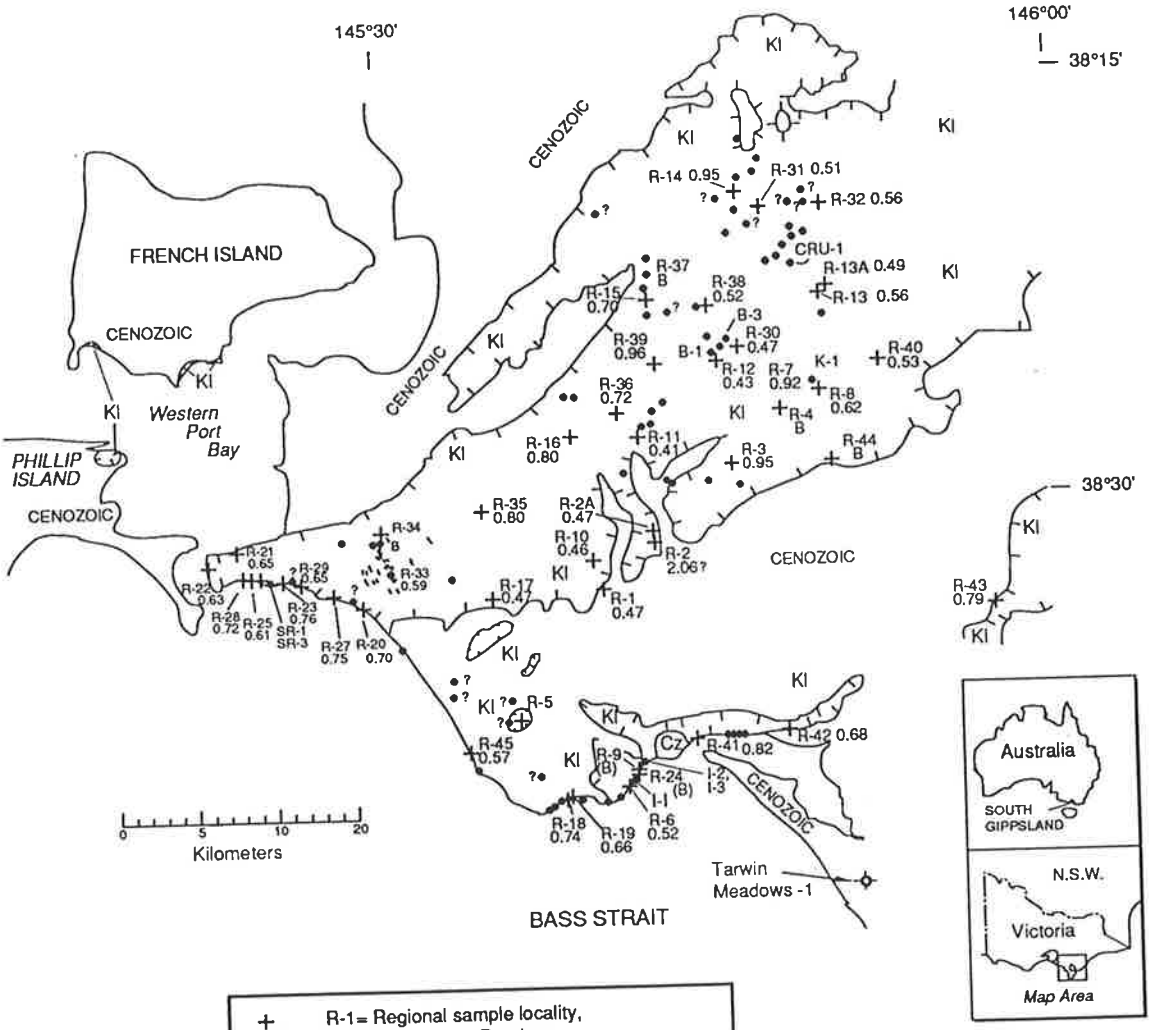

R-1 0.47	R-1= Regional sample locality, if available, mean Random vitrinite reflectance (in %) shown. (B) = Barren of vitrinite
	Dry oil well
•B-3	Dike with identifying code used in text
•R-37	Dikes, not sampled. If close to regional locality, this number given next to dike.
	Dike swarm near Kilcunda shown as lines
•?	Dike reported but location not well established
Kl	Lower Cretaceous Strzelecki Group
Cz	Cenozoic

Chapter 4.

Physical and Geochemical Conditions of Contact Metamorphism by Dikes, Strzelecki Group

4.1 A MID-CRETACEOUS DIKE SWARM

In the Western onshore Gippsland Basin, the Strzelecki Group is intruded by a mostly northwest-trending dike swarm (Fig. 3- 12). These dikes are Early to mid-Cretaceous age (Duddy and Green, 1992) and are now known to be unrelated to the Eocene age Older Volcanics despite some compositional affinities (Price et al., 1988). The mid-Cretaceous age dikes are locally well exposed in the Strzelecki Ranges and the coastal zone of the western onshore Gippsland Basin. There about 100 dikes recorded in the area but the dike exposures are limited because of deep soil and vegetation cover. The dike thicknesses range from 6 cm to about 40 m thick and some can be traced along their length up to 1 km (Edwards, 1934). The dikes typical northwest to north trend is apparently controlled by a regional joint set preferentially intruded by the dikes (Singleton, 1973). A few dikes, including Korumburra 1, appear to intrude a complementary northeast to east trending joint set. Petrographic observations for this study are limited as the dikes are often deeply weathered and thus are unsuitable for determining much about the original rock mineralogy. Many of the earlier studies of these igneous rocks used fresh samples collected from mines or newly opened railroad cuts and the petrographic data from these studies are used to reconstruct the intrusion temperature of the dikes.

4.2 ESTIMATES OF INTRUSION TEMPERATURE

Petrological and geochemical studies indicate that the dikes studied are mostly olivine basalt with minor alkaline basalt (Edwards, 1934; Day, 1983, Price et al., 1988). Edwards (1934) indicates that the dike magmas were mostly liquid when intruded and that olivine is the earliest phenocryst. Based on reconstruction of the crystallization sequence and experimental evidence, Edwards (1934) estimated intrusion temperatures from 1100°C to 1350°C with the temperature range attributed to compositional differences in the rocks.

As in Chapter 2, an estimate of intrusion temperature is made based on the liquidus temperatures of model basalts (Basaltic Volcanism Study Project, 1981). A basaltic melt in which only olivine has crystallized suggests a temperature of about 1250 °C (Fig. 2-9) at an apparent hydrostatic pressure of 20 to 25 MPa reached at a 2 km burial depth (Fig. 3-4). This liquidus-based intrusion temperature estimate is near midrange for the estimates made by Edwards (1934) and 1250 °C is used to initially characterize the expected temperature range next to the dike during contact metamorphism.

The initial dike and host rock contact temperature ($T_{contact}$) can be estimated using the equation presented in Chapter 2: $T_{contact} = (T_{magma} + T_{host})/2$. T_{host} in the western onshore Gippsland is estimated to have been about 100 °C (Fig. 3-4) and if the dike was intruded at 1250 °C, $T_{contact}$ was about 675°C. $T_{contact}$ calculated using this equation is based on a simplified model of dike cooling that is used here just to show the magnitude of the temperature change across the contact aureole. As discussed in Chapter 2, the range of physical and chemical properties found in the host rocks are set by $T_{contact}$ only near the dike contact and in the Gippsland Basin case, temperatures decrease rapidly to a T_{host} of 100°C about two dike widths away.

Table 4-1. Information Available for Selected Dikes, Western Onshore Gippsland Basin

Dike Name and Acronym	Latitude (°south)	Longitude (°east)	Thickness (meters)	Analyses available; Notes
Bena 1 (B1)	38.4113	145.7646	3.4	apatite fission track (AFT) analysis, ^{13}C CP MAS nuclear magnetic resonance (NMR), Rock-Eval (RE), vitrinite reflectance (VR), whole rock elemental composition (ICP-AES)
Bena 2 (B2)	----------	----------	0.7	Not sampled.* Similar in thickness to SR-1. Location just north of Bena 1.
Bena 3 (B3)	38.409	145.7563	20.1	AFT, fluid inclusions (FI), ICP-AES, Carbonate C and O isotopes (ISO), RE, VR
Bena 4 (B4)	-------	----------	<1	Not sampled* too close to Bena 3.
Cruickston 1 (Cru1)	38.358	145.807	41	VR, RE, ICP-AES, ISO
Inverloch 1 (I1)	38.657	145.6865	1.7 at VR, AFTA sample line	AFT, fracture count (FC), ICP-AES, RE, VR, porosity-permeability (P-P), thermal conductivity (TC), X-Ray diffraction (XRD).
Inverloch 2 (I2)	38.653	145.6902	0.4	VR, RE, NMR, ISO
Inverloch 3 (I3)	38.653	145.6902	0.17 at sample line	ISO, RE, VR, XRD; Same dike as I2 but sampled after it splits into two.
Korumburra 1 (K1)	38.431	145.8227	35	VR, RE, P-P, TC
San Remo 1 (SR1)	38.538	145.3965	0.6	AFT, ICP-AES, FC, FI, Gas chromatography, hydrous pyrolysis NMR, RE, VR
San Remo 2 (SR2)	38.538	145.3902	4 ?	Not sampled.* Mostly covered by rock debris. Thickness given in Edwards (1942)
San Remo 3 (SR3)	38.538	145.3963	0.06	VR, RE, ISO
San Remo 4 (SR4)	38.538	145.3963	0.4	Not sampled*In cliff face above SR1 and SR3

*Although not sampled, the presence of these dikes is noted because they influence the direction of the sample lines. The sample lines were oriented away from the known dikes so that the thermal history remains as simple as possible.

The Dike Width Rule

The dike width rule describes the empirical observation that the contact aureole in sedimentary rocks can often be detected by Rv-r measurements extending out to about one dike thickness (Bostick, 1973). The heat flow theory model developed to explain the dike width rule is based on models of a dike cooling in wet host rocks developed by Jaeger (1959, 1964; see review by Middleton, 1991). The conditions of dike cooling embodied in the dike width rule are used here as a reference system to compare the cooling conditions between dikes. The dike width rule is based on a model (termed here the 'wet-rock' model) in which the cooling magma initially releases a latent heat of crystallization as it cools and this heat acts to increase $T_{contact}$. The heat from this conductively cooling magma is in part absorbed by the pore water in the host rock. Because of the additional heat sink constituted by the pore water, temperatures in the contact aureole decease rapidly from $T_{contact}$. Advection of the heated pore water may occur next to the dike contact drawing in cool formation waters which further reduces heating of the host rocks away from the immediate dike contact (Delaney, 1987). This dike cooling model predicts that temperature should monotonically increase from the level of the initial host rock temperature to the level of $T_{contact}$ across a contact metamorphic zone that extends out a distance equal to that of the dike thickness. Because T_{peak} is a major control on Rv-r when temperature increases above the regional T_{peak} during contact metamorphism, Rv-r follows temperature and shows a monotonic increase towards the dike. Thus, the form of the Rv-r profile can be used to infer cooling conditions because if natural conditions during contact metamorphism diverge much from those assumed in dike cooling model, then the width of the contact aureole will vary from that predicted from the dike width rule. For example, purely conductive models of dike cooling predict Rv-r profiles that monotonically decrease to T_{host} some 3-4 dike widths away from the dike contact (Peacock, 1990). Further, thicker dikes or any dike intruding into permeable rocks may cool by convection (Delaney, 1982;1987) and the

contact metamorphic aureole because of the development of hydrothermal circulation would also be more extensive than predicted by the dike width rule and not show a monotonic decrease in the Rv-r profile.

Heat flow theory also a dimensionless distance parameter X/D, which is the distance from the dike margin divided by the dike thickness, can describe temperature, heating duration and Rv-r relative to a dike by normalizing the measurements to dike thickness (Jaeger, 1959). Heat flow models are discussed in detail in Chapter 5, but this parameter is introduced here to develop comparisons of contact metamorphism using X/D for this suite of dikes that vary over three orders of magnitude in thickness.

The monotonic increase of Rv-r as the dike is approached is often disrupted in the immediate vicinity of the dike (X/D <0.3) because of an increase in the molecular disorder of the vitrinite (Khovasani et al., 1990) making thermal maturation prediction using Rv-r inaccurate.

As found by the lack of response to intrusion at Buchan, the dike width rule also assumes a relatively reactive, low thermal maturity organic matter in a water saturated host rock that is capable of adequately responding to heating.

4.3 DIKES IN THE STRZELECKI RANGES

This group of dikes including Bena 1, Bena 3, Cruickston 1, and Korumburra 1 are exposed in the Strzelecki Ranges, just inland from the dikes exposed along the coast. These two groups of dikes are distinguished because the rate of erosion in these hills is much less than that occurring along the coast. Thus, the host and dike rocks in the Strzelecki Ranges are more weathered than that found in the coastal group.

4.4 BENA 1

The Bena 1 dike is in a group of 4 parallel dikes exposed in a railroad cut to the west and north of Bena, Victoria (Fig. 3-5). Only two dikes on the outside edges of the group (Bena 1 and Bena 3) were sampled to avoid overlapping metamorphic effects from adjacent dikes. Bena 1 is a 3.4 m thick northwest trending, near-vertical dike at the western edge of this group (Figs 4-1a,c) some 25 m away from the nearby Bena 2 dike. The Bena 1 dike intrudes weathered Strzelecki Group sandstone, mudstone and thin coal beds. The dike rock is deeply weathered at Bena 1. The sample suite extended outward on a perpendicular line from the western dike margin (Fig. 4-1d). The extensive degree of soil development and the succession of the vegetation cover at Bena 1 is indicated by comparison of the present photographs (Fig. 4-1a) and a sketch made in 1890 by Stirling (Fig. 4-2).

Host Rock Thermal Maturity and Organic Geochemistry

Vitrinite reflectance at Bena 1 (Fig. 4-3) varies from a level of about 0.5% Rv-r from 2 to 6 m from the dike, to 4.0% at the contact. However, the increase in Rv-r above background level occurs at X/D = 0.4 or 1.5 m from the 3.4 m thick dike. According to the dike width rule, the contact aureole as shown by an increase in Rv-r should commence at X/D = 1.. Rock-Eval T_{max} (Fig. 4-3) and the production index (PI; see tabular values in Appendix 5), both thermal maturity parameters like Rv-r, do show an increase from about X/D = 1 before decreasing near the dike contact. This decrease in T_{max} and PI is because the reduced S_2 peak caused by a reduction in the pyrolysiable (reactive) TOC and high thermal maturity near the dike makes these thermal maturation parameters inaccurate.

Fig 4-1 Dikes intruding the Strzelecki Group exposed in railroad cuts, Strzelecki Ranges, western onshore Gippsland Basin, Victoria. These railroad cuts were made in the late nineteenth century.

A) Bena 1 (right side set of arrows) and Bena 2 (left arrows) exposed in a cut just south of the South Gippsland Highway and just southwest of the town of Bena, Victoria.

B) A frontal view of the 0.7 m thick Bena 2 dike. The arrows point to the dike margins. The dike and host rocks are weathered to a soil-like consistency. The dike is differentiated by a color change from a light gray in the host rock to a orange-brown color in the dike, the adjacent darkened bake zones in the host sandstone and the subvertical subplanar dike margins. This dike was not sampled because it occurs in the middle of the dike group which may make its thermal history complex.

C) An oblique view of the 3.4 m thick Bena 1 dike looking approximately along strike. The arrows point to the dike margins. Again the dike and host rocks at the surface are weathered to a soil-like consistency.

D) An oblique view of the southerly contact of the 3.4 m thick Bena 1 dike. Arrow shows the southern dike margin. About 0.2 to 0.4 m of soil and host rock have been removed to better expose the host rock for sampling. At this sample depth, the thinly bedded coals had taken on a glossy, fresh-looking appearance. Later organic petrography showed that these coals were deeply weathered with even the fusinite degraded to a low reflectance material. This area was apparently the most weathered host rock sampled during this study.

E) Oblique view of the 35 m thick Korumburra 1 dike looking west-southwest. This cut is just northwest of the Korumburra town center. The arrow points to the western dike margin.

F) View of the 35 m thick Korumburra 1 dike looking south at the western dike margin and the results of the initial digging out of the sample pits. The arrow points to the western dike margin. Note the dark vegetable-matter-rich soil and thick vegetation covering the rocks.

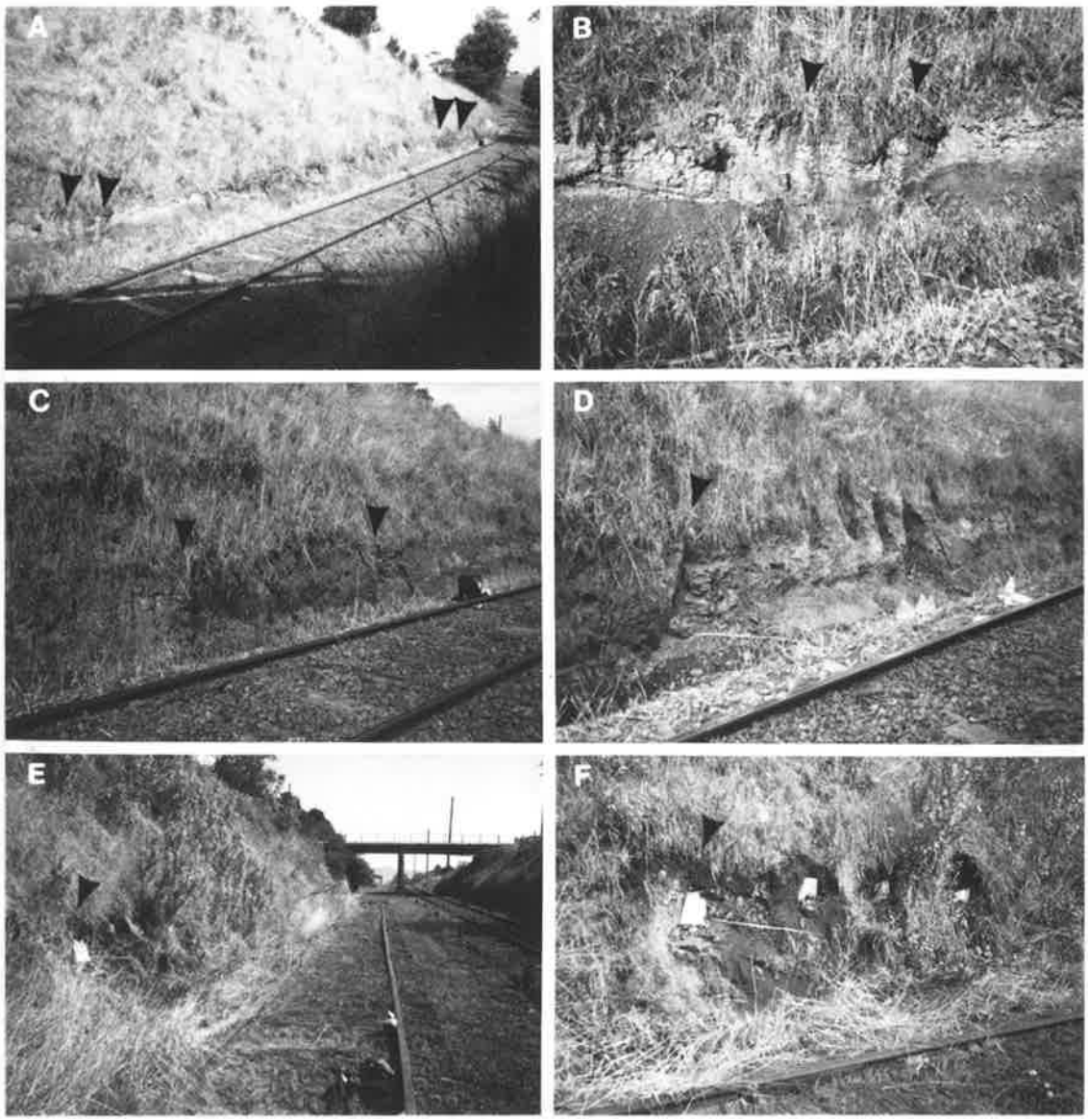
A
B
C
D
E
F

Fig. 4-2. Sketch of the railroad cut just west of Bena, Victoria, shown soon after opening in the late nineteenth century. Figure reproduced from Stirling (1890). Note how the Bena 1 dike thins upwards when traced along the face of the cut. Similar changes in dike thickness hidden from the observer and occurring just below the sample level may account for the lack of agreement between Rv-r profiles measured on either side of a dike at some of the studied dikes. Tickell (1971) also notes upward thinning of an intrusion near San Remo, Victoria.

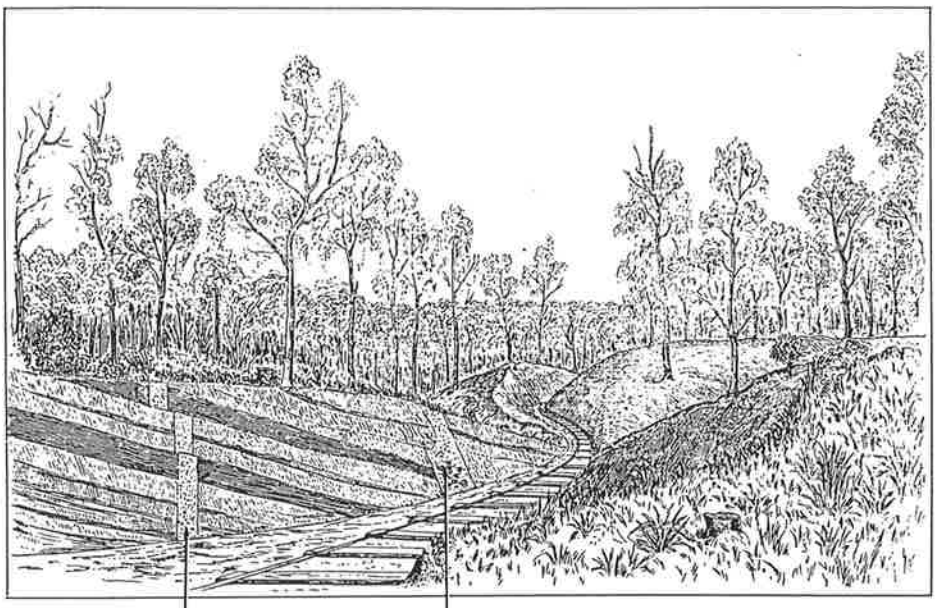

SKETCH OF CUTTING NEAR BENA SHEWING DYKES

From Stirling (1890)

For these reasons, the Rock-Eval S_1 levels, like S_2 levels are very low to zero over the thermal maturation range found next to the dike. S_1, a measure of the generated hydrocarbon (HC) and S_2, measure of remaining HC generation capacity would usually be expected to change substantially when thermal maturation increases over a Rv-r range of 0.5 to 4.0% in the TOC rich rocks like that found next to Bena 1. The hydrogen index (HI), which is the S_2 peak normalized to TOC, is also much reduced at Bena 1 from the levels found in less weathered coals such as R5 (HI = 270 mg HC/ g C) taken at 60 m depth in the State Coal mine at Wonthaggi. The oxygen index (OI) at Bena 1 is much higher than the OI of 9 mg CO_2/ g C found in sample R-5.

^{13}C CP MAS NMR response shows a generally lower level of aliphatic carbon compared to sample R-5 at low thermal maturity levels (Fig. 4-4). Further, the aliphatic carbon + aromatic spinning side bands (ssb) area shows little change over the thermal maturation increase near the dike. The reduced aliphatic carbon content, in good agreement with the reduced Rock-Eval S_1 and S_2 peak values, seems to be a reflection of a reduction in the mobile, largely aliphatic carbon compounds in a weathered coal sample (Barker et al., 1993).

A larger carbonyl carbon peak near 180 ppm and a minor peak at 200 ppm in the NMR spectrum is also assigned to carbonyl carbon (Wilson, 1987). Carbonyl carbon although usually present in immature coals of the area persists to unusually high thermal maturation levels of over 1.1% Rv-r. Other studies have shown that moderate rank coals show considerable carbonyl carbon at the high levels of natural oxidation (Wilson, 1987).

Fig. 4-3. Comparison of vitrinite reflectance and Rock-Eval pyrolysis results from coaly rocks in the Strzelecki Group next to the Bena 1 dike, western onshore Gippsland Basin, Victoria.

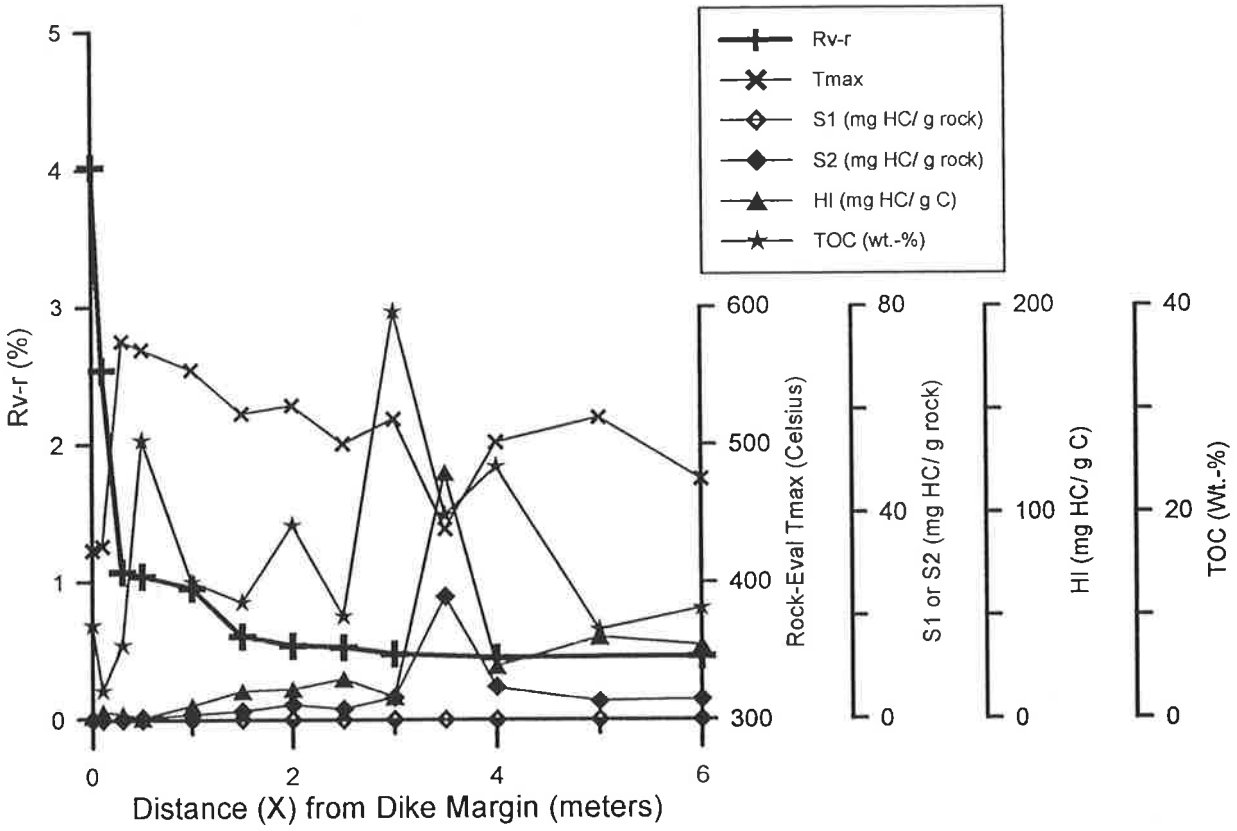
Rv-r
Tmax
S1 (mg HC/ g rock)
S2 (mg HC/ g rock)
HI (mg HC/ g C)
TOC (wt.-%)
Rv-r (%)
Rock-Eval Tmax (Celsius)
S1 or S2 (mg HC/ g rock)
HI (mg HC/ g C)
TOC (Wt.-%)
Distance (X) from Dike Margin (meters)

Fig. 4-4. ^{13}C CP MAS NMR spectra, Rv-r and aromatic fraction (fa) versus distance (X) from the dike margin, Bena 1 dike, western onshore Gippsland Basin, Victoria. The regional sample R-5 is presented as an example of a relatively unweathered coal because it was sampled underground at an active mine face and some 60 m below the present surface, in the State Coal mine near Wonthaggi, Victoria. Sample R-5 is marginally mature (Fig. 5-16).

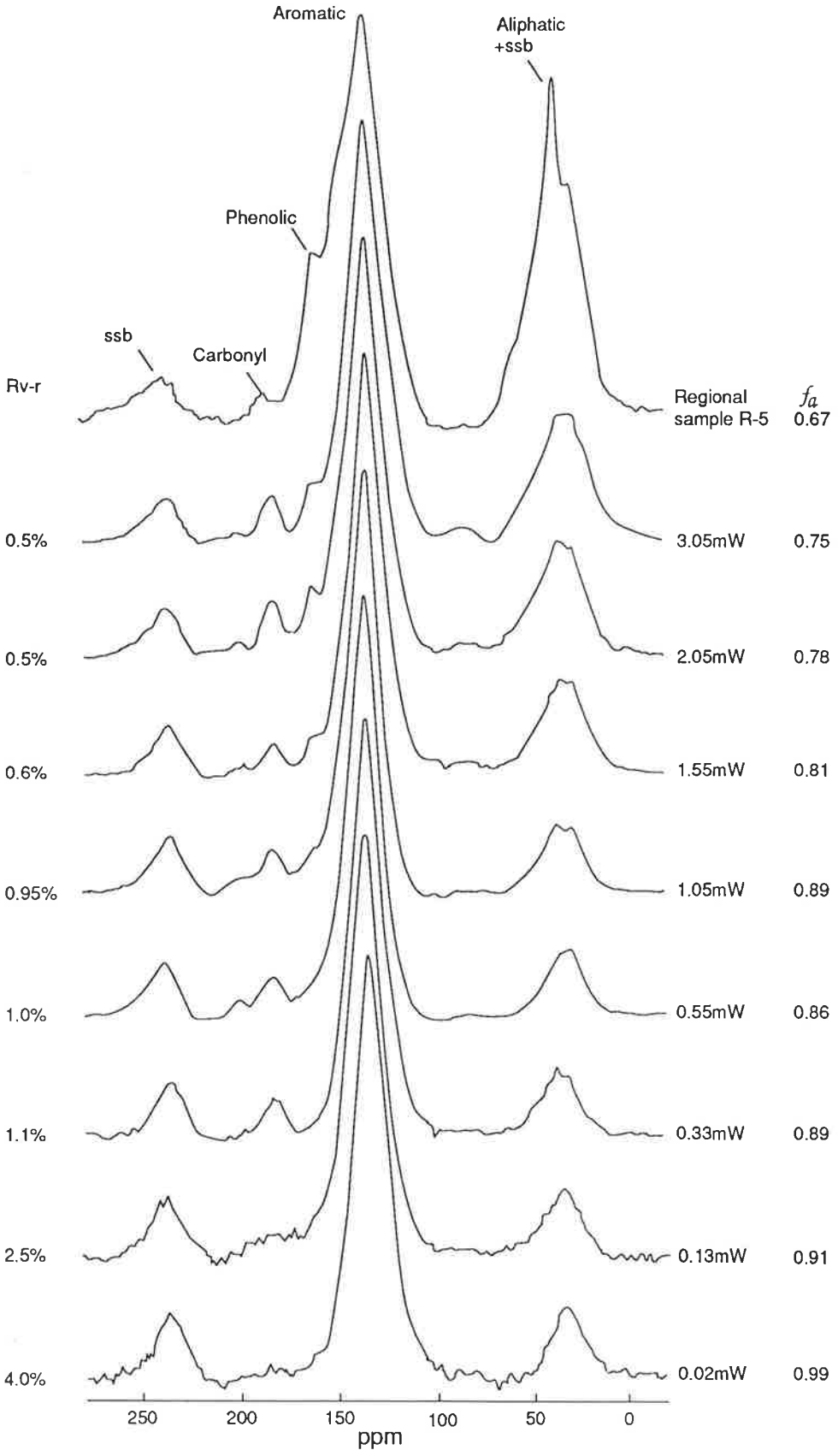
Aromatic
Aliphatic
+ssb
Phenolic
ssb
Carbonyl
Rv-r
Regional
sample R-5
f_a
0.67
0.5%
3.05mW
0.75
0.5%
2.05mW
0.78
0.6%
1.55mW
0.81
0.95%
1.05mW
0.89
1.0%
0.55mW
0.86
1.1%
0.33mW
0.89
2.5%
0.13mW
0.91
4.0%
0.02mW
0.99
250
200
150
100
50
0
ppm

Discussion of Thermal Maturation and Organic Geochemistry

Vitrinite reflectance is clearly not responding as far away from the dike as the other thermal maturation parameters, T_{max} and PI (Fig. 4-3). Vitrinite reflectance is a physical measurement dependent on polish quality and consequently is different in its response to weathering than the chemically based T_{max} and PI parameters. Usually adequate Rv-r determinations can be made by making the measurements near the grain center and avoiding the grain edge (Ingram and Rimstidt, 1984). Another set of polished whole rock mounts were made for the Bena 1 coals in the hopes of finding larger pieces preserved in the large rock grains that would give improved reflectance. However, comparable Rv-r levels were found in the picked coal and whole rock mounts (Appendix 2). It is concluded that in deeply weathered coals at Bena 1, the deterioration of the vitrinite grains has apparently approached completion and accurate Rv-r cannot be measured. The preservation of increased Rv-r near the dike is attributed to decreased porosity and permeability near the dike margin apparently protecting the vitrinite near the dike from weathering. This decreased porosity and permeability is later shown to occur at other dikes in the area.

Weathering of SOM at Bena 1

The spuriously low Rv-r, muted Rock-Eval S_1 and S_2 response, decreased HI and increased OI, and ^{13}C CP MAS NMR peaks suggesting the persistence of carbon-oxygen groups at high thermal maturity, all suggest deeply weathered, oxidized coals. The vitrinite also shows pitted, microfractured polished surfaces on grains occasionally rimmed with degraded low-reflecting material. Fusinite can also be degraded to a low-reflecting material recognizable only by its remnant bogen or cellular structure. The geochemical signatures have been severely altered by weathering after contact metamorphism. These results and those at Cruickston 1 and Korumburra 1 discussed below suggest the inland dikes are poor candidates for more

intensive organic geochemical of fluid inclusion studies. After the pilot study at Bena 3, intensive fluid inclusion studies are limited to dikes that are in relatively unweathered host rocks at the coastal sites because it is at these sites that the organic geochemistry study can be based on relatively unweathered rocks.

AFT Annealing

The overlap in error in the age determination suggested by the ±1σ bars suggests there is no statistically significant difference in the AFT apparent ages as the dike is approached (Fig. 4-5). Thus, the apparent decrease in the pooled apatite age from 130 Ma at X = 6 m to 105 Ma at X = 1.5 m is not considered statistically significant. Further, the ages near the dike are not significantly different than the AFT ages found regionally for the Strzelecki Group (Appendix 9). The apatite age near the dike is not distinguishable from the Early Cretaceous sediment apparent age because burial history reconstruction (Chapter 3) suggests the dikes intruded at burial temperatures high enough that AFT were unstable and annealing rapidly erased any tracks. Generally, the fission track length histograms (Appendix 9, page 9) for the samples from Bena 3 show a strong mode at 15 μm and few measurements away from this mode. This distribution is interpreted as indicating some time after deposition of the Strzelecki Group, at about 120 to 98 Ma, and after intrusion, the dike and host rock package cooled fairly rapidly to a burial temperature low enough for good AFT retention. Because the dike intruded into the host rocks when they were at a temperature where tracks were unstable, the heating duration next to the dike, described in Chapter 1, was not recorded by AFT annealing.

Fig. 4-5. Apparent apatite fission track age and Rv-r versus distance (X) from the Bena 1 dike margin, western onshore Gippsland Basin, Victoria. The fission track ages plotted are the pooled values, as the single grain age data passed the X^2 test at the 5% level. The error bars are ± 1σ. A discussion of terms used in AFT annealing studies is in Appendix 9.

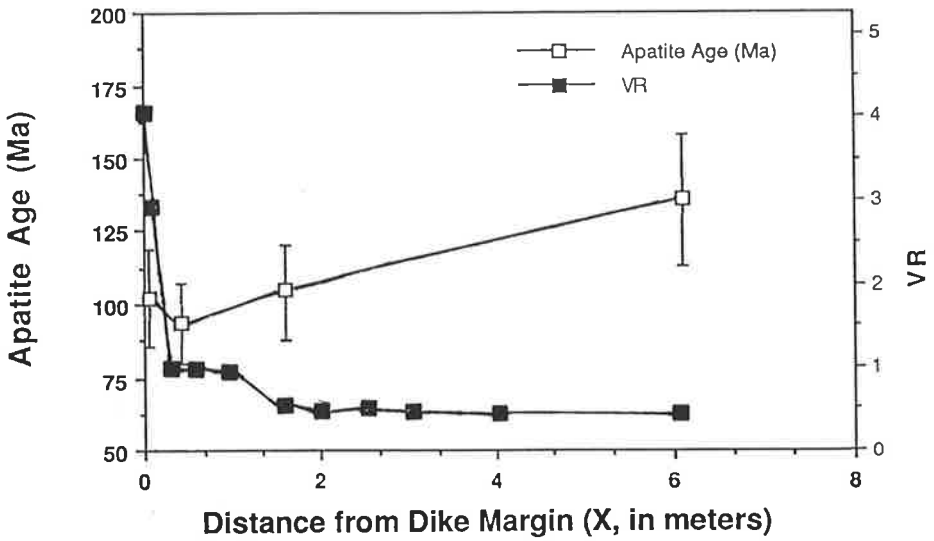
Apatite Age (Ma)
VR
200
175
150
125
100
75
50
0
2
4
6
8
5
4
3
2
1
0
Apatite Age (Ma)
VR
Distance from Dike Margin (X, in meters)

4.5 BENA 3

Bena 3 is exposed some 200 m north of Bena 1 in the same railroad cut near Bena, Victoria. Bena 3 is a 20.1 m thick, northwest trending, near-vertical dike at the eastern edge of the Bena group of dikes (Figs 4-1a,c). The dike rock is locally preserved near the dike center as rounded blocks consisting of a coarse-grained, holocrystalline gabbro. The dike rock at its margin consists of a felted mass of acicular plagioclase in what was probably a glassy groundmass. There are no large olivine phenocrysts in this quenched sample of the magma at the dike margin. The lack of large phenocrysts at the quenched dike margin is consistent with Edwards (1934) observation that these magmas were mostly liquid when intruded.

The sample suite extended outward on a perpendicular line from the eastern dike margin for 30 meters in a Strzelecki Group sandstone. Because Bena 3 is about 50 m away from the nearest dike (Bena 4, about 0.8 m thick), no overlapping contact metamorphism effects are expected.

Host Rock Thermal Maturity and Geochemistry

Vitrinite reflectance in the Bena 3 samples varied from 1.3 % at X = 30 m to 5.8 % at the dike contact. Except for the mudstone found at X = 30 m, organic matter was sparse in the Bena 3 rocks with the TOC in the sandstones always less than 0.5 wt.-% (Fig. 4-6). Rock-Eval data is generally inaccurate at such a low TOC and no interpretation is attempted.

The Rv-r profile at Bena 3 has a marked slope break near X = 13 m and therefore does not monotonically decrease to background levels. The Rv-r at Bena 3 does not reach the background level of 0.5-0.6% Rv-r (Fig. 3-12) even at X/D = 1.5 where the sample line ended. There is no other dike known to the east of Bena 3 and these effects are apparently solely due to this single dike.

Fig. 4-6. Comparison of Rv-r and Rock-Eval pyrolysis results from coaly rocks in the Strzelecki Group next to the Bena 3 dike, western onshore Gippsland Basin, Victoria.

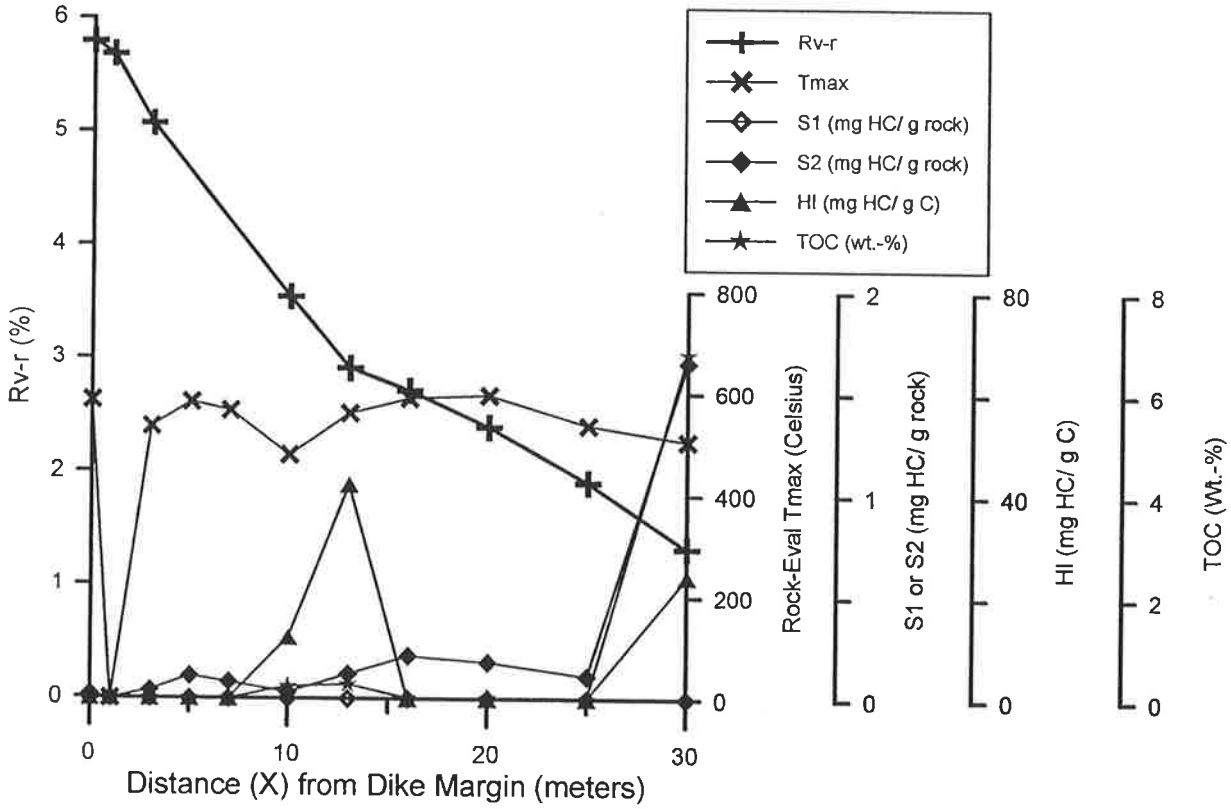
Rv-r
Tmax
S1 (mg HC/ g rock)
S2 (mg HC/ g rock)
HI (mg HC/ g C)
TOC (wt.-%)
Rv-r (%)
Rock-Eval Tmax (Celsius)
S1 or S2 (mg HC/ g rock)
HI (mg HC/ g C)
TOC (Wt.-%)
Distance (X) from Dike Margin (meters)

This marked divergence does not seem to be that Bena 3 thickens just below the sample line as does Bena 1 (Fig. 4-2) which would extend the contact aureole to greater distances than the expected X/D = 1 from the dike width rule. As shown below, the extended Rv-r profile seems to be related to an embryonic convection system that developed next to this thick dike. An extended Rv-r profile is also seen next to the Cruickston 1, so this type of profile seems favored in the thicker dikes of this study.

Next to Bena 3, the dike cooling model upon which the dike width rule is based (Jaeger, 1959; 1964) does not fit well. The poor fit of the dike width rule near this thicker dike may be due to the contact metamorphism persisting for much longer times, causing more extensive hydrothermal alteration and possibly enhancing permeability, which allows the onset of convection (Delaney, 1987). Thin dikes often cool to rapidly for convection to be established.

Another key to the onset of convection is a pre-existing or induced permeability caused by chemical reactions or physical changes in the rock during contact metamorphism. Adequate permeability allows the development of a more open system style of hydrothermal alteration expressed as a mobility of chemical species like that seen in convecting geothermal systems (Browne, 1978). Barker's (1989) compilation of data on igneous intrusive sheets and geothermal systems suggests that some of the thicker intrusions produce a style of thermal maturation more like that observed in open system, convecting geothermal systems. It is well known that geothermal systems are usually associated with young intrusions and that hot water flow caused by convection can produce increased Rv-r well away from the heat source (Barker, 1983; Gonsalez, 1985; Struckmeyer and Browne, 1988).

To test for a convection system and the associated water-rock reactions that may leave an imprint on the rocks, the use of oxygen isotopes in the carbonate cement was considered. However, most samples showed no reaction in concentrated hydrochloric acid (Appendix 7). Therefore, the entire Bena 3 sample suite was not analyzed for isotopes.

Another test for an open system used inductively coupled plasma atomic emission spectroscopy (ICP-AES) analysis of whole rock powders (Appendix 6) . In a closed system, the mass and bulk elemental composition in the system remain fixed. In an open system, these parameters are not fixed and the transport of mass and changes in the bulk elemental composition can occur. By examining element mobility, extended Rv-r profiles caused by open systems can be differentiated from extended Rv-r profiles caused by the dike thickening below the sample line. If the system remains closed, element mobility would not be observed in the rock showing an extended Rv-r profile.

ICP-AES

ICP-AES results indicate mostly small changes in elemental composition from X= 30 m to X = 15 m (Fig. 4-7) . At X = 15 m to 0.1 m, some important perturbations in the elemental composition occurs. Closer to the dike than X = 15 m, there is a general trend of diminishing loss on ignition (LOI). Although a minor proportion of LOI is due to water physically held in the sample, most of it is water chemically bound in minerals. A decreasing LOI suggests dehydration reactions are occurring. MgO content decreases in proportion towards the dike, while SiO_2, CaO, Na_2O and K_2O increase. Al_2O_3 content fluctuates towards the dike contact but shows little net change. The proportion of Fe_2O_3 decreases and then increases as the dike is approached. The Ba content increases in proportion from 360 ppm to 550 ppm as the dike is approached and Sr increases from 290 to 470 ppm (Appendix 6; not plotted as they would be indistinguishable at this scale). Trace elements, Nb, Rb, Y and Zr show little change in content as the dike is approached (not plotted as they would be indistinguishable at this scale).

Fig. 4-7. A comparison of selected element oxide abundances versus distance from the dike margin (X), Bena 3 dike, western onshore Gippsland Basin. The element oxides plotted were selected for their tendency to respond to hydrothermal alteration. SiO_2 content was plotted as SiO_2 minus 50 wt.-% so it would fit on this expanded scale with the minor oxides. SiO_2 actually increases from 62 to 66 wt.-% near the dike. Cr_2O_3, MnO, P_2O_5, and TiO_2 contents are low, fluctuate but show no trend, or are zero and these values were not plotted (Appendix 6). Note that correction of the analyses to a water-free basis was not done. This correction would increase the percentage changes in element oxide content but not the general form of the changes. Steel tools were used for sampling in the field and preparation of these samples. The basic sample size used for ICP-AES analysis was about 100 g of rock broken and selected for cleanliness minimizing any contamination effects to a few tenths of a weight percent Fe_2O_3.

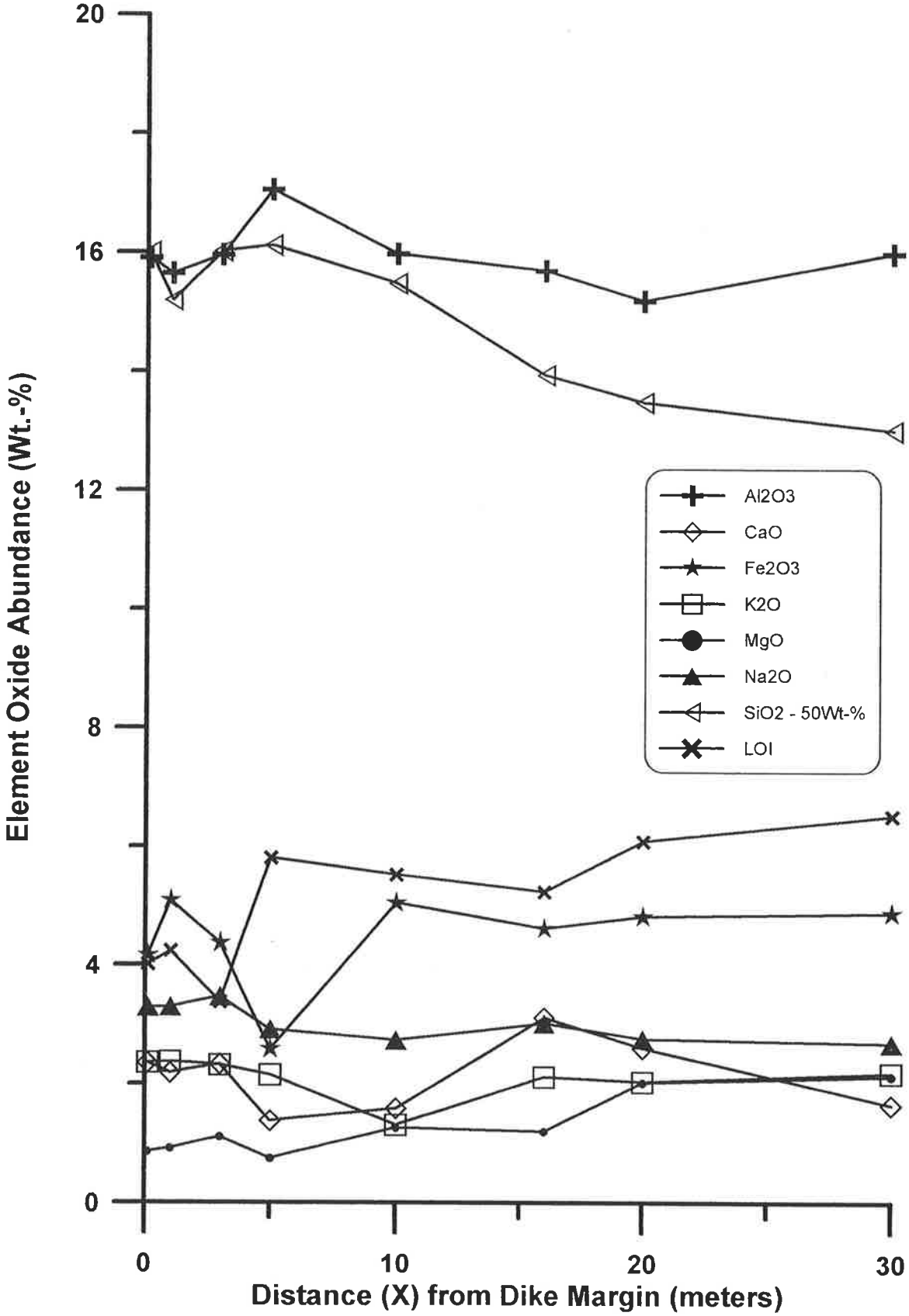
20
16
12
8
4
0
0
10
20
30
Element Oxide Abundance (Wt.-%)
Distance (X) from Dike Margin (meters)
Al2O3
CaO
Fe2O3
K2O
MgO
Na2O
SiO2 - 50Wt-%
LOI

In terms of assessing the conditions of hydrothermal alteration, the often sharp changes at the dike contact may not be as significant as the ones occurring further away from the dike. Delaney (1987) points out that thermal expansion of water causes buoyant advection near the dike even in rocks with 1% porosity and regardless of whether convection is established before the dike cools. The typical increase in the proportion of SiO_2 as the dike is closely approached is seemingly caused by the strong thermal control of silica aqueous solubility and a rapid approach of hydrothermal solutions to near equilibrium with SiO_2 (Ellis and Mahon, 1977). During the rapid temperature increase after intrusion, SiO_2 seems to be capable of rapid dissolution and mobility towards the dike in the advective flow near the dike. With the rapid passage of the heat pulse that occurs next to dikes, the SiO_2 is soon precipitated out during cooling near the dike and this is the record that ICP-AES analysis detects. This process may be ongoing along with the relative increases in element oxide abundance simply caused by the loss of TOC and LOI near these dikes. However, these sharp changes may also be the result of element exchange with the hot intrusive at the dike contact or later reactions over geologic time with ground water in the brecciated host and dike rocks at the contact. In this discussion, the changes at the dike contact are not weighted as heavily as those occurring away from the dike contact.

Studies of rock alteration by geothermal systems show that, in general, K and SiO_2 are added and Na and Ca are removed during open system hydrothermal alteration (Ellis and Mahon, 1977). In general, next to Bena 3, these elements show some mobility seemingly attributable to such hydrothermal alteration. Changes in CaO proportion may be influenced by the late diagenetic carbonate veins and cement in these host rocks. However, changes in CaO proportion do show some correlation with the other elements that change as the dike is approached, so these changes seem to be a real signal. Further, during acid testing for carbonates before isotopic analysis, the host rocks showed no reaction from X = 0.1 to X = 10

m and at X =30 m but showed reaction in acid at X = 16 and 20 m. The changes in CaO proportion at X < 10 m are not due to the late carbonate and are attributed to hydrothermal alteration.

Other elemental changes support an open system conditions of hydrothermal alteration. MgO concentration in aqueous solution at very low levels is temperature dependent and is controlled by silicate equilibria between mainly chlorite and montmorillonite (Ellis and Mahon, 1977). Because chlorite and mixed layer clays are common in the host sandstone matrix (Lindsay, 1982), the observed MgO content decrease as the dike is approached is probably due to reactions involving these common minerals. Similarly, the decrease in LOI as the dike is approached is inferred to be a result of the dehydration of minerals, such as laumontite, which is common in these host rocks (Lindsay, 1982).

In general, hydrothermally altered rocks show no change in the rare earth element content (Michard, 1989) which is consistent with the little change seen in the content of Nb and Y found by this study. Essentially no change or small changes in the content of rare earth elements is typical of host rocks at every dike suite in this study (Appendix 6) and changes in these elements are not discussed further.

Reaction with the hot magma may be the source of the Sr and Ba increases and possibly other changes essentially at host rock contact with Bena 3. Increasing Ba and Sr content as the dike is approached is typical of the entire dike suite and changes in these elements are not emphasized in the following discussions.

The muted elemental changes observed at Bena 3 seem consistent with an embryonic open hydrothermal system, that, next to a 20 m thick dike, would have only on the order of tens of years to develop (Mundry, 1968). In the discussion above, the changes next to Bena 3 are being compared to geothermal systems that are much longer lived, persisting up to 10^5 or 10^6 yr (Browne, 1978; Barker, 1983). The hydrothermal effects observed in geothermal systems are

consequently much more pervasive than observed at Bena 3. The low permeability rocks of the Strzelecki Group in general (Edwards and Baker, 1943) and those documented near the dike margins of other dikes in this study (Appendix 10) also mute the chemical changes because permeability is a critical factor in the development of hydrothermal mineral assemblages and fluid (Browne, 1978). However, some of the dehydration reaction seen next to Bena 3 may locally enhance permeability during contact metamorphism.

Decisive changes in element oxide content are not seen in this conjectured embryonic geothermal system, but what is observed is the increased mobility of hydrothermally active elements as the dike is approached (Fig. 4-7). Note that in general, hydrothermal alteration either decreases or increases the element oxide proportions of the mobile elements. These roughly monotonic general trends agree well with the increasing Rv-r. An increasing Rv-r suggests increasing temperatures towards the dike and a greater potential for hydrothermal alteration seen in the changes of element oxide proportions.

Fluid Inclusion Geothermometry

A pilot fluid inclusion study at Bena 3 was instituted to investigate the thermal underpinnings of the anomalous Rv-r profile. This pilot study was based on fracture bound type A and B fluid inclusions that are locally common (Appendix 4) at Bena 3. However, studies at the other dikes show that the number of fractures found are considerably more common away from the dike. The more common fracturing of the host rock may have occurred during the intrusion of the 20 m thick dike. The fracturing may be a factor in allowing the incipient hydrothermal system to develop or the fractures may be an expression of alteration caused by that system. In this pilot fluid inclusion study, the T_h of each fracture bound fluid inclusion indicates a minimum temperature of formation if it has not necked below the two phase boundary and trapped more than one phase. Such necked fluid inclusions may be

petrographically detectable (Goldstein and Reynolds, 1994). Necking is a major concern because undetected necked fluid inclusions can have anomalously high T_h caused by the disproportionate separation of the vapor bubble into one of the vacuoles. As disucssed in Chapter 1, by analyzing a series of fluid inclusion- bearing fractures, and considering that the fracturing and healing are enhanced at higher temperature (Somerton, 1992), the upper data edge of a series of T_h measurements is conjectured to approach T_{peak}. A limitation in accurately estimating T_{peak} using fractures is that type A and type B fractures are rare in the Strzelecki Group. The lack of fractures is particularly evident in the fine grained, matrix-rich sandstones found next to the Inverloch dikes. The chlorite, clay mineral and zeolite rich matrix is thought to plastically deform under stress and cushion the embedded grains from fracturing. Thus, a check on the T_h results is made using Rv-r to estimate temperature.

The paucity of fractures in the Strzelecki Group at Bena 3, is shown by the common experience of spending 6 hours searching one thin section and still not finding one unambiguous type A or B fracture that bears fluid inclusions.

Another limitation of fluid inclusion studies in general is that vapor-rich(?) inclusions near the dike formed at such high temperatures that they appear to contain only vapor. If vapor-rich fluid inclusions formed at the high temperatures next to the dike, at room temperature such fluid inclusions can contain little or no visible liquid. Further, refraction of light at the vacuole-liquid contact can hide this small amount of liquid that forms a meniscus about the vacuole boundary. Such inclusions may be the dark vapor-rich or gas-rich (?) fluid inclusions seen next to the Bena 3 dike (Fig. 1-6e). Even if fluid can be seen in these extremely vapor-rich fluid inclusions, the T_h data gathered from them can be inaccurate (Sterner, 1992b). T_{peak} based on vapor-rich fluid inclusions may be determined only in special cases when inclusions trap enough fluid or the vacuole has a shape such that T_h can be observed. When T_h is clearly observed in vapor-rich fluid inclusions, the vacuole often has a narrow shelf-like area that

seems to collect and hold the small amount of liquid to near T_h where it can clearly be seen to homogenize over a small temperature range.

The melting point of ice for salinity determinations is also difficult to see in vapor-rich inclusions because the volume change upon melting can be small and the vacuole wall can obscure phase changes.

The results of the pilot study show a good agreement between T_{peak} from type A and B fracture bound fluid inclusions and T_{peak} predicted from Rv-r (Fig. 4-8). Away from the dike margin, the agreement between the two types of geothermometers suggests that the temperature estimated by measuring T_h in a series of type A and B fluid inclusions does approach T_{peak}.

Near the dike margin, however, T_{peak} estimated from Rv-r is considerably lower than that estimated from T_h . This reduced temperature estimate near the dike is attributed to the difficulty in attaining large, uniformly polished surfaces because of increasing granular anisotropy and increasing molecular disorder at high temperatures near the dike (Khovasani et al., 1990). Near the dike, fluid inclusion estimates of T_{peak} are in better agreement when compared to the T_{peak} suggested by heat flow (Fig. 2-10) than those made from Rv-r up to the temperature range where vapor-rich fluid inclusions become unmeasurable.

Fig. 4-8. Homogenization temperature T_h from fluid inclusions along healed fractures in sandstone and T_{peak} estimated from Rv-r, Strzelecki Group next to the Bena 3 dike, western onshore Gippsland Basin, Victoria. T_{peak} estimated from Rv-r and a vitrinite reflectance geothermometer (VRG) for hydrothermal systems based on regression analysis of fluid inclusion and Rv-r data from ancient and active hydrothermal systems (Barker and Pawlewicz, 1994).

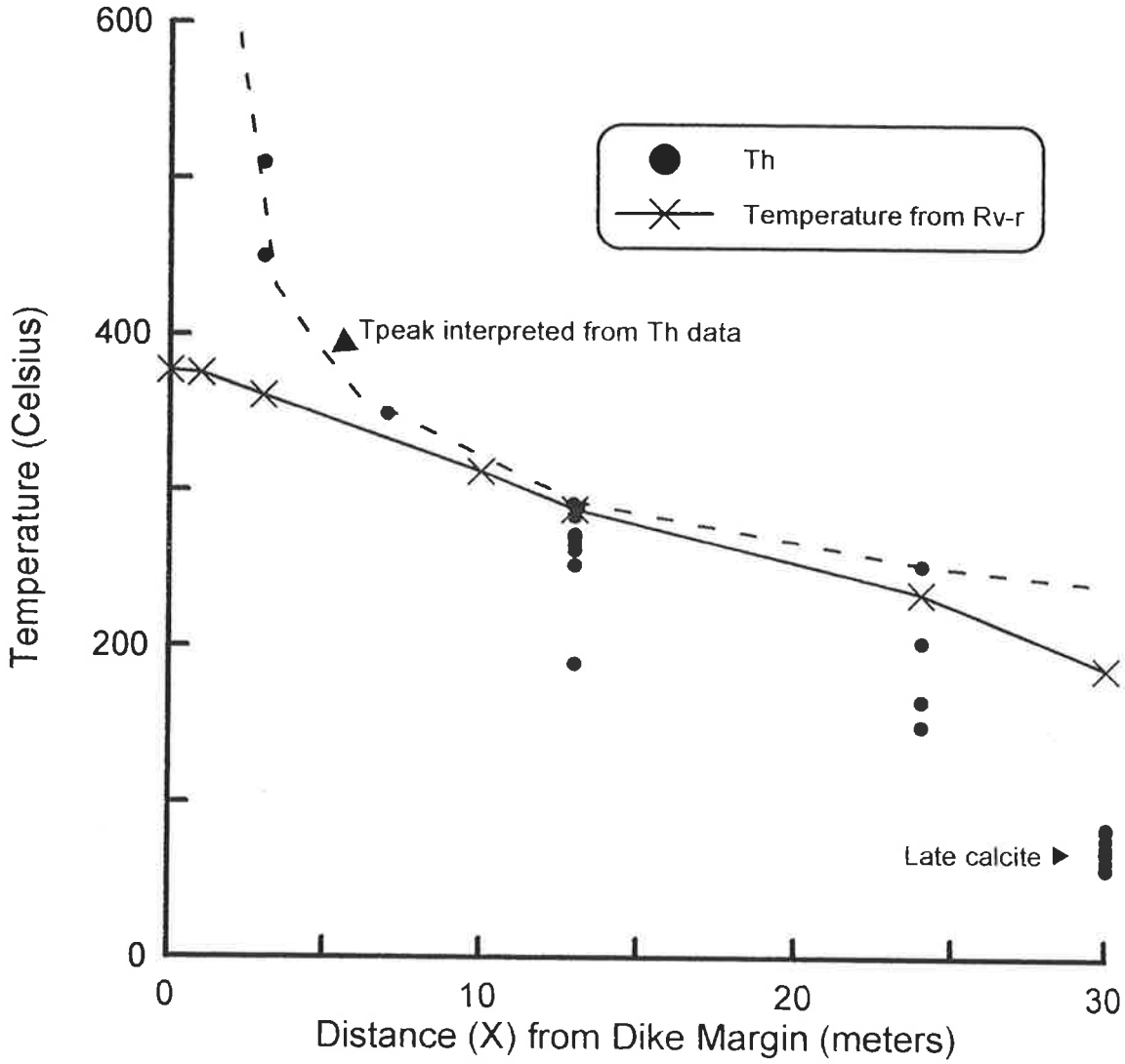
600
400
200
0
Temperature (Celsius)
Th
Temperature from Rv-r
Tpeak interpreted from Th data
Late calcite
0
10
20
30
Distance (X) from Dike Margin (meters)

The fluid inclusion results also confirm that T_{peak} is considerably higher away from the Bena 3 dike than predicted by the dike width rule. The element oxide, vitrinite reflectance, and fluid inclusion data available suggest that during contact metamorphism at Bena 3, the system may have partially opened and incipient hydrothermal convection developed. The possible convection would have been aided by an increase in fractures next to the dike suggested by the apparently more common type A and B fractures at this site. The onset of convective cooling extended the zone of increased temperature seen by their Rv-r and fluid inclusion data.

Away from the dike, the good agreement of T_{peak} estimated from fluid inclusions and Rv-r based on the hydrothermal VRG is consistent with the observation of Barker (1989) that thicker intrusive sheets seem to have a hydrothermal alteration conditions more like convecting geothermal systems.

AFT Annealing

Samples for AFT annealing study proved to be barren of apatite near the dike margin where the critical annealing levels would occur and though the rest of the dike was processed for apatite concentrates, the apatite was not counted for tracks.

4.6 CRUICKSTON 1

The Cruickston 1 dike is exposed in a cut along the road from Poowong to Ranceby, some 4 km east of Poowong, Victoria (Fig. 3-5). Cruickston 1 is a 40 m thick, northerly trending, near vertical dike or elongated volcanic plug. The dike rock is locally preserved near the dike center as rounded blocks consisting of a coarse-grained, holocrystalline gabbro. The Cruickston 1 dike intrudes a dark gray mudstone in the Strzelecki Group. The sample line extended outward from the eastern dike margin for 65 meters to near the end of the exposed mudstone in the road cut. There are no other dikes in the immediate area of Cruickston 1 and no overlapping contact

metamorphism effects are expected in these samples. Samples for AFT annealing were not analyzed because these mudstones were poor candidates for organic geochemistry. Fluid inclusion analysis is not possible at Cruickston 1 because there are no grains of transparent minerals of sufficient size.

Host Rock Thermal Maturity and Geochemistry

Vitrinite reflectance in the Cruickston 1 samples fluctuates in a wave-like manner between 3.3 % and 4.4 % (Fig. 4-9). Near the dike contact, Rv-r rapidly decreases from the highest observed value at 4.4% at X = 2 m to the lowest value found, 3.3% at X = 0.4 m. Organic matter was mostly sparse in the Cruickston 1 rocks with the TOC averaging 0.4 wt.-% (standard deviation, s =0.35 wt.-%) but varying from 1.4 to 0.04 wt.-%. The lowest TOC value is observed in the sample nearest the dike.

Rock-Eval data is generally inaccurate at low TOC and such high thermal maturation levels, and no meaningful interpretation is possible. The lack of interpretable Rock-Eval data is a surprise because the mudstones away from the immediate contact zone are a medium to dark gray color and do not look highly altered. A full range of thermal maturation and observation in changes of the organic matter through the hydrocarbon generation window was expected in these mudstones.

Another unexpected aspect of the Rv-r analyses at Cruickston 1 is the wave-like form and overall high Rv-r values in the vitrinite reflectance profile. There is no other dike known to the east of Cruickston 1 and these effects are apparently solely due to this single dike. This marked divergence may be due to the Cruickston 1 dike thickening just below the sample line, as seen at Bena 1 (Fig. 4-2), thereby extending the contact aureole to greater distances (>X/D =1.5) than the expected X/D = 1. However, as shown below, merely thickening the dike below the sample line would extend the Rv-r profile but would not greatly cause the significant changes in

the element oxide distribution observed next to the dike if a closed system is maintained.

ICP-AES

At Cruickston 1, ICP-AES results indicate important fluctuations in elemental composition throughout the sampled range from X= 65 m to X = 0.4 m (Fig. 4-10) . Again, the sharp changes near the dike contact may not be as significant in terms of assessing hydrothermal alteration as the ones occurring further away from the dike and these are discounted in the discussion. At Cruickston 1, the changes in element proportions follow the wave-like form of the Rv-r profile suggesting a temperature control on the degree of alteration. This apparent hydrothermal alteration in not obvious in the host rock: except for a few meter thick band of hornfels at the dike margin, the strata has constant medium to dark gray mudstone lithology.

The Rv-r values when converted to T_{peak} using the hydrothermal VRG of Barker and Pawlewicz (1994) suggests fluctuating temperatures in the host rock next to the dike: from 340°C at X = 2m decreasing to 300°C at X = 10 m, followed by an increase to 340°C at X = 30 m and a decrease to 300°C at X = 65 m. This fluctuation implies a variable degree of hydrothermal alteration that is also suggested by changes in element oxide proportions.

Fig. 4-9. Comparison of Rv-r and Rock-Eval pyrolysis results from mudstone within the Strzelecki Group next to the Cruickston 1 dike, western onshore Gippsland Basin, Victoria.

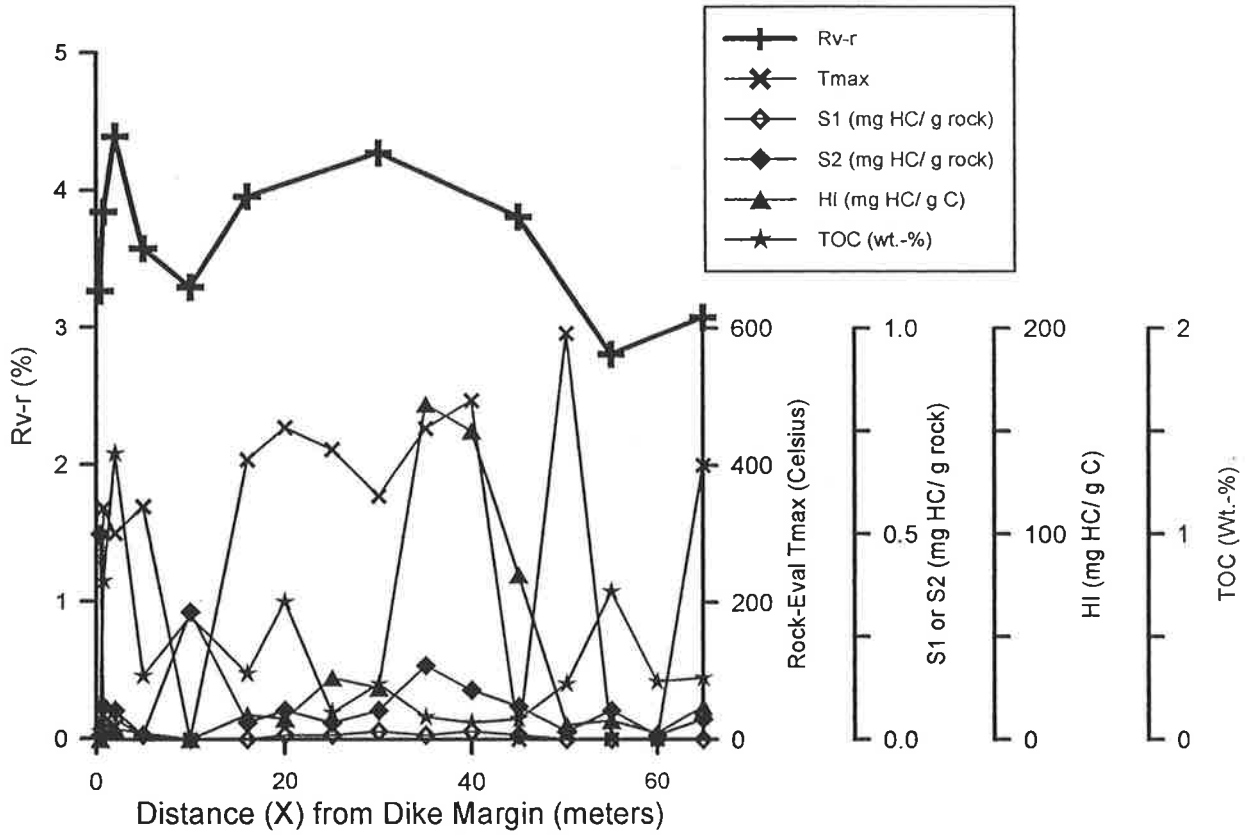
Rv-r
Tmax
S1 (mg HC/ g rock)
S2 (mg HC/ g rock)
HI (mg HC/ g C)
TOC (wt.-%)
Rv-r (%)
Rock-Eval Tmax (Celsius)
S1 or S2 (mg HC/ g rock)
HI (mg HC/ g C)
TOC (Wt.-%)
Distance (X) from Dike Margin (meters)

Fig 4-10. A comparison of selected element oxide abundances versus distance from the dike margin (X), Cruickston 1 dike, western onshore Gippsland Basin. The element oxides plotted were selected for their tendency to respond to hydrothermal alteration. SiO_2 content was plotted as SiO_2 minus 50 wt.-% so it would fit on the expanded scale with the minor oxides. Cr_2O_3, MnO, P_2O_5, and TiO_2 contents are low, fluctuate but show no trend, or are zero and these values were not plotted (Appendix 6). Note that correction of the analyses to a water-free basis was not done. This correction would increase the percentage changes in element oxide content but not the general form of the changes. Steel tools were used for sampling in the field and preparation of these samples. The basic sample size used for ICP-AES analysis was about 100 g of rock broken and selected for cleanliness minimizing any contamination effects to a few tenths of a weight percent Fe_2O_3.

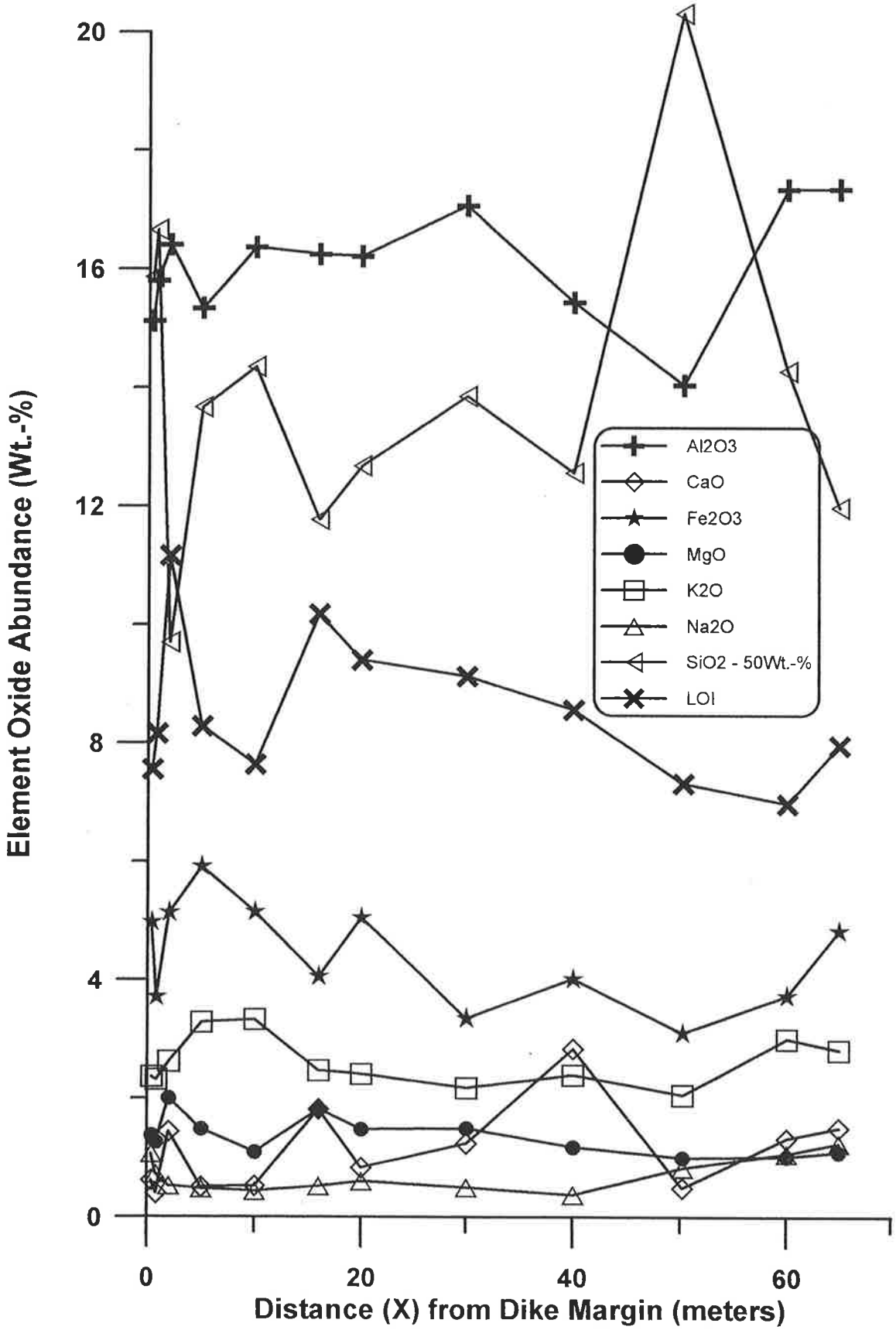
20
16
12
8
4
0
Element Oxide Abundance (Wt.-%)
0
20
40
60
Distance (X) from Dike Margin (meters)
Al2O3
CaO
Fe2O3
MgO
K2O
Na2O
SiO2 - 50Wt.-%
LOI

Thus, In many instances, the increase or decrease in element oxide proportions mirrors the changes in T_{peak} indicated by Rv-r. Most conspicuous is SiO_2 which tends to change inversely with the inferred T_{peak} computed from Rv-r. This relationship is again attributed to the direct temperature dependence of SiO_2 solubility which enriches the fluid and depletes the rock in proportion to temperature. Thus, at low Rv-r and T_{peak}, SiO_2 is not been dissolved as much from the host rock as compared to the zones of high Rv-r and T_{peak} where SiO_2 values are low, reflecting increased dissolution at high temperature. At Cruickston 1, the silica in aqueous solution may have been redeposited away from the dike near X = 50 m rather than at the dike contact. If a convection cell did develop near the dike, silica would be expected to be precipitated away from the dike, where cooled hydrothermal fluids would be descending. Near the dike, silica dissolution would occur as the hydrothermal fluid was being heated up, become buoyant and rise. This pattern is observed near Cruickston 1 (Fig. 4-10).

Hydrothermal alteration is also reflected in changes of the oxygen isotope composition of carbonate (Appendix 7). Oxygen isotopes in carbonate, during either precipitation or exchange with hydrothermal fluids, become more negative with increasing temperature (Ellis and Mahon, 1977). Thus, the more negative $\delta^{18}O$ values correlate with higher Rv-r (Fig. 4-11). Because no record of the $\delta^{18}O$ values of the water that the calcite was in equilibrium with is available, the oxygen isotope values cannot be used as a geothermometer for comparison to the VRG. However, an apparent T_{peak} control is indicated by the good agreement between increasingly negative $\delta^{18}O$ values and increased Rv-r. The strong shifts in oxygen isotopes at relatively high temperature is strong evidence for an open system and hydrothermal influence on the resulting rock compositions.

The $\delta\ ^{13}C$ values mirror the changes observed in Rv-r (Fig. 4-11). The observed enrichment of the carbonate in ^{13}C with increasing Rv-r is the attributed to a two part process 1) thermal cracking process which produces methane that is markedly enriched in ^{12}C (McKirdy

and Powell, 1974; Faure, 1977) and leaves the SOM enriched ^{13}C; and 2), the ^{13}C enriched carbon in the SOM evidently reacts at the higher temperatures to produce ^{13}C enriched CH_4 and CO_2. It has been shown that graphite may react with water at 250°C to form CH_4 and CO_2 (Landais et al., 1987). The high rank SOM next to the Cruickston 1 dike has a bronze reflection color like that seen in graphite. Thermodynamically, high rank SOM is probably little different from graphite as it differs mainly in the degree of ordering and is inferred to react in a similar manner to graphite during metamorphism. The thermodynamics of the reaction:

$$2C_{graphite} + 2H_2O = CH_4 + CO_2$$

favors gaseous products with increasing temperature. Evidence for this reaction is supported by the apparent decrease of TOC to near zero near the dike where this reaction would have its greatest expression. A decrease in TOC towards the dike margin is commonly observed in this study (Appendix 5) and in others (Degens, 1965; Peters et al., 1978; Cooles et al., 1986, Bishop and Abbott, 1995). The ^{13}C enrichment process in the CO_2 produced by this reaction is temperature driven and at higher temperatures, as indicated by the increased Rv-r, apparently precipitates or exchanges with existing carbonate to form an increasingly ^{13}C enriched carbonate. Rapid precipitation of carbonate as the CO_2 is evolved from this reaction is favored by the low aqueous solubility at high temperatures. CH_4 is mobile even in the relatively closed geologic systems represented by mudstone sealed gas traps. It presumably migrates upward and does not accumulate and retard reactions. The extent of this decarbonation reaction indicated by the considerable TOC loss near the Cruickston 1 dike argues for an open system where the products can escape and not inhibit continuing reaction. The isotopic equilibration of SOM and reaction products during hydrothermal alteration experiments has also been observed in the laboratory (Price, 1994).

Discussion of Results at Cruickston 1

The wave-like form of Rv-r at Cruickston 1 suggests that the system was not cooling as predicted by the dike width rule which would yield a monotonic increase in Rv-r as the dike is approached. The pattern of temperature dependent element mobility and apparent equilibrium exchange of oxygen and carbon isotopes suggest hydrothermal alteration occurred in a relatively open system. This evidence with the wave like pattern of thermal alteration is interpreted to be related to heating and cooling caused by convection cells operating next to the dike during contact metamorphism.

The extent of these apparent hydrothermal processes suggest a much more permeable system than expected in a mudstone. The evolution of the hydrothermal system may have increased permeability by volume changes related to dehydration and decarbonation reactions suggested by changes in LOI and TOC or perhaps enhanced fracturing of the baked and brittle mudstone. The techniques used to study fractures in transparent mineral grains at Inverloch 1 and San Remo 1 are not applicable to mudstone and these fractures are not investigated further.

Fig. 4-11. Comparison of Rv-r and $\delta^{18}O$ and $\delta^{13}C$ values from calcite cement in a mudstone of the Strzelecki Group, Cruickston 1 dike, western onshore Gippsland Basin

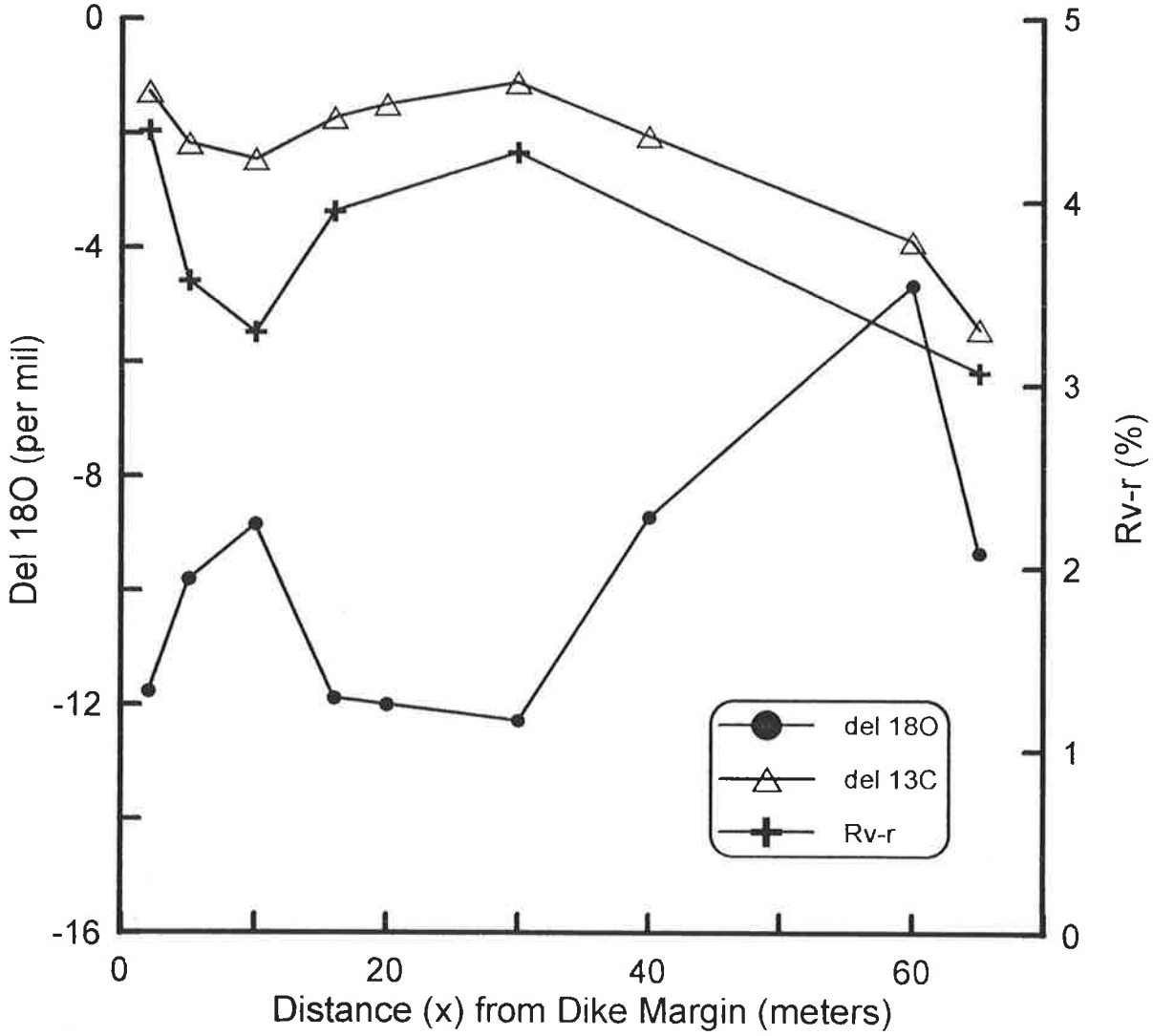
0
-4
-8
-12
-16
Del 18O (per mil)
5
4
3
2
1
0
Rv-r (%)
0
20
40
60
Distance (x) from Dike Margin (meters)
del 18O
del 13C
Rv-r

4.7 KORUMBURRA 1

Korumburra 1 is a 35 m thick, northeast trending, near-vertical dike exposed in a railroad cut just northeast of Korumburra, Victoria. The dike is more deeply buried to the east and it was only reasonable to dig in and sample host rocks on the west side (Figs 4-1e,f). The Korumburra 1 dike intrudes Strzelecki Group strata that has a moderate dip to the east. The strata are composed of hornfels near the dike, then massive sandstone followed by locally coaly sandstone with mudstone or coaly mudstone interbeds. The sample line extended outward from the western dike margin for 60 meters. There are no other dikes known in the vicinity of Korumburra 1 and no overlapping contact metamorphism effects are expected.

Host Rock Thermal Maturity and Geochemistry

Rv-r in the Korumburra 1 samples varied from 0.6% at X = 50 m to 5.2% % at X = 2 m (Fig. 4-12). As at Bena 1, there is evidence of weathering reducing Rv-r at Korumburra 1. The measured Rv-r at X = 60 m is only 0.3 %, far below the regional values of 0.5-0.6% (Fig 3-12) or background values of 0.5-0.6% nearer the dike. Also the increase in Rv-r above background levels as the dike is approached commences at X/D = 0.6 or 20 m away from the 35 m thick dike instead of at X/D = 1 as expected from the dike width rule. Rock-Eval T_{max} also starts to increase at about X/D = 0.6 but towards the dike TOC drops mostly to below 0.5 wt.-% and the T_{max} values are inaccurate. The Rock-Eval S_1 and S_2 levels are very low to zero over the thermal maturation range found next to the dike. S_1 and S_2 were expected to change substantially next to Korumburra 1 where Rv-r increases from 0.6 to 5.2 %.

Fig. 4-12. Comparison of Rv-r and Rock-Eval pyrolysis results from coaly rocks in the Strzelecki Group next to the Korumburra 1 dike, western onshore Gippsland Basin, Victoria.

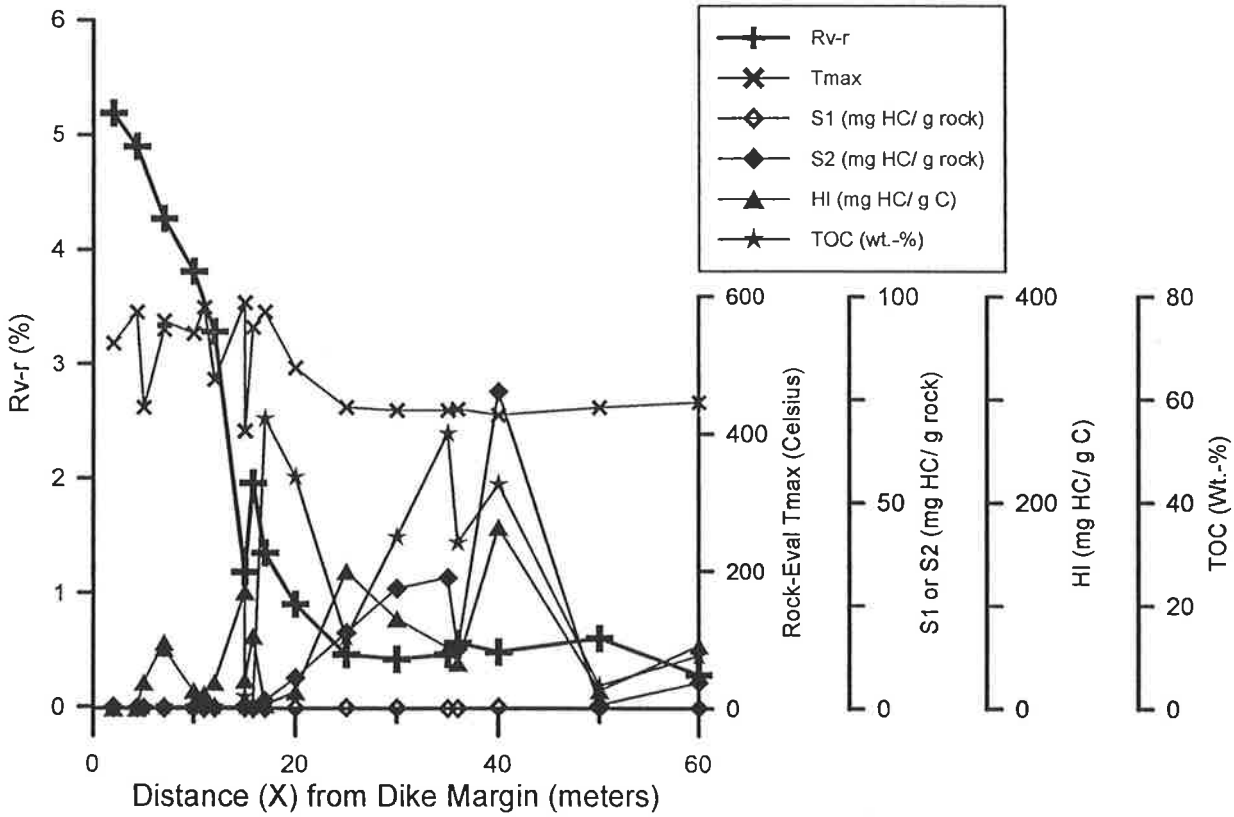
Rv-r
Tmax
S1 (mg HC/ g rock)
S2 (mg HC/ g rock)
HI (mg HC/ g C)
TOC (wt.-%)
Rv-r (%)
Rock-Eval Tmax (Celsius)
S1 or S2 (mg HC/ g rock)
HI (mg HC/ g C)
TOC (Wt.-%)
Distance (X) from Dike Margin (meters)

The hydrogen index (HI) which is also based on the S_2 peak is generally reduced at Korumburra 1 from the levels found in unweathered coals such as R5 (HI = 270 mg HC/g C) taken at depth in the State Coal mine at Wonthaggi. Conversely the oxygen index (OI) at Korumburra 1 is much higher than the OI of 9 mg CO_2 / g C found in sample R-5. As pointed out in the discussion of Bena 1, such geochemical trends are a signature of weathered coal and SOM. Consequently, the Korumburra 1 dike is not studied as intensively as the other Strzelecki Ranges dikes. No AFT annealing, whole rock element or fluid inclusion studies were done. However, porosity and permeability and thermal conductivity measurements were completed before it was realized that weathering limited the usefulness of the inland dikes in the organic geochemistry study.

Geophysics

Porosity at Korumburra 1 some 25 m away from the dike is about 30% and only decreases to 13% at the dike contact (Fig. 4-13). These porosity values are quite high compared to those values reported for unweathered portions of the Strzelecki Group (Edwards and Baker, 1943) and rock porosity is thought to be enhanced given the weathered look of the host rock at Korumburra 1. Porosity at the dike contact is also enhanced by vesicles in the host rock. Permeability, however, remains low to very low, measuring 2.72 md at X = 11 m and 0.008 md at X = 0.5. Similarly, bulk density increases near the dike contact probably due to formation of a dense hornfels. Thermal conductivity remains nearly constant at about 1.6 W/m-K as the dike is approached. The lack of change in thermal conductivity is surprising because the other geophysical parameters, especially porosity, are changing. Thermal conductivity is a bulk property, a function of the thermal conductivity of the pore fluid and the rock grains. The thermal conductivity of the rock is much higher than that of the aqueous fluids and a decrease in porosity of about 15 % would seem sufficient to cause a measurable increase in thermal

conductivity as the proportion of rock is much greater nearer the dike.

Discussion of Results at Korumburra 1

The roughly monotonic increase of Rv-r as the dike is approached is as predicted by the dike width rule. It appears that the host rock next to Korumburra 1 because of the low permeability do not allow convection to develop. Thus, the opening of a system is not solely due to the size of the dike as is demonstrated in these low permeability, apparently unfractured rocks. The much longer heating duration next to a 35 m dike as compared to a <4 meter thick dike, still does not produce an open hydrothermal system. This result is consistent with the conclusions of Browne (1978) that permeability is a key factor in controlling hydrothermal alteration.

Fig. 4-13. Comparison of porosity, permeability, bulk density and thermal conductivity measured on Strzelecki Group sandstones next to the Korumburra 1 dike, western onshore Gippsland Basin, Victoria. Permeability could not be measured in the sample at X = 24.8 m because an appropriate plug of sandstone could not be cut due to the friability of the sample. Thermal conductivity values shown were measured at 20°C (see appendix 1 for methods and Appendix 10 for numerical results) .

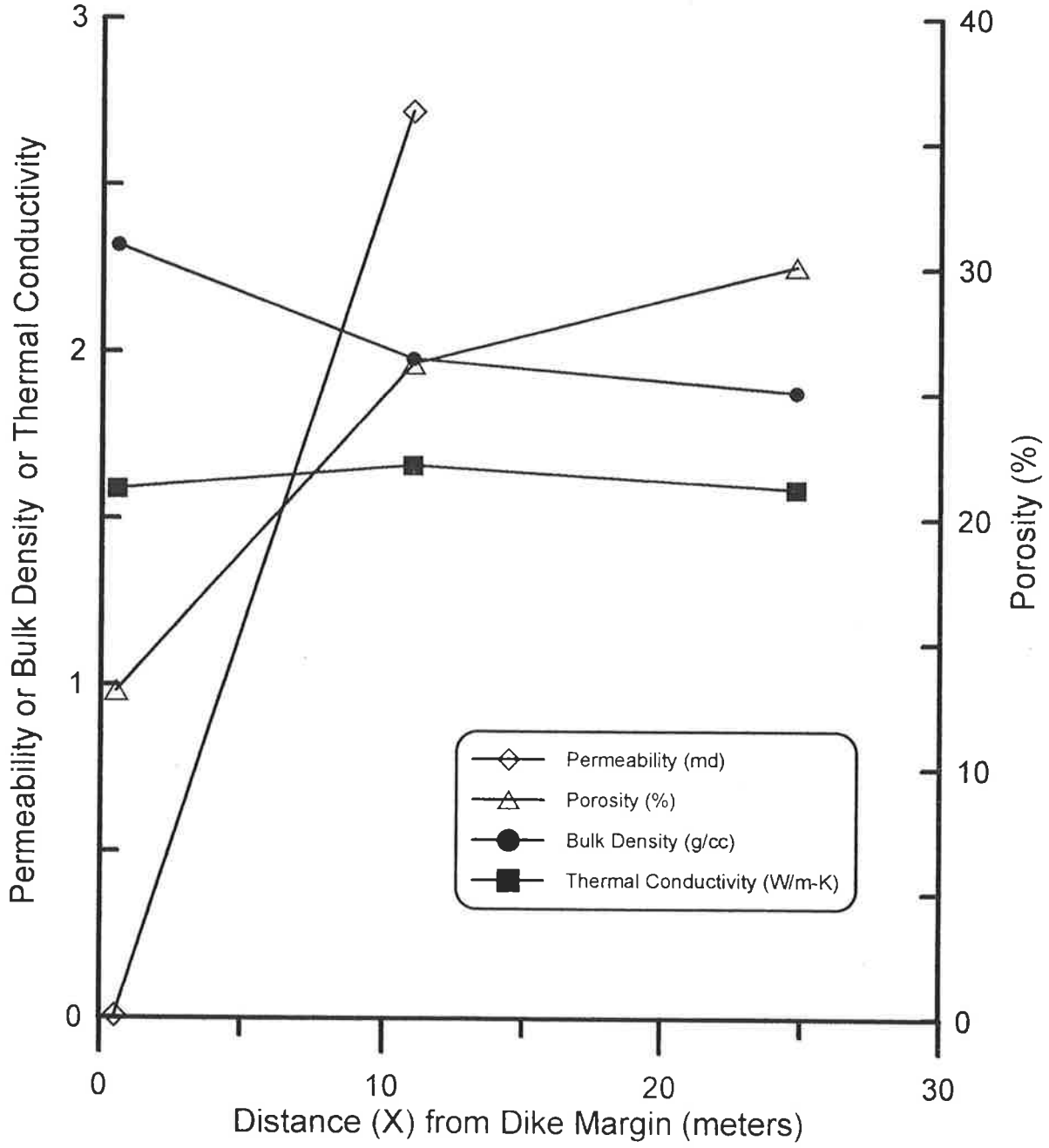
Permeability or Bulk Density or Thermal Conductivity
Porosity (%)
Distance (X) from Dike Margin (meters)
Permeability (md)
Porosity (%)
Bulk Density (g/cc)
Thermal Conductivity (W/m-K)
0
1
2
3
0
10
20
30
40

4.8 THE COASTAL DIKES

The coastal dikes are well exposed in the intertidal zone and coastal cliffs at several localities from San Remo to Inverloch, Victoria. These dikes, in general, seem to be less weathered than those exposed in the Strzelecki Ranges. Consequently, these dikes were targeted for intensive study.

4.9 INVERLOCH 1

Inverloch 1 is a 1.7 to 2.0 m thick, northwest trending dike that dips 85°E. The dike is well exposed across a wave cut platform and the coastal cliff (Fig 4-14 c, d) south southwest of Inverloch, Victoria. The dike intrudes a thin to thick bedded sandstone that locally contains reworked coal fragments and charcoal deposited along bedding planes. Within the intertidal zone, the host rock does not appear to be significantly weathered. Most samples for organic geochemistry analysis were picked from unweathered coal bearing rock fragments composed mostly of vitrinite. Although active erosion by wave and tidal action, the exposed basaltic dike rock is deeply weathered (Fig 4-15b). The AFT annealing, Rv-r, whole rock element and organic geochemistry sample suite extended outward on a perpendicular line from the western dike margin for 3.5 m and for 2 m Rv-r samples were taken from the eastern dike margin. There are no other dikes exposed near Inverloch 1 and no overlapping contact metamorphism effects are expected.

Figure 4-14. Strzelecki Group hosted dikes exposed on wave cut terraces and coastal cliffs, western onshore Gippsland Basin

A) Looking north at the 0.6 m thick San Remo 1 dike, San Remo Peninsula, Victoria. The single arrows point to the dike margins. The triple arrows point to a post-dike coarse grained sparry calcite partially filling the dike center. Fluid inclusion analyses of the calcite shows that it precipitated at about 70°C from very low salinity fluids. The San Remo 2 dike occurs to the left side of the photograph out of the field of view and is exposed high on the sea cliff face.

B) Looking north at the 0.06 m thick San Remo 3 dike, San Remo Peninsula, Victoria. Double arrow is along the western dike margin which is also marked by a thin calcite vein. The line of arrows shows the horizontal line of 5 mm diameter drill holes used to sample coaly SOM for analysis. The eastern dike margin is partially visible where it is marked by a thin calcite vein. The isotopic signature of these veins are like those found in calcite throughout the region and they formed after the dike.

C) Looking northeast at the 1.7 m thick Inverloch 1 dike, Cape Paterson, Victoria. The arrows point to the dike margins. Although partially buried in the sand of the shore, the dike reemerges in the intertidal zone where most samples for analysis were collected.

D) Close up view of the 1.7 m thick Inverloch 1 dike, Cape Paterson, Victoria. The double arrows point to the western dike margin. The single arrow points to a pit were a sample was cut out of the outcrop using a water-cooled saw. The spheroidally weathered and discolored dike rock is discernable to the right side of the frame.

E) Looking southwest at the 0.4 m thick Inverloch 2 dike exposed in the intertidal zone, Cape Paterson, Victoria. The single arrows point to the dike. A fault truncates the dike near the southerly single arrow. The double arrows point to the sample line trending east from the dike margin. The Inverloch 1 dike is located about 1 km to the southwest near where the drop in the coastal cliffs skyline occurs. The Inverloch 3 dike sample line is located about 25 meters north of the northerly single arrow in this photograph.

F) Looking down at the 0.17m thick Inverloch 3 dike exposed in the intertidal zone, Cape Paterson, Victoria. The single arrows point to the eastern dike margin. The chisel blade is about 3 cm wide. The chisel blade lies next to a channel where a sample was chipped out.

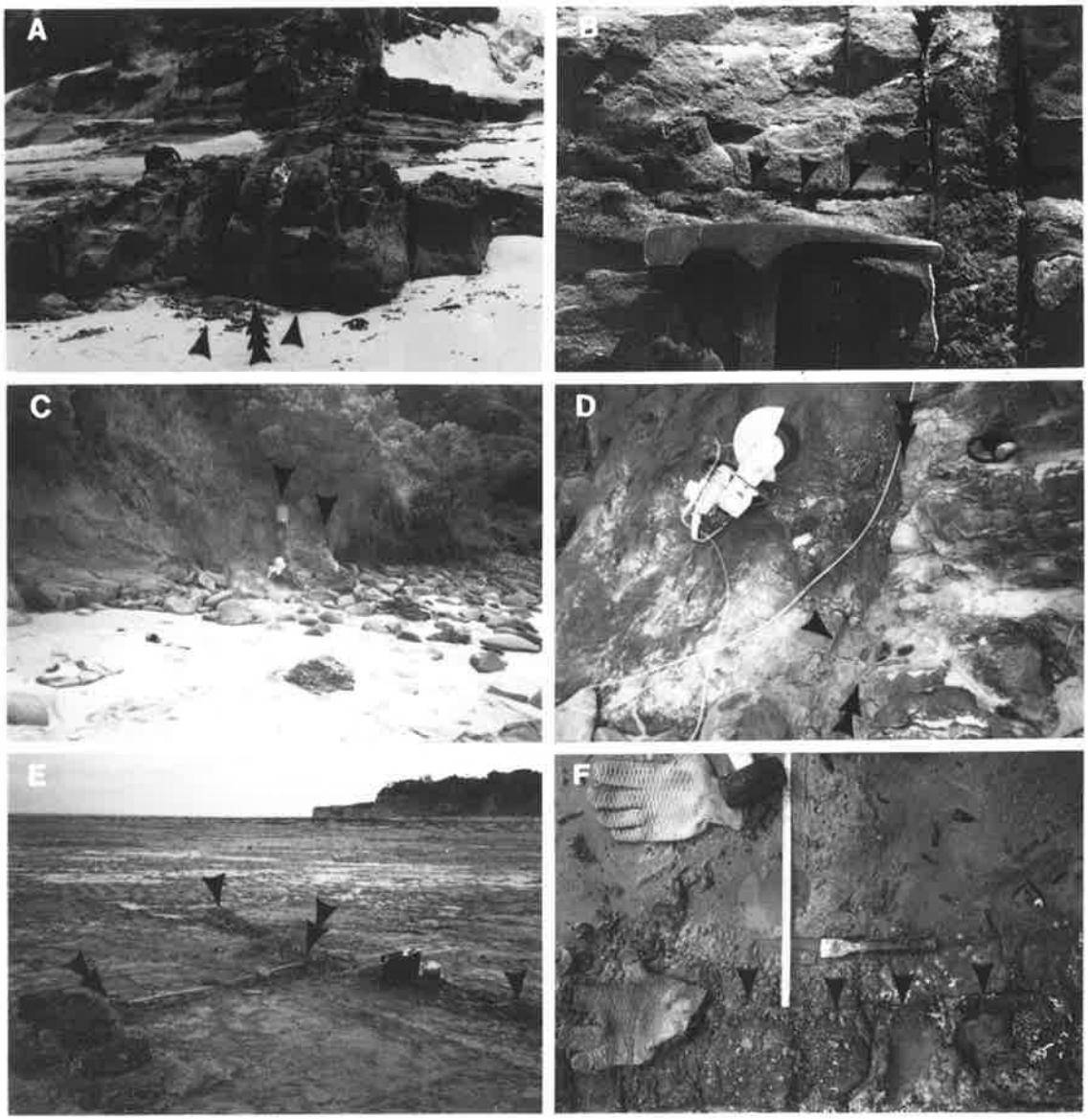
A
B
C
D
E
F

Figure 4-15. Photographs of flat surfaces ground on dike rocks and the Strzelecki Group sandstones that host the dikes.

A) Brecciated sandstone cut by a later fracture set parallel to the dike plane. The sample is from the west contact of the 1.7 m thick Inverloch 1 dike, Cape Paterson, Victoria. The fractures were present before sampling as the sample block was made by sawing it out of the outcrop. The horizontal field of view is 11 cm.

B) A dark weathering rind about 1 to 2 cm thick on the Inverloch 1 dike. The rind has developed even though the sample was exposed to vigorous erosion by wave action in the intertidal zone. This photograph illustrates how the rate of chemical weathering exceeds physical erosion even on the wave cut terraces in South Gippsland. Inland within the Strzelecki Ranges chemical weathering apparently far exceeds physical erosion and the dikes and host rocks at the surface are weathered to a soil-like consistency. Centimeter scale shown in the photograph.

C) The host rock contact with the 0.17 m thick Inverloch 3 dike, Cape Paterson, Victoria. Petrography and X-Ray diffraction shows the post-intrusion cement (white veinlets) precipitated in the sheared sandstone at the contact to be composed of mixture of calcite, feldspar and quartz with a vesiculated coke derived from the adjacent coal. Note the 1 to 2 cm thick darkened bake zone in the sandstone host next to the contact. Centimeter scale shown in the photograph.

D) A bedding plane view of vitrinite-rich coaly debris at x = 0.54 to 0.61 m east from the 0.4 m thick Inverloch 2 dike margin, Cape Paterson, Victoria. The horizontal field of view is 11 cm.

E) Rounded coal, carbonaceous mudstone and mudstone with wisps of coaly debris in an polymictic intraformational conglomerate, Inverloch 2 dike at X = 0.54 m east. Centimeter scale shown in the photograph.

F) Vitrinite-rich coaly debris lining bedding planes in the host sandstone at X = 1.43 m east, Inverloch 2 dike. Centimeter scale shown in the photograph.

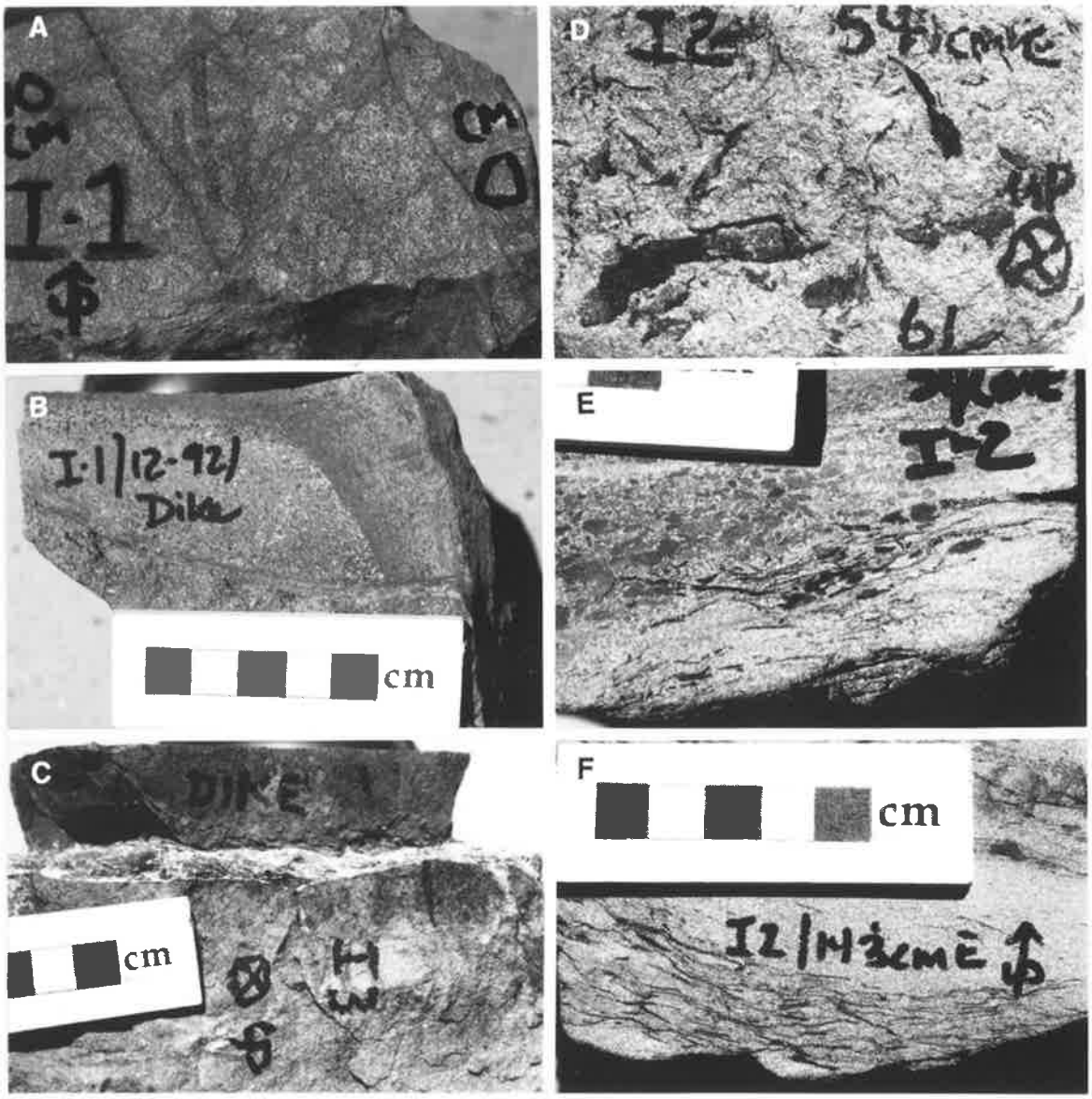
A
I·1
B
I·1/12-92/
Dike
cm
C
DIKE
cm
D
I2
54½cmE
61
E
I·2
F
cm
I2/M½cmE

At the Inverloch 1 dike, on the western sample line, Rv-r varied from 0.6 % at X = 3.5 m to a peak of 4.9% at X = 0.2 m and decreased to 4.4 % at X = 0.1 m near the dike contact (Fig. 4-16). The increase in Rv-r as the dike is approached commences between X = 2 m and 1.5 m or an X/D of about 1.0 consistent with the dike width rule. Overall, organic matter was sparse in the Inverloch 1 host sandstones but TOC on selected coaly fragments ranged from 2.5 to 9.1 wt.-%. Again, TOC tends to decrease towards the Inverloch 1 dike.

Rock-Eval T_{max} starts to increase at about X/D = 1.0, as happens with Rv-r, but as the dike is approached, TOC decreases or becomes too thermally mature to react (loss of pyrolysiable carbon). By about X= 0.7 m or X/D = 0.5, the T_{max} values as well as other Rock-Eval parameters become inaccurate and these values near the dike are not considered in the following discussion. Similarly, the Rock-Eval S_2 levels start to increase at about X = 2 m or X/D = 1 to 1.5 and then decrease to near zero. S_1 is very low to zero throughout most of the sampled range but shows a slight increase from X= 2 m to X=1 m and then again becomes very low near the dike. Again, a generally low S_1 is typical of weathered rocks. Also, S_1 and S_2 should change substantially, reflecting the opening and closing of the oil window when thermal maturation increases from 0.6% to near 5% Rv-r. The general failure of Rock-Eval in detecting hydrocarbon generation near the dike is in part attributed to the lack of pyrolysiable carbon. At Inverloch 1, the lack of reactive carbon is attributed to the fusinite (essentially fossil charcoal) common in the sandstone host. Fusinite was more common here than at the other dikes studied.

At Inverloch 1, the host rocks were well exposed in the wave cut terrace and samples were taken along perpendicular lines on both sides of the dike. The classical presumption in studying dikes is that the contact aureoles are symmetrical and only one side need be sampled because the far side will be a mirror image. Comparison of Rv-r measured on samples from the

west and east side of Inverloch 1 dike (Fig. 4-17) shows a significant difference in Rv-r. The difference in the profiles seems to be related to the 85°E dip of the Inverloch 1 dike because, as discussed below, such differences in the east and west Rv-r lines are not seen next to the near vertical dikes at Inverloch 2, Inverloch 3 and San Remo. The degree of heating on either side of Inverloch 1 even though it is inclined to the east should be equal because at a given X along the near horizontal sample lines on either side of the dike, the dike margin is at an equal distance above (west side), or below (east side), the symmetrical sample points. Contact metamorphic reaction products trapped below sills apparently can inhibit thermal maturation there (Peters et al., 1978). This effect extended to an inclined dike, that would at best only trap a small portion of reaction products below it, predicts that the west side Rv-r would be lower than that on the east side--the opposite of what is observed. Therefore the difference in the Rv-r lines cannot be explained by attributing it to differences in position relative to the dike.

The Inverloch 1 dike thickens seaward across the wave cut platform from 1.7 m to 2.0 m. The difference in Rv-r profiles may be due to the fact the dike thickening just below the sample line on the east side of the dike, as seen at Bena 1 (Fig. 4-2).

Fig. 4- 16. Comparison of Rv-r and Rock-Eval pyrolysis results from coaly rocks in the Strzelecki Group next to the Inverloch 1 dike, western onshore Gippsland Basin, Victoria.

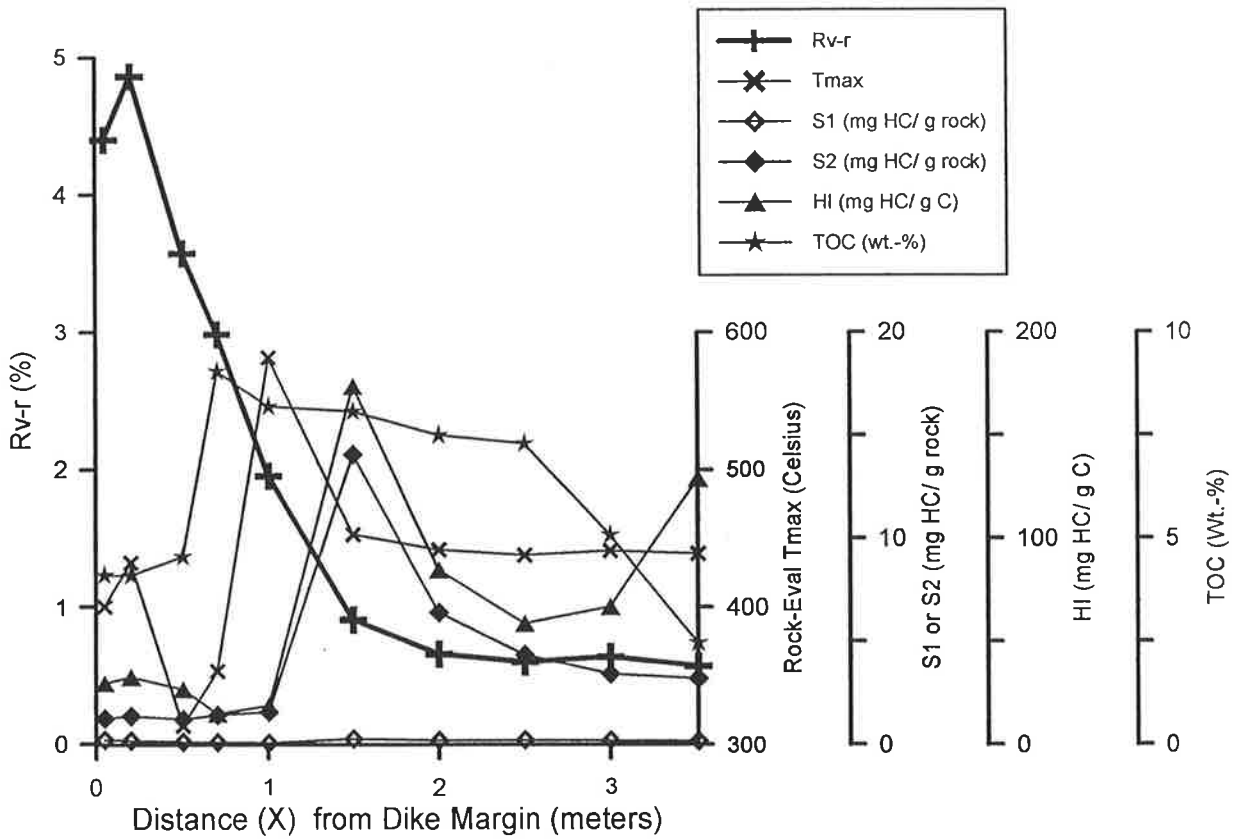
Rv-r
Tmax
S1 (mg HC/ g rock)
S2 (mg HC/ g rock)
HI (mg HC/ g C)
TOC (wt.-%)
Rv-r (%)
Rock-Eval Tmax (Celsius)
S1 or S2 (mg HC/ g rock)
HI (mg HC/ g C)
TOC (Wt.-%)
Distance (X) from Dike Margin (meters)

Fig. 4- 17. Comparison of Rv-r measured on samples from the west and east side of Inverloch 1 dike, Strzelecki Group, western onshore Gippsland Basin, Victoria.

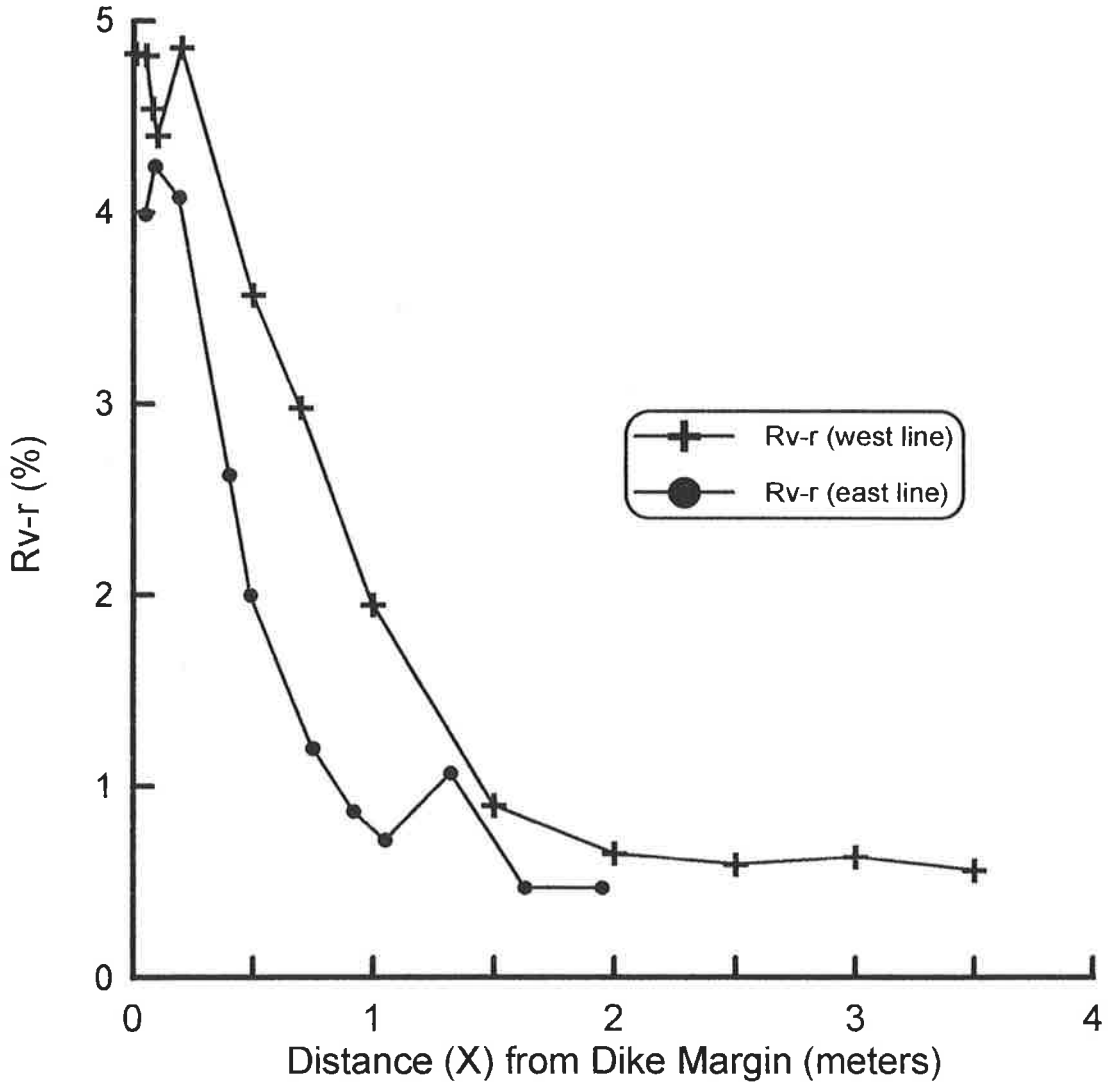
5
4
3
2
1
0
Rv-r (%)
0
1
2
3
4
Distance (X) from Dike Margin (meters)
Rv-r (west line)
Rv-r (east line)

Fig 4-18. A comparison of selected element oxide abundances versus distance from the dike margin (X), Inverloch 1 dike, western onshore Gippsland Basin. The element oxides plotted were selected for their tendency to respond to hydrothermal alteration. SiO_2 content was plotted as SiO_2 minus 50 wt.-% so it would fit on the expanded scale with the minor oxides. Cr_2O_3, MnO, P_2O_5, and TiO_2 contents are low, fluctuate but show no trend, or are zero and these values were not plotted (Appendix 6). Note that correction of the analyses to a water-free basis was not done. This correction would increase the percentage changes in element oxide content but not the general form of the changes. Steel tools were used for sampling in the field and preparation of these samples. The basic sample size used for ICP analysis was about 100 g of rock broken and selected for cleanliness minimizing any contamination effects to a few tenths of a weight percent Fe_2O_3.

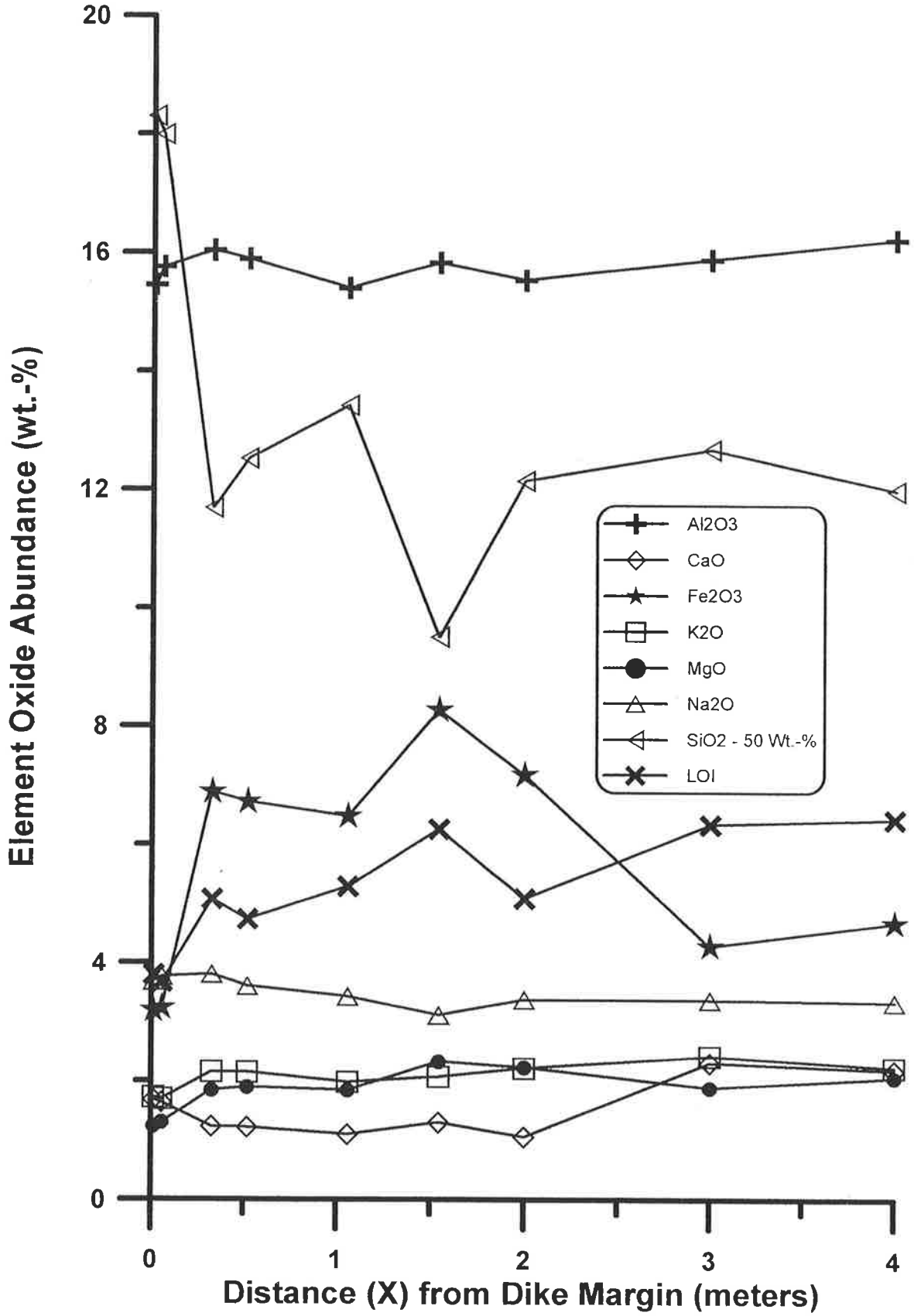
20
16
12
8
4
0
0
1
2
3
4
Element Oxide Abundance (wt.-%)
Distance (X) from Dike Margin (meters)
Al2O3
CaO
Fe2O3
K2O
MgO
Na2O
SiO2 - 50 Wt.-%
LOI

ICP-AES

At Inverloch 1, ICP-AES results indicate little fluctuation in elemental composition in most of the hydrothermally reactive elements throughout the sampled range from X= 4 m to X = 0.01 m (Fig. 4-18). Again, the often sharp changes essentially at the dike contact may not be as significant in terms of assessing hydrothermal alteration as the changes occurring further away from the dike and these are discounted in the discussion. Most elements show little change and element mobility seems small except for SIO_2, Fe_2O_3 and LOI. Except at the dike contact, SiO_2 fluctuates but shows little net change. Fe_2O_3 varies in a similar fashion to MgO and LOI and may be caused by reactions occurring in clay minerals and zeolites as the dike is approached.

To investigate these mineralogic changes in what visually appears to be mostly unweathered rock, X-Ray diffraction (XRD) analyses were completed using the powders remaining after ICP-AES analysis. Lindsay (1982) has completed a regional study of clay minerals in the Strzelecki Group. This study focuses only on using illite content as a indicator of contact metamorphism caused by dikes (Pytte and Reynolds, 1989). The XRD traces show the persistence of mixed-layer clays, chlorite and kaolinite from X = 1.05 m to the dike contact (Fig 4-19). Increasing temperatures near the dike contact should transform mixed-layer clay minerals by increasing their content of illite (Pytte and Reynolds, 1989). However, the amount of illite in these clays does not change much as the dike is approached as the mixed layer clays contain some 90% illite at X=1.55 m and X=1.05 m (peak at 9.0 °2Θ), 80% (peak at 9.1 °2Θ) at X = 0.30m and again 90% at X =0.01 m (peak at 9.0 °2Θ). This pattern may be just a reflection of an illite-rich detrital source area or, before the dike intruded, burial diagenesis caused a regional increase in illite content. Such illite-rich rocks would not show much change in illite content of the mixed-layer clays during contact metamorphism. Further, given the considerable K-feldspar content in these strata (Edwards and Baker, 1943), there is no lack of potassium to

inhibit the formation of illite from kaolinite. The lack of change in mineral assemblage as the dike is approaches is attributed to weathering. Weathering can apparently reverse the prograde sequence of increasing amounts of illite in the mixed layer clay minerals caused by heating (Moore and Reynolds, 1989). The presence of kaolinite at the dike contact would be introduced after intrusion as a weathering product of feldspar. Whether imposed by weathering or inherited from the source area or acquired during burial diagenesis, changes in the clay mineral assemblage do not seem to be a sensitive tool to investigate changes next to these dikes and was not extensively used in this study.

Carbon and oxygen isotopes were not measured on the host rocks as tests with concentrated hydrochloric acid indicated that carbonate was not common enough for analysis (Appendix 7).

Discussion of Results from Inverloch 1

The general lack of element mobility in the host rocks coupled with the apparently low permeability and observation that Rv-r monotonically increases as expected by the dike width rule suggests convection did not develop at Inverloch 1. A lack of convection is typical of thin dikes (Delaney,1987).

Fig. 4-19. X-Ray diffraction traces of the < 2 μm fraction versus distance (X) from the dike margin, Inverloch 1 dike, western onshore Gippsland Basin. The traces are dotted to show their trend when they project into the next plot. Clay mineral abbreviations: Chl = chlorite, Kao = kaolinite, ML = mixed layer clay minerals.

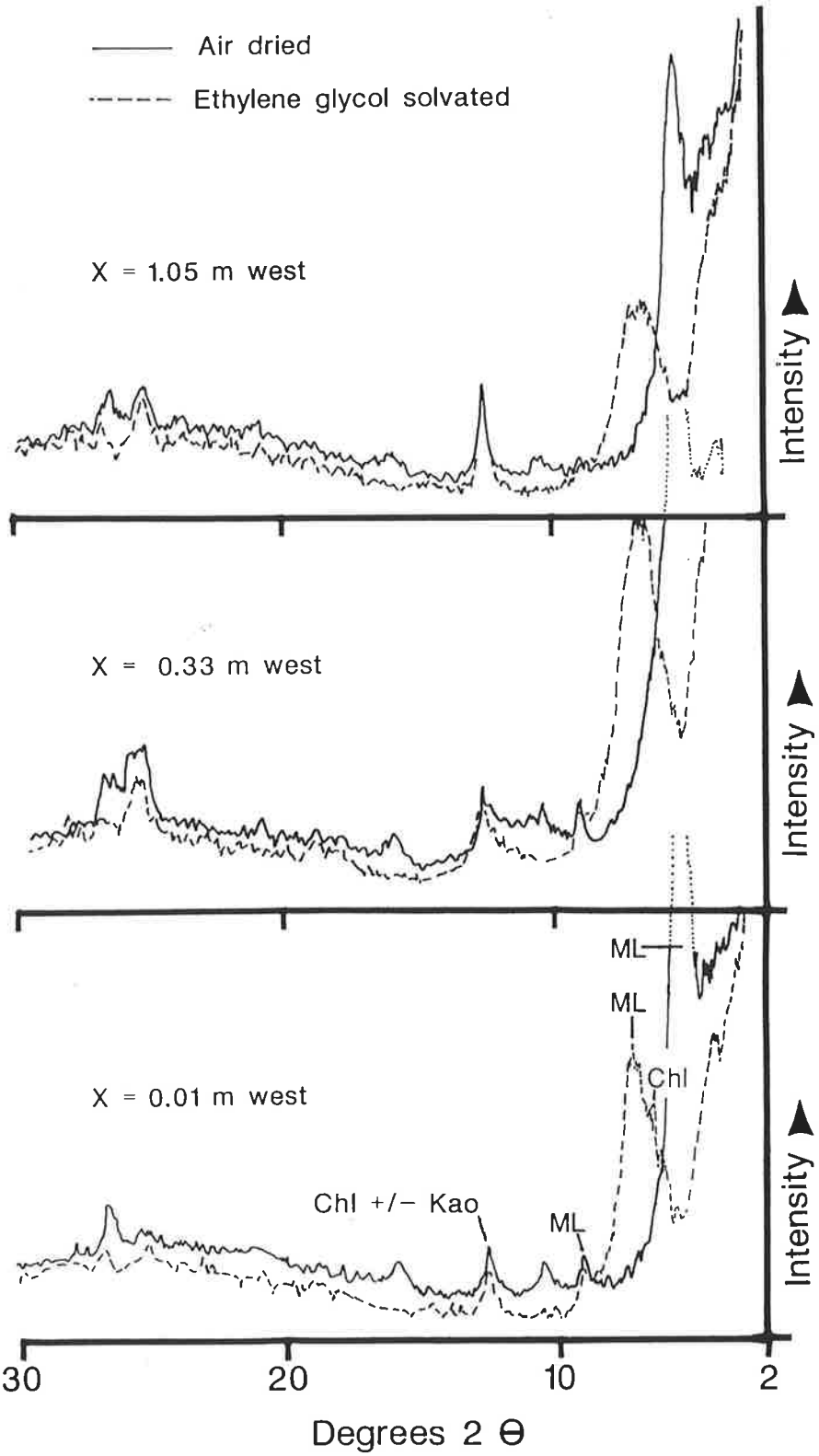
Air dried
Ethylene glycol solvated
X = 1.05 m west
X = 0.33 m west
X = 0.01 m west
Intensity
Intensity
Intensity
ML
ML
Chl
Chl +/− Kao
ML
30
20
10
2
Degrees 2 Θ

Geophysics

Permeability measurements mostly failed on host rocks from the Inverloch 1 dike because of the friable condition of the samples, even though they were sawn out of the outcrop in a effort to preserve them. In most cases, the rock disaggregated during plug cutting. Only in the baked rock at the dike contact was an adequate plug cut and a permeability of 0.02 md was measured. Porosity varies from 26% at X = 1 m to 15% at X= 0.03 in a similar fashion to that seen at Korumburra 1 and it is inferred that permeability at Inverloch 1 would also decrease towards the dike contact. Likewise, thermal conductivity is about 1.6 W/m-K measured at 20°C and does not systematically vary as the dike is approached. As at Korumburra 1, these host rocks seem to be mostly low permeability rocks whose porosity may be enhanced by weathering and thermal conductivity does not vary much as the dike is approached.

Undulosity Study

Because the rocks at Inverloch 1 did not undergo hydrothermal convection during contact metamorphism, they are good candidates for observing purely thermal effects on the host sandstones. Further, the Strzelecki Group in the vicinity of Inverloch 1 contain densely cemented, early diagenetic concretions (Gregory et al., 1989) that preserve early diagenetic features and thus should minimize burial diagenetic effects on undulosity (see appendix 1 for methods). The changes in undulosity within concretions as the dike is approached will mostly be caused by heating related to the dike. A study of undulosity in quartz was undertaken by Lewis (1993) as a Senior Thesis topic (M.R. Owen, thesis advisor) based on concretion samples supplied by the author. As noted by Lewis (1993), Bailey et al. (1958) established that recrystallization occurring during increasing metamorphism causes a reduction in undulosity. The expected response of these rocks is confirmed in this study where undulosity generally decreases towards the dike. The significance of the apparent annealing as the dike is

approached is that fluid inclusions contained in the quartz grains may reequilibrate if overheated during the annealing process. This mechanism may explain why inherited fluid inclusions appear to reequilibrate at the relatively low P_{eff} caused by the lower degrees of overheating present near X/D = 0.8 next to the San Remo 1 dike (Barker et al., 1992a).

Fig. 4-20. Comparison of Lewis (1993) undulosity measurements and mean fracture count measured in this study versus distance (X) from the dike margin in the Strzelecki Group host sandstones, Inverloch 1 dike, onshore Gippsland Basin, Victoria.

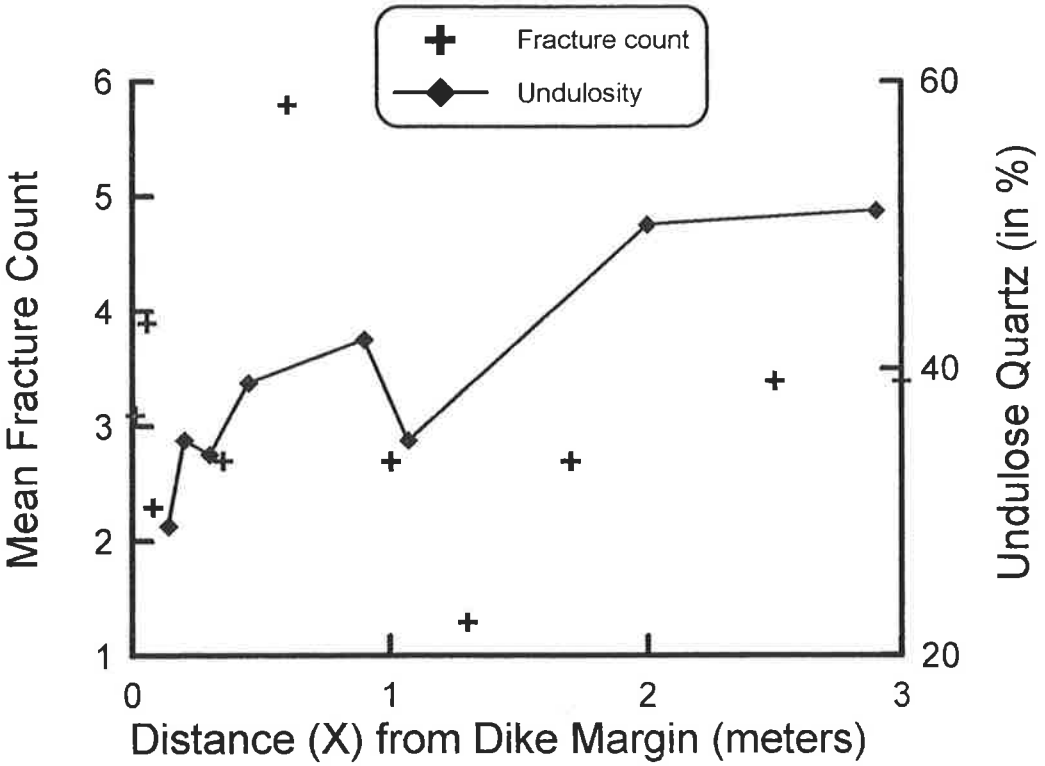
Fracture count
Undulosity
Mean Fracture Count
Undulose Quartz (in %)
Distance (X) from Dike Margin (meters)
6
5
4
3
2
1
60
40
20
0
1
2
3

Fig 4-21. Heating experiments on sandstone (Bandera Formation) and the resulting changes in permeability index and fracture index (Somerton, 1992). These indices are computed as the ratio of permeability or mean fracture count in the heated sample compared to the respective value in the unheated sample. The experiments were run dry.

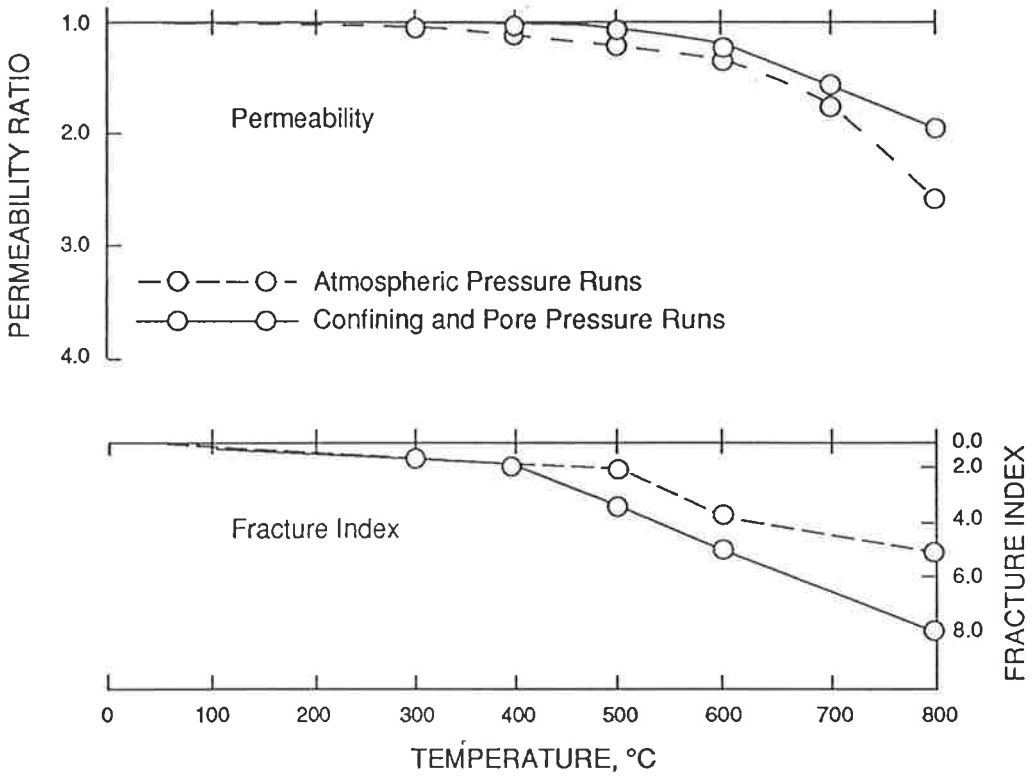
PERMEABILITY RATIO
1.0
2.0
3.0
4.0
Permeability
Atmospheric Pressure Runs
Confining and Pore Pressure Runs
Fracture Index
0.0
2.0
4.0
6.0
8.0
FRACTURE INDEX
0
100
200
300
400
500
600
700
800
TEMPERATURE, °C

Fracture Study

Heating experiments on sandstones by Somerton (1992) show a trend of increasing number of fractures and increasing permeability during heating from 300°C to 800°C (Fig. 4-21). The increased permeability is thought to be an expression of major structural damage to the rocks caused by differential thermal expansion of the framework grains. Under the microscope, this damage is expressed as an increasing number of fractures within the framework grains as T_{peak} is increased. Fracturing by differential thermal expansion seemingly must occur in nature when a basaltic dike induces temperatures near 700°C (Peacock, 1990). In some respects, Somerton's (1992) experiments are poor models of nature because they were run dry and heated at 3°C/minute to the peak temperature and then held for one hour. Healing of induced fractures and trapping fluid inclusions would be difficult under the dry experimental conditions. In nature, next to dikes, healing and annealing of the framework grains would be favored because water is present and the heating at near T_{peak} is maintained much longer than the one hour allowed in the experiments. The expected degree of fracturing suggested by Somerton's experiments may also be reduced by enhanced plastic deformation of quartz in the presence of water and under normal burial pressure. Nevertheless, as discussed below at San Remo 1, at X/D <0.1, open fractures or fluid inclusion lined healed fractures (type A and B) are increasingly common as the dike is approached. Thus, the following trapping mechanisms are proposed for detrital grains during contact metamorphism. Initially, fracturing by differential thermal expansion occurs during contact metamorphism, followed by healing of the fractures and sealing-in of the aqueous pore fluids to make type A or B fluid inclusions. The process of making synthetic fluid inclusions is similar in that quartz is heated and fractured, then new fluid inclusions are formed in hydrothermal bombs over a few days at temperature ranges similar to those found next to dikes (Sterner and Bodnar, 1984). Inherited fluid inclusions that do not decrepitate in the contact metamorphic aureole may still

reequilibrate by the grain annealing process detected by Lewis (1993). This healing and annealing process predicts that as the dike is approached, increased heating should cause a reduction in the number of fractures-- not the increase seen by Somerton (1992). Permeability should also decrease as open fractures are increasingly healed towards the dike as observed at Korumburra 1 and Inverloch 1. Because healing of fractures appears to be quite rapid in aqueous solutions (Brenan, 1991) many of these fractures could trap fluids at near T_{peak} .

This trapping along healed fractures at near T_{peak} is observed in this study. Increasingly higher T_h is measured on fluid inclusions along type A and B healed fractures as the dike is approached as is shown at Bena 3 and is discussed below at San Remo 1.

Fracture counts made using thin sections prepared from the host sandstone (no concretions) show that the mean fracture count (FC, essentially mean fracture density per microscope field of view) generally decreases as the Inverloch 1 dike is approached (Fig. 4-20). Superimposed on this trend are local increases in the mean FC in the immediate vicinity of the dike. Local increases in FC are thought to be an expression, at the thin section level, of exposed veins and fractures that parallel the trend of the Inverloch 1 dike (Fig 4-15a). The overall decrease in fractures near the dike, when viewed in the light of the undulosity study, suggest that grain annealing and(or) a fracture healing process, rather than fracturing processes alone increasingly dominate at high temperatures. Presumably the locally increased number of open fractures next to the dikes must be superimposed on samples after annealing-- probably after cooling and during dilation of the rocks during exhumation. These later fractures, many now calcite filled, appear to exploit the same northwest trending joints that the dike used during intrusion because they parallel the dike trends at each locality in the onshore Gippsland Basin.

Fluid Inclusion Geothermometry

The fluid inclusion study at Inverloch 1 failed because the sandstones are fine grained (50-100 μm size), pseudomatrix or matrix rich, and the transparent framework grains are mostly composed of monocrystalline quartz grains of volcanic origin that characteristically contain no or rare type C inclusions (Blatt et al., 1972). Further, these quartz grains did not later develop recognizable type A and B fluid inclusions. The lack of fracturing is attributed to the fine grained nature of the rocks and the reduced number of quartz to quartz grain contacts in these mudstone clast and matrix-rich sandstones (Fig. 4-15e). These combined effects may have cushioned grains from compaction effects. Further, the relatively closed system that apparently existed at Inverloch 1 appears to have reduced the chances of trapping of fluid inclusions during contact metamorphism as SiO_2 mobility, perhaps needed to heal the fractures, was relatively low adjacent to this dike.

Thin sections along three different sample lines were prepared without finding any identifiable type A and B fluid inclusions and this aspect of the study at Inverloch 1 was abandoned.

Fig. 4-22. Apparent apatite fission track age and Rv-r versus distance (X) from the Inverloch 1 dike margin, western onshore Gippsland Basin, Victoria. The fission track ages plotted are the pooled values as the single grain data passed the X^2 test at the 5% level. The error bar is $\pm 1\sigma$.

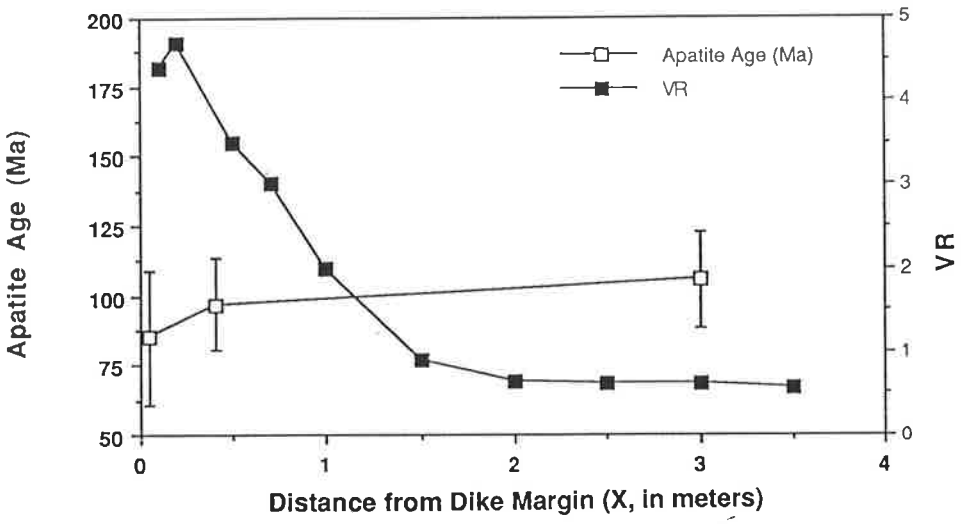
Apatite Age (Ma)
VR
Apatite Age (Ma)
VR
200
175
150
125
100
75
50
5
4
3
2
1
0
0
1
2
3
4
Distance from Dike Margin (X, in meters)

AFT Annealing

As at Bena 1, the apparent decrease in apatite age from 108 Ma at X = 3 m to 85 Ma at X = 0.025 m (Fig. 4- 22), considering the scatter in the age determinations, is not significantly different than the ages away from the dike. The apatite age near the dike is not distinguishable from the Early Cretaceous stratigraphic age because the dikes intruded when host rock temperatures were high enough that the AFT were unstable and were being rapidly annealed. Thus, the AFT age only records the cooling age of the sediment and dike package. Because the heating duration next to the dike was apparently not recorded by AFT annealing and the fluid inclusion studies failed, no other work, such as ^{13} C CP MAS NMR studies, was done at the Inverloch 1 dike.

4.10 INVERLOCH 2

Inverloch 2 was primarily studied to determine the Rv-r profile next to thin dikes where heating duration is quite short. This aspect is covered in detail in chapter 5, but the purpose of this portion of the study is to identify the dike thickness required to produce a heating duration so short during contact metamorphism that Rv-r cannot fully react. Thus, the Rv-r profile would begin to fall below the clustered Rv-r profiles from the thicker dikes when plotted against X/D. The dikes at Inverloch 3 and San Remo 3 were also specifically sampled for the same reason as they are exceptionally thin at 0.17 m and 0.06 m wide, respectively.

Inverloch 2 is a 0.4 m thick, near vertical, northerly trending dike. The dike is well exposed in the intertidal zone on a broad wave cut platform (Fig. 4-14e) south of Inverloch, Victoria. The host rock does not appear to be significantly weathered. The exposed dike rock is weathered. The dike intrudes a locally crossbedded sandstone that contains allochthonous coal fragments and shale pebble conglomerates (Fig. 4-15 d, e, f). Unweathered-looking coal fragments composed mostly of vitrinite were picked for organic geochemistry analysis. The Rv-

r and organic geochemistry sample line extended on a perpendicular from the eastern dike margin to X = 2 m and an Rv-r sample line extended in the opposite direction from the western dike margin to X = 0.8 m. The 0.17 m thick Inverloch 3 dike is located about 20 m north of Inverloch 2 along the same dike trend and no overlapping contact metamorphism effects are expected.

Host rock Thermal Maturity and Geochemistry

Vitrinite reflectance in the Inverloch 2 samples on the eastern sample line varied from 0.5 % at X = 2 m to a peak of 4.7% at X = 0.01 m (Fig. 4- 23). Contact metamorphic heating next to this dike is relatively uniform as is shown by the generally overlapping east and west Rv-r profiles (Fig. 4-24). Overall, organic matter is common in the Inverloch 2 host sandstones; TOC varies from 1.5% to 60 wt.-%. Because coal is common here and the rock appears to be relatively unweathered, hydrocarbon generation occurring as the dike is approached is discussed in detail.

As observed at Cruickston 1 and Inverloch 1, TOC tends to decrease as the dike is approached, but as coaly material is more common in this case, adequate TOC for organic geochemical analysis persisted up to the Inverloch 2 dike contact. The lowest TOC observed along the eastern sample line, 1.48 wt.-%, is at the dike contact. In part, the reduction in TOC is attributed to reaction of the carbon with water to produce mobile gases. Then through migration, carbon is lost to the system. Also with increasing thermal maturation, the movement of generated hydrocarbons can reduce the amount of carbon remaining in the system. On the Inverloch 2 east sample line, Rv-r increases from 0.5% near X/D =1 between X=0.4 m and X = 0.3 m to 4.7% at the dike contact, in general accord with predictions from the dike width rule. Rock-Eval T_{max} also starts to increase at about X/D = 1.0 from about 430°C to 550°C at X/D = 0.25 and then decreases as the dike is approached. Near the dike, pyrolysiable carbon content

appears to be too low and the T_{max} values, as well as the other Rock-Eval parameters, become inaccurate and are excluded from further consideration. The Rock-Eval S_1 values range from 0.7 to 0.4 mg HC/ g rock from X/D = 5 to X/D = 0.25 and then approach zero. S_1 should increase from X/D = 1 towards the dike as thermal maturation increases into the hydrocarbon generation window but probably remains low due to hydrocarbon migration or weathering. S_2 or HI would usually be expected to decrease inward from X/D = 1, where thermal conversion of SOM to free hydrocarbon commences, to near the dike contact where no pyrolysiable carbon remains. The data from Inverloch 2 generally follow this trend, suggesting that hydrocarbon generation has occurred near the dike.

C and O isotopes analyses on vein calcite next to Inverloch 2 dike shows a composition of $\delta^{18}O$ of -20.24 $^{o}/_{oo}$ and $\delta\ ^{13}C$ of -3.93 $^{o}/_{oo}$ and a calcite vein at X=0.33 had a $\delta^{18}O$ of -16.36$^{o}/_{oo}$ and $\delta\ ^{13}C$ of -0.23$^{o}/_{oo}$ (Appendix 7). A post-dike calcite that fills vesicles in a coal coke formed during contact metamorphism had a $\delta^{18}O$ of -14.52$^{o}/_{oo}$ and $\delta\ ^{13}C$ of -4.52 $^{o}/_{oo}$. All of these isotopic compositions are within the range of those found for early diagenetic concretions in the region suggesting they have precipitated from similar ^{18}O depleted meteoric fluids or fluids derived from the dissolution of such cements (Gregory et al., 1989; Fig. 3-11).

Fig. 4- 23. Comparison of Rv-r and Rock-Eval pyrolysis results from coaly sandstones in the Strzelecki Group next to the Inverloch 2 dike, western onshore Gippsland Basin, Victoria.

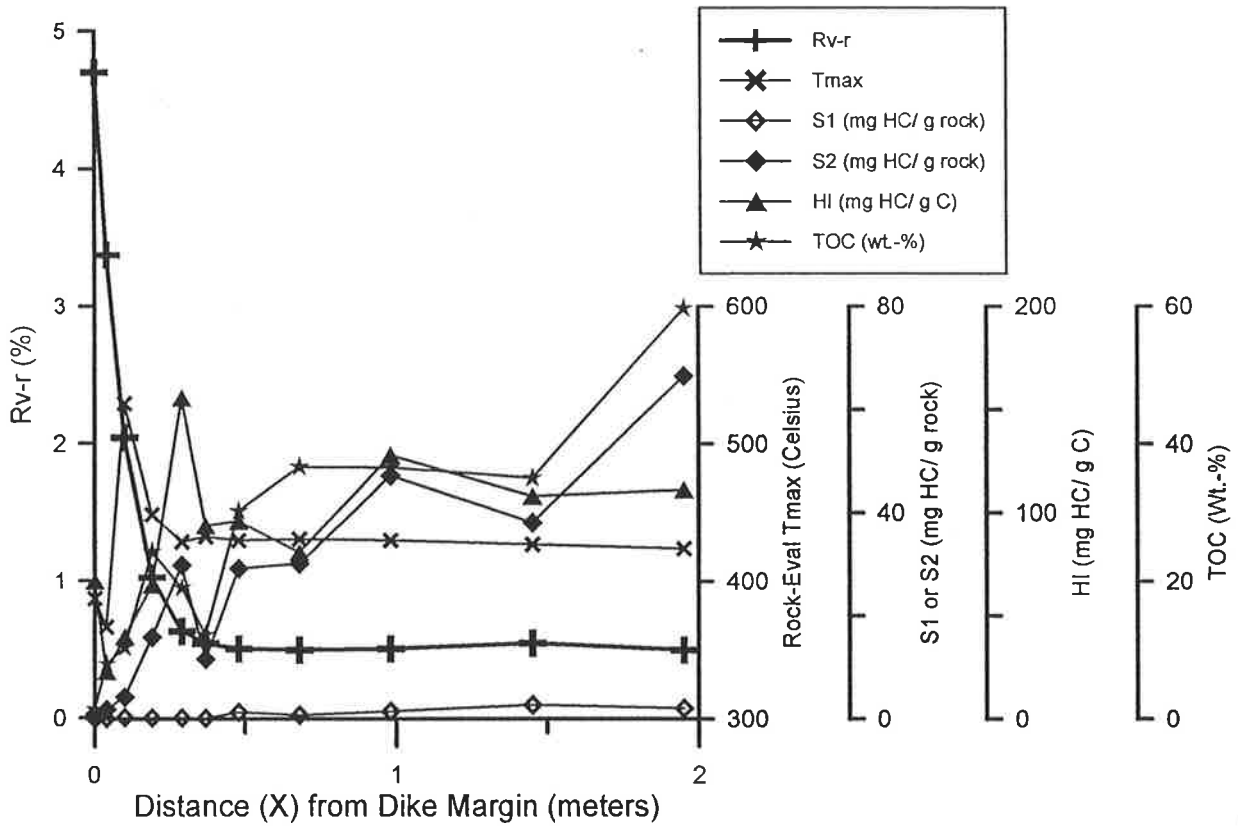
Rv-r
Tmax
S1 (mg HC/ g rock)
S2 (mg HC/ g rock)
HI (mg HC/ g C)
TOC (wt.-%)
Rv-r (%)
Rock-Eval Tmax (Celsius)
S1 or S2 (mg HC/ g rock)
HI (mg HC/ g C)
TOC (Wt.-%)
Distance (X) from Dike Margin (meters)

Fig. 4-24. Comparison of Rv-r measured on samples from the west and east side of Inverloch 2 dike, Strzelecki Group, western onshore Gippsland Basin, Victoria.

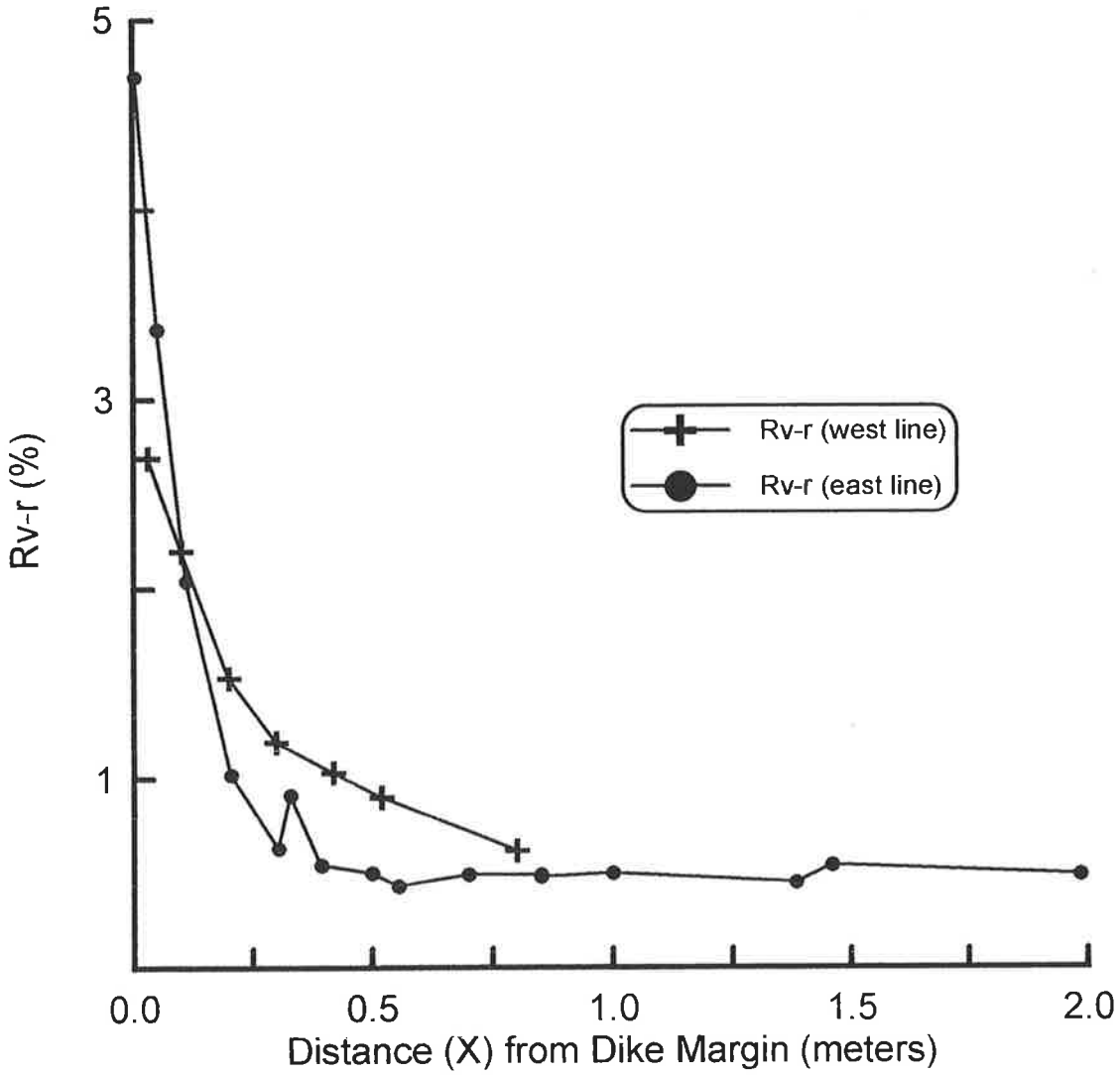
5
3
1
Rv-r (%)
Rv-r (west line)
Rv-r (east line)
0.0
0.5
1.0
1.5
2.0
Distance (X) from Dike Margin (meters)

^{13}C CP MAS NMR results are generally consistent with the onset of hydrocarbon generation as the dike is approached, marked by a rapid decrease in aliphatic carbon content. This is shown by an increase in fa from 0.73 commencing at about X = 0.3 m, X/D = 0.75 to an fa of about 1 at an X/D of near zero (Fig. 4-25). An fa of 1 indicates an aromatic carbon rich material that has essentially no remaining H-C bonded carbon and is incapable of further hydrocarbon generation. After X = 0.3 m or X/D = 0.75 and Rv-r increases from 0.6% to 2.0%, hydrocarbon generation is marked by the loss of: 1) methyl groups attached to aromatic carbon denoted by the decrease in the peak shoulder at 20-30 ppm; 2) a narrowing of the aromatic peak by loss of intensity in the range of 148-170 ppm marking the loss of heteroatomic groups bonded to aromatic carbon and an increasing size, or less substitution on, the aromatic rings (Garcia-Gonzalez et al., 1993); and 3) a narrowing of the aliphatic + aromatic side spinning band (ssb) peak by loss of intensity in the range of 50-90 ppm marking the loss of aliphatic carbon bonded to oxygen (Table A1-2 in Appendix 1). The peak remaining in the former aliphatic region near fa =1 is mostly due to ssb. The loss of the carbonyl carbons, phenolic carbons also occurs with increasing thermal maturation and along with the evolution of the heteroatomic compounds along with the generation of CO_2, H_2O and hydrocarbons with increasing thermal maturation.

Fig. 4- 25. ^{13}C CP MAS NMR spectra, Rv-r , and aromatic fraction (fa) versus distance (X) from the dike margin, Inverloch 2 dike, western onshore Gippsland Basin, Victoria. The regional sample R-5 is presented as an example of a relatively unweathered coal because it was sampled 60 m underground at an active mine face in the State Coal mine near Wonthaggi, Victoria. Sample R-5 is marginally mature (Fig. 5-16).

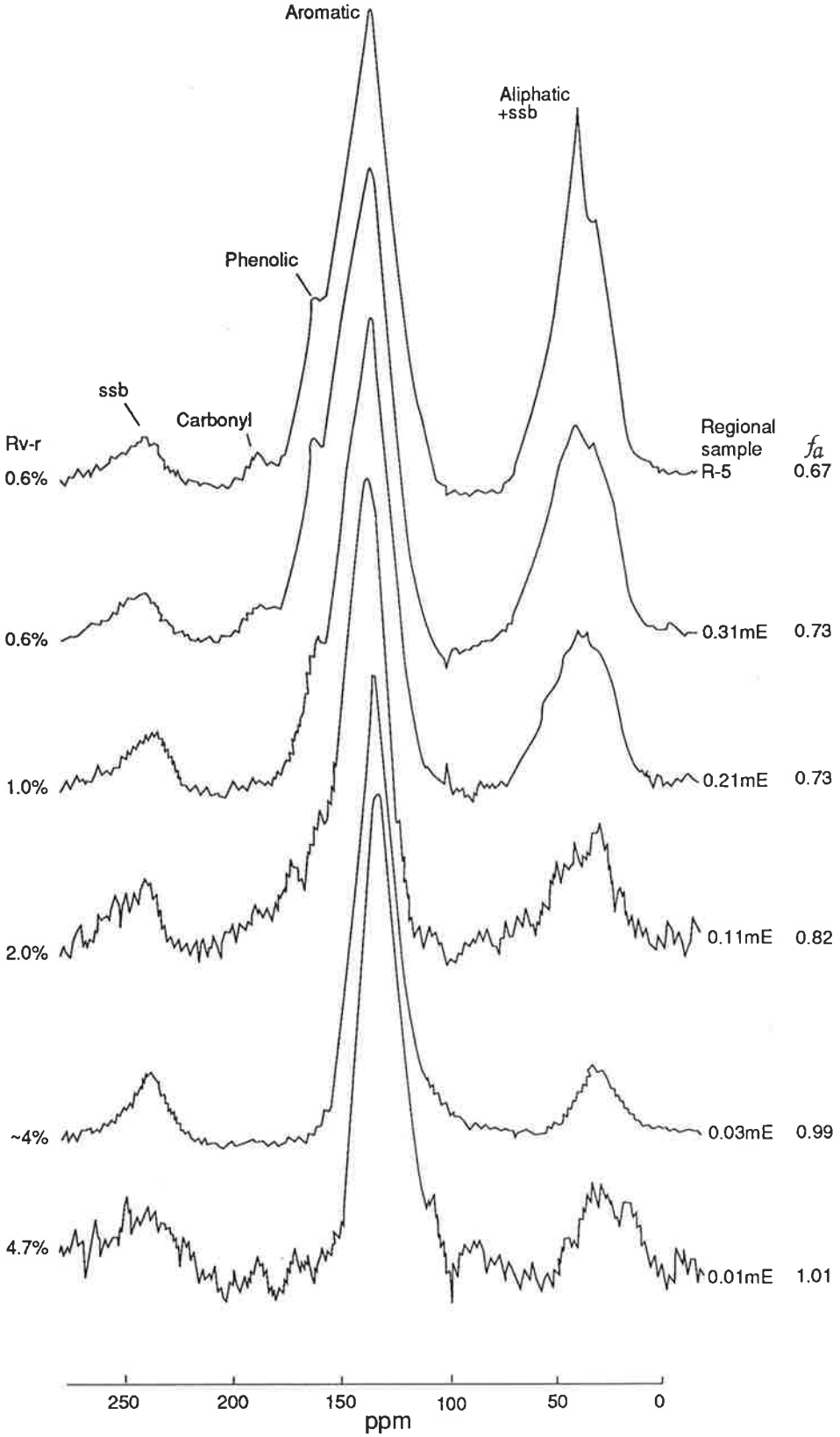
Aromatic
Aliphatic
+ssb
Phenolic
ssb
Carbonyl
Rv-r
Regional
sample
f_a
0.6%
R-5
0.67
0.6%
0.31mE
0.73
1.0%
0.21mE
0.73
2.0%
0.11mE
0.82
~4%
0.03mE
0.99
4.7%
0.01mE
1.01
250
200
150
100
50
0
ppm

4.11 INVERLOCH 3

Like Inverloch 2 and San Remo 3, Inverloch 3 was primarily studied to determine the Rv-r profile next to thin dikes where heating duration is quite short.

Inverloch 3 is a 0.17 m thick, near vertical northwest-trending dike about 20 m north of Inverloch 2. The dike is well exposed across a broad wave cut terrace (Fig 4-14 f) south of Inverloch, Victoria. Inverloch 3 is located on the eastern branch of the Inverloch 2 dike after it splits into two thinner branches. The dike intrudes a sandstone that contains allochthonous coal fragments. The host rock appears unweathered. The exposed dike rock is thoroughly weathered. For organic geochemistry analysis the samples were picked for unweathered vitrinite bearing rock or coal fragments. The Rv-r and organic geochemistry sample line extended out perpendicular to the eastern dike margin for 0.5 m. The other dike in the area, Inverloch 2, is exposed along the same dike trend due south-southeast of Inverloch 3 and no overlapping contact metamorphism effects are expected as the sample lines for both dikes are separated by about 20 m.

Host rock Thermal Maturity and Geochemistry

Vitrinite reflectance in the host sandstone east of the Inverloch 3 dike varied from 0.6 % at X = 0.5 m to a peak of 3.7 % at X = 0.01 m (Fig. 4-26). Overall, organic matter was moderately abundant in the Inverloch 3 host sandstones and TOC reached from 2 to 58 wt.-% in selected coaly fragments. As observed at other dikes in the area, TOC tends to decrease towards the dike. Because coal is common here and the rock appears to be relatively unweathered, hydrocarbon generation occurring as the dike is approached is discussed in detail.

Fig. 4-26. Comparison of Rv-r and Rock-Eval pyrolysis results from coaly sandstones in the Strzelecki Group next to the Inverloch 3 dike, western onshore Gippsland Basin, Victoria.

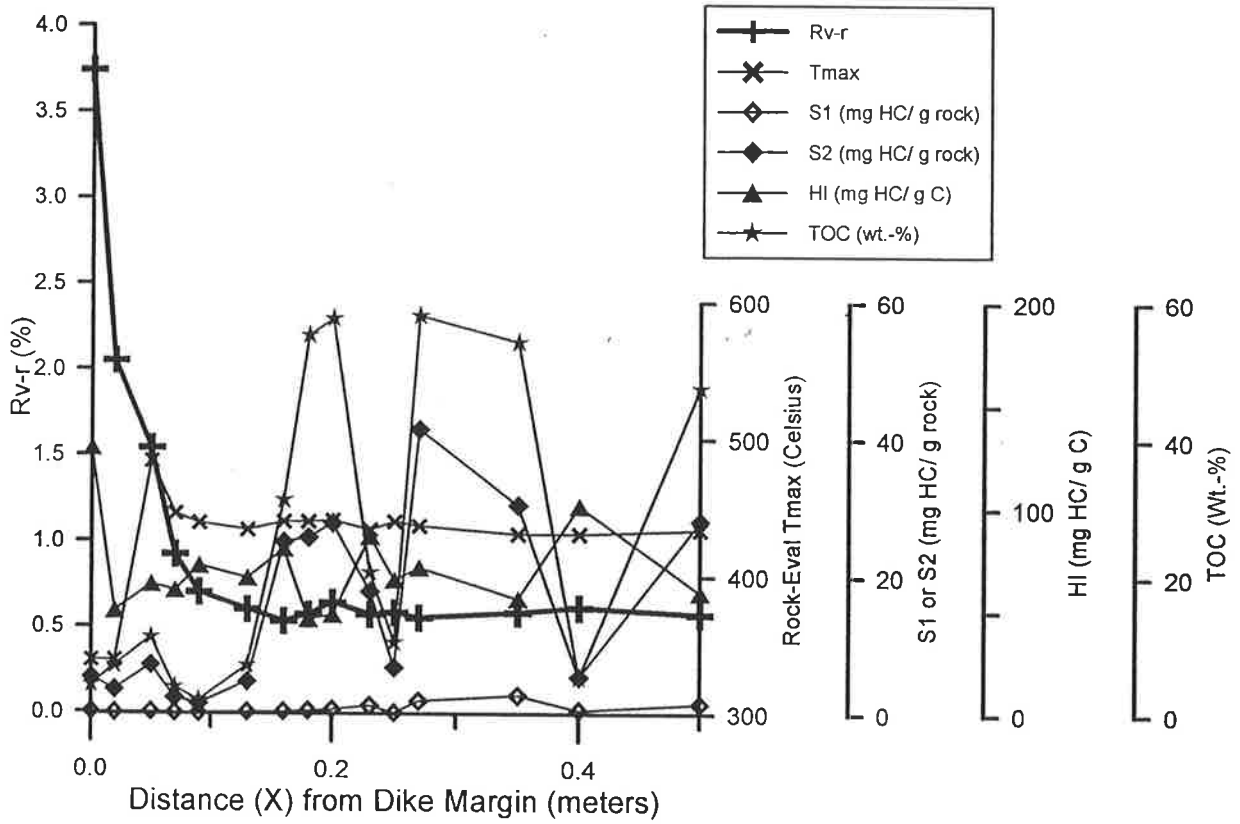
Rv-r
Tmax
S1 (mg HC/ g rock)
S2 (mg HC/ g rock)
HI (mg HC/ g C)
TOC (wt.-%)
Rv-r (%)
4.0
3.5
3.0
2.5
2.0
1.5
1.0
0.5
0.0
0.0
0.2
0.4
Distance (X) from Dike Margin (meters)
600
500
400
300
Rock-Eval Tmax (Celsius)
60
40
20
0
S1 or S2 (mg HC/ g rock)
200
100
0
HI (mg HC/ g C)
60
40
20
0
TOC (Wt.-%)

At Inverloch 3, Rv-r increases above background at about X = 0.17 m, X/D =1 as expected from the dike width. Rock-Eval T_{max} starts to increase at about X = 0.1 m but quickly decreases again as the dike is approached. Near the dike, the T_{max} values as well as all other Rock-Eval parameters become inaccurate because of increasing thermal maturation and a lack pyrolysiable carbon. Rock-Eval S_1 and S_2 levels are moderate to high as the dike is approached. HI varies over a narrow range from 50 to 100 mg HC/ g C as the dike is approached and tends to decrease near the dike as thermal maturity increases and hydrocarbon generation occurs. S_1 would usually be expected to change substantially next to Inverloch 3 when thermal maturation increases over a Rv-r range of 0.6% to 3.7%. However, S_1, remains low as the dike is approached and thermal maturation increases probably due to loss of hydrocarbon by migration or due to weathering.

Isotopic analysis of vein calcite at the dike contact (Fig 4-15c) shows a composition of $\delta^{18}O$ of -18.42 $^{o}/_{oo}$ and $\delta\ ^{13}C$ of -3.82 $^{o}/_{oo}$ and a calcite vein at X=0.42 had a $\delta^{18}O$ of -19.84 $^{o}/_{oo}$ and $\delta\ ^{13}C$ of -1.53 $^{o}/_{oo}$. Both of these isotopic compositions are within the range of the isotopic composition found regionally for early diagenetic concretions suggesting they have precipitated from similar ^{18}O depleted meteoric fluids or fluids derived from the dissolution of such cements (Gregory et al., 1989; Fig. 3-11). Petrography and XRD shows the post-intrusion cement (white veinlets in Fig 15c) that precipitated in the sheared sandstone at the Inverloch 3 contact to be composed of a mixture of calcite, feldspars and quartz with a vesiculated coke. These silicates and coke are apparently from crushing and formation of a mylonite-like material from the host coaly sandstone during intrusion.

4.12 SAN REMO 1

San Remo 1 intrudes coarse grained lithic sandstones and polymictic conglomerates that were deposited closer to the rift margin than the other host sandstones used in this study. Within the San Remo 1 host rocks, the larger framework grains contained abundant fluid inclusions. The host rocks also appear to be relatively unweathered where exposed in the shore face. However, the thin coal beds exposed in the cliff face were deeply weathered and accurate Rv-r could not be measured on them (Appendix 2). Fortunately, a thin discontinuous coal bed composed largely of vitrinite was found in the middle portion of the east sample line and a partial sample suite of relatively unweathered coal was obtained. The dike rock shows some preserved feldspar laths but most other minerals are weathered and unrecognizable. Because of the apparent freshness of the host rock and the presence of usable fluid inclusions, San Remo 1 was studied intensively to constrain T_{peak} for making heating duration estimates using AFT annealing data.

San Remo 1 is a 0.6 m thick, near-vertical, northerly trending dike. The dike is well exposed (Fig. 4-14 a) south of Inverloch, Victoria. The samples for organic geochemistry analysis were picked for unweathered-looking coal fragments composed mostly of vitrinite, so adequate analysis could be performed. The exposed basaltic dike rock is weathered and no fresh samples were available for petrography. The Rv-r, Rock-Eval, NMR, GC and hydrous pyrolysis sample line extended perpendicular to the eastern dike margin to X = 2.45 m. An AFT , Rv-r, ICP-AES, Rock-Eval, isotope and fluid inclusion sample line extended in the opposite direction from the western dike margin to X = 4 m. Numerous calcite veins that parallel the dike on either side of it were also sampled. Although San Remo 1 occurs in a cluster of three dikes, no overlapping contact metamorphism is expected because all three dikes are <0.6 m thick and spaced about 10 m apart.

Host rock Thermal Maturity and Geochemistry

Vitrinite reflectance in the San Remo 1 samples on the eastern sample line varied from 0.6 to 0.7% % at X = 2 m to 2.45 m to a peak of 3.7% at X = 0 m (Fig. 4- 27). Rv-r increases above background near X = 1 m or X/D = 1.7 which is in poor agreement with the dike width rule. Contact metamorphic heating on either side of this dike is relatively uniform as shown by the generally overlapping east and west Rv-r profiles (Fig. 4-28). Organic matter is moderately common to abundant in the San Remo 1 host sandstones; TOC varies from 2.9 wt.-% to 73 wt.-%. Because TOC is adequate and the rock appears to be relatively unweathered, hydrocarbon generation occurring as the dike is approached is discussed in detail.

As observed at most other dikes in the area, TOC tends to decrease as the dike is approached, but as coaly material is more common in this case, adequate TOC for organic geochemical analysis persisted up to the San Remo 1 dike contact. The lowest TOC observed along the eastern sample line, 2.9 wt.-% is at the immediate dike contact. As discussed above the reduction in TOC is caused by: 1) reaction of the carbon with water to produce gases which are mobile and through migration, carbon is lost to the system; and 2) increasing thermal maturation which causes hydrocarbon generation whose mobile phases can escape, reducing the carbon remaining in the system.

Fig. 4- 27. Comparison of Rv-r and Rock-Eval pyrolysis results from coaly rocks in the Strzelecki Group next to the San Remo 1 dike, western onshore Gippsland Basin, Victoria.

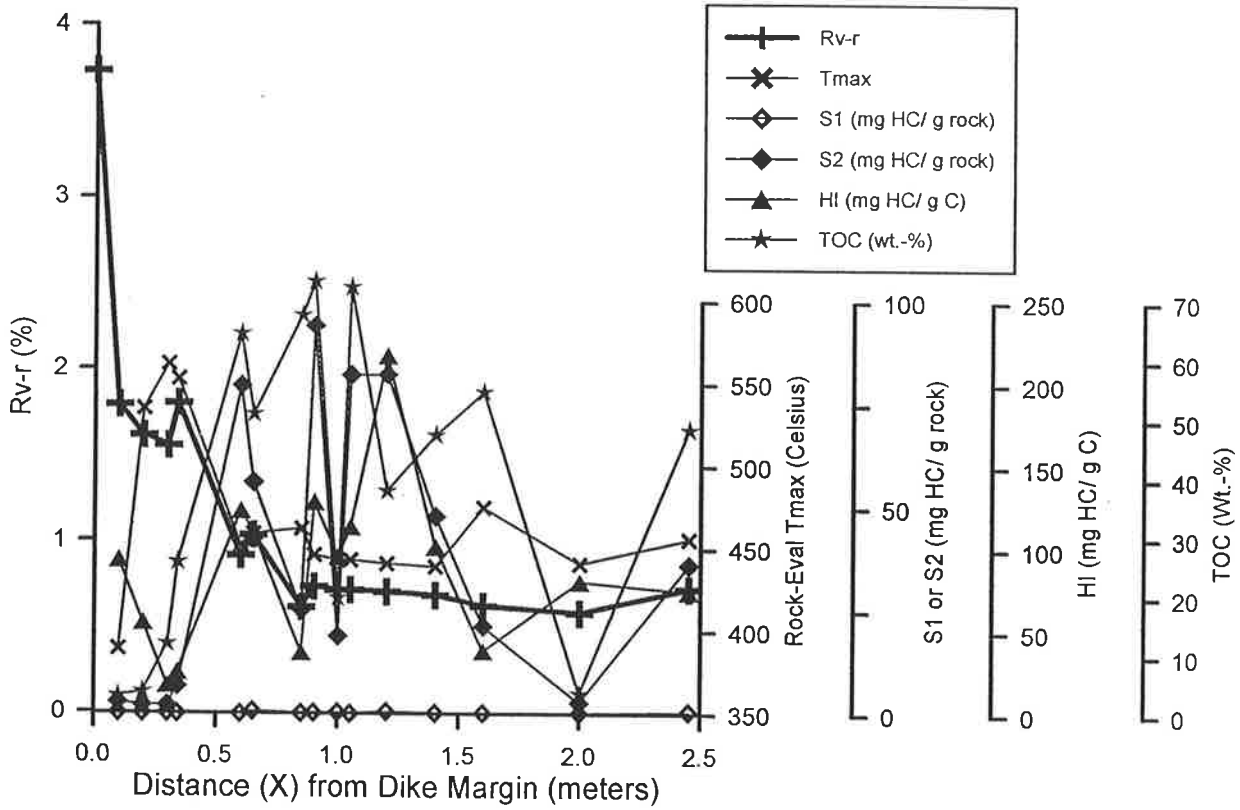
Rv-r
Tmax
S1 (mg HC/ g rock)
S2 (mg HC/ g rock)
HI (mg HC/ g C)
TOC (wt.-%)
Rv-r (%)
Rock-Eval Tmax (Celsius)
S1 or S2 (mg HC/ g rock)
HI (mg HC/ g C)
TOC (Wt.-%)
Distance (X) from Dike Margin (meters)

Fig. 4- 28. Comparison of Rv-r measured on samples from the west and east side of San Remo 1 dike, Strzelecki Group, western onshore Gippsland Basin, Victoria. Mean Maximum vitrinite reflectance (Rv-m) analyses of the AFT sample suite by A. C. Cook commissioned by Geotrack International. After conversion of Rv-m to Rv-r using the equation of Ting (1978), these independently measured data are in good agreement with those measured in this study.

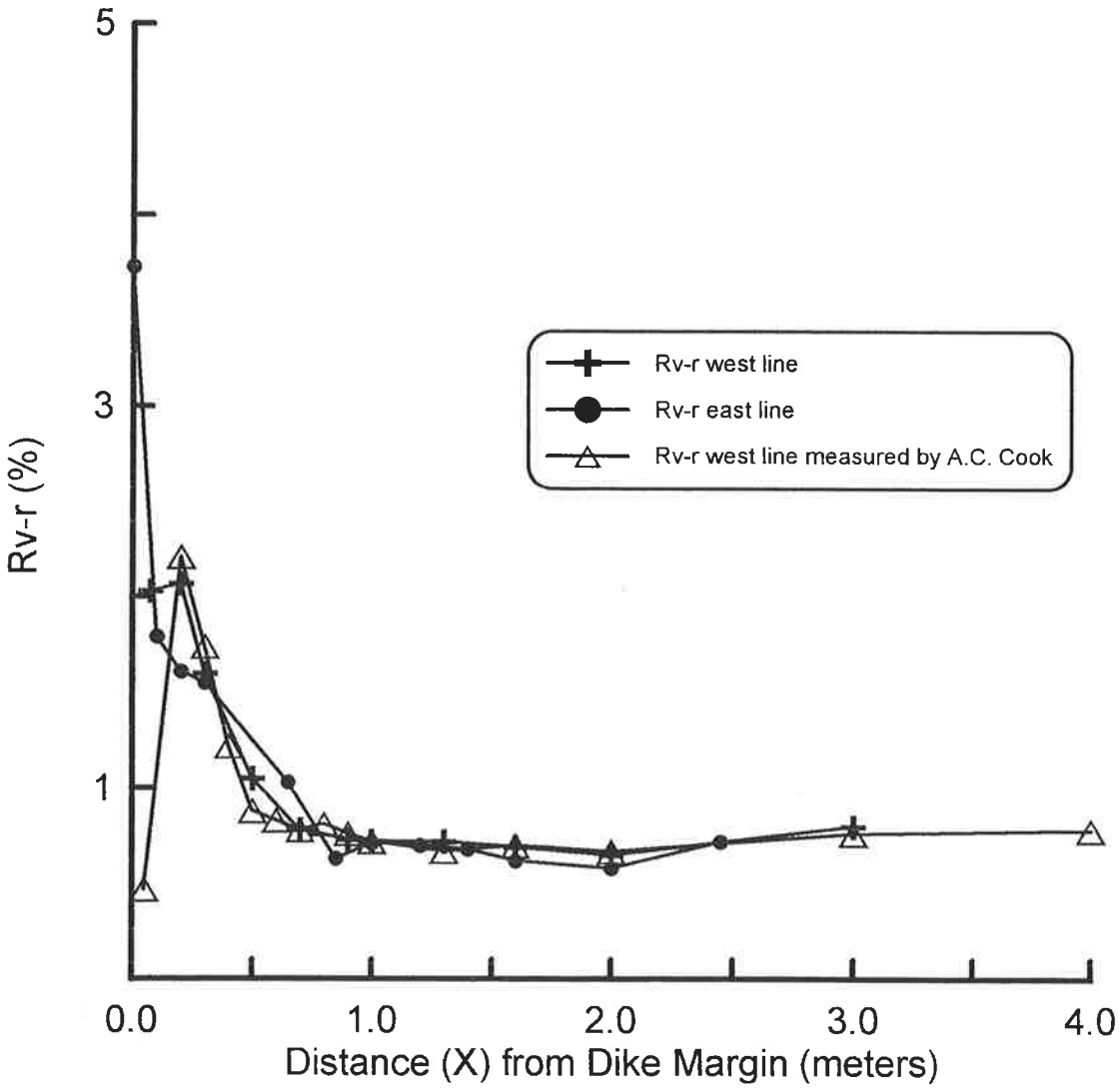
5
3
1
Rv-r (%)
Rv-r west line
Rv-r east line
Rv-r west line measured by A.C. Cook
0.0
1.0
2.0
3.0
4.0
Distance (X) from Dike Margin (meters)

Like Rv-r, Rock-Eval T_{max} also starts to increase from 440°C at about X/D = 1.7 to 560°C at X/D = 0.5 and then decreases as the dike is closely approached. Near the dike, pyrolysiable carbon content appears to be too low and the T_{max} values, as well as the other Rock-Eval parameters, become inaccurate and are excluded from further consideration. The Rock-Eval S_1 values range from 0.7 to 0 from X/D = 4 to X/D = 1.8 and then increase again. The decrease in S_1 to 0 at X/D = 1.8 is not well understood but may be attributed to losses occurring during weathering but not to a decrease in TOC, which is 72 wt.-% in this sample. S_1 increases from X/D = 1.7 as thermal maturation increases into the hydrocarbon generation window. Inspection of S_1 increases with Rv-r suggests the onset of hydrocarbon generation occurs at about 0.7%, peaks near 1.0%, and ends near 1.8% (Chapter 5). Near the dike, any generated hydrocarbons are probably destroyed during contact metamorphism or escape from the system as natural gases. S_2 and HI would usually be expected to decrease from X/D = 1.7, where thermal conversion of the SOM to free hydrocarbon commences, to the near dike contact where no pyrolysiable carbon remains. The data from San Remo 1 generally follow this trend, suggesting that hydrocarbon generation has occurred near the dike.

^{13}C CP MAS NMR results are consistent with continuing hydrocarbon generation and thermal maturation as the dike is approached, marked by a rapid decrease in aliphatic carbon content. This is further demonstrated by an increase in fa from 0.82 at Rv-r = 1.0% commencing with the initial sample at X = 0.65, X/D = 1.1 to an fa of 0.89 and a Rv-r of 3.7 % at an X/D of near zero (Fig. 4-29). The regional Rv-r near the San Remo dikes is about 0.7 % and further away from the dike marginally mature SOM is expected with an fa of about 0.7, somewhat higher than that of the regional sample R-5 shown on Fig. 4-30. Near the dike, an fa of 0.9 indicates an aromatic carbon rich material that has essentially little remaining H-C bonded carbon and is capable of little hydrocarbon generation. After X= 0.65 m or X/D = 0.75 and Rv-r increases from 0.7% to 3.7%, hydrocarbon generation, like that seen at Inverloch 2, is

marked by the loss of: 1) methyl groups attached to aromatic carbon denoted by the decrease in the peak shoulder at 20-30 ppm; 2) a narrowing of the aromatic peak by loss of intensity in the range of 148-170 ppm marking the loss of heteroatomic groups bonded to aromatic carbon and an increasing size, or less substitution on, the aromatic rings (Garcia-Gonzalez et al., 1993); and 3) a narrowing of the aliphatic +ssb peak by loss of intensity in the range of 50-90 ppm marking the loss of aliphatic carbon bonded to oxygen (Table A1-2 in Appendix 1). The peak remaining in the former aliphatic region near fa =0.9 is mostly due to aromatic side spinning band (ssb). The loss of the carbonyl and phenolic carbons, along with the loss of the heteroatomic groups with increasing thermal maturation occurs along with the evolution of CO_2, H_2O and hydrocarbon.

Fig. 4-29. ^{13}C CP MAS NMR spectra, Rv-r, and fa versus distance (X) from the dike margin Rv-r, San Remo 1 dike, western onshore Gippsland Basin, Victoria. The regional sample R-5 is presented as an example of a relatively unweathered coal because it was sampled underground in the State Coal mine near Wonthaggi, Victoria. Sample R-5 is marginally mature (Fig. 5-16).

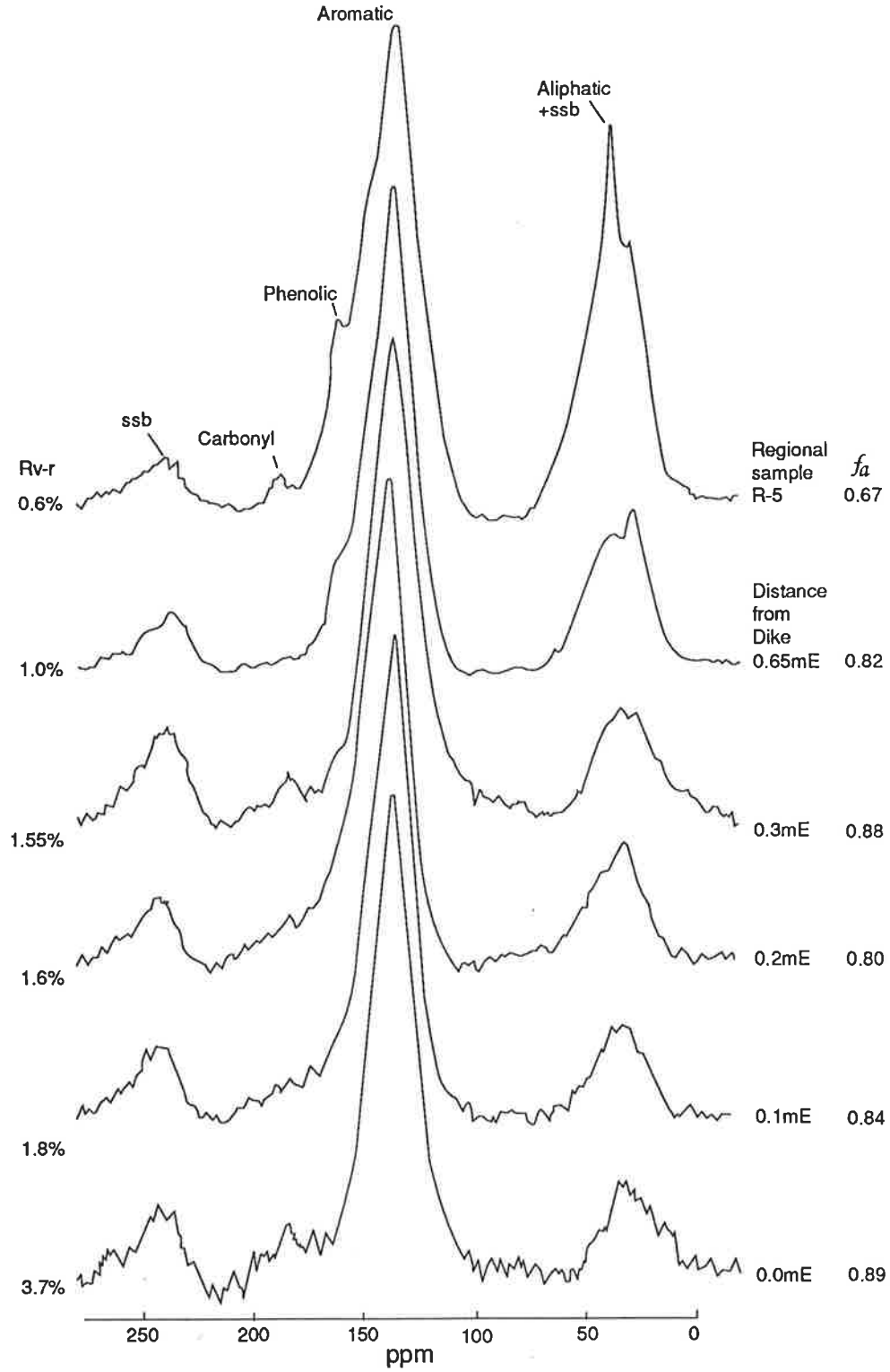
Aromatic
Aliphatic
+ssb
Phenolic
ssb
Carbonyl
Rv-r
0.6%
1.0%
1.55%
1.6%
1.8%
3.7%
Regional
sample
R-5
f_a
0.67
Distance
from
Dike
0.65mE
0.82
0.3mE
0.88
0.2mE
0.80
0.1mE
0.84
0.0mE
0.89
250
200
150
100
50
0
ppm

Fig 4-30. A comparison of selected element oxide abundances versus distance (X) from the west dike margin, San Remo 1 dike, western onshore Gippsland Basin. The element oxides plotted were selected for their tendency to respond to hydrothermal alteration. SiO_2 content was plotted as SiO_2 minus 50 wt.-% so it would fit on the expanded scale with the minor oxides. Cr_2O_3, MnO, P_2O_5 and TiO_2 contents are low, fluctuate but show no trend or are zero and these values were not plotted (Appendix 6). Note that correction of the analyses to a water-free basis was not done. This correction would increase the percentage changes in element oxide content but not the general form of the changes. Steel tools were used for sampling in the field and preparation of these samples. The basic sample size used for ICP-AES analysis was about 100 g of rock broken and selected for cleanliness minimizing any contamination effects to a few tenths of a weight percent Fe_2O_3.

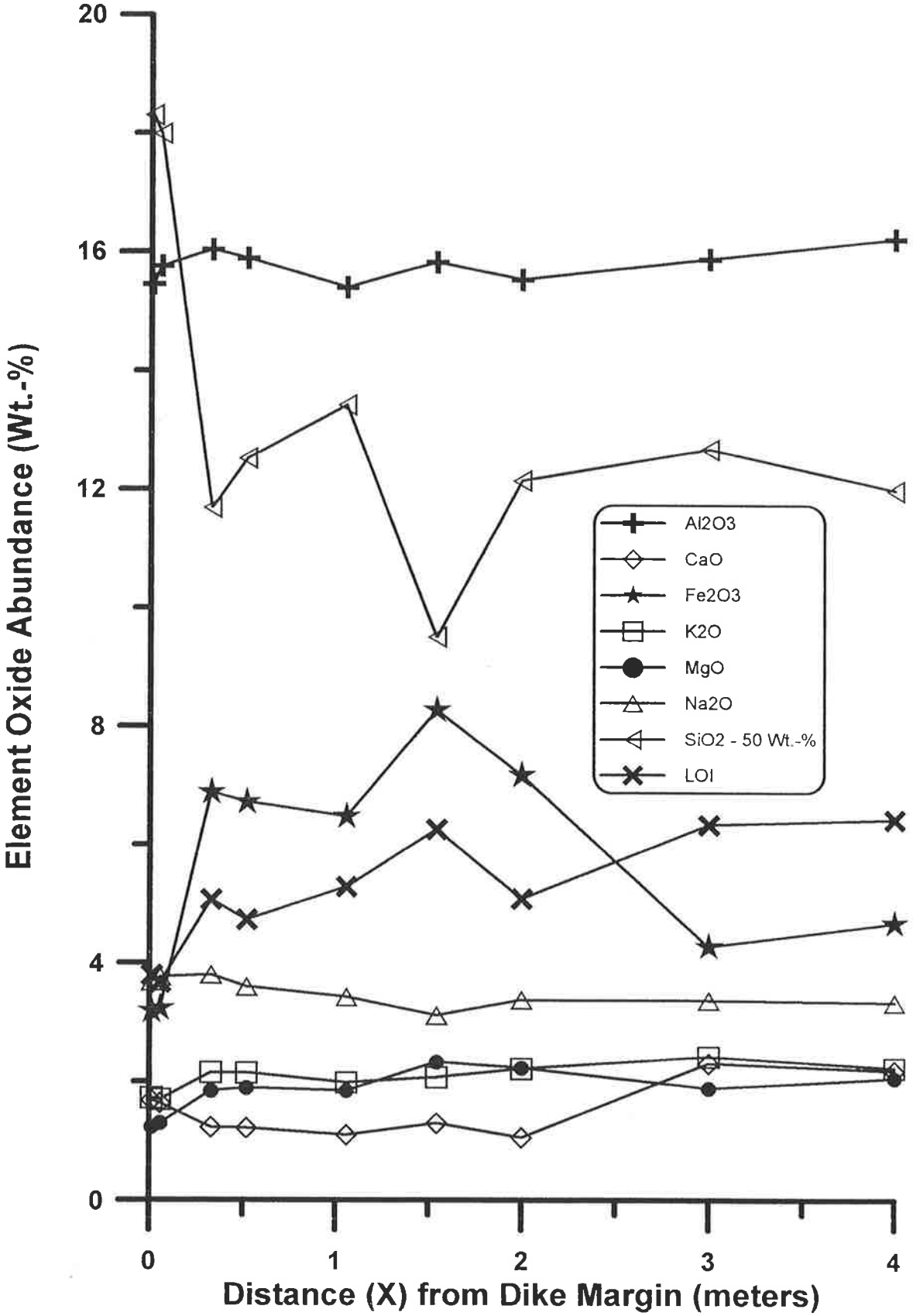
20
16
12
8
4
0
0
1
2
3
4
Element Oxide Abundance (Wt.-%)
Distance (X) from Dike Margin (meters)
Al2O3
CaO
Fe2O3
K2O
MgO
Na2O
SiO2 - 50 Wt.-%
LOI

ICP-AES

ICP-AES analysis of the host rock next to San Remo 1 suggest considerable fluctuation in proportion of MgO and LOI. The typically hydrothermally active elements K_20 and Na_2O show little change in proportion throughout the sampled range from X= 1.0 m to X = 0.02 m (Fig. 4-30). Again, the often sharp changes essentially at the dike contact may not be as significant in terms of assessing hydrothermal alteration as the changes occurring further from the dike and these are discounted in the discussion. SiO_2 content probably shows the most change as it increases from 4 to 12 wt.-% towards the dike. LOI undergoes strong fluctuations but makes little net change. Fe_2O_3 proportion varies in a similar fashion to CaO and LOI (although somewhat out of phase with LOI). MgO proportion decreases toward the dike and this change, along with the change in Fe_2O_3 and LOI are again attributed to reactions occurring in clay minerals and zeolites as the dike is approached. Given the ubiquitous late calcite near this dike, the fluctuation of CaO proportion was initially discounted but CaO does follow the changes in SIO_2 and Fe_2O_3 and seem to reflect contact metamorphic alteration.

Other suggestions of possible limited convection are that the Rv-r profile is not quite monotonic and Rv-r increases above background at X/D = 1.5 rather than the expected X/D = 1. The Rock-Eval parameters show considerable fluctuation but this change follows TOC content suggesting that is the cause rather than convection.

The host rocks are also different at San Remo 1 compared to the other dikes. Firstly, before late calcite cementation, the host rock appeared to be more porous and is inferred to be more permeable than seen at the other dikes. Increased permeability perhaps favored convection next to this thin dike. However, the host rock samples used for ICP-AES analysis are lithic sandstone and polymictic conglomerate. The lithic clasts in the host rock vary from coarse grained granite and volcanic rock fragments to mudstone clasts. This diverse assemblage of clasts probably imparts an initial heterogeneity in the whole rock composition

not seen at the other dikes which intrude more homogeneous rocks. Overall, the changes in element oxide proportions that occur next to San Remo 1 are thought to largely reflect the inherited change in host rock composition rather than significant hydrothermal activity extending away from the dike, but limited convection cannot be excluded as a factor.

Isotopes

C and O isotopes analyses from vein calcite next to the San Remo 1 dike show a composition range of $\delta^{18}O$ from -13.2 to -21.0 $^{o}/_{oo}$ and $\delta\ ^{13}C$ from -3.0 to -4.7 $^{o}/_{oo}$ (Appendix 7). The late calcite filling a vug in the dike had a $\delta^{18}O$ of -22.8 $^{o}/_{oo}$ and $\delta\ ^{13}C$ of -5.6 $^{o}/_{oo}$. All of these isotopic compositions are within the range of the isotopic composition found for early diagenetic concretions and calcite cement in the Strzelecki Group of the region suggesting they have precipitated from similar ^{18}O depleted meteoric fluids or fluids derived from the dissolution of host rock cements (Gregory et al., 1989; Fig. 3-11). The host sandstone at San Remo 1 was not sampled for isotopes because of the likelihood that abundant late calcite cement and veins would confuse any contact metamorphic signature.

Fracture Count

As at Inverloch 1, thin sections prepared from the host sandstone were used to measure the mean fracture count (FC). At San Remo 1, FC generally decreases as the dike is approached (Fig. 4-31). The overall decrease in fractures near the dike, considering the implications of the undulosity study at Inverloch 1, suggests that a healing and annealing process increasingly dominates at the high temperatures reached next to the dike. Presumably, as at Inverloch 1, the increased number of open fractures found in a few samples is superimposed on samples after annealing. These later fractures, many now calcite filled, appear to exploit the same joints that the dike used during intrusion because they parallel the

dike trends at each locality in the onshore Gippsland Basin.

Fluid Inclusion Geothermometry

As explained in Chapter 1, T_{peak}, when estimated from inherited fluid inclusions trapped along a type C fracture that have a variable V/L ratio, was taken to be near the low mode of the T_h distribution. T_h data from the early pilot study of San Remo 1 used mostly undifferentiated type C fluid inclusions (Barker et al., 1992b). These data were also used in estimating T_{peak} (Fig. 4-32) if from the fluid inclusion description it could be categorized into the fracture type classification that was developed later in this study. T_h data measured on isolated inclusions that could not be categorized were not used to estimate T_{peak}.

Fig. 4-31. Mean fracture count (FC) versus distance (X) from the dike margin in the Strzelecki Group host sandstones, San Remo 1 dike, western onshore Gippsland Basin, Victoria.

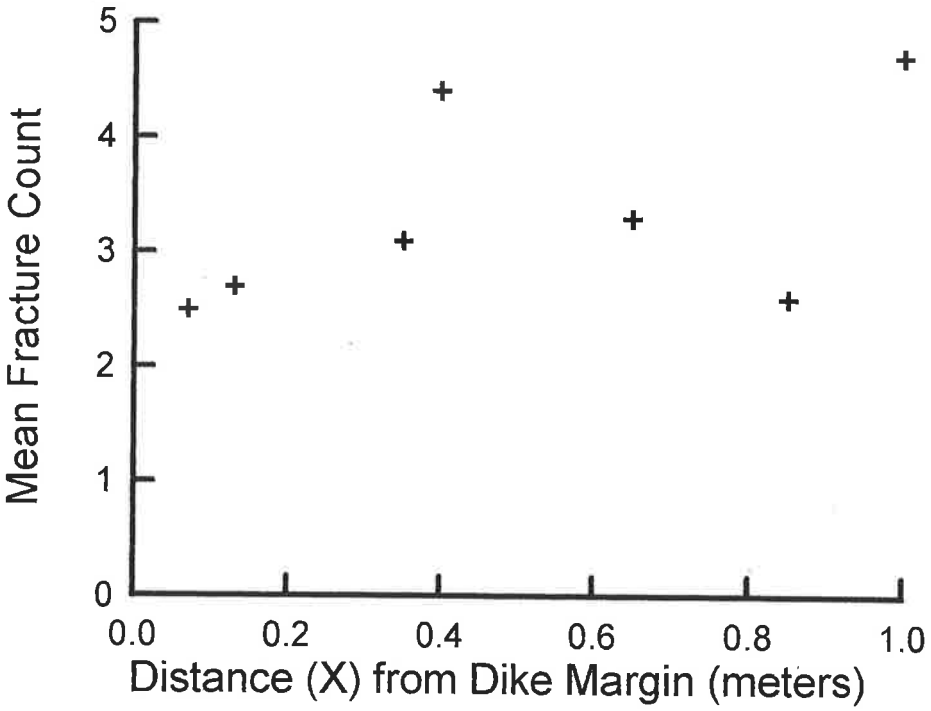
Mean Fracture Count
5
4
3
2
1
0
0.0
0.2
0.4
0.6
0.8
1.0
Distance (X) from Dike Margin (meters)

Fig. 4-31 SR-1

Fig. 4-32. Homogenization temperature (T_h) from fluid inclusions along healed fractures in sandstone and T_{peak} estimated from Rv-r, Strzelecki Group next to the San Remo 1 dike, western onshore Gippsland Basin, Victoria. All data rated as poor in quality (Appendix 4) not plotted. T_{peak} is estimated from Rv-r and a vitrinite reflectance geothermometer (VRG) for hydrothermal metamorphism based on data from ancient and active hydrothermal systems (Barker and Pawlewicz, 1994). T_h of type A, etc. in the legend refers to data from a fluid inclusion trapped along a fracture of this kind. The sample at 0.7 m was barren of type A and B fluid inclusions. The dashed line indicating the T_{peak} interpreted from fluid inclusion data is fixed at the dike contact by projecting to the dike margin the T_{peak} measured towards the center of the dike in the sandstone xenolith.

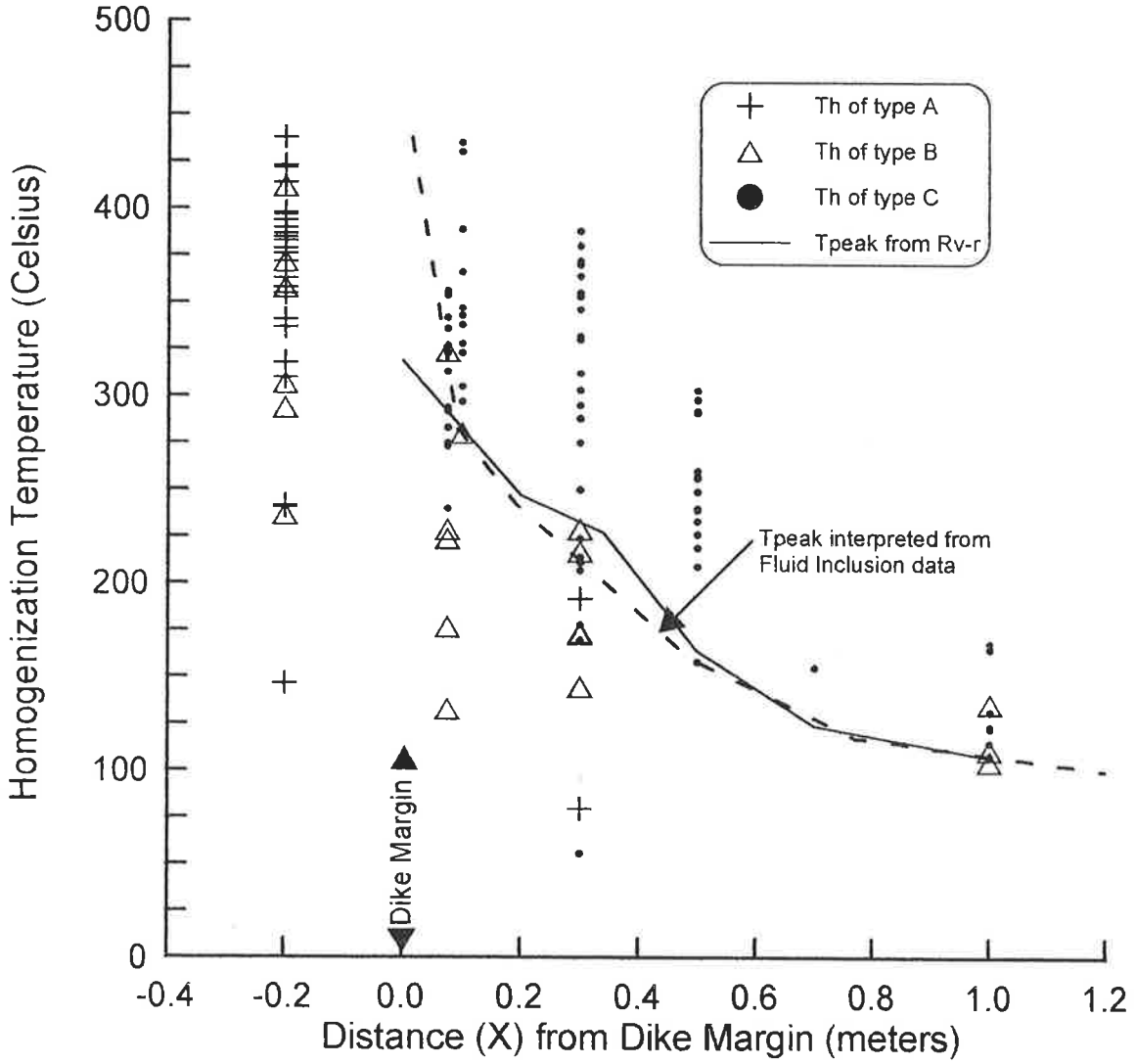
Homogenization Temperature (Celsius)
500
400
300
200
100
0
-0.4
-0.2
0.0
0.2
0.4
0.6
0.8
1.0
1.2
Distance (X) from Dike Margin (meters)
Dike Margin
Th of type A
Th of type B
Th of type C
Tpeak from Rv-r
Tpeak interpreted from
Fluid Inclusion data

12-94 Fig. 4.32

Fig. 4-33. An illustration of shape factors for fluid inclusion vacuoles in quartz based on Bodnar et al. (1989) and Osborne and Haszeltine (1993). The small circle inside each shape represents the vapor bubble. A shape factor = 10 is also termed a negative crystal.

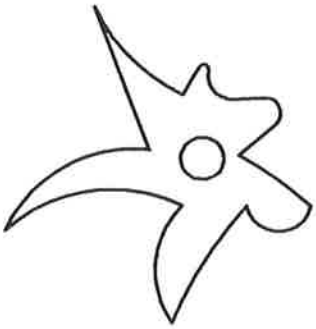

Shape Factor = 1

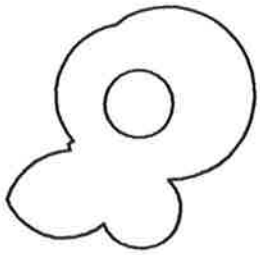

Shape Factor = 5

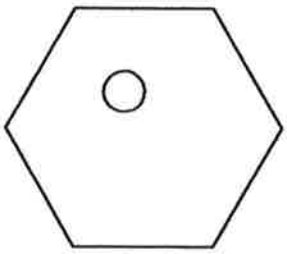

Shape Factor = 10

Fig 4-34. Shape factor versus distance (X) from the dike margin in the Strzelecki Group host sandstones, San Remo 1 dike, onshore Gippsland Basin, Victoria. Type A, B, or C in the legend refers to the T_h and shape factor for a fluid inclusion trapped along a fracture of this kind.

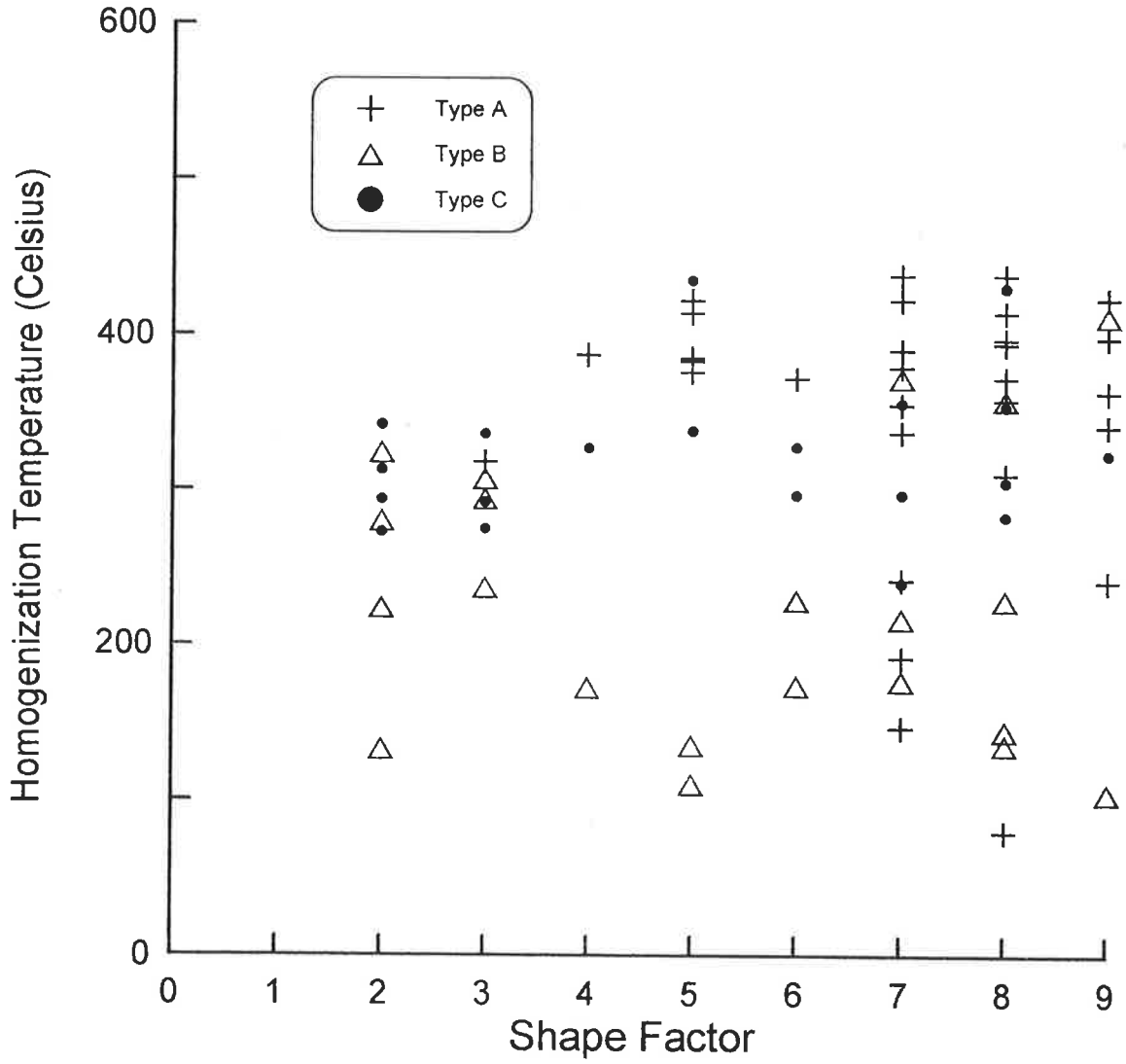
600
400
200
0
Homogenization Temperature (Celsius)
Type A
Type B
Type C
0
1
2
3
4
5
6
7
8
9
Shape Factor

As done at Bena 3, type A and B fluid inclusions used the UDE of the T_h population to estimate T_{peak}. T_h data from type A and B were combined with those from type C fractures to constrain T_{peak}.T_{peak} is interpreted to be the position where the low mode of the type C T_h and UDE from the type A and B T_h population approach each other and usually overlap. Overlap may occur because of inadvertently measuring fluid inclusions that have necked down, have leaked during sample preparation, or are inappropriately assigned to the wrong fracture type. The T_h from UDE of type A and B near the area of overlap with the low mode shows a generally monotonic increase as the dike is approached (Fig. 4-32) similar in form to that seen in the Rv-r data. Away from the immediate dike contact there is fair to good agreement of the T_{peak} suggested by T_h and the T_{peak} predicted from the hydrothermal VRG, which lends some confidence to the fluid inclusion based estimate. Of course, near the dike margin where Rv-r starts to decrease there is poor agreement between the VRG and T_{peak} estimated from UDE of T_h from type A and B fluid inclusions. As seen at Bena 3, the fluid inclusion data appear to give a more accurate T_{peak} estimate near the dike.

The use of T_h from type A and B fluid inclusions is particularly important near X/D of 1 where little overheating of the fluid inclusions is expected next to thin dikes. Thus, type C fluid inclusions would necessarily not be reequilibrated and record no information about post-depositional thermal history.

An important observation found in this portion of the study is that type C fluid inclusions apparently can exist essentially at the type A or B fracture boundary and not reequilibrate. It is crucial that it be determined that in fact the post-depositional fracture does in fact cut the fluid inclusion definitely making it a type A or B fluid inclusion. Otherwise it is better to ignore such fluid inclusions. If a type C fracture bound fluid inclusion, which could have formed at very high temperature, is erroneously assigned to a type A or B fracture, the result is a large error in T_{peak}. The error occurs because UDE based on the T_h of type A or B fluid inclusions strongly

influences the resulting T_{peak} estimate. The assignment of origin can be checked by using only type C fractures that include several measurable fluid inclusions along their length. A type C that is in close proximity to a type A or B fracture and has not reequilibrated, will have T_h value and fluid inclusion contents (salinity, V/L ratio and so forth) similar to that of the other fluid inclusions trapped along the type C fracture. If reequilibration has occurred, then the type C that is in close proximity to a type A or B fracture will have a T_h value and fluid inclusion contents similar to that of the other fluid inclusions trapped along the type A and B fracture.

The regular increase in T_h as suggested by the increasing low mode of the type C fracture-bound fluid inclusions as the dike is approached (Fig. 4- 32) suggests reequilibration of preexisting fluid inclusions has occurred near the San Remo 1 dike margin. Reequilibration during overheating has increased the T_h of inherited fluid inclusions such that T_h low mode seems to approach T_{peak}. The type C fracture-bound fluid inclusions found below T_h low mode are not unexpected in a reequilibrated fluid inclusion population, because all fluid inclusions may not reequilibrate.

Evidence for Reequilibration of Fluid Inclusions during Contact Metamorphism

Experimental work suggests that the shape of the fluid inclusion can change during reequilibration (Bodnar et al., 1989; Vityk et al., 1994). In quartz, reequilibration by stretching is typically followed by the reformation of the vacuole into a negative crystal shape (shape factor 10, Fig. 4-33). At San Remo 1, however, fluid inclusion shape factors within each fluid inclusion type show no relationship with temperature (Fig. 4-34). Similarly, Robinson et al. (1992) found that fluid inclusion size (maximum dimension of the vacuole) showed little correlation with T_h. The reason for the lack of correlation in shape and, apparently, size, is two fold: 1) type A and B fluid inclusions may form during or after intrusion and may not have been overheated or reequilibrated; 2), If a fluid inclusion reequilibrates by decrepitation at a relatively low P_{eff}, the

vacuole may not change shape.

As conjectured in the undulosity and fracture count sections, evidence for fracture healing during intrusion is the apparent increase in fracture-bound fluid inclusions at the immediate dike contact and in a sandstone xenolith found within the dike. Type A fluid inclusions with a high T_h are common near the dike and in the sandstone xenolith (Fig 4-32). The increase in fractures available for trapping fluid inclusions at the high temperatures found in the immediate vicinity of the dike may reflect crystal breakage due to thermal expansion suggested by the experiments of Somerton (1992) or stress caused by dike intrusion.

The nature of the reequilibration process, however, was not elucidated by salinity measurements. As discussed in chapter 1, salinity measurements by freezing point depression are usually not possible on extremely vapor-rich fluid inclusions, so the T_f data is biased towards fluid inclusions trapped at lower temperature. This limitation also reduces the amount of data available for interpretation.

The salinity measurements by freezing point depression focused on the samples near the dike from X = 0.075 to 0.3 m and in the sandstone xenolith at X = -0.2 m. Samples near the dike were used as the fluid inclusions in them are most likely to decrepitate or be trapped during contact metamorphism and thus record salinity of fluids present. At X = -0.2 m, T_f ranged from -3.1 to -4.4°C, indicating a salinity range of 5.1 to 7 wt.-% NaCl equivalent for six type A and B fluid inclusions (Bodnar and Vityk, 1994). From X= 0.1 to 0.3 m, seven type B and C fluid inclusions showed an ice melting point of -2.7 to -8.1°C indicating a salinity range of 4.5 to 12 wt.-% NaCl equivalent. The type C fluid inclusions within this T_f data have a measured salinity range of 4.5 to 12 wt.-% NaCl equivalent which completely overlaps the range seen in the type A and B fractures near, and in the dike.

An interesting aspect of the fluid inclusion study at San Remo 1 was that measurements could be made on a sample of a sandstone xenolith was partially embedded in

the dike. This sample was locally derived as it was still partially attached to the host rock at the dike margin. Therefore, fluid inclusion measurements made on the xenolith sample are related to the hydrothermal alteration in the adjacent host rock. The sandstone in the xenolith was metamorphosed, as shown by the numerous type A and B fractures that were lined with a greenish mineral, presumed to be chlorite. The type A and B fluid inclusions trapped along a single fracture often showed a wide range in T_h and displayed different homogenization behaviors: at over 400°C, by critical point fading, and at 370 to 440°C to a vapor phase and at 376°C or lower to a liquid phase. The T_h range and the variable homogenization behavior is interpreted as indicating trapping during the rapid cooling of the dike after intrusion. Further, the trapping of fluid inclusions with widely variable T_h behavior but similar temperature range in one or related FIA suggests that separate vapor and liquid phases evolved in the dike.

The T_h of C.P. fading also increases with salinity. The range of homogenization by C.P. fading for six fluid inclusions from 412 to 423°C suggests a salinity of 4 to 5 wt.-% NaCl equivalent (Bodnar and Vityk, 1994). One fluid inclusion in this sample that showed C.P. fading at 387°C, which suggests 1 wt.-% NaCl equivalent, is discounted given the problem of working with vapor rich fluid inclusions. In any case, these data generally indicate a lower salinity at 5.1 to 7 wt.-% NaCl equivalent at higher temperatures than those found by measuring by T_f in lower temperature type A and B fluid inclusions in the sandstone xenolith. Homogenization behavior by C.P. fading also suggests the evolution of a supercritical fluid in the sandstone xenolith during contact metamorphism.

The problem with using a change in fluid inclusion salinity as evidence of reequilibration is establishing the salinity of the pore fluid present during contact metamorphism. The type A and B fluid inclusions in the xenolith suggest a fluid of 4 to 7 wt.-% NaCl equivalent was present soon after intrusion. This salinity is similar to that found in a type B fluid inclusion with 8.5 wt.-% NaCl equivalent at X = 0.3 m. However, these salinities mostly overlap the range

found in the type C fluid inclusions (4.5 to 12 wt.-% NaCl equivalent) and thus, no clear evidence of reequilibration is found, as it cannot be determined whether this is an inherited salinity range or one developed during reequilibration.

The salinity data for the type A and B fluid inclusions do suggest that the higher temperature fluid inclusions have trapped lower salinity fluid relative to the later, more saline fluid inclusions that generally formed at lower temperatures. This observation is consistent with hydrothermal bomb experiments using rock and water mixtures that show the concentration of dissolved ions, and therefore salinity measured as wt.-% NaCl equivalent, increases with heating duration (Ellis and Mahon, 1977). Unfortunately, the indication of evolving salinity during contact metamorphism limits the usefulness of salinity studies in establishing that reequilibration has occurred.

Fluid inclusions trapped along type C fractures in the sandstone xenolith had commonly had a negative crystal shape (shape factors of 8-9) and small fractures are commencing at the points of the hexagonal negative crystals. Similar fluid inclusion shapes, T_h range and homogenization features are also observed in the sandstone sample at X = 0.1 m or less. These petrographic features are common in reequilibrated fluid inclusions in quartz (Bodnar et al., 1989; Vityk et al. 1994).

At X > 0.1 m or X/D > 0.15 these petrographic features that suggest reequilibration become increasingly rare. Fracturing and features suggesting reequilibration related to the dike rapidly decrease as distance from the dike increases.

Ultraviolet Microscopy

Although searches of the polished rock sections under blue light or peak ultraviolet excitation from San Remo 1 and other dikes were made, no fluorescent hydrocarbon inclusions were observed. The studies of hydrocarbon generation at other dikes in the area suggest the

hydrocarbon generation process near the dike during contact metamorphism favors methane, which is not fluorescent. Trapping of fluorescent hydrocarbons may not occur near the dikes during contact metamorphism. A.C. Cook (1992, Keiraville Konsultants report to Geotrack International) notes the common presence of oil or bitumen in the SOM sampled next to San Remo 1. As the observation of these fluorescent materials continues up to the dike contact, and because this study shows that no hydrocarbon generation potential remains there, it is inferred that these fluorescent hydrocarbon phases represent post-intrusion migration towards the dike.

Apatite Fission Track Ages

The AFT ages and associated error on samples measured next to San Remo 1 may show a small statistical difference at the dike contact compared to the apparent sediment age measured away from the dike (Fig. 4-35). Although only a slight, or perhaps no, difference in apparent AFT age exists in the sample near the dike it was decided to interpret the data as if it is significant and compare the results to estimates of heating duration from a heat flow model.

This trial interpretation of the AFT age data is based on the assumption that when half the fission tracks are annealed the apparent age is reduced by 50% (Fig. 1-10). So, well away from the dike, the apparent age of the strata is dominated by the Early Cretaceous age of the dominantly volcanic source terrains (Gleadow and Duddy, 1981). For the purpose of a trial calculation of heating duration, the age difference is assumed significant and the AFT age next to the dike would then indicate resetting during the mid-Cretaceous.

The trial calculation involves interpolating the point where the apparent sediment age is reduced by one half and projecting this point down the X-axis, the point where 50% age decrease occurs is at a Rv-r of 2.7% (Fig. 4-35). An Rv-r of 2.7% using a hydrothermal system VRG (Barker and Pawlewicz 1994) suggests a T_{peak} of about 280°C. Because of the

assumption that 50% age decrease = 50% track loss, 50% track loss occurred at about 280°C. Using the 50% track loss line on the fan model of AFT annealing (Fig. 4-36), this trial calculation indicates that it would take 1.2×10^6 sec. (14 days) heating duration to accomplish this track loss at 280°C.

This trial heating duration value is comparable in magnitude to that made using a heat flow model for a 0.6 m dike (chapter 5, this paper) so the trial calculation seems to fit theory.

At San Remo 1, the mean track lengths are fairly consistent ranging from 14.3 ±0.25µm to 14.9 ± 0.15 µm and are near those found in a regional sample (15.2 ± 0.39 µm) that is far removed from the dike heating (Appendix 9, RD20-19). The age of this regional sample at 116.3 ± 28.1 Ma) overlaps that found in the dike sample at 94.1± 8.1 Ma which supports the interpretation that temperatures were too high to record the dike intrusion and that all of the samples near San Remo 1 were in the temperature range where track were unstable and rapidly annealed.

Fig. 4-35. Apparent apatite fission track age and Rv-r versus distance (X) from the San Remo 1 dike margin, western onshore Gippsland Basin, Victoria. The fission track ages plotted are the pooled values as the single grain data passed the X^2 test at the 5% level. The error bar is ±1σ.

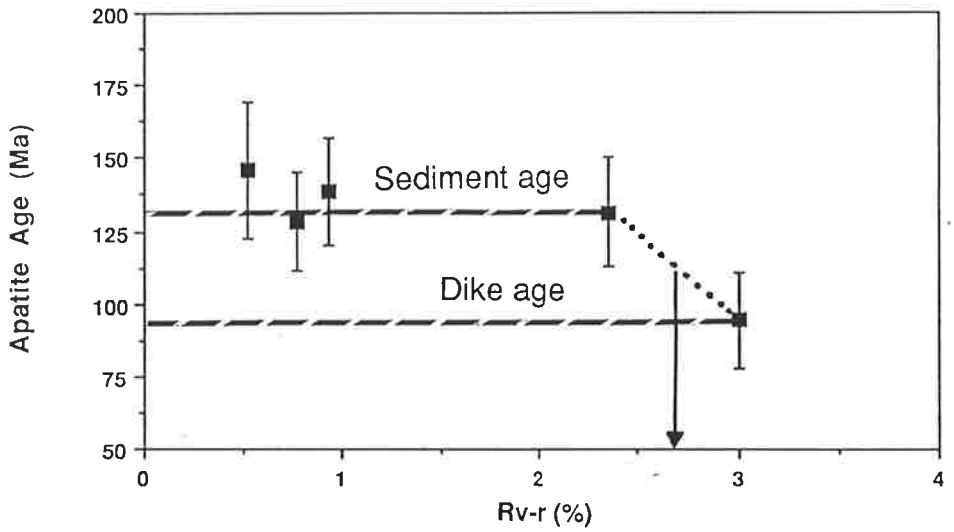
Apatite Age (Ma)
200
175
150
125
100
75
50
0
1
2
3
4
Rv-r (%)
Sediment age
Dike age

Fig 4-36. The straight line and fan model of apatite fission track annealing from Laslett et al. (1987). The solid lines and arrows indicates estimated T_{peak} projected to the 50% track loss curve and then onto the time axis. See Green et al. (1988) for a discussion of the problems of modeling AFT annealing.

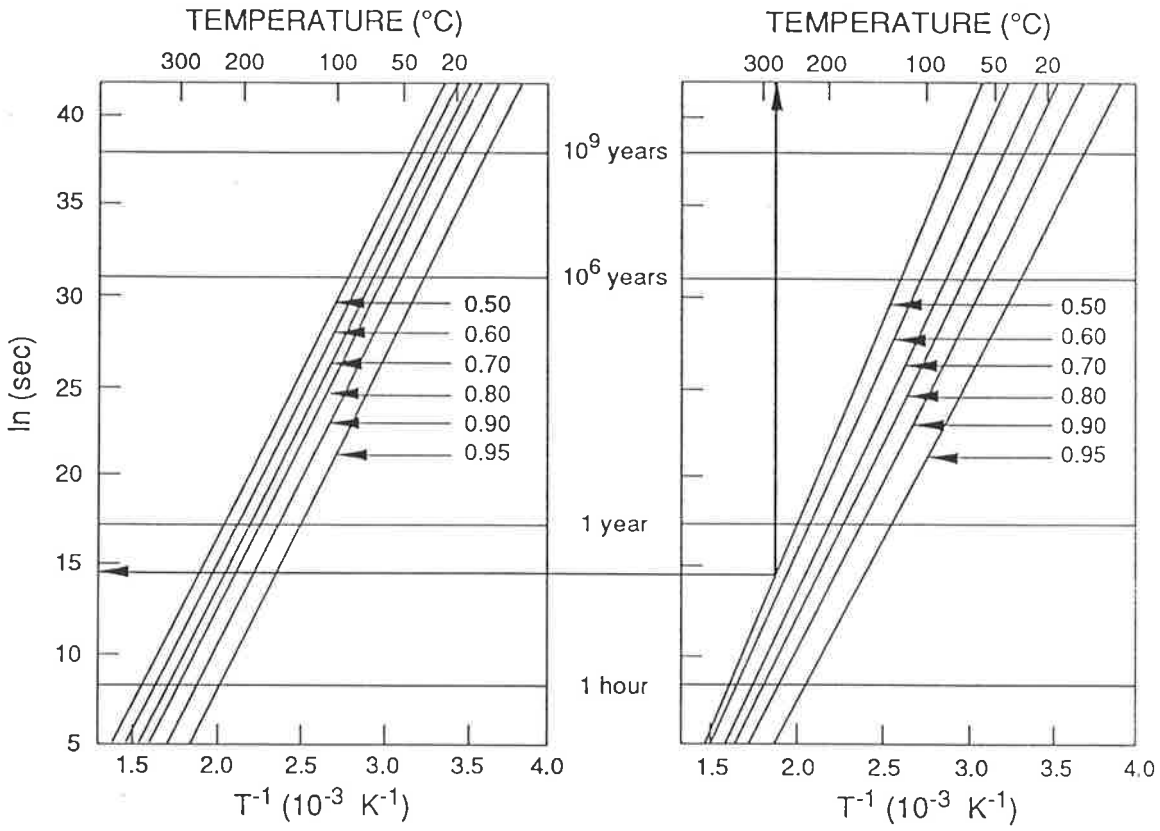
TEMPERATURE (°C)
300 200 100 50 20
40
35
30
25
20
15
10
5
ln (sec)
0.50
0.60
0.70
0.80
0.90
0.95
10^9 years
10^6 years
1 year
1 hour
1.5 2.0 2.5 3.0 3.5 4.0
T^{-1} (10^{-3} K^{-1})
TEMPERATURE (°C)
300 200 100 50 20
0.50
0.60
0.70
0.80
0.90
0.95
1.5 2.0 2.5 3.0 3.5 4.0
T^{-1} (10^{-3} K^{-1})

4.13 SAN REMO 3

Together with Inverloch 2 and 3, San Remo 3 was primarily studied to determine the Rv-r profile next to thin dikes where heating duration is quite short.

San Remo 3 is a 0.06 m thick, near-vertical northwest-trending dike that parallels San Remo 1 which is exposed about 20 m to the east. San Remo 2 , an approximately 0.2 m thick dike is located about 10 m east of San Remo 3 but is only exposed in the cliff face well above the shore face where the samples were taken. The 4 m thick San Remo 4 (Edwards, 1942) is located about 150 m west of San Remo 3. San Remo 3 is exposed in the shore face (Fig 4-14 b) southeast of San Remo, Victoria. The dike intrudes a sandstone that contains large pieces of allochthonous coal fragments. The host rock appears unweathered. The exposed dike rock is thoroughly weathered and no fresh samples were available for petrography. For organic geochemistry analysis, coal samples were drilled out of the outcrop using a 5 mm diameter drill. The recovered coal bearing rock fragments are composed mostly of vitrinite and sufficiently concentrated that accurate Rock-Eval analysis could be performed. The Rv-r and organic geochemistry sample line extended outward from the eastern dike margin for about 1.4 m or X/D = 7. Although San Remo 3 occurs in a cluster of three dikes, no overlapping contact metamorphism is expected because all three dikes are <0.6 m thick and spaced about 10 m apart.

Host rock Thermal Maturity and Geochemistry

Vitrinite reflectance in the host sandstone east of the San Remo 3 dike varied from 0.7 % at X = 1.4 m to a peak of 3.1 % at X = 0.003 m (Fig. 4-26). Rv-r starts to increase at about X = 0.07 m or near X/D = 1 but Rv-r only increases from 0.7 to 0.8% there, as predicted by the dike width rule. However, marked increase in Rv-r is delayed until X= 0.4 m or X/D = 0.6.

Overall, organic matter was moderately abundant in the San Remo 3 host sandstones

and the TOC of the drilled out coal and sandstone powder reached from 3.2 to 42 wt.-%. As observed at other dikes in the area, TOC tends to decrease as the dike is approached but at this dike coaly material is abundant enough that this decease makes little difference in the Rock-Eval results. The lowest TOC value in the suite is found at X= 0.003 m, the sample closest to the dike contact. Because of the appreciable TOC content up to the dike and the relatively low Rv-r of 3.0% at the dike contact, T_{max} continues to increase to the dike margin where it reaches 493°C. T_{max} starts to increase as the dike is approached at X = 0.03 m or X/D = 0.5 much closer than expected from the dike width rule. S_1 is generally low and remains relatively constant at about 0.2 to 0.4 mg HC/g rock as the dike is approached and decreases from X=0.017 m to the dike contact, which, as explained above, is probably due to hydrocarbon generation and migration occurring during contact metamorphism or loss during weathering. S_2 and HI decrease towards the dike near X= 0.09 m, apparently related to an Rv-r increase from 0.7 to 0.8% and the onset of oil and gas generation. The decrease in S_2, HI and TOC from X = 0.03 m or X/D = 0.5 is attributed to reactions occurring during contact metamorphism.

OI is much higher at 20-40 mg CO_2/g C than the less weathered R-5 regional coal that has an OI of 9 mg CO_2/ g C. The delayed and muted onset of hydrocarbon generation at San Remo 3 until about X/D =0.5 may be due to the relatively short heating duration of contact metamorphism next to this thin dike. The present observation of consistently low S_1 with increasing thermal maturation is thought to be a combination of the exposed condition of the rocks and apparently weathered character of the SOM, conditions which tend to remove free hydrocarbon.

Fig. 4- 37. Comparison of vitrinite reflectance and Rock-Eval pyrolysis results from coaly rocks in the Strzelecki Group next to the San Remo 3 dike, western onshore Gippsland Basin, Victoria.

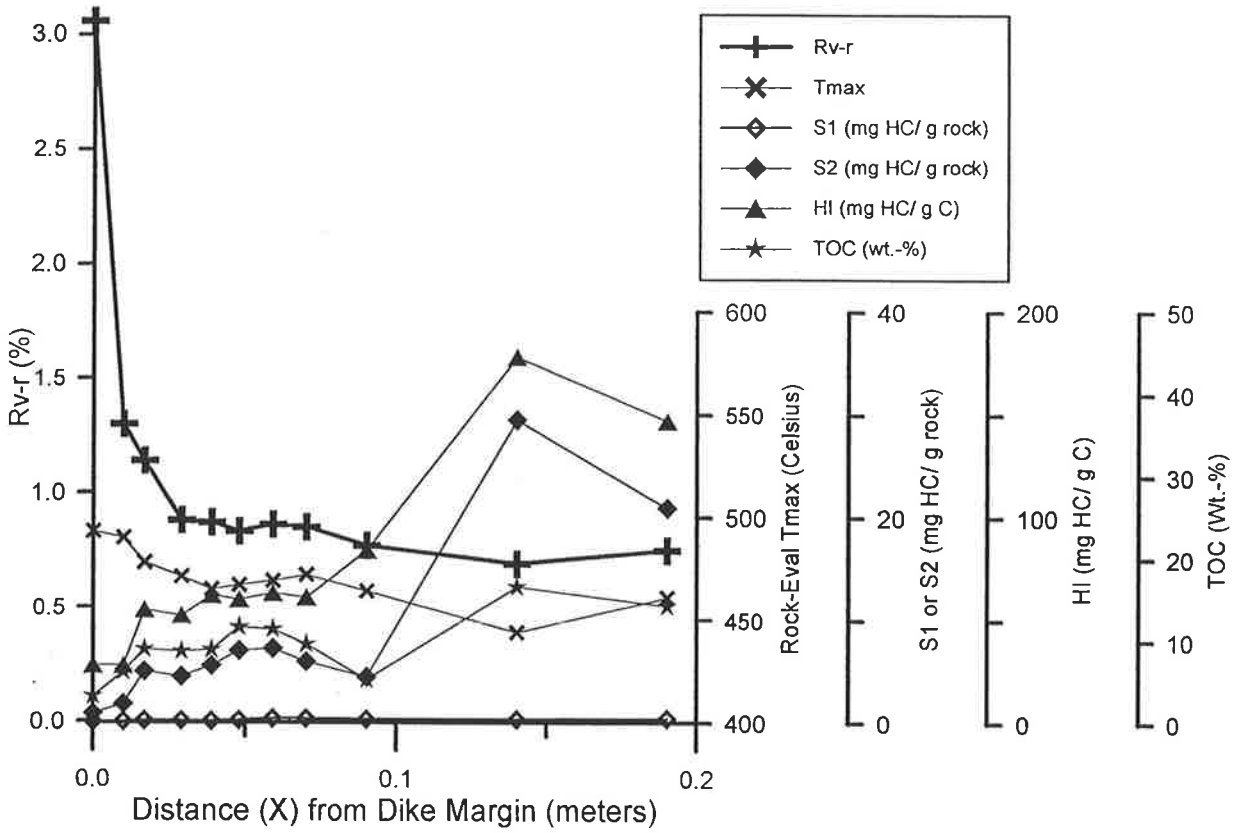
Rv-r
Tmax
S1 (mg HC/ g rock)
S2 (mg HC/ g rock)
HI (mg HC/ g C)
TOC (wt.-%)
Rv-r (%)
3.0
2.5
2.0
1.5
1.0
0.5
0.0
0.0
0.1
0.2
Distance (X) from Dike Margin (meters)
600
550
500
450
400
Rock-Eval Tmax (Celsius)
40
20
0
S1 or S2 (mg HC/ g rock)
200
100
0
HI (mg HC/ g C)
50
40
30
20
10
0
TOC (Wt.-%)

4. 14 DISCUSSION

Petrography of the Contact Metamorphosed Samples

The zone of brecciated, fractured and(or) mylonitic rock immediately adjacent to most of these dikes is thought to be caused by the dike intrusion process which mechanically disrupts the host rock at the dike margin. Generally, the host rock sandstone or mudstone does not seem to have melted near the dikes. Sedimentary rock textures are preserved in the sandstones very near the dike contact or at least next to thin dikes, where samples very near the contact were still recognizable as sandstones.

Next to thicker dikes, the immediate contact with the host rock is typically a hornfels or mylonite that looks superficially like a mudstone. This mylonite/hornfels zone extends only to about X/D = 0.05. The hornfels zone is often calcite rich but the calcite is isotopically related to regional carbonates of low temperature origin and thus, postdate the dike intrusion. Although difficult to assess because of the general lack of SOM near the dikes, vesiculation in vitrinite is restricted to X/D < 0.3. (Fig. 4-38). Vesiculation marks the evolution of gases in the vitrinite when it is hot enough to show plastic behavior or melting. These changes are similar to those observed in the industrial process of coking coal.

The darkened rock next to the dike, known as the bake zone, which probably represents mineralogic changes in the host rock, extends out from the dike to about X/D = 0.3. Even at Cruickston 1, where extended hydrothermal alteration in the rock is documented, the bake zone is still only a few meters thick and is restricted to the immediate dike contact zone.

Fig. 4-38. Summary of physical metamorphism observed in the host rocks versus the percentage of dike thickness (X/D x100%).

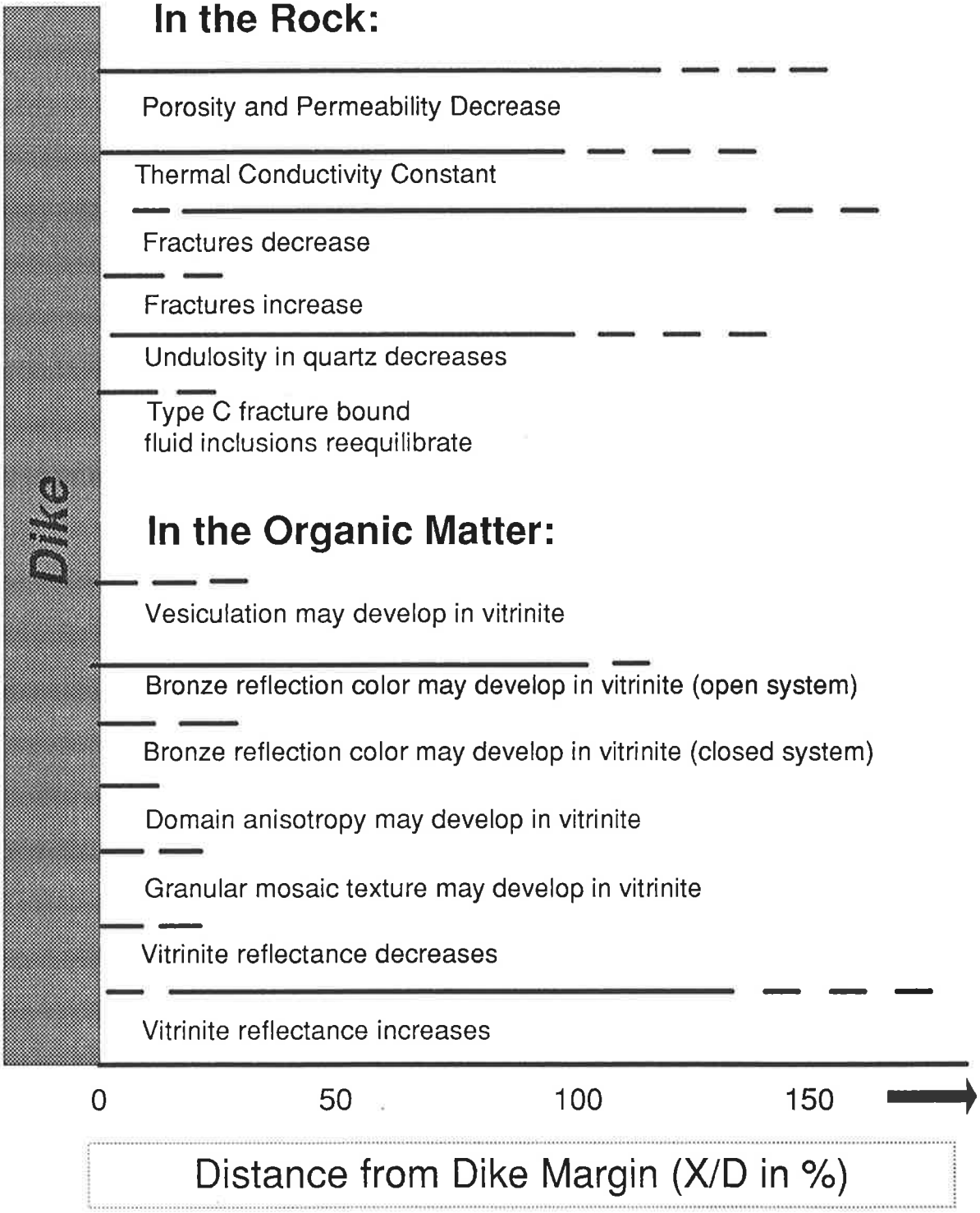
In the Rock:
Porosity and Permeability Decrease
Thermal Conductivity Constant
Fractures decrease
Fractures increase
Undulosity in quartz decreases
Type C fracture bound
fluid inclusions reequilibrate
Dike
In the Organic Matter:
Vesiculation may develop in vitrinite
Bronze reflection color may develop in vitrinite (open system)
Bronze reflection color may develop in vitrinite (closed system)
Domain anisotropy may develop in vitrinite
Granular mosaic texture may develop in vitrinite
Vitrinite reflectance decreases
Vitrinite reflectance increases
0
50
100
150
Distance from Dike Margin (X/D in %)

Near the dikes, vesiculation in vitrinite often occurs with the development of zoned optical anisotropy in vitrinite as shown by the development of granular mosaic textures or the larger domains of anisotropy. Associated with these changes is the development of a bronze reflection color in the vitrinite. The onset of the bronze color occurred very near the dikes that appear to remain as relatively closed systems during contact metamorphism. Bronze color was noted much further from the dike margin at Bena 3 and Cruickston 1, which are thought to be examples of incipient to open hydrothermal convection systems that developed during contact metamorphism (Fig. 4-38). The bronze reflection color is similar to that observed in graphite and its development may be an indicator of incipient graphitization of the SOM.

The other features of physical metamorphism occurring during contact were discussed in the body of this chapter and are only summarized in Fig. 4-38.

Fluid Inclusion Petrography

The low proportion of quartz or quartz feldspar grain contacts has produced a generally limited opportunity for the brittle grain failure that produces type A fractures, making identifiably post-depositional fluid inclusions a generally rare occurrence. Type A fractures can be common near the dike contact where other processes, possibly related to the intrusion or thermal expansion fractures that develop at high temperatures, increase the number of fractures available for trapping fluid inclusions.

Type B fractures caused by post-depositional fracturing must be differentiated from those that may be related to the embayed grains derived from the volcanic source rocks. Usually the fissures related to the embayed quartz grains are wide opening and would not be confused with a healed microfracture. However, it was felt that there could be cases of much thinner embayments that may have healed before deposition in the Strzelecki Group and these needed to be excluded from consideration. This was accomplished by using only type B fractures that

are lined by diagenetic minerals also found in the matrix or that show the incorporation of matrix materials as the fracture approaches the grain boundary. Even these criteria are not foolproof, but the fluid inclusion results from type B fluid inclusions that are in agreement with temperature predictions from hydrothermal VRG suggests it is a largely effective technique.

In retrospect it is felt that selecting the host rocks for this type of study is critical for success. A pilot study should have been done at every dike before any other analyses were completed. Further, quartz arenites with a high degree of grain to grain contacts would be better candidates for detecting type A fractures. Type A fluid inclusions are in my estimation the least ambiguous types for use in predicting T_{peak} . The use of type B and C fluid inclusions was in part to help establish T_{peak} , once it was discerned that few type A fluid inclusions would be found. If common type A fluid inclusions were present, no other fluid inclusion types would be needed to make a minimum estimate of T_{peak}.

Type C fluid inclusions were studied primarily to document if reequilibration does occur during contact metamorphism. This effort had a mixed result. Type C fluid inclusions in the sandstone xenolith almost certainly reequilibrated. But after about X/D = 0.1, the evidence becomes increasingly ambiguous. For example, many of the type C fluid inclusions well away from the dike show features consistent with being reequilibrated during their thermal history before being deposited in the Strzelecki Group strata. Type C fluid inclusions give the most ambiguous and error-prone data of the all the fluid inclusions studied.

To avoid major errors in T_{peak} estimates, it is essential to determine that a fracture actually cuts the fluid inclusion before assigning it to a type A or B fracture post-depositional origin. Fluid inclusions positioned near, but not on, fractures are best not used unless evidence relates them to a specific origin. It is also important that the type C fractures used contain several measurable fluid inclusions and that they show evidence of reequilibration by the heating caused by the dike.

Feldspars and carbonate are the only other common transparent or semi-transparent minerals present that are amenable to fluid inclusion analysis. However these minerals in the host rocks are fluid inclusion poor or barren. Calcite in the late veins is usually fluid inclusion-bearing.

Crushing stage studies are difficult to interpret when working with inherited fluid inclusions, as fluid inclusions of diverse origin may also break during crushing and the source of the evolved gases becomes obscured. For example, CO_2 or CO_2 - H_2O are common in some metamorphic rocks and cracking open inherited fluid inclusions with this composition would produce much gas unrelated to post depositional contact metamorphism or diagenesis.

General Results

1. Weathering seems pervasive in the near surface Strzelecki Group of the western onshore Gippsland Basin. Some evidence for weathering is also present in the coastal dikes and host rocks exposed to erosion by wave action. Weathering is expressed in many of the Rock-Eval parameters but especially by a muted S_1 response with increasing thermal maturity, a decreased HI and an increased OI. Pitting and microfracturing of polished surfaces in the SOM mounts is common and usually indicates weathering. Locally, the effect is severe enough to reduce Rv-r. Weathering effects are also suggested by XRD studies of clay minerals, and an apparent increase in porosity in the near-surface samples. Weathering related problems limit the success of the study especially for determining the character of hydrocarbon generation during contact metamorphism.
2. The decrease in TOC and a high degree of thermal maturation near the dikes limit observations of the response of SOM to contact metamorphism and of the hydrocarbon generation process. ^{13}C CP MAS NMR data seems to reveal the most information about hydrocarbon generation in the weathered and high thermal maturity samples close to the dikes.

3. Limited organic geochemical and Rv-r data suggest the onset of hydrocarbon generation at an Rv-r of about 0.7%, a peak near 1.0%, and is largely complete 1.8%. The hydrocarbon produced is dominantly aliphatic as shown by the sharp decrease in aliphatic carbon content with increasing Rv-r in the ^{13}C CP MAS NMR analyses.
4. Isotope, Rv-r, fluid inclusion and ICP-AES data suggest that the large 20-40 m thick dikes tend to become open systems and in some cases initiate convection. The onset of convection seems to explain the extended Rv-r profile compared to that observed next to thin dikes. Permeable rocks next to thin dikes may also show evidence of hydrothermal alteration well away from the dike contact suggesting incipient convection may have occurred.
5. Rv-r, fluid inclusion, and ICP-AES data suggest thin dikes cool in accordance with the dike width rule. The dike cooling model upon which the dike width rule is based suggests thin dikes cool by conductive heating of a porous host rock and that advection may occur next to the dike.
6. Usable fluid inclusions of determinable origin appear to be rare in the framework grains of fine grained sandstones. Fluid inclusions are thought to show reequilibration at lower P_{eff} because of annealing in quartz grains that occurs during contact metamorphism
7. The UDE of type A and B fluid inclusion populations seems to monotonically increase to the dike contact in a fashion similar to that predicted by heat flow theory. The T_{peak} estimated using fluid inclusions is in good agreement with T_{peak} estimated from a VRG for calibrated hydrothermal systems except near the dike contact at about X/D <0.3 where Rv-r fails as a thermal maturation parameter. At X/D > 0.3, the hydrothermal VRG seems to adequately predict T_{peak} given the precision of the fluid inclusion data.
8. In the xenolith within the dike or at the dike contact most measurable fluid inclusions seem to have been trapped during rapid cooling after intrusion. In fractured quartz grains, fracture

bound fluid inclusions may preferentially heal during cooling because of the decreasing solubility of silica.

9. AFT annealing apparently failed to record heating duration information as the rocks were too warm to clearly be annealed by the intrusion event;
10. As the dike is approached, thermal conductivity remains constant even though porosity and permeability decrease. This result has implications to modeling dike intrusions using heat flow theory taken up in the next chapter.

Chapter 5.

Thermal and Hydrous Pyrolysis Modeling of Contact Metamorphism and Hydrocarbon Generation Caused by Dikes

5.1 SIMPLE CONDUCTIVE HEAT FLOW MODELS OF DIKE COOLING

The cooling of dike-like igneous bodies using modern heat flow theory was initially addressed by Lovering (1935). Lovering's model, however, did not consider the latent heat of crystallization, an important factor that can increase predicted temperatures in the contact aureole on the order of 100°C (Jaeger, 1957). Bostick and Pawlewicz (1984) showed that T_{peak} estimated from Rv-r and a VRG calibrated by laboratory heating experiments generally is 50-100°C higher than those predicted by the Lovering (1935) model. Because of its oversimplification of the heat content of the magma, the Lovering model is not used further in this study.

A heat flow theory that considers the effects of both latent heat and pore fluids forms the basis of current models for cooling by dikes (Jaeger 1957, 1959, 1964; Delaney, 1982, 1987; Delaney and Pollard, 1982). The major difference from the simple models of Lovering (1935) is that Jaeger's (1957) simple model considers the heat of crystallization of the magma. The initial simple conductive model used in this study assumes no fluid flow or heat-absorbing phase changes in pore water.

For this study, the numerical simulation of contact metamorphism uses a computer program developed by Peacock (1990). This program models the temperature produced at a distance (X) from the dike margin for an igneous sheet of width (D), that is inserted at an initial temperature (T_{magma}) into a host rock at temperature (T_{host}), and instantly begins cooling solely by conductive heat transfer. The latent heat of crystallization in the magma is considered by

computing an effective thermal diffusivity rather than using the method of increasing T_{magma} to account for it (Jaeger, 1959, 1964). Pore water movement or in situ vaporization of the pore water is not considered. This type of conductive model yields the maximum theoretical temperatures reached next to a dike as no heat is absorbed or removed by the pore water. As discussed below, the wet-rock conductive model considered in this study involves intrusions into a low-temperature host rock in which the effect of heating the pore water is considered. Because of heat absorbed by vaporizing pore water, the wet-rock model predicts much lower temperatures and can also consider an open system with heat loss by vapor or liquid escape.

Construction of the initial simple conductive numerical model requires that several thermal and physical values relevant to the Gippsland Basin to be assessed prior to modelling (Table 5-1). One of the most important values measured in this study is the thermal conductivity of the dike and host rock, which may change with increasing temperature. The dike and host rock thermal conductivity values are assumed equal in the simplest models of Jaeger (1959) and in the one by Peacock (1990) used in this study. Therefore, if these values are significantly different, the predicted temperature will be inaccurate.

Thermal Conductivity

Thermal conductivity was measured using water-wet at sample temperatures of 20 to 150°C and at a constant 35 kPa pressure, using the method of Sass et al. (1992). As the bomb temperature was increased, some of the Strzelecki Group sandstone samples started to deform, as shown by a thermal conductivity reversal. Analyses were not run above 150°C (Appendix 10). Data from samples that showed damage during heating were not used. The thermal conductivity (K) values for all these rock types are initially similar at 1.6-1.7 W/m-K at 20°C (Fig. 5-1). With increasing temperature, K increases slowly and approaches 2.0 W/m-K at 150°C. The increase in K seems to be leveling off with increasing temperature, so the

expectation is that the K of both the dike and host rock will increase to near 2.1 W/m-K as temperatures increase towards the dike contact. This good agreement of K in the dike and host rock and the small change with temperature is consistent with one of the major simplifying assumptions in the heat flow models.

Peacock's (1990) program models the temperature produced at a point (X) from the dike margin for an igneous sheet of width (D), that is intruded at an initial temperature (T_{magma}) into a host rock at temperature (T_{host}), and instantly begins cooling solely by conductive heat transfer. The thermal diffusivity (κ) of the country rock and solidified magma is defined by the relationship $\kappa = K/\rho C$, where K is the thermal conductivity, ρ is the bulk density, and C is the heat capacity. The thermal diffusivity is dependent on K and ρ which both seem to approach or maintain constant values, as well as C which is a function of temperature. Bethke et al. (1993) calculate that the heat capacity of sandstone changes by about 20% over the temperature range of 0 to 300°C. Given the other uncertainties in the variable input into these models, the relatively small variation of κ with temperature is neglected.

Fig. 5-1. Thermal conductivity as a function of hydrothermal bomb temperature. Bomb pressure was held at 35 kPa pressure. Hydrothermal bomb apparatus and method described by Sass et al. (1992).

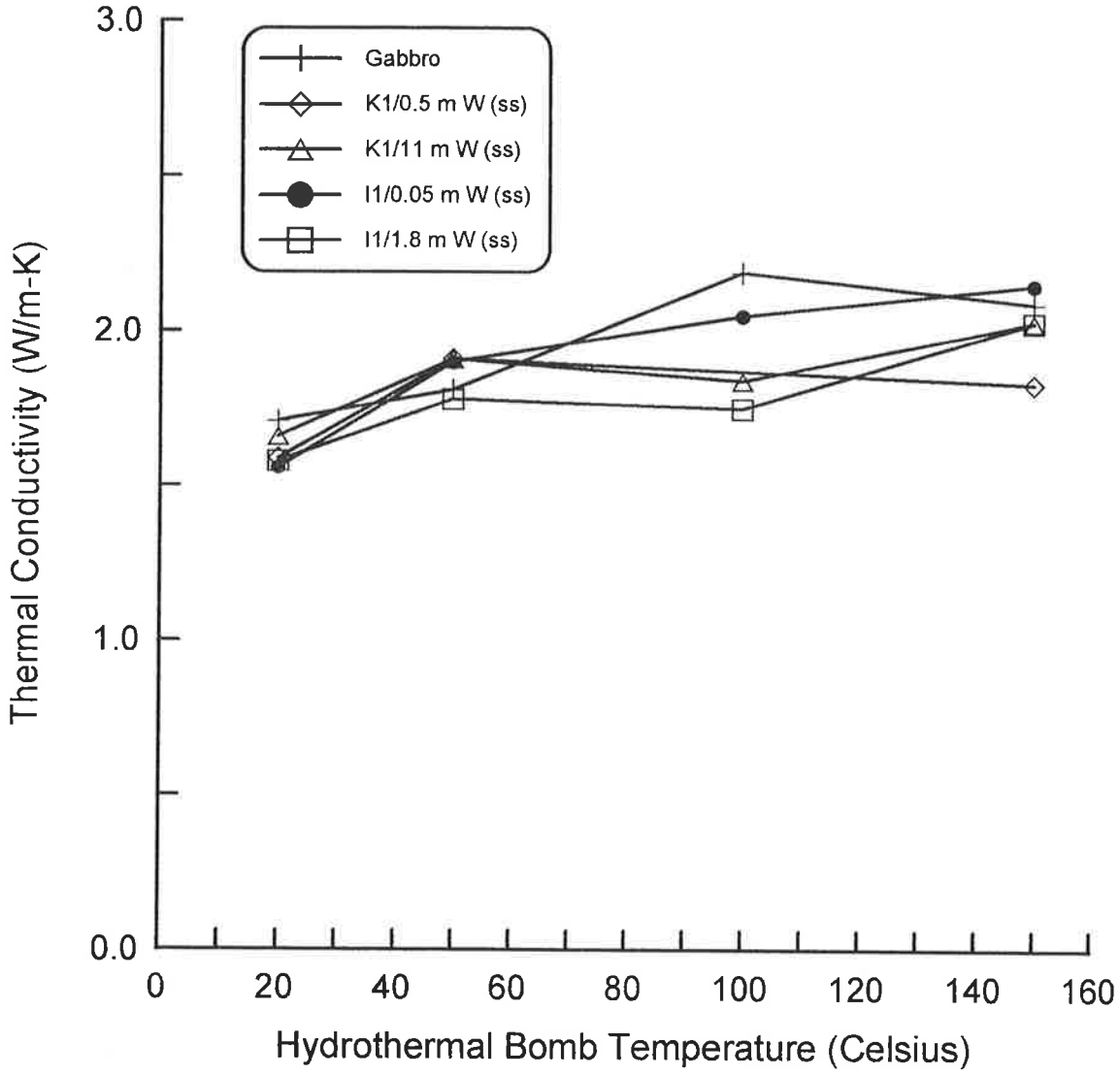
Gabbro
K1/0.5 m W (ss)
K1/11 m W (ss)
I1/0.05 m W (ss)
I1/1.8 m W (ss)
Thermal Conductivity (W/m-K)
3.0
2.0
1.0
0.0
0
20
40
60
80
100
120
140
160
Hydrothermal Bomb Temperature (Celsius)

Table 5-1. Thermal Parameters for a Simple Conductive Model of Dike Intrusion

Thermal Parameter /Value used	Model sensitivity to value used	Method/Notes
Dike Width: 20 m for Bena 3 0.6 m for San Remo 1	A key factor in determining the width of the contact aureole.	Fixed by field measurements.
Host Rock Temperature: 100°C	The baseline value that the modeled temperatures approach away from the dike margin	Temperature from reconstruction made in Chapter 3. The value simulates a shallow level intrusion
Magma Temperature: 1250°C for Bena 3 1200°C San Remo 1	A key factor in determining T_c and T_{peak} away from the dike. The value used is based on a liquidus of 1235°C with respect to olivine in mafic magmas (Fig. 2-9).	Quenched magmas that contain olivine phenocrysts were intruded below the liquidus temperature and those that appear to be all liquid when intruded are above it.
Temperature Interval of Crystallization: 100°C	Increasing the temperature range of crystallization seems to mostly effect T_c . T_{peak} away from dike contact changes little.	A range of 100-300°C suggested by Spear and Peacock (1990). Delaney and Pollard (1982) report an observed ratio of solidifaction temperature to T_{magma} of 0.95 or about 60°C at 1200°C
Degree of Crystallization: 0% Bena 3 10% San Remo 1	Large effect on heat of crystallization	Degree of crystallization at time of Intrusion is estimated from proportion of phenocrysts of olivine in quenched magma at dike margin.
Heat of Crystallization: 400,000 J/kg, Bena 3 360,000 J/kg, San Remo 1	Decreasing heat of crystallization reduces temperatures away from dike	Spear and Peacock (1990) suggest 400,000 J/kg for completely liquid mafic magmas and adjusting this value based on degree of crystallization
Thermal Conductivity: 2.1 W/m-K	Assumed in the model to be equal in dike and host rock. Fig. 5-1 indicates this is a reasonable assumption(Fig. 5-1).	This value is fairly typical for basalt and ultramafic rocks (Robertson, 1988) and near the measured value for Strzelecki Group sandstones.
Heat Capacity: 820 J/kg-K	Assumed in model to be equal in dike and host rock. The measured values indicate this is a reasonable assumption.	Roy et al. (1981)for Gabbro: 775±60 J/kg-K. Haenel (1983) and Erren and Bredewout (1991) for coaly clastic rocks; 840 J/kg-K
Density: 2600 kg/m^3	Assumed in model to be equal in dike and host rock. The measured values suggests this is a tenuous assumption but the model shows little sensitivity respect to density.	Typical basalts are 3000 kg/m^3 and sandstones are 2500 kg/m^3 However, measured values of Strzelecki Group sandstone average 2100 kg/m^3 and the value for the dike/host rock system was lowered overall.

Peak Temperatures Predicted by Simple Conductive Models

Numerical models, based on conductive cooling only, were prepared for dike thicknesses of 0.6 m and 20 m representing the San Remo 1 and Bena 3 dikes. These dikes were selected because they have reliable fluid inclusion data available to allow a comparison of model results.

Because Bena 3 dike apparently intruded at above liquidus temperatures, estimated to be about 1250°C, the model predicts a high $T_{contact}$ of 840°C (Fig. 5-2a). At San Remo 1, $T_{contact}$ is somewhat lower at 800°C, as the dike had a higher degree of crystallization at intrusion and a lower latent heat content (Fig. 5-3). Away from the dikes, cooling from $T_{contact}$ appears to occur relatively slowly because the model which uses a high T_{magma} and heat of crystallization, and a relatively low thermal diffusivity, computed from the low measured thermal conductivity (Fig 5-2b). An effect of considering latent heat is shown below for Bena 3 where $T_{contact}$ initially increases for some time after intrusion (Fig. 5-7). The effect of latent heat is to increase $T_{contact}$ to about 150°C higher than the value computed using the equation:

$$T_{contact} = (T_{magma} + T_{host})/2$$

as this equation does not consider latent heat (Chapter 2). These predicted higher temperatures approach the anatexis temperature for water-wet rocks that have a bulk composition similar to the Strzelecki Group sandstones (Winkler, 1976) yet no fusion is normally observed in the host sandstones that are preserved (non-mylonitic) immediately adjacent to the dike margins. The rock at the Korumburra 1 contact is vesiculated, suggesting the evolution of a plastic host rock/dike rock mass, but generally no flow features are observed next to the dikes and bedding continues relatively undeformed into the dike contact. This suggests that overall $T_{contact}$ for the dikes intruding the Strzelecki Group is less than the predicted temperature from this simple conductive model.

Fig. 5-2. A. Peak temperature as a function of distance from the dike margin predicted for a 20 m thick dike, such as the Bena 3 dike, western onshore Gippsland Basin. Note how the simple conductive model predicts T_{peak} to rise above the assumed regional temperature of 100°C out to about X = 80 m or X/D = 4; this extended zone of cooling may be a signature of simple conductive cooling. B. Temperature as a function of distance from the dike margin and time. Note that T_{peak} out to X = 30 m, the limit of the sample range for Bena 3, took about 20 yrs to attain and then decline slightly. These numerical models were constructed using Peacock (1989) and the data in Table 3-1.

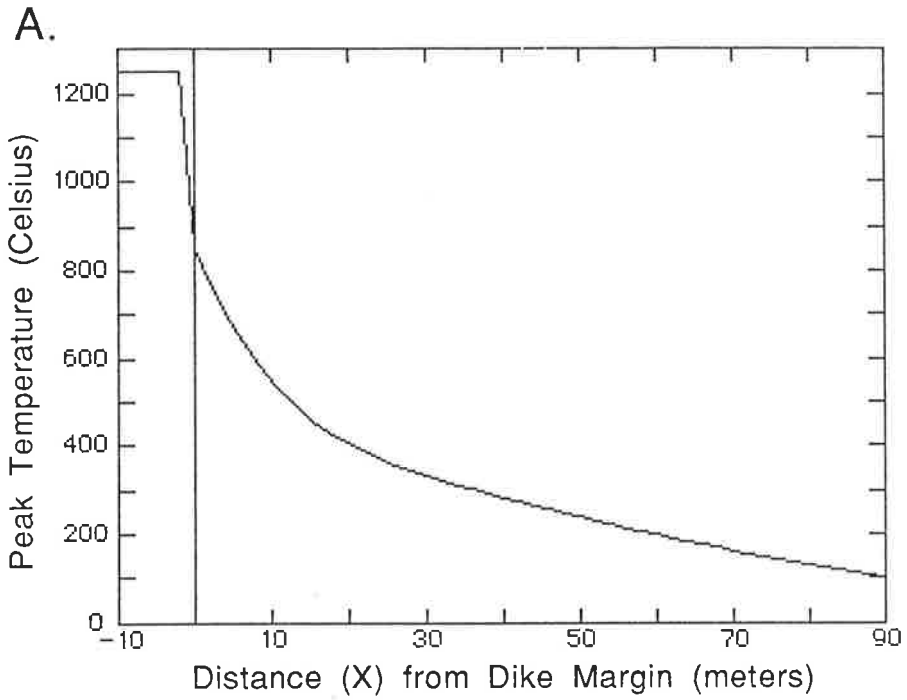
A.
Peak Temperature (Celsius)
0
200
400
600
800
1000
1200
−10
10
30
50
70
90
Distance (X) from Dike Margin (meters)

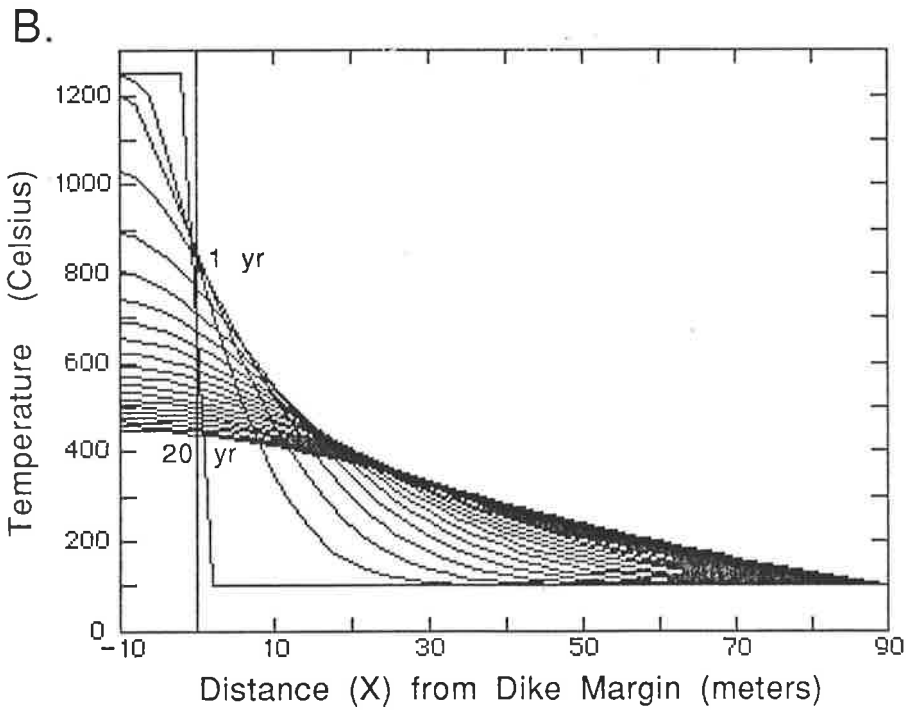
B.
Temperature (Celsius)
0
200
400
600
800
1000
1200
1 yr
20 yr
−10
10
30
50
70
90
Distance (X) from Dike Margin (meters)

Fig. 5-3. A. Peak temperature as a function of distance from the dike margin predicted for a 0.6 m thick dike, like the San Remo 1 dike, western onshore Gippsland Basin. Note how the simple conductive model predicts T_{peak} will persist above the assumed regional temperature of 100°C out to about x = 2.4 m or X/D = 4; this extended zone of heating may be a signature of simple conductive cooling by the dike. B. Temperature as a function of distance from the dike margin and time. These numerical models were constructed using Peacock (1989) and the data in Table 3-1.

A.

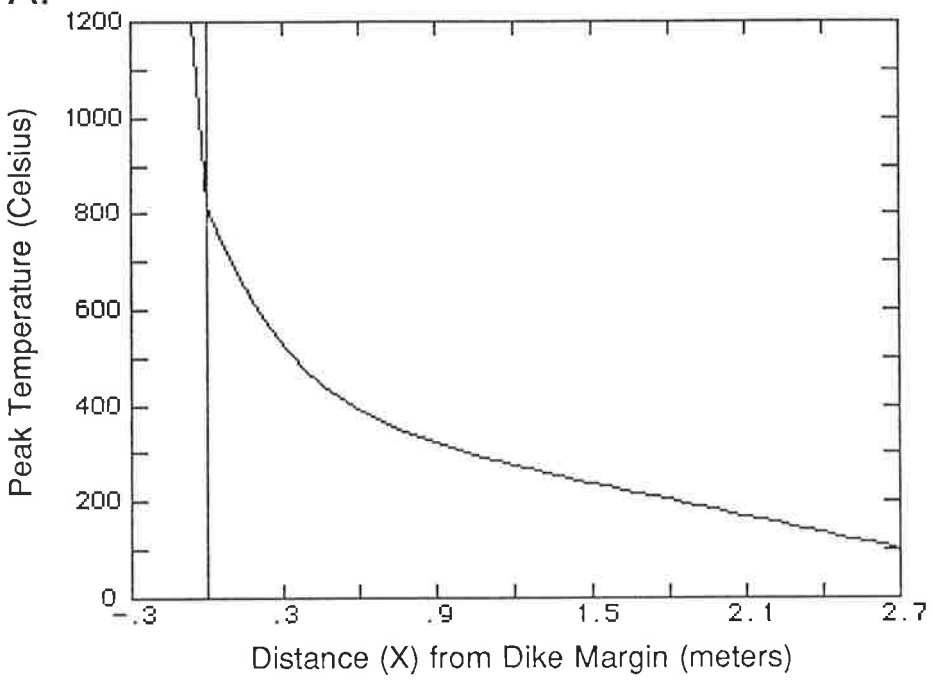
Peak Temperature (Celsius)
1200
1000
800
600
400
200
0
-.3
.3
.9
1.5
2.1
2.7
Distance (X) from Dike Margin (meters)

B.

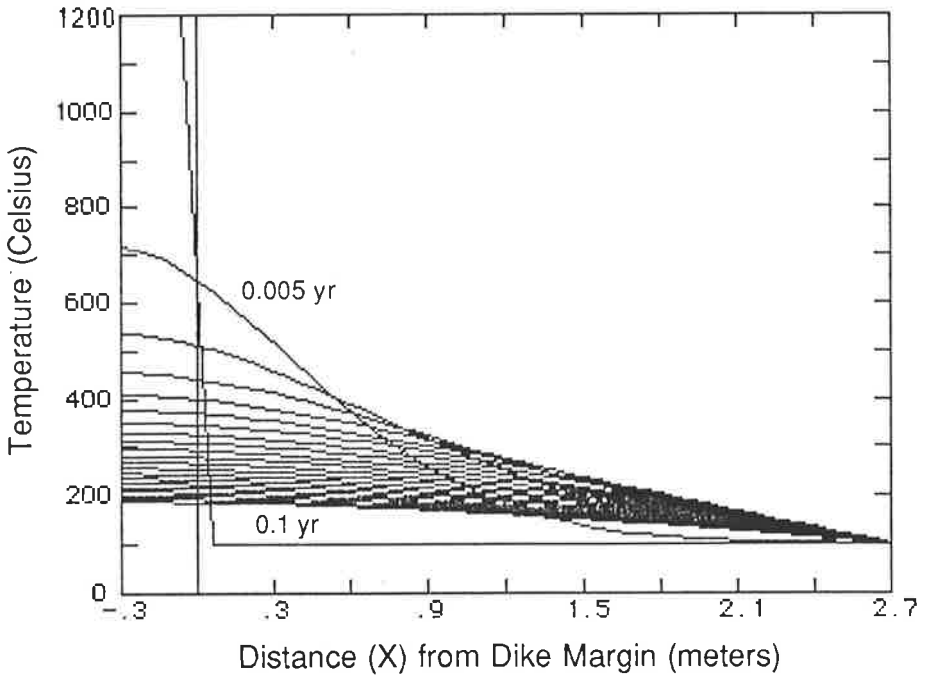
Temperature (Celsius)
1200
1000
800
600
400
200
0
0.005 yr
0.1 yr
-.3
.3
.9
1.5
2.1
2.7
Distance (X) from Dike Margin (meters)

Using a T_{magma} of 1000°C for basalt, 100,000 J/kg heat of crystallization and a temperature interval of crystallization of 60°C, would reduce $T_{contact}$ to 600°C but increased heating of the host rocks still continues out to about X/D = 3 or 4 (Fig. 5-4). While the 1000°C intrusion temperature has been suggested for basalts (Jaeger, 1959; Hughes, 1982; among others), the other thermal parameters used are unrealistic in this low temperature case (Simon and Peacock, 1989). Note that this case is based on unrealistic thermal parameters in that a heat of crystallization of 100,000 J/kg in a basaltic magma suggests that these dikes were intruded with 75% of the magma crystallized. This is not the case for the western onshore Gippsland Basin dikes that were apparently intruded in a near liquid state. This curve is an attempt to compare the heat flow model predictions by shifting the simple conductive model values (solid squares in Fig 5-4) to near those computed by the wet-rock curve (solid triangles). In the simple heat flow model, the continued heating of the host rocks far from the contact, even with the unrealistic reduction in heat content of the magma, occurs because the heat introduced by the dike can dissipate only into the heat sink formed by the host rocks. The heat sink represented by the vaporization of the pore fluids or migration of the heated fluids after intrusion is not allowed for in this model.

The values of these thermal parameters could be modified to change the temperatures and cooling history predicted by the model but given the number of assumptions in developing the model, this approach is not used in this study. Unless more of the variables can be measured at each dike suite, arbitrarily changing thermal parameters until a fit is made may obscure the fact that the model itself does not adequately fit nature.

The model results are used in this study by comparing the form of the predicted conductive cooling curves to determine the type of cooling inherent suggested by T_{peak} measurements next to the dike. The simple conductive model, if reasonable T_{magma} values are used, suggests that significant heating above background regional temperature occurs out to

from X/D = 2 to 4. Dow (1977) reports that dikes and sills increase the Rv-r of host sedimentary rock in a zone about two times the thickness of the igneous sheet (a double dike thickness rule).

This observation and the simple conductive model presented here suggest that dikes cooling predominantly by conduction appear to heat the host rocks from 2 to 4 dike thicknesses. A more sophisticated model of a basaltic dike that intrudes impermeable evaporites and apparently cools mostly by conduction gives an apparent $T_{contact}$ value of 790°C which is similar to those calculated here for this simple model (Knipping, 1989). This more sophisticated model also predicts a contact aureole that extends out to several dike thicknesses in the host rock.

In summary, a contact aureole that consists of an extended zone of monotonic temperature decrease reaching out to well over X/D = 2 and a $T_{contact} \approx (T_{magma}+T_{host})/2$ appears to be a signature of simple conductive cooling.

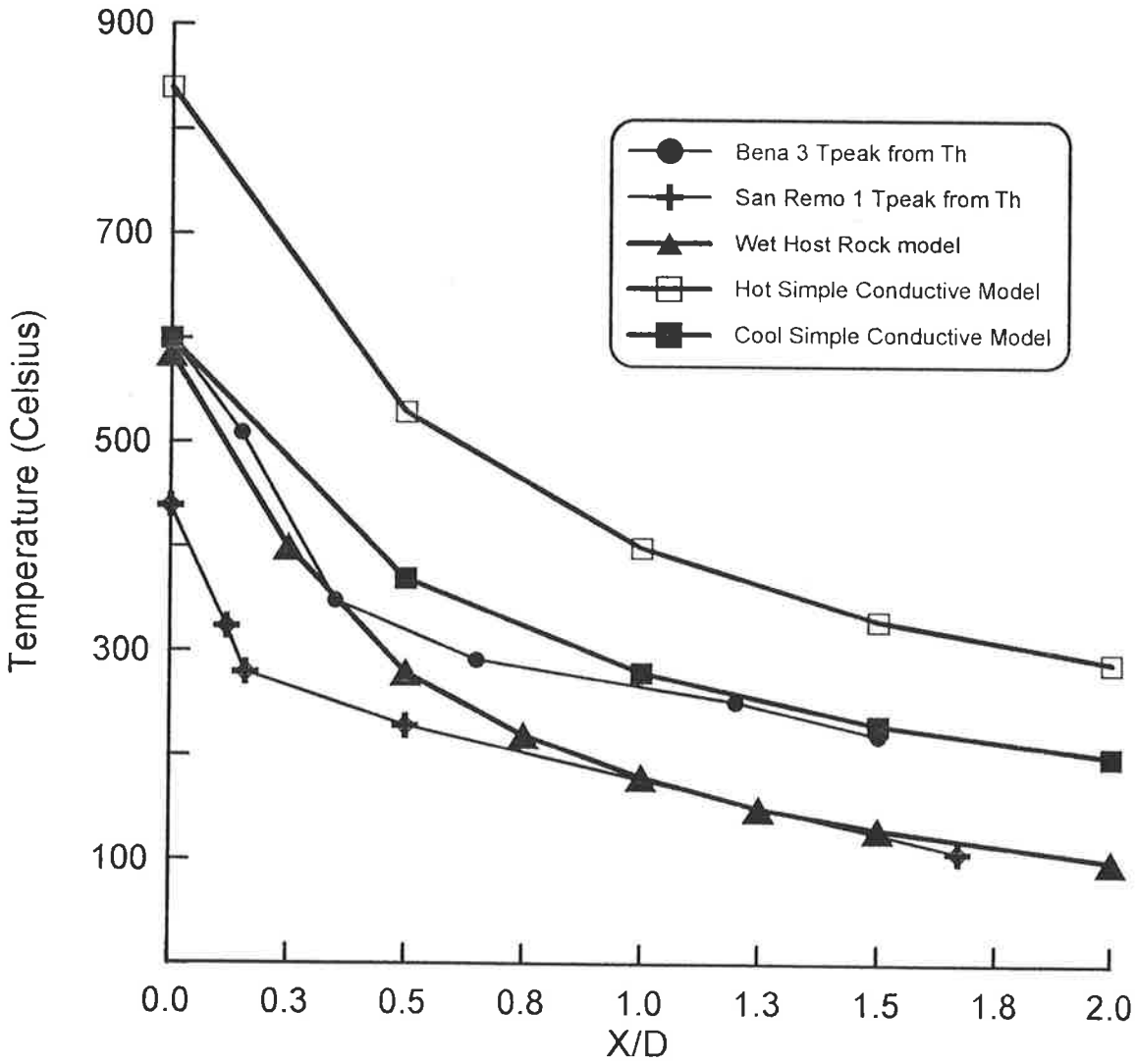
900
700
500
300
100
Temperature (Celsius)
0.0
0.3
0.5
0.8
1.0
1.3
1.5
1.8
2.0
X/D
Bena 3 Tpeak from Th
San Remo 1 Tpeak from Th
Wet Host Rock model
Hot Simple Conductive Model
Cool Simple Conductive Model

Comparing the form of the model temperature predictions to the form of the T_{peak} curves interpreted from the fluid inclusion data (Fig. 5-4) suggests that, in the western onshore Gippsland Basin, the dikes are not cooling by simple conduction. The T_{peak} curves more closely follow the cooling curves predicted by a model developed by Jaeger (1959) that considers the effects of pore water vaporization and shows increased heating at X/D < 2. As pointed out by Spear and Peacock (1990), evidence for hydrothermal advection or convection next to shallow intrusions is commonly found. As shown by the wet-rock heat flow model below, pore water vaporization and potential loss by fluid flow can significantly decrease temperatures next to dikes (Jaeger, 1959; Delaney 1982, 1987). The pore water is in effect acting as a heat sink that absorbs some of the heat added to the host rocks from the heat of crystallization of the magma.

Heating Duration Predicted by Simple Conductive Models

A heating duration estimate can also be developed from the simple conductive cooling model and compared to the trial heating duration value computed from the AFT age data at San Remo 1. To review the AFT age and track length data presented in Chapter 4, they are summarized using interpretive plots developed by Arne et al. (1990b) (Figs 5-5 and 5-6). These plots are based on the theory that if the AFT age data show a progression towards total annealing, the trend of younger AFT ages will be observed in samples with longer mean track lengths and a smaller track length standard deviation. This trend reflects the accumulation of unannealed 15 µm tracks after intrusion, partial or total annealing, and then rapid cooling to temperatures where tracks show good stability. A plot of all the dike AFT data shows that the mean track length varies over a small range of about 1 µm and there is no trend in the AFT age and track length standard deviation (Fig. 5-5). In all of these samples, track length standard deviation is relatively small and suggests a relatively rapid cooling sometime after intrusion that

has produced a small degree of annealing after tracks became partially or completely stable.

AFT annealing effects can also be detected by plotting the mean track length and standard deviation versus AFT age (Fig. 5-6). If the host rocks are initially cool during intrusion, the apparent sample age will decrease by the annealing of tracks until a zero age is indicated near the dike. Tracks accumulated after rapid dike cooling (presuming that the host rocks are cool enough for track retention) will show an unannealed length about 15 μm. The apparent sediment age of the completely reset sample near the dike will equal the age of the intrusion. When the samples are studied sometime after intrusion, the annealing trend observed is an increasing average track length with decreasing age as the dike is approached. This trend is observed in the Inverloch 1sample suite (Fig. 5-6) but the trend seen in the Inverloch samples is apparently not statistically significant as the error in the measurements overlaps the range of the adjacent samples. The data from the other dikes show no trend of age and track length as the samples approach the dike margin. Thus, as in Chapter 4, the conclusion is reached that AFT data apparently only record the cooling of the dike and host rock package sometime after intrusion. However, Fig. 5-6 does suggest the latest time for this cooling was about 80 to 90 Ma, marked by the lower boundary of the AFT ages. The date is consistent with the burial history of Duddy and Green (1992) as documented in Chapter 3. These AFT ages are not corrected for the decreased age due to track length reduction (Green, 1988) because the mean track length in these samples is close to that of an unannealed track length distribution and the correction is negligible (Appendix 9).

Fig. 5-5. Mean track length with an error bar equal to ± 1σ . Data shown from the Bena 1, Inverloch 1, San Remo 1 dikes, western onshore Gippsland Basin. Data point label is pooled AFT age.

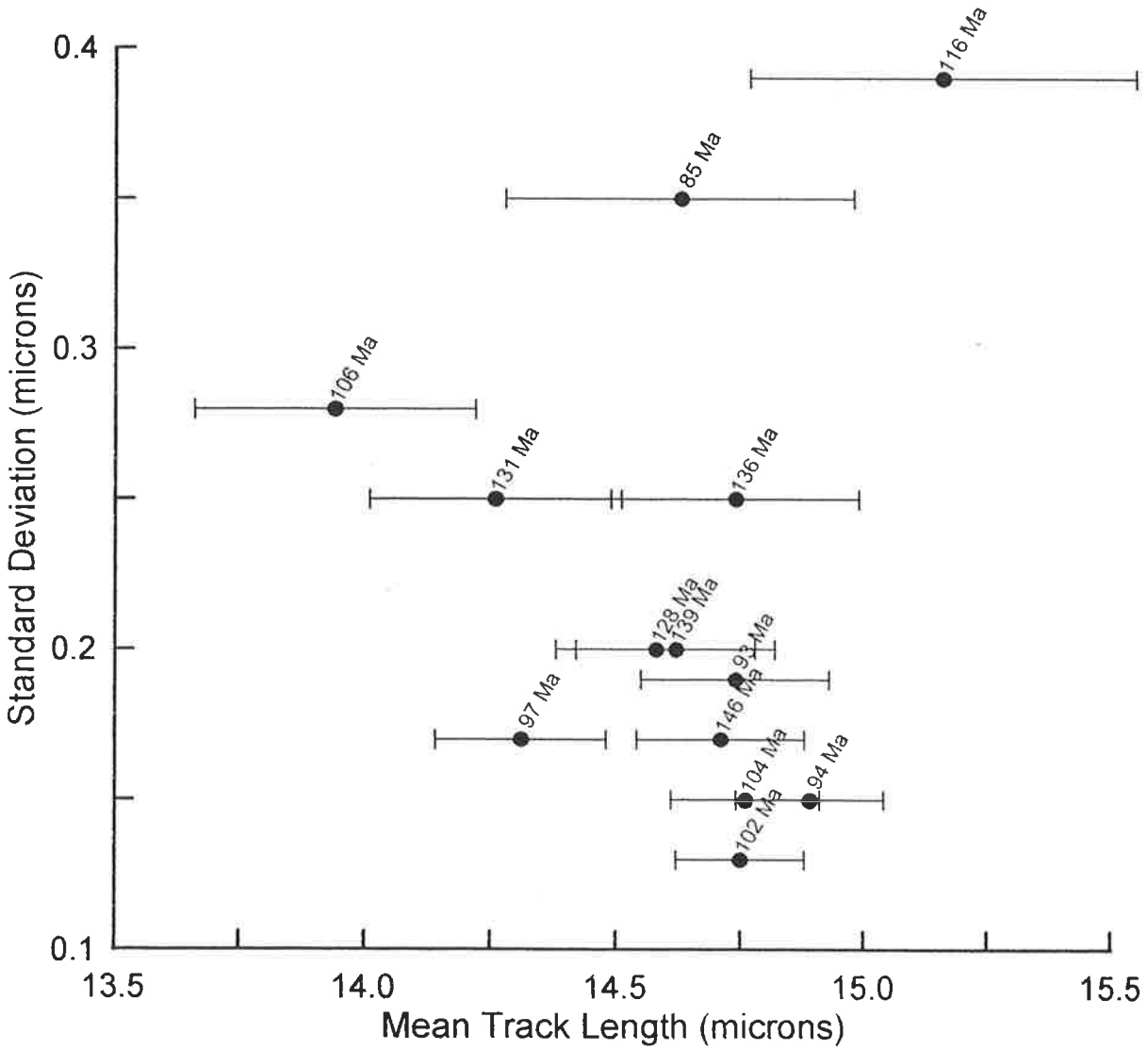
0.4
0.3
0.2
0.1
Standard Deviation (microns)
13.5
14.0
14.5
15.0
15.5
Mean Track Length (microns)
116 Ma
85 Ma
106 Ma
131 Ma
136 Ma
128 Ma
139 Ma
93 Ma
97 Ma
146 Ma
104 Ma
94 Ma
102 Ma

Fig. 5-6. Mean track length and pooled AFT age with error bars equal to ± 1σ. For dikes from the western onshore Gippsland Basin. Data point label is dike code and distance (X) from the dike margin. Dike codes = B1 = Bena 1; I1 = Inverloch 1; SR1 = San Remo 1.

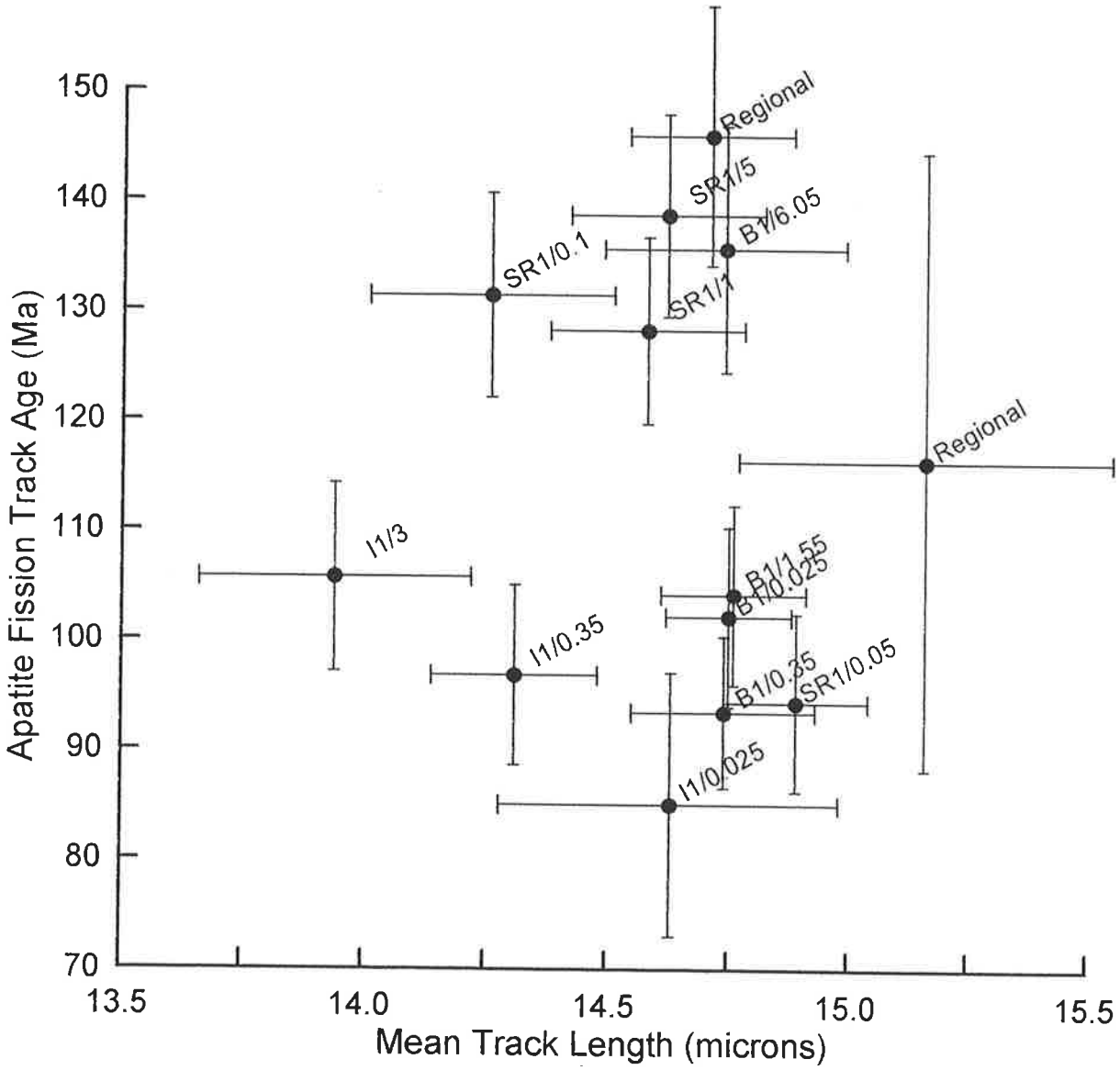
Regional
SR1/5
B1/6.05
SR1/0.1
SR1/1
Regional
I1/3
B1/1.55
B1/0.025
I1/0.35
B1/0.35
SR1/0.05
I1/0.025
150
140
130
120
110
100
90
80
70
13.5
14.0
14.5
15.0
15.5
Apatite Fission Track Age (Ma)
Mean Track Length (microns)

Heating duration can also be estimated from the simple conductive models (Fig. 5-7). A key problem is defining the heating duration in the case of dike intrusions. In this definition, we consider only the zone of intense contact metamorphism at about $X/D \leq 0.5$ which is where the AFT ages apparently decrease to 50%. Within this zone, the heating duration is taken to be the sum of the time to reach T_{peak} and elapsed time at this temperature before cooling commences. Using this definition, at Bena 3 the heating duration near the dike is about 3 yr and at San Remo 1 it is about 0.01 yr or 4 days. This value of heating duration estimated from heat flow models is roughly the same as the 8 day value speculatively estimated from AFT data at San Remo 1 in Chapter 4.

Fig. 5-7. Temperature at a distance (X) from the dike margin as a function of time. A. A simple conductive model for a 20 m thick dike which emulates the Bena 3 dike. The curves between X= 0 m and X = 45 m are at 3, 9, 15 and 30 m. Note the initial increase in $T_{contact}$ defined by the X =0 m curve. B. A simple conductive model for a 0.6 m thick dike which emulates the San Remo 1 dike. The curves between X= 0 m and X = 1.2 m are at 0.1, 0.3, 0.6, and 0.9 m. Both of these cooling curve computed from a simple conductive model with T_{magma} = 1200°C, heat of crystallization = 400,000 J/kg, and a temperature interval of crystallization = 100°C.

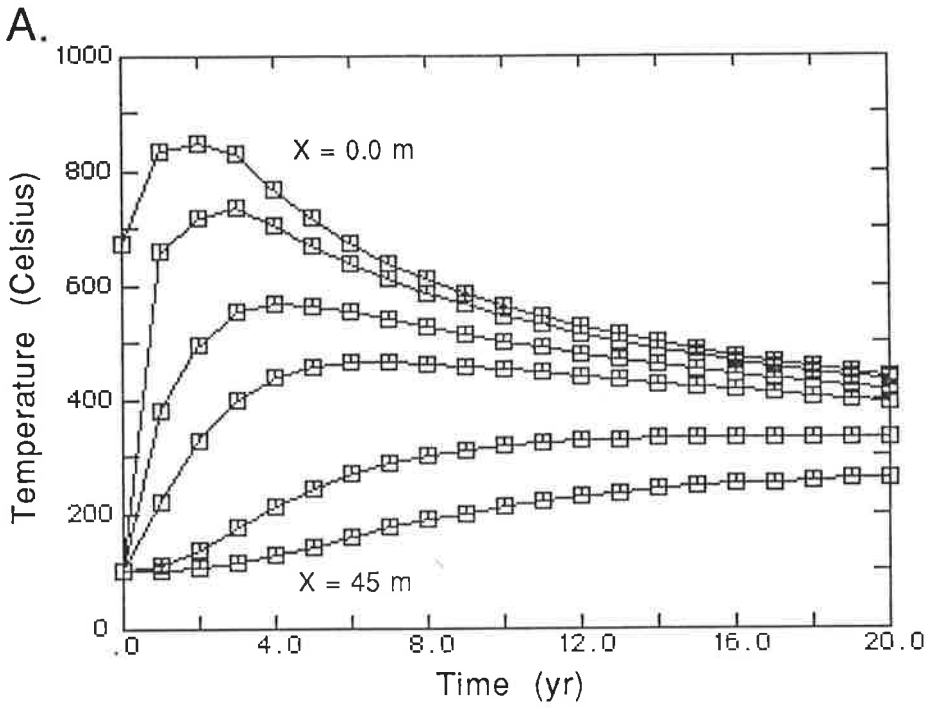
A.
1000
800
600
400
200
0
Temperature (Celsius)
X = 0.0 m
X = 45 m
.0
4.0
8.0
12.0
16.0
20.0
Time (yr)

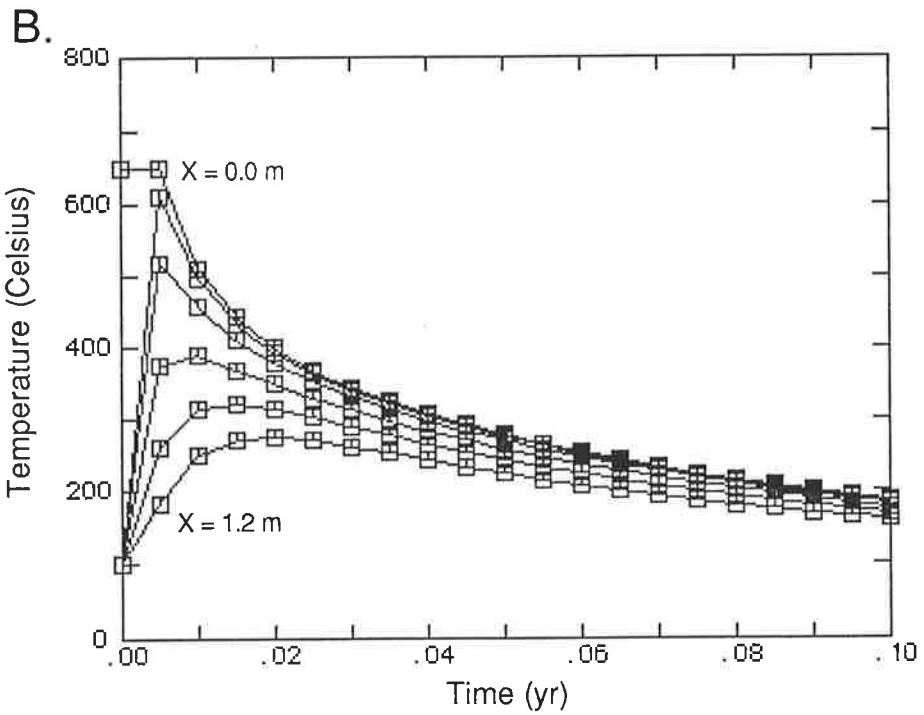
B.
800
600
400
200
0
Temperature (Celsius)
X = 0.0 m
X = 1.2 m
.00
.02
.04
.06
.08
.10
Time (yr)

5.2 CONDUCTIVE HEAT FLOW MODELS OF DIKES INTRUDING WET HOST ROCKS

In Chapter 2, the reaction duration and temperature in rock which was contact metamorphosed by an intrusive igneous dike were estimated from a heating duration-temperature model derived from heat-flow theory (Jaeger, 1959). In these one-dimensional heat flow models, the intrusive sheet is assumed to be instantly emplaced at 1000°C into a water-wet, porous sedimentary rock at a depth where water would boil at 200°C. Vaporization of the fluid absorbs heat reducing the T_{peak} as distance from the dike increases. Further, the dike may also cool by the advective loss of vapor from the system and the migration of cool ground water towards the dike (Jaeger 1959, 1964; Delaney, 1982, 1987; Delaney and Pollard, 1982). Thus, the model was designed for the case of a dike intruded into shallowly-buried water-wet host rock, similar to the situation in the Gippsland basin as established in Chapter 3.

The Strzelecki Group, at the time of intrusion was at about 100°C and a depth of 2 km, representing hydrostatic pressure of about 20 MPa. Aqueous fluid inclusions trapped during the thermal pulse at the time of intrusion suggest the sediments were water saturated. The boiling point of fresh water, indicated by the fluid inclusion salinity measurements at this depth and pressure, is about 300°C (White, 1973), somewhat higher than in the wet-rock model as set-up by Jaeger (1959). The effect of the increased boiling point is to reduce the thickness of the band of vaporized pore water next to the dike. Intrusion temperatures of the Gippsland Basin dikes are also thought to be somewhat higher, about 1200°C. However, as discussed above, the point of this model is not to exactly fit the prediction to nature by arbitrarily adjusting thermal parameters that are not very well known, but to show that the style of cooling is similar based on the simplifications used to construct the model.

Results from the Wet-Rock Model

The profile of the predicted dike temperatures from Jaeger's (1959) wet-rock model and the fluid inclusion data from Bena 3 are in good agreement close to the dike and become somewhat hotter away from the dike (Fig. 5-4). Conversely, the profile of the predicted dike temperatures from the wet-rock model and the fluid inclusion data from San Remo 1 initially are somewhat cooler but agree well away from the dike (Fig. 5- 4). Overall, the plot of these modeled temperatures and the predicted $T_{contact}$ are in good agreement with T_{peak} interpreted from fluid inclusions.

After intrusion, the wet-rock model considers that as heat is transferred to the pore water in the host rocks, thermal expansion occurs and initially water moves away from the dike margin (Delaney, 1987). In some cases, a portion of the water near the dike contact may vaporize (Jaeger, 1959). This study confirms the generation of vapor and also supercritical fluids during contact metamorphism caused by dikes.

After the initial expansion of the fluids, Delaney (1987) shows that with continued heating of the host rocks, buoyant forces are generated in the pore fluids and advection (fluid flow) commences near the dike. Advection commencing near the dike draws relatively cool pore water towards the dike and consequently reduces the T_{peak} reached in the host rock. In most cases, the host rock is too impermeable and(or) cooling is too rapid next to thin dikes for convection, a special case of advection where a hydrothermal fluid circulation system develops, to become established.. Next to thick dikes cooling is much slower, mineral reactions that may increase permeability are more extensive and convection can develop (Delaney, 1987). The inferences from this analysis and the earlier results from the simple conductive model are that if the rocks are permeable enough, most of the heat from an intrusion is dissipated by advection next to thin dikes and convection next to thick dikes.

As Delaney (1982, 1987) and Delaney and Pollard (1982) point out thin dikes may

initiate advection but normally cool before convection ensues. Thin dikes in the Strzelecki Group typically develop the monotonic decrease in T_{peak}, as suggested by Rv-r profiles out to one dike thickness or X/D = 1 (Fig. 5-8). Thick dikes, or thin intrusions into permeable rocks, may show the convection-like effects of the transitional advection-to-convection profile seen at the Bena 3 dike and perhaps at the San Remo 1 dike. Thick dikes can heat long enough to produce an increase in permeability to the point where an apparent convective system develops, even in mudstone, as shown at Cruickston 1. This is not always the case with intrusions into mudstone, however, as Norland (1986) reports that a Cretaceous shale near El Paso, Texas, that was intruded by a middle Eocene pluton averaging 1680 m thick, only produced a zone of increased thermal maturation 600 m wide. This is an X/D of about 0.35 and far less than that predicted by heat flow models (Mundry, 1968) for cylindrical intrusions. Although details of the degree of crystallization of the magma is unknown in this case, this magma could have been intruded in a significantly crystallized state or have a composition with a lower heat of crystallization (Spear and Peacock, 1990). The magma may have released little heat of crystallization during solidification and the resulting contact aureole is thinner than expected. The evaluation of magma temperature alone is insufficient to determine the width of the contact aureole.

This analysis also indicates a problem with overemphasizing intrusion temperature and conductive cooling in determining the width of the contact metamorphic aureole (Dow, 1977; Raymond and Murchison, 1988; Wang et al., 1989). The latent heat of crystallization and the occurrence of advection or convection seem to be more influential in predicting contact metamorphism away from the dike. Whereas considering the latent heat of crystallization adds a significant heat source to the system, the effect of pore water is to act as a heat sink that can absorb and transport (remove) considerable heat. Further, chemical reactions occurring in the host rock may act to increase or decrease permeability and in part control the fluid movement

after intrusion. Among other dehydration and decarbonization reactions, a well-documented chemical reaction causing volume loss is the strong loss of TOC seen as the dike margin is approached in the western onshore Gippsland Basin. Thus, contact metamorphism caused by dikes is not a simple system that can be completely modeled without at least some consideration of the physical and chemical conditions at each dike at the time of intrusion.

Evaluation of Physical Factors Affecting the Width of Contact Aureole

Physical factors thought important in controlling the extent of contact metamorphism by dikes are numerous. Besides the obvious heat flow factors listed in Table 5-1 and prior burial history, including host rock temperature at the time of intrusion, discussed in Chapter 2, the other critical factors in determining the width of the contact aureole are: 1) continuing magma flow in the dike conduit after intrusion; 2) overburden pressure at the time of intrusion as it influences vaporization of the pore fluid; and 3) fluid movement by advection or convection (Jaeger, 1959, 1964; Delaney 1982, 1987; Delaney and Pollard, 1982). The importance of burial history prior to intrusion is that it determines the reactivity of the host rocks and its water content (Raymond and Murchison, 1988) as well as its temperature at the time of intrusion. The effect of continuing magma flow in the dike conduit is to preheat the host rock before the magma stops flowing. Subsequently, the dike follows a cooling history suggested by these heat flow models.

System closure is not assessed in most previous studies of thermal maturation caused by intrusions (an exception is Pytte, 1982). The width of the contact aureoles suggested by thermal models of closed (Jaeger, 1959) and open systems (Jaeger, 1959; Delaney, 1982; 1987) as well as the heat content of the magma are significantly different (Fig. 5- 4). So the idea of Raymond and Murchison (1988) of pore water content of the host rock minimizing the contact aureole needs to be modified to make it compatible with the results of this study. The

minimal aureoles in the water-rich host rocks observed by Raymond and Murchison could result from the fact that pore water by its heat capacity and through phase changes absorbs heat. The resulting advection of pore water towards the intrusion minimizes the width of the contact aureole in the host rocks. Such hydrothermal effects have been reported in highly-porous young sediments (Einsele et al., 1980). Further, these apparently cool host rocks. The heat flow models suggest this would give a much greater temperature drop from the dike contact to the ambient temperature extant at the time of intrusion. The wide aureoles in the drier, more mature rocks observed by Raymond and Murchison(1988) could be caused by conductive cooling in relatively impermeable host rocks that were more deeply buried at the time of intrusion. Also, in the more deeply buried rocks, metamorphic temperatures are maintained much further away from the dike contact, T_{host} was much higher, and consequently the observed contact metamorphism is more extensive. The conclusion that the degree of sediment compaction is a significant control on the width of the contact aureole is consistent with the heat flow models presented here, in the sense that compacted rocks are less permeable and may cool by conduction, thus producing a wide contact aureole. However, Raymond and Murchison might have also considered the effect of the heat of crystallization and other thermal conditions at the time of intrusion as well as considering that the temperatures of the magmas may be similar. Heat flow modeling presented above shows that the temperature decrease is much faster in the contact aureole of an intrusion that has a low heat of crystallization content, as in a magma that is mostly crystallized at intrusion, compared to an intrusion of a magma with a high heat of crystallization content, even though the initial magma temperatures may have been similar.

The changes in the width of the contact aureole, as shown by Rv-r increases, are not strongly time dependent (Fig. 5-8). The heat flow model of Peacock (1990) shows that the heating duration next to a cooling dike is strongly dependent on dike thickness. However, the

Rv-r profiles of the dikes that appear to cool by advection are in a relatively narrow band, whereas the thickness of the dikes varies widely, from 0.06 m thick to 35 m. Heat flow modeling suggests heating durations for these dike thicknesses would range from hours to decades. Thus, heating duration seems to be a minor factor in determining the width of the contact aureole as measured by Rv-r.

Comparison of Vitrinite Reflectance Geothermometry and T_{peak} from Fluid Inclusions

T_{peak} values interpreted from fluid inclusion data and vitrinite reflectance geothermometry (VRG) are in good agreement up to temperatures of about 300°C (Fig. 5-9). Above this temperature, Rv-r becomes inaccurate near the dike (Chapter 4) and consequently the VRG T_{peak} estimate becomes inaccurate. The inaccuracy of vitrinite reflectance measurements near the dike makes them useless for calibrating a geothermometer specifically for dike contact metamorphism. It is possible that the evolution of a vapor or supercritical fluids near the dike cause the degradation of vitrinite reflectance by a changing the type of reactions that occur or their reaction rate. Evidence for this change is a variation in the extent and type of reactions occurring in organic matter which are seen during pyrolysis experiments, if vapor or super critical fluids evolve during the experiment (Lewan, 1994).

Fig. 5-8. Comparison of Rv-r and X/D for all dikes studied in the western onshore Gippsland Basin. Also shown is the interpreted cooling environment, derived from the form of the Rv-r profile.

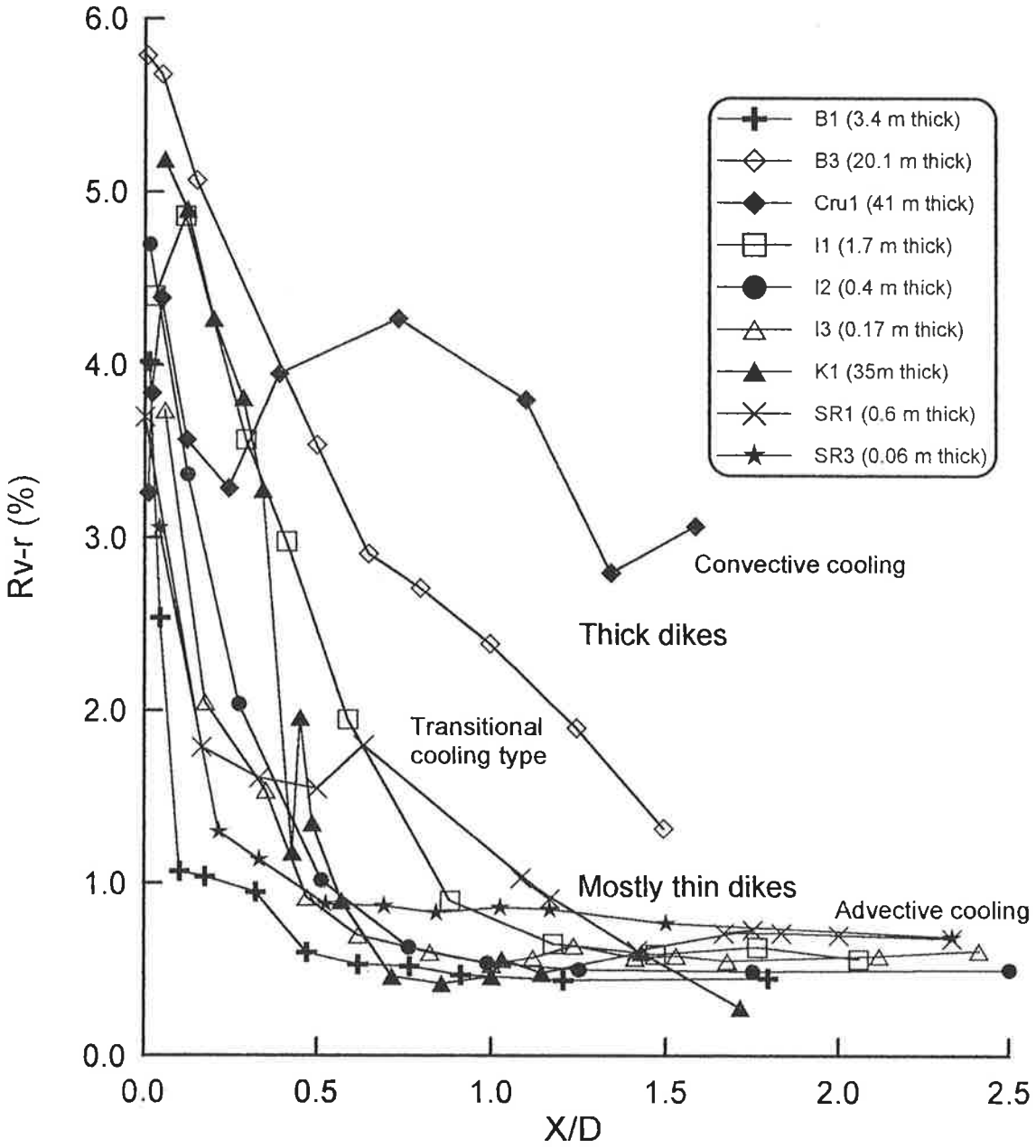
6.0
5.0
4.0
3.0
2.0
1.0
0.0
Rv-r (%)
0.0
0.5
1.0
1.5
2.0
2.5
X/D
B1 (3.4 m thick)
B3 (20.1 m thick)
Cru1 (41 m thick)
I1 (1.7 m thick)
I2 (0.4 m thick)
I3 (0.17 m thick)
K1 (35m thick)
SR1 (0.6 m thick)
SR3 (0.06 m thick)
Convective cooling
Thick dikes
Transitional
cooling type
Mostly thin dikes
Advective cooling

Fig. 5-9. T_{peak} from the vitrinite reflectance geothermometer (VRG) for hydrothermal metamorphism compared to T_{peak} interpreted from fluid inclusion data. VRG for hydrothermal metamorphism from Barker and Pawlewicz (1994). T_{peak} from fluid inclusion data interpreted from Figs 4-8 and 4-32. The dashed line represents perfect 1:1 agreement between the two types of T_{peak} estimates.

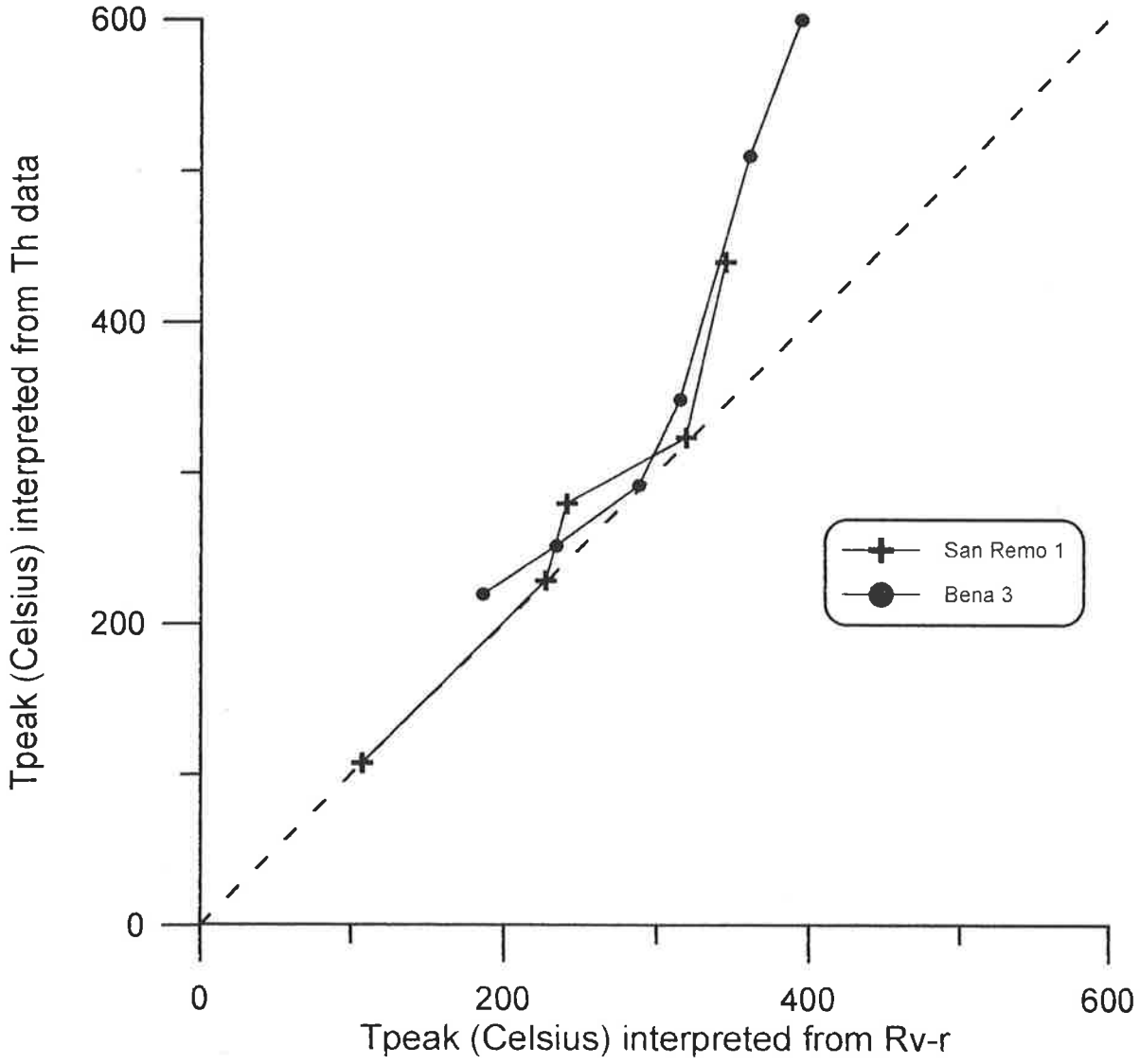
600
400
200
0
0
200
400
600
Tpeak (Celsius) interpreted from Th data
Tpeak (Celsius) interpreted from Rv-r
San Remo 1
Bena 3

Even though the fluid inclusion data show a consistent trend above 300°C, suggesting direct geothermometry is possible, the trend is not well enough established because of the limited number of cases. In any case, away from the dike and below T_{peak} of about 300°C, an accurate T_{peak} can be predicted for contact metamorphism by dikes using the hydrothermal metamorphism VRG of Barker and Pawlewicz (1994) and direct determinations by fluid inclusions measurements. Above 300°C, fluid inclusion geothermometry is more accurate, as determined by comparison to the prediction of the heat flow models for temperatures reached near the dike contact (Fig 5-4). The fit of the VRG of the hydrothermal metamorphism is consistent with the apparent advective cooling of these dikes which is typical of geothermal systems.

5.3 HYDROUS PYROLYSIS MODELING

Contact metamorphism by dikes was chemically modeled using hydrous pyrolysis (Lewan, 1993a; 1994). Hydrous pyrolysis uses a closed reaction vessel to heat an aliquot of coarsely crushed source rock in the presence of liquid water under controlled temperature, pressure, and heating duration conditions. The experimental parameters of temperature and heating duration used in this study were designed to simulate a range found next to thin dikes. Pressure was not controlled and the value reached is dependent on the vapor pressure of water and generated gases at the experimental temperatures. Table 5-2 shows that the Rv-r measured after the experiments is in good agreement with those found in the natural samples next to the 0.6 m San Remo 1 dike, suggesting the selected experimental conditions were appropriate.

The objective of hydrous pyrolysis experiments is to emulate the natural conditions normally encountered during burial diagenesis (Lewan, 1993a, 1994). Consequently, the experimental T and P reached in the reaction vessel is tightly controlled during the experiments to keep water vapor from contacting the sample or supercritical fluids from developing in the

reaction vessel. Avoiding the evolution of other than liquid water in the reaction vessel is crucial as organic compounds have very high solubilities in supercritical fluids (Lewan, 1994) and a vapor phase is not usually present during burial diagenesis. The trapping of vapor and supercritical fluids in some fluid inclusions at San Remo 1 is evidence that these phases can evolve during contact metamorphism. However, fluid inclusion evidence indicates these phases are restricted to approximately X/D < 0.2 where the organic matter usually has a high Rv-r and is incapable of generating much hydrocarbon other than methane. Therefore, hydrous pyrolysis experiments are a useful tool in studying contact metamorphism of source rocks away from the immediate dike contact zone.

Table 5-2. Comparison of Experimental and Natural Hydrous Pyrolysis

Sample Number	Rv-r (%)	S_1 mg /g	PI	TOC wt-%	HI mg /g	T (°C)	P (MPa)	Expelled Oil (wt.-% rock)	Bitumen Extract (wt.-% rock)	Oil Plus Bitumen (wt.-% rock)	Gas (wt.-% rock)
HYDROUS PYROLYSIS:											
R5, Raw	0.6	0.2	0.0	63.5	268	ca.100	ca.20	N/A	0.04	0.04	N/A
HP2182	0.9	2.6	0.01	80.3	218	295.4	8.6	1.4	1.8	3.2	1.1
HP2183	1.2	15.5	0.11	76.9	158	330.0	13.2	2.2	1.8	4.0	2.3
HP2184	1.7	19.0	0.21	73.1	99	365.4	21	3.7	6.4	10.1	5.2
NATURAL PYROLYSIS next to the San Remo 1 dike:											
0.98m E	0.7	0.2	0.02	73.4	128	105*	20	oil lost	0.36	N/D,oil lost	gas lost
0.65m E	0.9	0.6	.01	50.8	110	130*	20	oil lost	0.09	N/D,oil lost	gas lost
0.36m E	1.8	0	0	25.6	25	230*	20	oil lost	0.009	N/D,oil lost	gas lost

* T_{peak} estimated from T_h, Fig. 4-32.

The important advantage of hydrous pyrolysis is that expelled oil and gas are retained in the reaction vessel and can be analyzed (Table 5-2 and 5-3). Next to these dikes, the bulk of the generated hydrocarbons have been lost. The remnants of the naturally generated hydrocarbons observed next to the dikes are microscopic particles of fluorescent oil, bitumen and exsudatinite in the coals.

Otherwise geochemical and thermal maturation results between the natural pyrolysis by the dikes and hydrous pyrolysis are generally in good agreement if allowance is made for the differences in the conditions of reaction. For example, Rv-r in the hydrous pyrolysis samples follows the same trend as the natural samples from the San Remo 1 dike (Fig. 5-10). The difference in the two curves is probably due to system closure and heating duration differences. The hydrous pyrolysis is a closed system whereas these dikes are at least a semi-open system. The hydrous pyrolysis samples were heated for 72 hours whereas the natural samples were heated on the order of 2 to 3 times longer.

Fig. 5-10. Rv-r of the hydrous pyrolysis residues plotted at the experimental temperature of hydrous pyrolysis. These data are compared to the Rv-r and T_{peak} interpreted from fluid inclusion T_h from the San Remo 1 dike. Hydrous pyrolysis and Rv-r data from a Latrobe Group lignite reported in Yin et al. (1993).

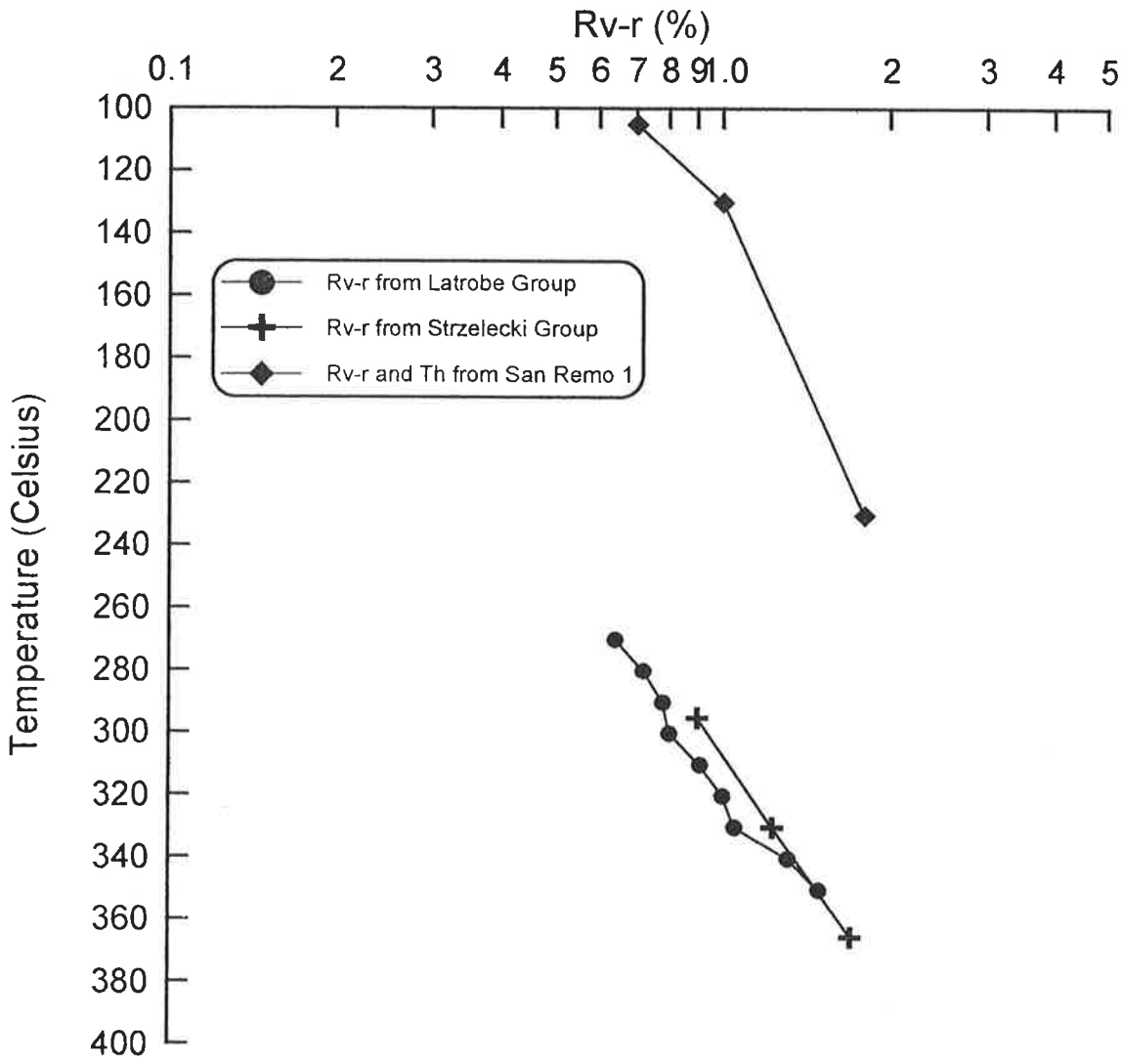
Rv-r (%)
0.1
2
3
4
5
6
7
8
9
1.0
2
3
4
5
100
120
140
160
180
200
220
240
260
280
300
320
340
360
380
400
Temperature (Celsius)
Rv-r from Latrobe Group
Rv-r from Strzelecki Group
Rv-r and Th from San Remo 1

Hydrocarbon generation indicated by the production index ($PI = S_1/(S_1+S_2)$) also follows the same trend in the Strzelecki Group and Latrobe Group hydrous pyrolysis samples but is essentially zero in the San Remo samples (Table 5-2). The lower yield of the Strzelecki Group coal is attributed to a lower yield of distillable hydrocarbons for a similar degree of heating. The lower hydrocarbon yield in the Strzelecki Group coal is probably related to its organic matter composition, with the mostly non-fluorescent vitrinite, and a lower content of liptinite group macerals compared to the Latrobe Group lignite. In the San Remo coal samples, the low PI value is attributed to a loss of S_1 during contact metamorphism or weathering.

Fig. 5-11. Production index in the hydrous pyrolysis residues plotted at the experimental temperature of hydrous pyrolysis. Hydrous pyrolysis PI data from a Latrobe Group lignite reported in Yin et al. (1993).

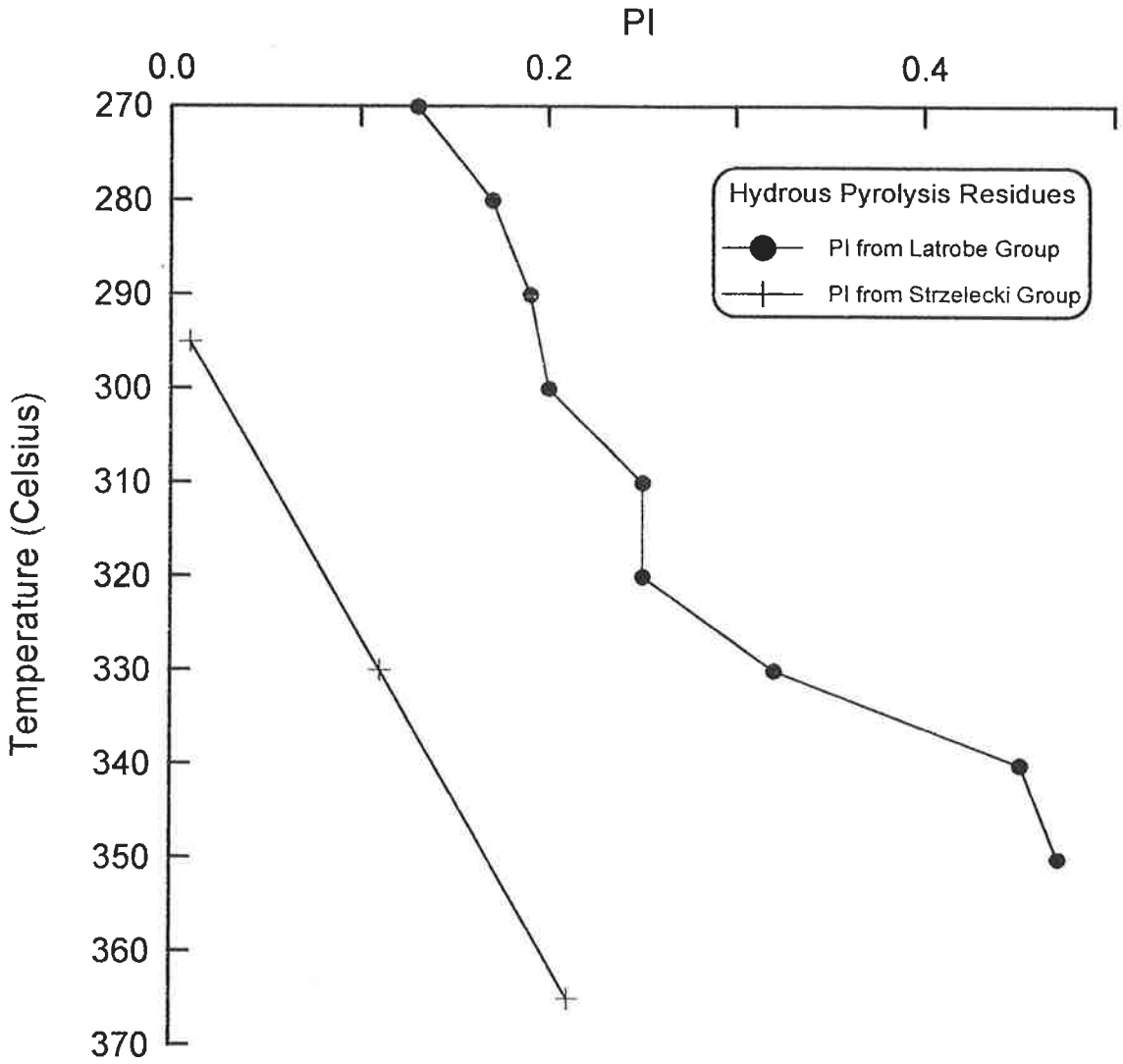
PI
0.0
0.2
0.4
270
280
290
300
310
320
330
340
350
360
370
Temperature (Celsius)
Hydrous Pyrolysis Residues
PI from Latrobe Group
PI from Strzelecki Group

Nuclear Magnetic Resonance

^{13}C CP MAS NMR results from the hydrous pyrolysis samples heated at 295°C, 330°C and 365°C using the Strzelecki coal, show a pattern consistent with hydrocarbon generation which is marked by a rapid decrease in aliphatic carbon content. The decrease in aliphatic carbon content shown by an increase in fa from 0.67 in the unheated R-5 sample to near 0.9 in the sample heated to 365°C (Fig. 5-12) (note that $f$aliphatic = 1- fa). An fa of 0.9 indicates an aromatic-carbon rich material that is only capable of limited hydrocarbon generation, most likely methane. In the hydrous pyrolysis series, as Rv-r increases from 0.6% to 1.8% and temperatures increase from 295°C to 365°C, hydrocarbon generation is marked by: 1) a narrowing of the aromatic peak by loss of intensity in the range of 148-170 ppm, marking the loss of heteroatomic groups bonded to aromatic carbon, and an increasing size, or less substitution on, the aromatic rings (Garcia-Gonzalez et al., 1993); and 2) a narrowing of the aliphatic + aromatic side spinning band (ssb) peak by loss of intensity in the range of 50-90 ppm marking the loss of aliphatic carbon bonded to oxygen (Table A1-2 in Appendix 1). The peak remaining in the former aliphatic region near fa = 0.9 is mostly due to ssb and minor aliphatic carbon, mostly methyl groups attached to aromatic carbon denoted by the peak shoulder at 20-30 ppm. The loss of the carbonyl carbons, probably by decarboxylation reactions, and phenolic carbons also occurs with increasing thermal maturation. These losses along with the evolution of other heteroatomic compounds probably is marked by the generation of CO_2, H_2O, nitrogen-bearing and sulfur-bearing compounds, and hydrocarbons with increasing thermal maturation.

Corresponding to the changes shown by ^{13}C CP MAS NMR in the hydrous pyrolysis samples, Rock-Eval pyrolysis shows marked decreases in both HI and TOC as hydrous pyrolysis temperatures increase (Table 5-2), similar to the natural changes observed as the dike is approached(Figs 5-13 and 5-14). The sharp loss of HI and TOC as the dike margins are approached, interpreted in the light of the hydrous pyrolysis results above, suggests

considerable oil, methane, CO_2 and other heteroatomic compounds have been generated next to these dikes. However, this hydrocarbon, as shown by the increasing loss of S_1 closer to the dike than X/D = 1 has not been retained (Fig. 5-15). While some of this loss may be due to weathering, the relationship of the low S_1 near the dike suggests it may be related to advection occurring at the time of intrusion, as hydrocarbons show considerable solubility in hydrothermal fluids. Besides possible transport in solution, the hydrothermal fluids may also physically transport hydrocarbons as a separate phase.

Fig. 5-12. ^{13}C CP MAS NMR spectra, Rv-r and aromatic fraction (fa) from a series of hydrous pyrolysis experiments on sample R-5, western onshore Gippsland Basin, Victoria. The regional sample R-5 is presented as an example of a relatively unweathered coal because it was sampled underground in the State Coal mine near Wonthaggi, Victoria. Fig. 5-13 shows sample R-5 is marginally mature.

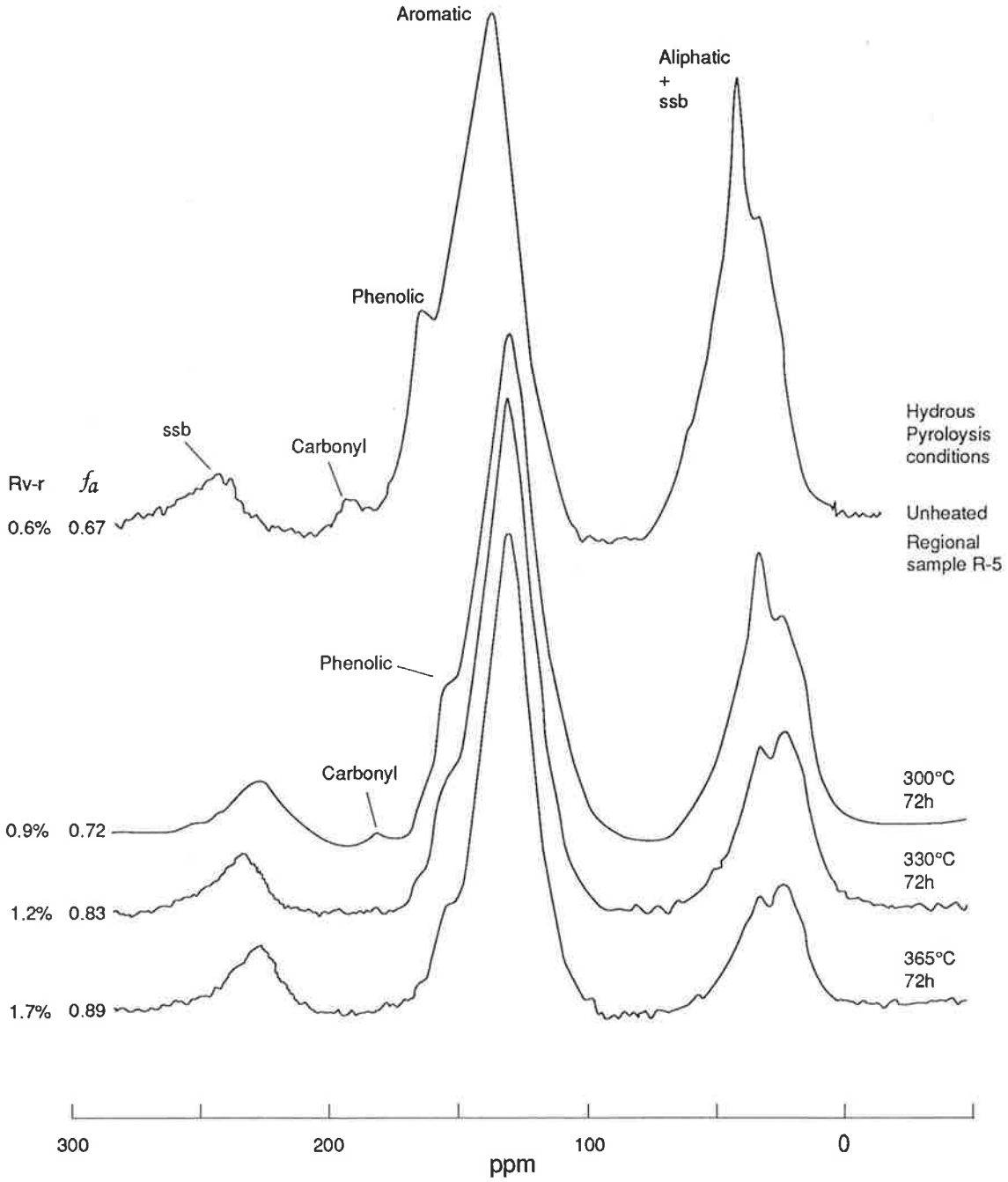
Aromatic
Aliphatic
+
ssb
Phenolic
ssb
Carbonyl
Rv-r
f_a
0.6%
0.67
Hydrous
Pyroloysis
conditions
Unheated
Regional
sample R-5
Phenolic
Carbonyl
0.9%
0.72
300°C
72h
1.2%
0.83
330°C
72h
1.7%
0.89
365°C
72h
300
200
100
0
ppm

Fig. 5-13. Hydrogen Index (HI) versus X/D, for all dikes studied in the western onshore Gippsland Basin. Samples with a TOC < 0.5 wt.-% not plotted as they can give inaccurate results. As discussed in Chapter 4, samples near the dike with very high thermal maturity have little pyrolysiable carbon and give spuriously high HI values. The arrow suggests a trend of decreasing HI that ignores the spurious data.

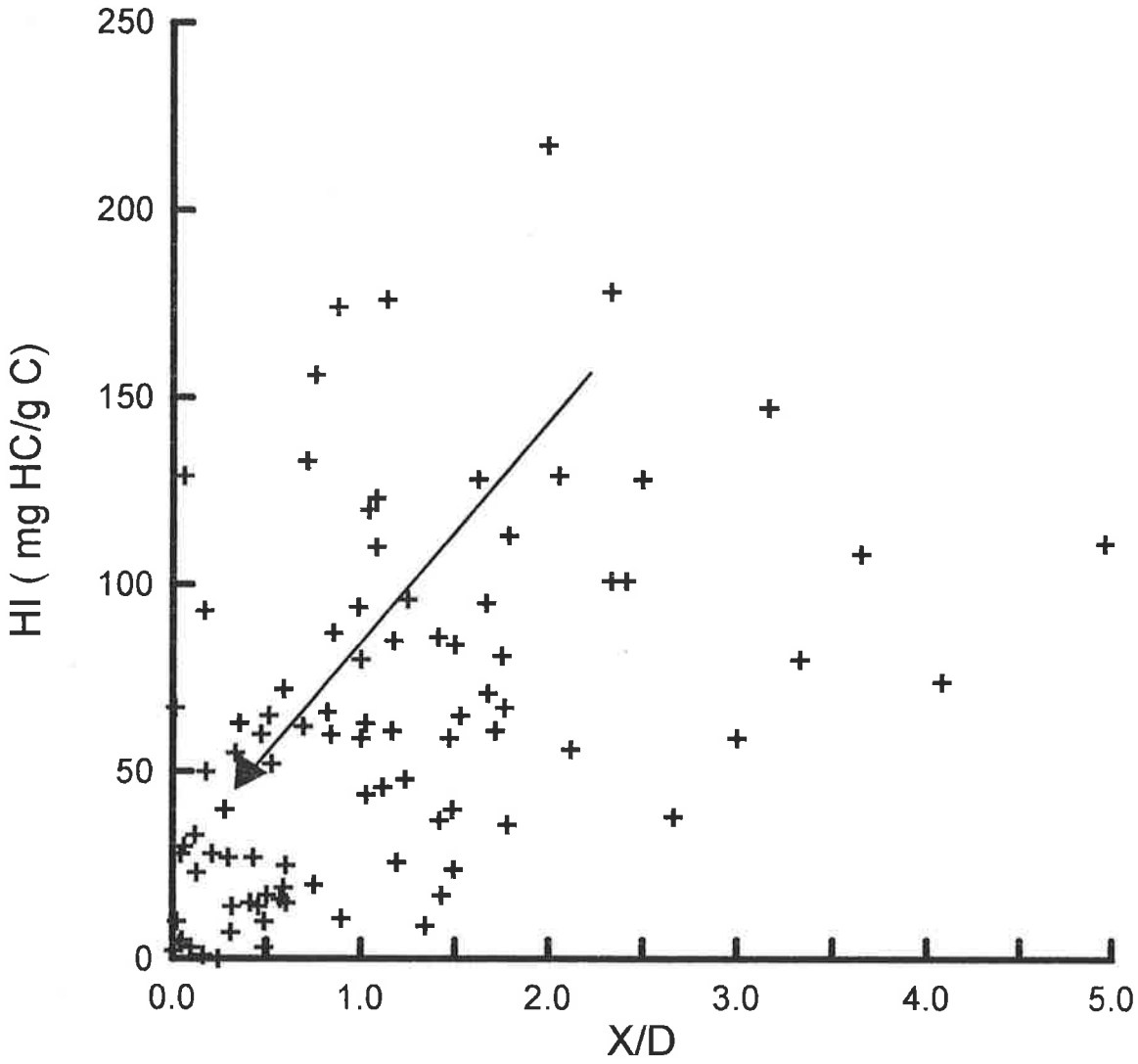
250
200
150
100
50
0
HI (mg HC/g C)
0.0
1.0
2.0
3.0
4.0
5.0
X/D

Fig. 5-14. Total organic carbon (TOC) versus X/D, for all dikes studied in the western onshore Gippsland Basin. Samples with a TOC < 0.5 wt.-% not plotted as they can give inaccurate Rock-Eval pyrolysis results. The arrow suggests a trend of decreasing TOC that ignores the spurious data.

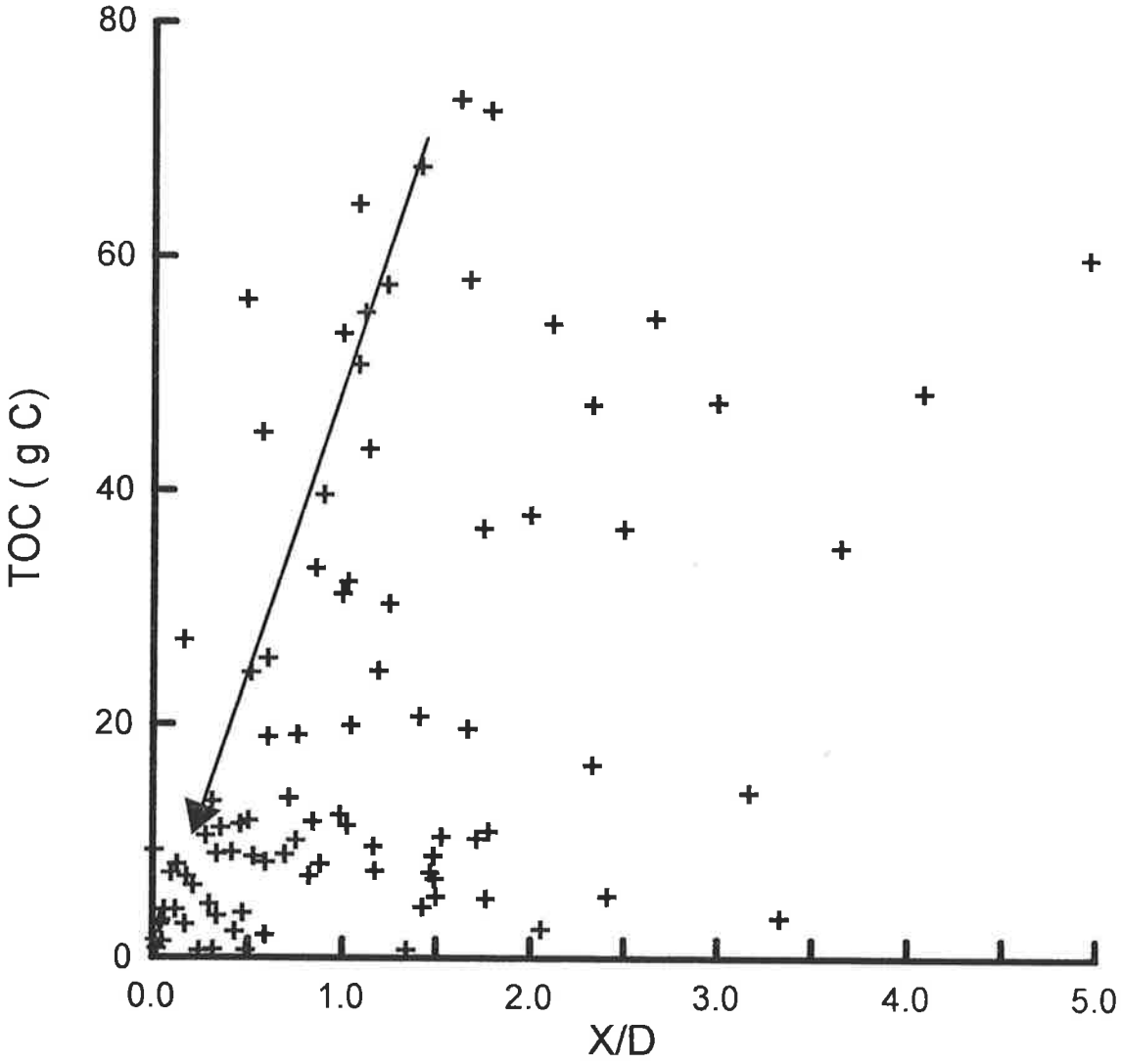
80
60
40
20
0
TOC (g C)
0.0
1.0
2.0
3.0
4.0
5.0
X/D

Fig. 5-15. S_1 versus X/D, for all dikes studied in the western onshore Gippsland Basin. Samples with a TOC < 0.5 wt.-% not plotted as they can give inaccurate Rock-Eval pyrolysis results.

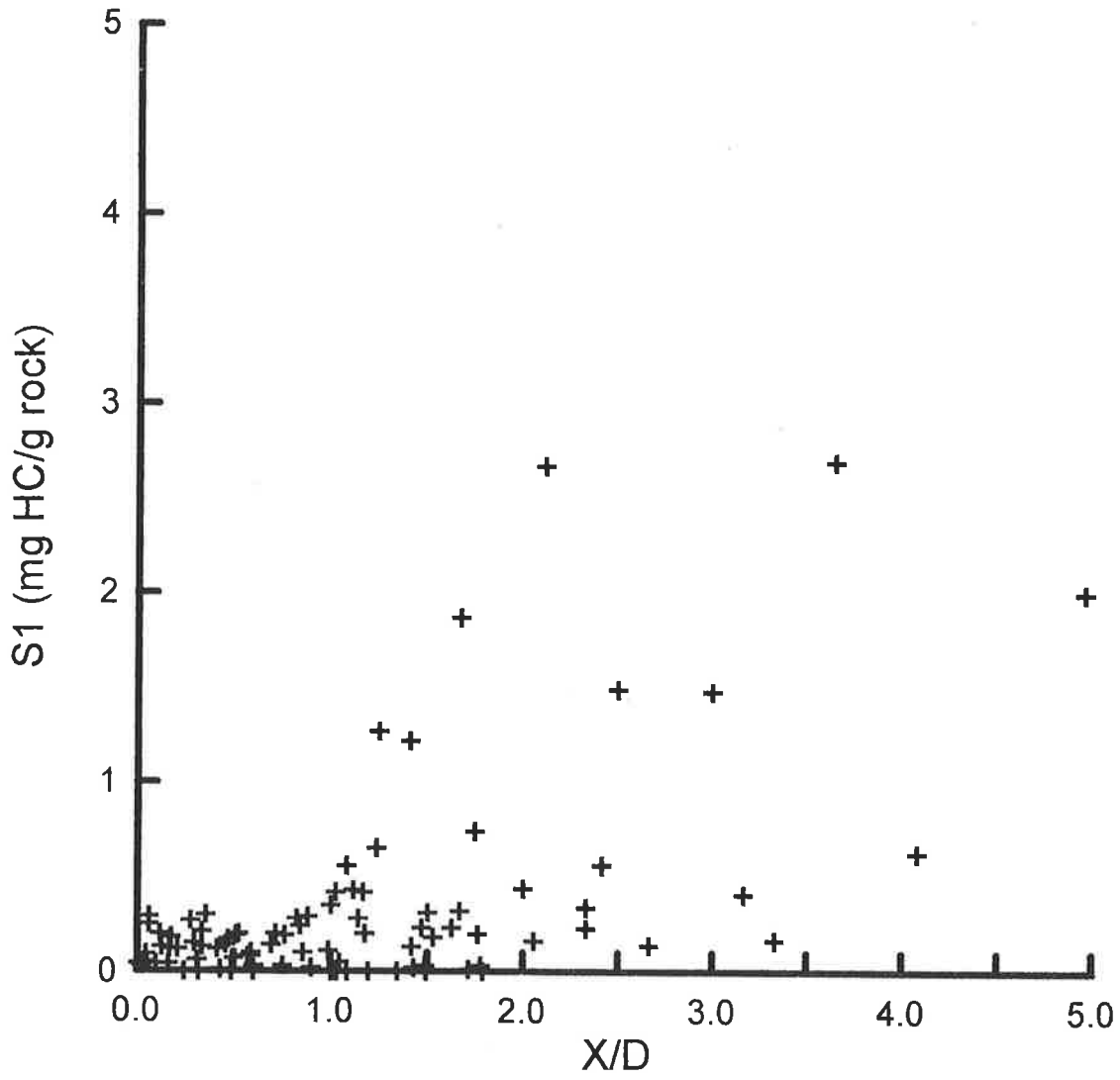
S1 (mg HC/g rock)
5
4
3
2
1
0
0.0
1.0
2.0
3.0
4.0
5.0
X/D

Comparison of Expelled Oils and Rock Extracts

As the naturally expelled hydrocarbons have been lost, the remaining generated hydrocarbons can be studied by preparing the source rock solvent extracts for examination by gas chromatography (GC). For this study, the coals next to the San Remo 1 dike were compared to the oils and gases expelled during hydrous pyrolysis, as well as solvent extracts of the artificially generated bitumens that remained in the heated coal after the experiment. The bitumens are extracted from the natural samples and hydrous pyrolysis residues by the Soxhlet method (Appendix 1).

The sample R-5 is the unheated sample used for comparison of all of these GC data because it appears to be immature (Rv-r =0.6%) and relatively unweathered (Fig. 5-16). The solvent extracts from R-5 are very lean, yielding only 360 ppm bitumen. The low yield of extractable hydrocarbons in this unweathered sample is also taken to indicate the sample is immature. The GC analysis shows the presence of a small proportion of nC_{18} (a normal alkane with 18 carbons annotated nC_n, where the subscript n = the number of carbon atoms in the hydrocarbon structure). The n-alkanes range up to to nC_{28}. Some isoprenoids iC_{16} and iC_{19} (phytane) (Isoprenoids are annotated iC_n) are also present. These isoprenoids are thought to be reaction products of phytol which is derived from chlorophyll in sediments and so are commonly found in SOM. Typically, the peaks of the isoprenoids are small relative to n-alkanes in extracts from thermally mature samples. Thus, the large proportion of isoprenoids relative to n-alkanes suggests that the coal is immature with respect to hydrocarbon generation (L.C. Price, U.S. Geological Survey, Denver, personal comunication, 1994).The peaks that elute beyond nC_{28} in part contain a class of compounds termed biomarkers. Biomarkers are less useful in source rock-oil correlation at the high temperatures found next to dikes and so are not discussed in detail here.

At the San Remo 1 dike, the saturate fraction extracted from the contact metamorphosed coal reaching a Rv-r = 0.7% and 0.9% at a T_{peak} of 110 and 150°C, respectively, appear marginally mature or possibly biodegraded with isoprenoid peaks dominating the chromatogram. Apparently, these compounds are inherited from the source material (Fig. 5-16) before contact metamorphism (Fig. 5-17). Laboratory heating of isoprenoid precursors has been shown to generate iC_{20}, iC_{19}, iC_{18}, iC_{16}, iC_{15} saturated isoprenoids (Tissot and Welte, 1984). Some of these saturated isoprenoid reaction products are observed in the natural compounds with increasing thermal maturation (Fig 5-18) as well as the hydrous pyrolysis samples with increasing temperature (Fig. 5-19).

The n-alkanes seen in the sample R-5 chromatogram have been lost during weathering or by biodegradation in the San Remo 1 samples at X = 0.98 m and X = 0.65 m. The high content of the isoprenoids relative to the n-alkanes in the San Remo 1 samples is consistent with an immature sample. However, the chromatogram of saturates from the sample at X = 0.36 m and Rv-r = 1.8% shows a mature oil. Generally, mature oils are rich in saturates (alkanes), relatively lean in aromatics, and with increasing thermal maturation, the n-alkane distribution shifts to shorter carbon chain lengths as cracking occurs. The maximum of the n-alkane distribution in this oil is at nC_{16} for a range from nC_{10} to nC_{23}. The chromatogram shows no predominance of odd-numbered carbon-chain lengths over even-numbered carbon-chain lengths (termed odd predominance) in the peak heights of the alkanes. These geochemical signatures indicate an extract generated by a mature source rock (termed a mature oil). This oil would have a high API gravity if found in nature. It is interesting to note that the concentration of bitumen in this sample series decreases from 3650 ppm in the sample at X =0.98 m to 900 ppm at X = 0.65 m and 94 ppm at X = 0.36 m. This decrease is consistent with the decreasing S_1 values as the dike is approached (Fig. 5-15). The small amount of extract found is seemingly not biodegraded and the reduced S_1 and bitumen

concentration as the dike is approached may be due to a hydrothermal extraction process induced by contact metamorphism.

The saturates extracted from the hydrous pyrolysis residues show a consistent maximum in the n-alkane distribution at about nC_{23} over an increasing Rv-r from 0.6 to 1.7% and temperatures from ca. 100°C to 365°C (Figs 5-16 and 5-18; Table 5-2). The lower limit of the n-alkanes changes markedly with increasing Rv-r from nC_{16} at 100°C to nC_{10} at 365°C. The decreasing carbon numbers are the result of cracking reactions at higher pyrolysis temperatures breaking down the longer carbon chains and producing the shorter carbon chain alkanes and gas. As shown in Table 5-2, an increasing amount of gas is recovered with increasing temperature during hydrous pyrolysis. This trend of increasing gas generation is probably true for the samples next to the San Remo-1 dike, although this gas is now lost. For the lower Rv-r samples at San Remo 1, the hydrous pyrolysis experiments also suggest that liquid hydrocarbons were generated. These hydrocarbons were apparently only preserved at X =0.36 m and Rv-r = 1.8% near the San Remo 1 dike (Fig. 5-17). This preservation may be due to the typical decrease in permeability and porosity near the dike that was documented in Chapter 4.

The extracts from the hydrous pyrolysis also show a increasingly even predominance with increasing temperature (Figs 5-16 and 5-18). The initial odd to even predominance is typical of lignites and coals (Tissot and Welte, 1984). The change from strong odd predominance to weak odd or no predominance is typical of a sequence of oils generated from increasingly more mature coals. This process seems to have progressed further in the natural samples as is shown by the San Remo 1 chromatogram from the sample at X = 0.36 m and Rv-r = 1.8% (Fig. 5-17). This chromatogram shows little or no odd predominance whereas the hydrous pyrolysis sample at Rv-r 1.7% still shows weak odd predominance (Fig. 5-18).

Fig. 5-16. Gas chromatogram of the saturate fraction isolated from bitumen extracted from the regional sample R-5 (coal) from the Strzelecki Group. The sample was taken in the subsurface from an active mine face and appears unweathered. This sample has an Rv-r of 0.6% and yielded only 360 ppm hydrocarbon during Soxhlet extraction. The coal is interpreted to be marginally mature with respect to hydrocarbon generation. The alkanes are annotated $nC_{n,}$ where the subscript n = the number of carbon atoms in the hydrocarbon structure. Likewise, iC_{19} indicates an isoprenoid hydrocarbon with 19 carbon atoms in its structure.

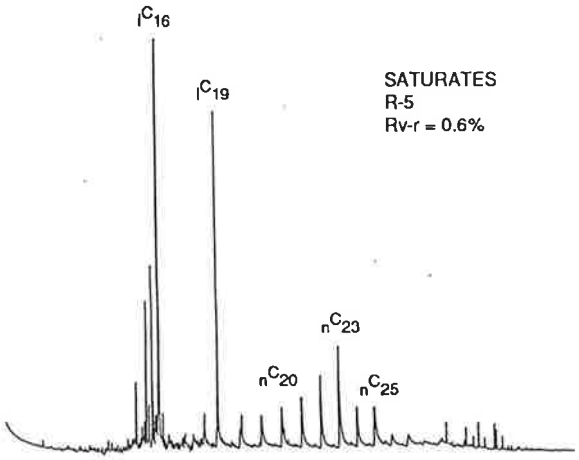
$^{i}C_{16}$
$^{i}C_{19}$
SATURATES
R-5
Rv-r = 0.6%
$_{n}C_{23}$
$_{n}C_{20}$
$_{n}C_{25}$

Fig. 5-17. Gas chromatogram of the saturate fraction isolated from bitumen extracted from San Remo 1 Strzelecki Group coals. Dike code, distance (X) from the dike margin and Rv-r is shown next to each chromatogram.

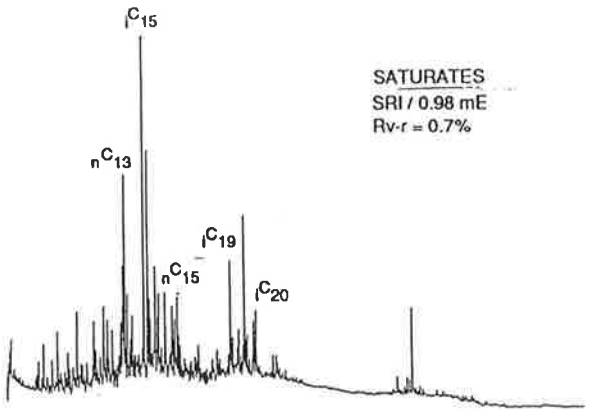
iC15
SATURATES
SRI / 0.98 mE
Rv-r = 0.7%
nC13
iC19
nC15
iC20

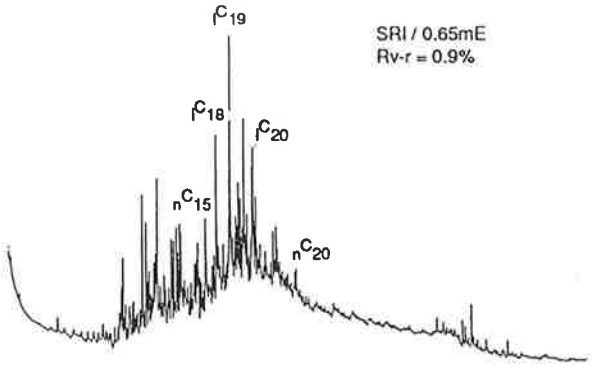
iC19
SRI / 0.65mE
Rv-r = 0.9%
iC18
iC20
nC15
nC20

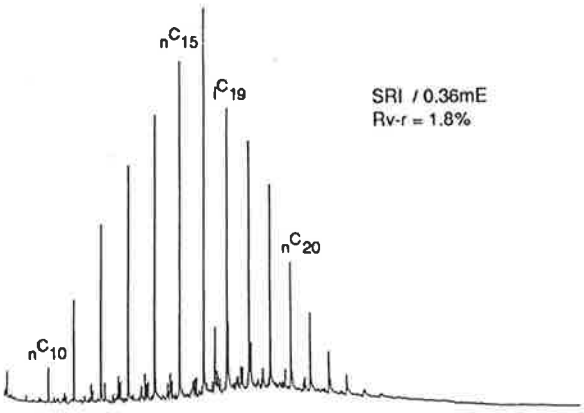
nC15
iC19
SRI / 0.36mE
Rv-r = 1.8%
nC20
nC10

Fig. 5-18. Gas chromatogram of the saturate fraction isolated from bitumen extracted from the coaly residues of hydrous pyrolysis experiments. Experiments based on sample R-5, a coal from the Strzelecki Group. Details of the experiments given in Table 5-2. Rv-r of the hydrous pyrolysis residue shown after the experiment number.

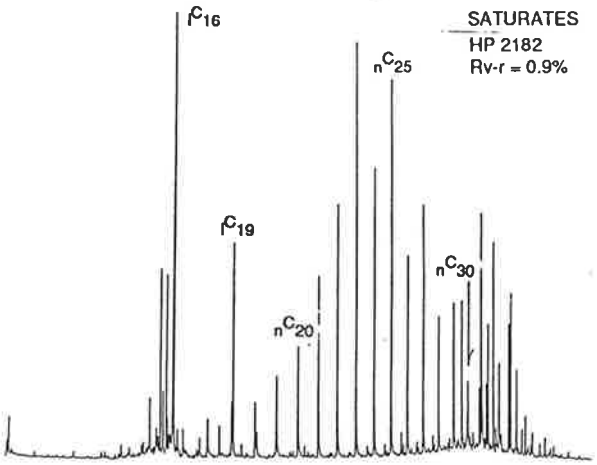
SATURATES
HP 2182
Rv-r = 0.9%
iC16
nC25
iC19
nC30
nC20

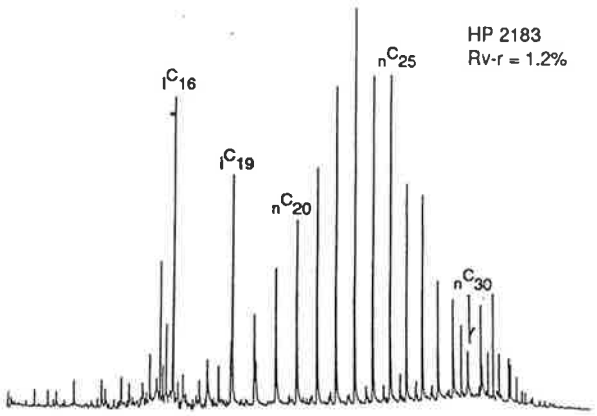
HP 2183
Rv-r = 1.2%
nC25
iC16
iC19
nC20
nC30

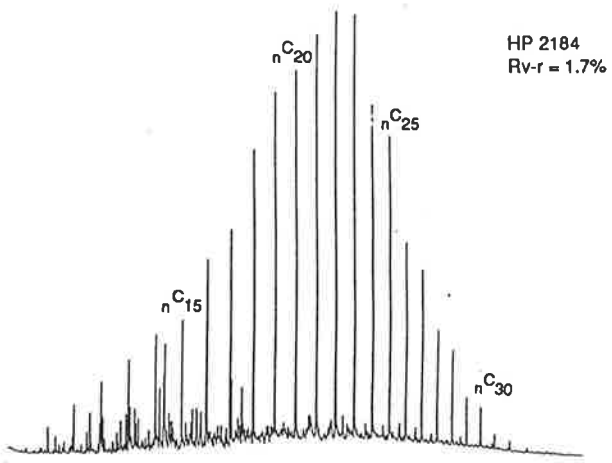
HP 2184
Rv-r = 1.7%
nC20
nC25
nC15
nC30

Another feature of the hydrous pyrolysis extracts is the decreasing proportion of isoprenoids as n-alkanes are generated during increasing thermal maturation and temperature (Fig. 5-18). L.C. Price (U.S. Geological Survey, Denver, personal communication, 1994) suggests that the isoprenoids are relatively stable with increasing thermal maturation and temperature and the decrease in their relative abundance in Fig. 5-18 is because they are being diluted by the n-alkanes, rather than showing much reaction with increasing thermal maturation and temperature.

The expelled oils generally show similar features to the extracts from the hydrous pyrolysis residues with increasing thermal maturation and temperature (Fig. 5-19). The expelled oil gathered from the 295°C at Rv-r = 0.9 % is a very close match to the extract from sample R-5 (Fig. 5- 16) and suggests that the hydrous pyrolysis sample is still immature. All the oils again show a maximum in the n-alkane distribution at nC_{23} and a shift to lower carbon number n-alkanes from nC_{18} to nC_8 with increasing thermal maturation and temperature. Isoprenoids also show a decrease in relative abundance with increasing thermal maturation and temperature. However, significant odd predominance remains in all the expelled oils. This persistent odd predominance may be due to the short duration of the hydrous pyrolysis experiments relative to the estimated heating duration next to the dikes, leaving the oils with a greater apparent immaturity that is not supported by the other geochemical signatures that indicate a fairly mature oil. For example, Altebaumer et al. (1983) recorded a shift in peak hydrocarbon generation from Rv-r = 0.9 % during what is conjectured to be more normal burial heating to 1.7% in rapidly heated rocks. This concept is also illustrated by Rock-Eval pyrolysis, which heats the sample at very high rates, and the experimental temperatures must exceed 400°C to reach maximum hydrocarbon generation which is represented by the parameter T_{max}. Thus, the maturation of the organic matter with respect to oil generation appears to occur at somewhat elevated Rv-r and temperature, during contact metamorphism caused by the dikes

and during the hydrous pyrolysis experiments, compared to burial diagenesis. The shift in maximum petroleum generation occurs because the kinetics of vitrinite reflectance are not necessarily parallel to the kinetics of oil generation. Thus, to attain the same degree of oil generation during rapid heating requires higher reaction temperatures. These higher reaction temperatures, however, drive vitrinite reflectance evolution further than observed during burial heating and consequently, the same degree of oil generation is found at much higher Rv-r values during rapid heating.

Fig. 5-19. Gas chromatogram of expelled oils collected floating on the water in the hydrous pyrolysis reaction vessel. Experiments based on sample R-5, a coal from the Strzelecki Group. Details of the experiments are given in Table 5-2. Rv-r of the hydrous pyrolysis residues shown after the experiment number.

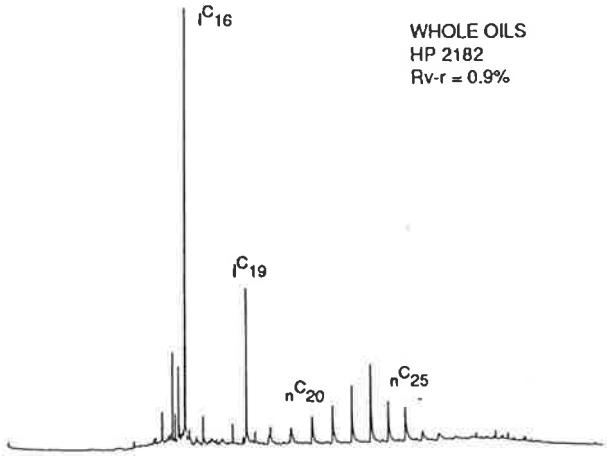

WHOLE OILS
HP 2182
Rv-r = 0.9%

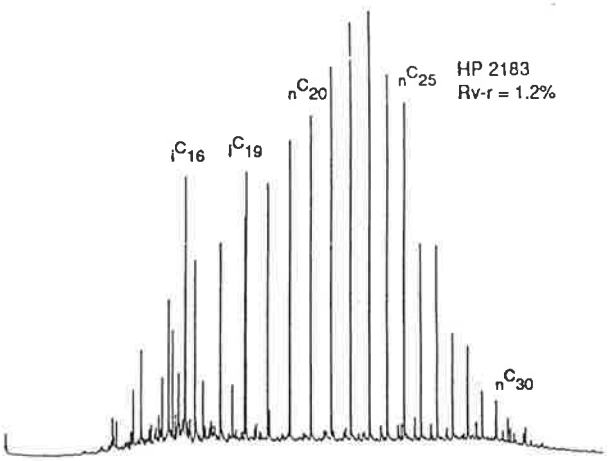

HP 2183
Rv-r = 1.2%

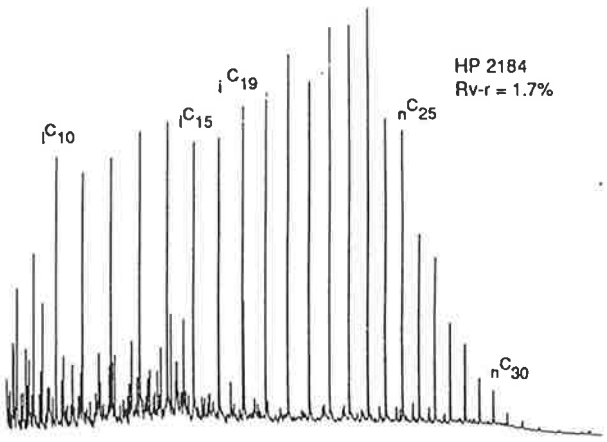

HP 2184
Rv-r = 1.7%

Fig. 5-20. Gas chromatogram of expelled oils collected floating on the water in the hydrous pyrolysis reaction vessel. Figure based on the chromatograms of saturate hydrocarbons produced from the hydrous pyrolysis experiments from Yin et al. (1993) and a chromatogram of a produced oil from the Kingfish well, eastern offshore Gippsland basin (Powell and McKirdy, 1975). Conditions of the hydrous pyrolysis experiment shown next to the chromatogram. The Yin et al. (1993) hydrous pyrolysis experiments are based on a lignite sample from the Latrobe Group, eastern onshore Gippsland Basin. The lignite before heating has a Rv-r of 0.2%, TOC = 59 wt. -%, and HI = 167 mg HC/ g C. Pr = Pristane = iC_{19} and Ph = Phytane = iC_{20}.

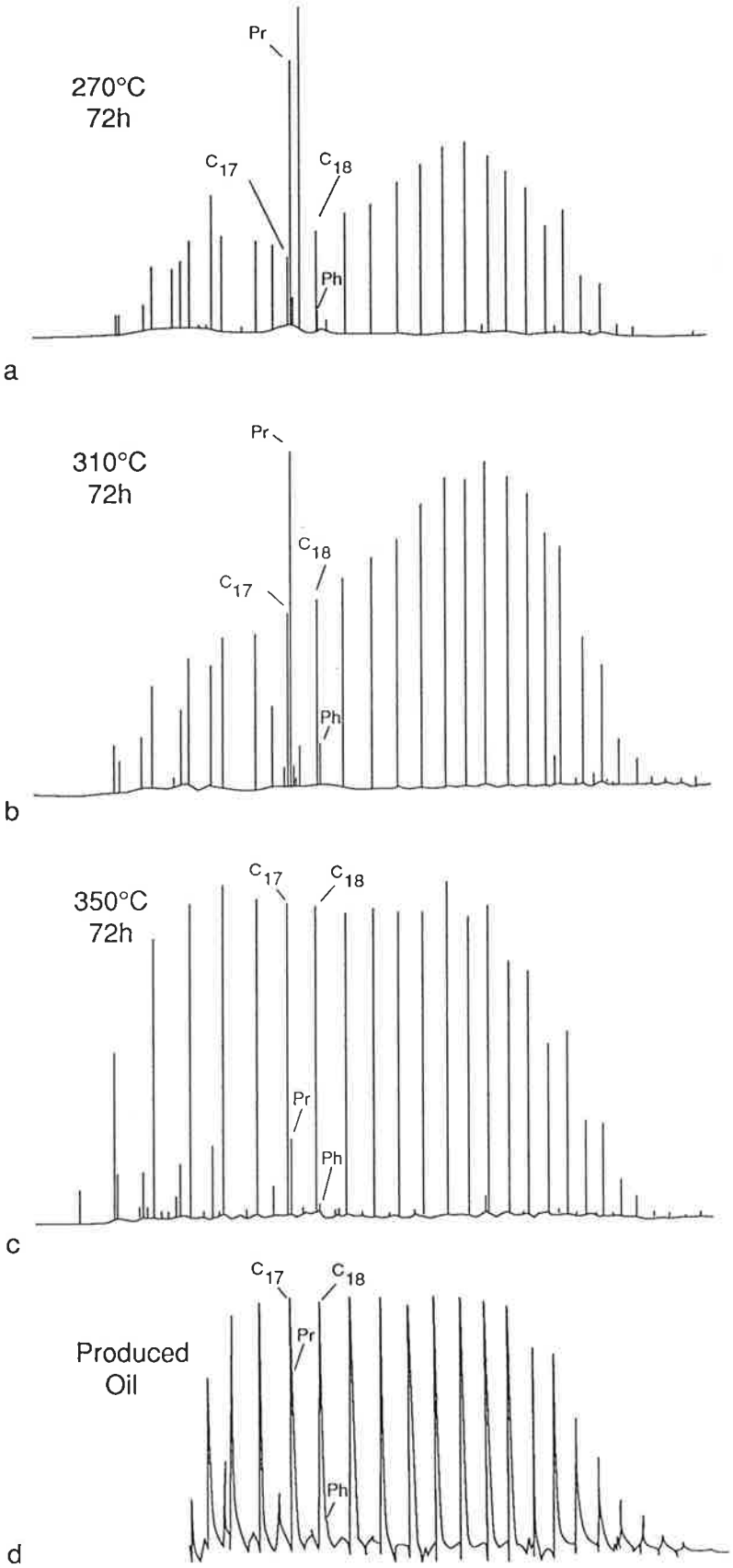
270°C
72h
Pr
C17
C18
Ph
a
310°C
72h
Pr
C18
C17
Ph
b
350°C
72h
C17
C18
Pr
Ph
c
Produced
Oil
C17
C18
Pr
Ph
d

The oils expelled from the Strzelecki Group (Fig. 5-19) at 295°C (Rv-r = 0.9%), 330°C (Rv-r = 1.2%) and 365°C (Rv-r = 1.8%) are a good match with the oils expelled from a Latrobe Group lignite at 270°C (Rv-r = 0.6 %), 310°C (Rv-r = 0.9 %) and 350°C (Rv-r = 1.5%) as reported by Yin et al. (1993) (Fig. 5-20). The peak of the n-alkanes is about nC_{23}-nC_{25} for the oils expelled from the Latrobe Group lignite. The range of the hydrocarbons in the lignite also shifts to shorter chain n-alkanes with increasing temperature is similar to the shifts seen in the Strzelecki Group coal. The upper range of n-alkanes is about nC_{30} in both the lignite and the coal.

The highest temperature pyrolysis sample in both the Strzelecki Group coal and the Latrobe Group lignite are also a good match to the produced oil (Fig. 5-20). Thus, the oils in the eastern Gippsland basin that have been attributed solely to a Latrobe Group lignite could also contain a contribution from the Strzelecki Group coal. Analysis of gases sampled after hydrous pyrolysis supports this correlation. The gases recovered from hydrous pyrolysis show a $\delta\ ^{13}C$ range of -32.3 to -36.1 $^{o}/_{oo}$ and the natural methane recovered from the Gippsland Basin which shows a $\delta\ ^{13}C$ range of -31.4 to -35.4 $^{o}/_{oo}$ (Table 5-3). The gases from hydrous pyrolysis become more negative (lighter) with increasing temperature. The natural gases from the Gippsland Basin may tend to become lighter with increasing depth of production and probably temperature. This trend towards isotopically lighter methane with depth is less clear in the Gippsland Basin because of the ease with which methane can vertically migrate in natural systems emplacing isotopically light gases at shallow depths. Nevertheless, these data are interpreted to suggest some of the gases are probably sourced at relatively high burial temperatures in the offshore Gippsland Basin. Further, as observed in the chromatograms, the isotopic signature of the gases does not preclude them from being, in part, sourced from a Strzelecki Group coal.

Table 5-3. Comparison of carbon isotopic composition of gases from hydrous pyrolysis experiments (this paper) and non-biodegraded natural gas from the Gippsland Basin reported by Burns et al. (1987).

Hydrous Pyrolysis of a Strzelecki Group Coal	**Hydrous Pyrolysis Experimental Conditions**	**$\delta^{13}C$ from CH_4 (‰)**
R5 (HP 2182)	295°C for 72 hr	-32.27
R5 (HP 2183)	330°C for 72 hr	-34.84
R5(HP 2184)	365°C for 72 hr	-36.12
Offshore Well	**Sample Depth**	
Veilfin 1	3194	-31.4
Tuna 4	3118	-32.5
Marlin A11	1361.9	-34.8
Grunter 1	3400.5	-35.4
Flounder 6	2504	-35.7

5.4 THE STRZELECKI GROUP AS A SOURCE OF HYDROCARBONS IN THE EASTERN OFFSHORE GIPPSLAND BASIN

The Strzelecki Group has previously been considered as a self source of oil and gas for charging basal strata of the Group where porosity is preserved. (Holdgate and McNichol, 1992). In the Otway Basin, the Strzelecki Group is the time equivalent of the Eumeralla Formation of the Otway Group that had minor gas production in a medium to poor quality reservoir (Carmody, 1992). In general, however, commercial quality reservoirs have not yet been found in the Strzelecki Group.

The studies of the dike contact aureoles and hydrous pyrolysis experiments show that

the Strzelecki Group has potential as a source of oil and gas. Further, this oil and gas has a similar geochemical signature to oil and gas thought to be sourced in the Latrobe Goup lignite. The Strzelecki Group is thought to mainly contribute hydrocarbons to the known good-quality reservoirs in major traps located along faulted anticlines in the overlying Golden Beach and Latrobe Groups. The vertical migration from the deeply buried, higher thermal maturity Strzelecki Group would occur along the faults that cut the section from the basement to the shallower anticlines or other traps (Mebberson, 1989).

Burns et al.(1987) showed that some of the recoverd oils or condensates have a high API and a vitrinite relfectance equivalent (Rv) computed from the methylphenanthrene index that suggest a deep high thermal maturity source of about 1.6 to 1.9% Rv (Fig. 5-21). Measured Rv-r profiles from the offshore Gippsland basin, all of the profiles shown in Fig. 5-22 except Wellington Park-1, are measured in Latrobe Group and related strata. Extrapolation of these Rv-r profiles suggests that Rv levels needed for the generation of the high API gravity oils will generally not be present in the Latrobe Group. Further, the measured Rv-r profile in the Wellington Park-1 well from the eastern onshore Gippsland Basin does reach 1.9% Rv-r at 3.2 km within the Strzelecki Group (Appendix 5).

As discussed in Chapter 3, most of the oil found so far in the Gippsland Basin is in the upper Latrobe Group. The geochemical data presented in this report suggests that much deeper traps in the basin should be reconsidered as a play based on charging from the Strzelecki Group.

Fig. 5-21. API gravity of produced oils and a vitrinite reflectance equivalent (Rv) computed from the methylphenanthrene index. Data from Burns et al. (1987) .

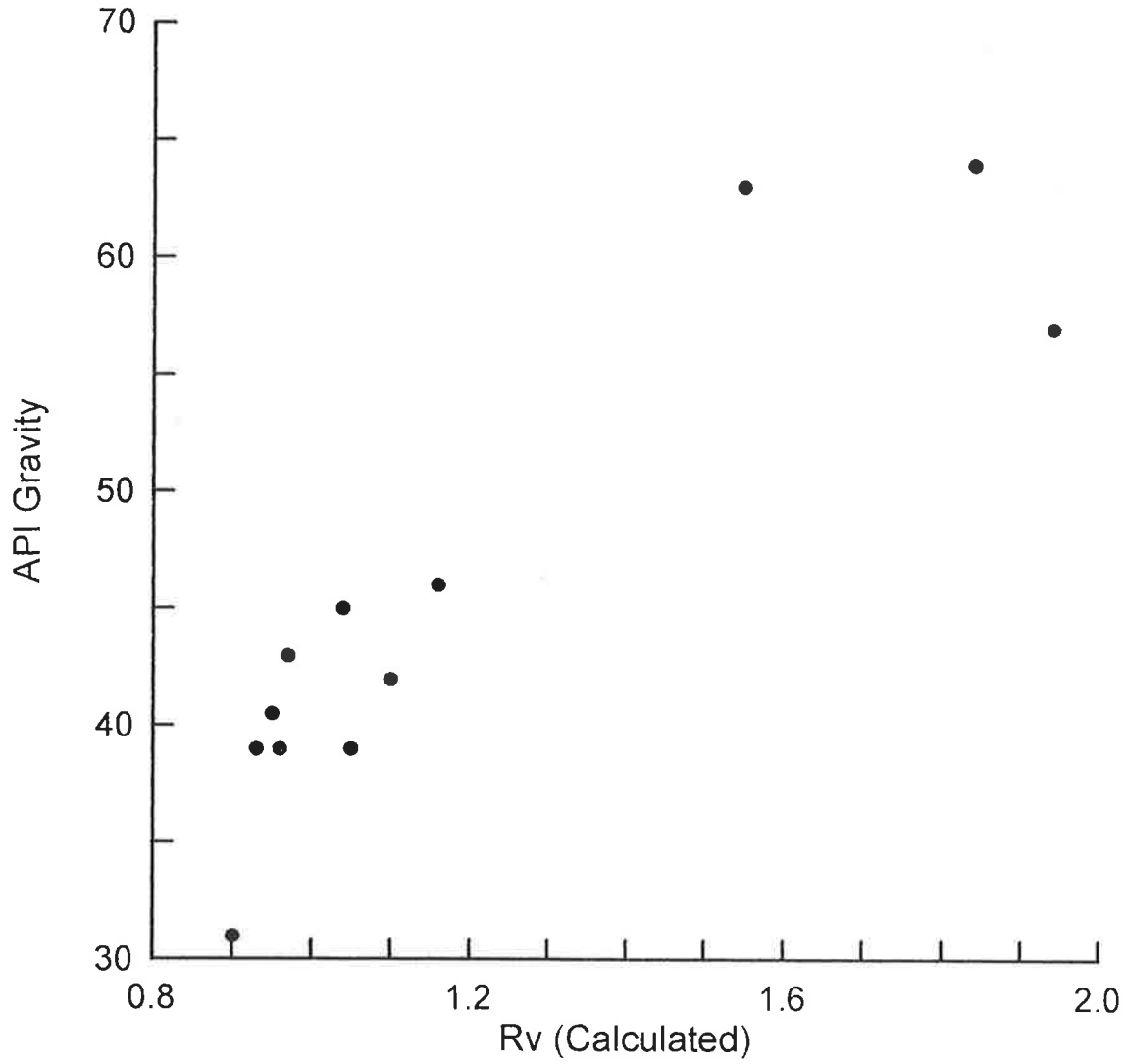
70
60
50
40
30
API Gravity
0.8
1.2
1.6
2.0
Rv (Calculated)

Fig 5-22. Rv-r measured on some deep wells, Gippsland Basin. The offshore well data and the base figure is fro Smith and Cook (1984). The data for the only onshore well, Wellington Park -1 are from this study.

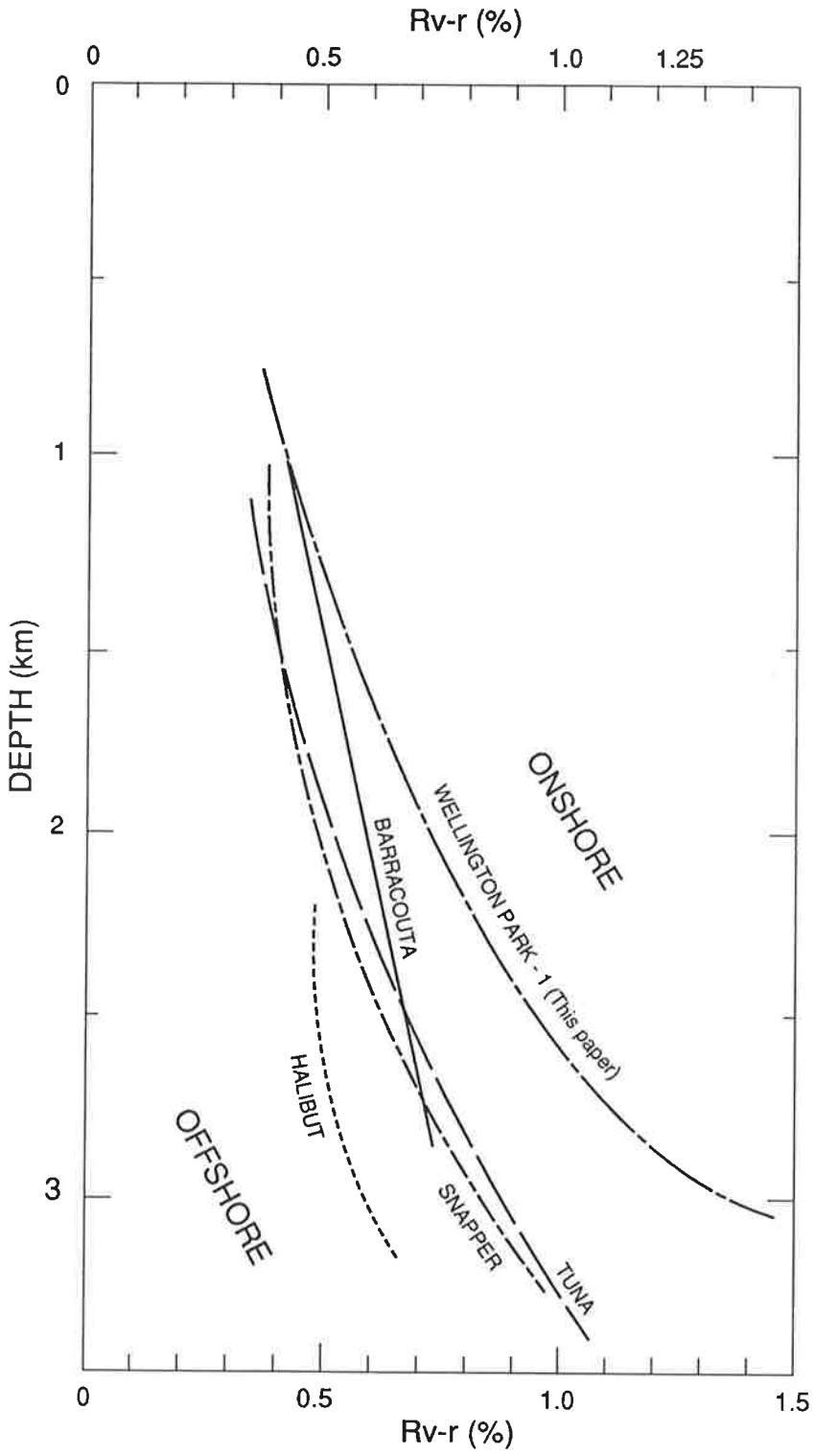
Rv-r (%)
0
0.5
1.0
1.25
0
1
2
3
DEPTH (km)
ONSHORE
WELLINGTON PARK - 1 (This paper)
BARRACOUTA
HALIBUT
OFFSHORE
SNAPPER
TUNA
0
0.5
1.0
1.5
Rv-r (%)

5.5 IMPLICATIONS

Comparing the fit of heat flow models to T_{peak} interpreted from fluid inclusions suggests that the contact aureoles next to the dikes in the Strzelecki Group are strongly influenced by cooling by the advection of pore water. GC analysis of natural and hydrous pyrolysis samples shows good agreement in their geochemical signatures. The recovered oils and residues from hydrous pyrolysis can be used to study the natural products that have been lost from the contact aureole in exposed dikes. The GC, isotope, oil gravity and thermal maturity data also suggest that the Strzelecki Group may have been a source of oil and gas in the deep Gippsland Basin.

Finaly, most gas maturation schemes suggest that methane carbon-isotopes become heavier with increasing thermal maturation (Tissot and Welte, 1984). The hydrous pyrolysis and natural data from the Gippsland basin show that this generalization is not true (Table 5-3).

Chapter 6.

Discussion and Conclusions

6.1 DISCUSSION

Implications of the Fluid Inclusion Results

Published experimental data, fluid inclusion measurements, and petrographic observations in these igneous intrusive systems show that reequilibration almost certainly occurs in fluid inclusions within the host rock near a dike contact. However, the study also shows that based on textural information alone, unambiguously identifying these reequilibrated fluid inclusions can be difficult. Near the dike (X/D< 0.1), fluid inclusions that seem to have existed before the dike intrusion have T_h that is close to that predicted by the heat flow model. Further, some of these fracture bound inherited fluid inclusions have highly variable V/L ratios and a negative crystal shape. This evidence strongly suggests that many of the preexisting fluid inclusions in quartz host grains have reequilibrated.

The Fluid Inclusion Method of Determining T_{peak}

Fluid inclusions work is very time consuming because of the ambiguity on determining fluid inclusion origin. In any sandstone there are always numerous fluid inclusions found in the detrital quartz grains but only a few of those grains have any demonstrable meaning in the context of post-depositional processes. This work demonstrates however, that there is a thermal signal embedded in the wide range of fluid inclusion T_h found in type C fluid inclusions. The temperature information may, however, be a weak signal that cannot be detected in the absence of a strong thermal event. In the absence of a strong thermal event such as a dike intrusion, I do not think that reequilibration could be easily distinguishable within the T_h range inherited from the detrital source rocks. Thus, fluid inclusion based studies of post-depositional temperatures are restricted to using type A and type B fluid inclusions.

This study documents that fluid inclusions in quartz must be strongly overheated by hundreds of degrees past T_h to markedly reequilibrate. At relatively low degrees of overheating (<200°C) such as is possible in normal diagenetic P-T conditions temperatures, P_i remains close enough to P_c that most fluid inclusions will not reequilibrate. Reequilibration at relatively low temperatures may be enhanced by crack-seal and annealing mechanisms caused by contact metamorphism.

Dikes as Oil Generators During Contact Metamorphism

The hydrocarbon prospects next to deeply buried dikes are poor. Vitrinite reflectance studies generally indicate that hydrocarbon generation is contained in a relatively small volume of rock near the dike. During contact metamorphism, the oil window is rapidly passed and before significant oil can migrate, the oil cracking reactions predominate and the primary product seems to be natural gases. However, the penetration and probable corruption of any hydrocarbon seals by the dike means that little gas can be trapped near the dike. Trapping of hydrocarbons generated by contact metamorphosed rocks apparently requires accessible geological structure with an effectively sealed closure.

The regional vitrinite reflectance studies in the Gippsland Basin suggest broad areas of increased Rv-r near the dike swarm. This widespread heating is thought to occur by: 1) enhanced conductive heat flow, apparently from deep seated magmas; 2) vertical transport of heat in the magma during the intrusion of dike swarms; and 3) advection causing vertical heat transfer along with the spreading of heat by lateral fluid flow at impermeable barriers encountered at shallower levels in the crust. These long range thermal effects can apparently produce regional heating of source rocks and possibly widespread hydrocarbon generation well outside of the immediate contact zone.

Heat Flow Modeling

This study demonstrates that the degree of system closure with respect to fluid movement is one of several key factors in determining the temperature distribution next to a dike. The degree of system closure as it influences temperatures is also more important than heating duration in determining the Rv-r resulting from contact metamorphism.

The temperatures predicted by heat flow modeling are fairly comparable to those measured by geothermometry if the degree of system openness is determined before selecting which model to use. The petrography of the dike should be studied to suggest the degree of crystallization from the mineral assemblage, and the heat of crystallization likely to be released during cooling, as these are also important controls on temperature. Similarly, burial history reconstruction is important to establish the initial host rock temperature during intrusion. The water content of the rocks, their porosity and their permeability are also important controls on the T_{peak} reached during contact metamorphism by dikes. It is probably necessary to measure the key thermal parameters for the host and dike rock at each dike. The key parameters should be selected by testing which values show significant sensitivity in that particular model. Note that the theory of fluid flow next to dikes is not well constrained. The mathematical models still cannot quantitatively account for fluid flow, so this factor remains an uncontrolled variable in accurately predicting temperatures (Gretener, 1981).

The method of estimating initial temperature of basalt used in this study is insensitive as pressures in the shallow crust are small compared to pressures at the depths of magma generation in the lower crust and mantle. Thus, shallow magmas intruded over a depth range from the surface to several kilometers would all have similar predicted T_{magma}.

Hydrous Pyrolysis Modeling

This study also confirms that contact metamorphism by thin dikes can be represented by short-term laboratory hydrous pyrolysis experiments. In particular, the hydrocarbons generated by hydrous pyrolysis and Rv-r seem to be comparable to those derived from contact metamorphism caused by dikes. The heating duration indicated next to thick dikes and their tendency to induce open system convection in the host rocks may make them unsuitable for modeling by short-term hydrous pyrolysis experiments. Thick dikes would require an increase in experiment duration to several years, which is probably not feasible.

The Gippsland Basin study used only one type of organic matter (coaly) to avoid major differences in results of the studies caused by differences in organic matter composition. In particular, suppression effects (Price and Barker, 1985) were not studied and so no conclusion can be drawn on the influence of organic matter composition and its response to thermal stress. However, the similarity of the results from contact metamorphsim by dikes and hydrous pyrolysis found in this study suggests that Rv-r and temperature measurements on source rocks near dikes should indicate if the organic matter is following a suppressed or normal thermal maturation path (Lewan, 1993b).

The Buchan study, as a natural pyrolysis experiment, tells us that further heating of mature to overmature rocks leads to little increase in thermal maturation and, by inference, little additional hydrocarbon generation.

6.2 CONCLUSIONS

At the end of each chapter, the conclusions important to each portion of the study were discussed or listed. These specific conclusions are not reiterated here. The conclusions that this study set out to investigate are:

1. In the Buchan Rift, this study : A) confirmed the importance of burial heating prior to intrusion in determining the response of the rocks to contact metamorphism ; B) found that when an intrusion apparently occurs in the unsaturated zone, the lack of free water may greatly inhibit the extent of contact metamorphism; and C) showed that a calibration of a geothermometer based on solid bitumen reflectance seems to give realistic results in predicting peak burial temperatures.
2. AFT annealing studies used to estimate heating duration in contact metamorphosed sedimentary rocks proved to be ineffective in these particular host rocks because when the dike intruded , T_{host} was too high and the event was not recorded. A trial calculation suggests that the technique would give appropriate results as shown by a heat flow model, if a cooler study area was selected.
3. Dike contact aureoles are not necessarily symmetrical on either side of the dike.
4. Type A fluid inclusions are the most reliable in terms of giving a minimum estimate of T_{peak} and, with enough measurements, the UDE seems to approach T_{peak}. Type B fluid inclusions can be as reliable as type A fluid inclusions if it can be established that the fracture is post-depositional. In this study, the post-depositional origin was established by observing mineral matter along the fracture that can be inferred to be diagenetic. It is critical that the fluid inclusion is actually cut by the fracture and is not merely close to it before classifying the measurements as coming from a type A or B fracture.

4. Type C fluid inclusions seem reliable when selected using several criteria: a) they are fracture bound; b) these fractures contain several fluid inclusions that can be studied to demonstrate reequilibration; and c), it can be established that they have reequilibrated in response to the present T_{peak}. Thus, the use of type C fluid inclusions requires so much qualification that the data measured from them can become suspect. Further, the use of type C fluid inclusions will probably not work in the absence of a strong thermal event, because although they may have reequilibrated at relatively low P_{eff} because of annealing and(or) a crack-seal process in the host grain, this fact can not necessarily be recognized without other evidence.
5. Heat flow models based on simple conductive cooling in a closed geologic system do not always adequately describe the temperatures reached during contact metamorphism. The conditions of contact metamorphism, especially with respect to system closure need to be established at each dike before making temperature predictions.
6. The form of the Rv-r profile, as it indicates T_{peak} , can be interpreted using temperature profiles predicted from various heat flow models to infer whether the dike cooled by advection, convection, or conduction.
7. The dikes studied in the Gippsland Basin seem to have cooled in at least semi-open advective environment to open convection systems. These conditions are similar to those found in the systems used to calibrate the hydrothermal VRG. Thus, it is not surprising that at distances of approximately X/D = 0.3 or greater, where vitrinite reflectance values remain accurate, the hydrothermal VRG is in good agreement with estimates of T_{peak} interpreted from fluid inclusion data.
8. In the Gippsland Basin, Rock-Eval pyrolysis, gas chromatography, Rv-r and ^{13}C NMR responses of vitrinite-rich SOM to contact metamorphism caused by dikes show that this system is fairly well characterized by laboratory pyrolysis, especially with respect

to the composition of the generated hydrocarbons. Near the dike contact, hydrous pyrolysis may not compare to natural pyrolysis by dikes because of the extensive development of water vapor, rather than liquid water, near the dike. Supercritical fluids may also be formed if pressure and temperature reach the appropriate levels near the dike.

8. The western onshore Gippsland Basin study also suggests that the Strzelecki Group SOM at higher Rv-r is capable of generating hydrocarbons that are geochemically similar to the oils and gases reservoired in the deep Gippsland Basin and those that published studies have shown to be generated from the Latrobe Group lignites. While these studies do not demonstrate that these hydrocarbons are from the Strzelecki Group, they do not exclude this source either. This newly recognized source of hydrocarbons in the Gippsland Basin indicates that the deeper reservoirs within the basin need to be reevaluated.

ADDENDUM: Apatite Fission Track (AFT) Age Data

Clarification of selected Hypotheses and Assumptions

The AFT age data were treated as: 1) indicating heating duration hrough a trend of decreasing age data and, 2) showing no significant age lifferences between samples. The first hypothesis is considered by assuming ı data trend of decreasing AFT age exists as the dike is approached, and naking a simple heating duration calculation. As discussed in the thesis, the :omputed heating duration value, although fitting well with heat flow modelling vas subsequently rejected because this trend of decreasing age does not ıave a firm statistical basis. For this trend to be accepted, the AFT age data nust show statistically significant changes in mean track lengths between the samples near the dike and the regional samples that is well removed from the effect of intrusive heating. The fission track ages of the samples near the dike are indistinguishable from the stratigraphic age of the Strzelecki Group because of the large uncertainty in this determination. Even though a viable ıeating duration estimate would greatly complement this study, the lack of significant differences in the AFT age makes any inferences on the heating duration next to the dike statistically invalid.

This study show that the lack of differences in the AFT annealing between samples was due to dike intrusion at or near T_{peak}. Burial history reconstruction, discussed in the thesis, suggests that AFT annealing at T_{peak} was severe enough on a regional scale that no contact effect next to the dikes was recorded. Thus, the track length distributions reflect regional cooling rather than contact metamorphism.

Fluid Inclusion Data

Pressure correction of the fluid inclusion data, as discussed in Chapter 1, s an error-prone procedure that was not used in this study. In fluid inclusions :hat have not re-equilibrated, the objective of pressure correction is to estimate :he trapping temperature from the homogenization temperature (T_h) measured n the laboratory. The phase diagrams illustrated in Chapter 1 show that pressure corrections would be of the order of 10-20°C for trapping at the inferred 2 km burial depth for the generally low salinity fluid inclusions encountered in these samples. This is a relatively small pressure correction and, given the low precision of burial history reconstruction upon which it is based, it is not used. Further, in re-equilibrated fluid inclusions, the T_h is an estimator of T_{peak}, not the original trapping temperature. Thus, in the latter case, a pressure correction is not relevant.

Calibration of vitrinite reflectance geothermometers based on re-equilibrated fluid inclusions uses the approach of T_h to T_{peak} caused by heating past the original trapping temperature. As discussed in the thesis, the basis for hypothesizing this relationship is based on phase chemistry and empirical observations. P-T relationships indicate that internal pressure within the fuid inclusions during overheating can be sufficient to permanently increase the vacuole volume or cause decrepitation, both of which decrease fluid density, and consequently increase T_h. In the absence of decrepitation, the finite strength of the mineral limits these fluid density changes such that T_h only approaches T_{peak}. However, a fluid inclusion that decrepitates and heals at T_{peak} records these later trapping conditions. Heating caused by an intrusion is sufficient to decrepitate most fluid inclusions. Thus, given sufficient sample size, the T_h of re-equilibrated fluid inclusions are a direct T_{peak} determination based on the upper data edge of the T_h measurements made on the samples near the dike. This theoretical relationship is empirically demonstrated by comparison to heat flow models and other geothermometers, such as vitrinite reflectance, that are also thought to be set by T_h.

References

Abele, C., 1988, Mesozoic and Cainozoic stratigraphy of Victoria, *in* Clark, I., Cook, B. and Cochrane, G.C., eds., Victorian Geology Excursion Guide: Australian Academy of Science and the Victorian Division of the Australian Geological Society, p. 39-45.

Aizenshtat, Z., Miloslavki, I. and Tannenbaum, E. ,1986, Thermal behavior of immature asphalts and related kerogens. Organic Geochemistry, v. 10, p. 537-546.

Allen, P.A. and Allen, J.R., 1990, Basin Analysis. Blackwell Scientific, Oxford, 451 p.

Altebaumer, F.J., Leythaeuser, D. And Schaefer, R.G., 1983, Effect of geologically rapid heating on maturation and hydrocarbon generation in Lower Jurassic shales from NW-Germany: Advances in Organic Geochemistry, 1981. John Wiley and Sons, New York, p. 80-86.

Arne, D.C., 1991, Regional thermal history of the Pine Point area, Northwest Territories, Canada, from apatite fission track analysis: Economic Geology, v. 86, p. 428-435.

Arne, D., 1992, Evidence from apatite fission-track analysis for regional Cretaceous cooling in the Ouachita Mountain Fold Belt and the Arkoma Basin of Arkansas: The American Association of Petroleum Geologists Bulletin, v. 76, no. 3, p. 392-402.

Arne, D.C., Green, P.F. and Duddy, I.R., 1990a, Thermochronologic constraints on the timing of Mississippi Valley-type ore formation from apatite fission track analysis: Nuclear track and Radiation Measurements, v. 17, p. 319-323.

Arne, D.C., Duddy, I.R. and Sangster, D.F., 1990b, Thermochronologic constraints on ore formation at the Gays River Pb-Zn deposit, Nova Scotia, Canada, from apatite fission track analysis: Canadian Journal of Earth Sciences, v. 27, p. 1013-1022.

Arne, D.C., Cromie, P., Webb, J.A. and Richards, J.R., 1994, The genesis of Pb-Zn sulphide occurrences in the Lower Devonian Buchan Group, Victoria: Australian Journal of Earth Sciences, v. 41, p. 75-90.

Arne, D.C. and Zentilli, M., 1994, Apatite fission track thermochronology integrated with vitrinite reflectance: a review, *in* Mukhopadhyay, P.K. and Dow, W.G., eds., Vitrinite Reflectance as a Maturity Parameter: American Chemical Society Symposium Series no. 570, p. 249-268.

Arthur, M.A., Anderson, T.F., Kaplan, I.R. and Veizer, J., 1983, Stable Isotopes in Sedimentary Geology: Society of Economic Paleontologists and Mineralogists Short Course 10, 435 p.

Axelson, D.E., 1985, Solid State Nuclear Magnetic Resonance of Fossil Fuels: An Experimental Approach: Multiscience Publications, Ottawa. 226 p.

Bailey, S.W., Bell, R. A., Peng, C.J., 1958, Plastic deformation of quartz in nature: Geological Society of America Bulletin, v. 69, p. 1441-1466.

Barker, C. E., 1983, The influence of time on metamorphism of sedimentary organic matter in selected geothermal systems, western North America: Geology, v. 11, p. 384-388.

Barker, C.E., 1989, Temperature and time in the thermal maturation of sedimentary organic matter, *in* Naeser, N.D. and McCulloch, T., eds., Thermal History of Sedimentary Basins: Methods and Case Histories. Springer-Verlag, Berlin. p. 74-98.

Barker, C.E., 1990, Reconnaissance fluid inclusion study, Amoco Eischeid #1 well, Defiance Basin, Mid-continent rift system, Iowa: Iowa Geological Survey Special Report Series no. 2, p. 169-173.

Barker, C.E., 1991, Implications for organic maturation studies of evidence for a geologically rapid increase and stabilization of vitrinite reflectance at peak temperature: Cerro Prieto geothermal system, Mexico: American Association of Petroleum Geologists Bulletin, v. 75, p. 1852-1863.

Barker, C.E., 1992, Sample temperatures reached during cathodoluminescence observations--preliminary measurement using reequilibrated fluid inclusions in calcite:

Society for Luminescence Microscopy and Spectroscopy, v. 4, p. 3.

Barker, C.E., 1994, Vitrinite reflectance of whole-rock versus dispersed organic matter mounts: what's the difference?: Extended Abstracts, The Society for Organic Petrology, v. 11, p. 1-4.

Barker, C.E., Bartke, T.C., Hatcher, P.G. and Daws, T.A., 1993, An empirical correlation between coal bed gas with Rock-Eval pyrolysis and ^{13}C NMR results, Cretaceous Mesaverde and Meeteetse Formations, Wind River Basin, Wyoming, *in* Strook, B. and Andrew, S. , eds., Wyoming Geological Association Fifitieth Anniversary Guidebook, p. 243-256.

Barker, C.E., Bone, Y. and Dalgarno, C.R., 1992a, Contact metamorphism of organic matter in the Buchan Caves Limestone, Buchan Trough, Victoria, Australia: Abstracts, 11th Australian Geology Congress, Ballarat, Victoria, Australia. p. 127-128.

Barker, C.E., Bone, Y., Duddy, I.R., Marshallsea, S.J. and Green, P.F., 1992b, Peak temperature estimated from fluid inclusions and vitrinite reflectance next to a thin dike near San Remo, Victoria, Australia: Extended Abstracts, The Society for Organic Petrology, v. 9, p. 102-104,

Barker, C.E. and Bone, Y., 1995, The minimal response to contact metamorphism by the Devonian Buchan Caves Limestone, Buchan Rift, Victoria, Australia: Organic Geochemistry, v. 22, p. 151-164.

Barker, C.E. and Goldstein, R.H., 1990, Fluid inclusion technique for determining maximum temperature in calcite and its comparison to the vitrinite reflectance geothermometer: Geology, 18, 1003-1006.

Barker, C.E. and Pawlewicz, M.J., 1986a, The correlation of vitrinite reflectance with maximum temperature in humic organic matter, *in* Buntebarth, G. and Stegena, L. eds., Paleogeothermics, Lecture Notes in Earth Sciences, v. 5, Springer-Verlag, New York. p.

80-93.

Barker, C.E. and Pawlewicz, M.J., 1986b, Concentration of dispersed sedimentary organic matter for vitrinite reflectance analysis using a simple crush and float technique: The Society for Organic Petrology Newsletter, v. 3, no. 3, p. 3.

Barker, C.E. and Pawlewicz, M.J., 1993, An empirical determination of the minimum number of measurements needed to estimate the mean random vitrinite reflectance of disseminated Organic Matter: Organic Geochemistry, vol. 20, p. 643-651.

Barker, C.E. and Pawlewicz, M.J. ,1994, Calculation of vitrinite reflectance from thermal histories and peak temperature: a comparison of methods, *in* Mukhopadhyay, P.K. and Dow, W.G., eds., Vitrinite Reflectance as a Maturity Parameter: American Chemical Society Symposium Series no. 570, p. 216-229.

Barker, C.E. and Reynolds, T.J., 1984, Preparing doubly polished sections of temperature sensitive sedimentary rocks: Journal of Sedimentary Petrology. v. 54, p. 635-636.

Barker, C.E. and Wood, T., 1986, A review of the Technosyn and Nuclide cathodoluminescence stages and their application to sedimentary geology, *in* Hagni, R.D., 1986, Process Mineralogy VI: The Metallurgical Society of the American Institute of Mining Engineers, Warrendale, PA. p. 137-158.

Basaltic Volcanism Study Project , 1981, Basaltic Volcanism on Terrestrial Planets. Pergamon Press, New York, p. 509.

Basu, A., Young, S.W., Suttner, L.J., James, W.C., Mack, G.H., 1975, Re-evaluation of the use of undulatory extinction and polycrystallinity in detrital quartz for provenance interpretation: Journal of Sedimentary Petrology, v. 45, p. 873-882.

Bethke, C. M., Ming-Kuo, L., Quinodoz, H. A. M. and Kreiling, W. N., 1993, Basin Modeling with Basin2: University of Illinois, Urbana, 225 p.

Bishop, A.N. and Abbott, G..D., 1993, The interrelationship of biological marker maturity parameters and molecular yields during contact metamorphism: Geochimica et Cosmochimica Acta, v. 57, p. 3661-3668.

Bishop, A.N. and Abbott, G.D., 1994, Vitrinite reflectance and molecular geochemistry of Jurassic sediments: the influence of heating by Tertiary dykes (northwest Scotland): Organic Geochemistry, v. 22, No. 1, p. 165-177

Blatt, H., Middleton, G and Murray, R., 1972, Origin of Sedimentary Rocks: Prentice-Hall, Inc., Englewood Cliffs, New Jersey. 634 p.

Bodnar, R.J., Binns, P.R. and Hall, D.L., 1989, Synthetic fluid inclusions--VI. Quantitative evaluation of decrepitation behavior of fluid inclusions in quartz at one atmosphere confining pressure: Journal of Metamorphic Geology, v. 7, p. 229-242.

Bodnar, R.J. and Vityk, M.O., 1994, Interpretation of microthermometric data for H_2O-NaCl fluid inclusions, *in* De Vito, B., Frezzotti, M.L., 1994, eds., Fluid Inclusions in Minerals: Methods and Applications: Short Course, International Mineralogical Association Working Group, "Inclusions in Minerals", p. 117-130

Bolger, P.F., 1991, Lithofacies variations as a consequence of Late Cainozoic tectonic and palaeoclimatic events in the onshore Gippsland Basin, *in* Williams, M.A.J., DeDeckker, P., Kershaw, A.P., eds., The Cainozoic in Australia: A Re-appraisal of the Evidence: Geological Society of Australia Special Publication 18, p. 158-180.

Bone, Y. and Russell, N.J., 1988, Correlation of vitrinite reflectivity with fluid inclusion microthermometry: assessment of the technique in the Cooper/Eromanga Basins, South Australia: Australian Journal of Earth Sciences, V. 35, p. 567-570.

Boullier, A.-M., Michot, G., Pecher, A. and Barres, O., 1989, Diffusion and(or) plastic deformation around fluid inclusions in synthetic quartz: new investigations, *in* Bridgwater, D., ed., Fluid Movements--Element transport and the Composition of the

Deep Crust: Kluwer, Dordrecht, p. 345-360.

Borg, I. Friedman, M., Handin, J. and Higgs, D.V., 1960, Experimental deformation of the St. Peter Sandstone, *in* Griggs, D. and Handin, J., eds., Rock Deformation: Geological Society of America Memoir 79, p. 133-192.

Bostick, N.H., 1973, Time as a factor in thermal metamorphism of phytoclasts (coaly particles), *In* Congress International de Stratigraphie et de Geologie Carbonifere, Septieme, Krefeld, August, 1971, Compte Rendu, v. 2, p. 183-193.

Bostick, N.H., 1979, Microscopic measurement of the level of catagenesis of solid organic matter in sedimentary rocks to aid exploration for petroleum and to determine former burial temperatures--a review, *in* Scholle, P. A. and Schluger, P. R., eds., Aspects of Diagenesis: Society of Economic Paleontologists and Mineralogists Special Publication, No. 26, p. 17-44.

Bostick, N.H. and Pawlewicz, M.J., 1984, Paleotemperatures based on vitrinite reflectance of shales and limestones in igneous dike contact aureoles in the Upper Cretaceous Pierre Shale, Walsenburg, Colorado, *in* Woodward, J.G., Meissner, F.F. and Clayton, J.L., eds., Hydrocarbon Source Rocks of the Greater Rocky Mountain Region: Rocky Mountain Association of Geologists, p. 387-392.

Bray, R.J., Green, P.F. and Duddy, I.R., 1992, Thermal history reconstruction using apatite fission track analysis and vitrinite reflectance: a case study from the UK East Midlands and Southern North Sea, *in* Hardman, R.F., ed., Exploration Britain: Geological Insights for the Next Decade: Geological Society Special Publication no. 67, p. 3-25.

Brenan, J. M., 1991, Development and maintenance of metamorphic permeability: Implications for fluid transport, *in* Kerrick, D.M., ed., Contact Metamorphism, Mineralogical Society of America, Reviews in Mineralogy, v. 26, p. 291-320.

Brooks, J. D., 1970, The use of coals as indicators of the occurrence of oil and gas: Australian

Petroleum Exploration Association Journal, v. 10, p. 35-40.

Browne, P.R.L., 1978, Hydrothermal alteration in active geothermal fields: Annual Review of Earth and Planet Science, v. 6, p. 229-250

Burns, B.J., Bostwick, T.R. and Emmet, J.K., 1987, Gippsland terrestrial oils--recognition of Compositional variations due to maturity and biodegradation effects: Australian Petroleum Exploration Association (APEA) Journal, v. 27, p. 73-84.

Burruss, R.C., 1989, Paleotemperatures from fluid inclusions: advances in theory and technique, *in* Naeser, N.D. and McCulloch, T., eds., Thermal History of Sedimentary Basins: Methods and Case Histories. Springer-Verlag, Berlin. p. 119-132.

Burruss, R.C. and Hollister, L.S., 1979, Evidence from fluid inclusions for a paleogeothermal gradient at the geothermal test well site, Los Alamos, New Mexico: Journal of Volcanic and Geothermal. Res. 5, p.163-177.

Bustin, R.M., Cameron, A.R., Grieve, D.A. and Kalkreuth, W.D., 1983, Coal Petrology, its Principles, Methods and Applications: Geological Society of Canada, Short Course Notes, v. 3, 230 p.

Carmichael, I.S.E., Turner, F.J. and Verhoogen, J., 1974, Igneous Petrology: McGraw-Hill, New York. 739 p.

Carmody, J., 1992, Recent Petroleum Exploration Activity- Onshore Gippsland Basin: Gippsland Basin Symposium, Australasian Institute of Mining and Metallurgy, Melbourne. p. 157-163.

Carr, A.D. and Williamson, J.E., 1990, The relationship between aromaticity, vitrinite reflectance and maceral composition of coals: Implications for the use of vitrinite reflectance as a maturation parameter: Organic Geochemistry, v.16, p. 313-323.

Carslaw, H.S., and Jaeger, J.C., 1959, Conduction of Heat in Solids: Oxford University Press, London. 510 p.

Cas, R., 1983, A review of the palaeogeographic and tectonic development of the Palaeozoic Lachlan fold belt of southeastern Australia: Geological Society of Australia Special Publication 10. 104 p.

Cas, R., 1988, Tectonic history of Victoria, *in* Clark, I., Cook, B. and Cochrane, G.C., eds., Victorian Geology Excursion Guide, p. 47-79.

Clayton, J.L. and Bostick, N.H., 1986, Temperature effects on kerogen and molecular and isotopic composition of organic matter in Pierre Shale near an igneous dike: Organic Geochemistry, v. 10, p. 135-143.

Cook, A.C., 1981, Organic petrology of a suite of samples from the Neocomian of the Gippsland Basin: Keiraville Konsultants Report to Bell Cochrane and Associates Pty, Ltd. (Unpublished). 18 p.

Cooles, G.P., Mackenzie, A.S. and Quigley, T.M., 1986, Calculation of petroleum masses generated and expelled from source rocks: Organic Geochemistry, v. 10, p. 235-245.

Cooper, R.A. and Grindley, G.W., editors, 1982, Late Proterozoic to Devonian sequences of southeastern Australia, Antarctica and New Zealand and their correlation: Geological Society of Australia Special Publication 9. 103 p.

Cornelius, C.D., 1987, Classification of natural bitumen: a physical and chemical approach, *in* Meyer, R.F., ed., Exploration for Heavy Crude Oil and Natural Bitumen: American Association of Petroleum Geologists Studies in Geology, v. 25, p. 165-174.

Corrigan, J.D., 1993, Apatite fission-track analysis of Oligocene strata in South Texas, U.S.A.: Testing annealing models: Chemical Geology, v. 104, p. 227-249.

Cortial, F., Gauthier-Lafaye, F., Lacrampe-Couloume, G., Oberlin, A. and Weber, F., 1990, Characterization of organic matter associated with uranium deposits in the Francevillian Formation of Gabon (Lower Proterozoic): Organic Geochemistry, v. 15, p. 73-85.

Crawford, M.L., 1981, Phase equilibria in aqueous fluid inclusions, *in* Hollister, L.S. and

Crawford, M.L., ed., Fluid inclusions: applications to petrology: Mineralogical Association of Canada Short Course Handbook v. 6, p. 75-97.

Crawford, M.L. and Hollister, L.S., 1986, Metamorphic fluids: the evidence from fluid inclusions, *in* Walther, J.V. and Wood, B.J., eds., Fluid-Rock Interactions During Metamorphism: Springer-Verlag, Berlin, p. 1-35.

Crick, I.H., 1992, Petrological and maturation characteristics of organic matter from the Middle Proterozoic McArthur Basin, Australia: Australian Journal of Earth Sciences, v. 39, p. 501-519.

Cromie, P. ,1990, Base metal occurrences of the Buchan Caves Limestone, Victoria: Honours Thesis, Department of Geology, University of Melbourne. 72 p.

Cull, J.P. and Beardsmore, G.R., 1992, Estimates of heat flow and geothermal gradients in the Gippsland Basin: Gippsland Basin Symposium, Australasian Institute of Mining and Metallurgy, Melbourne. p. 15-24.

Day, R.A. ,1983, Petrology and geochemistry of Older Volcanics, Victoria: Ph.D. thesis, Monash University, Melbourne. 372 p.

Degens, E.T., 1965, Geochemistry of Sediments- A Brief Survey: Prentice-Hall Inc. Englewood Cliffs, New Jersey. 346p.

Delaney, P.T., 1982, Rapid intrusion of magma into wet rock: groundwater flow due to pore pressure increases: Journal of Geophysical Research.,v. 87, p. 7739-7756.

Delaney, P.T., 1987, Heat transfer during emplacement and cooling of mafic dykes, *in* Halls, H.C. and Fahrig, W.F., eds., Mafic Dyke Swarms: Geological Association of Canada Special Paper 34, p. 31-46.

Delaney, P.T. and Pollard, D.D., 1982, Solidification of basaltic magma during flow in a dike: American Journal of Science, v. 282, p. 856-885.

Dembicki, H., Jr., 1984, An interlaboratory comparison of source rock data: Geochimica et

Cosmochimica Acta, v. 48, p. 2641-2649.

Douglas, J.G., compiler, 1976, Geological map of Victoria: Australia 1:1 000,000 map series.

Douglas, J.G., Abele, C., Benedek, S., Dettman, M.E., Kenley, P.R., Lawrence, C.R., Rich, T.H.V. and Rich, P.V., 1988, Mesozoic, *in* Douglas, J.G. and Ferguson, J.A., eds., Geology of Victoria: Victorian Division, Geological Society of Australia, p. 213-250.

Dow, W.G., 1977, Kerogen studies and geological interpretations: Journal of Geochemical Exploration, v. 7, p. 79-99.

Duba, D. and Williams-Jones, A.E., 1983, The application of illite crystallinity, organic matter reflectance and isotopic techniques to mineral exploration: A case study in southwestern Gaspe, Quebec: Economic Geology, v. 78, p. 1350-1353.

Duddy, I.R., 1983, The geology, petrology and geochemistry of the Otway Formation volcanigenic sediments: Ph.D. thesis, Melbourne University, 426 p.

Duddy, I.R., Green, P.F. and Laslett, , G.M., 1988, Thermal annealing of fission tracks in apatite 3. Variable temperature behavior: Chemical Geology, v. 73, p. 25-38.

Duddy, I.R. and Green, P.F., 1992, Tectonic development of the Gippsland Basin and environs: identification of key episodes using apatite fission track analysis (AFTA): Gippsland Basin Symposium, Australasian Institute of Mining and Metallurgy, Melbourne. p. 111-121.

Duddy, I.R., Green, P.F., Bray, R.J. and Hegarty, K. A., 1994, Recognition of the thermal effects of fluid flow in sedimentary basins, *in* Parnell, J., ed., Geofluids: Origin, Migration and Evolution of Fluids in Sedimentary Basins: Geological Society Special Publication, no. 78, p. 325-345.

Dumitru, T.A., Hill, K.C., Coyle, D.A., Duddy, I.R., Foster, D.A., Gleadow, A.J.W., Green, P.F., Kohn, B.P., Laslett, G.M. and O'Sullivan, A.J., 1991, Fission track thermochronology: Application to continental rifting in southeast Australia: The Australian Petroleum

Exploration Association (APEA) Journal, v. 31 , p. 131-142.

Eakin, P.A., 1989, Isotopic and petrographic studies of uraniferous hydrocarbons from around the Irish Sea basin: Journal of the Geological Society, London, v. 146, p. 663-673.

Eakin, P.A. and Gize, A.P., 1992, Reflected-light microscopy of uraniferous bitumens: Mineralogical Magazine, v. 56, 85-99.

Edwards, A.B., 1934, Tertiary Dykes and Volcanic necks of south Gippsland, Victoria: Proceedings, Royal Society of Victoria, v. 47, p. 112-133.

Edwards, A.B., 1938. Petrology of the Tertiary Older Volcanic rocks of Victoria: Proceedings, Royal Society of Victoria, v. 51, p. 73-98.

Edwards, A.B., 1942, The San Remo Peninsula: Proceedings, Royal Society of Victoria, v. 54, p. 59-74.

Edwards, A.B. and Baker, G., 1943, Jurassic Arkose in southern Victoria: Proceedings, Royal Society of Victoria, v. 55, p. 195-228.

Edwards, A.B., Baker, G. and Knight, J.L., 1944, The geology of the Wonthaggi coalfield, Victoria: Australasian Institute of Mining and Metallurgy Proceedings number 129, p. 1-54.

Einsele, G., Gieskes, J. M., Curray, J., Moore, D. M., Aguayo, E., Aubry, M.-P., Fornari, D., Guerrero, J., Kastner, M., Kelts, K., Lyle, M., Matoba, Y., Molina- Cruz, A., Niemitz, J., Rueda, J., Saunders, A., Schrader, H., Simoneit, B. and Vacquier, V., 1980, Intrusion of basaltic sills into highly porous sediments and resulting hydrothermal activity: Nature, v. 283, p. 441-445.

Ellis, A. J., 1979, Explored Geothermal Systems, *in* Barnes, H. L., ed. Geochemistry of Hydrothermal Ore Deposits, second Edition: J. Wiley and Sons, New York, p. 632-683.

Ellis, A.J. and Mahon, W.A.J., 1977, Chemistry and Geothermal Systems: Academic Press, New York, 392 p.

Erren, H. and Bredewout, J.W., 1991, Model calculations on intrusive cooling and related coalification of the Peel-Erkelenz coalfield (The Netherlands and Germany): Geologie en Mijnbouw, v. 70, p. 243-252.

Espitalie, J., Laporte, J.L., Madec, M., Marquis, F., Leplat, P., Paulet, J., Boutefeu, A., 1977, Rapid method of characterizing source rocks and their petroleum potential and degree of maturity: Revue de l'Institut Francais du Petrole, v. 32, p. 23-42.

Fan, D., Liu, T., Yang, P. and Ye, J., 1993, Occurrence of anthraxolite (bitumen) spheroids in Xiangtan-type manganese carbonate deposits of south China, *in* Parnell, J., Kucha, H. and Landais, P., eds., Bitumen in Ore Deposits: Springer-Verlag, Berlin. p. 447-458.

Faure, G., 1977, Principles of Isotope Geology: J. Wiley and Sons, New York.

Ferguson, W.H., 1909, Report on the lower Powlett, Cape Paterson, and Inverloch Quarter Sheets: Victoria Geological Survey Memoir 8, 14 p.

Finlayson, B., Webb, J.A. and Ellaway, M., 1992, The Buchan Karst, *in* Gillieson, D., ed., Geology, Climate, Hydrology and Karst Formation: Field Symposia in Australia: Guidebook, Special Publication 4, Department of Geography and Oceanography, University College, Australian Defense Force Academy, Canberra, p. 3-24.

Fisher, J.R., 1976, The volumetric properties of H_2O -- a graphical portrayal: Journal of Research, U.S. Geological Survey, v. 4, p. 189-193.

Fleischer, R. L., Price, P. B. and Walker, R. M., 1975, Nuclear Tracks in Solids: University of California Press, Berkeley, 605 p.

Frakes, L.A. and Rich, P.V., 1982, Paleoclimatic setting and paleogeographic links of Australia in the Phanerozoic, *in* Rich, P.V. and Thompson, E.M., eds., The Fossil Vertebrate Record of Australasia, Monash University Press, Melbourne, Victoria, p. 28-52.

Garcia-Gonzalez, M., MacGowan, D.B. and Surdam, R.C., 1993, Coal as a source rock of petroleum and gas--A comparison between natural and artificial maturation of the

Almond Formation coals, greater Green River Basin in Wyoming: U.S. Geological Survey Professional Paper 1570, p. 405- 437.

Gauthier-Lafaye, F. and Weber, F., 1993, Uranium-hydrocarbon association in Francevillian Uranium ore deposits, Lower Proterozoic of Gabon, *in* Parnell, J., Kucha, H. and Landais, P., eds., Bitumen in Ore Deposits: Springer-Verlag, Berlin. p. 276-286.

Gentzis, T. and Goodarzi, F., 1990, A review of the use of bitumen reflectance in hydrocarbon exploration with examples from Melville Island, Arctic Canada, *In* Nuccio, V.F. and Barker, C.E., eds., Applications of Maturity Studies to Energy Exploration: Rocky Mountain Section, Society of Economic Paleontologists and Mineralogists, p. 23-36.

Gize, A.P., 1986a, The development of a thermomesophase in bitumens from high temperature ore deposits, *in* Dean, W.E., ed., Organics and Ore Deposits: Denver Region Exploration Geologists Society, p. 137-150.

Gize, A.P., 1986b, Analytical approaches to organic matter in ore deposits, *in* Dean, W.E., ed., Organics and Ore Deposits: Denver Region Exploration Geologists Society, p.21-32.

Gize, A.P., 1990, Petroleum derived cokes in sedimentary basins, *in* Fermont, J.J. and Weegink, J.W., eds., International Symposium on Organic Petrology: Mededelingen Rijks Geologische Dienst, v. 45, p. 65-73.

Gize, A.P. and Rimmer, S. M., 1983, Mesophase development in a bitumen from the Nanisivik Mississippi Valley-type deposit: Carnegie Institute, Washington, Year Book 82, p. 414-419.

Gleadow, A.J.W. and Duddy, I.R., 1981, Early Cretaceous volcanism and the early breakup history of southeastern Australia: evidence from fission track dating of volcaniclastic sediments, *in* Cresswell, M.M. and Vella, P., eds., Godwana Five: Balkema, Rotterdam.

Gleadow, A.J. W., Duddy, I.R., Green, P.F. and Lovering, J.F., 1986, Confined fission track lengths in apatite; a diagnostic tool for thermal history analysis: Contributions to

Mineralogy and Petrology, v. 94, p.405-415.

Goldstein, R.H. and Reynolds, T.J., 1994, Systematics of fluid inclusions in diagenetic minerals: Society of Economic Paleontologists and Mineralogists, Short Course 31, 199 p.

Gonsalez, R.C., 1985, Vitrinite reflectance of cores and cuttings from the Ngatamariki Well NM-2, New Zealand: Geothermal Institute Report 85.10, 60p.

Goodarzi, F. and Murchison, D. G., 1977, Effect of prolonged heating on the optical properties of vitrinite: Fuel, v. 56, p. 89-96.

Goodarzi, F., Gandi, S.S. and Snowdon, L.R., 1989, Bitumen in a Lower Proterozoic dolomite hosting Pb-Zn-Cu occurrences, Artillery Lake, Northwest Territories: Geological Survey of Canada Paper 89-1C, p. 369-376.

Gratier, J.P. and Jenatton, L., 1984, Deformation by solution-deposition, and re-equilibration of fluid inclusions in crystals depending on temperature, internal pressure and stress: Journal Structural Geology, v. 6, p. 189-200.

Gratz, J.F. and Misra, K.C., 1987, Fluid inclusion study of the Gordonsville zinc deposit, central Tennessee: Economic Geology, 82, p. 1790-1804.

Green, P.F., 1988, The relationship between track shortening and fission track age reduction in apatite--combined influences of inherent instability, annealing anisotropy, length bias and system calibration: Earth and Planetary Science Letters, v. 89, p. 335-352.

Green, P.F., Duddy, I.R., Gleadow, A.J.W. and Tingate, P.R., 1985, Fission track annealing in apatite: track length measurements and the form of the Arrhenius plot, Nuclear Tracks, v.10, p. 323-328.

Green, P.F., Duddy, I.R., Gleadow, A.J.W., Tingate, P.R. and Laslett, G.M., 1986, Thermal annealing of fission tracks in apatite 1. A qualitative description: Chemical Geology, v. 59, p. 237-253.

Green, P.F., Duddy, I.R. and Laslett, G.M., 1988, Can fission track annealing in apatite be described by first order kinetics?: Earth and Planetary Science Letters, v. 87, p. 216-228.

Green, P.F., Duddy, I.R., Gleadow, A.J.W. and Lovering, J.F., 1989, Apatite fission-track analysis as a paleotemperature indicator for hydrocarbon exploration, *in* Naeser, N.D. and McCulloh, T.H., eds., Thermal History of Sedimentary Basins, Springer-Verlag, Berlin, p. 181-195.

Gregory, R.T., Douthitt, C.B., Duddy, I.R., Rich, P.V. and Rich, T.H., 1989, Oxygen isotopic composition of carbonate concretions from the lower Cretaceous of Victoria, Australia: Implications for the evolution of meteoric waters on the Australian continent in a paleopolar environment: Earth and Planetary Science Letters, v. 92, p. 27-42.

Gretener, P.E., 1981, Geothermics: using temperature in hydrocarbon exploration: American Association of Petroleum Geologists Education Course Note Series no. 17, 156 p.

Haenel, R., 1983, Geothermal investigations in the Rhenish Massif, *in* Fuchs, K., Von Gehlen, K., Maltzer, H., Murawski, H. and Semmel, A., eds, Plateau uplift, the Rhenish shield, a case history: Springer Verlag, Berlin, p. 228-246.

Hallbauer, D.K. and Kable, E.J.D., 1982, Fluid inclusions and trace element content of quartz and pyrite pebbles from Witwatersrand conglomerates: their significance with respect to the genesis of primary deposits, *in* Amstutz, G.C. et al., eds., Ore Genesis-- The State of the Art: Springer Verlag, Berlin, p. 742-752.

Hanor, J.S., 1980, Dissolved methane in sedimentary brines: potential effect on the PVT properties of fluid inclusions: Economic Geology, v. 75, p. 603-609.

Haq, B.U. and Eysinga, F.W.B., 1994, Geological Time Table, Fourth edition: Elsevier, Amsterdam.

Harrington, C.L., 1993, Origin of dolomitization and MVT sulphides in the Lower Devonian

Buchan Group, Eastern Victoria: Honours Thesis, Department of Earth Sciences, University of Melbourne, 66p.

Harrison, W.J., 1989, Modeling fluid/rock interactions in sedimentary basins, *in* Cross, T.A., ed., Quantitative Dynamic Stratigraphy. Prentice Hall, New York, p. 195-231.

Haskell, T.R., 1972, Hydrocarbon potential of the Mesozoic and basal Tertiary of the Gippsland Basin-- a stratigraphic analysis: Journal Australian Petroleum Exploration Association, v. 12, p. 138-143.

Hausen, D.M. and Park, W.C., 1986, Observations on the association of gold mineralization with organic matter in Carlin-type ores, *in* Dean, W.E., ed., Organics and Ore Deposits: Denver Region Exploration Geologists Society, p. 119-135.

Hegarty, K.A., Duddy, I.R., Green , P.F., Gleadow, A.J.W., Fraser, I. and Weissel, J.K., 1986, Regional evaluation of the tectonic and thermal history of the Gippsland Basin, *in* Glenie, R.C., ed., Second South-Eastern Australia Oil Exploration Symposium, Melbourne, November, 1985. Petroleum Exploration Society of Australia, p. 65-74.

Henry, A.L., 1988, Alteration of organic matter in the Viburnum Trend lead/zinc District of southeastern Missouri: M.Sc. thesis, University of Toronto. 130 p.

Heydari, E. and Moore, C.H., 1989, Burial diagenesis and thermochemical sulfate reduction, Smackover Formation, southeastern Mississippi Salt basin: Geology, v. 17, p. 1080-1084.

Hofstra, A.H., Leventhal, J.S., Northrop, H.R., Landis, G.P., Rye, R.O., Birak, D.J. and Dahl, A.R., 1991, Genesis of sediment-hosted disseminated-gold deposits by fluid mixing and sulfidization: chemical-reaction-path modeling of ore-depositional processes documented in the Jerritt Canyon District, Nevada: Geology, v. 19, p. 36-40.

Holdgate, G.R., 1991, Gippsland Basin Excursion Notes: Australian Petroleum Exploration Association Guidebook. 28 p.

Holdgate, G.R. and McNicol, M.D., 1992, New Directions - Old Ideas; Hydrocarbon Prospects of th Strezlecki Group, onshore Gippsland Basin: Gippsland Basin Symposium, Australasian Institute of Mining and Metallurgy, Melbourne. p. 121-131.

Hollister, L.S., 1981, Information intrinsically available from fluid inclusions, *in* Hollister, L.S. and Crawford, M.L., ed., Fluid inclusions: applications to petrology. Mineralogical Association of Canada short course handbook v. 6, p. 1-12.

Horváth, F., Dövényi, P., Szalay, Á. and Royden, L.H., 1988, Subsidence, thermal and maturation history of the Great Hungarian Plain, *in* Royden, L.H. and Horváth, F., eds., The Pannonian Basin--a Study in Basin Evolution: American Association of Petroleum Geologists Memoir 45, p. 355-372.

Hughes, C.J., 1982, Igneous Petrology: Elsevier, Amsterdam, 356 p.

Hunt, J. M., 1979, Petroleum Geochemistry and Geology. Freeman, San Francisco. 617 p.

Hurford, A. J. and Green, P. F., 1982, A users' guide to fission track dating calibration: Earth and Planetary Science Letters, v. 59, p. 343-354.

Ingram, G. R. and Rimstidt, J. D., 1984, Natural weathering of coal: Fuel, v. 63, p.292-296.

Islam, S. and Hesse, R., 1983, The P-T conditions of late stage diagenesis and low grade metamorphism in the Taconic Belt of the Gaspe Peninsula from fluid inclusions: preliminary results: Geological Survey of Canada Paper 83-1b, p. 145-150.

Jacob, H., 1975, Mikroskopphotometrische Analyse naturlicher fester Erdolbitumina, in, Alpern, B., ed., Petrographie Organique et Potentiel Petrolier. Coll. int., CNRS, Paris. p. 103-113.

Jacob, H., 1989, Classification, structure, genesis and practical importance of natural solid oil bitumen ("migrabitumen"): International Journal of Coal Geology, v. 11, p. 65-79.

Jaeger, J. C., 1957, The temperature in the neighborhood of a cooling intrusive sheet: American Journal of Science, v. 255, p. 306-318.

Jaeger, J.C., 1959, Temperatures outside a cooling intrusive sheet: American Journal of Science, v. 257, p. 44-54.

Jaeger, J. C., 1964, Thermal effects of intrusions: Reviews of Geophysics, v. 2, p. 443-466.

Jakobsen, U.H. and Ohmoto, H., 1993, Bitumen associated with precipitation of sulphides in carbonate-hosted vein mineralization, north Greenland, *in* Parnell, J., Kucha, H. and Landais, P., eds., Bitumen in Ore Deposits: Springer Verlag, Berlin. p. 398-414.

Jenkin, J.J., 1962, The Geology and Hydrology of the Western Port Area: Geological Survey of Victoria Underground Water Investigation report no. 5, 53 p.

Jowett, E.C., 1986, Genesis of Kuperschiefer Cu-Ag deposits by convective flow of Rotliegende brines during Triassic rifting: Economic Geology, v. 81, p. 1823-1837.

Joyce, E.B. and King, R.L., editors, 1980, Geological features of the National estate in Victoria: Victorian Division, Geological Society of Australia, 210 pp.

Katz, B.J., 1983, Limitations of 'Rock-Eval' pyrolysis for typing organic matter: Organic Geochemistry, v. 4, p. 195-199.

Kerrich, R., 1976, Some effects of tectonic recrystallization on fluid inclusions in quartz: Contribution to Mineralogy and Petrology, v. 59, p. 195-202.

Khavari-Khorasani, G. and Murchison, D.G., 1978, Thermally metamorphosed bitumen from Windy Knoll, Derbyshire, England: Chemical Geology, v. 22, p. 91-105.

Khavari-Khorasani, G.K., Murchison, D.G. and Raymond, A.C., 1990, Molecular disordering in natural cokes approaching dyke and sill contacts: Fuel, v. 69, p. 1037-1045.

King, R.L., Ford, A.J., Stanley, D.R., Kenley, P.R. and Cecil, M.K., 1985, Geothermal resources of Victoria: A discussion paper: Victorian Solar Energy Council, Department of Industry, Technology and Resources, Report. 129p.

Kitson, A.E., 1917, The Jumbunna and Powlett plains district, south Gippsland: Geological Survey of Victoria, Bulletin 40, 25 p.

Kitson, A.E., 1903, Volcanic necks at Anderson's inlet, south Gippsland, Victoria: Proceedings, Royal Society of Victoria, p. 154-176.

Knipping, B., 1989, Basalt Intrusives in Evaporites: Springer-Verlag, Berlin. 132 p.

Kribek, B., Holubar, V., Parnell, J., Pouba, Z. and Hladikova, J., 1993, Interpretation of thermal mesophase in vanadiferous bitumens from Upper Proterozoic lava flows (Mitov, Czechoslovakia), *in* Parnell, J., Kucha, H. and Landais, P., eds., Bitumen in Ore Deposits: Springer-Verlag, Berlin. p. 61-77.

Kribek, B., Hrabal, J., Landais, P. and Hladikova, J., 1994, The association of poorly ordered graphite, coke and bitumens in greenschist metamorphosed rock of the Ponikla Group, Lugicum, Czech Republic: the result of graphitization of various types of organic matter: Metamorphic Geology, v. 12, p. 493-503.

Kucha, H., 1993, Noble metals associated with organic matter, Kupferschiefer, Poland, *in* Parnell, J., Kucha, H., and Landais P., eds., Bitumen in Ore Deposits: Springer-Verlag, Berlin, p. 153-170.

Kuttan, K., Kulla, J.B. and Neumann, R.G., 1986, Freshwater influx in the Gippsland Basin: impact on formation evaluation, hydrocarbon volumes, and hydrocarbon migration: Australian Petroleum Exploration Association Journal, v. 26, p. 242-249.

Lacazette, A., 1990, Application of linear elastic fracture mechanics to the quantitative evaluation of fluid inclusion decrepitation: Geology, v. 18, p. 782-785.

Landais, P., 1993, Bitumens in Uranium Deposits, *in* Parnell, J., Kucha, H. and Landais, P., eds., Bitumen in Ore Deposits. Springer-Verlag, Berlin. p. 213-238.

Landais, P. and Connan , J., 1986, Source rock potential and oil alteration in the Uraniferous Basin of Lodeve (Herault, France): Sciences Geologiques Bulletin v. 39, p. 293-314.

Landais, P., Connan, J., Dereppe, J. M., George, E., Meunier, J.D., Monthioux, M., Pagel, M., Pironon, J. and Poty, B., 1987, Alterations of Organic Matter: A Clue for Uranium

Ore Genesis: Uranium, v. 3, p. 307-342.

Langford, F.F. and Blanc-Valleron, M.-M., 1990, Interpreting Rock-Eval pyrolysis data using graphs of pyrolizable hydrocarbons vs. total organic carbon: American Association of Petroleum Geologists Bulletin, v. 74, no. 6, p. 799-804.

Laslett, G.M., Green, P.F., Duddy, I.R. and Gleadow, A.J.W., 1987, Thermal annealing of fission tracks in apatite 2. A quantitative analysis: Chemical Geology, v. 65, p. 1-13.

Leroy, J., 1979, Contribution a l'etalonnage de la presion interne des inclusions fluides lors de leur decrepitation: Societe Francaise, Mineralogie et Cristallographie, Bulletin, v. 102, p. 584-593.

Leventhal, J.S., Grauch, R.I., Threlkeld, C.N., Lichte, F.E. and Harper, C.T., 1987, Unusual organic matter associated with uranium from the Claude deposit, Cluff Lake, Canada: Economic Geology, v. 82, p. 1169-1176.

Levine, J.R., Samson, I.M. and Hesse, R., 1991 Occurrence of fracture-hosted impsonite and Petroleum fluid inclusions, Quebec City Region, Canada: American Association of Petroleum Geologists Bulletin, v. 75, p. 139-155.

Lewan, M.D., 1985, Evaluation of petroleum generation by hydrous pyrolysis experimentation: Philosophical Transactions of the Royal Society of London, v. A315, p. 123-134.

Lewan, M.D., 1993a, Laboratory simulation of petroleum formation: Hydrous Pyrolysis, *in* Engel, M.H. and Macko, S.A., eds., Organic Geochemistry, Plenum Press, New York, p. 419-442.

Lewan, M.D., 1993b, Identifying and understanding suppressed vitrinite reflectance through hydrous pyrolysis experiments: Extended Abstracts, The Society of Organic Petrology, v. 10, p. 1-3.

Lewan, M.D., 1994, Assessing natural oil expulsion form source by laboratory pyrolysis, *in* Magoon, L.B. and Dow, W.G., eds., The Petroleum System from Source to trap:

American Association of Petroleum Geologists Memoir 60., p. 201-209.

Lewis, L..J., 1993, Undulosity and cathodoluminescence of quartz adjacent to a dolerite dike, Victoria, Australia: B.Sc. thesis, St. Lawrence University, New York, 50 p.

Lindsay, N.M., 1982, the burial history of the Strzelecki Group sandstones, S.E. Australia: M.Sc thesis, University of Melbourne, 153 p.

Liu, D., Fu, J. and Jia, R., 1993, Bitumen and dispersed organic matter related to mineralization in stratabound deposits, south China, *in* Parnell, J., Kucha, H. and Landais, P., eds., Bitumen in Ore Deposits: Springer-Verlag, Berlin. p. 171-177.

Lobzova, R.V. and Ziborova, T.A.,1988, Behavior of high carbon solids during metamorphism: International Geological Reviews, v. 30, p. 187-196.

Lovering, T.S., 1935, Theory of heat conduction applied to geological problems: Geological Society of America, v. 46, p. 69-94.

Lowry, D.C., 1988, Alternative Cretaceous history of the Gippsland Basin: Australian Petroleum Exploration Association Journal , v. 28, p. 181-194.

Lowry, D.C. and Longley, I.M., 1991, A new model for the mid-Cretaceous structural history of the northern Gippsland basin: Australian Petroleum Exploration Association Journal , v. 31, p. 143-153.

Marshall, D.J., 1978, Suggested standards for the reporting of cathodoluminescence results: Journal of Sedimentary Petrology, v. 48, p. 635.

Marshallsea, S.J., 1988, The thermal history of the Bowen Basin (Qld): An apatite fission track study: Ph.D. thesis, University of Melbourne, 291 p.

McAndrew, J. and Marsden, M.A.H. , 1968, A Regional Guide to Victorian Geology: Geology Department, University of Melbourne, 219 p.

McKirdy, D. M. and Powell, T. G., 1974, Metamorphic alteration of carbon isotopic composition in ancient sedimentary organic matter: New evidence from Australia and South Africa:

Geology, v. 2, p. 591- 596.

McNaughton, K.C., 1983, A fluid inclusion study of the Nanisivik lead-zinc deposit, Baffin Island, Northwest Territories: M.Sc. thesis, University of Windsor, Ontario. 94 p.

McQueen, R.W., 1986, Origin of Mississippi Valley-type lead-zinc ores by organic matter-sulfate reactions: the Pine Point example, *in* Dean, W.E., ed., Organics and Ore Deposits: Denver Region Exploration Geologists Society, p. 151-156.

Mebberson, A.J.,1989, The future for exploration in the Gippsland Basin: Australian Petroleum Exploration Association Journal, v. 29, p. 430-439.

Megallaa, M.,1993, Tectonic evolution of the Gippsland Basin and hydrocarbon potential of its lower Continental shelf: Australian Petroleum Exploration Association Journal, v. 33, p. 45-61.

Michard, A., 1989, Rare earth element systematics in hydrothermal fluids: Geochimica et Cosmochimica Acta, v. 53, p. 745-750.

Middlemost, E.A.K., 1985, Magmas and Magmatric Rocks; an introduction to Igneous Petrology: Longman, London and New York, 266 p.

Middleton, M. F.,1991, Thermal effects of intrusions on coal: Permian Coals of Eastern Australia: Bureau of Mineral Resources Bulletin 231, p. 395-400.

Middleton, M., 1993, A transient method of measuring the thermal properties of rocks: Geophysics, v. 58, p.357-365.

Mill, L., White, S. and Mackey, P., editors, 1980, Victorian Caves and Karst. Guidebook, 13th conference of the Australian Speleological Association. 86 p.

Miyazaki, S., 1989, Characterization of Australia's oil fields by fluid and reservoir properties and conditions: Australian Petroleum Exploration Association Journal, v. 29, p. 287-297.

Moore, D.M. and Reynolds, R.C., Jr., 1989, X-Ray Diffraction and the Identification and Analysis of Clay Minerals: Oxford University Press, 332 p.

Morrow, D.W. and Issler, D.R., 1993, Calculation of vitrinite reflectance from thermal histories: A comparison of some methods: American Association of Petroleum Geologists Bulletin, v. 77, p. 610-624.

Moser, M.R., Rankin, A.H. and Milledge, H.J., 1992, Hydrocarbon-bearing fluid inclusions in fluorite associated with the Windy Knoll bitumen deposit, UK: Geochimica et Cosmochimica Acta, v. 56, p. 155-168.

Mossman, D.J., Nagy, B., Rigali, M.J., Gauthier-Lafaye, F. and Holliger, P., 1993, Petrography and paragenesis of organic matter associated with the natural fission reactors at Oklo, Republic of Gabon: a preliminary report: International Journal of Coal Geology, v. 24, p. 179-194.

Muir, M.D., Donnelly, T.h., Wilkins, R.W.T. and Armstrong, K.J., 1985, Stable isotope, petrological, and fluid inclusion studies of minor mineral deposits from the McArthur Basin: implications for the genesis of some sediment-hosted base metal mineralization from the Northern Territory: Australian Journal of Earth Sciences, v. 32, p. 239-260.

Mundry, E., 1968, Ueber die Abkuhlung magmatischer Koper: Geologisches Jahrbuch, v. 85, p. 755-766.

Naeser, C.W., 1979, Fission track dating and geologic annealing of fission tracks, *in* Jager, E. and Hunsiker, J.C., eds., Lectures in Isotope Geology: Springer-Verlag, Berlin, p. 154-169.

Naeser, C.W., 1981, The fading of fission tracks in the geologic environment: data from deep drill holes: Nuclear Tracks, v. 5, p. 248-250.

Naeser, N.D., Naeser, C.W., McCulloh, T.H., 1989, The application of fission track dating to the depositiional and thermal history of rocks in sedimentary basins, *in* Naeser, N.D. and McCulloh, T.H., eds., Thermal History of Sedimentary Basins: Springer-Verlag, Berlin, p. 157-180.

Norland, W.D., 1986, Thermal maturation of the Mesilla Valley Shale (Late Albian) on the north and east flanks of the Cerro De Cristo Rey Pluton, Dona Ana County, New Mexico: M.Sc. Thesis, The Univeristy of Texas, El Paso. 164 p.

North, F.K., 1985, Petroleum Geology: Allen and Unwin, London. 607 p.

Orth, K. and VandenBerg, A.H.M., Nott, R.J. and Simons, B.A., in press, Murrindal 1:100,000 Map, Geological Report: Geological Survey of Victoria.

Osborne, M. And Haszeldine, S., 1993, Evidence for resetting of fluid inclusion temperatures from quartz cements in oil fields: Marine and Petroleum Geology, v. 10, p. 271-278.

O'Shea, P.J., 1980, Mineral potential of the Snowy River Volcanics and Buchan Caves Limestone: Geological Survey of Victoria Report number 63, 29 p.

Ozimic, S., Nicholas, E.M., Pain, L. and Vuckovic, V., 1987, Gippsland Basin, Victoria: Bureau of Mineral Resources, Australian Petroleum Accumulations Report 3, 252 p.

Pagel, M., Poty, B. and Sheppard, S.M.F., 1980, Contributions to some Saskatchewan uranium deposits mainly from fluid inclusions and isotopic data, *in* Ferguson, J. and Goleby, A.B., eds., Uranium in the Pine Creek Geosyncline: International Atomic Energy Agency Proceedings series, p. 639-654.

Parnell, J., 1989, Hydrocarbon potential of Lower Palaeozoic of the British Isles: Oil and Gas Journal, v. 87, p. 82-86.

Parnell, J., 1993, Metal enrichments in bitumens from the Carboniferous of Ireland: potential in exploration for ore deposits, *in* Parnell, J., Kucha, H. and Landais, P., eds., Bitumen in Ore Deposits: Springer-Verlag, Berlin. p. 475-489.

Parnell, J. and Monson, B., 1990, Sandstone-hosted thorium-bitumen mineralization in the Northwest Irish Basin: Sedimentology, v. 37, p. 1011-1022.

Parnell, J., Kucha, H. and Landais, P., editors, 1993, Bitumen in Ore Deposits: Springer-Verlag, Berlin. 520 p.

Paton, M., 1982, Gippsland basin, post-depositional adjustments in buried sediments: B.Sc. Honours thesis, Monash University. Unkown pages.

Pawlewicz, M.J., 1986, Polishing method for dispersed vitrinite and coal slides: The Society for Organic Petrology Newsletter, v. 5, p.3.

Peacock, S.M., 1989, Thermal modeling of metamorphic pressure-temperature-time paths: a forward approach, *in* Spear, F.S. and Peacock, S.M., Metamorphic Pressure-Temperature-Time Paths: American Geophysical Union Short Course In Geology, v. 7, p. 57-102.

Peacock, S.M., 1990, Numerical simulation of regional and contact metamorphism using the Macintosh microcomputer: Journal of Geological Education, v. 38, p. 132-137.

Pecher, A., 1981, Experimental decrepitation and re-equilibration of fluid inclusions in synthetic quartz: Tectonophysics, v. 78, p. 567-584.

Peters, K.E., Simoneit, B.R.T., Brenner, S. and Kaplan, I.R., 1978, Vitrinite reflectance temperature determination for intruded cretaceous black shale in the eastern Atlantic, *in* Oltz, D.F., ed., Low Temperature Metamorphism of Kerogen and Clay Minerals: Pacific Section, Society of Economic Paleontologists and Mineralogists, p. 53-58.

Peters, K.E., 1986, Guidelines for evaluating petroleum source rock using programmed pyrolysis: American Association of Petroleum Geologists Bulletin, v. 70, no. 3, p. 318-329.

Philip, G.M., 1958, The Jurassic sediments of the Tyers Group, Gippsland, Victoria: Proceedings, Royal Society of Victoria, v. 70, p. 181-199.

Pollastro, R.M., 1982, A recommended procedure for the preparation of oriented clay mineral specimens for X-Ray diffraction analysis: Modifications to Drever's filter membrane peel technique: U.S. Geological Survey, Open File Report 82-71. 10 p.

Powell, T.G. and Boreham, C.J., 1994, Terrestrially sourced oils: where do they exist and

what are the limits of knowledge?--A geochemical perspective, *in* Scott, A.C. and Fleet, A.J., eds., Coal and Coal-Bearing Strata as Oil-Prone Source Rocks?: Geological Society Special Publication 77, p. 11-29.

Powell, T.G. and McKirdy, D.M., 1975, Geological factors controlling crude oil composition in Australia and Papua New Guinea: American Association of Petroleum Geologists Bulletin, v. 59, p. 1176-1197.

Price, L.C. and Barker, C. E., 1985, Suppression of vitrinite reflectance in amorphous rich kerogen--a major unrecognized problem: Journal of Petroleum Geology, v. 8, p. 59-84.

Price, L. C., 1983, Geologic time as a parameter in organic metamorphism and vitrinite reflectance as an absolute paleogeothermometer: Journal of Petroleum Geology, v. 6, p. 5-38.

Price, L. C., 1994, Metamorphic free-for-all: Nature, v. 370, p. 253-254.

Price, R.C., Gray, C.M., Nichols, I.A. and Day, A., 1988, Cainozoic volcanic rocks, *in* Douglas, J.G. and Ferguson, J.A., eds., Geology of Victoria: Victorian Division, Geological Society of Australia, p. 439-451.

Pytte, A.M., 1982, The kinetics of smectite to illite reaction in contact metamorphic shales. M.A. Thesis, Dartmouth College, Hanover, New Hampshire, 78p.

Pytte, A.M. and Reynolds, R.C., 1989, The thermal transformation of smectite to illite, *in* Naeser, N.D. and McCulloch, T., eds., Thermal History of Sedimentary Basins: Methods and Case Histories. Springer-Verlag, Berlin. p. 133-140.

Rahmanian, V.D., Moore, P.S., Mudge, W.J. and Spring, D.E., 1990, Sequence stratigraphy and the habitat of hydrocarbons, Gippsland Basin, Australia, *in* Brooks, J, ed., Classic Petroleum Provinces. Geological Society Special Publication no. 50, p. 525-541.

Ramsay, W.R.H. and VandenBerg, A.H.M., 1990, Lachlan Fold Belt in Victoria--regional geology and mineralization, *in* Hughes, F.E, ed., Geology of the Mineral Deposits of

Australia and Papua New Guinea: Australasian Institute of Mining and Metallurgy, Melbourne, p. 1269-1273.

Raymond, A.C. and Murchison, D.G., 1988, Development of organic maturation in the thermal aureoles of sills and its relation to sediment compaction: Fuel, v. 67, p. 1599-1608.

Richards, J.R. and Singleton, O.P., 1981, Palaeozoic Victoria, Australia: igneous rocks, ages, and their interpretation: Geological Society of Australia Journal , v. 28, p. 395-421.

Riediger, C.L., 1993, Solid bitumen reflectance and Rock-Eval Tmax as maturation indices: an example from the "Nordegg Member", Western Canada sedimentary basin: International Journal of Coal Geology, v. 22, p. 295-315.

Riediger, C.L. and Coniglio, M., 1992, Early diagenetic calcites and associated bitumens in the "Nordegg Member": implications for Jurassic paleogeography of the western Canada sedimentary basin: Bulletin of Canadian Petroleum Geology, v. 40, p. 381-394.

Robbins, E.I., D'Agostine, J.P., Hass, J.L., Jr., Larson, R.R. and Delong, F.T., 1990, Palynological assessment of the organic tissues and metallic minerals in the Jerritt Canyon gold Deposit, Nevada (U.S.A.): Ore Geology Reviews, v. 5, p. 399-422.

Robert, P., 1988, Organic metamorphism and geothermal history: Reidel, Dordrecht, Netherlands. 311 p.

Robinson A., Grant, S. and Oxtoby, N., 1991, Evidence against natural deformation of fluid inclusions in diagenetic quartz: Marine and Petroleum Geology, v. 9, p. 568-572.

Roedder, E., 1968, Temperature, salinity, and origin of the ore-forming fluids at Pine Point, Northwest Territories, Canada, from fluid inclusion studies: Economic Geology, v. 63, p. 439-450.

Roedder, E., 1984, Fluid Inclusions: Mineralogical Society of America, Reviews in Mineralogy, v. 12, 644 p.

Roedder, E. and Bodnar, R.J., 1980, Geologic pressure determinations from fluid inclusions:

Annual Reviews of Earth and Planetary Sciences, v. 8, p. 263-301.

Rosengren, N., 1984, Sites of geological and geomorphological significance in the Westernport Bay catchment: Environmental Studies Division, Victoria Department of Conservation, Forests and Lands, Publication 84-1., 513p.

Roy, R. F., Beck, A. E. And Touloukian, Y.S., 1981, Thermophysical properties of rocks, *in* Touloukian, Y. S. , Judd, W. R. and Roy, R. F., eds., Physical Properties of Rocks and Minerals, vol II-2: McGraw-Hill, New York, p. 409-502.

Russell, N.J. and Bone, Y., 1989, Cooper/Eromanga Basin paleogeothermometry, *in* O'Neil, B.J., ed., The Cooper/Eromanga Basins, Australia. Proceedings, Petroleum Exploration Society of Australia, SPE and ASEG (South Australia branches), Adelaide, p. 559-581.

Samson, I.M. and Russell, M.J., 1983, Fluid inclusion data from the Silvermines base metal/baryte deposits, Ireland: Institute Mining and Metallurgy Transactions, v. 92, p. B67-B71.

Sanyal, S.P., 1965, Nature of a thin vein of solidified tarry matter formed during natural carbonization of coal from the Victoria West Colliery, Raniganj coalfield, India: Fuel, v. 44, p. 333-338.

Sass, J.H., Kennelly, J.P., Jr., Williams, C.F. and Lachenbuch, A.H., 1992, Thermal conductivity of water saturated crystalline rocks as a function of temperature: Proceedings, Conference on Thermal properties of Crustal Materials, Badhonnef, Germany, April 1-3, 1992.

Sassen, R., 1988, Geochemical and carbon isotope studies of crude oil destruction, bitumen precipitation, and sulfate reduction in the deep Smackover Formation: Organic Geochemistry, v. 12, p. 351-361.

Savin, S.M., 1977, The history of the earth's surface temperature during the past 100 million years: Annual Reviews of Earth and Planetary Sciences, v. 5, p. 319-355.

Shibaoka, M., Saxby, J. D. and Taylor, G. H., 1978, Hydrocarbon generation in Gippsland basin, Australia--comparison with Cooper basin Australia: American Association of Petroleum Geologists Bulletin, v. 62, p. 1151-1158.

Singleton, O.P., 1973, Geology of the Macedon District, *in* McAndrew, J.and Marsden, M.A.H., eds., Regional Guide to Victorian Geology: School of Geology, University of Melbourne, Publication no. 1.

Skibo, D.N., Harrison, C., Gentzis, T. and Goodarzi, F., 1991, Organic maturity/time-temperature models of the Ellesmerian (Paleozoic) Orogeny, Melville island, Northwest Territories: Geological Survey of Canada Paper 91-1E, p. 165-175.

Simmons, G. and Richter, D., 1976, Microcracks in rocks, *in* Strens, R.G.J., ed., The Physics and Chemistry of Minerals and Rocks: Wiley, New York, p. 105-137.

Smith, A.G. and Briden, J.C., 1977, Mesozoic and Cenozoic paleocontinental Maps: Cambridge University press, Cambridge, 63 p.

Smith, G.C., 1986, Bass Basin geology and petroleum exploration, *in* Glenie, R.C., ed., Second South-Eastern Australia Oil Exploration Symposium, Melbourne, November, 1985. Petroleum Exploration Society of Australia, p. 257-283.

Smith, G.C., 1988, Oil and Gas, *in* Douglas, J.G. and Ferguson, J.A., eds., Geology of Victoria: Victorian Division, Geological Society of Australia. p. 514-546.

Smith, G.C. and Cook, A.C., 1984, Petroleum occurrence in the Gippsland Basin and its relationship to rank and organic matter type: Australian Petroleum Exploration Association Journal, v. 24, p. 196-218.

Smith, J.W., Rigby, D., Gould, K.W., Hart, G. and Hargraves, A.J, 1985, An isotopic study of hydrocarbon generation processes: Organic Geochemistry, v. 8, p. 341-345.

Smith, J.W., Rigby, D., Binjie, L., Zhiguang, S., and Wang, Y., 1994, The determination of the petroleum potential of terrestrial source rocks: Organic Geochemistry, v. 21, p. 287-

301.

Sofer, Z., 1991, Stable isotopes in Petroleum Exploration, *in* Merrill, R.K., ed., Source and Migration Processes and Evaluation Techniques, American Association of Petroleum Geologists, Treatise of Petroleum Geology Series, p. 103-106.

Somerton, W. H., 1992, Thermal properties and temperature-related behavior of rock/fluid systems: Elsevier, Amsterdam. 257 p.

Spear, F.S. and Peacock, S.M., 1990, Metamorphic P-T-t paths: Computer Program Manual. Published by Spear and Peacock. 188 p.

Spencer-Jones, D., Marsden, M.A.H., Barton, C.M. and Carrillo-Rivera, J.J., 1975, Geology of the Westernport sunkland: Proceedings of the Royal Society of Victoria, v. 87, p. 43-67.

Spiegel, M.G., 1961, Theory and Problems of Statistics: Schaum Publishing Co., New York.

Stach, E., Mackowsky, M.-TH., Teichmuller, M., Taylor, G. H., Chandra, D. and Teichmuller, R., 1982, Stach's Textbook of Coal Petrology, third edition: Gebruder Borntraeger, Berlin. 535 p.

Sterner, S.M., 1992a, Synthetic fluid inclusions: part XI. Notes on the application of synthetic fluid inclusions to high P-T experimental aqueous geochemistry: American Mineralogist, v. 77, p. 156-167.

Sterner, S.M., 1992b, Homogenization of fluid inclusions to the vapor phase: the apparent homogenziation phenomenon: Economic Geology, v. 87, 1616-1623.

Sterner, S.M. and Bodnar, R.J., 1984, Synthetic fluid inclusions in natural quartz I. Compositional types synthesized and applications to experimental geochemistry: Geochimica et Cosmochimica Acta, v. 48, p. 2659-2668.

Sterner, S.M. and Bodnar, R.J., 1989, Synthetic fluid inclusions--VII. Re-equilibration of fluid inclusions in quartz during laboratory-simulated metamorphic burial and uplift: Journal

of Metamorphic Geology, v. 7, p. 243-260.

Stirling, J., 1890, First progress report on geological survey of carboniferous area in south Gippsland: Reports and Statistics, Victoria Mining Department, For the Quarter ending December 31, 1890. p. 35-40.

Stirling, J., 1892, Special report on the Victorian coal-fields: Victoria Department of Mines Special Report 2. p. 1-16.

Stirling, J., 1893, Topographical and Geological survey of Gippsland carbonaceous area: [contains map of Korumburra, Jeetho and Jeetho West Parishes]: Victorian Department of Mines, Reports on the Victorian Coalfields Special Report 3. 1 sheet.

Struckmeyer, H. and Browne, P.R.L., 1988, Application of the vitrinite reflectivity method to samples from the Wairakei-Tauhara and Ohaaki geothermal fields: Proceedings, 10th New Zealand Geothermal Workshop. p. 251-255.

Suggate, R. P., 1982, Low-rank sequences and scales of organic metamorphism: Journal of Petroleum Geology, v. 4, p. 377-392.

Swanenberg, H.E.C., 1980, Phase equilibria in carbonic systems and their application to freezing studies of fluid inclusions: Contributions to Mineralogy and Petrology, v.68, p.303-306.

Taitt, S. and Jaupart, C. ,1990, Physical processes in the evolution of magmas: Mineralogical Society of America, Reviews in Mineralogy, v. 24, p. 125-152.

Tannenbaum, E. and Aizenshtat, Z. ,1985, Formation of immature asphalt from organic-rich carbonate rocks: Organic Geochemistry, v. 8, p. 181-192.

Teichert, C. and Talent, J.A., 1958, Geology of the Buchan Area, East Gippsland: Geological Survey of Victoria Memoir 21, 56 p.

Teichmüller, M., 1987, Recent advances in coalification studies and their application to geology, *in* Scott, A.C., ed., Coal and Coal-bearing Strata: Recent Advances:

Geological Society Special Publication 32, p. 127-169.

Thompson, B.R., 1986, The Gippsland Basin- Development and *Stratigraphy, in* Glenie, R.C., ed., Second South-Eastern Australia Oil Exploration Symposium, Melbourne, November, 1985. Petroleum Exploration Society of Australia, p. 57-64.

Tickell, S.J., 1971, The geology of the Bass River area: B.Sc. Honours thesis, Department of Geology, University of Melbourne. 20 p.

Ting, F.T.C., 1978, Petrographic techniques in coal analysis, *in* Karr, C., Jr., ed., Analytical Methods for Coal and Coal Products: Academic Press, New York, p. 3-26.

Tissot, B.P. and Welte, D.H., 1984, Petroleum Formation and Occurrence, Second Edition: Springer-Verlag, Berlin. 699 p.

Turner, F.J. ,1981, Metamorphic Petrology: McGraw-Hill, New York, 524 p.

Veevers, J.J., editor, 1984, Phanerozoic Earth History of Australia: Oxford Science Publications, Oxford , 418 p.

Vityk, M.O., Bodnar, R.J. and Schmidt, C.S., 1994, Fluid inclusions as tectonothermobarometers: relation between pressure-temperature history and reequilibration morphology during crustal thickening: Geology, v. 22, p. 731-734.

Wang, X. Leche, I. and Walter, C., 1989, the effect of igneous intrusive bodies on sedimentary thermal maturity: Organic Geochemistry, v. 14, p. 571-584.

Webb, J.A., 1991, Geological history of Victoria, *in* Cochrane, G.W., Quick, G.W. and Spencer-Jones, D., ed., Introducing Victorian Geology: Victorian Division, Geological Society of Australia, p. 97-168.

Webb, J.A., Finlayson, B.L., Fabel, D. and Ellaway M., 1991, The geomorphology of the Buchan Karst- implication for the landscape history of the Southeastern Highlands of Australia, *in* Williams, M.A.J., DeDeckker, P. And Kershaw, A.P., eds, The Cainozoic in Australia: A Re-appraisal of the Evidence: Geological Society of Australia Special

Publication 18, p. 210-234.

Whelan, J.K., Seewald, J., Eglinton, L. and Miknis, F., in press, Time-temperature histories of kerogen and mineral ammonia from ODP leg 139 (Middle Valley) sediments: Initial Reports, Ocean Drilling Program. 18 p.

White, D. E., 1973, Characteristics of geothermal resources, in Kruger, P. and Otte, C., eds., Geothermal Energy: Stanford University Press, Stanford, California, p. 69-94.

Whitelaw, O.A.L., 1922, Geologically coloured parish plans, Poowong parish: Geological Survey of Victoria. 1 sheet.

Willcox, J.B., Colwell, J.B. and Constantine, A.E., 1992, New ideas on Gippsland Basin regional tectonics: Gippsland Basin Symposium, Australasian Institute of Mining and Metallurgy, Melbourne. p. 93-109.

Williams-Jones, A.E. and Ferreira, D.R., 1989, Thermal metamorphism and H_2O-CO_2-NaCl immiscibility at Patapedia, Quebec: evidence from fluid inclusions: Contributions to Mineralogy and Petrology, v. 102, p. 247-254.

Wilson, M.A., 1987, NMR Techniques and Applications in Geochemistry and Soil Chemistry: Pergamon Press, Oxford. 353 p.

Winkler, H.G.F., 1976, Petrogenesis of Metamorphic Rocks, fourth edition: Springer-Verlag, Berlin. 334 p.

Yang, C. and Hesse, R., 1993, Diagenesis and anchimetamorphism in an overthrust belt, external domain of the Taconian Orogen, southern Canadian Appalachians--II. Paleogeothermal gradients derived from maturation of different types of organic matter: Organic Geochemistry, v. 20, p. 381-403.

Yang, W. And Liu, Y., 1993, Geochemcial data for organic matter in stratabound sulphide and other ore deposits in China, *in* Parnell, J., Kucha, H. and Landais, P., eds., Bitumen in Ore Deposits: Springer-Verlag, Berlin. p. 415-430.

Yin, P., Surdam, R.C., Boese, S.W., MacGowan, D.B. and Miknis, F.P., 1993, Simulation of hydrocarbon source rock maturation by hydrous pyrolysis, *in* Stroock, B. and Andrew, S., eds., Wyoming Geological Association Fifitieth Field Conference Guidebook. p. 359-373.

Appendix 1: Methods

A1.1 SAMPLING AND SAMPLE PREPARATION

Field treatment

For this study, coals or coaly rocks were selected along a line perpendicular to the dike plane. The sample intervals varied depending on dike thickness, but generally were taken out to a distance equal to one or two dike thicknesses as allowed by the rock exposure. To expose the fresher rock and minimize contamination by soil and plant material, the samples were taken as far below the present surface as digging conditions and time would reasonably allow. In general, the soil was scraped away and a pit was dug about 20 to 50 cm below the present rock surface. If possible, rocks were discarded when they did not have the color of the unweathered host rock, showed Liesegang-like banding, were friable, or were coated with accumulations of soil zone materials.

At each dike, several sample series were collected. These sample series included the typical host rock for clay mineral, whole rock element, thermal conductivity, or porosity and permeability analyses; more sand-rich host rock for fluid inclusion, fracture or AFT annealing studies, coals or coaly rock for organic petrography and geochemistry. These samples were air dried soon after collection and stored in polyethylene plastic bags.

Samples taken for analyses that would be sensitive to fracturing were sawn out of the outcrop or sawn from the center of larger samples using water cooled blades or core plug equipment.

Laboratory Treatment

The samples for vitrinite reflectance, organic geochemistry and ^{13}C NMR analyses were washed and dried. The fresher coal or coaly mudstone chips picked out while examining the sample under a binocular microscope. Using picked samples for organic geochemistry eliminates any visible foreign materials, such as plastic or recent plant materials, that could be a contamination problem. These samples were finely pulverized using a glass mortar and pestle which is more easily cleaned of organic matter. If no coaly rock was present, the

darker, finer-grained rocks were picked out for analysis . When using whole rock samples, my experience shows that the best chance of finding adequate TOC for analysis is in the darker colored mudstones.

Analyses requiring whole rock samples were treated according to established practice for that analysis as described below. Processing whole rock samples usually involves pulverizing the rock to about 100 μm grain size while taking care not to fractionate the sample. All whole rock samples were passed through a grinder until over 90% of the sample passed the appropriate screen for the analytical equipment.

The samples for thermal properties analysis were sawn or cored, using water cooled equipment, to a shape appropriate for the analytical equipment. Fluid inclusion, CL and general petrography samples were prepared by a method evolved from that of Barker and Reynolds (1984).

Buchan Rift

The sampled dike is about 10 km north from Buchan, Victoria and is exposed in a road cut along Gelantipy Road just west southwest of Murrindal, Victoria Deep soil and vegetation cover obscures the dike away from the road cut. The Murrindal dike is 2.2 m thick where sampled. The dike trends N80°E with near vertical orientation.

The strata hosting Murrindal dike are exposed in the road cut for some distance, making it possible to sample the same bed well away from the dike contact. Samples for analysis were prepared in the laboratory by cutting off exposed surfaces in order to obtain the less weathered cores. Some polished sections made for the ore deposit study by Cromie (1990) were made available to us for bitumen reflectance analysis (by D.C. Arne, now at Dalhousie University, Halifax, Nova Scotia).

Bulk chip samples were chiseled out of one bed at increasing horizontal distance from the near-vertical dike margin. The distances from the dike contact were marked on the well exposed outcrop using a felt tip pen. Within this one bed, the chambers of articulated brachiopods that contained sparry cements were preferentially removed for fluid inclusion

analysis. Regional background measurements were made on samples far removed from known intrusions. Regional samples were collected in road cuts, mine pits and stream beds where the strata were well exposed.

Western Onshore Gippsland Basin

The dikes used in this study were exposed in railroad cuts or on coastal wave cut platforms or cliffs in the western onshore Gippsland Basin. These exposures of the contact metamorphosed Strzelecki Group provided what may be the least weathered samples available. Most samples were taken next to dikes exposed within the intertidal zone from San Remo to Inverloch, Victoria. The Strzelecki Group coals near the Bena, Korumburra, and Cruickston dikes are deeply weathered. Sampling in this area was limited to relatively unweathered exposures in railroad and road cuts.

All of these sampled dikes, except Korumburra 1, have a subvertical orientation and trend northerly to northwest. Korumburra 1 trends northeast and has a near vertical orientation.

To assess the weathering problem, well core samples of mudstone, coal and coaly fossils were also taken for source rock analysis and used to compare to the regional samples and the contact metamorphosed sample suites. These regional samples were analyzed from localities across the western onshore Gippsland Basin.

A1.2 PETROGRAPHIC METHODS

Vitrinite Reflectance

Vitrinite reflectance was measured on the vitrinite group maceral, telocollinite, using conventional methods (Stach et al., 1982; Bustin et al., 1983; Robert, 1988). In samples where reflectance was rerun to check the data, the first value measured was still used for plotting and data analysis.

During this study, three aspects of vitrinite reflectance method were examined:

1) Comparison of Rv-r measurements made using mounts made from rocks and SOM concentrates .

   This comparison was needed because, although only humic SOM was used for vitrinite reflectance, the study used diverse sample types consisting of coals, whole rock mounts made from sandstone and mudstone, as well as SOM concentrates made from these rocks (Barker, 1994; see appendix 11). This study shows that vitrinite reflectance when measured by a single operator, shows fair to good agreement regardless of the sample preparation method. This factor is considered negligible in comparison to the other potential errors in vitrinite reflectance (Dembicki, 1984).

2) Calibration of photometers when using multiple reflectance standards.

   Measuring Rv-r over the extremely wide thermal maturation range found next to dikes requires using several reflectance standards. Multiple standards are necessary in this case because photometers can have a non-linear response when measuring light intensity over a wide range. The question is how comparable are Rv-r measurements made by calibrating the photometer using different standards? This study is presented below in this appendix.

3) Number of reflectance measurements needed to determine precisely measure Rv-r.

   Given that this study required thousands of reflectance determinations, assessing the minimum sample size required to effectively determine Rv-r was crucial to efficiently completing the study (Barker and Pawlewicz, 1993; see appendix 11).

Preparation of Whole Rock Mounts

Whole rock samples for vitrinite reflectance analysis were prepared by coarse crushing in a jaw crusher set with 3 mm plate gap and sieving out that portion that passed through a 0.85 mm mesh screen and remained trapped on a 0.18 mm mesh screen. Coals were just pulverized using a mortar and pestle. The crushed and screened rock was vacuum impregnated and embedded in a plug made of Epotek 301 plastic (Epoxy Technology Corp,

Massachusetts, USA). Epotek 301 is a low viscosity, room temperature setting plastic. The hardened plug was polished using the method of Pawlewicz (1986). This technique of using small rock fragments randomly embedded in plastic, gives random reflectance measurements more comparable to the results of the Rv-r analyses on SOM concentrates.

In some very lean samples (TOC <<0.5 wt-%), the whole rock samples contained only rare SOM or were barren of measurable SOM. In these cases, SOM concentrates were made using a sink-float technique (Barker and Pawlewicz, 1986). The isolated SOM was rinsed, freeze dried, mounted on glass slides with epoxy, and polished (Pawlewicz, 1986). However, in most cases, the concentrate mounts provided no better results than the whole rock analyses and this additional step was later abandoned.

Instrumentation

Reflectance was measured using vertical illumination on a Zeiss Universal microscope fitted with a MPM-01 microphotometric system. The photometer was restricted with a pinhole diaphragm to read a 3 μm spot on the sample at 500x total magnification, using a 40x/0.85 n.a. lens under oil immersion. The standard was oriented perpendicular to the optical axis of the microscope and reflectance measurements were made under oil immersion (Cargille PCB free Type A immersion oil, n_e = 1.5180). The system was calibrated by synthetic crystal standards in filtered 546 nm light. Thermal maturity was estimated in this study using Rv-r (mean-random vitrinite reflectance) data. When using published vitrinite reflectance analyses that report the results in Rv-m (mean maximum vitrinite reflectance) conversion to Rv-r was by using the equation in Ting (1978; Rv-r = Rv-m/1.066).

Reflectance Standards and Calibration

The reflectance standards were synthetic isotropic single crystals of leucosapphire (LS), 0.58%Ro; gadolinium gallium garnet (GGG), 1.73%Ro; cubic zirconia (CZ), 3.26%Ro; and silicon carbide (SiC), 7.49%Ro from Zeiss (LS) and McCrone Research (GGG, CZ, SiC). Crystal based standards, unlike glass standards, are scratch resistant and do not require

quarterly or semiannual repolishing. These reflectance standards are calibrated for use at 23°C and a change of immersion oil temperature of a few degrees away from this value produces a detectable change in reflectance. Thus, the typical temperature change over the course of a day mostly caused by the increase in microscope temperature during photometer operation, cause small but detectable changes in reflectance at the second decimal place level. However, such changes are not significant at the precision level of one decimal place for SOM Rv-r measurements (Robert, 1988) although the precision of the microphotometer operation is 2 decimal places. Daily laboratory temperature variations are thought to be the cause of the observed instrumental drift on the order of a few hundredths detected by measuring a standard before and after scanning a sample.

Linearity of the microphotometer response was tested by calibrating the photometer using selected standards and measuring other standards (Table A1-1). These studies show that the error in measured reflectance is negligible, at least up to the reflectance of the next higher standard. The procedure used in this paper is to recalibrate the microphotometer after a few pilot measurement on a sample, if the apparent sample Rv-r is close to that of the next higher standard.

In conclusion, these experiments show that at the level of precision (one decimal place) possible for SOM reflectance studies, the microphotometer response is quite linear. Nevertheless, in this study, the reflectance standard nearest the range of a sample's apparent Rv-r was usually employed to calibrate the microphotometer.

Table A1-1. Tests of Photometer Linearity.

Photometer Standardized at: (Ro in %)	Measuring Standard (Ro in %)	Measured Ro (Ro in %)	Difference (in %)
LS (0.58)	0.58	0.58	0.00 (Observed Ro measurement after LS series completed)
LS	1.73	1.71	0.03
LS	3.26	3.13	0.13
LS	7.49	7.26	0.26
GGG(1.73)	1.73	1.75	0.02 (Observed Ro measurement after GGG series completed)
GGG	0.58	0.6	0.02
GGG	3.26	3.18	-0.08
GGG	7.49	7.52	0.03
CZ (3.26)	3.26	3.26	0.00 (Observed Ro measurement after CZ series completed)
CZ	0.58	0.63	0.05
CZ	1.73	1.8	0.07
CZ	7.49	7.53	0.04
SiC (7.49)	0.58	0.61	0.03
SiC	1.73	1.76	0.03
SiC	3.26	3.21	0.05
SiC	7.49	7.56	0.06 (Observed Ro measurement after SiC series completed)

Note: The photometer was warmed up for one hour before tests were initiated. Three to five measurements were taken at different spots on each standard. The tests were completed over several days and laboratory room temperature varied by several degrees during this time.

Sample Quality

In an effort to assess the quality of a coal for vitrinite reflectance analysis and the confidence level in the measurements a list of sample qualities was devised. A sample with most of these qualities would be considered a good analysis. A sample with few of these qualities would be considered a poor analysis. For each sample an assessment is made as to whether the sample quality is good, fair or poor. However, this qualitative assessment of the sample quality still does not preclude an erroneous vitrinite reflectance value because in a sample with a high score it is still possible for the wrong population of vitrinite to be selected by the microscopist. Further, a sample with a low score could give an entirely reasonable and useful result.

The checklist used to evaluate sample quality in this study is as follows:

1. Sample from deeper subsurface (versus surface exposure)
2. Sample from core or whole rock (versus drill cuttings)
3. Sample is a humic coal (versus a rock sample that contains disseminated organic matter which may be suppressed).
4. Coal plug or whole rock polish relatively smooth, scratch free, and has a low relief.
5. The vitrinite has identifiable telocollinite that is relatively clean, i.e., few inclusions of mineral matter, other macerals, or polishing compound. The surface not porous or pitted, gelified and sufficiently homogeneous to have spots large to measure.
6. Measurable vitrinite, as defined above, is common enough to reach the target sample size.
7. Organic matter common enough to allow easy reflectance range comparisons.
8. Vitrinite reflectance distribution is monomodal.
9. The vitrinite has a cellular, plied (interlayered with other macerals), or other texture, structure, or associations that positively identify it as vitrinite (versus bitumen) and as

telocollinite.

10. In very high thermal maturity samples, as found near a dike, is the vitrinite distinguishable from semi-fusinite and(or) fusinite.

To evaluate sample quality using this list, each attribute that the sample possessed was scored as one point. Using this system, a summed score of 8 to 10 was ranked as good, 5 to 7 as fair and 0-4 as poor.

Sample Size

Barker and Pawlewicz (1993; see appendix 11) found that after only 30 measurements the mean Rv-r is generally known to within 5 % and always to within 12 % of the mean Rv-r calculated using all of the measured particles. Thus, even in the worst case, the precision after measuring only 30 particles is in good agreement with the general precision of one decimal place recommended for mean Rv-r measurements on DOM. In some cases, especially close to the dike contact, only a few vitrinite grains were found for measurement. In these cases, the coefficient of variation (V = standard deviation/mean) was proposed by Barker and Pawlewicz (1993) as a statistic to indicate the reliability of the mean Rv-r estimates made at $n << 20$. Their preliminary study suggests a $V < 0.1$ indicates a reliable mean and a $V > 0.2$ suggests an unreliable mean in such small samples.

In this study, the coefficient of variation was computed for each sample and is used in assessing the sample quality given in appendix 2. Samples assessed to be of poor quality and with a $V>0.2$ were queried in the regional compilations and ignored in the analyses of measured Rv-r and T_{peak}.

Bitumen Reflectance

Bitumen reflectance was measured on samples from the Buchan Rift using the same sample preparation for concentrates, microphotometric system and standards as vitrinite reflectance. Whole rock mounts were made using the method of Barker and Reynolds (1984). After Rb-r measurement, the samples were used for fluid inclusion analyses.

For calibration of a geothermometer based on Rb (Appendix 3), the Rb-r values used are the upper limit of the measurements (upper data edge), and if known, the value measured away from radioactive inclusions. The reasons for using the upper data edge value are discussed in Chapter 2.Conversion of Rb-r to Rv-r equivalents for use in the burial history modeling program employed the calibration in Jacob (1989). Note that Jacob uses the lowest reflecting population for both vitrinite and solid bitumen and thus, the conversion to the upper data edge value used in this study is only approximate. As discussed below, the lowest reflecting bitumen population is poorly suited for use in geothermometry because this population, which formed last in the burial history, is least likely to have recorded T_{peak}.

Fluid Inclusion Analysis

Instrumentation, Calibration and Sample Preparation

Phase transition temperatures in fluid inclusions were determined in a Fluid Inc. heating/freezing stage. The stage was calibrated using SYNFLINC synthetic fluid inclusion standards in the range of -56.6°C (triple point of CO_2) to +374.1°C (critical temperature of H_2O). These measurements indicate the accuracy of the temperature determinations is at least +/- 1°C in heating mode and +/-0.2°C in freezing mode. Dismountable doubly polished thin sections (Barker and Reynolds, 1984) were used for fluid inclusion studies.

General Heating Procedure

Small, about 4 mm by 4 mm, doubly polished chips of rock were broken or cut off of the thin section and centered in the heating stage. After perusing the slide, the fluid inclusions selected by the microscopist to be measured were monitored during heating to assure that the T_h of each fluid inclusion was not exceeded before measurement. The microscopist recorded the host mineral, the occurrence of the inclusion, dimensions of the fluid inclusion, V/L ratio, and nearby associated fluid inclusions (Appendix 4).

All T_h measurements were repeated at least once. If the measurements were in good agreement (about 2°C or less) then no more measurements were made on this fluid inclusion. When using the cycling method (Roedder, 1984; Goldstein and Reynolds, 1994) measurements continued until the microscopist was confident that the measurements were reproducible within a reasonable temperature range (generally less than +/- 3°C) dependent mostly on the visibility of the vapor bubble during heating.

Determination of Fracture Origin

Fluid inclusions formed during diagenesis or fluid inclusions identifable as reequilibrated found within framework grains of sandstones are essentially all fracture-bound "secondary" fluid inclusions. Evidence for trapping during crystal growth is rarely seen in detrital grains. Therefore, a key element of this study is the determination of the origin of the fractures that contain fluid inclusions. Framework grains in sandstones contain ubiquitous fracture bound and primary fluid inclusions inherited from their source area. These inherited fluid inclusions, unless reequilibrated during contact metamorphism, are irrelevant to the diagenesis of the rocks. Thus, discrimination of inherited versus diagenetic fluid inclusions is also a key element of this fluid inclusion study.

In some ambiguous cases of fluid inclusion origin, cathodoluminescence microscopy was used after heating of the fluid inclusions in a sample to gather more information on fluid

inclusion origin. Fractured and healed portions of a crystal can often be clearly observed under CL by the tendency of quartz cements formed during diagenesis to have little or no luminescence.

Fracture Types

Type A. The fracture cross cuts several sedimentary features such as framework grains, cement, lithified matrix and so forth. These fluid inclusions are post-depositional because of their crosscutting relationship to grain associations and contacts created during deposition of the sediment. Type A fractures may be formed during diagenesis or contact metamorphism. However, Type A fractures may also form after dike intrusion and thus may not have experienced contact metamorphism.

Type B. These fractures clearly involve grain edge and(or) apparent lithified matrix breakage but do not noticeably crosscut other framework grains in the field of view. In the best examples, diagenetic mineral matter may precipitate along the fracture. CL may show that the cement healing the fracture has a CL color or character like other demonstrably diagenetic materials in the rock. Type B fractures appear to be formed after sediment deposition. Type B fractures may also form after dike intrusion and thus may not have experienced contact metamorphism.

Type C. A fracture in a grain that, within the plane of the thin section, does not show any connection to features at framework grain edge or in the matrix adjacent to the grain. If observed at grain edge the fracture is clearly truncated and contained wholly within the framework grain. A type C fracture is apparently an inherited fracture and because it has been present since sediment deposition, the fluid inclusions trapped along it have definitely experienced contact metamorphism. These fractures are only used for paleotemperature determination when: (1) they are demonstrably reequilibrated by showing highly variable V/L

ratios and (2), A similar T_{peak} is indicated by several Type C fractures within several different grains in a sample.

Identification of Introduced Fractures

Identification of fractures introduced during sampling, processing into thin sections, and cutting up for use in the heating stage are identified by the presence of plastic if they were introduced during impregnation or the lack of epoxy if they were formed after. These fractures when sealed with epoxy may contain realistic-looking fluid inclusions but of course these inclusion do not respond in a normal way to heating. Further introduced fractures contain no diagenetic mineralization, I. e. cement. and fractures caused by dismounting form the glass for insertion into the heating stage have no real fluid inclusions or epoxy. Note that this study used small chips prepared for the heating stage by cutting up or scrubbing and breaking up the mounted thin section and glass slide as a unit.

Rules of T_h Measurement

1. Peruse slide and find the FIA with lowest V/L ratio and, if possible, determine its origin. If a fluid inclusion of this origin is significant in study design, then measure T_h. For this study the lowest V/L diagenetic or inherited fluid inclusions were measured first.
2. Cycling runs continue until T_h is bracketed to the limit made possible by clarity of host mineral and the inclusion itself -- but generally not more than +/- 3°C.
3. Edge up the cycling temperature by about 3°C increments until the vapor bubble does not grow back, the temperature of the final cycle is accepted as T_h.
4. Fluid inclusions lining fractures were preferentially used if they occur along a sharply defined fracture versus fluid inclusions along an intertwining fracture zone or diffuse wide band of inclusions. Only fluid inclusions along sharp fractures planes were measured

because this tactic may avoid fluid inclusions that are from another, possibly post-dike generation, or necked fluid inclusions. In a fracture zone unless the fluid inclusion is clearly trapped along the fracture there is a possibility of measuring an inherited fluid inclusion not reset by heating related to the dike.

5. Ideally study fractures containing three or more measurable fluid inclusions.

   T_h measurements on these related fluid inclusions to can demonstrate that reequilibration has occurred. The working hypothesis in this study is that when originally trapped most fracture bound inclusions initially trap a single phase of similar density because the vacuoles close over a narrow temperature range. Of course, the T_h of such fracture bound inclusions would initially be very consistent. After trapping, reequilibration of a fluid inclusion can modify the density of its contents. The extent to which each fluid inclusion will reequilibrate is dependent on size, position, shape and so forth. At room temperature, the variation in density is observed as a variable V/L ratio between fluid inclusions along the fracture. Upon heating, a wide variation in measured T_h confirms a variable V/L ratio and suggests that reequilibration has occurred. In fluid inclusions along inherited fractures, reequilibration may have occurred in the detrital source area. However, if a spatial and a reasonable temperature relationship to the dike is found, the T_h of reequilibrated fluid inclusions data is inferred to be the result of post-depositional contact metamorphism.

Mean Fracture Count

Measuring the mean fracture count in a sample involved using the method of Borg et al. (1960; as modified by Somerton, 1992) developed for studies of quartz and feldspar rich grain-supported rocks. The Somerton method counts the number of fractures (fracture count, FC) cutting quartz and feldspar grains along the ocular cross hairs at 400 x total magnification in 20 fields of view (FV) and computing the average Fracture count (FC/20).

Somerton's fracture index is computed by dividing the average FC in the heated sample by the corresponding number in the unheated sample before laboratory experiments. Thus, the Somerton fracture index cannot be computed for natural samples as it is not possible to measure the number of fractures in a sample before it was heated by contact metamorphism. This study just uses the average fracture count. Somerton's technique also needed to be adapted to the matrix rich Strzelecki Group sandstones.

In a Strzelecki Group sandstone, the number of quartz and feldspar grains in a given field of view can be low, sometimes with no such grains observed. Thus, an estimate based on a few fields of view could be significantly in error. Replicate runs on the same sample using 20 fields of view suggest a precision of analysis of -/+ 0.25 (FC/FV) which was considered poor. The number of fields of view counted was increased to 40 for this study. The nature of the Strzelecki sandstones also made it necessary to consider fractures in lithic fragments (mostly volcanic source) as well as quartz and feldspar framework grains.

To minimize operator bias in counting fractures, the samples were assigned numbers and polished sections made. These numbers were covered, and several samples were mixed up in order, so that the relation of the sample to the dike was not known during counting. Each field of view was selected without the microscopist looking down the microscope to avoid bias.

Introduced fractures were minimized by preparing the thin section being using low speed saws, cold-setting epoxy and procedures that avoid heating the sample (Barker and Reynolds, 1984). In addition, the first 5 mm or so at the edge of the polished thin section was not counted. Fractures in partially plucked grains were ignored. The stage was racked up and down on each fracture to assure that it is a planar feature and not a surface defect in the polish.

What the operator assesses as a fracture is the major variable in such studies. Only

intragranular fractures (those cutting framework grains) were counted. Intragranular fractures are considered to be any break, healed or open, that cut at least one framework grain somewhere in the field of view and also crossed the cross hairs. A fracture that curved and crossed the cross hairs multiple times was counted each time it crossed the hairs. Healed fractures are those filled with cement or delineated by fluid inclusion planes. Open fractures are detected as mechanical breaks at the thin section surface that are not lined by fluid inclusions or cement. Problematic grains are those that are cloudy or solid inclusion rich making it difficult to assess whether a fracture is present or not.

All of these procedural differences make my average fracture count different than the fracture index used by Somerton (1992). As stated above, Somerton's value is not comparable in any case because it is calculated by dividing his fracture count by the number of fractures in his unheated samples. This baseline fracture value is not available in natural samples. I consider these fracture counts at best to be internally consistent in that the same operator would get similar values, but another operator may find values that vary in magnitude while showing similar relative changes.

Quartz Undulosity

Samples of polished thin sections of concretions taken from next to the I-1 dike were supplied to L.J. Lewis to study for a Bachelor's of Science thesis (Saint Lawrence University, New York, Dr. Michael R. Owen, supervisor). Lewis (1993) analyzed the changes in quartz undulosity to determine if annealing of the quartz grains occurs as the dike is approached.

Lewis (1993) determined undulosity by measuring the extinction angle in some 100 quartz grains on a standard single axis rotating stage mounted on a petrographic microscope. Extinction angle is defined as the apparent angle between maximum extinction and no extinction. A grain was classed as non-undulose if the apparent extinction angle was less

than 5°. Undulose grains had an apparent extinction angle of greater than 5° (Basu et al., 1975). Basu et al. found that the apparent extinction angle is a good estimator of the true extinction angle. In over 90% of the grains studied by Basu et al., grains with a true extinction angle of >5° also had an apparent extinction angle of >5°.

Apatite Fission Track Annealing

AFT annealing samples were taken as large 1 to 3 kg bulk samples. At the laboratory, 100-200 g splits were pulverized and apatite concentrates prepared using heavy liquid separation at the Geotrack laboratories. AFT etching, counting, age dating and track length determination (annealing) in sedimentary rocks as used in this study are described by Marshallsea (1988), Green et al. (1989) and Naeser et al. (1989) among others.

Cathodoluminescence

The polishing and cathodoluminescence (CL) microscopy procedures used in this study are discussed in Barker and Wood (1986). Operating conditions of the Technosyn mark II cathodoluminescence stage were: 10-15 kv beam potential; 400-500 microampere beam current; and 0.05-0.1 torr pressure. As noted by Marshall (1978) these operating specifications do not describe conditions at the sample surface, so reproducing the exact conditions of measurement is difficult. However, CL is best generally used as a qualitative observational tool and relative operating conditions are adequate in this case.

Thermal Alteration of Rocks Caused by CL

Unfortunately, samples used for cathodoluminescence study appear to be unsuitable for use in subsequent fluid inclusion studies. Any CL observations potentially alter the fluid inclusions in the sample and render them useless. For example, on the Gippsland samples,

observation by CL beam produced color changes in the matrix and epoxy similar to those observed by heating chips to about 250°C during fluid inclusion observations. A pilot fluid inclusion study of sample temperatures reached during CL observations involved using single-phase aqueous fluid inclusions in calcite. These calcite samples consist of phreatic cements formed at low temperatures and trapped fluid inclusions that contained only liquid. These cements contained large single phase inclusions, a feature considered useful for this study because of their greater tendency to reequilibrate. The idea behind this kind of study is that heating caused by the electron beam impinging on the sample during CL observations causes the fluid inclusions to reequilibrate by exceeding their original trapping temperature. After sufficient heating in the electron beam and subsequent cooling, the single phase fluid inclusions may contain two-phase fluid inclusions caused by reequilibration. Cleavage fragments of the calcite were placed in a Technosyn stage at 15 kv and 300 microamperes for about 15 minutes. After cooling, fluid inclusions in the area under CL observation now contained two phase fluid inclusions. Using reequilibrated fluid inclusions, the peak temperature is measured by the uppermost mode of the homogenization temperature histogram. This simple exercise shows that sample temperatures can reach 220°C during typical CL observations (Barker, 1992).

X-Ray Diffraction

Sample preparation for XRD involved picking out the material of interest and finely pulverizing it. Both whole rock and <2 micron clay mineral fractions were used for mineral identification as appropriate to the sample characteristics. At the I-1 and I-2 dikes of the Gippsland Basin, the powder X-ray diffraction method was used to identify unknown minerals occurring in the host rock near the near dike contact. Analyses were done in the USGS laboratories, Denver, Colorado by Tom Finn. The sample preparation and XRD

instrumentation used are described in Pollastro (1982). Interpretation of clay mineral assemblages used the methods outlined in Moore and Reynolds (1989).

A1.3 GEOCHEMISTRY

Rock-Eval

Rock-Eval samples were prepared by selecting the more carbon-rich and least weathered looking material in a sample and finely pulverizing it. Analyses were performed on a Delsi Rock-Eval II instrument in the USGS Laboratories, Denver, by T.A. Daws . The Rock-Eval method is described by Espitalie et al. (1977; among others). Recent general discussions of the interpretation of Rock-Eval data include: Katz, 1983; Peters, 1986; and Langford and Blanc-Valleron, 1990. These reports are used extensively as a broad guideline for the interpretations made in this study.

Rock-Eval instrument initially heats the sample to 300°C causing a release of hydrocarbons that are quantified by the flame ionization detector response as the S_1 peak. The S_1 peak in Rock-Eval analyses is interpreted as indicating previously generated hydrocarbons (bitumen) that have accumulated over the geologic history of the sample and can be mobilized by this initial thermal distillation. The S_1 peak can be enhanced by the presence of migrated hydrocarbons that were generated elsewhere. The migrated hydrocarbons produce an anomalously high PI for the samples thermal maturation. The S_2 peak is produced by increased temperature produced by continuing the heating program beyond the S_1 distillation temperature range. The S_2 peak is produced by the remaining pyrolyzable hydrocarbon in the sample and is a measure of the hydrocarbon generation potential still remaining in the SOM. In practical terms, the S_2 peak is a measure of the volume of hydrocarbon that would be produced by further heating of the rock in nature. The S_3 peak measures CO_2 generated by the sample during the entire temperature program. The

CO_2 trapped by the device is analyzed after the temperature program is complete. The S_2 and S_3 peaks (or HI and OI which are normalized to TOC (annotated gC)) are proportional to hydrocarbon and oxygen content, respectively, in the organic matter (Espitalie et al., 1977).

Nuclear Magnetic Resonance

Solid state ^{13}C CP MAS NMR analysis was applied to coals from selected dikes samples, regional samples away from the dikes, a coal (sample R5) sampled from within the State coal mine (at Wonthaggi) and well core. The selected samples were prepared for NMR analysis by picking out clean coal chips from coal, coaly sandstone or mudstone, followed by crushing and pulverizing the chips. NMR analysis uses about 500 mg of powdered sample split of the picked coaly material. The ^{13}C NMR analyses were performed by G. P. Jones, Waite Solid State NMR Facility, The University of Adelaide.

In this study, ^{13}C NMR spectra were obtained by use of a Chemagnetics M-100 solid NMR spectrometer operating at a carbon frequency of 25.2 Mhz. The samples were packed in a 9 mm bullet rotor and spun at a frequency of approximately 3.5 kHz in the coils of a solids probe. A standard cross-polarization and magic angle-spinning sequence was employed, with a contact time of 1 msec, a pi/2 pulse of 6 μsec, and a pulse delay of 1 sec. These conditions were established to render the NMR spectra quantitative. The areas under aromatic and aliphatic signals were integrated. The aromatic spinning sideband areas were also integrated and added to the area for the aromatic carbons.

NMR is another form of absorption spectroscopy in which, under appropriate instrumental conditions, the susceptible nuclei in a sample selectively adsorb radiation and respond by attempting to align themselves within the magnetic field (Gize, 1986). The magnetic field affecting the susceptible nuclei will depend on the density of electrons between it and nearby nuclei. Electron density is controlled by the bond types between the

nuclei. The differences in bonding types are expressed as the chemical shift relative to a standard. The chemical shift is reported relative the standard compound tetramethysilane which by definition has a chemical shift of zero.

Solids can be analyzed by the use of cross polarization to enhance sensitivity and elimination of anisotropic chemical effects by "magic angle" spinning at 54.7° with respect to the external magnetic field (Gize, 1986). The solid state ^{13}C NMR spectra of coal samples examined here all contained two major peaks denoting aromatic and aliphatic carbons. The aromatic carbons in coal show a broad peak that stretches from about 100 ppm to 160 ppm (Table A1- 2). A shoulder at 150 ppm is assigned to aromatic carbons having an attached oxygen, as in phenolic structures. At about 175 ppm, a peak assigned to carboxyl carbons can be observed. At a higher chemical shift, a broad peak is observed and this peak is due to spinning side bands of aromatic carbons. An equivalent peak of equal intensity and of equidistant position on the other side of the aromatic peak is commonly found. In the case of this spectra, however, this peak is buried under the aliphatic-carbon peak, the other large peak extending from 0 to 80 ppm. A shoulder at approximately 15 ppm denotes aliphatic methyl groups.

A widely used parameter used to characterize thermal maturation is aromaticity (Appendix 8). The aromaticity is the ratio of the aromatic carbons to total summed carbons in the sample. Aromaticity in this study is computed as the sum of carbons (area) in the aromatic-phenolic peak, the two aromatic spinning side bands and the aromatic carbon-carbon and carbon-hydrogen peak. The aliphatic fraction in a sample is computed as the area of the aliphatic carbon peak minus the aromatic spinning side band that occurs in a chemical shift range similar to the aliphatic peak.

Table A1-2. Chemical Shift Assignments for ^{13} C CP MAS Nuclear Magnetic Resonance. (Modified from Axelson, 1985)

Chemical Shift Range	Carbon Bond Type
0 - 70	ALIPHATIC CARBONS ©
13 - 15	terminal methyls
17 - 19	CH_3 of ethyl
20 - 45	napthenic C
22 - 24	branched CH_3 groups; sterically crowded CH_2
23 - 30	certain Carbon-β to aromatic ring
29 -	sterically crowded CH ; branched CH_3 cyclic, acyclic CH_2; long chain CH_2
30 - 37	CH α to aromatic ring other than CH_3
30 - 55	branched centers; alicyclic C
37 - 53	methylene bridge C, bridgehead C of napthenes and branched alkyls
45 - 55	aliphatic C, CH, CH_2 at or adjacent to highly branched centers
50 - 90	ALIPHATIC CARBONS BONDED TO OXYGEN
51 - 67	methoxy carbons
50 - 75	aromatic, aliphatic ethers, esters
60 - 80	branched aliphatic ethers, thio-ethers; highly branched amines; acetylenic, thioacetylenic and allene type carbons
67 - 93	aliphatic ether or alcohol
75 - 95	glucoside, pyranoside moieties associated with cellulose, lignin, and so forth
93 - 129	AROMATIC C BOUND TO OXYGEN
108 - 118	aromatic CH ortho to ether-O and OH
112 - 117	pyrrole, furan ring structures; vinyl, substituted vinyl and alkylated aromatic rings
110 - 120	alkene structures; β -C in aromatic cyclic ethers (furans); ortho-C in phenols; phenolic ethers
129 - 137	METHYL SUBSTITUTED AROMATIC C
129 - 148	AROMATIC C-C; quaternary C in alkylated rings; bridgehead C; thio-ethers; aromatic C two bonds removed from N
148 - 158	phenol O-H
150 - 155	oxygen functional groups and aromatic C adjacent to N
137 - 160	alkyl substituted aromatic C
148 - 171	AROMATIC C BOUND TO O; hydroxy, methoxy and O atoms of diphenylether group
187 - 205	CARBONYLS in aldehydes, quinones, phenyl ketones
>205	CARBONYLS in alkanones, cycloalkanones

Hydrous Pyrolysis

The Gippsland basin regional sample R-5 was used for the hydrous pyrolysis experiments. R-5 is a coal sampled at about 60 m vertical depth and 300 m down an inclined shaft into the State Coal Mine at Wonthaggi, Victoria. This coal was from a recently exposed face in a new drift being cut by the miners at the time of my visit. For the experiments a total of about 10 kg of coal was coarsely crushed to 1-2 cm size. Fine sized coal was removed by screening with a 5.5 mm mesh sieve. A 150 g aliquot from this larger mass was split out for loading into the reactors. The experiments were performed under the supervision of M. D. Lewan in the USGS Organic Geochemistry Laboratories, Denver, Colorado using a method evolved from that described by Lewan (1985; 1993a, 1994).

Gas Chromatography

Gas chromatography analysis used selected samples of coals found on the east side of the SR1 dike, and the R5 coal from the subsurface. These rocks were prepared for extraction by finely pulverizing them. The sample R5 used in the hydrous pyrolysis experiments and the unheated sample were also extracted. These hydrous pyrolysis samples were not finely pulverized but were extracted directly using the 1-2 cm size particles prepared for hydrous pyrolysis, so that the pyrolysate and extracts would be more comparable. Solvent soluble material was extracted over 1-2 days using Soxhlet reflux chambers and chloroform. The extraction continued until the solvent color was clear, or in the extract-rich samples essentially clear.

Sample extraction, isolation of extract fractions, and gas chromatography (GC) analysis were performed by the author at the U.S. Geological Survey, Denver under the guidance of Paul Lillis and Mark Monk. The GC analysis used the C_{10+} plus saturated hydrocarbon fraction, that after removing asphaltene, was isolated from the extract by silica-alumina

column chromatography. Free oils recovered from the hydrous pyrolysis experiments were diluted in carbon disulfide to about 1-2 ppm concentration and injected directly into the GC. GC analysis was performed on a Hewlett-Packard 5880A GC equipped with a 50 m by 0.25mm, 5% phenyl methyl silicone (D) capillary column using hydrogen as the carrier gas. The GC was programmed to hold at 50°C for two minutes then from 50°C to 320°C at 4°C per minute and then held for 10 minutes.

Stable Isotope Analysis

Selected calcite veins, concretions and host rock were sampled for carbon and oxygen isotopic analysis (listed in Appendix 7). The calcite veins were sued whole for isotopic analyses because they showed little or no zonation under cathodoluminescence. The veins were sampled by drilling out calcite from freshly broken open surfaces or pieces were picked out of broken pieces of veins. Whole rock samples for stable isotope analysis were cut down to a unweathered core, using a water cooled diamond saw. the whole rock sample were cut to include only the host rock and exclude any visible vein material and burial cement. Weathered rock or vein calcite (often seen as stained or discolored) was removed by breaking it off the sample exterior to get fresh material at the core of the sample, and(or) grinding it off the exposed face, and(or) dissolving it off using hydrochloric acid.

Carbon dioxide gas for analysis was produced from 10-50 mg split of the ground sample. The CO_2 analyzed was liberated during reaction in anhydrous phosphoric acid at 25°C . Isotopic analyses used a MAT 251 PM ratio mass spectrometer run by Augusta Warden, U.S. Geological Survey Organic Geochemistry Laboratory, Denver, Colorado. In this system samples that produce gas yields of less than 0.5 ml should be used with caution. Those samples with less than 0.5 ml CO_2 yield from acid digestion were typically rerun using

larger sample masses. If CO_2 yield was still low (0.2 ml or less) the sample was listed as having insufficient yield and no analyses were reported. Methane and CO_2 gases recovered from hydrous pyrolysis experiments were analyzed directly by injection into the mass spectrometer port.

The mass spectrometer is calibrated through a laboratory standard gas produced from the U.S. National Bureau of Standards, carbonate standard TS NBS-19. Routine replicate analysis of TS NBS-19 in this laboratory have a precision of +/- 0.2 $^{o}/_{oo}$ (1 standard deviation) for oxygen and +/-0.1 for carbon. Carbonate analyses are reported relative to the PDB standard.

Carbon and oxygen isotopic analyses of CO_2 from carbonate minerals, CO_2 gas, and C in CH_4 gas are reported in δ annotation:

$$\delta\ ^{13}C \text{ or } \delta\ ^{18}O \text{ (in } ^{o}/_{oo}) = [R_{sample}/(R_{standard}-1)] \times 1000.$$

R_{sample} is the ratio of heavy to light isotope. the ratio for $\delta\ ^{13}C$ it is $^{13}CO_2/\ ^{12}CO_2$ and for $\delta\ ^{18}O$ it is $C(^{8}O_2\ /C^{16}O_2$ (Sofer, 1991). $R_{standard}$ is the respective ratio in an internationally accepted standard (in this study, PDB). By convention, All standards have δ values of 0.00 $^{o}/_{oo}$.

Whole Rock Elemental Analysis

One to two hundred grams of the least weathered-appearing host rock was pulverized using tungsten carbide or ceramic plates (composed of 85% aluminum oxide) until about 90% of the sample passed a brass 140 mesh (106 micron) screen. The fraction was submitted to Chemex Laboratories, Reno, Nevada for whole rock analysis by inductively coupled plasma atomic emission spectroscopy (ICP-AES). This analysis package includes the major element oxides: Al_2O_3, Fe_2O_3, MgO, CaO, Na_2O, K_2O, as well as the minor element oxides P_2O_5, Cr_2O_3, MnO, and loss on ignition (LOI) all reported to +/-0.01 wt.-% (Appendix 6). The trace elements Ba, Nb, Rb, Sr, Y and Zr are reported to +/- 10 ppm. Total

organic carbon analyses are available from Rock-Eval pyrolysis assay method. The analyses sum to near 100% in each case suggesting the analytical errors are small. Nevertheless, the major and minor element analyses were recomputed to 100% to distribute the error.

A1.4 GEOPHYSICS

Thermal Properties

Samples for thermal conductivity analysis were taken from the western onshore Gippsland Basin, Victoria, Australia (Appendix 10). The Gippsland sedimentary rock samples are all from the Strzelecki Group sandstones near the I1 and K1 dikes. The samples were taken on a line perpendicular to the I-1 and K-1 dike plane. A power saw with a water cooled blade was used to cut out the sample block. Where possible, the bedding plane, up direction, and direction to the dike were marked on the sample. This orientation procedure was used so that thermal conductivity measured in the sample would be measured in the same direction as heat flow from the dike. The sedimentary rock samples series from K-1 and I-1 are friable and somewhat water-sensitive in that they can disintegrate when wet. These rocks were finally sawn to shape using alcohol as a coolant.

Oriented samples with both up arrow and dike direction marked were taken at I1 at 0-10cm west; 100-112 cm west.; and 185 cm west. The K1 samples were all marked with an up arrow and bedding marked if obvious at 0.5 m west, 11 m west and 24.8 m west. The last sample is a relatively fresh gabbro from the B3 dike. The fresh gabbro is found in the cores of spheroidally weathered masses near the center of the dike exposed in a railroad cut. These rocks were analyzed by Colin F. Williams, USGS, Menlo Park, using the method of Sass et al. (1992). The samples were run water saturated at 20, 50, 100, and 150°C at a confining pressure of 34.5 MPa. At an average lithostatic pressure gradient of 24.4 MPa/Km (Hunt, 1979), this confining pressure equals a depth of 1.4 km. At a freshwater hydrostatic

pressure gradient of 9.8 MPa/km this confining pressure equals a depth of 3.5 km.

The samples were only run to 150°C because the samples had a tendency to flow at elevated temperature and pressure. Beyond 150°C, the sample began to disintegrate and further measurements would have been inaccurate.

Density, Permeability and Porosity

Samples for density, permeability and porosity measurement were cut out from the same rock blocks sawn out for thermal conductivity measurement. Rock plugs for analysis were cut out of these blocks using a 2.5 cm diameter diamond core barrel with water as a coolant. These plugs were dried and analyzed by Joe Weir, Core Laboratories, Houston, Texas, USA. (Appendix 10).

A1.5 BURIAL AND TEMPERATURE HISTORY RECONSTRUCTION

The burial and temperature history reconstruction for the Buchan Rift uses Platte River Associates (Denver, Colorado) BASINMOD for Windows computer program for burial depth, heat flow, porosity, thermal conductivity, temperature and thermal maturation (vitrinite reflectance) computations. Within BASINMOD, all models used: (1) Falvey and Middleton Compaction; (2) LLNL kinetic model for vitrinite reflectance predictions; and (3) a 5 m.y. time interval for computations. Formation thicknesses for estimating burial depth were compiled from the literature. Estimates of eroded thicknesses are discussed for each model in the text. The geologic age of the formation boundaries, times of erosion, or change in heat flow were converted to absolute time using the correlations of Haq and Eysinga (1994). If not measured directly, the lithology of the rocks was used for computing thermal conductivity in BASINMOD. The surface temperature history reconstructed from paleoclimate also remained constant. In the models, burial temperatures were changed by varying heat flow

within geologically reasonable limits until agreement was made between the temperature computed in BASINMOD and the T_{peak} or paleotemperature measured from fluid inclusion geothermometry, present day temperatures or T_{peak} predicted by a vitrinite reflectance geothermometer for burial diagenesis (Barker and Pawlewicz, 1994). The limits of heat flow variation were estimated from the reconstructed changes in tectonic regime over geologic time and the heat flow range to tectonic regime correlation of Allen and Allen (1990).

Appendix 2. Sample Locality and Organic Petrography Data

Appendix 2-1. Sample Locality and Rb-r Data, Buchan Rift

Regional Locality, Lithology	Latitude (°south)	Longitude (°east)	Rb-r	s	n	s/mean	Range	BMode	Quality
91-1, mdst	37.4983	148.1688	-----	------	----	------	-----	-----	B
91-2, mdst	37.4901	148.1707	1.80	0.20	13	0.11	1.3-2.03	2.2**	F
91-3, mdst	37.4875	148.1707	2.03	0.33	6	0.13	1.73-2.60	2.7**	P
91-4, mdst	37.4567	148.1957	----	-----	----	------	-----	-----	B
91-5, mdst, Cromie (1990)	37.4575	148.2125	2.48	0.52	41	0.11	1.99-2.99	3.0**	F
Dike/ X, in meters with direction	Rock Type	Mount type	mean Rb-r	s	n	s/mean	Range	BMode	Quality
Murrindal Dike (M1)	Latitude: 37.4192°S	Longitude: 148.2058°E							
M1/ 0.45 S	Limestone	Concentrate	2.60	0.36	34	0.14	1.73-3.16	3.2	F
M1/ 0.45 S	Limestone	Concentrate	2.36*	0.20	7	0.07	2.05-2.70	2.7	P
M1/ 0.93 S	Limestone	Concentrate	2.43*	0.22	11	0.09	2.11-2.72	2.7	P
M1/ 2.18 S	Limestone	Concentrate	2.75*	0.20	15	0.25	2.30-3.10	3.10	F
M1/ 3.03 S	Limestone	whole rock	2.13	0.40	26	0.16	1.08-2.69	2.7	F
M1/ 3.03 S	Limestone	Concentrate	2.52*	0.09	31	0.04	2.36-2.66	2.66	G
M1/ 5.45 S	Limestone	Concentrate	2.92*	0.07	25	0.02	2.80-3.05	3.05	G
M1/ 6.28 S	Limestone	Concentrate	2.62*	0.15	21	0.06	2.11-2.86	2.86	G
M1/ 0.54 N	Limestone	Whole Rock	2.84	0.27	3	0.10	2.53-3.04	3.0	P
M1/ 9.8 N	Limestone	Whole Rock	2.46*	0.14	6	0.06	2.27-2.60	2.6	P
M1/ 16 N	Limestone	Vitrinite	1.87*	0.36	10	0.20	1.45-2.38	2.4	P
M1/ 21 N	Limestone	Whole Rock	-----	-----	----	------	-----	-----	B

*Analyses by M.J. Pawlewicz, USGS, Denver. Applicable to this page only.

** UDE from range or established using polished fluid inclusion sections--this Rb-r data has been used in chapter 2.

Appendix 2-2. Location and Regional Rv-r data, Western Onshore Gippsland Basin

Locality, Lithology	Latitude (°south)	Longitude (°east)	mean	s	n	s/mean	Range	BM e o d s t e	Quality
R-1, mdst	38.5503	145.6603	0.47	0.02	32	0.04	N/R	N/R	G
R-2, coaly mdst	38.5222	145.7001	2.06	0.33	34	0.16	1.5-3.0	1.9	F
R-2A, coaly ss	38.5212	145.7010	0.47	0.03	38	0.06	0.42-0.54	0.55	P
R-3, sltst	38.4794	145.7617	0.95	0.28	24	0.30	0.4- 1.6	1.0	?
R-4, coaly ss	38.4469	145.8009	----	----	----	----	----	----	B
R-5, coal	38.6249	145.5939	0.62	0.04	30	0.06	0.56-0.69	0.62	G
R-6, coaly ss	38.6639	145.6795	0.52	0.02	50	0.04	0.48-0.59	0.55	G
R-7, coaly ss	38.4284	145.8193	0.92	0.11	35	0.12	0.75-1.22	0.85	P
R-8, coal	38.4352	145.8276	0.62	0.05	31	0.08	0.52-0.70	0.65	G
R-9, coal	38.6555	145.6847	----	----	----	----	----	----	B
R-10, coaly ss	38.5339	145.6515	0.46	0.02	31	0.04	0.41-0.49	0.47	G
R-11, coaly ss	38.4610	145.6917	0.41	0.03	30	0.07	0.36-0.45	0.42	F
R-12, coal	38.4176	145.7500	0.43	0.03	30	0.06	0.33-0.48	0.43	F
R-13, coaly ss	38.3774	145.8328	0.56	0.04	30	0.07	N/R	0.55	F
R-13A, coal	38.3765	145.8355	0.49	0.04	31	0.08	0.42-0.31	0.48	F
R-14, coaly sltst	38.3195	145.7691	0.95	0.13	24	0.14	0.75-1.16	1.05	F
R-15, coaly ss	38.3833	145.7016	0.70	0.08	17	0.11	0.55-0.87	0.75	P
R-16, coaly mdst	38.4610	145.6404	0.80	0.10	31	0.13	0.62-1.04	0.80	F
R-17, ss	38.5563	145.5777	0.47	0.05	31	0.11	0.40-0.56	0.48	F
R-18, coal	38.6748	145.6308	0.74	0.05	31	0.07	0.61-0.84	0.76	F
R-19, coaly mdst	38.6748	145.6380	0.66	0.04	30	0.06	0.56-0.77	0.68	G
R-20, coaly mdst	38.5572	145.4799	0.70	0.03	40	0.04	0.60-0.74	0.70	G
R-21, coal	38.5232	145.3903	0.65	0.05	12	0.08	0.59-0.73	0.70	P
R-22, coal	38.5331	145.3689	0.63	0.03	20	0.05	0.56-0.70	------	p

Appendix 2-2. Location and Regional Rv-r data, Western Onshore Gippsland Basin

Locality, lithology	Latitude (°south)	Longitude (°east)	mean	s	n	s/mean	Range	Best Mode	Quality
R-23, coal	38.5378	145.3966	0.76	0.03	51	0.04	0.69-0.81	0.75	G
R-24, coaly mdst	38.6577	145.6840	----	----	----	----	----	----	B
R-25, coal	38.5378	145.3895	0.61	0.03	31	0.05	0.56-0.66	0.63	F
R-26, cc vein	38.5378	145.3965	N/A				vein only		-
R-27, coal	38.5514	145.4603	0.75	0.04	30	0.05	0.64-0.81	0.78	G
R-28, coal	38.5378	145.3859	0.72	0.04	30	0.06	0.65-0.85	0.70	G
R-29, coaly ss	38.5392	145.4054	0.65	0.07	16	0.11	0.55-0.78	0.70	P
R-30, coaly ss	38.4122	145.7617	0.47	0.02	32	0.04	0.44-0.53	0.47	P
R-31, coaly mdst	38.3337	145.7876	0.51	0.06	30	0.12	0.32-0.65	0.53	F
R-32, mdst	38.3281	145.8289	0.56	0.03	25	0.05	0.51-0.62	0.57	F
R-33, mdst	38.5415	145.5054	0.59	0.05	5	0.08	0.54-0.68	0.6	P
R-34, coaly ss	38.5145	145.4965	0.45	----	1				B
R-35, ss	38.5020	145.5698	0.80	0.09	30	0.11	0.68-1.00	0.9	F
R-36, ss	38.4468	145.6741	0.72	0.06	14	0.08	0.62-0.80	0.7	P
R-37, mdst	38.3705	145.7016	----	----	----	----	----	-----	B
R-38, coal	38.3897	145.7443	0.52	0.03	50	0.06	0.43-0.61	0.5	G
R-39, coaly ss	38.4207	145.7038	0.96	0.14	31	0.14	0.58-1.19	1.1	P
R-40, coaly ss	38.4185	145.8747	0.53	0.03	15	0.06	0.49-0.59	0.53	F
R-41, coaly ss	38.6404	145.7239	0.62	0.08	13	0.13	0.46-0.74	0.7	P
R-42, ss	38.6342	145.7948	0.68	0.09	12	0.13	0.56-0.89	0.65	P
R-43, coaly ss	38.5648	145.9524	0.79	0.07	16	0.09	0.69-0.91	0.7	P
R-44, ss	38.4777	145.8393	----	----	----	----	----	----	B
R-45, coal	38.6444	145.5540	0.57	0.05	31	0.02	0.49-0.73	0.60	P

Appendix 2-2. Dike Related Rv-r Data, Western Onshore Gippsland Basin

Dike/ X, in meters with direction	Rock Type	Mount type	mean	s	n	s/mean	Range	Best Mode	Quality
Bena 1 (B1) (3.4 m thick)	Latitude: 38.4113°S	Longitude: 145.7646°E							
B1/ 0.025 W	coaly ss	picked coal	4.02	0.20	50	0.05	3.54-4.38	4.05	G
B1/ 0.125 W	coaly ss	picked coal	2.54	0.07	50	0.03	2.39-2.66	2.6	G
B1/ 0.30 W	coaly ss	picked coal	1.07	0.09	21	0.08	0.88-1.23	1.05	P
B1/ 0.55 W	coaly ss	picked coal	0.95	0.06	50	0.06	0.75-1.04	0.95	F
B1/ 1.05 W	coaly ss	picked coal	0.95	0.04	31	0.04	0.87-1.04	0.95	F
B1/ 1.5 W	coaly ss	picked coal	0.60	0.09	41	0.15	0.41-0.72	0.68	P
B1/ 2.05 W	coaly ss	picked coal	0.53	0.02	50	0.04	0.45-0.56	0.55	F
B1/ 2.55 W	coaly ss	picked coal	0.52	0.03	39	0.06	0.46-0.57	0.55	F
B1/ 3.05 W	coaly ss	picked coal	0.48	0.02	50	0.04	0.41-0.53	0.45	F
B1/ 4.25 W	coaly ss	picked coal	0.44	0.03	50	0.07	0.39-0.50	0.43	P
B1/ 6.25 W	coaly ss	picked coal	0.45	0.04	23	0.09	.35-0.50	0.47	P
Bena-1 (B1) whole rock	Latitude: 38.4113°S	Longitude: 145.7546°E							
B1/ 0.11 W	coaly ss	whole rock	2.34	0.94	19	0.40	1.13-5.02	2.7	P
B1/ 0.4 W	ss	whole rock	3.68	0.31	30	0.08	3.07-4.18	4.1	F
B1/ 0.55 W	coaly ss	whole rock	1.59	0.36	28	0.23	1.03-2.14	2.0	P
B1/ 1.05 W	coaly ss	whole rock	1.05	0.06	30	0.06	0.89-1.15	1.1	G
B1/ 1.55 W	coal	whole rock	0.80	0.09	9	0.11	0.68-0.92	0.75	P
B1/ 2.05 W	coal	whole rock	0.54	0.03	30	0.06	0.49-0.59	0.55	P
Bena-3 (B-3) (20.1 m thick)	Latitude: 38.4090°S	Longitude: 145.7563°E							
B3/ 0-0.01 E	ss	whole rock	5.79	0.61	31	0.11	4.59-6.74	6.2	G

Appendix 2-2. Dike Related Vitrinite Reflectance Data, Western Onshore Gippsland Basin

Dike/ X, in meters with direction	Rock Type	Mount type	mean	s	n	s/mean	Range	Best Mode	Quality
B3/ 1.0 E	ss	whole rock	5.68	0.34	17	0.06	5.24-6.44	5.7	G
B3/ 3 E	ss	whole rock	5.07	0.36	32	0.07	4.37-5.61	5.1	F
B3/ 5 E	ss	whole rock	----	----	----	----	----	----	B
B3/ 7 E	ss	whole rock	----	----	----	----	----	----	B
B3/ 10 E	ss	whole rock	3.54	0.38	16	0.11	2.88-4.32	3.4	P
B3/ 13 E	ss	whole rock	2.91	0.32	25	0.32	2.46-3.50	3.1	A
B3/ 16 E	ss	whole rock	2.71	0.18	4	0.07	2.53-2.96	-----	P
B3/ 20 E	ss	whole rock	2.39	0.25	10	0.10	2.12-2.75	-----	P
B3/ 25 E	ss	whole rock	1.90	0.71	10	0.37	0.79-2.82	-----	P
B3 /30 E	mdst	whole rock	1.32	0.10	22	0.08	1.12-1.49	1.40	G
Cruickston-1 (41 m thick)	Latitude: 38.3580°S	Longitude: 145.8070°E							
Cru1/ 0.4 E	mdst	whole rock	3.26	0.59	5	0.18	2.26-3.78	-----	P
Cru1/ 0.8 E	mdst	whole rock	3.84	0.24	11	0.06	3.57-4.35	3.9	F
Cru1/ 2 E	mdst	whole rock	4.39	0.38	30	0.09	3.84-5.35	4.0	G
Cru1/ 5 E	mdst	whole rock	3.57	0.35	26	0.10	3.02-4.33	3.7	F
Cru1/ 10 E	mdst	whole rock	3.29	0.14	32	0.04	2.90-3.65	3.3	G
Cru1/ 16 E	mdst	whole rock	3.95	0.37	23	0.09	3.18-4.93	4.1	F
Cru!/ 30 E	mdst	whole rock	4.44	0.62	22	0.14	3.73-6.36	4.4	F
Cru1/ 45 E	mdst	whole rock	4.21	1.10	6	0.26	3.28-6.29	-----	P
Cru1/ 55 E	mdst	whole rock	2.99	0.94	26	0.31	1.78-5.52	3.1	P
Cru1/ 65 E	mdst	whole rock	3.07	0.68	32	0.22	2.01-5.38	3.5	G

Appendix 2-2. Dike Related Vitrinite Reflectance Data, Western Onshore Gippsland Basin

Dike/ X, in meters with direction	Rock Type	Mount type	mean	s	n	s/mean	Range	Best Mode	Quality
Inverloch 1 (I1) (1.7 m thick)	Latitude: 38.6572°S	Longitude: 145.6865°E							
I1/0-0.02W	coaly ss	picked coal	4.83	0.36	6	0.07	4.36-5.24	-----	P
I1/0.04-0.07W	coaly ss	picked coal	4.82	0.23	8	0.05	4.35-5.31	-----	P
I1/0.07-0.09W	coaly ss	picked coal	4.54	0.43	30	0.09	3.48-5.38	-----	G
I1/0.10W	coaly ss	picked coal	4.40	0.41	10	0.09	3.06-5.23	-----	G
I1/0.20W	coaly ss	picked coal	4.86	0.25	11	0.05	4.56-5.38	-----	G
I1/0.50W	coaly ss	picked coal	3.57	0.31	16	0.09	2.90-3.92	-----	A
I1/0.70W	coaly ss	picked coal	2.98	0.14	32	0.05	2.58-3.21	-----	A
I1/1.0W	coaly ss	picked coal	1.95	0.15	25	0.08	1.60-2.21	-----	A
I1/1.5W	coaly ss	picked coal	0.90	0.07	16	0.08	0.78-1.02	-----	P
I1/2.0W	coaly ss	picked coal	0.65	0.09	14	0.14	0.53-0.87	-----	P
I1/2.5W	coaly ss	picked coal	0.59	0.07	16	0.12	0.50-0.77	-----	P
I1/3.0W	coaly ss	picked coal	0.63	0.07	8	0.11	0.52-0.73	-----	P
I1/3.5W	coaly ss	picked coal	0.56	0.14	5	0.25	0.38-0.71	-----	P
I-1 east									
I1/0.04-0.05E	coaly ss	picked coal	3.99	0.71	11	0.18	3.04-5.11	-----	P
I1/0.08-0.09E	coaly ss	picked coal	4.24	0.48	20	0.11	3.05-4.83	-----	A
I1/0.17-0.21E	coaly ss	picked coal	4.08	0.26	22	0.06	3.61-4.65	-----	A
I1/0.38-0.41E	coaly ss	picked coal	2.63	0.15	31	0.06	2.38-3.13	-----	G
I1/0.48-0.50E	coaly ss	picked coal	2.00	0.04	31	0.02	2.17-2.35	-----	G
I1/0.70-0.80E	coaly ss	picked coal	1.20	0.04	30	0.03	1.08-1.25	-----	G
I1/0.90-0.94E	coaly ss	picked coal	0.87	0.09	30	0.10	0.68-.1.08	-----	G
I1/1.0-1.1E	coaly ss	picked coal	0.72	0.02	31	0.03	0.67-0.76	-----	G

Appendix 2-2. Dike Related Vitrinite Reflectance Data, Western Onshore Gippsland Basin

Dike/ X, in meters with direction	Rock Type	Mount type	mean	s	n	s/mean	Range	Best Mode	Quality
I1 East									
I1/1.30-1.35E	coaly ss	picked coal	1.07	0.12	30	0.11	0.85-1.28	-----	A
I1/1.60-1.65E	coaly ss	picked coal	0.47	0.03	30	0.06	0.40-0.54	-----	A
I1/1.90-2.00E	coaly ss	picked coal	0.47	0.05	30	0.11	0.37-0.57	-----	P
Inverloch 2 (I2) (0.4 m thick)	Latitude:38.653°S	Longitude: 145.6902°E							
I2/0.0-0.01E	coaly ss	picked coal	4.70	0.21	31	0.05	4.13-5.00	-----	G
I2/0.04-0.06E	coaly ss	picked coal	3.37	0.49	35	0.15	2.39-3.85	-----	G
I2/0.10-0.12E	coaly ss	picked coal	2.04	0.15	30	0.07	1.79-2.45	-----	G
I2/0.19-0.22E	coaly ss	picked coal	1.02	0.06	30	0.06	0.87-1.15	-----	G
I2/0.29-0.32E	coaly ss	picked coal	0.63	0.03	30	0.05	0.58-0.70	-----	G
I2/0.31-0.35E	coaly ss	picked coal	0.91	0.03	30	0.03	0.84-0.97	-----	G
I2/0.37-0.42E	coaly ss	picked coal	0.54	0.04	30	0.07	0.47-0.62	-----	A
I2/0.48-0.52E	coaly ss	picked coal	0.50	0.02	26	0.04	0.46-0.55	-----	A
I2/0.54-0.57E	coaly ss	picked coal	0.43	0.02	30	0.05	0.38-0.51	-----	P
I2/0.68-0.72E	coaly ss	picked coal	0.49	0.03	30	0.06	0.44-0.57	-----	A
I2/0.84-0.86E	coaly ss	picked coal	0.49	0.02	30	0.04	0.46-0.56	-----	A
I2/0.82-0.88E	coaly ss	picked coal	0.48	0.03	30	0.06	0.44-0.58	-----	A
I2/0.98-1.02E	coaly ss	picked coal	0.50	0.04	30	0.08	0.45-0.63	-----	A
I2/1.37-1.40E	coaly ss	picked coal	0.45	0.02	30	0.04	0.39-0.49	-----	P
I2/1.45-1.47E	coaly ss	picked coal	0.54	0.04	21	0.07	0.41-0.59	-----	A
I2/1.95-2.02E	coaly ss	picked coal	0.49	0.03	30	0.06	0.45-0.57	-----	P

Appendix 2-2. Dike Related Rv-r Data, Western Onshore Gippsland Basin

Dike/ X, in meters with direction	Rock Type	Mount type	mean	s	n	s/mean	Range	Best Mode	Quality
I-2 west									
I2/0.01-0.04W	coaly ss	picked coal	2.69	0.14	30	0.05	2.46-2.98	-----	G
I2/0.08-0.12W	coaly ss	picked coal	2.20	0.11	30	0.05	2.04-2.55	-----	G
I2/0.18-0.22W	coaly ss	picked coal	1.53	0.09	30	0.06	1.42-1.78	-----	G
I2/0.28-0.32W	coaly ss	picked coal	1.19	0.04	32	0.03	1.10-1.26	-----	G
I2/0.39-0.44W	coaly ss	picked coal	1.03	0.04	37	0.04	0.90-1.10	-----	G
I2/0.50-0.54W	coaly ss	picked coal	0.90	0.02	40	0.02	0.85-0.94	-----	G
I2/0.78-0.82W	coaly ss	picked coal	0.62	0.02	31	0.03	0.57-0.65	-----	G
Inverloch 3 (I3) (0.17 m thick)	Latitude:38.653°S	Longitude: 145.6902°E							
I3/0.0-0.02E	coaly ss	picked coal	3.74	0.44	40	0.12	3.09-4.62	-----	A
I3/0.02-0.04E	coaly ss	picked coal	2.05	0.20	33	0.10	1.55-2.43	-----	G
I3/0.05-0.07E	coaly ss	picked coal	1.54	0.07	31	0.05	1.33-1.64	-----	G
I3/0.07-0.09E	coaly ss	picked coal	0.92	0.07	30	0.08	0.78-1.08	-----	A
I3/0.09-0.11E	coaly ss	picked coal	0.70	0.05	30	0.07	0.58-0.82	-----	A
I3/0.13-0.15E	coaly ss	picked coal	0.60	0.03	30	0.05	0.55-0.65	-----	A
I3/0.16-0.18E	coaly ss	picked coal	0.53	0.04	31	0.08	0.46-0.63	-----	G
I3/0.18-0.20E	coaly ss	picked coal	0.57	0.05	33	0.09	0.48-0.70	-----	G
I3/0.20-0.22E	coaly ss	picked coal	0.64	0.04	30	0.06	0.57-0.74	-----	G
I3/0.25-0.27E	coaly ss	picked coal	0.58	0.04	31	0.07	0.48-0.68	-----	G
I3/0.27-0.30E	coaly ss	picked coal	0.55	0.04	31	0.07	0.50-0.68	-----	A
I3/0.35-0.37E	coaly ss	picked coal	0.58	0.04	25	0.07	0.51-0.68	-----	P
I3/0.40-0.42E	coaly ss	picked coal	0.61	0.05	30	0.08	0.52-0.74	-----	P
I3/0.50-0.52E	coaly ss	picked coal	0.57	0.03	30	0.05	0.50-0.64	-----	P
I3/0.23-0.25E	coaly ss	picked coal	0.57	0.03	21	0.05	0.53-0.64	-----	A

Appendix 2-2. Dike Related Rv-r Data, Western Onshore Gippsland Basin

Dike/ X, in meters with direction	Rock Type	Mount type	mean	s	n	s/mean	Range	Best Mode	Quality
Korumburra 1 (K1) (35 m thick)	Latitude: 38.431°S	longitude: 145.8227°E							
K1/ 2W	ss	whole rock	5.19	0.52	10	0.10	4.26-6.02	-----	P
K1/ 4.3W	mdst	whole rock	4.90	0.32	5?	0.07	4.50-5.37	-----	P
K1/ 7W	mdst	concentrate	4.27	0.22	30	0.05	3.90-4.80	-----	P
K1/ 7W	mdst	whole rock	3.43	0.42	10	0.12	2.80-3.90	-----	P
K1/ 10W	carb mdst	picked coal?	3.81	0.27	18	0.07	3.21-4.27	-----	A
K1/ 11W	ss	concentrate	-----	-----	----	-----	-----	-----	B
K1/ 12W	carb ss	picked coal	3.28	0.37	15	0.11	2.41-3.76	-----	A
K1/ 15W	ss	picked coal	1.18	0.13	31	0.11	0.94-1.59	-----	P
K1/ 15.8W	carb mdst	whole rock	1.96	0.38	36	0.19	1.38-2.94	-----	G
K1/ 17W	carb mdst	picked coal	1.35	0.12	31	0.09	1.13-1.68	-----	A
K1/ 20W	ss	picked coal	0.90	0.06	30	0.07	0.82-1.05	-----	A
K1/ 25W	carb mdst	picked coal	0.46	0.05	9	0.11	0.39-0.56	-----	P
K1/ 30W	carb mdst	picked coal	0.42	0.03	18	0.07	0.37-0.50	-----	P
K1/ 35W	carb mdst	picked coal	0.41	0.05	17	0.12	0.35-0.56	-----	P
K1/ 36W	carb mdst	picked coal	0.56	0.05	9	0.09	0.50-0.64	-----	P
K1/ 40W	carb mdst	picked coal	0.48	0.07	31	0.15	0.36-0.61	-----	P
K1/ 50W	coaly mdst	picked coal	0.60	0.06	7	0.10	0.49-0.67	-----	P
K1/ 60W	coaly ss	picked coal	0.28	0.03	30	0.11	0.23-0.34	-----	A

Appendix 2-2. Dike Related Rv-r Data, Western Onshore Gippsland Basin

Dike/ X, in meters with direction	Rock Type	Mount type	mean	s	n	s/mean	Range	Best Mode	Quality
San Remo-1 (SR1) (0.6 m thick)	Latitude: 38.538°S	Longitude: 145.3965°E							
SR1/ 0.075 W	coaly ss	picked coal	2.03	0.46	18	0.22	1.25-3.03	-----	A
SR1/ 0.2 W	coaly ss	picked coal	2.07	0.18	31	0.09	1.70-2.51	-----	G
SR1/ 0.3 W	coaly ss	picked coal	1.60	0.17	14	0.11	1.23-1.85	-----	A
SR1/ 0.5 W	coaly ss	picked coal	1.05	0.04	50	0.04	0.97-1.14	-----	G
SR1/ 0.7 W	coaly ss	picked coal	0.78	0.06	50	0.08	0.69-0.88	-----	G
SR1/ 0.9 W	coaly ss	picked coal	0.73	0.05	50	0.07	0.61-0.83	-----	G
SR1/ 1.0 W	coaly ss	picked coal	0.72	0.06	50	0.08	0.61-0.84	-----	G
SR1/ 1.3 W	coaly ss	picked coal	0.72	0.06	50	0.08	0.59-0.81	-----	G
SR1/ 1.6 W	coaly ss	picked coal	0.69	0.07	50	0.10	0.56-0.83	-----	G
SR1/ 2.0 W	coaly ss	picked coal	0.65	0.05	48	0.08	0.53-0.78	-----	G
SR1/ 3.0 W	coaly ss	picked coal	0.80	0.08	31	0.10	0.62-0.91	-----	A
SR 1 east GC series									
SR1/ 0.36 E	coal	whole rock	1.80	0.14	25	0.08	1.39-1.99	-----	G
SR1/0.65 E	coal	whole rock	0.91	0.06	33	0.07	0.82-1.09	-----	G
SR1/0.98 E	coal	whole rock	0.73	0.06	33	0.08	0.63-0.87	-----	G
SR1/ 1.07 E	coal	whole rock	0.71	0.02	30	0.03	0.66--0.75	-----	G

Appendix 2-2. Dike Related Rv-r Data, Western Onshore Gippsland Basin

Dike/ X, in meters with direction	Rock Type	Mount type	mean	s	n	s/mean	Range	Best Mode	Quality
SR1 east symmetry series									
SR1/0.0E	coaly ss	picked coal	3.73	0.28	28	0.08	3.24-4.50	-----	A
SR1/0.10E	coaly ss	picked coal	1.79	0.21	18	0.12	1.48-2.16	-----	P
SR1/0.20E	coaly ss	picked coal	1.61	0.14	36	0.09	1.33-1.86	-----	G
SR1/0.30E	coaly ss	picked coal	1.55	0.20	36	0.13	1.29-1.99	-----	G
SR1/0.65E	coaly ss	picked coal	1.03	0.05	30	0.05	0.95-1.18	-----	G
SR1/ 0.85E	coaly ss	picked coal	0.63	0.03	33	0.05	0.58-0.68	-----	G
SR1/ 1.00E	coaly ss	picked coal	0.71	0.03	30	0.04	0.66-0.76	-----	G
SR1/ 1.20E	coaly ss	picked coal	0.70	0.02	30	0.03	0.66-0.75	-----	G
SR1/ 1.40E	coaly ss	picked coal	0.68	0.03	32	0.04	0.63-0.74	-----	G
SR1/ 1.60E	coaly ss	picked coal	0.62	0.02	30	0.03	0.58-0.70	-----	G
SR1/ 2.00E	coaly ss	picked coal	0.58	0.03	32	0.05	0.53-0.65	-----	G
SR1/ 2.45E	coaly ss	picked coal	0.72	0.03	30	0.04	0.65-0.76	-----	G

Appendix 2-2. Dike Related Rv-r Data, Western Onshore Gippsland Basin

Dike/ X, in meters with direction	Rock Type	Mount type	mean	s	n	s/mean	Range	Best Mode	Quality
San Remo 3 (SR3) 0.06 m thick	Latitude:38.538°S	Longitude: 145.3963°E							
SR3/0.0-0.005W	coaly ss	picked coal	3.06	0.14	4	0.05	2.86-3.20	-----	A
SR3/0.01-0.015W	coaly ss	picked coal	1.30	0.25	19	0.20	0.76-1.71	-----	A
SR3/0.017-0.023W	coaly ss	picked coal	1.14	0.08	50	0.07	1.04-1.40	-----	G
SR3/0.029-0.034W	coaly ss	picked coal	0.88	0.06	50	0.07	0.71-0.98	-----	G
SR3/0.039-0.044W	coaly ss	picked coal	0.87	0.04	51	0.05	0.78-0.96	-----	G
SR3/0.048-0.053W	coaly ss	picked coal	0.83	0.03	51	0.04	0.73-0.89	-----	G
SR3/0.059-0.064W	coaly ss	picked coal	0.86	0.03	52	0.03	N/R	-----	G
SR3/0.07W	coaly ss	picked coal	0.85	0.04	30	0.05	0.70-0.87	-----	G
SR3/0.09W	coaly ss	picked coal	0.77	0.04	50	0.05	0.70-0.87	-----	G
SR3/0.14W	coaly ss	picked coal	0.69	0.04	52	0.06	0.50-0.77	-----	G
SR3/0.19W	coaly ss	picked coal	0.75	0.04	37	0.05	0.70-0.83	-----	G
SR3/1.40W	coaly ss	picked coal	0.71	0.05	39	0.07	0.58-0.80	-----	G
SR3 east									
SR3/0.4E	coaly ss	picked coal	0.64	0.04	50	0.06	0.55-0.72	-----	G

Appendix 2-2. Well Related Rv-r Data, Western Onshore Gippsland Basin

Well name/ Depth in meters	Rock Type	Mount type	mean	s	n	s/mean	Range	Best Mode	Quality
Tarwin Meadows 1 (TM1)	Latitude: 38.7239°S	longitude: 145.8600°E							
TM1/ 94.5	coaly ss	whole rock	0.61	0.07	30	0.11	0.45-0.77	-----	G
TM1/ 490	coaly ss	picked coal	0.5 ?	0.04	30	0.08	0.42-0.58	-----	G
TM1/ 782.5	mdst	picked coal	0.72	0.03	30	0.04	0.67-0.81	-----	G
TM1/ 953	coaly mdst	picked coal	1.11	0.17	17	0.15	0.70-1.30	-----	P
The TM1/ 490 sample contained abundant liptinite that reduces the reflectance of the vitrinite and the resulting Rv-r is suppressed. The Rv-r data from this sample was not used in further data analysis.									
Wellington Park 1 (WP1)	Latitude: 38.1404°S	Longitude: 147.375°E							
WP1/ 753	coaly mdst	whole rock	0.36	0.03	31	0.08	0.29-0.44	-----	P
WP1/ 1010	coal	picked coal	0.40	0.03	31	0.07	0.35-0.45	-----	G
WP1/ 1134	coaly ss	picked coal	0.45	0.03	31	0.07	0.40-0.49	-----	G
WP1/ 1323	coaly ss	picked coal	0.51	0.06	13	0.12	0.39-0.61	-----	P
WP1/ 2088	coaly mdst	picked coal	0.77	0.03	30	0.04	0.71-0.82	-----	G
WP1/ 2564	coaly mdst	picked coal	0.94	0.04	31	0.04	0.84-1.01	-----	G
WP1/3050	coaly ss	picked coal	1.46	0.06	31	0.04	1.34-1.57	-----	G
WP1/3649	coaly ss	picked coal	1.89	0.13	30	0.07	1.66-2.18	-----	G

Appendix 3. A Compilation of Temperature and Solid Bitumen Reflectance Data.

Abbreviations specific to this table: max = microscope stage rotation to maximum reflectance and this value measured; N/A = not applicable; N/R = not reported; ran = no rotation, random reflectance measured; Texture = temperature estimated from coke texture; Type III used in this case as a type of solid bitumen; A query mark next to a data point suggests some uncertainty in which distribution statistic or measurement method was used.

Appendix 3-1. A Compilation of Temperature and Solid Bitumen Reflectance Data.

Locality Reference(s)	**FI type, occurrence, host mineral, country rock [notes]**	**Th (°C)**	**Rb (%)**
Abbeytown, Ireland Parnell (1993)	N/R, veins, dolomite, sandstone	175 UDE	3.1 N/R
Apollo well, Canada Skibo et al. (1991)	N/A, N/A, carbonate and anhydrite	170 Tpeak	2.6 max
Artillery Lake, Canada Goodarzi et al. (1989)	primary, N/A, quartz, dolostone. [The quartz is post bitumen].	202 ave	4.53 ave
Buchan Rift, Australia Arne et al. (1994) Barker and Bone (1995)	primary, cement, fluorite, limestone	200 est UM	3.0 UDE
Carlin Mine, Nevada Hausen and Park (1986)	primary, quartz and calcite, limestone and dolostone	295 UDE	4.9 UDE
Claude deposit, Canada. Leventhal et al. (1987) Pagel et al. (1980)	secondaries, fracture filling, quartz, gneiss. [Rb may be enhanced by radiation]	172 UDE	2.91 UDE
Danchang, China. Liu et al. (1993); Yang and Liu (1993)	N/R, N/R, calcite, limestone and shale	300 N/R	6 max
Dundas well, Canada. Skibo et al. (1991)	N/A, N/A, N/A, carbonates	160 Tpeak	3.1 max
Eischeid well, Iowa. Barker (1990)	secondary, calcite and quartz, sandstone	200 UDE	2.3 ran
Elmwood, Tennessee Gratz and Misra (1987); Gize (1990)	primary, gangue, early calcite, dolostone	1.3 N/R	107 UDE
Gaspe, Canada Duba and Williams-Jones (1983)	primary, veins, calcite, limestone and shale	355 UM	5.0 UM ran?

Appendix 3-1. A Compilation of Temperature and Solid Bitumen Reflectance Data.

Locality **Reference(s)**	**FI type, occurrence, host mineral, country rock [notes]**	**Th (°C)**	**Rb (%)**
Gaspe, Canada. Islam and Hesse (1983)	N/R, veins, quartz, limestone, sandstone, mudstone	170, UDE 269, UDE 197, UDE 250, UDE 212, UDE 223, UDE 213, UDE 206, UDE 217, UDE 210, UDE 182, UDE 212, UDE 118, UDE 220, UDE 319, UDE	2.0 ran 3.75 ran 5.3 ran 3.8 ran 3.3 ran 3.3 ran 3.2 ran 3.2 ran 2.6 ran 2.6 ran 2.5 ran 2.7 ran 2.2 ran 2.0 ran 5.6 ran
HYC Mine, Australia Muir et al. (1985); Crick (1992)	N/R, veins, dolomite, evaporites	168 UDE	2.6 UDE
Irish Basin, Parnell and Monson (1990)	N/R, veins, fluorite, limestone.	140, UDE 140, UDE	2.3 max 2.96 max
Jerritt Canyon, Nevada Robbins et al. (1990) Hoefstra et al. (1991)	N/R, ore stage calcite and barite, carbonaceous limestone	300, UDE est	6.5 N/R
Kongsberg, Norway Gize (1986)	N/R, veins?, calcite?, gneiss and quartzite	300 ave?	5.9 max
Laxey, Wales, U.K. Eakin (1989)	N/R, N/R, calcite, limestone [Rb measured away from u-bearing grain]	115 UDE	1.4 max?
Lodeve Basin, France Landais (1993) Landais & Connan (1986)	N/R, cement, calcite, N/R [Rb from low U content sample]	150 UDE	1.2 UDE
Lubin District, Poland Kucha (1993); Jowett (1986)	N/A, N/A, N/A, shale [Rb from low U content sample] [Rb used in regression was 1.7ave]	140 UDE	2.5 UDE

Appendix 3-1. A Compilation of Temperature and Solid Bitumen Reflectance Data.

Locality Reference(s)	**Fl type, occurrence, host mineral, country rock [notes]**	**Th (°C)**	**Rb (%)**
Lugicum, Czech Republic Kribek et al. (1994)	N/R, N/R, greenschist grade schist and gneiss with volcanics and limestone. [Rb from their Type III DOM]	450 Tpeak	7.7 max
Mitov, Czech Republic Kribek et al. (1993)	N/R, gangue, quartz and calcite, meta-sedimentary rock within pillow lava	400 texture	6.46 max
Nanisivik, Canada. Gize and Rimmer (1983); McNaughton (1983)	secondary, healed fracture, dolomite, dolostone. [measured next to gabbroic dike]	350 UDE	5.9 max
Navarana Fjord, Greenland Jakobsen and Ohmoto (1993)	N/R, veins, quartz, carbonate rock	200 ave?	4.16 ave
Oklo, Gabon Cortial et al (1990) Mossman et al. (1993) Gauthier-Lafaye and Weber (1993)	N/R, N/R, quartz and dolomite, sandstone. [Rb from high reflecting population and was measured away from a U-bearing grain]	180 ave	2.65 UDE
Patapedia, Quebec Duba and Williams-Jones (1983); Williams-Jones and Ferreira (1989)	Secondaries, metamorphosed phenocrysts in dikes, quartz, limestone and shale	375 UM	4.7 ave? ran
Pine Point, Canada Mcqueen (1986); Roedder (1968)	primary, cement, sphalerite and dolomite, dolostone [lower Tpeak is a regional value; higher Tpeak is within the ore deposit]	65 est, regional 100 UDE in ore deposit	0.5 UM, regional 1.12 UDE in ore
Quebec City, Canada. SA locality. Levine et al. (1991)	secondary oil Fl, quartz, limestone, sandstone, mudstone	130, UDE	2.05
Raniganj, India Sanyal (1965)	N/A, N/A, vein, coal	175 est	1.7 N/R
SE Salt Basin, Mississippi Sassen (1988); Heydari and Moore (1989)	N/A, N/A, post-bitumen calcite, limestone	200 ? Tpeak	3.2 UDE?

Appendix 3-1. A Compilation of Temperature and Solid Bitumen Reflectance Data.

Locality Reference(s)	**FI type, occurrence, host mineral, country rock [notes]**	**Th (°C)**	**Rb (%)**
Silvermines, Ireland Samson & Russell (1983); Parnell (1989)	N/R, N/R, carbonate, limestone	260, UDE	3.7 N/R
Tongren, China. Liu et al. (1993); Yang and Liu (1993)	N/R, N/R, gangue minerals, limestone	150 N/R	3.25 max
Tyangh, Ireland Parnell (1993)	N/R, veins, dolomite, sandstone	207 UDE	3.6 N/R
Viburnum Trend, Missouri Henry (1988)	N/R, gangue, carbonates and sphalerite, dolomite	137 UDE	1.39 UDE
Wanshan, China. Liu et al. (1993); Yang and Liu (1993)	N/R, quartz, limestone	183 UDE	3.2 max
Western Canada Basin Riediger (1983); Riediger and Coniglio (1992)	N/A, N/A, calcite, calcareous mudrocks	60 Tpeak 90 Tpeak	0.1 ran 1.1 ran
Windy Knoll, U.K. Kharvari-Khorosani and Murchinson (1978); Moser et al (1992)	secondaries, veins, fluorite, limestone	156 UDE	1.9 max
Witwatersrand, South Africa Hallbauer and Kable (1982); Eakin (1989)	post-depositional secondaries, healed fractures, quartz, conglomerate [Rb measured away from U-bearing grain]	180 UDE	1.75 max?
Xiangtan, China Fan et al. (1993)	veinlets, quartz and Mn-carbonate, shale	200 est.	2.3 UDE

Appendix 4. Fluid inclusion data

Abbreviations used in this table:

FIA = fluid inclusion assemblage
FI = fluid inclusion(s)

T_e = eutectic temperature
T_h = temperature of total fluid inclusion homogenization to a single phase. A single temperature is reported in the table but this value is usually the result of three measurements in the typical determination sequence.

Th-phase = The phase to which homogenization occurs-- liquid, vapor or by C.P. fading

C.P. fading = homogenization by loss of the distinction between liquid and vapor phases at the critical point. This loss is observed as a fading of the meniscus.

T_f = temperature of melting
T_t = temperature of trapping

V/L = vapor to liquid volume ratio

Size = the dimensions of an imaginary rectangle scribed about the greatest length and width of the fluid inclusion vacuole

SF = shape of the fluid inclusion vacuole. Shape is an empirical determination made by the microscopist based on geometric forms suggested by Bodnar et al. (1989).

Q = Quality. Quality is an subjective assessment of how accurate the data is compared to the rest of the sample suite.

B = assessed to be barren
P = assessed to be poor for sample suite
F = assessed to be average for sample suite
G= assessed to be good for sample suite

Host Rock Lithology:
cc = calcite
Q-d = Quartz -detrital. meaning the fluid inclusion host mineral is a framework grain of quartz within a sandstone

Fracture Type:
Type A. Fracture cross cuts several sedimentary features such as framework grains, cement, matrix and so forth. Type A fractures are clearly diagenetic.
Type B. Fractures which involve grain edge and perhaps matrix breakage.
Type C. A fracture wholly contained within a detrital grain and is likely an inherited fracture.

General note: The T_h values rate to be poor quality were not used for determining T_{peak}.

Appendix 4-1. Fluid Inclusion data, Buchan Rift, Victoria

Dike/ X (in m) / chip no./ inclusion	Host rock; host mineral; fracture type; related FI	Size in μm; V/L	SF	T_h (°C); T_h phase	T_f (°C)	Q	Notes
Murrindal 1 M1/ 30N/1/1	Limestone;cc; A; no two phase, but 1/2 to 1/5 single phase	40x12; 20	3	230.6; liquid	-0.1	G	associated with single phase fluid inclusions that nucleated a bubble upon heating and cooling of 1/1.
M1/30N/1/2	Limestone;cc; A;1/ 1. see note for 1/1	20x30; 20	3	N/A	-0.0	G	T_e =-23.2°C
M1/30N/1/3	Limestone;cc; A;1/ 1. see note for 1/1	11x20; 15	3	N/A	0.0 to 0.2 ?	G	T_e about -24 to -21°C
M1/30N/1/4	Limestone;cc; A;1/ 1. see note for 1/1	21x15; 30	1	N/A	-0.0	G	T_e = -23.7°C
M1/30N/1/5	Limestone;cc; A;1/ 1. see note for 1/1	12x10; 20	6	N/A	0.1	G	
M1/30N/ 2/1	Limestone;cc; A; 2/2	11x11; 5	5	75.4; liquid	N/A	F	bubble did not renucleate
M1/30N/ 2/2	Limestone;cc; A; 2/1	16x30; 15	7	N/A	-0.6 ?	P	bubble nucleated after heating 2/1; however, bubble is very large and T_f is indefinite.
M1/30N/ 2/3	Limestone;cc; A; N/R	14x20	6	73; liquid	N/A	P	decrepitated after heating to T_h 3 times
M1/30N/ 2/4	Limestone;cc; A; 2/2 is 350 μm away	N/R; 10	4	101.7; liquid	N/A	P	monitored FI before heating 2/1; decrepitated after heating to T_h 3 times.

Appendix 4-1. Fluid Inclusion data, Buchan Rift, Victoria

Dike/ X (in m) / chip no./ inclusion	**Host rock; host mineral; fracture type; related FI**	**Size in μm; V/L**	**S F**	**T_h (°C); T_h phase**	**T_f (°C)**	**Q**	**Notes**
M1/0.2N/1/1	Limestone; cc;A; 1/2	8.5x24; 30	2	315	N/A	P	cement in biomoldic porosity; Decrepitated after heating to T_h 3 times
M1/0.2N/1/2	Limestone; cc;A; 1/1	10x40; N/R	3	>284; liquid	N/A	P	decrepitated.
M1/0.2N/1/3	Limestone; cc; A; 1/1 is 70 μm away	5x14; 30	6	355.4	-0.2	P	

Appendix 4-2. Fluid inclusion data, western onshore Gippsland Basin

Dike/ X (in m) / chip no./ inclusion	Host Rock; host mineral; fracture type; related FI	Size in μm; V/L	SF	T_h (°C); T_h phase	T_f (°C)	Q	Notes
B3/3E/1/1	ss;q-d; A; 1/2	10x 5; 95	7	450; vapor		A ?	Th obscure; but this is typical of High T_h vapor rich FI
B3/3E/1/2	ss;q-d; A; 1/1	10x 10; 95	9	510; vapor		A ?	Th obscure; see note above
B3/3E/3/-							chip barren
B3/3E/4/-							chip barren
B3/3E/5/-							chip barren
B3/3E/6/-							chip barren
B3/7E/1/1	ss;q-d; A; N/A	5x5; 50	9	349.4; liquid		G	
B3/7E/2/-							chip barren
B3/7E/3/-							chip barren
B3/13E/1/1	ss;q-d; A; N/A	1.5X1.5; 20	8	N/A		P	decrepitated
B3/13E/2/1	ss;q-d; A; 2/1 to 2/8	4.5x3; 50	9	262; liquid		A	
B3/13E/2/2	ss;q-d; A; 2/1 to 2/8	1x3; 50	9	252; liquid		A	
B3/13E/2/3	ss;q-d; A; 2/1 to 2/8	3x5; 50	9	284; liquid		A	green mineral lining fracture
B3/13E/2/4	ss;q-d; A; 2/1 to 2/8	3x3; 50	9	N/A		A	bubble too hidden to see T_h
B3/13E/2/5	ss;q-d; A; 2/1 to 2/8	3x6; 40	9	292; liquid		G	
B3/13E/2/6	ss;q-d; A; 2/1 to 2/8	3x5; 30	8	189; liquid		G	
B3/13E/2/7	ss;q-d; A; 2/1 to 2/8	4x3; 40	9	262; liquid		G	

Appendix 4-2. Fluid inclusion data, western onshore Gippsland Basin

Dike/ X (in m) / chip no./ inclusion	**Host Rock; host mineral; fracture type; related FI**	**Size in μm; V/L**	**S F**	**T_h (°C); T_h phase**	**T_f (°C)**	**Q**	**Notes**
B3/13E/2/8	ss;q-d; A; not measurable	2x4; 30	8	290; liquid		A	related to vapor rich FI
B3/13E/3/1	ss;q-d; A; 3/1 to 3/4	6x4; 25	5	272; liquid	see note	A	freezing not observed; cooled to -196°C; fresh?
B3/13E/3/2	ss;q-d; A; 3/1 to 3/4	1.5x1.5; 40	7	266; liquid		G	too small to freeze
B3/13E/3/3	ss;q-d; A; 3/1 to 3/4	2x2; 25	7	272; liquid			
B3/13E/3/4	ss;q-d; A; 3/1 to 3/4	3x4; 25	8	270?; liquid		P	indeterminate T_h
B3/13E/3/5	ss;q-d; A; no	1x3; 25		285; liquid		A	
B3/13E/4/-							chip barren
B3/13E/5/-							chip barren
B3/13E/6/-							chip barren
B3/13E/7/-							chip barren
B3/13E/8/1	ss;q-d; A; no	5x5; 45	9	290; liquid		A	Th difficult to see.
B3/24E/1/1	ss;q-d; A; 1/1 to 1/2	1x4; 5		149;		A ?	heater stuck on, slightly overheated chip
B3/24E/1/2	ss;q-d; A; 1/1 to 1/2	N/R		252.4		A ?	
B3/24E/2/-							chip barren
B3/24E/3/1	ss;q-d; A; 3/2	1x1; 5	6	165; liquid		A	
B3/24E/3/2	ss;q-d; A; 3/1	2x2; 5	6	203; liquid		A	

Appendix 4-2. Fluid inclusion data, western onshore Gippsland Basin

Dike/ X (in m) / chip no./ inclusion	Host Rock; host mineral; fracture type; related FI	Size in μm; V/L	SF	T_h (°C); T_h phase	T_f (°C)	Q	Notes
B3/30E/1/1	ss; cc (vein); B; no	5x8; 5	9	109; liquid		P	Gas rich and some vapor rich FI in this section; this Th may reflect two phase trapping
B3/30E/1/2	ss; cc (vein); B; 1/3	4x6; 5	5	69; liquid		A	1/2 and 1/3 on same fracture.
B3/30E/1/3	ss; cc (vein); B; 1/2	11x5; 5	5	68; liquid		A	
B3/30E/1/4	ss; cc (vein); B; no measurable	3x3; 3	5	58; liquid		P	associated with single phase in one fracture
B3/30E/1/5	ss; cc (vein); B; 1/6	3x9; 5	9	84; liquid		A	FIA in another fracture
B3/30E/1/6	ss; cc (vein); B; 1/5	5x5; 5	0	83; liquid		A	Associated with single phase FI
B3/30E/1/7	ss; cc (vein); B; no	11x6; 5	3	77; liquid		A	
B3/30E/2/1	ss; cc (vein); B; one phase	11x2; 1	8	72; liquid		A	Associated with single phase FI
B3/30E/2/2	ss; cc (vein); B; one phase	5x5; 5	7	63; liquid		A	Associated with single phase FI
B3/30E/2/3	ss; cc (vein); B; one phase	5x2; 3	8	69; liquid		A	Associated with single phase FI
B3/30E/2/4	ss; cc (vein); B; one phase	11x5; 2	7	68; liquid		A	Associated with single phase FI
Best to use fractures that have FI with consistent V/L ratios --these FI indicate a Th of about 70-80°C in the Bena 3, X= 30 m east late calcite vein. Note that at these low trapping temperatures the single phase fluid inclusions simply may not have nucleated a vapor bubble.							

Appendix 4-2. Fluid inclusion data, western onshore Gippsland Basin

Dike/ X (in m) / chip no./ inclusion	**Host Rock; host mineral; fracture type; related FI**	**Size in μm; V/L**	**S F**	**T_h (°C); T_h phase**	**T_f (°C)**	**Q**	**Notes**
SR1/-0.2W/1/1 (ss xenolith within the dike)	ssQ-d; A; none	10x10; 30	4	>400?; liquid		P	T_h indefinite, poor visibility.
SR1/-0.2W/2/1	ss; Q-d; A; none	15 x 6; N/R	3	318; liquid		A	
SR1/-0.2W/3/1	ss; Q-d; A; 3/1-3/7	4 x 9; 20	7	422; C.P.Fading		G	
SR1/-0.2W/3/2	ss; Q-d; A; 3/1-3/7	6 x 12; 20	5	422; C.P. fading		G	
SR1/-0.2W/3/3	ss; Q-d; A; 3/1-3/7	4 x 9; 50	5	414; C.P. fading		G	
SR1/-0.2W/3/4	ss; Q-d; A; 3/1-3/7	6 x 8; 20	5	376; liquid		G	
SR1/-0.2W/3/5	ss; Q-d; A; 3/1-3/7	5 x 15; 30	5	383; vapor		G	
SR1/-0.2W/3/6	ss; Q-d; A; 3/1-3/7	5 x 7; 30	9	423; C.P. fading?		G	
SR1/-0.2W/3/7	ss; Q-d; A; 3/1-3/7	21x 27; N/R	7	438; vapor		G	
SR1/-0.2W/4/1	ss; Q-d; A; no	6 x 9; 50	8	372; N/R		G	
SR1/-0.2W/5/1	ss; Q-d; A; no	6 x 9; 40	7	355; N/R		G	associated with vapor rich FI
SR1/-0.2W/5/2	ss; Q-d; A; no	5 x 4; 60	8	438; vapor?		G	associated with vapor rich FI
SR1/-0.2W/5/3	ss; Q-d; A; no	7 x 9; 50	8	414; N/R		G	trapped on a mineral matter lined fracture

Appendix 4-2. Fluid inclusion data, western onshore Gippsland Basin

Dike/ X (in m) / chip no./ inclusion	Host Rock; host mineral; fracture type; related FI	Size in μm; V/L	SF	T_h (°C); T_h phase	T_f (°C)	Q	Notes
SR1/-0.2W/6/1	ss; Q-d; A; ---	7 x 21; 30	6	----		P	decrepitated
SR1/-0.2W/6/2	ss; Q-d; A; ---	7 x 9; 80	5	375; vapor		G	associated with vapor rich FI
SR1/-0.2W/7/1	ss; Q-d; B; 7/1-7/6	6x6; 50	3	307; liquid		G	this FIA trapped on a chlorite? lined fracture
SR1/-0.2W/7/2	ss; Q-d; B; 7/1-7/6	1x6; 20	3	237; liquid		G	
SR1/-0.2W/7/3	ss; Q-d; B; 7/1-7/6	2x4; 60	8	358; liquid		G	
SR1/-0.2W/7/4	ss; Q-d; B; 7/1-7/6	3x3; N/R	3	294; liquid		G	vapor bubble hidden at 298K
SR1/-0.2W/7/5	ss; Q-d; B; 7/1-7/6	4x6; 70	7	372; liquid		G	appears vapor rich at 298K
SR1/-0.2W/7/6	ss; Q-d; B; 7/1-7/6	3x3; 80	9	412; C.P. fading		G	
SR1/-0.2W/8/1	ss; Q-d; A; no measurable	5x8; 25	9	241; liquid		G	
SR1/-0.2W/8/2	ss; Q-d; A; 8/2-8/7	6x9; 80	7	379; vapor		G	
SR1/-0.2W/8/3	ss; Q-d; A; 8/2-8/7	4x3; 60	9	405; vapor		G	
SR1/-0.2W/8/4	ss; Q-d; A; 8/2-8/7	2x3; 40	9	341; liquid		G	
SR1/-0.2W/8/5	ss; Q-d; A; 8/2-8/7	3x5; N/R	7	242; liquid		G	
SR1/-0.2W/8/6	ss; Q-d; a; 8/2-8/7	5x8; 30	8	310; N/R	-4.3	G	

Appendix 4-2. Fluid inclusion data, western onshore Gippsland Basin

Dike/ X (in m) / chip no./ inclusion	Host Rock; host mineral; fracture type; related FI	Size in μm; V/L	S F	T_h (°C); T_h phase	T_f (°C)	Q	Notes
SR1/-0.2W/8/7	ss; Q-d; A; 8/2-8/7	6x9; 80	7	337; N/R	-4.3	G	T_e = -35.5°C?
SR1/-0.2W/9/1	ss; Q-d; A?; no	6x12; 5	7	147; liquid		G	
SR1/-0.2W/10/ 1	ss; Q-d; A; 10/1-10/3	10x11; 50	5	----------		G	decrepitated
SR1/-0.2W/10/ 2	ss; Q-d; A; 10/1-10/3	10x23; 60	5	385; vapor	-3.1 ?	G	FIA in chlorite? lined fracture
SR1/-0.2W/10/ 3	ss; Q-d; A; 10/1-10/3	8x9; 40	8	358; liquid	-4.1	G	FIA in chlorite? lined fracture
SR1/-0.2W/10/ 4	ss; Q-d; A; 10/4-10/8	5x7; 50	9	363; liquid	N/R	G	
SR1/-0.2W/10/ 5	ss; Q-d; A; 10/4-10/8	7x9; 70	6	372; vapor	-4.4	A	
SR1/-0.2W/10/ 6	ss; Q-d; A; 10/4-10/8	7x14; 70	7	390; vapor		A	
SR1/-0.2W/10/ 7	ss; Q-d; A; 10/4-10/8	5x15; 70	8	397; vapor		G	cooled to -150°C; no change
SR1/-0.2W/10/ 8	ss; Q-d; A; 10/4-10/8	5x9; 70	9	398; vapor		A	
SR1/-0.2W/10/ 9	ss; Q-d; A; 10/10	7x30; 35	4	387; C.P. fading	-3.3	A	
SR1/-0.2W/10/ 10	ss; Q-d; A; 10/9	10x13; 70	8	394; vapor		A	no obvious change upon freezing

Appendix 4-2 Fluid inclusion data, western onshore Gippsland Basin

Dike/ X (in m) / chip no./ inclusion	Host Rock; host mineral; fracture type; related FI	Size in μm; V/L	SF	T_h (°C); T_h phase	T_f (°C)	Q	Notes
SR1/0.075W/1/1	ss; Q-d; B; no	5x14;15	2	224; liquid		G	
SR1/0.075W/1/2	ss; Q-d; C; 1/3	4x7;20	7	336; liquid		G	
SR1/0.075W/1/3	ss; Q-d; C; 1/2	2x3;25	8	275; liquid		G	
SR1/0.075W/1/4	ss; Q-d; C; 1/5	2x3;30	8	354; liquid		G	
SR1/0.075W/1/5	ss; Q-d; C; 1/4	2x2;25	8	292; liquid			
SR1/0.075W/1/6	ss; Q-d; C; none measurable	3x3;20	9	240; liquid			type C in what appears to be a halo of smaller FI --a decrepitation texture.
SR1/0.075W/1/7	ss; Q-d; C; 1/8	4x7;25	6	323; liquid			
SR1/0.075W/1/8	ss; Q-d; C; 1/7	2x2; 30	5	294; liquid			
SR1/0.075W/2/1	ss; Q-d; B; no	4x3;10	7	177; liquid			
SR1/0.075W/2/2	ss; Q-d; B; no	2x2;10	2	133; liquid			
SR1/0.075W/2/3	ss; Q-d; C; 2/3-2/5	5x5;30	9	356; liquid			
SR1/0.075W/2/4	ss; Q-d; C; 2/3-2/5	3x4;25	7	342; liquid			
SR1/0.075W/2/5	ss; Q-d; C; 2/3-2/5	5x7;15	7	283; liquid			
SR1/0.075W/2/6	ss; Q-d; B; no	14xN/R; 15	8	229; liquid			

Appendix 4-2. Fluid inclusion data, western onshore Gippsland Basin

Dike/ X (in m) / chip no./ inclusion	Host Rock; host mineral; fracture type; related FI	Size in μm; V/L	S F	T_h (°C); T_h phase	T_f (°C)	Q	Notes
SR1/0.075W/ 2/7	ss; Q-d; C; 2/8	4x5;15	8	273; liquid			
SR1/0.075W/ 2/8	ss; Q-d; B; 2/7	4x6;25	2	324; liquid			
SR1/0.075W/ 2/9	ss; Q-d; C;2/10	4x4;20	4	313; liquid			
SR1/0.075W/ 2/10	ss; Q-d; C; 2/9	4x4;30	8	327; liquid			
SR1/0.10/1/1	ss; Q-d; B; no	9x18;20	2	280; liquid		A	In fracture that cuts matrix
SR1/0.10W/2/1	ss; Q-d; B; no	9x15;60	3	N/R		P	
SR1/0.10W/2/2	ss; Q-d; C; 2/2-2/4	6x12;30	8	328; liquid		G	Type C fracture with variable V/L
SR1/0.10W/2/3	ss; Q-d; C; 2/2-2/4	13x15; 20	6	297; liquid		G	
SR1/0.10W/2/4	ss; Q-d; C; 2/2-2/4	7x18; 20	5	297; liquid		G	
SR1/0.10W/3/1	ss; Q-d; B; 3/1-3/5	6x15; 30	4	402; liquid		P	necked?
SR1/0.10W/3/2	ss; Q-d; B; 3/1-3/5	7x12;30	3	390; liquid		P	necked?
SR1/0.10W/3/3	ss; Q-d; B; 3/1-3/5	15x27; 30	6	443; liquid		P	necked?
SR1/0.10W/3/4	ss; Q-d; B; 3/1-3/5	3x6; 20	6	345; liquid		P	necked?
SR1/0.10W/3/5	ss; Q-d; B; 3/1-3/5	2x4; 30	8	N/R		P	could not see T_h
SR1/0.10W/3/6	ss; Q-d; B; not measured	6x9; 60	5	418; liquid		P	necked?

Appendix 4-2. Fluid inclusion data, western onshore Gippsland Basin

Dike/ X (in m) / chip no./ inclusion	Host Rock; host mineral; fracture type; related FI	Size in μm; V/L	S F	T_h (°C); T_h phase	T_f (°C)	Q	Notes
SR1/0.10W/ 3/7	ss; Q-d; C; 3/7-3/9	4x6; 10	6	305; liquid		G	in same grain as 3/1-3/6
SR1/0.10W/ 3/8	ss; Q-d; C; 3/7-3/9	3x9; 10	9	323; liquid		G	in same grain as 3/1-3/6
SR1/0.10W/ 3/9	ss; Q-d; C; 3/7-3/9	5x8; 10	9	338; liquid		G	in same grain as 3/1-3/6
SR1/0.10W/ 3/10	ss; Q-d; C; 3/7-3/9	12x12; 80	2	435;vapor	-4	G	In a fracture that crosses the 3/7-3/9 fracture
SR1/0.10W/ 3/11	ss; Q-d; C; 3/7-3/9	6x9; 40	7	430; N/R		G	In a fracture that crosses the 1/1- 2/1 fracture
SR1/0.10W/ 3/11	ss; Q-d; C; 3/7-3/9	6x9; 40	9	366; N/R		G	In a fracture that crosses the 1/1- 2/1 fracture
SR1/0.10W/ 4/1	ss; Q-d; C; no	9x21; 80	7	389; N/R		G	
SR1/0.10W/ 4/2	ss; Q-d; b; no	7x9; 60	9	----------		P	indeterminate T_h
SR1/0.10W/ 4/3	ss; Q-d; C; no	7x6; 30	8	347; liquid		G	
SR1/0.10W/ 4/4	ss; Q-d; C; 4/5	9x24; 40	3	----------		P	indeterminate T_h
SR1/0.10W/ 4/5	ss; Q-d; C; 4/4	5x10; 70	8	366; vapor		G	
SR1/0.10W/ 5/1	ss; Q-d; C; none measured	7x6; 30	9	343; liquid		G	
SR1/0.30W/ 1/1	ss; Q-d; C; no measurable	7x5; 20	6	207; liquid		G	

Appendix 4-2. Fluid inclusion data, western onshore Gippsland Basin

Dike/ X (in m) / chip no./ inclusion	Host Rock; host mineral; fracture type; related FI	Size in μm; V/L	S F	T_h (°C); T_h phase	T_f (°C)	Q	Notes
SR1/0.30W/ 1/2	ss; Q-d; B; no	14x6; 20	4	173; liquid	-5.5	G	
SR1/0.30W/ 1/3	ss; Q-d; C; no	6x12; 20	6	170; liquid	-4.8	G	
SR1/0.30W/ 1/4	ss; Q-d; C; no	12x25; 20	6	214; liquid	-6.0	G	
SR1/0.30W/ 1/5	ss; Q-d; B; no	4x9; 15	6	229; liquid		G	
SR1/0.30W/ 1/6	ss; Q-d; C; no measurable	7x5; 20	7	388; N/R		P	Reassessed origin--close but not actually cut by fracture, so its a type C
SR1/0.30W/ 2/1	ss; Q-d; A; 2/1-2/3	5x8; 20	8	80; liquid		P	Th indefinite
SR1/0.30W/ 2/2	ss; Q-d; A; 2/1-2/3	3x6; 20	7	192; liquid		G	
SR1/0.30W/ 2/3	ss; Q-d; C; 2/1-2/3	3x4;20	6	250?; liquid		P	fracture type indefinite; Th indefinite
SR1/0.30W/ 3/1	ss; Q-d; B; 3-2	6x15; 2	7	217; liquid		p	stretching during heating; Th indefinite
SR1/0.30W/ 3/2	ss; Q-d; B; 3-1	5x20; 5-10	6	174; liquid		G	
SR1/0.30W/ 3/3	ss; Q-d; C; no	4x5; 60	9	370; liquid	-2.7	G	Reassessed origin--close but not actually cut by fracture, so its a type C
SR1/0.30W/ 3/4	ss; Q-d; C; not measurable	5x7; 60	4	380; liquid		G	

Appendix 4-2. Fluid inclusion data, western onshore Gippsland Basin

Dike/ X (in m) / chip no./ inclusion	Host Rock; host mineral; fracture type; related FI	Size in μm; V/L	SF	T_h (°C); T_h phase	T_f (°C)	Q	Notes
SR1/0.30W/ 3/5	ss; Q-d; C; 3/5-3/7	2x6; 60	8	303; liquid		G	
SR1/0.30W/ 3/6	ss; Q-d; C; 3/5-3/7	6x11; 50	1	380; liquid	?	G	Reassessed origin--close but not actually cut by fracture, so its a type C
SR1/0.30W/ 3/7	ss; Q-d; C; 3/5-3/7	2x6; 60	8	346; liquid		G	
SR1/0.30W/ 4/1	ss; Q-d; C; 4/1-4/6	6x15; 20	3	178; N/R		G	
SR1/0.30W/ 4/2	ss; Q-d; C; 4/1-4/6	5x20; 10	7	212; N/R		G	
SR1/0.30W/ 4/3	ss; Q-d; C; 4/1-4/6	7x8; 10	6	224; N/R		G	
SR1/0.30W/ 4/4	ss; Q-d; C; 4/1-4/6	4x5; 20	8	275; N/R		G	
SR1/0.30W/ 4/5	ss; Q-d; C; 4/1-4/6	7x10; 60	3	371; N/R		G	
SR1/0.30W/ 4/6	ss; Q-d; C; 4/1-4/6	3x4; 40	8	353; N/R		G	
SR1/0.30W/ 5/1	ss; Q-d; B;	5x20; 15	8	145; liquid		G	Fluid inclusion on chlorite? lined fracture
SR1/0.30W/ 5/2	ss; Q-d; C: 5/2-5/7	4x5; 10	5	212; liquid		G	
SR1/0.30W/ 5/3	ss; Q-d; C: 5/2-5/7	4x7; 15	5	211; liquid		G	
SR1/0.30W/ 5/4	ss; Q-d; C: 5/2-5/7	5x8; n/r	5	212; liquid		G	

Appendix 4-2. Fluid inclusion data, western onshore Gippsland Basin

Dike/ X (in m) / chip no./ inclusion	**Host Rock; host mineral; fracture type; related FI**	**Size in μm; V/L**	**S F**	**T_h (°C); T_h phase**	**T_f (°C)**	**Q**	**Notes**
SR1/0.30W/ 5/5	ss; Q-d; C: 5/2-5/7	7x8; 50	4	372; liquid		G	
SR1/0.30W/ 5/6	ss; Q-d; C: 5/2-5/7	6x8; 30	4	288; liquid		G	
SR1/0.30W/ 5/7	ss; Q-d; C: 5/2-5/7	7x9; 20	3	250; liquid		G	
SR1/0.30W/ 6/1	ss; Q-d; C: 6/1-6/7	3x7; 1	4	56; liquid	-7.3	G	T_e <-30
SR1/0.30W/ 6/2	ss; Q-d; C: 6/1-6/7	6x7; 30	8	330; liquid	-8.1	G	
SR1/0.30W/ 6/3	ss; Q-d; C; 6/1-6/7	4x6; 30	8	295; liquid		G	
SR1/0.30W/ 6/4	ss; Q-d; C; 6/1-6/7	3x4; 30	9	312; liquid		G	
SR1/0.30W/ 6/5	ss; Q-d; C; 6/1-6/7	3x5; 30	9	364; liquid		G	
SR1/0.30W/ 6/6	ss; Q-d; C; 6/1-6/7	2x3; 30	8	332; liquid		G	
SR1/0.30W/ 6/7	ss; Q-d; C; 6/1-6/7	1.5x6; 20	7	355; liquid		G	
SR1/0.50W/ 1/1	ss; Q-d; C; 1/1-1/3	6x6; 20	8	257; liquid		A	
SR1/0.50W/ 1/2	ss; Q-d; C; 1/1-1/3	N/R	N R	>>270; liquid		P	
SR1/0.50W/ 1/3	ss; Q-d; C; 1/1-1/3	2x4; 10	N R	239; liquid		A	
SR1/0.50W/ 1/4	ss; Q-d; C; 1/4-1/6	6x20; N/R	N R	298; liquid		A	
SR1/0.50W/ 1/5	ss; Q-d; C; 1/4-1/6	2x5; N/R	N R	317?; liquid		P	T_h indefinite

Appendix 4-2. Fluid inclusion data, western onshore Gippsland Basin

Dike/ X (in m) / chip no./ inclusion	Host Rock; host mineral; fracture type; related FI	Size in μm; V/L	SF	T_h (°C); T_h phase	T_f (°C)	Q	Notes
SR1/0.50W/ 1/6	ss; Q-d; C; 1/4-1/6	6x14; N/R	NR	292; liquid		A	
SR1/0.50W/ 1/7	ss; Q-d; C; 1/8	5x5; N/R	8	219; liquid		A	
SR1/0.50W/ 1/8	ss; Q-d; C; 1/7	2x3; N/R	3	233; liquid		A	
SR1/0.50W/ 1/9	ss; Q-d; C; 1/10	5x12; N/R	3	303; liquid		A	
SR1/0.50W/ 1/10	ss; Q-d; C; 1/9	2X3; N/R	NR	291; liquid		A	
SR1/0.50W/ 2/1	ss; Q-d; C; 2/1-2/4	10x10; 20	9	226; liquid		G	
SR1/0.50W/ 2/2	ss; Q-d; C; 2/1-2/4	6x20; 10	5	158; liquid		G	
SR1/0.50W/ 2/3	ss; Q-d; C; 2/1-2/4	4x4; 15	6	209; liquid		G	
SR1/0.50W/ 2/4	ss; Q-d; C; 2/1-2/4	8x8; 15	8	226; liquid		G	
SR1/0.50W/ 2/5	ss; Q-d; C; 2/6	4x12; 10	5	240; liquid		G	associated with vapor rich FI with T_h>325°C
SR1/0.50W/ 2/6	ss; Q-d; C; 2/5	4x10; 15	9	256; liquid		G	
SR1/0.50W/ 2/7	ss; Q-d; C; 2/8	6x8; 20	3	260; liquid		G	
SR1/0.50W/ 2/8	ss; Q-d; C; 2/7	4x8; N/R	8	249; liquid		G	
SR1/0.50W/ 3/1	ss; Q-d; C; 3/2	6x10; N/R	9	226; liquid		G	

Appendix 4-2. Fluid inclusion data, western onshore Gippsland Basin

Dike/ X (in m) / chip no./ inclusion	Host Rock; host mineral; fracture type; related FI	Size in μm; V/L	S F	T_h (°C); T_h phase	T_f (°C)	Q	Notes
SR1/1W/1/1	ss; Q-d; C; 1/2	3x9; N/R	3	168; liquid		G	
SR1/1W/1/2	ss; Q-d; C; 1/1	4x6; N/R	8	>>275; liquid		P	
SR1/1W/2/1	ss; Q-d; B;	4x4;10	9	105; liquid		G	
SR1/1W/2/2	ss; Q-d; C; in same grain as 2/1	3x4; N/R	8	>>136; liquid		P	Stopped heating to preserve the other low T_h FI
SR1/1W/2/3	ss; Q-d;C; 2/4	3x4;5	7	115; liquid			
SR1/1W/2/4	ss; Q-d; C;2/3	4x6; 10	3	108; liquid			
SR1/1W/2/5	ss; Q-d; B; 2/6	6x6; 20	5	136; liquid			vapor bubble did not renucleate
SR1/1W/2/6	ss; Q-d; B; 2/5	13x26; 15	5	111; liquid			
SR1/1W/2/7	ss; Q-d; C;2/8	9x9; 10	6	124; liquid			
SR1/1W/2/8	ss; Q-d; C;2/7	7x7; N/R	5	165; liquid			
SR1/1W/2/9	ss; Q-d; C;2/7-2/8	4x6; 10	8	123; liquid			In the same grain as 2/7-2/8
SR1/1W/2/10	ss; Q-d; B;2/11	3x5; 10	8	136; liquid			
SR1/1W/2/11	ss; Q-d; C;2/10	2x4; 10	8	132; liquid			

Appendix 5. Rock-Eval Pyrolysis Results.

Definitions for the Rock-Eval data are as follows: S_1 and S_2 are the first and second pulses of hydrocarbon (HC) yield occurring during pyrolysis of the sample; T_{max} is the temperature of maximum pyrolysis yield during the S_2 pulse; S_3 is the amount of CO_2 generated during pyrolysis; TOC is total organic carbon; Hydrogen index (HI) = $(S_2/TOC)x100$; Oxygen index (OI) = $(S_3/TOC)x100$; PI = transformation ratio = $S_1/(S_1+S_2)$.

Unit definitions for Rock-Eval data are as follows: mg = milligrams; gC = grams carbon; HC = hydrocarbon; rk = rock; wt.-% = weight percent.

Rb-r = mean random bitumen reflectance

Rv-r = mean random vitrinite reflectance

Basin Dike name Dike code Thickness Sample line	Initial X from Dike Contact (m)	Final X from Dike Contact (m)	Rock type	Rb-r mean (%)	Tmax Celsius	S1 mgHC/ g rock	S2 mgHC/ g rock	S3 mg CO2/ g rock	PI	S2/S3 HC/CO2	TOC wt-%	HI mgHC/ g C	OI mg CO2/ gC
Buchan Rift													
Murrindal-1	0.10	0.10	limestone		0	0.0	0.0	0.2	0.0	0.0	0.2	0	126
(M1)	0.15	0.15	limestone		0	0.0	0.0	0.2	0.0	0.0	0.1	0	187
2.2 meters	0.45	0.45	limestone	2.36	0	0.0	0.0	0.1	0.0	0.0	0.2	0	66
south	0.72	0.72	limestone		0	0.0	0.0	0.1	0.0	0.0	0.2	4	59
	0.93	0.93	limestone	2.43	0	0.0	0.0	0.1	0.0	0.0	0.2	0	50
	1.36	1.36	limestone		0	0.0	0.0	0.1	0.0	0.0	0.1	0	76
	1.47	1.47	limestone		0	0.0	0.0	0.1	0.0	0.0	0.2	5	31
	1.70	1.70	limestone		0	0.0	0.0	0.1	0.0	0.0	0.1	20	100
	2.10	2.10	limestone		0	0.0	0.0	0.1	0.0	0.0	0.1	0	150
	2.18	2.18	limestone	2.75	0	0.0	0.0	0.1	0.0	0.0	0.1	16	75
	2.35	2.35	limestone		0	0.0	0.0	0.1	0.0	0.0	0.2	5	76
	3.03	3.03	limestone	2.52	0	0.0	0.0	0.1	0.0	0.0	0.3	11	40
	3.44	3.44	limestone		0	0.0	0.0	0.2	0.0	0.0	0.1	0	190
	4.30	4.30	limestone		0	0.0	0.0	0.1	0.0	0.0	0.2	6	86
	5.23	5.23	limestone		0	0.0	0.0	0.1	0.0	0.0	0.1	10	100
	5.45	5.45	limestone	2.92	0	0.0	0.0	0.1	0.0	0.0	0.2	4	36
	6.28	6.28	limestone	2.62	0	0.0	0.0	0.1	0.0	0.0	0.2	12	62
	6.61	6.61	limestone		0	0.0	0.0	0.1	0.0	0.0	0.1	15	61

Gippsland Regional Sample	Rock type	Rv-r (%) mean	Tmax Celsius	S1 mgHC/ g rock	S2 mgHC/ g rock	S3 mg CO2/ g rock	PI	S2/S3 HC/CO2	TOC wt-%	HI mgHC/ g C	OI mg CO2/ gC
R-1	mdst	0.47	405	0.32	1.4	1.35	0.19	1.03	1.89	74	71
R-2A	coaly ss	0.47	445	0.03	2.99	12.53	0.01	0.23	9.61	31	130
R-2	coaly mdst	2.06	566	0.1	0.46	0.5	0.18	0.92	0.93	49	53
R-3	sltst	0.95	446	0.01	0.03	0.41	0.25	0.07	0.57	5	71
R-4	coaly ss	B	479	0.02	4.05	5.41	0	0.74	10.83	37	49
R-5	coal	0.62	430	0.16	170.84	6.21	0	27.51	63.54	268	9
R-6	coaly ss	0.52	440	0.15	33.45	9.2	0	3.63	13.08	255	70
R-7	coaly ss	0.92	440	0.01	0.33	1.21	0.03	0.27	1.18	27	102
R-8	coal	0.62	433	1.23	135.22	10.26	0.01	13.17	57.2	236	17
R-9	coal	B	435	0.1	47.13	26.93	0	1.75	48.3	97	55
R-10	coaly ss	0.46	469	0.02	1.85	4.15	0.01	0.44	6.13	30	67
R-11	coaly ss	0.41	425	0.33	61.98	14.3	0.01	4.33	34.44	179	41
R-12	coal	0.43	480	0	15	48	0	0.31	31.19	48	153
R-12A	coaly mdst	N/R	442	0.03	3.81	4.66	0.01	0.81	7.57	50	61
R-13	coaly ss	0.56	457	0.01	1.55	6.16	0.01	0.25	6.61	23	93
R-13A	coal	0.49	433	0.08	80.99	25.22	0	3.21	44.86	180	56
R-14	coaly sltst	0.95	596	0.01	0.38	0.31	0.03	1.22	0.38	100	81
R-15	ss	0.7	592	0	0.03	0.21	0	0.14	0	0	0
R-16	coaly mdst	0.8	432	0.08	8.15	1.54	0.01	5.29	3.33	244	46
R-17	coaly ss	0.47	455	0.02	2.03	4.15	0.01	0.48	6.21	32	66
R-18	coal	0.74	463	8.56	67.72	10.89	0.11	6.21	49.93	135	21
R-19	coal y mdst	0.66	456	0.13	20.4	7.05	0.01	2.89	10.03	203	70

Gippsland Regional Sample	Rock type	Rv-r (%) mean	Tmax Celsius	S1 mgHC/ g rock	S2 mgHC/ g rock	S3 mg CO2/ g rock	PI	S2/S3 HC/CO2	TOC wt-%	HI mgHC/ g C	OI mg CO2/ gC
R-20	coaly mdst	0.7	474	0.05	3.31	4.2	0.01	0.78	6.3	52	66
R-21	coal	0.65	449	0.06	2.72	29.38	0.02	0.09	50.73	5	57
R-22	coal	0.63	592	0.4	16	30.47	0.02	0.52	16.38	97	186
R-23	coal	0.76	438	0.09	103.84	4.13	0	25.14	46.64	222	8
R-25C	coal	0.61	478	0	19.21	22.45	0	0.85	67.12	28	33
R-27	coal	0.75	442	0.44	31.01	4.66	0.01	6.65	13.92	222	33
R-28	coal	0.72	455	0.03	17.64	9.89	0	1.78	12.35	142	80
R-29	coal	0.65	581	0	1.83	37.33	0	0.04	44.06	4	84
R-30	coal	0.47	419	0.07	19.53	51.25	0	0.38	42.65	45	120
R-31	coal	0.51	437	0	1.85	15	0	0.12	16.07	11	93
R-32	mdst	0.56	442	0.02	0.23	1.13	0.08	0.2	1.25	18	90
R-33	mdst	0.59	353	0.02	0.01	0.09	1	0.11	0	0	0
R-34	coaly ss	0.45?	598	0	2.28	2.05	0	1.11	1.74	131	117
R-35	ss	0.8	450	0.09	3.22	3.16	0.03	1.01	9.68	33	32
R-36	ss	0.72	539	0	0.15	1.26	0	0.11	0.78	19	161
R-37	mdst	B	440	0.02	0.73	3.36	0.03	0.21	5.14	14	65
R-38	coal	0.52	431	0.06	99.07	17.74	0	5.58	56.62	174	31
R-39	coaly ss	0.96	538	0.01	0.23	0.68	0.04	0.33	0.79	29	86
R-40	coaly ss	0.53	481	0.03	1.04	10.15	0.03	0.1	9.41	11	107
R-41	coal	0.62	579	0	1.98	23.35	0	0.08	39.12	5	59

Gippsland Regional Sample	Rock type	Rv-r (%) mean	Tmax Celsius	S1 mgHC/ g rock	S2 mgHC/ g rock	S3 mg CO2/ g rock	PI	S2/S3 HC/CO2	TOC wt-%	HI mgHC/ g C	OI mg CO2/ gC

Regional Rock-Eval Statistical Summary

Mean	0.6	472	0.3	23.5	11.2	0.1	2.9	20.2	85	69
Standard Deviation	0.3	60	1.3	40.2	13.0	0.2	5.9	21.4	85	42

Basin Well	Initial Sample Depth (m)	Final Sample Depth (m)	Rock type	Rv-r mean (%)	Tmax Celsius	S1 mgHC/ g rock	S2 mgHC/ r rock	S3 mg CO2/ g rock	PI	S2/S3 HC/CO2	TOC wt-%	HI mgHC/ g C	OI mg CO2/ gC
Gippsland													
Tarwin Meadows-1													
	93	96	mdst	0.61	433	0.05	0.88	0.2	0.05	4.4	1.09	80	18
	490	490	coaly mdst	0.51*	N/R	N/R	N/R	N/R	N/R	N/R	N/R	N/R	N/R
	782	783	mdst	0.72	438	0.03	0.74	0.18	0.04	4.11	1.22	60	14
	953	953	coaly mdst	1.11	420	0.6	6.76	1.59	0.08	4.25	13.31	50	11
Wellington Park-1													
	750	756	coaly mdst	0.36	408	0.86	83.39	13.42	0.01	6.21	36.18	230	37
	1009	1012	picked coal	0.4	417	2.8	179.33	16.4	0.02	10.93	66.6	269	24
	1134	1134	coaly ss	0.45	419	0.79	19.96	6.12	0.04	3.26	15.97	124	38
	1322	1324	coaly ss	0.51	432	0.1	8.28	1.48	0.01	5.59	4.96	166	29
	1923	1924	mdst	NA	442	0.02	0.41	0.13	0.05	3.15	0.37	110	35
	2086	2088	coaly mdst	0.77	440	0.07	7.21	0.68	0.01	10.6	6.38	113	10
	2562	2566	coaly mdst	0.94	451	1.26	24.86	3.2	0.05	7.76	14.88	167	21
	3050	3051	coaly ss	1.46	475	0.69	67.06	2.65	0.01	25.3	66.9	100	3
	3211	3214	coaly ss	1.89	483	0.03	0.33	0.08	0.08	4.12	0.71	46	11
	3648	3650	coaly ss	NA	515	0.16	6.35	0.71	0.02	8.94	19.68	32	3

* The sample at 490m is a thin liptinite rich coaly mudstone and the Rv-r is suppressed. This value was not used in plotting the data.

Basin Dike name Dike code Thickness Sample line	Initial X from Dike Contact (m)	Final X from Dike Contact (m)	Rock type	Rv-r mean (%)	Tmax Celsius	S1 mgHC/ g rock	S2 mgHC/ g rock	S3 mg CO2/ g rock	PI	S2/S3 HC/CO2	TOC wt-%	HI mgHC/ g C	OI mg CO2/ gC
Gippsland													
Bena 1	0.00	0.04	coaly ss	4.02	424	0.04	0.21	2.63	0.17	0.07	9.24	2	28
B1	0.10	0.15	coaly ss	2.54	427	0.04	0.14	1.48	0.22	0.09	2.86	4	51
3.4m	0.30	0.35	coaly ss	1.07	576	0.04	0.26	13.04	0.13	0.01	7.28	3	179
west	0.50	0.60	coal	1.04	570	0.04	0.41	11.06	0.09	0.03	27.18	1	40
	1.00	1.10	coaly ss	0.95	555	0.06	1	20.62	0.06	0.04	13.41	7	153
	1.50	1.60	coaly ss	0.6	523	0.14	1.7	16.84	0.08	0.1	11.43	14	147
	2.00	2.10	coaly ss	0.53	529	0.03	2.91	35.61	0.01	0.08	18.92	15	188
	2.50	2.60	coaly ss	0.52	501	0.03	2.08	13.62	0.01	0.15	10.07	20	135
	3.00	3.10	coal	0.47	519	0.02	4.37	30.32	0	0.14	39.63	11	76
	3.50	3.60	coaly ss	N/R	439	0.05	23.91	36.52	0	0.65	19.9	120	183
	4.00	4.10	coal	0.44	502	0	6.41	47.36	0	0.13	24.55	26	192
	5.00	5.10	coaly ss	N/R	520	0.03	3.58	27.86	0.01	0.12	8.75	40	318
	6.00	6.10	coaly ss	0.45	475	0.03	3.96	15.54	0.01	0.25	10.81	36	143

Basin Dike name Dike code Thickness Sample line	Initial X from Dike Contact (m)	Final X from Dike Contact (m)	Rock type	Rv-r mean (%)	Tmax Celsius	S1 mgHC/ g rock	S2 mgHC/ g rock	S3 mg CO2/ g rock	PI	S2/S3 HC/CO2	TOC wt-%	HI mgHC/ g C	OI mg CO2/ gC
Gippsland													
Bena 3	0	0.1	ss	5.79	586	0	0.02	0.3	0	0.06	0	0	0
B3	1	1	ss	5.68	0	0	0	0.09	0	0	0	0	0
20.1 m	3	3	ss	5.07	535	0	0.04	0.04	0	1	0	0	0
east	5	5	ss	B	582	0	0.11	0.28	0	0.39	0	0	0
	7	7	ss	B	566	0	0.08	0.05	0	1.6	0	0	0
	10	10	ss	3.54	479	0	0.03	0.23	0	0.13	0.24	12	95
	13	13	ss	2.91	561	0	0.12	0.36	0	0.33	0.28	42	128
	16	16	ss	2.71	590	0	0.21	0.04	0	5.25	0.01	0	400
	20	20	ss	2.39	596	0	0.18	0.03	0	6	0.01	0	300
	25	25	ss	1.9	537	0	0.11	0.05	0	2.2	0	0	0
	30	30	mdst	1.32	506	0	1.65	2.68	0	0.61	6.77	24	39

Basin Dike name Dike code Thickness Sample line	Initial X from Dike Contact (m)	Final X from Dike Contact (m)	Rock type	Rv-r mean (%)	Tmax Celsius	S1 mgHC/ g rock	S2 mgHC/ g rock	S3 mg CO2/ g rock	PI	S2/S3 HC/CO2	TOC wt-%	HI mgHC/ g C	OI mg CO2/ gC
Gippsland													
Cruickston-1	0.4	0.4	mdst	3.26	0	0.01	0.5	0	0	0	0.04	0	1250
Cru-1	0.8	0.8	mdst	3.84	338	0.03	0.08	0.51	0.3	0.15	0.77	10	66
41 m	2	2	mdst	4.39	301	0.05	0.07	0.61	0.42	0.11	1.39	5	43
east	5	5	mdst	3.57	340	0.01	0.01	0.56	0.5	0.01	0.31	3	180
	10	10	mdst	3.29	0	0	0.31	0	0	0	0.6	0	51
	16	16	mdst	3.95	408	0	0.04	0.34	0	0.11	0.32	12	106
	20	20	mdst	N/R	455	0.01	0.07	0.38	0.12	0.18	0.67	10	56
	25	25	mdst	N/R	423	0.01	0.04	0.38	0.25	0.1	0.13	30	292
	30	30	mdst	4.27	355	0.02	0.07	0.32	0.25	0.21	0.27	25	118
	35	35	mdst	N/R	454	0.01	0.18	0.5	0.06	0.36	0.11	163	454
	40	40	mdst	N/R	494	0.02	0.12	0.4	0.14	0.3	0.08	150	500
	45	45	mdst	3.8	0	0.01	0.08	0.13	0.12	0.61	0.1	80	130
	50.2	50.2	mdst	N/R	592	0	0.02	0.33	0	0.06	0.27	7	122
	55	55	mdst	2.8	0	0	0.07	0.24	0	0.29	0.72	9	33
	60	60	mdst	N/R	0	0	0.01	0.21	0	0.04	0.28	3	75
	65	65	mdst	3.07	400	0	0.05	0.28	0	0.17	0.3	16	93

Basin Dike name Dike code Thickness Sample line	Initial X from Dike Contact (m)	Final X from Dike Contact (m)	Rock type	Rv-r mean (%)	Tmax Celsius	S1 mgHC/ g rock	S2 mgHC/ g rock	S3 mg CO2/ g rock	PI	S2/S3 HC/CO2	TOC wt-%	HI mgHC/ g C	OI mg CO2/ gC
Gippsland													
Inverloch-1	0.05	0.1	picked coal	4.4	401	0.25	1.28	0.26	0.16	4.92	4.13	30	6
I1	0.2	0.2	picked coal	4.86	433	0.2	1.4	0.39	0.12	3.58	4.12	33	9
1.7 m	0.5	0.5	picked coal	3.57	314	0.15	1.24	2.76	0.11	0.44	4.58	27	60
west	0.7	0.7	picked coal	2.98	354	0.12	1.44	0.71	0.08	2.02	9.07	15	7
	1.0	1.0	picked coal	1.95	582	0.08	1.59	1.32	0.05	1.2	8.21	19	16
	1.5	1.5	picked coal	0.9	453	0.29	14.09	1.23	0.02	11.45	8.09	174	15
	2.0	2.0	picked coal	0.65	442	0.2	6.43	1.49	0.03	4.31	7.51	85	19
	2.5	2.5	picked coal	0.59	438	0.23	4.35	1.04	0.05	4.18	7.3	59	14
	3.0	3.0	picked coal	0.63	441	0.2	3.43	0.83	0.06	4.13	5.08	67	16
	3.5	3.5	picked coal	0.56	439	0.16	3.19	0.88	0.05	3.62	2.47	129	35
Inverloch-1	0.04	0.05	picked coal	3.99	461	0	1.38	0.04	0	34.5	0.57	242	7
I1	0.08	0.09	picked coal	4.24	358	0	0.56	0	0	0	0.22	254	0
1.7 m	0.17	0.21	picked coal	4.08	417	0	0.46	0	0	0	0.43	106	0
east	0.38	0.41	picked coal	2.63	574	0.02	2.38	0	0.01	0	6.14	38	0
	0.46	0.5	picked coal	2.25	466	0	0.6	0	0	0	0.56	107	0
	0.5	0.6	picked coal	N/R	562	0.01	0.91	0.02	0.01	45.5	0.79	115	2
	0.7	0.8	picked coal	1.2	462	0.04	8.5	1.53	0	5.55	9.91	85	15
	0.9	0.94	picked coal	0.87	395	0.07	0.69	0.18	0.09	3.83	0.43	160	41
	1.0	1.1	picked coal	0.72	434	0.01	1.31	0.01	0.01	131	0.48	272	2
	1.3	1.35	picked coal	1.07	434	0	0.39	0.01	0	39	0.3	130	3
	1.6	1.65	picked coal	0.47	440	0.01	1.79	1.44	0.01	1.24	2.47	72	58
	1.9	2.0	picked coal	0.47	427	0.05	9.28	1.25	0.01	7.42	8.55	108	14

Basin Dike name Dike code Thickness Sample line	Initial X from Dike Contact (m)	Final X from Dike Contact (m)	Rock type	Rv-r mean (%)	Tmax Celsius	S1 mgHC/ g rock	S2 mgHC/ g rock	S3 mg CO2/ g rock	PI	S2/S3 HC/CO2	TOC wt-%	HI mgHC/ g C	OI mg CO2/ gC
Gippsland													
Inverloch 2	0	0.01	picked coal	4.7	388	0.04	1	0.59	0.04	1.69	1.48	67	39
I2	0.04	0.06	picked coal	3.37	367	0.13	1.85	0.99	0.07	1.86	8.03	23	12
0.4 m	0.1	0.12	picked coal	2.04	530	0.27	4.26	0.59	0.06	7.22	10.47	40	5
East	0.19	0.22	picked coal	1.02	449	0.19	15.94	1.39	0.01	11.46	24.41	65	5
	0.29	0.32	picked coal	0.63	429	0.19	29.86	3.47	0.01	8.6	19.12	156	18
	0.37	0.42	picked coal	0.54	433	0.11	11.63	1.92	0.01	6.05	12.27	94	15
	0.48	0.52	picked coal	0.5	430	1.27	29.19	7.91	0.04	3.69	30.29	96	26
	0.68	0.72	picked coal	0.49	431	0.74	30.09	7.87	0.02	3.82	36.71	81	21
	0.98	1.02	picked coal	0.5	430	1.49	47.21	15.86	0.03	2.97	36.64	128	43
	1.45	1.47	picked coal	0.54	427	2.69	38.08	8.7	0.07	4.37	35.05	108	24
	1.95	2.02	picked coal	0.49	424	2	66.46	14.97	0.03	4.43	59.75	111	25
Inverloch 2	0.01	0.04	picked coal	2.69	519	0	0.32	0.04	0	8	0.56	57	7
I2	0.08	0.12	picked coal	2.2	554	0.08	1.05	0.23	0.07	4.56	3.17	33	7
0.4 m	0.18	0.22	picked coal	1.53	497	0.09	2.17	0.22	0.04	9.86	4.47	48	4
West	0.28	0.32	picked coal	1.19	457	0.12	11.71	0.5	0.01	23.42	15.69	74	3
	0.39	0.44	picked coal	1.03	457	0.07	27.37	0.72	0	38.01	45.7	59	1
	0.5	0.54	picked coal	0.9	452	0	14.22	0.17	0	83.64	21.5	66	0
	0.78	0.82	picked coal	0.62	436	0.3	17.37	1.73	0.02	10.04	16.75	103	10
	0.82	0.84	picked coal	N/R	425	0.75	84.5	11.18	0.01	7.55	69.58	121	16
	1.37	1.39	picked coal	N/R	426	1.28	74.02	10.29	0.02	7.19	60.05	123	17

Basin Dike name Dike code Thickness Sample line	Initial X from Dike Contact (m)	Final X from Dike Contact (m)	Rock type	Rv-r mean (%)	Tmax Celsius	S1 mgHC/ g rock	S2 mgHC/ g rock	S3 mg CO2/ g rock	PI	S2/S3 HC/CO2	TOC wt-%	HI mgHC/ g C	OI mg CO2/ gC
Gippsland													
Inverloch 3	0	0.02	picked coal	3.74	339	0.29	5.28	0.87	0.05	6.06	4.09	129	21
I3	0.02	0.04	picked coal	2.05	339	0.18	3.5	0.68	0.05	5.14	6.95	50	9
0.2 m	0.05	0.07	picked coal	1.54	484	0.3	7.11	1.18	0.04	6.02	11.15	63	10
east	0.07	0.09	picked coal	0.92	446	0.17	2.33	0.59	0.07	3.94	3.86	60	15
	0.09	0.11	picked coal	0.7	439	0.1	1.43	0.31	0.07	4.61	1.97	72	15
	0.13	0.15	picked coal	0.6	434	0.28	4.65	1.37	0.06	3.39	7.03	66	19
	0.16	0.18	picked coal	0.53	440	0.35	25.04	16.2	0.01	1.54	31.13	80	52
	0.18	0.2	picked coal	0.57	440	0.43	25.7	15.76	0.02	1.63	55.19	46	28
	0.2	0.22	picked coal	0.64	441	0.65	27.82	16.46	0.02	1.69	57.57	48	28
	0.23	0.25	picked coal	0.57	434	1.22	17.82	3.55	0.06	5.01	20.63	86	17
	0.25	0.27	picked coal	0.58	440	0.18	6.75	2.34	0.03	2.88	10.38	65	22
	0.27	0.3	picked coal	0.55	437	1.87	41.45	13.95	0.04	2.97	58.01	71	24
	0.35	0.37	picked coal	0.58	431	2.67	30.39	14.45	0.08	2.1	54.16	56	26
	0.4	0.42	picked coal	0.61	431	0.56	5.36	1.17	0.09	4.58	5.3	101	22
	0.5	0.52	picked coal	0.57	434	1.48	28.13	14.09	0.05	1.99	47.44	59	29

Basin Dike name Dike code Thickness Sample line	Initial X from Dike Contact (m)	Final X from Dike Contact (m)	Rock type	Rv-r mean (%)	Tmax Celsius	S1 mgHC/ g rock	S2 mgHC/ g rock	S3 mg CO2/ g rock	PI	S2/S3 HC/CO2	TOC wt-%	HI mgHC/ g C	OI mg CO2/ gC
Gippsland													
Korumburra1	2	2	ss	5.19	532	0.01	0.33	0.08	0.03	4.12	0.02	0	400
K1	4.3	4.3	ss	4.9	577	0.01	0.05	0	0.17	0	0	0	0
35 m	7	7	ss	NA	552	0.01	0.16	0.06	0.06	2.66	0.25	64	24
west	7	7	mdst	4.27	564	0	0.18	0.09	0	2	0.31	58	29
	5	5	ss	N/A	438	0.01	0.04	0.17	0.25	0.23	0.16	25	106
	10	10	ss	3.81	546	0	0.06	0.58	0	0.1	0.34	17	170
	11	11	ss	B	584	0	0.1	0.27	0	0.37	0.71	14	38
	12	12	ss	3.28	479	0.01	0.08	1.64	0.12	0.04	0.32	25	512
	15	15	ss	1.18	591	0.01	0.34	0.32	0.03	1.06	0.3	113	106
	15	15	ss	1.18	404	0.01	0.62	2.32	0.02	0.26	2.27	27	102
	15.8	15.8	picked coal	1.96	555	0	0.12	0.41	0	0.29	0.17	70	241
	17	17	picked coal	1.35	577	0	1.84	21.07	0	0.08	56.27	3	37
	20	20	picked coal	0.9	496	0.08	7.36	17.52	0.01	0.42	44.96	16	38
	25	25	picked coal	0.46	438	0.2	18.33	6.4	0.01	2.86	13.75	133	46
	30	30	picked coal	0.42	434	0.1	29.16	19.68	0	1.48	33.32	87	59
	35	35	picked coal	0.46	434	0	31.68	22.97	0	1.37	53.36	59	43
	36	36	picked coal	0.56	436	0	14.46	20.42	0	0.7	32.17	44	63
	40	40	picked coal	0.48	427	0.28	76.82	9.13	0	8.41	43.53	176	20
	50	50	picked coal	0.6	438	0.02	0.77	1.35	0.03	0.57	4.39	17	30
	60	60	picked coal	0.28	446	0.01	6.22	3.69	0	1.68	10.19	61	36

Basin Dike name Dike code Thickness Sample line	Initial X from Dike Contact (m)	Final X from Dike Contact (m)	Rock type	Rv-r mean (%)	Tmax Celsius	S1 mgHC/ g rock	S2 mgHC/ g rock	S3 mg CO2/ g rock	PI	S2/S3 HC/CO2	TOC wt-%	HI mgHC/ g C	OI mg CO2/ gC
Gippsland													
San Remo-1	0.1	0.1	coaly ss	1.79	389	0.12	2.66	0.77	0.04	3.45	2.86	93	26
SR-1	0.2	0.2	coaly ss	1.61	535	0.13	1.98	1.05	0.06	1.88	3.6	55	29
0.6 m	0.3	0.3	coaly ss	1.55	562	0.07	2	3.05	0.03	0.65	11.75	17	25
east	0.34	0.38	coal	1.8	553	0	6.61	3.72	0	1.77	25.63	25	14
	0.6	0.7	coal	0.91	452	0	79.51	4.51	0	17.62	64.45	123	6
	0.65	0.65	coal	1.03	459	0.56	56.05	3.66	0.01	15.31	50.78	110	7
	0.85	0.85	coal	0.61	462	0.13	25.06	19.2	0.01	1.3	67.62	37	28
	0.9	1.05	coal	0.73	446	0.23	94.04	8.57	0	10.97	73.35	128	11
	1	1	coal	0.71	443	0.32	18.75	2.96	0.02	6.33	19.57	95	15
	1.05	1.1	coal	0.71	443	0	82.08	8.75	0	9.38	72.34	113	12
	1.2	1.2	coal	0.7	441	0.44	82.22	8	0.01	10.27	37.83	217	21
	1.4	1.4	coal	0.68	439	0.23	47.84	4.88	0	9.8	47.27	101	10
	1.6	1.6	coal	0.62	475	0.14	21.16	19.02	0.01	1.11	54.62	38	34
	2	2	coaly ss	0.58	441	0.17	2.77	1.57	0.06	1.76	3.43	80	45
	2.45	2.45	coal	0.72	456	0.63	36.08	6.46	0.02	5.58	48.32	74	13
SR-1	5	10	picked coal	2.03	550	0.06	0.35	1.16	0.15	0.3	2.5	14	46
west	20	20	picked coal	2.07	320	0.09	0.97	0.46	0.08	2.1	1.85	52	24
AFTA	30	30	picked coal	1.6	528	0.17	1.55	0.69	0.1	2.24	4.23	36	16

Basin Dike name Dike code Thickness Sample line	Initial X from Dike Contact (m)	Final X from Dike Contact (m)	Rock type	Rv-r mean (%)	Tmax Celsius	S1 mgHC/ g rock	S2 mgHC/ g rock	S3 mg CO2/ g rock	PI	S2/S3 HC/CO2	TOC wt-%	HI mgHC/ g C	OI mg CO2/ gC
series	40	40	picked coal	N/R	492	0.03	0.98	1.25	0.03	0.78	4.2	23	29
	50	50	picked coal	1.05	457	0.08	2.76	0.47	0.03	5.87	3.55	77	13
	60	60	picked coal	N/R	465	0.05	1.55	0.97	0.03	1.59	3.64	42	26
	70	70	picked coal	0.78	461	0.03	2.81	0.79	0.01	3.55	4.57	61	17
	80	80	picked coal	N/R	451	0.02	2.4	0.79	0.01	3.03	3.7	64	21
	90	90	picked coal	0.73	446	0.06	8.41	1.93	0.01	4.35	4.26	197	45
	100	100	picked coal	0.72	439	0.08	7.41	1.31	0.01	5.65	4.56	162	28
	130	130	picked coal	0.72	451	0.09	4.37	0.97	0.02	4.5	3.94	110	24
	160	160	picked coal	0.69	458	0.06	4.53	1.58	0.01	2.86	7.2	62	21
	200	200	picked coal	0.65	438	0.05	1.59	0.49	0.03	3.24	2.68	59	18
	300	300	picked coal	0.8	446	0.29	7.61	1.08	0.04	7.04	8.8	86	12
	400	400	picked coal	N/R	455	0.11	5.12	1.58	0.02	3.24	8.49	60	18
SR-1													
west	0.1	0.15	coal	1.51?	517	0	0.13	1.75	0	0.07	3.73	3	46
coals	0.25	0.3	coal	NA	477	0	0.83	0.78	0	1.06	2.68	30	29
	0.34	0.34	coaly ss	1.6?	553	0	6.61	3.72	0	1.77	25.63	25	14
	0.35	0.4	coal	NA	490	0	0.96	2.51	0	0.38	5.08	18	49
	0.4	0.5	coal	NA	479	0	0.75	1.62	0	0.46	3	25	54

Basin Dike name Dike code Thickness Sample line	Initial X from Dike Contact (m)	Final X from Dike Contact (m)	Rock type	Rv-r mean (%)	Tmax Celsius	S1 mgHC/ g rock	S2 mgHC/ g rock	S3 mg CO2/ g rock	PI	S2/S3 HC/CO2	TOC wt-%	HI mgHC/ g C	OI mg CO2/ gC
	0.55	0.6	coal	NA	463	0	11.53	13.65	0	0.84	33.64	34	40
	0.6	0.6	coaly ss	0.73?	452	0	79.51	4.51	0	17.62	64.45	123	6
	0.9	0.9	coaly ss	0.73?	446	0.23	94.04	8.57	0	10.97	73.35	128	11
	0.9	1	coal	NA	487	0	17.32	21.4	0	0.8	57.78	29	37
	1	1.1	coaly ss	0.72?	443	0	82.08	8.75	0	9.38	72.34	113	12

NA or ? in this sample series means samples too weathered for Rv-r determination or source rock geochemist
The SR1 west coal series is not used for plotting purposes.

Basin Dike name Dike code Thickness Sample line	Initial X from Dike Contact (m)	Final X from Dike Contact (m)	Rock type	Rv-r mean (%)	Tmax Celsius	S1 mgHC/ g rock	S2 mgHC/ g rock	S3 mg CO2/ g rock	PI	S2/S3 HC/CO2	TOC wt-%	HI mgHC/ g C	OI mg CO2/ gC
Gippsland													
San Remo 3	0	0.005	picked coal	3.06	493	0.09	0.92	1.26	0.09	0.73	3.19	28	39
SR 3	0.01	0.015	picked coal	1.3	490	0.12	1.79	1.54	0.06	1.16	6.21	28	24
0.06 m	0.017	0.023	picked coal	1.14	478	0.21	4.98	1.78	0.04	2.79	8.91	55	19
west	0.029	0.034	picked coal	0.88	471	0.2	4.52	1.63	0.04	2.77	8.69	52	18
	0.039	0.044	picked coal	0.87	465	0.14	5.58	2.14	0.02	2.6	8.86	62	24
	0.048	0.053	picked coal	0.83	467	0.24	7.04	2.45	0.03	2.87	11.65	60	21
	0.059	0.064	picked coal	0.86	469	0.42	7.23	2.6	0.05	2.78	11.36	63	22
	0.07	0.07	picked coal	0.85	472	0.42	5.93	2.13	0.07	2.78	9.58	61	22
	0.09	0.09	picked coal	0.77	464	0.31	4.47	1.82	0.06	2.45	5.28	84	34
	0.14	0.14	picked coal	0.69	444	0.34	29.46	5.58	0.01	5.27	16.54	178	33
	0.19	0.19	picked coal	0.75	461	0.41	20.92	5.97	0.02	3.5	14.22	147	41
	1.4	1.4	picked coal	0.71	481	0.08	10.8	11.78	0.01	0.91	42.47	25	27
San Remo 3 SR 3 east	0.4	0.4	picked coal	0.64	505	0.04	4.36	7.59	0.01	0.57	22.61	19	33

Basin Sample Number	Reactor Temperature Celsius	Heating Duration hr	Rock type	Rv-r mean %	Tmax Celsius	S1 mgHC/ g rock	S2 mgHC/ r rock	S3 mg CO2/ g rock	PI	S2/S3 HC/CO2	TOC wt-%	HI mgHC/ g C	OI mg CO2/ gC
Gippsland													
R-5	Before Hydrous Pyrolysis		coal	0.62	430	0.16	170.84	6.21	0.00	27.51	63.54	268	9
HP 2182	295	72	coal	0.90	441	2.60	175.06	5.89	0.01	29.72	80.28	218	7
HP 2183	330	72	coal	1.23	454	15.53	121.80	5.53	0.11	22.02	76.93	158	7
HP 2184	365	72	coal	1.69	478	19.01	72.45	7.70	0.21	9.40	73.12	99	10

Appendix 6. Whole Rock Elemental data

Definitions for terms used in this tabulation of inductively coupled plasma atomic emission spectroscopy (ICP-AES) data in Appendix 6 are :

X = distance from dike contact in meters. X maybe annotated with the direction from dike margin, if appropriate. X may also be given as the sample interval relative to the dike margin on the side of the dike suggested by the direction (i.e. 0.1 to 0.2 m west) . If a single number is given, X indicates the sample interval midpoint from the dike contact.

ppm = parts per million

wt.-% = weight percent.

LOI = Loss on ignition (sample fusion) for ICP-AES analysis

Rock type:

ss = sandstone

ss-west = sandstones sampled on the west side of the dike

Basin Dike Name Host Rock X, in m	Al2O3 wt.-%	CaO wt.-%	Cr2O3 wt.-%	Fe2O3 wt.-%	K2O wt.-%	MgO wt.-%	MnO wt.-%	Na2O wt.-%	P2O5 wt.-%	SiO2 wt.-%	TiO2 wt.-%	L.O.I. wt.-%	Total wt.-%
Gippsland		Analyses After Correction to 100 wt-%											
Bena 3													
sandstone													
0.1	15.91	2.35	0.00	4.17	2.36	0.86	0.03	3.29	0.21	66.00	0.81	4.01	100.0
1.0	15.65	2.19	0.00	5.09	2.37	0.91	0.06	3.30	0.21	65.20	0.78	4.24	100.0
3.0	15.96	2.33	0.00	4.38	2.32	1.11	0.03	3.47	0.23	66.02	0.76	3.38	100.0
5.0	17.05	1.38	0.00	2.59	2.15	0.75	0.00	2.91	0.27	66.12	0.97	5.81	100.0
10.0	15.97	1.59	0.00	5.05	1.31	1.26	0.03	2.73	0.23	65.47	0.83	5.52	100.0
16.0	15.69	3.12	0.00	4.62	2.12	1.20	0.06	3.02	0.23	63.94	0.76	5.23	100.0
20.0	15.19	2.61	0.00	4.82	2.03	2.02	0.08	2.76	0.21	63.48	0.72	6.09	100.0
30.0	15.99	1.65	0.00	4.88	2.19	2.13	0.05	2.69	0.19	63.01	0.72	6.52	100.0
Gippsland													
Cruickston-1													
mudstone													
0.4	15.13	0.63	0.00	4.98	2.37	1.39	0.04	1.07	0.20	65.87	0.77	7.56	100.0
0.8	15.81	0.41	0.00	3.72	2.32	1.27	0.03	0.73	0.12	66.66	0.77	8.16	100.0
2.0	16.41	1.45	0.00	5.14	2.63	2.01	0.06	0.53	0.13	59.70	0.77	11.17	100.0
5.0	15.34	0.51	0.00	5.92	3.28	1.49	0.07	0.48	0.21	63.68	0.74	8.29	100.0
10.0	16.37	0.53	0.00	5.15	3.34	1.10	0.05	0.44	0.25	64.36	0.77	7.64	100.0
16.0	16.25	1.82	0.00	4.06	2.48	1.82	0.06	0.52	0.20	61.78	0.82	10.18	100.0
20.0	16.22	0.84	0.00	5.05	2.41	1.48	0.12	0.61	0.34	62.69	0.85	9.40	100.0
30.0	17.08	1.24	0.00	3.35	2.18	1.50	0.04	0.50	0.21	63.87	0.90	9.13	100.0
40.0	15.45	2.84	0.00	4.02	2.40	1.18	0.09	0.38	1.78	62.58	0.70	8.57	100.0
50.2	14.05	0.49	0.00	3.11	2.06	1.00	0.03	0.83	0.13	70.32	0.66	7.32	100.0
60.0	17.35	1.33	0.00	3.74	3.01	1.02	0.05	1.07	0.24	64.29	0.91	6.98	100.0
65.0	17.36	1.51	0.00	4.84	2.82	1.10	0.06	1.25	0.21	61.99	0.92	7.97	100.0
Gippsland													
Inverloch-1													
ss (west)													
0.0	15.45	1.68	0.02	3.19	1.72	1.24	0.01	3.68	0.17	68.30	0.74	3.79	100.0
0.1	15.76	1.63	0.03	3.23	1.70	1.30	0.01	3.76	0.18	67.99	0.75	3.66	100.0
0.3	16.04	1.23	0.01	6.88	2.15	1.84	0.04	3.80	0.21	61.69	1.04	5.07	100.0
0.5	15.89	1.22	0.01	6.71	2.15	1.89	0.04	3.60	0.21	62.52	1.04	4.73	100.0
1.1	15.40	1.10	0.01	6.47	1.98	1.84	0.13	3.42	0.17	63.42	0.77	5.29	100.0
1.5	15.83	1.30	0.00	8.27	2.07	2.33	0.17	3.11	0.19	59.50	0.97	6.26	100.0
2.0	15.54	1.06	0.01	7.17	2.22	2.23	0.10	3.38	0.18	62.15	0.89	5.08	100.0
3.0	15.88	2.31	0.00	4.28	2.42	1.88	0.06	3.37	0.15	62.68	0.63	6.34	100.0
4.0	16.22	2.18	0.00	4.67	2.23	2.05	0.06	3.33	0.16	61.98	0.67	6.43	100.0
San Remo-1													
ss (west)													
0.0	15.32	1.26	0.00	10.84	2.05	1.64	0.08	3.66	0.22	58.24	1.10	5.60	100.0
0.1	14.61	1.49	0.00	6.64	2.24	1.37	0.11	3.38	0.16	61.63	0.74	7.62	100.0
0.1	15.31	1.19	0.00	11.36	1.65	2.07	0.09	3.59	0.19	59.43	0.84	4.28	100.0
0.3	14.86	5.55	0.00	10.17	1.69	1.98	0.18	3.28	0.19	53.24	0.82	8.04	100.0
0.5	15.20	3.53	0.00	8.83	1.92	1.93	0.12	3.69	0.20	57.13	0.81	6.66	100.0
0.6	15.44	2.02	0.00	13.73	1.45	2.47	0.11	3.21	0.22	54.86	0.80	5.69	100.0
1.0	15.44	4.42	0.00	11.63	1.78	2.32	0.16	3.20	0.19	52.61	0.79	7.45	100.0

Basin Dike name Host Rock X, in meters	Ba ppm	Rb ppm	Sr ppm	Nb ppm	Zr ppm	Y ppm
Gippsland						
Bena-3						
sandstone						
0.1	550	70	470	10	160	20
1	600	70	440	10	150	20
3	580	65	460	10	140	20
5	470	70	270	10	180	20
10	410	60	310	<10	180	20
16	460	60	290	<10	120	10
20	420	65	270	<10	130	10
30	460	70	290	<10	140	10
Gippsland						
Cruickston-1						
mudstone						
0.4	390	70	140	10	140	20
0.8	360	90	110	10	140	10
2	360	100	120	10	150	20
5	410	120	190	10	130	20
10	440	120	270	10	150	10
16	350	90	120	10	180	20
20	380	95	100	10	170	20
30	370	85	170	10	190	20
40	440	80	260	10	110	60
50.2	380	80	90	10	130	10
60	440	110	110	10	170	10
65	410	100	110	10	160	20
Gippsland						
Inverloch-1						
sandstone						
0.01	440	40	320	10	150	20
0.055	430	40	320	10	160	20
0.325	480	55	220	10	160	20
0.52	460	55	210	10	180	20
1.06	390	50	180	10	170	10
1.545	420	60	180	10	160	20
2	420	55	170	10	140	10
3	450	70	190	10	120	10
4	420	55	190	10	150	10
Gippsland						
San Remo-1						
sandstone						
0.02	350	45	220	10	200	20
0.075	1010	60	260	10	140	10
0.14	300	40	160	10	140	10
0.315	330	35	210	10	130	10
0.535	370	45	210	10	130	20
0.645	210	35	120	10	120	10
1	330	40	190	10	130	10

Appendix 7. Carbon and Oxygen Isotope Data.

Appendix 7-1. Isotope Data, Buchan Caves Limestone, Buchan Rift, Victoria

Dike/ X (in m) + direction	Sample Type	Gas Yield (ml)	$\delta^{13}C$ (‰)	$\delta^{18}O$ (‰)	Notes
M1/0.10 S	whole rock	N/R	-0.28	- 7.58	All M1 are host rock cut using a saw to avoid cements.
M1/0.15 S	whole rock	N/R	0.15	- 6.19	
M1/0.45 S	whole rock	N/R	0.10	- 7.41	
M1/0.72 S	whole rock	N/R	0.30	- 6.83	
M1/0.93 S	whole rock	N/R	0.23	-6.88	
M1/1.36 S	whole rock	N/R	0.12	- 7.32	
M1/1.47 S	whole rock	N/R	0.34	- 8.93	
M1/1.70 S	whole rock	N/R	0.27	- 6.80	
M1/2.10 S	whole rock	N/R	0.09	-6.24	
M1/2.18 S	whole rock	N/R	0.19	- 9.55	
M1/2.35 S	whole rock	N/R	0.30	- 8.16	
M1/3.03 S	whole rock	N/R	0.25	- 7.03	
M1/3.44 S	whole rock	N/R	-0.03	-6.79	
M1/4.30 S	whole rock	N/R	0.29	-6.91	
M1/5.13 S	whole rock	N/R	0.08	-7.00	
M1/5.45 S	whole rock	N/R	0.23	-6.40	
M1/6.28 S	whole rock	N/R	0.36	-6.61	
M1/6.61 S	whole rock	N/R	0.28	-6.25	
M1/6.97 S	whole rock	N/R	0.34	-6.13	

Appendix 7-2. Isotope Data, Strzelecki Group, Western Onshore GippslandBasin.

Regional Sample	Sample Type	Gas Yield (ml)	$\delta^{13}C$ (‰)	$\delta^{18}O$ (‰)	Notes
R4	picked calcite; whole vein	N/R	-1.96	-20.90	Calcite vein with near vertical trend in a coaly sandstone.
R5/calcite	picked calcite	9.5	+1.81	-16.33	Calcite in coal cleat. 90% cc; 10% coal. The same sample that was used for hydrous pyrolysis.
R5 (HP 2182)	CO_2 gas	3.7	-20.00	-21.80	Gas from hydrous pyrolysis of sample R5 coal; 295°C/ 72 hr
R5 (HP 2182)	CH_4 gas	0.8	-32.27	--------	Gas from hydrous pyrolysis of sample R5 coal; 295°C/ 72 hr
R5 (HP 2183)	CO_2 gas	4.6	-21.77	-17.37	Gas from hydrous pyrolysis of sample R5 coal; 330°C/ 72 hr
R5 (HP 2183)	CH_4 gas	1.1	-34.84	--------	Gas from hydrous pyrolysis of sample R5 coal; 330°C/ 72 hr
R5 (HP 2184)	CO_2 gas	3.6	-24.28	-21.66	Gas from hydrous pyrolysis of sample R5 coal; 365°C/ 72 hr
R5 (HP 2184)	CH_4 gas	3.2	-36.12	--------	Gas from hydrous pyrolysis of sample R5 coal; 365°C/ 72 hr
R6	picked calcite; whole vein	N/R	+2.01	-17.91	Calcite vein with a near vertical, NE orientation approximately parallel to the I1 dike.
R9A	picked calcite; whole vein	N/R	+3.84	-22.37	NNW set of veins exposed in coastal cliff near dikes I2 and I3. Vein is composed of coarse sparry calcite.
R9/ concretion	concretion, whole rock	4.4	+1.21	-20.76	Carbonate cement in ss
R10	picked calcite; whole vein	N/R	-0.15	-11.18	Calcite vein in a fracture oriented parallel to bedding planes in the in sandstone.
R12/ concretion	concretion, whole rock	------	--------	--------	Insufficient yield. Regional sample for B1 and B3 dikes.
R19	concretion, whole rock	N/R	-1.80	-22.24	Analysis of fresh rock taken from core of sample.

Appendix 7-2. Isotope Data, Strzelecki Group, Western Onshore Gippsland Basin

Regional Sample	Sample Type	Gas Yield (ml)	$\delta^{13}C$ (‰)	$\delta^{18}O$ (‰)	Notes
R19 country rock	concretion, whole rock	2.7	-0.82	-22.07	Calcite cemented sandstone.
R19 vein	picked calcite; whole vein	10.0	+2.48	-20.87	Vein in calcite cemented sandstone.
R20	picked calcite; whole vein	N/R	-6.37	-24.12	Calcite from NNW oriented vein at Bourne Creek, near Kilcunda, Victoria.
R20	ss, host rock	------	---------	--------	No reaction in concentrated hydrochloric acid; not submitted for isotope analysis.
R23	picked calcite; whole vein	N/R	-2.32	-20.20	Calcite vein in cove just east of SR1.
R25B	picked calcite; whole vein	N/R	-8.21	-12.62	Vein composed of sparry calcite. Host rock removed by grinding. regional sample for SR1 and SR3 dikes.
R25CR	whole rock	4.3	-4.87	-21.15	Calcite cemented massive sandstone; regional sample to SR1 and SR3 dikes
R25D	picked calcite; whole vein	N/R	-8.26	-12.63	Calcite veins trending north and near vertical.
R26	picked calcite; whole vein	N/R	-5.58	-22.76	Very coarse sparry calcite filling vug in SR1 dike. Definitely a post dike calcite. Fluid inclusion analysis shows this calcite to have formed near 70°C and from fresh water.
R27A	picked calcite, whole vein	N/R	-4.01	-14.68	Sample taken from a NW trending vein in sandstone at Shelley Beach SW of Kilcunda, Victoria; crushed and picked out unweathered calcite.
R27B	picked calcite	N/R	-5.33	-22.32	Calcite in coal. Location as above.
R-28	ss, host rock	------	---------	--------	No reaction in concentrated hydrochloric acid; not submitted for isotope analysis.

Appendix 7-2.Isotope Data, Strzelecki Group, Western Onshore Gippsland Basin

Regional sample	Sample Type	Gas Yield (ml)	$\delta^{13}C$ (‰)	$\delta^{18}O$ (‰)	Notes
R28	picked calcite; whole vein	N/R	-7.78	-8.88	Calcite vein in a sandstone. NW strike
R32 concretion	concretion; whole rock	3.4	+3.97	-24.19	Calcite cemented sandstone; weathered rind of rock removed.
R35	picked calcite; whole vein	N/R	-5.02	-21.70	Calcite vein in a sandstone.
R35	picked calcite; whole vein	N/R	-5.03	-21.62	Rerun
R37	picked calcite; whole vein	N/R			Thin calcite veins near 0.5m and 0.2 to 0.4 m thick dikes. The dikes are exposed in a road cut just west of Loch, Victoria.
R40	whole host rock	------	---------	--------	No reaction in concentrated hydrochloric acid; not submitted for isotope analysis.
Well / depth (in m)	**Sample Type**	**Gas Yield (ml)**	**$\delta^{13}C$ ‰**	**$\delta^{18}O$ ‰**	**Notes**
Wellington Park 1/ 4337	picked calcite; whole vein	8.2	-1.85	-23.33	Calcite vein, slickensided apparently caused by repeated fault movement.
Tarwin Meadows 1 / 3128	whole rock	0.5	+0.20	-23.96	Carbonate cemented massive light medium gray sandstone

Appendix 7-2. Isotope Data, Strzelecki Group, Western Onshore Gippsland Basin

Dike/ X (in m) + direction	Sample Type	Gas Yield (ml)	$\delta^{13}C$ (‰)	$\delta^{18}O$ (‰)	Notes
Bena 3 east B3/ 0.05m E B3/ 1m E B3/ 3m E B3/ 5m E B3/ 10m E B3/ 16m E B3/ 20m E B3/ 30m E	whole rock	 none none none none none yes yes none			Most samples showed no reaction in concentrated hydrochloric acid. Therefore, the entire sample suite was not analyzed for isotopes.
Cruickston 1 east CRU1/ 2 E	whole rock; all CRU1 isotope samples taken from powders prepared for whole rock element analysis	0.3	-1.27	-11.76	Calcareous mudstone. Mudstones at 0.4 m E and 0.8 m E had no reaction in concentrated hydrochloric acid and were not analyzed for isotopes.
CRU1/ 5 E	whole rock	0.3	-2.17	-9.79	Calcareous mudstone
CRU1/ 10 E	whole rock	0.5	-2.45	-8.83	Calcareous mudstone
CRU1/ 16 E	whole rock	1.8	-1.72	-11.87	Calcareous mudstone
CRU1/ 20 E	whole rock	0.6	-1.49	-11.99	Calcareous mudstone
CRU1/ 30 E	whole rock	1.1	-1.11	-12.27	Calcareous mudstone
CRU1/ 40 E	whole rock	0.6	-2.04	-8.71	Calcareous mudstone
CRU1/ 60 E	whole rock	1.0	-3.88	-4.65	Calcareous mudstone
CRU1/ 65 E	whole rock	0.8	-5.41	-9.33	Calcareous mudstone
Inverloch 1 west I1/ 0.01 W I1/ 0.055 W I1/ 0.32 W I1/ 0.52 W I1/ 1.06 W I1/ 1.55 W I1/ 2 W I1/3 W I1/4 W	 whole host rock whole host rock whole host rock whole host rock whole host rock whole host rock whole host rock whole host rock whole host rock	 none none none none none none little yes yes	N/A	N/A	Most samples showed no reaction in concentrated hydrochloric acid. Therefore, entire sample suite was not analyzed for isotopes.

Appendix 7-2. Isotope Data, Strzelecki Group, Western Onshore Gippsland Basin.

Dike/ X (in m) + direction	Sample Type	Gas Yield (ml)	$\delta^{13}C$ (‰)	$\delta^{18}O$ (‰)	Notes
I1/ 3.4 W	picked calcite; whole vein	5.6	+5.81	-22.69	Coarse sparry calcite from vein with a parallel orientation to dike. exposed at cliff face. 95% cc; 5% host rock
I1/ 6.5 W	picked calcite; whole vein	9.7	+5.18	-22.40	Coarse sparry calcite from vein with a parallel orientation to dike. Exposed at cliff face. 99% cc; 1% host rock.
Iverloch 2 east I2/ 0.0 e	picked calcite; whole vein	N/R	-3.93	-20.24	braided veins filled with acicular cc at dike host rock contact. Sample mixed with mdst; about 85-90% cc; rest host rock.
I2/ 0.30-0.35 E	picked calcite; whole vein	N/R	-0.23	-16.36	Thin calcite veins cutting host sandstone; 95% cc; 5 % host
I2/ 0.155-0.215 E	picked calcite	N/R	-4.52	-14.52	Coal (or coke) with pores filled by cc; 70% coal; 30% cc; 10% ss
Iverloch 3 East I3/ 0-0.02 E	picked calcite; whole vein	N/R	-3.82	-18.42	Selected vein fragments; 70% cc; 30% ss
I3/ 0.40-0.43 E	picked calcite; whole vein	N/R	-1.53	-19.84	Braided veins composed of acicular cc fibers oriented perpendicular to vein wall.
San Remo 1 east SR1/ 0.01 E	picked calcite; whole vein	N/R	-5.19	-15.43	Vein in mdst. 90% cc; 10% host.
SR1/ 0.19 E	picked calcite; whole vein	N/R	-4.63	-14.98	Thin discontinuous calcite vein lining fractures parallel to dike orientation.
SR1/ 0.20 E	picked calcite; whole vein	N/R	-3.59	-15.04	Thin discontinuous calcite vein lining fractures parallel to dike orientation
SR1/ 0.27 E	picked calcite; whole vein	N/R	-4.42	-13.96	Thin discontinuous calcite vein lining fractures parallel to dike orientation.
SR1/ 0.50 E	picked calcite; whole vein	N/R	-3.18	-20.69	Thin discontinuous calcite vein lining fractures parallel to dike orientation.

Appendix 7-2. Isotope Data, Strzelecki Group, Western Onshore Gippsland Basin

Dike/ X (in m) + direction	Sample Type	Gas Yield (ml)	$\delta^{13}C$ (‰)	$\delta^{18}O$ (‰)	Notes
San Remo 1 west SR1/0.01 W	picked calcite; whole vein	0.3	-6.47	-13.46	Thin discontinuous calcite vein lining fractures parallel to dike orientation.
SR1/ 0.04 W	picked calcite; whole vein	8.1	-4.18	-17.56	Thin discontinuous calcite vein lining fractures parallel to dike orientation.
SR1/0.05 W	picked calcite; whole vein	0.6	-4.65	-13.18	Braided veins in host sandstone. 80% cc; 20% host.
SR1/0.11 W	whole vein; cleaned calcite	9.8	-4.29	-18.89	2 mm thick vein. Trace of host sandstone remaining attached to vein contact after grinding.
SR1/ 0.12 W	picked calcite; whole vein	10.0	-4.01	-18.46	1 to 4 mm thick calcite vein that has incorporated host rock ripoff fragments making it look crudely zoned. CL microscopy suggests homogeneous composition. 95% cc; 5% host sandstone
SR1/ 0.14 W	picked calcite; whole vein	0.5	-4.49	-18.67	Thin discontinuous calcite vein lining fractures parallel to dike orientation.
SR1/ 0.3 W	picked calcite; whole vein	1.0	-2.94	-20.28	Thin discontinuous calcite vein lining fractures parallel to dike orientation.
SR1/ 0.47 W	picked calcite; whole vein	0.5	-3.44	-20.77	Thin discontinuous calcite vein lining fractures parallel to dike orientation.
SR1/ 0.61 W	picked calcite; whole vein	0.3	-3.60	-21.02	Thin discontinuous calcite vein lining fractures parallel to dike orientation.
SR1/ 0.61 W	picked calcite; whole vein	0.8	-3.61	-20.93	Rerun
SR1/ 1.0 W	picked calcite; whole vein	0.8	-2.96	-18.90	Thin discontinuous calcite vein lining fractures parallel to dike orientation.
San Remo 3 SR3/ 0.0 W	picked calcite; whole vein	N/R	+2.90	-12.03	Thin calcite vein at the dike contact with sandstone.

Appendix 8. Summary of ^{13}C CP MAS NMR Results

Appendix 8-1. ^{13}C NMR Results, selected picked coal samples, Western Onshore Gippsland Basin.

Basin: Dike / x (in meters) + direction	***f*a**	***f*ali**	**Aromatic spinning side band**	**Carbonyl-ketone?**	**Aromatic-phenolic**	**Aromatic C-C, C-H**
Gippsland:						
Bena 1 west						
B1/0.0-0.4 m W	0.99	0.02	0.10	0.01	0.04	0.75
B1/0.10-0.15mW	0.91	0.03	0.09	0.04	0.0	0.73
B1/0.3-0.35mW	0.89	0.05	0.08	0.04	0.01	0.72
B1/0.5-0.6mW	0.86	0.05	0.07	0.04	0.02	0.74
B1/1.0-1.1mW	0.89	0.06	0.08	0.04	0.03	0.70
B1/1.5-1.6mW	0.81	0.13	0.06	0.03	0.02	0.67
B1/ 2-2.1 m W	0.78	0.16	0.06	0.04	0.04	0.62
B1/3.0-3.1mW	0.75	0.20	0.05	0.04	0.0	0.65
Inverloch 2 east						
I2/0.00-0.01mE	1.01	-0.01	0.15	0.0	0.0	0.71
I2/0.04-0.06mE	0.99	0.02	0.09	0.0	0.0	0.81
I2/0.10-0.12mE	0.82	0.11	0.07	0.05	0.06	0.62
I2/0.19-0.22mE	0.73	0.20	0.06	0.0	0.0	0.61
I2/0.29-0.32mE	0.73	0.28	0.04	0.01	0.11	0.54
San Remo 1 west						
SR1/0.0mW	0.89	0.07	0.07	0.05	0.0	0.75
SR1/0.1mW	0.84	0.08	0.08	0.04	0.0	0.68
SR1/0.2mW	0.80	0.11	0.06	0.05	0.0	0.68
SR1/0.3mW	0.88	0.07	0.10	0.02	0.03	0.65
SR1/0.65mW	0.82	0.19	0.06	0.01	0.0	0.70

Appendix 8-1. ^{13}C NMR Results, selected picked coal samples,

Western Onshore Gippsland Basin.

Regional Samples	*fa*	*fali*	Aromatic spinning side band	Carbonyl-ketone?	Aromatic-phenolic	Aromatic C-C, C-H
R5	0.67	0.35	0.03	0.01	0.08	0.53
R5 -- hydrous pyrolysis: 300°C; 72 hr	0.72	0.28	0.04	0.0	0.0	0.64
R5 -- hydrous pyrolysis: 330°C; 72 hr	0.83	0.18	0.07	0.0	0.0	0.69
R5 -- hydrous pyrolysis: 365°C; 72 hr	0.89	0.11	0.08	0.0	0.0	0.73
R23	0.76	0.21	0.06	0.0	0.0	0.64
Basin: Well/ Depth (in meters)	***fa***	***fali***	**Aromatic spinning side band**	**Carbonyl-ketone?**	**Aromatic-phenolic**	**Aromatic C-C, C-H**
Gippsland: Tarwin Meadows 1/ 490m depth	0.61	0.39	0.04	0.0	0.04	0.49

Appendix 9. Geothermochronological data

Fission Track Age Data Sheets

Terms and Definitions

N_s = Number of spontaneous tracks in N_a grid squares

N_i = Number of induced tracks in N_a grid squares

N_a = Number of grid squares counted in each grain

RATIO = N_s/N_i

U(ppm) = Uranium content of each grain (= U content of standard glass . ρ_i/ρ_o)

Cl (wt%) = Weight percent chlorine content of each grain

Rho s (ρ_s) = Spontaneous track density (ρ_s) = N_s/ (N_a.area of basic unit)

Rho i (ρ_i) = Induced track density (ρ_i) = N_i/ (N_a.area of basic unit)

F. T. AGE = Fission track age, calculated using the fission track age equation (Marshallsea, 1988)

Area of basic unit = Area of one grid square

Chi squared = X^2 parameter, used to assess variation of single grain ages within the sample

P(X^2) = Probability of obtaining observed X^2 value for the relevant number of degrees of freedom, if all grains belong to a single population

Correlation coefficient = Correlation coefficient between N_s and N_i

Variance of √(Ns) = Variance of square root of N_s values- should be ~0.25 for Poisson distribution; greater if additional variation present

Variance of √(Ni) = Variance of square root of Ni values- should be ~0.25 for Poisson distribution; greater if additional variation present

Age dispersion	= % variation in single grain ages- see discussion on central age
N_s/N_i	= Pooled ratio, total spontaneous tracks divided by total induced tracks for all grains
Mean ratio	= Mean of (N_s/N_i) for individual grains
Zeta	= Calibration constant, determined empirically for each observer
Rho D (ρ_D)	= Track density ρ_D) from uranium standard glass (interpolated from values at each end of stack
ND	= Total number of tracks counted for determining ρ_D
POOLED AGE	= Fission track age calculated from pooled ratio Ns/Ni. Valid only when X^2>5%
CENTRAL AGE	= Alternative to pooled age when X^2<5%

This apatite fission track annealing and age data is from a cooperative study on heating duration near dikes with Susan Marshallsea, Geotrack International, Melbourne, Australia. Barker with Ian Duddy and Paul Green, Geotrack International, Melbourne, Australia, sampled the San Remo 1 dike. Barker sampled all other dikes.

Table 1: Details of AFTA samples and apatite yields - outcrop samples from the Gippsland Basin (Geotrack Report #RD20)

Sample number	Location	Source number	Stratigraphic subdivision	Stratigraphic age (Ma)	Raw weight (g)	Washed weight (g)	Apatite yield *1
San Remo Dyke							
RD20-1	0-10 cm West of dyke	9142-1	Strzelecki Gp	120-98	1160	-	Very Good
RD20-2	~20 cm West of dyke	9142-2	Strzelecki Gp	120-98	740	265	Excellent
RD20-10	~1.0 m West of dyke	9142-10	Strzelecki Gp	120-98	1220	465	Excellent
RD20-16	5.0 m West of dyke	9142-16	Strzelecki Gp	120-98	990	598	Very Good
RD20-18	regional sample	9142-18	Strzelecki Gp	120-98	15580	186	Excellent
RD20-19	-		Strzelecki Gp	120-98	1510	863	Fair
			Granite pebble				
Inverlock-1							
RD20-31	0-5 cm left of dyke		Strzelecki Gp	120-98	1400	409	Poor
RD20-32	30-40 cm left of dyke		Strzelecki Gp	120-98	2230	263	Excellent
RD20-35	300 cm left of dyke		Strzelecki Gp	120-98	1640	845	Very Good
Bena-1							
RD20-36	0-5 cm West of dyke		Strzelecki Gp	120-98	2740	840	Excellent
RD20-37	30-40 cm West of dyke		Strzelecki Gp	120-98	2470	1112	Excellent
RD20-38	1.5-1.6 m West of dyke		Strzelecki Gp	120-98	2430	1090	Excellent
RD20-39	6.0-6.1 m West of dyke		Strzelecki Gp	120-98	2650	1390	Excellent

*1 Yield based on quantity of apatite suitable for age determination. Excellent: >20 grains; Very Good: ~20 grains; Good: 15-20 grains; Fair: 10-15 grains; Poor: 5-10 grains; Very Poor: <5 grains.

Table 1: Summary of apatite fission track data - outcrop samples from the Gippsland Basin (Geotrack Report #RD20)

Sample number	Source number	Apatite fission track age (Ma)	Corrected age *1 (Ma)	Stratigraphic age (Ma)	Mean track length (µm)
San Remo Dyke					
RD20-1	9142-1	94.3 ± 8.1	94	120-98	14.89 ± 0.15
RD20-2	9142-2	131.4 ± 9.3	132	120-98	14.26 ± 0.25
RD20-10	9142-10	128.2 ± 8.5	128	120-98	14.58 ± 0.20
RD20-16	9142-16	138.7 ± 9.2	139	120-98	14.62 ± 0.20
RD20-18	9142-18	145.9 ± 11.8	146	120-98	14.71 ± 0.17
RD20-19		116.3 ± 28.1	116	120-98	15.16 ± 0.39
Inverlock-1					
RD20-31		85.0 ± 12.0	85	120-98	14.63 ± 0.35
RD20-32		96.8 ± 8.2	97	120-98	14.31 ± 0.17
RD20-35		105.7 ± 8.6	108	120-98	13.94 ± 0.28
Bena-1					
RD20-36		102.1 ± 8.2	102	120-98	14.75 ± 0.13
RD20-37		93.4 ± 6.9	93	120-98	14.74 ± 0.19
RD20-38		104.1 ± 8.2	104	120-98	14.76 ± 0.15
RD20-39		135.6 ± 11.2	136	120-98	14.74 ± 0.25

*1 See Appendix C for explanation of Corrected age. Corrected age is not calculated for mean lengths less than 7.5 µm.

Table B.2: Length distribution summary data - outcrop samples from the Gippsland Basin (Geotrack Report #RD20)

Sample number	Mean track length (µm)	Standard deviation (µm)	Number of tracks (N)	Number of Tracks in Length Intervals (µm) 1	2	3	4	5	6	7	8	9	10	11	12	13	14	15	16	17	18	19	20
San Remo Dyke																							
RD20-1	14.89 ± 0.15	1.18	58	-	-	-	-	-	-	-	-	-	-	-	2	1	5	24	18	6	2	-	-
RD20-2	14.26 ± 0.25	2.07	71	-	-	-	-	1	1	-	-	-	-	1	3	4	13	19	22	7	-	-	-
RD20-10	14.58 ± 0.20	2.03	100	-	-	-	2	-	-	-	-	-	-	1	-	8	10	35	25	18	1	-	-
RD20-16	14.62 ± 0.20	1.70	69	-	-	-	-	-	-	-	1	-	1	-	3	4	10	16	20	12	2	-	-
RD20-18	14.71 ± 0.17	1.35	61	-	-	-	-	-	-	-	-	-	-	2	1	3	8	21	17	7	2	-	-
RD20-19	15.16 ± 0.39	0.77	4	-	-	-	-	-	-	-	-	-	-	-	-	-	-	1	2	1	-	-	-
Inverlock-1																							
RD20-31	14.63 ± 0.35	0.85	6	-	-	-	-	-	-	-	-	-	-	-	-	-	1	3	2	-	-	-	-
RD20-32	14.31 ± 0.17	1.72	104	-	-	-	-	1	1	-	-	-	-	1	1	9	19	34	31	7	-	-	-
RD20-35	13.94 ± 0.28	2.39	72	-	-	-	1	-	1	-	1	1	1	1	2	5	16	17	16	9	1	-	-
Bena-1																							
RD20-36	14.75 ± 0.13	1.11	70	-	-	-	-	-	-	-	-	-	-	-	1	3	10	28	18	9	1	-	-
RD20-37	14.74 ± 0.19	1.65	76	-	-	-	-	-	1	-	-	-	-	-	1	6	12	21	21	10	4	-	-
RD20-38	14.76 ± 0.15	1.51	106	-	-	-	-	-	-	1	-	-	1	2	1	1	12	41	31	13	2	1	-
RD20-39	14.74 ± 0.25	1.84	55	-	-	-	-	1	-	-	-	-	1	-	-	-	11	14	21	4	3	-	-

Track length measurements by S.J. Marshallsea.

RD20-1

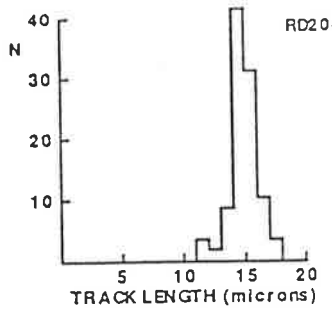

RD20-18

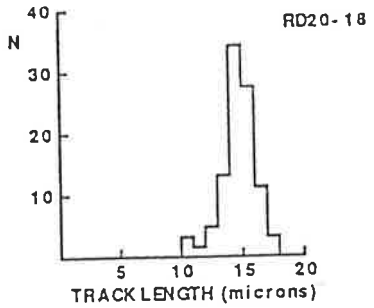

RD20-2

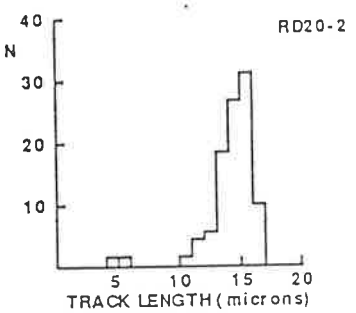

RD20-19

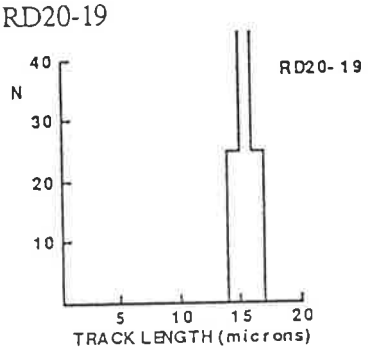

RD20-10

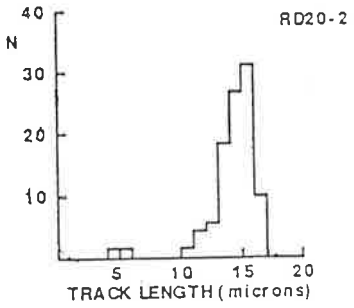

RD20-31

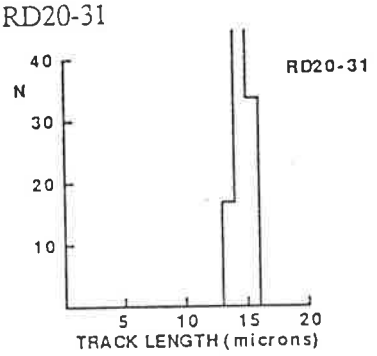

RD20-16

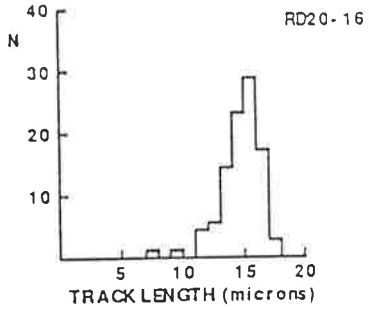

RD220-31

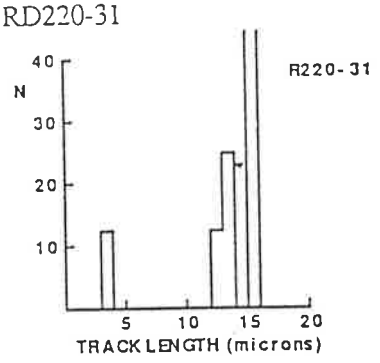

Figure B.4: Distributions of confined track lengths in outcrop samples from the Otway Basin.

RD15-32

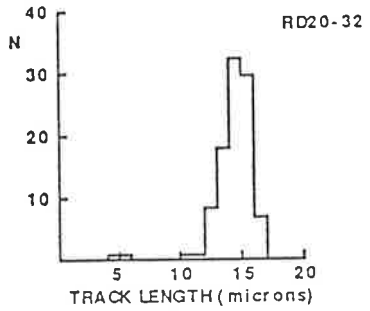

RD15-35

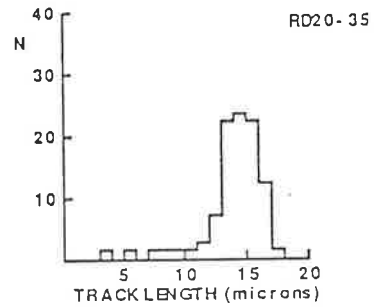

Figure B4: continued

RD20-36

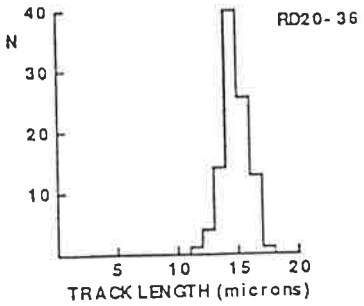

RD20-37

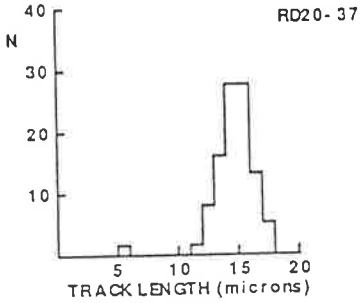

RD20-38

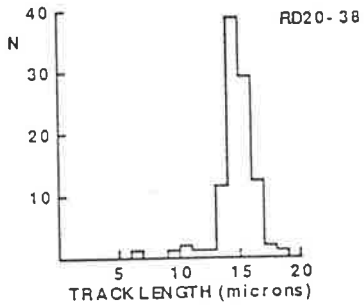

RD20-39

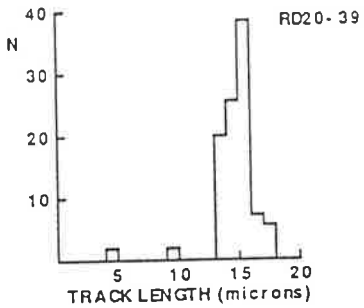

Figure B.4a: Distributions of confined track lengths in outcrop samples from the Gippsland Basin.

RD20-1

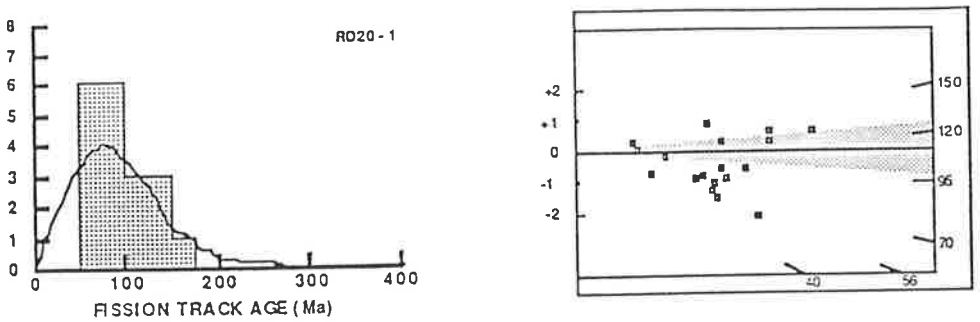

RD20-2

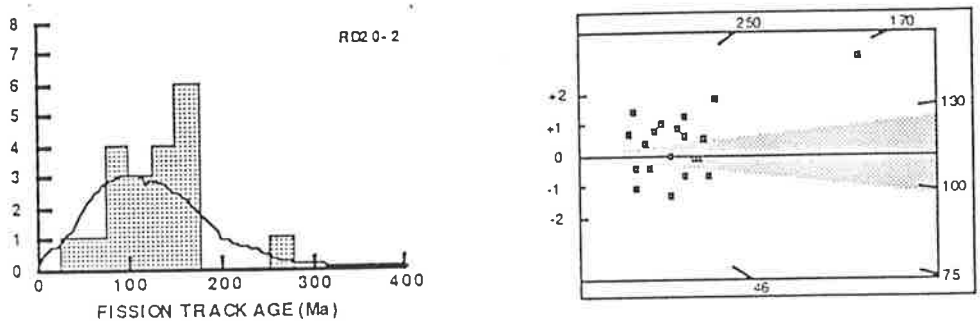

RD20-10

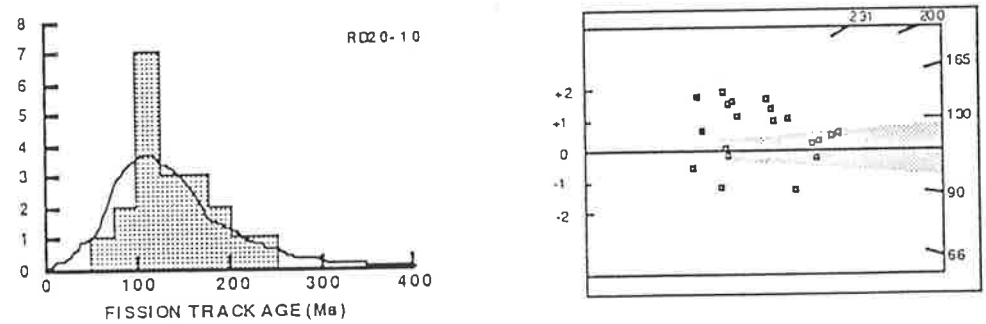

RD20-16

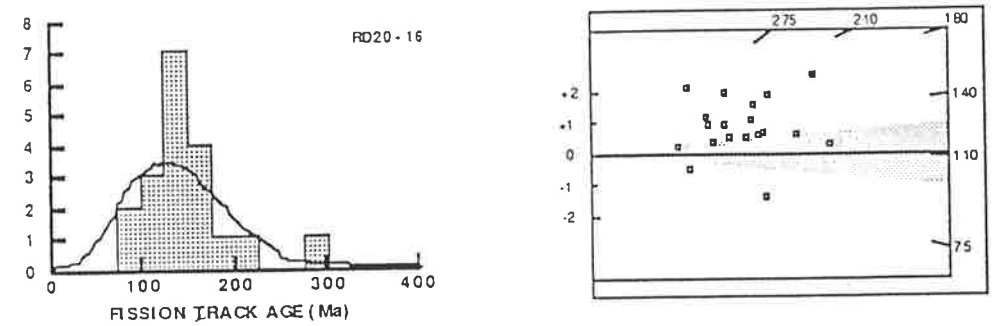

Figure B.3a: Single grain age figures for outcrop samples from the Gippsland Basin.

RD20-18

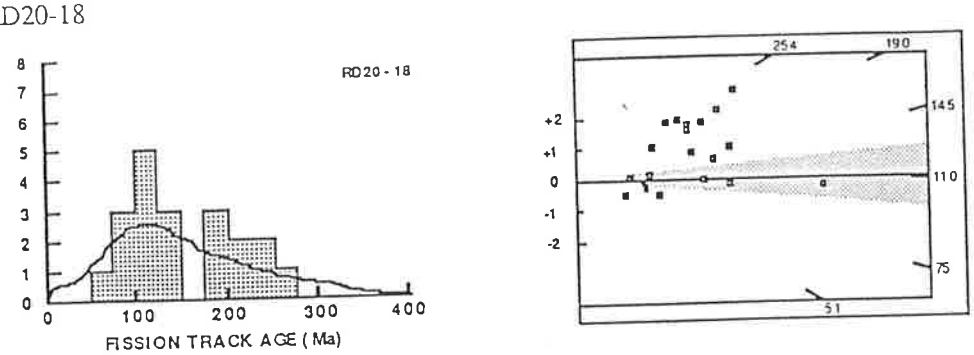

RD20-19

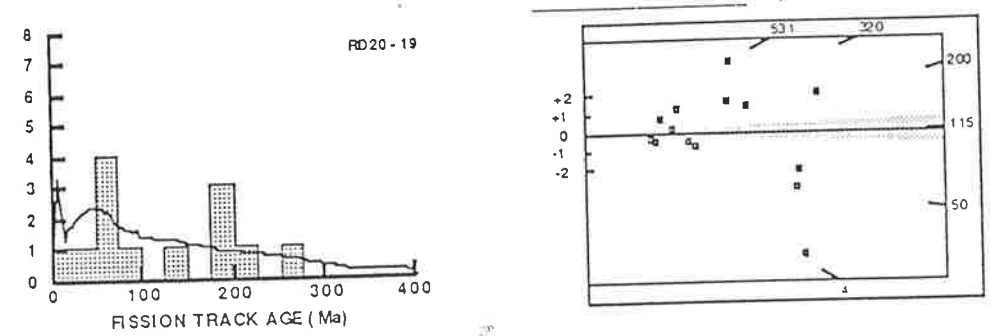

RD20-31

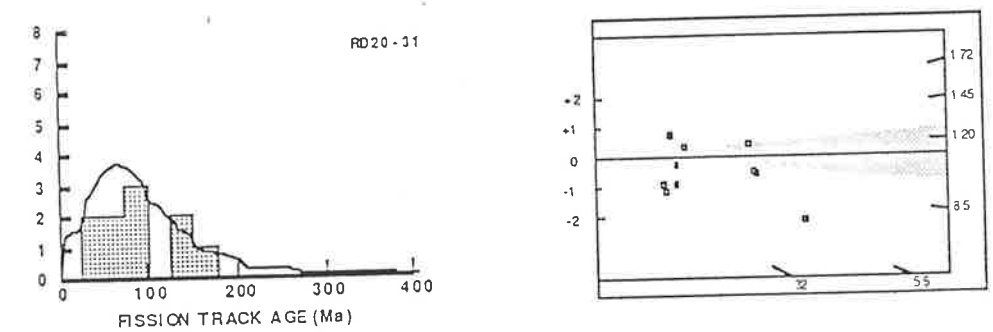

R220-31

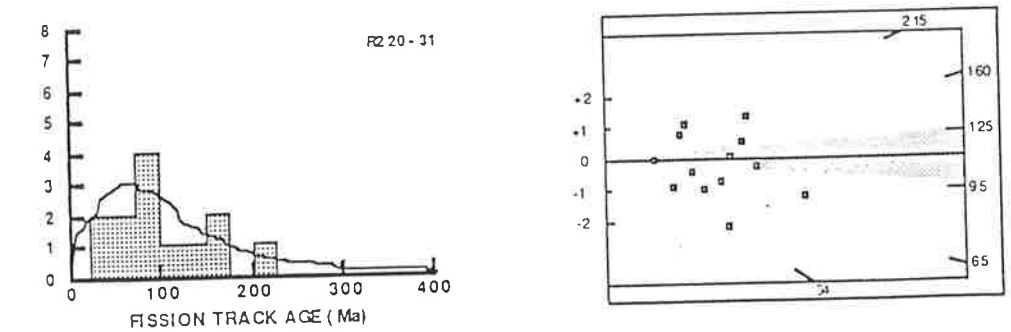

Figure B.3: continued

RD20-32

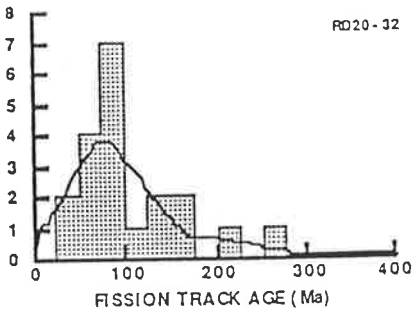

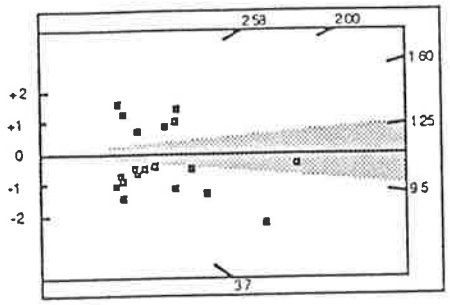

RD20-35

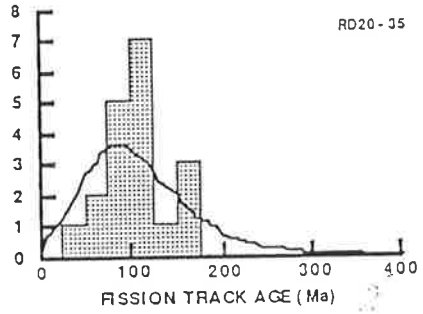

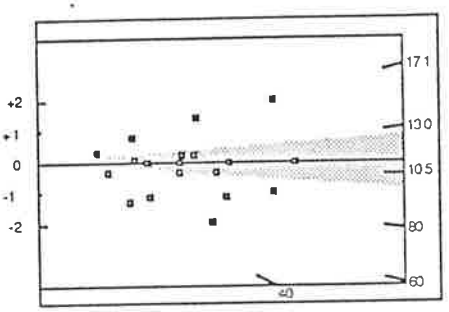

Figure B.3: continued

RD20-36

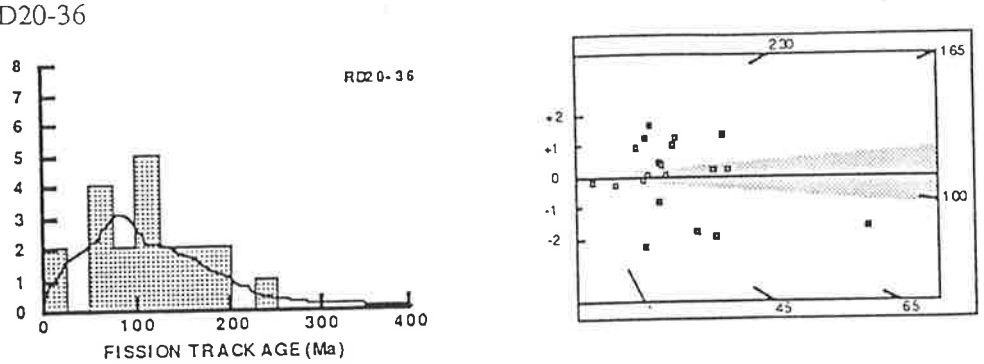

RD20-37

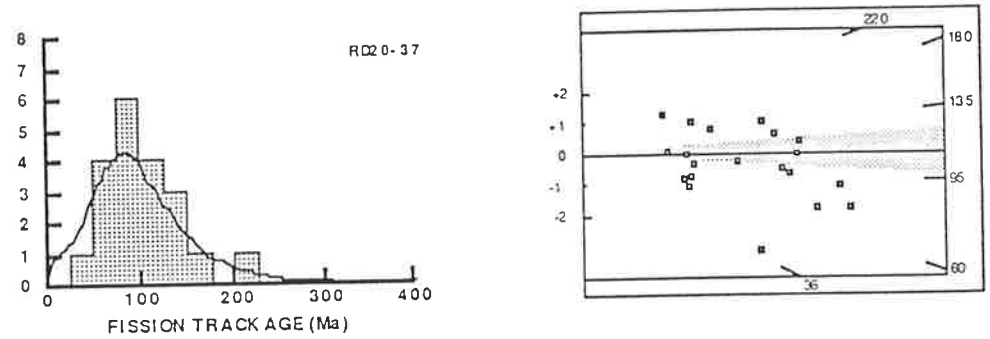

RD20-38

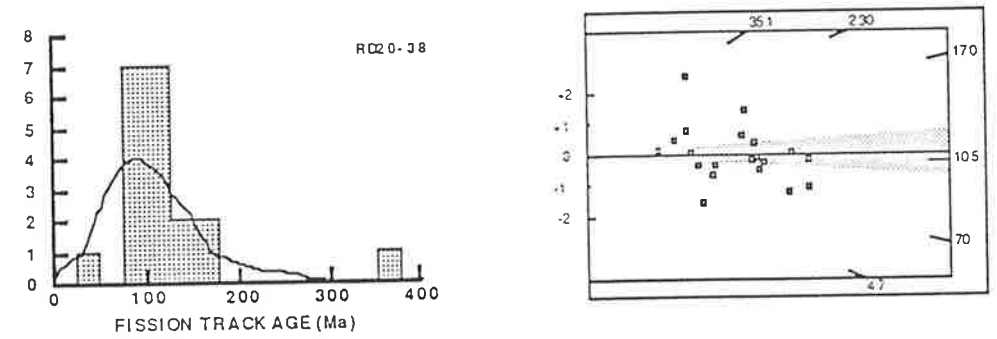

RD20-39

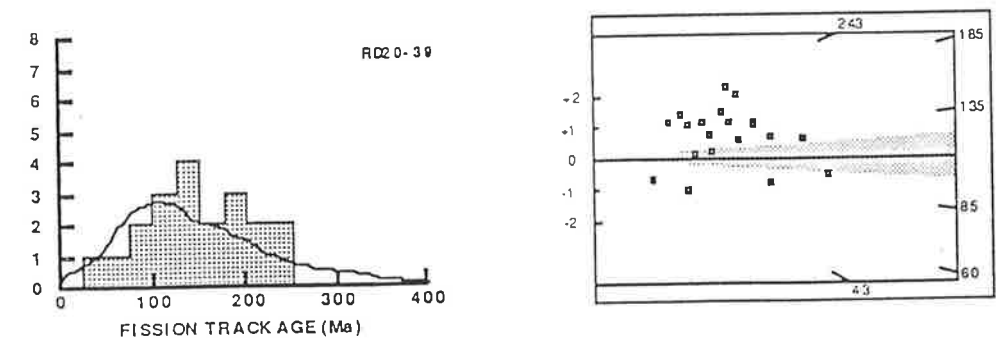

Figure B.3a: Single grain age figures for outcrop samples from the Gippsland Basin.

RD20-1 APATITE

IRRADIATION G344
SLIDE NUMBER 2
COUNTED BY: SJM

No.	Ns	Ni	Na	RATIO	U (ppm)	RHOs	RHOi	F.T. AGE (Ma)
1	12	20	64	0.600	4.5	2.980E+05	4.966E+05	150.8 ± 55.2
2	7	23	48	0.304	6.9	2.317E+05	7.614E+05	76.9 ± 33.3
3	2	5	40	0.400	1.8	7.945E+04	1.986E+05	100.9 ± 84.5
4	22	47	80	0.468	8.4	4.370E+05	9.336E+05	117.9 ± 30.6
5	10	32	80	0.312	5.7	1.986E+05	6.356E+05	79.0 ± 28.7
6	4	11	60	0.364	2.6	1.059E+05	2.913E+05	91.8 ± 53.6
7	7	23	40	0.304	8.3	2.781E+05	9.137E+05	76.9 ± 33.3
8	2	4	21	0.500	2.7	1.513E+05	3.027E+05	125.9 ± 109.1
9	13	27	42	0.481	9.2	4.919E+05	1.022E+06	121.3 ± 41.1
10	11	49	100	0.224	7.0	1.748E+05	7.786E+05	56.8 ± 19.0
11	10	29	60	0.345	6.9	2.648E+05	7.680E+05	87.1 ± 32.0
12	34	68	80	0.500	12.2	6.754E+05	1.351E+06	125.9 ± 26.6
13	6	21	50	0.286	6.0	1.907E+05	6.674E+05	72.2 ± 33.5
14	7	30	80	0.233	5.4	1.390E+05	5.959E+05	59.1 ± 24.8
15	8	28	80	0.286	5.0	1.589E+05	5.562E+05	72.2 ± 29.0
16	2	9	48	0.222	2.7	6.621E+04	2.980E+05	56.3 ± 44.0
17	7	28	36	0.250	11.2	3.090E+05	1.236E+06	63.3 ± 26.8
18	14	39	60	0.359	9.3	3.708E+05	1.033E+06	90.6 ± 28.3
19	23	45	50	0.511	12.9	7.310E+05	1.430E+06	128.7 ± 33.1
	201	538			6.9	2.854E+05	7.640E+05	

Area of basic unit = 6.293E-07 cm-2

Chi Squared = 13.195 with 18 degrees of freedom
P(chi squared) = 78.0 %
Correlation Coefficient = 0.895
Variance of SQR(Ns) = 1.37
Variance of SQR(Ni) = 2.63
Age Dispersion = 4.897 % (did not converge)

Ns/Ni = 0.374 ± 0.031
Mean Ratio = 0.366 ± 0.026

Ages calculated using a zeta of 350.7 ± 5 for SRM612 glass
Rho D = 1.450E+06cm-2; ND = 2343
Rho D interpolated between top of can; Rho D = 1.443E+06cm-2. ND = 1135
bottom of can; Rho D = 1.536E+06cm-2. ND = 1208

POOLED AGE = 94.3 ± 8.1 Ma
CENTRAL AGE = 94.1 ± 8.2 Ma

RD20-2 APATITE

IRRADIATION G344
SLIDE NUMBER 3
COUNTED BY: SJM

No.	Ns	Ni	Na	RATIO	U (ppm)	RHOs	RHOi	F.T. AGE (Ma)
1	2	11	16	0.182	9.8	1.986E+05	1.092E+06	46.3 ± 35.6
2	4	6	21	0.667	4.1	3.027E+05	4.540E+05	168.1 ± 108.6
3	21	42	100	0.500	6.0	3.337E+05	6.674E+05	126.5 ± 34.0
4	15	26	48	0.577	7.7	4.966E+05	8.607E+05	145.7 ± 47.4
5	31	46	56	0.674	11.7	8.797E+05	1.305E+06	169.9 ± 39.7
6	122	191	56	0.639	48.7	3.462E+06	5.420E+06	161.2 ± 19.1
7	9	15	38	0.600	5.6	3.764E+05	6.273E+05	151.5 ± 64.0
8	16	38	36	0.421	15.1	7.063E+05	1.677E+06	106.7 ± 31.9
9	3	10	35	0.300	4.1	1.362E+05	4.540E+05	76.2 ± 50.2
10	11	17	60	0.647	4.0	2.913E+05	4.502E+05	163.2 ± 63.3
11	18	28	64	0.643	6.2	4.469E+05	6.952E+05	162.2 ± 49.2
12	16	31	100	0.516	4.4	2.542E+05	4.926E+05	130.5 ± 40.3
13	12	35	20	0.343	25.0	9.534E+05	2.781E+06	87.0 ± 29.2
14	17	41	80	0.415	7.3	3.377E+05	8.144E+05	105.1 ± 30.4
15	5	15	70	0.333	3.1	1.135E+05	3.405E+05	84.6 ± 43.7
16	6	6	35	1.000	2.4	2.724E+05	2.724E+05	250.6 ± 144.8
17	18	50	60	0.360	11.9	4.767E+05	1.324E+06	91.3 ± 25.2
18	10	24	70	0.417	4.9	2.270E+05	5.448E+05	105.6 ± 39.8
19	7	28	80	0.250	5.0	1.390E+05	5.562E+05	63.6 ± 26.9
20	6	12	60	0.500	2.9	1.589E+05	3.178E+05	126.5 ± 63.3
	349	672			8.7	5.019E+05	9.664E+05	

Area of basic unit = 6.293E-07 cm-2

Chi Squared = 18.469 with 19 degrees of freedom
P(chi squared) = 49.1 %
Correlation Coefficient = 0.984
Variance of SQR(Ns) = 4.13
Variance of SQR(Ni) = 6.08
Age Dispersion = 11.645 %

Ns/Ni = 0.519 ± 0.034
Mean Ratio = 0.499 ± 0.042

Ages calculated using a zeta of 350.7 ± 5 for SRM612 glass
Rho D = 1.457E+06cm-2; ND = 2343
Rho D interpolated between top of can; Rho D = 1.443E+06cm-2, ND = 1135
bottom of can; Rho D = 1.536E+06cm-2, ND = 1208

POOLED AGE = 131.4 ± 9.3 Ma
CENTRAL AGE = 127.2 ± 10.2 Ma

RD20-10 APATITE

IRRADIATION G344
SLIDE NUMBER 4
COUNTED BY: SJM

No.	Ns	Ni	Na	RATIO	U (ppm)	RHOs	RHOi	F.T. AGE (Ma)
1	24	39	80	0.615	6.9	4.767E+05	7.747E+05	156.1 ± 40.7
2	9	16	56	0.562	4.1	2.554E+05	4.540E+05	142.8 ± 59.6
3	5	16	60	0.312	3.8	1.324E+05	4.238E+05	79.7 ± 40.9
4	16	22	60	0.727	5.2	4.238E+05	5.827E+05	184.1 ± 60.7
5	35	73	100	0.479	10.4	5.562E+05	1.160E+06	121.9 ± 25.3
6	11	12	100	0.917	1.7	1.748E+05	1.907E+05	231.2 ± 96.7
7	38	78	100	0.487	11.1	6.038E+05	1.239E+06	123.9 ± 24.7
8	19	61	100	0.311	8.7	3.019E+05	9.693E+05	79.5 ± 21.0
9	16	19	90	0.842	3.0	2.825E+05	3.355E+05	212.7 ± 72.4
10	28	68	100	0.412	9.7	4.449E+05	1.081E+06	104.9 ± 23.7
11	24	35	70	0.686	7.1	5.448E+05	7.945E+05	173.7 ± 46.2
12	7	27	100	0.259	3.8	1.112E+05	4.290E+05	66.2 ± 28.1
13	16	26	56	0.615	6.6	4.540E+05	7.378E+05	156.1 ± 49.8
14	11	27	56	0.407	6.9	3.121E+05	7.662E+05	103.8 ± 37.2
15	17	23	40	0.739	8.2	6.754E+05	9.137E+05	187.0 ± 60.0
16	29	64	70	0.453	13.0	6.583E+05	1.453E+06	115.3 ± 26.0
17	11	25	100	0.440	3.6	1.748E+05	3.973E+05	112.0 ± 40.6
18	27	48	88	0.562	7.8	4.876E+05	8.668E+05	142.8 ± 34.5
19	31	67	80	0.463	11.9	6.158E+05	1.331E+06	117.7 ± 25.7
20	23	41	90	0.561	6.5	4.061E+05	7.239E+05	142.5 ± 37.3
	397	787			7.0	3.953E+05	7.836E+05	

Area of basic unit = 6.293E-07 cm-2

Chi Squared = 18.593 with 19 degrees of freedom
P(chi squared) = 48.3 %
Correlation Coefficient = 0.892
Variance of SQR(Ns) = 1.24
Variance of SQR(Ni) = 2.95
Age Dispersion = 1.271 % (did not converge)

Ns/Ni = 0.504 ± 0.031
Mean Ratio = 0.543 ± 0.039

Ages calculated using a zeta of 350.7 ± 5 for SRM612 glass
Rho D = 1.464E+06cm-2; ND = 2343
Rho D interpolated between top of can: Rho D = 1.443E+06cm-2, ND = 1135
bottom of can: Rho D = 1.536E+06cm-2, ND = 1208

POOLED AGE = 128.2 ± 8.5 Ma
CENTRAL AGE = 128.3 ± 8.5 Ma

RD20-16 APATITE

IRRADIATION G344
SLIDE NUMBER 5
COUNTED BY: SJM

No.	Ns	Ni	Na	RATIO	U (ppm)	RHOs	RHOi	F.T. AGE (Ma)
1	13	20	70	0.650	4.0	2.951E+05	4.540E+05	165.6 ± 59.1
2	13	22	70	0.591	4.4	2.951E+05	4.994E+05	150.7 ± 52.8
3	6	18	60	0.333	4.2	1.589E+05	4.767E+05	85.4 ± 40.3
4	17	58	100	0.293	8.2	2.701E+05	9.217E+05	75.2 ± 20.8
5	12	11	40	1.091	3.9	4.767E+05	4.370E+05	275.5 ± 115.2
6	16	28	60	0.571	6.6	4.238E+05	7.416E+05	145.8 ± 45.8
7	25	49	100	0.510	6.9	3.973E+05	7.786E+05	130.3 ± 32.2
8	26	40	88	0.650	6.4	4.695E+05	7.223E+05	165.6 ± 41.9
9	12	25	100	0.480	3.5	1.907E+05	3.973E+05	122.7 ± 43.2
10	44	96	100	0.458	13.6	6.992E+05	1.526E+06	117.2 ± 21.5
11	50	71	100	0.704	10.0	7.945E+05	1.128E+06	179.2 ± 33.4
12	31	46	90	0.674	7.2	5.473E+05	8.122E+05	171.6 ± 40.1
13	6	13	60	0.462	3.1	1.589E+05	3.443E+05	118.0 ± 58.3
14	34	69	100	0.493	9.8	5.403E+05	1.096E+06	125.9 ± 26.6
15	16	32	60	0.500	7.5	4.238E+05	8.475E+05	127.7 ± 39.2
16	23	46	100	0.500	6.5	3.655E+05	7.310E+05	127.7 ± 32.8
17	20	25	54	0.800	6.5	5.885E+05	7.357E+05	203.2 ± 61.2
18	23	40	100	0.575	5.7	3.655E+05	6.356E+05	146.7 ± 38.6
19	20	40	60	0.500	9.4	5.297E+05	1.059E+06	127.7 ± 35.1
	407	749			7.0	4.277E+05	7.872E+05	

Area of basic unit = 6.293E-07 cm-2

Chi Squared = 16.255 with 18 degrees of freedom
P(chi squared) = 57.5 %
Correlation Coefficient = 0.885
Variance of SQR(Ns) = 1.54
Variance of SQR(Ni) = 2.97
Age Dispersion = 3.506 % (did not converge)

Ns/Ni = 0.543 ± 0.033
Mean Ratio = 0.570 ± 0.040

Ages calculated using a zeta of 350.7 ± 5 for SRM612 glass
Rho D = 1.471E+06cm-2; ND = 2343
Rho D interpolated between top of can; Rho D = 1.443E+06cm-2, ND = 1135
bottom of can; Rho D = 1.536E+06cm-2, ND = 1208

POOLED AGE = 138.7 ± 9.2 Ma
CENTRAL AGE = 138.7 ± 9.3 Ma

RD20-18 APATITE

IRRADIATION G344
SLIDE NUMBER 6
COUNTED BY: SJM

No.	Ns	Ni	Na	RATIO	U (ppm)	RHOs	RHOi	F.T. AGE (Ma)
1	17	22	40	0.773	7.7	6.754E+05	8.740E+05	197.3 ± 63.9
2	10	10	35	1.000	4.0	4.540E+05	4.540E+05	254.2 ± 113.9
3	2	5	50	0.400	1.4	6.356E+04	1.589E+05	102.9 ± 86.1
4	1	5	70	0.200	1.0	2.270E+04	1.135E+05	51.6 ± 56.6
5	12	13	49	0.923	3.7	3.892E+05	4.216E+05	235.0 ± 94.3
6	17	42	50	0.405	11.8	5.403E+05	1.335E+06	104.1 ± 30.0
7	3	9	60	0.333	2.1	7.945E+04	2.384E+05	85.8 ± 57.3
8	44	107	100	0.411	15.1	6.992E+05	1.700E+06	105.7 ± 19.1
9	14	17	48	0.824	5.0	4.635E+05	5.628E+05	210.1 ± 76.0
10	13	17	70	0.765	3.4	2.951E+05	3.859E+05	195.3 ± 72.1
11	4	9	50	0.444	2.5	1.271E+05	2.860E+05	114.2 ± 68.7
12	4	13	70	0.308	2.6	9.080E+04	2.951E+05	79.3 ± 45.4
13	12	29	63	0.414	6.5	3.027E+05	7.315E+05	106.4 ± 36.6
14	21	37	70	0.568	7.4	4.767E+05	8.399E+05	145.5 ± 39.9
15	3	8	60	0.375	1.9	7.945E+04	2.119E+05	96.5 ± 65.4
16	30	33	70	0.909	6.6	6.810E+05	7.491E+05	231.5 ± 58.7
17	6	8	40	0.750	2.8	2.384E+05	3.178E+05	191.6 ± 103.6
18	23	28	50	0.821	7.9	7.310E+05	8.899E+05	209.5 ± 59.2
19	12	21	60	0.571	4.9	3.178E+05	5.562E+05	146.5 ± 53.1
20	16	31	60	0.516	7.3	4.238E+05	8.210E+05	132.4 ± 40.9
	264	464			5.6	3.601E+05	6.329E+05	

Area of basic unit = 6.293E-07 cm-2

Chi Squared = 20.523 with 19 degrees of freedom
P(chi squared) = 36.4 %
Correlation Coefficient = 0.895
Variance of SQR(Ns) = 2.09
Variance of SQR(Ni) = 3.61
Age Dispersion = 15.705 %

Ns/Ni = 0.569 ± 0.044
Mean Ratio = 0.585 ± 0.053

Ages calculated using a zeta of 350.7 ± 5 for SRM612 glass
Rho D = 1.479E+06cm-2; ND = 2343
Rho D interpolated between top of can; Rho D = 1.443E+06cm-2, ND = 1135
bottom of can; Rho D = 1.536E+06cm-2, ND = 1208

POOLED AGE = 145.9 ± 11.8 Ma
CENTRAL AGE = 148.6 ± 13.6 Ma

RD20-19 APATITE

IRRADIATION G344
SLIDE NUMBER 7
COUNTED BY: SJM

No.	Ns	Ni	Na	RATIO	U (ppm)	RHOs	RHOi	F.T. AGE (Ma)
1	11	13	18	0.846	10.1	9.711E+05	1.148E+06	216.8 ± 89.0
2	1	5	16	0.200	4.4	9.932E+04	4.966E+05	51.9 ± 56.9
3	3	4	25	0.750	2.2	1.907E+05	2.542E+05	192.5 ± 147.1
4	3	12	24	0.250	7.0	1.986E+05	7.945E+05	64.8 ± 41.9
5	28	38	49	0.737	10.9	9.080E+05	1.232E+06	189.2 ± 47.4
6	5	5	20	1.000	3.5	3.973E+05	3.973E+05	255.4 ± 161.7
7	1	4	16	0.250	3.5	9.932E+04	3.973E+05	64.8 ± 72.5
8	3	6	30	0.500	2.8	1.589E+05	3.178E+05	129.0 ± 91.2
9	10	45	50	0.222	12.6	3.178E+05	1.430E+06	57.6 ± 20.2
10	17	8	30	2.125	3.7	9.005E+05	4.238E+05	531.1 ± 228.1
11	7	47	24	0.149	27.4	4.635E+05	3.112E+06	38.7 ± 15.7
12	13	18	15	0.722	16.8	1.377E+06	1.907E+06	185.5 ± 67.7
13	1	57	50	0.018	16.0	3.178E+04	1.812E+06	4.6 ± 4.6
14	3	10	16	0.300	8.8	2.980E+05	9.932E+05	77.7 ± 51.2
	106	272			10.0	4.398E+05	1.129E+06	

Area of basic unit = 6.293E-07 cm-2

Chi Squared = 66.381 with 13 degrees of freedom
P(chi squared) = 0.0 %
Correlation Coefficient = 0.257
Variance of SQR(Ns) = 1.69
Variance of SQR(Ni) = 4.00
Age Dispersion = 74.803 %

Ns/Ni = 0.390 ± 0.045
Mean Ratio = 0.576 ± 0.144

Ages calculated using a zeta of 350.7 ± 5 for SRM612 glass
Rho D = 1.486E+06cm-2; ND = 2343
Rho D interpolated between top of can; Rho D = 1.443E+06cm-2, ND = 1135
bottom of can; Rho D = 1.536E+06cm-2, ND = 1208

POOLED AGE = 100.7 ± 11.8 Ma
CENTRAL AGE = 116.3 ± 28.1 Ma

R220-31 APATITE S

IRRADIATION G344
SLIDE NUMBER 9
COUNTED BY: SJM

No.	Ns	Ni	Na	RATIO	U (ppm)	RHOs	RHOi	F.T. AGE (Ma)
1	4	6	15	0.667	5.6	4.238E+05	6.356E+05	173.0 ± 111.8
2	1	3	9	0.333	4.6	1.766E+05	5.297E+05	87.1 ± 100.6
3	8	19	21	0.421	12.6	6.054E+05	1.438E+06	109.8 ± 46.4
4	3	23	18	0.130	17.7	2.648E+05	2.030E+06	34.2 ± 21.0
5	5	6	40	0.833	2.1	1.986E+05	2.384E+05	215.5 ± 130.6
6	5	18	50	0.278	5.0	1.589E+05	5.721E+05	72.6 ± 36.8
7	3	10	42	0.300	3.3	1.135E+05	3.783E+05	78.4 ± 51.7
8	11	29	42	0.379	9.6	4.162E+05	1.097E+06	99.0 ± 35.1
9	14	21	30	0.667	9.7	7.416E+05	1.112E+06	173.0 ± 59.8
10	16	54	28	0.296	26.8	9.080E+05	3.065E+06	77.5 ± 22.1
11	11	22	42	0.500	7.3	4.162E+05	8.324E+05	130.2 ± 48.2
12	1	7	48	0.143	2.0	3.311E+04	2.317E+05	37.5 ± 40.1
13	3	14	40	0.214	4.9	1.192E+05	5.562E+05	56.1 ± 35.7
	85	232			7.6	3.178E+05	8.674E+05	

Area of basic unit = 6.293E-07 cm-2

Chi Squared = 12.382 with 12 degrees of freedom
P(chi squared) = 41.5 %
Correlation Coefficient = 0.806
Variance of SQR(Ns) = 0.97
Variance of SQR(Ni) = 2.28
Age Dispersion = 9.030 % (did not converge)

Ns/Ni = 0.366 ± 0.046
Mean Ratio = 0.397 ± 0.060

Ages calculated using a zeta of 350.7 ± 5 for SRM612 glass
Rho D = 1.500E+06cm-2; ND = 2343
Rho D interpolated between top of can; Rho D = 1.443E+06cm-2, ND = 1135
bottom of can; Rho D = 1.536E+06cm-2, ND = 1208

POOLED AGE = 95.7 ± 12.4 Ma
CENTRAL AGE = 95.8 ± 12.7 Ma

RD20-31 APATITE T

IRRADIATION G344
SLIDE NUMBER 8
COUNTED BY: SJM

No.	Ns	Ni	Na	RATIO	U (ppm)	RHOs	RHOi	F.T. AGE (Ma)
1	1	8	18	0.125	6.2	8.828E+04	7.063E+05	32.6 ± 34.6
2	14	29	16	0.483	25.3	1.390E+06	2.880E+06	125.1 ± 40.8
3	12	35	50	0.343	9.8	3.814E+05	1.112E+06	89.1 ± 29.9
4	2	10	21	0.200	6.6	1.513E+05	7.567E+05	52.1 ± 40.4
5	12	34	15	0.353	31.6	1.271E+06	3.602E+06	91.7 ± 30.9
6	4	6	10	0.667	8.4	6.356E+05	9.534E+05	172.2 ± 111.2
7	5	10	25	0.500	5.6	3.178E+05	6.356E+05	129.6 ± 71.0
8	15	63	40	0.238	22.0	5.959E+05	2.503E+06	62.0 ± 17.9
9	3	9	15	0.333	8.4	3.178E+05	9.534E+05	86.7 ± 57.8
10	1	7	16	0.143	6.1	9.932E+04	6.952E+05	37.3 ± 39.9
	69	211			13.0	4.852E+05	1.484E+06	

Area of basic unit = 6.293E-07 cm-2

Chi Squared = 6.567 with 9 degrees of freedom
P(chi squared) = 68.2 %
Correlation Coefficient = 0.898
Variance of SQR(Ns) = 1.31
Variance of SQR(Ni) = 3.55
Age Dispersion = 0.706 % (did not converge)

Ns/Ni = 0.327 ± 0.045
Mean Ratio = 0.338 ± 0.055

Ages calculated using a zeta of 350.7 ± 5 for SRM612 glass
Rho D = 1.493E+06cm-2; ND = 2343
Rho D interpolated between top of can; Rho D = 1.443E+06cm-2, ND = 1135
bottom of can; Rho D = 1.536E+06cm-2, ND = 1208

POOLED AGE = 85.0 ± 12.0 Ma
CENTRAL AGE = 85.0 ± 12.0 Ma

RD20-32 APATITE

IRRADIATION G344
SLIDE NUMBER 10
COUNTED BY: SJM

No.	Ns	Ni	Na	RATIO	U (ppm)	RHOs	RHOi	F.T. AGE (Ma)
1	2	11	56	0.182	2.7	5.675E+04	3.121E+05	47.9 ± 36.8
2	14	39	40	0.359	13.5	5.562E+05	1.549E+06	94.2 ± 29.4
3	13	23	36	0.565	8.8	5.738E+05	1.015E+06	147.7 ± 51.4
4	7	7	35	1.000	2.8	3.178E+05	3.178E+05	259.0 ± 138.6
5	2	14	49	0.143	3.9	6.486E+04	4.540E+05	37.6 ± 28.5
6	8	23	50	0.348	6.4	2.542E+05	7.310E+05	91.3 ± 37.5
7	7	9	60	0.778	2.1	1.854E+05	2.384E+05	202.3 ± 102.1
8	3	12	40	0.250	4.1	1.192E+05	4.767E+05	65.7 ± 42.5
9	15	26	40	0.577	9.0	5.959E+05	1.033E+06	150.7 ± 49.0
10	14	49	80	0.286	8.5	2.781E+05	9.733E+05	75.1 ± 22.8
11	9	33	40	0.273	11.4	3.575E+05	1.311E+06	71.7 ± 27.0
12	24	93	50	0.258	25.7	7.628E+05	2.956E+06	67.8 ± 15.6
13	5	17	70	0.294	3.4	1.135E+05	3.859E+05	77.3 ± 39.4
14	43	109	70	0.394	21.5	9.761E+05	2.474E+06	103.4 ± 18.8
15	8	14	28	0.571	6.9	4.540E+05	7.945E+05	149.3 ± 66.3
16	3	13	50	0.231	3.6	9.534E+04	4.132E+05	60.7 ± 38.9
17	5	16	50	0.312	4.4	1.589E+05	5.085E+05	82.1 ± 42.1
18	17	26	40	0.654	9.0	6.754E+05	1.033E+06	170.5 ± 53.4
19	5	16	70	0.312	3.2	1.135E+05	3.632E+05	82.1 ± 42.1
20	6	19	70	0.316	3.7	1.362E+05	4.313E+05	82.9 ± 38.9
	210	569			7.7	3.259E+05	8.830E+05	

Area of basic unit = 6.293E-07 cm-2

Chi Squared = 21.996 with 19 degrees of freedom
P(chi squared) = 28.4 %
Correlation Coefficient = 0.915
Variance of SQR(Ns) = 1.60
Variance of SQR(Ni) = 4.23
Age Dispersion = 10.066 % (did not converge)

Ns/Ni = 0.369 ± 0.030
Mean Ratio = 0.405 ± 0.049

Ages calculated using a zeta of 350.7 ± 5 for SRM612 glass
Rho D = 1.507E+06cm-2; ND = 2343
Rho D interpolated between top of can; Rho D = 1.443E+06cm-2, ND = 1135
bottom of can; Rho D = 1.536E+06cm-2, ND = 1208

POOLED AGE = 96.8 ± 8.2 Ma
CENTRAL AGE = 97.3 ± 8.7 Ma

RD20-35 APATITE

IRRADIATION G344
SLIDE NUMBER 11
COUNTED BY: SJM

No.	Ns	Ni	Na	RATIO	U (ppm)	RHOs	RHOi	F.T. AGE (Ma)
1	11	25	100	0.440	3.4	1.748E+05	3.973E+05	115.8 ± 42.0
2	18	44	97	0.409	6.2	2.949E+05	7.208E+05	107.7 ± 30.3
3	2	7	49	0.286	2.0	6.486E+04	2.270E+05	75.4 ± 60.5
4	14	47	90	0.298	7.2	2.472E+05	8.298E+05	78.6 ± 24.0
5	2	13	90	0.154	2.0	3.531E+04	2.295E+05	40.7 ± 30.9
6	23	70	100	0.329	9.6	3.655E+05	1.112E+06	86.7 ± 20.9
7	2	4	84	0.500	0.7	3.783E+04	7.567E+04	131.4 ± 113.9
8	15	40	63	0.375	8.7	3.783E+05	1.009E+06	98.8 ± 30.0
9	9	25	64	0.360	5.4	2.235E+05	6.207E+05	94.9 ± 37.0
10	6	10	60	0.600	2.3	1.589E+05	2.648E+05	157.4 ± 81.4
11	6	15	50	0.400	4.1	1.907E+05	4.767E+05	105.3 ± 51.0
12	37	57	90	0.649	8.7	6.533E+05	1.006E+06	170.1 ± 36.2
13	13	29	80	0.448	5.0	2.582E+05	5.760E+05	117.9 ± 39.5
14	4	18	100	0.222	2.5	6.356E+04	2.860E+05	58.7 ± 32.5
15	5	12	50	0.417	3.3	1.589E+05	3.814E+05	109.7 ± 58.5
16	33	79	100	0.418	10.9	5.244E+05	1.255E+06	110.0 ± 23.0
17	9	42	100	0.214	5.8	1.430E+05	6.674E+05	56.6 ± 20.9
18	10	25	60	0.400	5.7	2.648E+05	6.621E+05	105.3 ± 39.5
19	17	26	70	0.654	5.1	3.859E+05	5.902E+05	171.3 ± 53.6
	236	588			5.4	2.505E+05	6.242E+05	

Area of basic unit = 6.293E-07 cm-2

Chi Squared = 16.569 with 18 degrees of freedom
P(chi squared) = 55.3 %
Correlation Coefficient = 0.884
Variance of SQR(Ns) = 1.85
Variance of SQR(Ni) = 3.67
Age Dispersion = 10.506 % (did not converge)

Ns/Ni = 0.401 ± 0.031
Mean Ratio = 0.399 ± 0.031

Ages calculated using a zeta of 350.7 ± 5 for SRM612 glass
Rho D = 1.514E+06cm-2; ND = 2343
Rho D interpolated between top of can: Rho D = 1.443E+06cm-2, ND = 1135
bottom of can: Rho D = 1.536E+06cm-2, ND = 1208

POOLED AGE = 105.7 ± 8.6 Ma
CENTRAL AGE = 105.3 ± 9.1 Ma

RD20-36 APATITE

IRRADIATION G386
SLIDE NUMBER 1
COUNTED BY: SJM

No.	Ns	Ni	Na	RHOs	RHOi	RATIO	U (ppm)	F.T. AGE (Ma)
1	1	15	50	3.178E+04	4.767E+05	0.067	4.2	17.3 ± 17.9
2	12	52	100	1.907E+05	8.263E+05	0.231	7.3	59.8 ± 19.2
3	5	7	30	2.648E+05	3.708E+05	0.714	3.3	183.3 ± 107.4
4	8	16	42	3.027E+05	6.054E+05	0.500	5.3	128.9 ± 55.9
5	13	20	24	8.607E+05	1.324E+06	0.650	11.7	167.1 ± 59.7
6	23	53	80	4.569E+05	1.053E+06	0.434	9.3	112.0 ± 28.1
7	9	10	40	3.575E+05	3.973E+05	0.900	3.5	230.2 ± 105.9
8	9	40	50	2.860E+05	1.271E+06	0.225	11.2	58.3 ± 21.6
9	8	17	28	4.540E+05	9.648E+05	0.471	8.5	121.4 ± 52.1
10	19	43	50	6.038E+05	1.367E+06	0.442	12.1	114.0 ± 31.5
11	4	11	30	2.119E+05	5.827E+05	0.364	5.1	94.0 ± 54.9
12	0	1	35	0.000E+00	4.540E+04	0.000	0.4	0.0 ± 0.0
13	26	45	70	5.902E+05	1.022E+06	0.578	9.0	148.7 ± 36.8
14	1	4	25	6.356E+04	2.542E+05	0.250	2.2	64.8 ± 72.4
15	66	197	30	3.496E+06	1.043E+07	0.335	92.1	86.6 ± 12.5
16	8	19	40	3.178E+05	7.548E+05	0.421	6.7	108.7 ± 45.9
17	12	20	30	6.356E+05	1.059E+06	0.600	9.3	154.4 ± 56.5
18	5	19	36	2.207E+05	8.387E+05	0.263	7.4	68.2 ± 34.3
19	7	9	42	2.648E+05	3.405E+05	0.778	3.0	199.4 ± 100.6
20	5	12	40	1.986E+05	4.767E+05	0.417	4.2	107.6 ± 57.3
	241	610		4.392E+05	1.112E+06		9.8	

Area of basic unit = 6.293E-07 cm-2

Chi Squared = 24.574 with 19 degrees of freedom
P(chi squared) = 17.5 %
Correlation Coefficient = 0.961
Variance of SQR(Ns) = 2.97
Variance of SQR(Ni) = 7.67
Age Dispersion = 16.888 % (did not converge)

Ns/Ni = 0.395 ± 0.030
Mean Ratio = 0.432 ± 0.051

Ages calculated using a zeta of 350.7 ± 5 for SRM612 glass
Rho D = 1.485E+06cm-2; ND = 2408
Rho D interpolated between top of can; Rho D = 1.485E+06cm-2, ND = 1168
bottom of can; Rho D = 1.576E+06cm-2, ND = 1240

POOLED AGE = 102.1 ± 8.2 Ma
CENTRAL AGE = 105.4 ± 10.1 Ma

RD20-37 APATITE

IRRADIATION G386
SLIDE NUMBER 2
COUNTED BY: SJM

No.	Ns	Ni	Na	RHOs	RHOi	RATIO	U (ppm)	F.T. AGE (Ma)
1	5	18	50	1.589E+05	5.721E+05	0.278	5.0	72.3 ± 36.6
2	4	10	30	2.119E+05	5.297E+05	0.400	4.7	103.8 ± 61.5
3	28	97	74	6.013E+05	2.083E+06	0.289	18.3	75.1 ± 16.2
4	21	77	50	6.674E+05	2.447E+06	0.273	21.5	71.0 ± 17.6
5	6	15	49	1.946E+05	4.864E+05	0.400	4.3	103.8 ± 50.2
6	6	7	50	1.907E+05	2.225E+05	0.857	2.0	220.4 ± 122.8
7	22	45	50	6.992E+05	1.430E+06	0.489	12.6	126.6 ± 33.1
8	24	59	25	1.526E+06	3.750E+06	0.407	32.9	105.5 ± 25.7
9	11	20	48	3.642E+05	6.621E+05	0.550	5.8	142.3 ± 53.5
10	19	53	64	4.718E+05	1.316E+06	0.358	11.6	93.1 ± 25.0
11	29	88	100	4.608E+05	1.398E+06	0.330	12.3	85.6 ± 18.5
12	6	18	35	2.724E+05	8.172E+05	0.333	7.2	86.6 ± 40.9
13	12	32	80	2.384E+05	6.356E+05	0.375	5.6	97.4 ± 33.0
14	26	58	48	8.607E+05	1.920E+06	0.448	16.9	116.2 ± 27.6
15	9	14	60	2.384E+05	3.708E+05	0.643	3.3	166.0 ± 71.0
16	7	50	50	2.225E+05	1.589E+06	0.140	14.0	36.5 ± 14.8
17	20	57	70	4.540E+05	1.294E+06	0.351	11.4	91.1 ± 23.8
18	21	38	70	4.767E+05	8.626E+05	0.553	7.6	143.0 ± 39.0
19	4	16	48	1.324E+05	5.297E+05	0.250	4.7	65.1 ± 36.4
20	4	18	40	1.589E+05	7.151E+05	0.222	6.3	57.9 ± 32.0
	284	790		4.137E+05	1.151E+06		10.1	

Area of basic unit = 6.293E-07 cm-2

Chi Squared = 20.841 with 19 degrees of freedom
P(chi squared) = 34.6 %
Correlation Coefficient = 0.884
Variance of SQR(Ns) = 1.54
Variance of SQR(Ni) = 4.72
Age Dispersion = 7.635 % (did not converge)

Ns/Ni = 0.359 ± 0.025
Mean Ratio = 0.397 ± 0.036

Ages calculated using a zeta of 350.7 ± 5 for SRM612 glass
Rho D = 1.492E+06cm-2; ND = 2408
Rho D interpolated between top of can; Rho D = 1.485E+06cm-2, ND = 1168
bottom of can; Rho D = 1.576E+06cm-2, ND = 1240

POOLED AGE = 93.4 ± 6.9 Ma
CENTRAL AGE = 93.7 ± 7.1 Ma

RD20-38 APATITE

IRRADIATION G386
SLIDE NUMBER 3
COUNTED BY: SJM

No.	Ns	Ni	Na	RHOs	RHOi	RATIO	U (ppm)	F.T. AGE (Ma)
1	5	10	60	1.324E+05	2.648E+05	0.500	2.3	130.1 ± 71.3
2	16	42	42	6.054E+05	1.589E+06	0.381	13.9	99.4 ± 29.3
3	7	12	35	3.178E+05	5.448E+05	0.583	4.8	151.5 ± 72.2
4	15	30	56	4.256E+05	8.513E+05	0.500	7.4	130.1 ± 41.3
5	17	57	100	2.701E+05	9.058E+05	0.298	7.9	77.9 ± 21.6
6	14	36	30	7.416E+05	1.907E+06	0.389	16.7	101.4 ± 32.0
7	25	63	80	4.966E+05	1.251E+06	0.397	10.9	103.5 ± 24.6
8	8	23	35	3.632E+05	1.044E+06	0.348	9.1	90.8 ± 37.3
9	16	35	50	5.085E+05	1.112E+06	0.457	9.7	119.0 ± 36.0
10	18	28	28	1.022E+06	1.589E+06	0.643	13.9	166.8 ± 50.6
11	11	8	36	4.855E+05	3.531E+05	1.375	3.1	351.6 ± 163.6
12	4	22	40	1.589E+05	8.740E+05	0.182	7.6	47.6 ± 25.9
13	3	7	70	6.810E+04	1.589E+05	0.429	1.4	111.7 ± 77.1
14	14	40	35	6.356E+05	1.816E+06	0.350	15.9	91.3 ± 28.5
15	15	38	50	4.767E+05	1.208E+06	0.395	10.6	102.9 ± 31.5
16	6	15	80	1.192E+05	2.980E+05	0.400	2.6	104.3 ± 50.4
17	22	53	80	4.370E+05	1.053E+06	0.415	9.2	108.2 ± 27.6
18	21	66	100	3.337E+05	1.049E+06	0.318	9.2	83.1 ± 20.9
19	6	18	40	2.384E+05	7.151E+05	0.333	6.2	87.0 ± 41.1
20	7	23	48	2.317E+05	7.614E+05	0.304	6.7	79.5 ± 34.4
	250	626		3.628E+05	9.085E+05		7.9	

Area of basic unit = 6.293E-07 cm-2

Chi Squared = 17.144 with 19 degrees of freedom
P(chi squared) = 58.0 %
Correlation Coefficient = 0.880
Variance of SQR(Ns) = 0.93
Variance of SQR(Ni) = 2.79
Age Dispersion = 0.309 % (did not converge)

Ns/Ni = 0.399 ± 0.030
Mean Ratio = 0.450 ± 0.054

Ages calculated using a zeta of 350.7 ± 5 for SRM612 glass
Rho D = 1.499E+06cm-2; ND = 2408
Rho D interpolated between top of can; Rho D = 1.485E+06cm-2, ND = 1168
bottom of can; Rho D = 1.576E+06cm-2, ND = 1240

POOLED AGE = 104.1 ± 8.2 Ma
CENTRAL AGE = 104.1 ± 8.2 Ma

RD20-39 APATITE

IRRADIATION G386
SLIDE NUMBER 4
COUNTED BY: SJM

No.	Ns	Ni	Na	RHOs	RHOi	RATIO	U (ppm)	F.T. AGE (Ma)
1	8	18	60	2.119E+05	4.767E+05	0.444	4.1	116.3 ± 49.5
2	9	13	50	2.860E+05	4.132E+05	0.692	3.6	180.3 ± 78.3
3	13	26	100	2.066E+05	4.132E+05	0.500	3.6	130.7 ± 44.5
4	13	21	100	2.066E+05	3.337E+05	0.619	2.9	161.4 ± 57.1
5	1	6	28	5.675E+04	3.405E+05	0.167	3.0	43.9 ± 47.4
6	5	6	27	2.943E+05	3.531E+05	0.833	3.1	216.4 ± 131.1
7	6	14	60	1.589E+05	3.708E+05	0.429	3.2	112.2 ± 54.8
8	9	16	100	1.430E+05	2.542E+05	0.562	2.2	146.9 ± 61.3
9	14	43	100	2.225E+05	6.833E+05	0.326	5.9	85.4 ± 26.4
10	17	29	50	5.403E+05	9.217E+05	0.586	8.0	153.0 ± 46.9
11	7	8	40	2.781E+05	3.178E+05	0.875	2.8	227.0 ± 117.6
12	3	14	80	5.959E+04	2.781E+05	0.214	2.4	56.3 ± 35.9
13	13	18	100	2.066E+05	2.860E+05	0.722	2.5	187.9 ± 68.6
14	7	10	25	4.449E+05	6.356E+05	0.700	5.5	182.2 ± 89.9
15	19	38	56	5.391E+05	1.078E+06	0.500	9.4	130.7 ± 36.9
16	16	17	50	5.085E+05	5.403E+05	0.941	4.7	243.9 ± 85.2
17	17	21	100	2.701E+05	3.337E+05	0.810	2.9	210.3 ± 68.8
18	25	53	30	1.324E+06	2.807E+06	0.472	24.4	123.4 ± 30.1
19	17	30	70	3.859E+05	6.810E+05	0.567	5.9	147.9 ± 45.1
20	26	71	48	8.607E+05	2.350E+06	0.366	20.4	96.0 ± 22.1
	245	472		3.056E+05	5.887E+05		5.1	

Area of basic unit = 6.293E-07 cm-2

Chi Squared = 17.179 with 19 degrees of freedom
P(chi squared) = 57.8 %
Correlation Coefficient = 0.872
Variance of SQR(Ns) = 1.11
Variance of SQR(Ni) = 2.50
Age Dispersion = 4.720 % (did not converge)

Ns/Ni = 0.519 ± 0.041
Mean Ratio = 0.566 ± 0.048

Ages calculated using a zeta of 350.7 ± 5 for SRM612 glass
Rho D = 1.506E+06cm-2; ND = 2408
Rho D interpolated between top of can; Rho D = 1.485E+06cm-2, ND = 1168
bottom of can; Rho D = 1.576E+06cm-2, ND = 1240

POOLED AGE = 135.6 ± 11.2 Ma
CENTRAL AGE = 135.9 ± 11.4 Ma

Appendix 10. Geophysical data, Western Onshore Gippsland Basin.

Appendix 10-1. Permeability, Porosity and Density.

Basin: Dike or well/ x (meters) Direction,	Rock Description	Permeability K, in air, millidarcies	Porosity %, in He	Bulk density g/cc	Grain density g/cc
Gippsland:					
K1/ 0.5 W	metasandstone or hornfels	0.008	13.1	2.32	2.67
K1/ 11 W	ss, medium grain, thick bedded, moderately weathered	2.72	26.2	1.98	2.69
K1/ 24.8 W	ss, medium grain, thick bedded, moderately weathered	N/R, poor plug condition	30.1	1.88	2.69
I1/ 0.03 W	metasandstone or hornfels	0.02	15.7	2.28	2.71
I1/ 1.06 W	ss, medium grain, medium bedded.	N/R, poor plug condition	26.4	1.99	2.7

Appendix 10-2. Thermal Conductivity (K) measurements, water saturated, at 34.5 MPa confining pressure.

Dike/ x, in meters and direction	Rock Description	K (W/m·K) at 20°C	K (W/m·K) at 50°C	K (W/m·K) at 100°C	K (W/m·K) at 150°C
B3/ -10 W	Gabbro, coarse grained, holocrystalline	1.71	1.81	2.19	2.09
K1/ 0.5 W	dense metasandstone or hornfels	1.59	1.91	N/A	1.83
K1/ 11 W	ss, medium grain, thick bedded	1.66	1.91	1.84	2.03
K1/ 24.8 W	ss, medium grain, thick bedded	1.59	1.94*	1.69*	1.63*
I1/ 0-0.1 W	metasandstone or hornfels	1.56	1.90	2.05	2.15
I1/ 1.0-1.12 W	ss, medium grain, medium bedded.	1.51	1.94*	1.68*	1.97*
I1/ 1.75-1.85 W	ss, medium grain, medium bedded	1.58	1.78	1.75	2.03

* These samples had a thermal conductivity reversal at increased temperature interpreted to be due to irreversible sample damage caused by the measurement procedure (Written communication, Dr. Colin Williams, USGS, Menlo Park, California).

Appendix 11.

Publications by Charles E. Barker related to the thesis.

Peer Reviewed Papers

Barker, C.E. and Pawlewicz, M.J., 1993, An empirical determination of the minimum number of measurements needed to estimate the mean random vitrinite reflectance of disseminated Organic Matter: Organic Geochemistry, v. 20, p. 643-651.

Barker, C.E. and Pawlewicz, M.J. , 1994, Calculation of vitrinite reflectance from thermal histories and peak temperature: a comparison of methods, *In* Mukhopadhyay, P.K. and Dow, W.G., eds., Vitrinite Reflectance as a Maturity Parameter: American Chemical Society Symposium Series number 570, p. 216-229.

Barker, C.E. and Bone, Y., 1995, The minimal response to contact metamorphism by the Devonian Buchan Caves Limestone, Buchan Rift, Victoria, Australia: Organic Geochemistry, v. 22, p. 151-164.

Extended Abstracts

Barker, C.E., 1994, Vitrinite reflectance of whole-rock versus dispersed organic matter mounts: what's the difference?: Abstracts, The Society for Organic Petrology, v. 11, p. 1-4.

Barker, C.E., Bone, Y., and Dalgarno, C.R., 1992a, Contact metamorphism of organic matter in the Buchan Caves Limestone, Buchan Trough, Victoria, Australia : Abstracts, Eleventh Australian Geology Congress, Ballarat, Victoria, Australia. p. 127-128.

Publications by Charles E. Barker related to the thesis.

Extended Abstracts (continued)

Barker, C.E., Bone, Y., Duddy, I.R., Marshallsea, S.J., and Green, P.F., 1992b, Peak temperature estimated from fluid inclusions and vitrinite reflectance next to a thin dike near San Remo, Victoria, Australia: Abstracts, The Society for Organic Petrology, v. 9, p. 102-104.

Barker, C.E. and Bone, Y., 1993, A minimal response to contact metamorphism by the Devonian Buchan Group limestones, Buchan Trough, Victoria, Australia--evidence from impsonite reflectance, isotopic composition and fluid inclusions: Abstracts, The Society for Organic Petrology, v. 10 , p. 84-86

Barker, C.E. & Pawlewicz, M.J. (1993) An empirical determination of the minimum number of measurements needed to estimate the mean random vitrinite reflectance of disseminated organic matter.
Organic Geochemistry, v. 20(6), pp. 643-651

Barker, C.E. & Pawlewicz, M.J. (1994) Calculation of vitrinite reflectance from thermal histories and peak temperatures: a comparison of methods.
Presented at 206th National Meeting of the American Chemical Society, Chicago, Illinois, 22-27 August

Barker, C.E. and Bone, Y., 1995, The minimal response to contact metamorphism by the Devonian Buchan Caves Limestone, Buchan Rift, Victoria, Australia: Organic Geochemistry, v. 22, P.151-164.

Barker, C.E. (1994) Vitrinite reflectance of whole-rock versus dispersed organic matter concentrate mounts: what's the difference?.
Presented at: 11th Annual Meeting of the Society for Organic Petrology, Jackson, Wyoming, 25-30September

Barker, C.E., Bone, Y. & Dalgarno, C.R. (1992) Contact metamorphism of organic matter in the Buchan Caves limestone, Buchan Trough, Victoria Australia.
Presented at: 11th Australian Geology Congress, Ballarat, Victoria

NOTE: This publication is not included in the thesis

PARAMETERS OF TIME AND HEAT IN ORGANIC MATURATION: A CASE STUDY FROM THE BUCHAN LIMESTONE

C.E. Barker(1,2)*, Bone, Y.(1), and Dalgarno, C.R.(3)

(1) Department of Geology and Geophysics, University of Adelaide, South Australia
(2) U.S. Geological Survey, Denver, Colorado 80225 U.S.A.
(3) Geological Survey of Victoria, Melbourne, Victoria

It has long been established that there is a minimum time during which temperature must be elevated for organic material in sediments to mature into the oil/gas window. This work is based, in part, on models of thermal maturity that use measured vitrinite reflectance and the computed rock temperature profile from heat flow equations. These results can now be tested by a new technique using reequilibrated fluid inclusions in metamorphosed cements (Barker and Goldstein, 1990). Microthermometry of the reequilibrated fluid inclusions is used here to indicate the peak temperature reached in rocks adjacent to dykes. The test of thermal maturity models involves measuring peak temperature and vitrinite reflectance, and comparing them to the computed temperature, heating time, and thermal maturity. The expected vitrinite reflectance profile should be comparable to the measured values. Because peak temperature and vitrinite reflectance are measured, the influence of heating time in modeling thermal maturity can be clearly assessed.

This paper considers a Tertiary dyke that has intruded the Devonian Buchan Caves Limestone, near Murrindal, Victoria. Samples were taken from one bed at increasing horizontal distance from the near-vertical dyke margin. Regional background measurements were made on samples far removed from the intrusions. Vitrinite was sparse in these samples adjacent to the dyke, and reflectance

measurements was not practical on this maceral. However, fracture- and pore-lining bitumen (meso-impsonite), showing a well developed mosaic structure, is common in these samples. The bitumen has a reflectance of about 2.4 to 2.7% (equivalent to about 2.0% vitrinite reflectance--Jacob, 1975). Bitumen reflectance showed little change up to 6 m away from the dyke contact. This thermal maturity level suggests a peak temperature of over 200°C was reached during metamorphism. Other studies of fluid inclusions trapped in lead-zinc deposits indicate similar paleotemperatures were widespread throughout the Buchan trough.

Although these sample limitations negate a test of vitrinite-reflectance based thermal-maturity models at this site, it is important to note that bitumen was present in the Buchan Caves Limestone when the Tertiary dyke intruded. Thus, oil generation and subsequent formation of meso-impsonite occurred before the Tertiary dyke intruded the Buchan Trough.

References

Barker, C.E., and Goldstein, R.H., 1990, A fluid inclusion technique for determining maximum temperature in calcite and its comparison to the vitrinite reflectance geothermometer: Geology, v. 18, p. 1003-1006.

Jacob, H., 1975, Mikroskopphotometrische Analyse naturlicher fester Erdolbitumina, in, Alpern, B., ed., Petrographie Organique et Potentiel Petrolier. Coll. int., CNRS, Paris. p. 103-113.

Barker, C.E., Bone, Y., Duddy, I.R., Marshallsea, S.J. & Green, P.F. (1992) Peak temperature estimated from fluid inclusions and vitrinite reflectance next to a thin dike near San Remo, Victoria, Australia.
Presented at: 9th Annual Meeting of the Society for Organic Petrology

Barker, C.E. and Bone, Y., 1993, A minimal response to contact metamorphism by the Devonian Buchan Group limestones, Buchan Trough, Victoria, Australia - Evidence from impsonite reflectance, isotopic composition and fluid inclusions: Abstracts, The Society for Organic Petrology, v. 10 , p. 84-86